Modelling Stress-Dependent Effective Porosity-Permeability Relationships of Metre-Scale Heterogeneous Mudstones

Michael C. Drews

Submitted in fulfilment for the degree of Doctor of Philosophy in the Faculty of Science.

School of Civil Engineering and Geoscience
Newcastle University

August, 2012

Declaration

I hereby declare that this is my own work, except where otherwise acknowledged, and that it has not been submitted for a degree at this, or any other university.

Michael C. Drews

Abstract

The importance of shales and mudstones to applied geosciences and in particular to fluid migration in sedimentary basins has never been more recognized than today. Prominent examples are conventional or unconventional petroleum systems, where shales and mudstones act as source, reservoir or cap rock, but also CO_2 and nuclear waste storage or hydrogeology. Despite their importance, shales and mudstones are yet not as far well understood as sandstones or carbonate rocks. In particular, the influence of heterogeneity on fluid migration has been poorly addressed in the past, although many authors have identified and studied heterogeneities in shales and mudstones. Nevertheless, their flow properties are fairly well understood when treated as homogeneous on sample scale (centimetre-scale). Typical flow relevant heterogeneities are grain size and thus petrophysical property (e.g. porosity, permeability, capillary entry pressures) variations due to spatial lithological variation induced by primary and secondary sedimentary structures.

In this study we investigate flow relevant heterogeneities of shales and mudstones on sub-metre scale derived from core and borehole images from an off-shore gas field in the Western Nile Delta, Egypt. Thereby, we combine latest models and published measurements of sample-scale petrophysical properties with interpretation, quantitative analyses, advanced modelling and numerical fluid flow simulation to assess the influence of shale and mudstone heterogeneity on fluid flow and hence, fluid migration, retention and mudstone seal capacity. Additionally, the set of mudstone heterogeneities used in this study has been derived from a combined visual and geostatistical interpretation of more than 500 m of mud-rich core and borehole images.

As final results, we deliver stress-dependent effective porosity-permeability relationships for a broad range of shale and mudstone heterogeneities, representative model sizes and resolution as well as measures of uncertainty for each heterogeneity type. Moreover, probability density functions describing where and how these heterogeneities appear in larger scale geological units, such as seismic facies or local depositional environments, are provided. As a key result, heterogeneity and lithological variation have great influences on effective permeability and effective permeability anisotropy (K_h/K_v). Furthermore, our results indicate that mudstone heterogeneity is very common in all investigated larger scale geological units (hemipelagites, levees, channels). Modelling of fluid flow through mud-rich sedimentary basins without inclusion of these sub-metre scale heterogeneities of mudstones can therefore lead to misleading results. Thus, effective porosity-permeability (anisotropy) relationships are provided for different lithological variations and mudstone heterogeneities as a final result.

Acknowledgements

First of all I would like to express thanks to my supervisor Professor Andy Aplin, who always found the right words of encouragement, guidance and advice. Additionally, I would like to show gratitude to Dr Kuncho Kurtev for vital and enthusiastic discussions about geostatistics, maths and geology and for sharing his great ideas with me. Also, I would like to thank Dr Ulf Boeker for critical discussions about uncertainties of data and about the geology of the Western Nile Delta, Egypt. I would like to thank all three of you for your friendship and support during my time in Newcastle and beyond.

The participation in different industry founded projects allowed me to work with great researchers from different Universities throughout the UK and Canada. Dr Jing-Sheng Ma and Professor Gary Couples from Heriot-Watt University, Edinburgh, supported me with numerical know-how, whenever it was necessary and they thus had a great impact on my project. Also, I would like to thank Professor Joe Cartwright, Professor Quentin Fisher, Professor Steve Larter, Dr Tiago Alves, Dr Aggeliki Georgiopoulou, Dr Xiuwen Mo, and Dr Mohamed Rouainia for their kind support and for opening my mind for new approaches and aspects in Petroleum Geology.

This Ph.D. project has been part of and founded by the Caprocks Project. I would like to thank BP for providing a great data base and the sponsor representatives for their comments, criticism, encouragement and hospitality at various meetings in the past three years.

I would additionally like to thank my family for their fantastic support. Last but not least, I express my everlasting gratitude to my beloved wife Laura, who did not hesitate to make the move with me to Newcastle and who supported me ever since and before.

Table of Contents

List of Figures

List of Tables

Important Terminology

Anisotropy: The ratio between horizontal and vertical properties. For example, the permeability anisotropy A_K is given by K_h/K_v, where K_h is the horizontal permeability and K_v is the vertical permeability.

Borehole image: In this study referred to formation micro images obtained from a spatially resolved electrical resistivity well log.

Clay content: Sample specific grain size fraction summing all grains with a size < 2 µm.

Coarse silt: Sample specific grain size fraction summing all grains with a size 10-63 µm.

Cohesive content: Sample specific grain size fraction summing the cohesive grain size fractions (< 10 µm) clay and fine silts.

Covariance function: Can be used to model (fit) an *experimental semi-variogram* to approximate the *experimental semi-variogram* with a mathematical formulation.

Effective stress: Overburden subtracted by pore pressure. Effective stress is the main parameter driving mechanical compaction.

Experimental semi-variogram: Geostatistical tool to describe spatial variation (heterogeneity).

Fine silt: Sample specific grain size fraction summing all grains with a size 2-10 µm.

Geostatistical realisation: Geostatistical simulation reproduces stochastically defined spatial distributions. Each realisation of this simulation will be stochastically equal, but might vary in its visible appearance and thus effective properties.

Heterogeneity: Spatial lithological variation in a *mudstone* due to primary or secondary sedimentary processes.

Indicator distribution: A discrete distribution, which can be used to apply qualitative properties (e.g. assigning lithologies such as mud, silt and sand to cells of a model).

Sub-metre scale: centimetre-metre scale.

Model: *Geostatistical realisation* of a *structural template*.

Mud and mud content: Bulk lithological property on all scales beyond sample scale (centimetre-scale). A sample can be called mud, if its *cohesive content* is equal or greater than 50%. For example, a modelled *structural template* build up of sample sized cells has 100% of mud content, if all of its sample sized cells have *cohesive contents* equal or greater than 50%.

Mudstone: *Sub-metre scale* rock, which has a *mud content* equal or greater than 50%.

Percolation threshold: A heterogeneous system, which is described by spatial lithological variability is connected by a continuous network (e.g. a *sub-metre scale* sand network), when a certain ratio (the *percolation threshold*) of the involved lithologies (e.g. mud and

sand) is reached. Usually this threshold is assessed in a statistical way, by investigating the connectivity of several realisations of the *heterogeneity*.

Petrophysical modeling framework: All cells of a *model* are populated with lithological (grain size fractions) and petrophysical (porosity and permeability) properties. Hereby the cells are treated as homogeneous samples, whose properties can be modelled from *cohesive content* and effective stress by employing a *petrophysical modelling framework* derived from sample measurements, mechanical experimental compaction data, empirical and theoretical relationships.

Sand: Sample specific grain size fraction summing all grains with a size >63 µm.

Structural class: Definition of a geological *heterogeneity* present in mudstones

Structural template: Representative, real data (core and borehole images) end-member of a *sub-metre scale*, spatial heterogeneity, which is related to sedimentary structures present in *mudstones*.

Variography: Geostatistical analysis of the *experimental semi-variogram*. The analysis can be for interpretation of the shape of the *experimental semi-variogram* or for modelling the *experimental semi-variogram* with a *covariance function*.

Chapter 1: Introduction

Motivation

Shales and mudstones are not only the most abundant rock in the Earth's sedimentary basins, they also play an important role in conventional and unconventional petroleum systems, as well as in many other applied aspects of geosciences, such as hydrology, CO_2 and nuclear waste storage sites. Within the past years many author's studied, investigated and described shales and mudstones on different scales (e.g. Potter et al., 1980; Neuzil, 1994; Dewhurst et al., 1998, 1999a, 1999b; Schieber, 1999; Aplin et al., 1999; Macquaker and Adams, 2003; Mondol et al., 2007, 2008; Macquaker and Bohacs, 2007; Piper et al., 2010; Schieber et al., 2007, 2010; Yang and Aplin, 2004, 2007, 2010; Aplin and Macquaker, 2011). Thereby, shales and mudstones have been either investigated from sub-millimetre to millimetre (e.g. on micrographs and thin-sections) to centimetre-scale (e.g. core plug samples) for their textural and petrophysical properties, such as grain size and alignment, mineralogy, porosity and permeability or for their structural appearance (heterogeneity) related to sedimentary processes on micrographs, core (sub-metre scale), outcrops (metre-scale) and large scale geophysical measurements (10-100 m). Thereby, it is well known, that small scale (cm-m) heterogeneity can have a significant influence on larger scale fluid flow processes (e.g. Pickup et al., 2000; Eaton 2006). However, the interplay of both, mudstone petrophysical variety and beyond millimetre-scale mudstone heterogeneities in terms of fluid flow in sedimentary basins, has been only poorly studied, as Aplin and Macquaker (2011) pinpoint in their recent review on mudstone diversity: "*Although the petrophysical properties of homogeneous mudstones are reasonably well known, the quantitative implications of heterogeneity for* [fluid] *expulsion, retention,* […] *migration, seal capacity* [and] *acoustic anisotropy* […] *are essentially unexplored. Future work should seek to redress this position.*" Even more, in many cases of assessing fluid flow in sedimentary basins, the physical property derived from point-wise measurements (1D geophysical well log or sample measurement) is usually directly upscaled to the cell scale (10s to 100s of metres) of the basin model, neglecting the centimetre-to-metre-scale heterogeneities of mud-rich sequences. The work presented in this thesis contributes to this issue by investigating the influence of sub-metre-scale shale and mudstone heterogeneity derived from core and borehole images from an offshore gas field in the Nile Delta, Egypt, on stress-dependent, effective porosity-permeability relationships. Hereby, quantitative methods are used and the study can be seen as part of a complete upscaling process to describe mudstone heterogeneity and its influence on fluid flow from

sample to full field scale (Figure 1.1). The results of this study are therefore of direct relevance to "[...] *the quantitative implications of heterogeneity* […]" (Aplin and Macquaker, 2011) of shale and mudstones for fluid flow in sedimentary basins and its applied aspects such as prediction of groundwater contamination, petroleum production and CO_2 and nuclear waste storage site assessment.

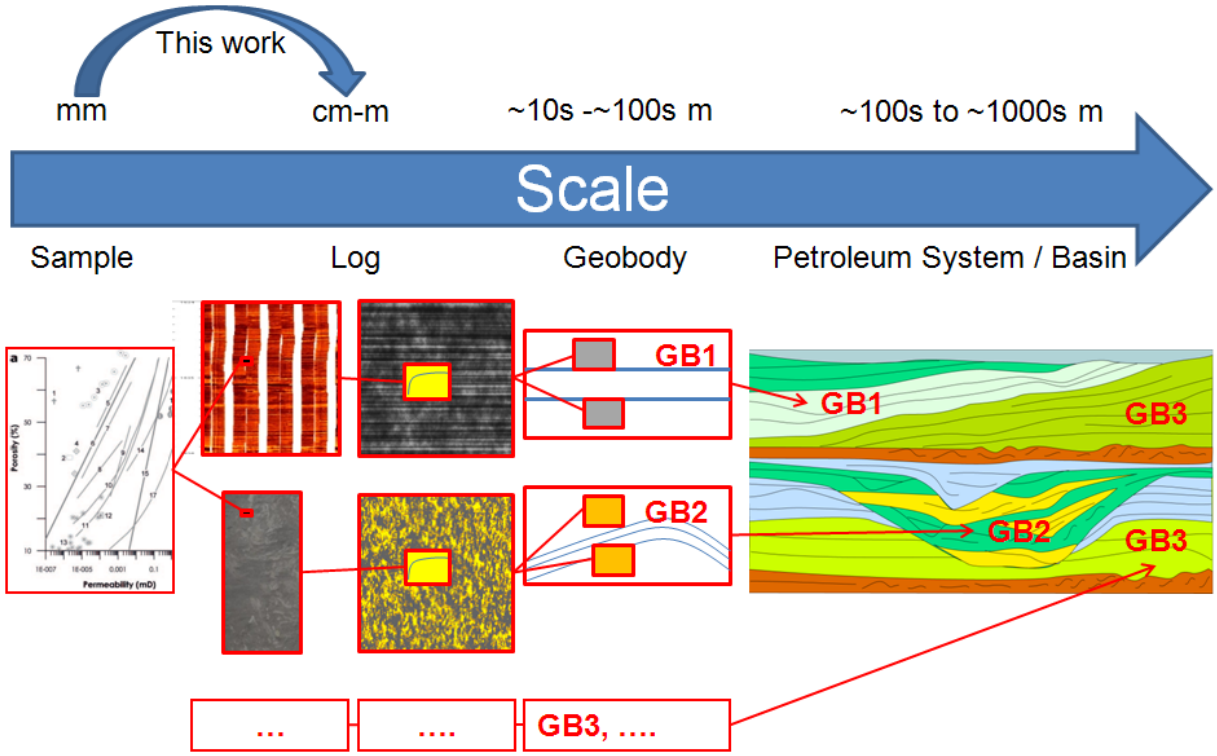

Figure 1.1: Upscaling process through different scales, which themselves depend on the scales of different measurements. The work of this study is the starting point in this process and covers the transition from millimetre (after Mondol et al., 2008) to metre scale. The resulting metre-scale effective properties are then used to populate models on the geobody (seismic) scale to further upscale the flow properties to full field or even basin scale.

Background

Porosity and Permeability of "Homogeneous" Shales and Mudstones

Published porosity (Aplin et al., 1995; Yang and Aplin, 1998, 2004, 2007; Dewhurst et al., 1998, 1999b) and permeability (Mesri and Olson, 1971; Coyner et al., 1993; Neuzil, 1994; Nagaraj et al., 1994; Yang and Aplin, 1998, 2007, 2010; Dewhurst et al., 1998, 1999a, 1999b; Hildenbrand et al., 2004; Kwon et al., 2004; Mallon et al., 2005) data on real rocks are available for clay-rich sediments, some of them even providing models as a function of effective stress and clay content (Aplin et al., 1995; Yang & Aplin, 1998, 2004, 2010). Most studies report sub-nano- to micro-darcy permeabilities and logarithmic porosity and permeability decrease with increasing effective stress for clay-rich sediments, which usually

have high initial porosities (Aplin et al., 1995; Mondol et al., 2007). Additionally, clay rich sediments show anisotropic behaviour for vertical and horizontal permeabilities (Yang and Aplin, 1998; Armitage et al., 2011). Thereby, shales and mudstones are either characterized by grain size (e.g. Yang and Aplin, 2004, 2010) or mineralogy (e.g. Mondol et al., 2007, 2008), both important parameters to be considered. However, as Yang and Aplin (1998) found a strong correlation between clay content and porosity and permeability, a grain size approach is used in this study. By doing so, the definition of clay sized particles is set to 0.002 mm, as this threshold, derived from soil mechanics, appears to be more appropriate (Skempton, 1944; Dewhurst et al., 1999a; Yang and Aplin, 2004) than the classical reciprocal exponent, where clay content is given by $1/2^8$ = 0.0039 mm (e.g. Wentworth, 1922).

Siltstones have a grain size between 10-63 µm and can either constitute a large fraction in mudstones or are often designated as shales themselves (e.g. Potter et al., 1980). Also, a division of cohesive (fine) and sortable (coarse) silt at 0.01 mm can be made as grains sized smaller than this threshold behave cohesively, while grains larger than this threshold remain sortable (McCave et al. 1995). Only a few silt datasets are available (Bryant et al., 1975; Mitchell, 1976; Heard et al., 1988; Kitajima et al., 2004) and are mostly for low pressures in the case of soil related studies (Heard et al., 1988) or uplifted sediments in the case of outcrop studies (Kitajima et al., 2004). For silt-rich sediments permeabilities in the micro- to lower millidarcy range are usually reported (Bryant et al., 1975; Mitchell, 1976; Heard et al., 1988; Kitajima et al., 2004), whereas porosity can span a wide range (Mitchell, 1976), which is probably due to the wide grain size spectrum of silts. However, from experimental mechanical compaction studies on fine silt sized Kaolinite and coarse silt sized Quartz grains it can be assumed that the compaction behaviour of fine silt tends to be more clay alike and the compaction behaviour of coarse silts tends to be more sand alike (Mondol et al., 2008; 2011; Fawad et al., 2010).

Mudstone Heterogeneity

Heterogeneities present in shales and mudstones have been investigated on different scales such as micrographs and thin sections (Potter et al., 1980; O'Brien and Slatt, 1990; Macquaker and Gawthorpe, 1993; Schieber, 1999; Rohl and Schmid-Rohl, 2005) and core slabs and images (e.g. Pe-Piper et al., 2005; Piper et al., 2010). Hereby, a range of sub-metre scale heterogeneities have been reported. Coarser grained material dispersed by storms and tides forms structures such as starved ripples (Macquaker and Bohacs, 2007; Schieber et al., 2007; Schieber and Southard, 2009) and intraclasts (Myrow, 1992; Schieber, 1994; Macquaker and Taylor, 1996; Macquaker et al., 2010; Schieber et al., 2010). Clay-dominated ripples have

been reported to form by flocculation (Schieber et al., 2007). Also, different forms of bioturbation (Droser and Bottjer, 1986), as well as coarser grained thin-beds as a result of turbiditic pollution of hemipelagites (e.g. Aplin and Macquaker, 2011) can be found. In addition, mass transport deposits, often incorporate chaotic and brecciated mud-rich structures at different scales (e.g. Tripsanas et al., 2008). Finally, overpressure release can be associated with forming of sand injections through mud-rich sections with thicknesses and extents ranging from few centimetres to hundreds of metres (Hurst et al., 2003, 2011).

Heterogeneity and Fluid Flow

Geological heterogeneity is literally always present and therefore fluid flow is always influenced by some scale of heterogeneity. Hence, the main task in investigating fluid flow through geological systems is to quantify the influence of heterogeneity on fluid flow on appropriate scales. To do so, the heterogeneities present at different scales have to be identified and their influence on fluid flow quantified and described individually for each scale and type of heterogeneity. The resulting effective properties for different heterogeneities at a certain scale can then be used to treat the respective scale incorporating the heterogeneity as homogeneous, which allows investigating the heterogeneity of the next larger scale without being troubled by the influence of the heterogeneity of the smaller scale. This important process is usually being referred to the term upscaling. Upscaling of sub-metre scale heterogeneities is crucial in complex geological settings (Pickup et al., 2000; Pickup et al., 2005), where heterogeneity is high on all scales. However, in some cases, it might be even neglectible, in particular when sub-metre scale heterogeneities are only scarcely distributed within a homogeneous larger scale context (Pickup et al., 2005). Hence it is vital to identify the heterogeneities on different scales and to identify their influence on fluid flow, before initiation of a complex upscaling process, when investigating the influence of heterogeneity on fluid flow in a geological environment (Marsily et al., 2005).

Different upscaling methods have been developed in the past. Effective media theory (Dagan, 1979), percolation theory, where, from a geological fluid flow point of view, a certain threshold of highly permeable material guarantees for connectivity through a system (Begg and King, 1985), and numerical methods are only the most prominent examples (compare Renard and Marsily, 1997). A critical parameter in upscaling, independent of the method, is the scale that the influence of heterogeneity should be upscaled to. This scale should ensure stable upscaling, and thus be a scale where the influence of the heterogeneity of interest is considered to be stochastically stationary, or homogeneous in other words. This yields to the continuum approach, where a representative element or, in 3D, a representative elementary

volume (Bear, 1972) fulfils these requirements. This approach is an approximation of the effective media theory, and thus assumes the representative element to be large enough to capture the relevant or representative heterogeneities (Bear, 1972). It is obvious that the size of the representative element is closely related to the length scales (correlation lengths) of the present heterogeneities. Thus, the results of the upscaling method might be unstable, when these correlation lengths approach the observed scale (Sahimi, 1995). In order to overcome this issue, a measure of uncertainty (e.g. standard deviation of different upscaled results, which form a distribution) together with the upscaled property can be provided. This is in particular important as in geological settings not always all occurrences of a certain structure appear at the size and scale of the respective representative scale (effective medium) mainly due to geological discontinuities such as faults, magmatic intrusions, injectites and erosion. An alternative to a representative elementary volume or domain would be the combination of a probability density function (PDF) of the size of a certain heterogeneity with its PDF of the property of interest as a function of heterogeneity size (compare Durlofsky, 1991 and Pickup et al. 1994 on fluctuating boundary conditions).

Thesis Structure

The reader of this thesis must be aware of the thesis structure, which is not supposed to be of a monographic nature. Instead, the individual technical chapters (Chapters 2-5) are written in publication style, each with sections such as introduction, methods and data, results, discussion, conclusions and references. Thus, repetitions might occur in some cases, as the individual technical chapters should be readable as stand-alone works. However, in combination the individual technical chapters build up a bigger picture and follow a superior workflow to model stress-dependent effective porosity-permeability relationships of metre-scale heterogeneous mudstones. The workflow implements all available data (core, image logs, sample measurements and published data and models) relevant to fluid flow simulation of heterogeneous shales and mudstones. Hereby, the workflow starts with the characterisation of porosity and permeability as a function of mechanical compaction and lithological variety of fine-grained sediments from samples on centimetre-scale and proceeds with identification and quantification of mudstone heterogeneity, which is then investigated for its influence on fluid flow on sub-metre scales. Finally, the outcomes of porosity and permeability characterisation, quantification of mudstone heterogeneity and investigation of model size and resolution dependence on fluid flow are integrated to calculate stress-dependent effective porosity-permeability relationships of different sub-metre scale mudstone heterogeneities.

References

Aplin, A. C., Yang, Y. L. & Hansen, S. 1995. Assessment of β, the compression coefficient of mudstones and its relationship to detailed lithology. Marine and Petroleum Geology, 12, 955–963.

Aplin, A. C., Fleet, A. J., MacQuaker, J. H. S. 1999. Muds and Mudstones: Physical and Fluid Flow Properties. Geological Society, Special Publications, 158. In: Aplin, A.C., Fleet, A.J. & MacQuaker, J.H.S. (eds) 1999. Muds and Mudstones: Physical and Fluid Flow Properties.Geological Society, Special Publications,158, 1-8.

Aplin, A. C., Macquaker, J. 2011. Mudstone diversity: Origin and implications for source, seal, and reservoir properties in petroleum systems. AAPG Bulletin, 95, 12, 2031-2059.

Armitage, P. J., Faulkner, D. R., Worden, R. H., Aplin, A. C., Butcher, A. R., Iliffe, J. 2011. Experimental measurement of, and controls on, permeability and permeability anisotropy of caprocks from the CO2 storage project at the Krechba Field, Algeria, J. Geophys. Res., 116, B12208, doi:10.1029/2011JB008385.

Bear, J. (1972). Dynamics of fluids in porous media. American Elsevier, New York.

Begg, S. H., King P. R. (1985). Modelling the effects of shales on reservoir performance: calculation of effective vertical permeability. Society of petroleum engineers paper 13529, presented at SPE symposium on reservoir simulation, Dallas, 10–13 February 1985.

Bryant, W. R., Hottmann, A., Trabant, P. 1975. Permeability of unconsolidated and consolidated marine sediments, Gulf of Mexico. Marine Geotechnology, 1, 1, 1-14.

Coyner, K., Katsube, T. J., Best, M. E., Williamson, M. 1993. Gas and water permeability of tight shales from the Venture gas Field offshore Nova Scotia. In: Current Research, Part D. Geological Survey of Canada, pp. 129–136.

Dagan, G. 1979. Models of groundwater flow in statistically homogeneous porous formations. Water Resour Res 15, 1, 47–63.

Dewhurst, D. N., Aplin, A. C., Sarda, J. P., Yang, Y. L. 1998. Compaction-driven evolution of poroperm in natural mudstones: an experimental study. J. Geophys. Res. 103, 651–661.

Dewhurst, D. N., Yang, Y. L., Aplin, A. C. 1999a. Permeability and fluid flow in natural mudstones, in Muds and Mudstones: Physical and Fluid Flow Properties, edited by A.C. Aplin et al., Geol. Soc. Spec. Publ., vol. 158, 23–43.

Dewhurst, D. N., Aplin, A. C., Sarda, J. P. 1999b. Influence of clay fraction on pore-scale properties and hydraulic conductivity of experimentally compacted mudstones. J. Geophys. Res. 104, B14, 29261–29274.

Droser, M. L., Bottjer, D. J. 1986. A semiquantitative field classification of ichnofabric. J Sed. Petr., 58, 558-559.

Durlofsky, L. J. 1991. Numerical calculation of equivalent grid block permeability tensors for heterogeneous porous media. Water Resour Res 27, 5, 699–708.

Fawad, M., Mondol, N. H., Jahren, J., Bjørlykke, K. 2010. Microfabric and rock properties of experimentally compressed silt-clay mixtures. Marine and Petroleum Geology, 27, 1698–1712.

Heard, J. R., Eileen, J. K., Mannering, J. V. 1988. Soil Macroporosity, Hydraulic Conductivity and Air Permeability of Silty Soils under Long-Term Conservation Tillage in Indiana. Soil & Tillage Research, 11, 1-18.

Hildenbrand, A., Schlomer, S., Krooss, B.M. 2004. Gas breakthrough experiments on fine-grained sedimentary rocks. Geofluids 2, 1, 3–23.

Hurst, A., Cartwright, J., Huuse, M., Jonk, R., Schwab, A., Duranti, D., Cronin, B. 2003. Significance of large-scale sand injectites as long-term fluid conduits: evidence from seismic data. Geofluids, 3, 4, 263–274.

Hurst, A., Scott, A., Vigorito, M. 2011. Physical characteristics of sand injectites. Earth-Science Reviews, 106, 215–246.

Kitajima, H., Shimamoto, T., Tanikawa, W. 2004. Permeability Structure and Basin Analysis of Miyazaki Group. International symposium on methane hydrates and fluid flow in upper accretionary prisms. Japan Drilling Earth Science Consortium.

Kwon, O., Kronenberg, A.K., Gangi, A.F., Johnson, B., Herbert, B.E. 2004. Permeability of illite-bearing shale: 1. Anisotropy and effects of clay content and loading. J. Geophys. Res., 109, B10, B10205.

Macquaker, J. H. S., Gawthorpe, R. L., 1993. Mudstone lithofacies in the Kimmeridge Clay Formation, Wessex Basin, southern England: Implications for the origin and controls of the distribution of mudstones. J. Sed. Petr., 63, 1129-1143.

Macquaker, J. H. S., Taylor, K. G. 1996. A sequence-stratigraphic interpretation of a mudstone-dominated succession: The Lower Jurassic Cleveland Ironstone Formation, United Kingdom. J. Geol. Soc., 153, 759-770.

Macquaker, J. H. S., Adams, A. E. 2003. Maximizing Information from Fine-Grained Sedimentary Rocks: an Inclusive Nomenclature for Mudstones. J. Sed. Res., 73, 5, 735–744.

Macquaker, J. H. S., Bohacs, K. M. 2007. On the Accumulation of Mud. Science 318, 1734-1735.

Macquaker, J. H. S., Bentley, S. J., Bohacs, K. M. 2010a. Wave-enhanced sediment gravity flows and mud dispersal across continental shelves: Reappraising sediment transport processes operating in ancient mudstone successions. Geology, 38, 947-950.

Mallon, A.J., Swarbrick, R.E., Katsube, T.J. 2005. Permeability of fine-grained rocks: new evidence from chalks. Geology 33, 21–24.

Marsily, G. de, Delay, F.Goncalves, J., Renard, P., Teles, V., Violette, S. 2005. Dealing with spatial heterogeneity. Hydrogeol J, 13, 161–183.

McCave, I. N., Manighetti, B., and Robinson, S. G. 1995. Sortable silt and fine sediment size/composition slicing: parameters for palaeocurrent speed and palaeoceanography. Paleoceanography, 10, 593-610.

Mesri, G., Olson, R. E. 1971. Mechanisms controlling the permeability of clays. Clays Clay Min. 19, 151–158.

Mitchell, J. K., 1976, Fundamentals of Soil Behavior, Wiley, New York, 422 p.

Mondol, N. H., Bjørlykke, K., Jahren, J., Høeg, K. 2007. Experimental mechanical compaction of clay mineral aggregates - changes in physical properties of mudstones during burial. Marine and Petroleum Geology 24, 289–311.

Mondol, N. H., Bjørlykke, K., Jahren, J. 2008. Experimental compaction of clays: relationship between permeability and petrophysical properties in mudstones. Petroleum Geoscience 14, 319–337.

Mondol, N. H., Jahren, J., Berre, T., Grande, L., Bjørlykke, K. 2011. Permeability Anisotropy in Synthetic Mudstones − An Experimental Study. EAGE Vienna 2011. EarthDoc – Extended Abstract, D030.

Nagaraj, T. S., Pandian, N. S., Narasimha Raju, P. S. R. 1994. Stress-state-permeability relations for overconsolidated clays. Geotechnique 44, 349–352.

Neuzil, C. E. 1994. How permeable are clays and shales? Water Resour. Res. 30, 145–150.

O'Brien, N. R., Slatt, R. M. 1990. Argilleceous rock atlas. New York, Springer-Verlag, 141 p.

Pe-Piper, G., Dolansky, L., Piper, D. J. W. 2005. Sedimentary Environment and Diagenesis of the Lower Cretaceous Chaswood Formation, Southeastern Canada: The Origin of Kaolin-Rich Mudstones. Sedimentary Geology, 178, 75–97.

Pickup, G. E., Ringrose, P. S., Jensen, J. L., Sorbie, K. S. 1994. Permeability tensors for sedimentary structures. Math Geol, 26, 2, 227–250.

Pickup, G. E., Ringrose, P. S., Sharif, A. 2000. Steady-state upscaling: from lamina-scale to full-field model. SPE J, 5, 2, 208–217.

Pickup, G. E., Stephen, K. D. Ma, J., Zhang, P., Clark, J. D. 2005. Multi-Stage Upscaling: Selection of Suitable Methods. Transp Porous Med, 58, 191–216.

Piper, D. J. W., Noftall, R., Pe-Piper, G. 2010. Allochtonous Prodeltaic Sediment Facies in the Lower Cretaceous at the Tantallon M-41 Well: Implications for the Deep-Water Scotian Basin. AAPG Bulletin, 94, 1, 87-104.

Potter, E. P., Maynard, J. B., Pryor, W. A. 1980. Sedimentology of Shale. Springer, New York, Berlin, Heidelberg, Tokyo, 306 p.

Renard, P., Marsily, G. de 1997. Calculating equivalent permeability: a review, Adv.Water Resour., 20, 5–6, 253–278.

Rohl, H.-J., Schmid-Rohl, A. 2005. Lower Toarcian (upper Liassic) black shales of the central European epicontinental basin: A sequence-stratigraphic case study from the southwestern German Posidonia Shale. In: Harris, N. (ed.). The deposition of organic-carbon-rich sediments: Models, mechanisms, and consequences. SEPM Special Publication, 82, 165-189.

Sahimi, M. 1995. Flow and transport in porous media and fractured rock. From classical methods to modern approaches. VCH, Weinheim.

Schieber, J. 1999. Distribution and Deposition of Mudstone Facies in the Upper Devonian Sonyea Group of New York. J. of Sedimentary Research, 69, 4, 909–925.

Schieber, J., Southard, J., Thaisen, K. 2007. Accretion of Mudstone Beds from Migrating Floccule Ripples. Science 318, 1760-1763.

Schieber, J., Southard, J. B. 2009. Bed-load transport of mud by floccule ripples: Direct observation of ripple migration processes and their implications. Geology, 37, 483-486.

Schieber, J., Southard, J. B., Schimmelmann, A. 2010. Lenticular shale fabrics resulting from intermittent erosion of water-rich muds: INterpreting the rock record in the light of recent flume experiments. J. Sed. Res., 80, 119-128.

Skempton, A.W. 1944. Notes on the compressibility of clay. Quarterly Journal of the Geological Society of London, 100, 119–135.

Tripsanas, E. K., Piper, D. J. W., Jenner, K. A., Bryant, W. R. 2008. Submarine mass-transport facies: new perspectives on flow processes from cores on the eastern North American margin. Sedimentology, 55, 97–136.

Wentworth, C. K. 1922. A scale of grade and class terms for clastic sediments. J. Geol. 30, 377-392.

Yang, Y. L., Aplin, A. C. 1998. Influence of lithology and effective stress on the pore size distribution and modelled permeability of some mudstones from the Norwegian margin. Mar. Petrol. Geol. 15, 163–175.

Yang, Y. L., Aplin, A. C. 2004. Definition and practical application of mudstone porosity–effective stress relationships. Petroleum Geoscience, 10, 153–162.

Yang, Y. L., Aplin, A. C. 2007. Permeability and petrophysical properties of 30 natural mudstones. Journal of Geophysical Research: Solid Earth, 112, B3, B03206.

Yang, Y. L., Aplin, A. C. 2010. A Permeability–Porosity Relationship for Mudstones. Marine and Petroleum Geology, 27, 8, 1692-1697.

Chapter 2: A Grain Size Fraction Dependent Modelling Framework to Predict Sample-Scale (Centimetre-Scale) Porosity and Permeability of Fine-Grained Sediments at Different Effective Stresses

Introduction

Fine grained sediments such as shales and mudstones comprise the largest fraction of fill in sedimentary basins (e.g. Aplin et al., 1999). They are important in many applied aspects of geosciences, and can serve as barrier rocks (groundwater and conventional petroleum systems, CO_2 storage, nuclear waste deposits), reservoir rocks (unconventional resources like shale gas) or source rocks (conventional petroleum systems). Shales and mudstones are heterogeneous (Schieber, 1999; Macquaker and Howell, 1999) yielding wide ranges of grain size (Aplin et al., 1999) and lithology through different scales (Potter, 1980; Aplin et al., 1999; Schieber, 1999). Lithological variability in shales and mudstones has a significant impact on flow properties, but has been addressed in only very few studies such as Yang's and Aplin's empirical models of effective stress-porosity (2004) and porosity-permeability (2010) relationships as a function of clay content. Despite, their usefulness for very clay-rich (clay > 30%) sections, Yang's and Aplin's models cannot predict porosity and permeability of coarse grained sections, which are common in heterogeneous mudstones and shales (e.g. Aplin and Macquaker, 2011). On the contrary, in previous studies, where mud-rich heterogeneous sediments have been modelled at various scales, the focus had been set to model only physical properties of sandy sections in an accurate way, while porosity and permeability of the finer material was assumed to be at a constant value or to follow a predefined distribution, such as normal or log-normal distributions independent of effective stress (e.g. Nordahl et al., 2005; Nordahl and Ringrose, 2008). Thereby, porosity and permeability have not been linked to grain size distributions, but have been assigned randomly to predefined lithological units, such as sandstone, siltstone and mudstone. It is thus crucial to model physical properties such as porosity and permeability of all different lithologies present in shales and mudstones as accurate as possible and with respect to lithological variation.

In this study we present a modelling framework to predict porosity and permeability as a function of grain size fractions and mechanical compaction by increasing effective stress. The modelling approach extends classical pore-filling models for porosity (Marion et al., 1992) and permeability (Revil and Cathles, 1999) by incorporating Yang's and Aplin's (2004, 2010) models for mudstones and published experimental mechanical compaction data of siltstones

(Fawad et al., 2010; Mondol et al., 2011) and sandstones (Chuhan et al., 2003) and stress-dependent sandstone permeability models (Pettersen, 2007). Thereby, we utilize natural grouping of the grain size fractions into cohesive and sortable fractions (McCave et al., 1995), which allows for cross-correlation of our approach with common measures such as vshale or net-gross (mud-sand) from wireline logging. The resulting modelling scheme thus allows for more flexibility and variety in porosity-permeability modelling workflows, as it honors all available grain size fractions (clay, cohesive silt, sortable silt, sand), while keeping the input data as close to previous approaches as possible. Also, by combination of the measured published data with the theoretical models, we are able to reproduce a theoretical porosity minimum based on quaternary grain size mixing. The strength of the modelling framework is that it allows calculation of realistic porosities and permeabilities of siliclastic sediments, once the much simpler to be measured grain size fractions and stress state of a rock sample have been determined. The porosity permeability model is compared to existing grain size and porosity data from our data base.

As our model requires grain size as input, we show how grain size databases can be utilized to reliably reproduce regional grain size trends and relationships, by using a simple simulation algorithm. For demonstration purposes the algorithm was applied to a grain size fraction data base from the Nile Delta, Egypt. We suggest using the algorithm in combination with our porosity permeability modelling framework to allow for maximum flexibility in modelling of stress-dependent, lithologically varying porosities and permeabilities of heterogeneous fine-grained sediments.

Background

Grain Size

Common grain size classifications (e.g. Wentworth, 1922) are based on the principle $gs = 1/2^x$, where gs is the grain size in millimetres and x takes on values from 1-8 for different transitions between grain size classes (e.g. 1 for medium-coarse sand, 4 for coarse silt-very fine sand and 8 for clay-very fine silt, yielding grain sizes of 0.5 mm, 0.0625 mm and 0.0039 mm, respectively). However, in this study the transition between clay and silt has been set to a diameter of 0.002 mm, as this threshold, derived from soil mechanics, correlates better with measurements of physical properties such as porosity and permeability (Skempton, 1944; Dewhurst et al., 1999a; Yang and Aplin, 2004). Also, a division of fine and coarse silt at 0.01 mm has been chosen, as this threshold separates sortable from cohesive grain support behaviour (McCave et al. 1995). Thus, sand and coarse silt can be grouped to a sortable grain

size fraction and clay and fine silt can be unified to a cohesive grain size fraction. This grouping has the advantage of being directly comparable to common quantitative measures such as vshale from wireline. Table 2.1 summarizes the grain size classification used in this study.

Table 2.1: Grain size classification used in this study.

Grain size [mm]	Class	Unified Class
> 0.063	Sand	Sortables
0.010-0.063	Coarse (sortable) silt	
0.002-0.010	Fine (cohesive) silt	Cohesives
< 0.002	Clay	

Porosity and Permeability of Clays, Silts and Sands

Published porosity (Aplin et al., 1995; Yang and Aplin, 1998, 2004, 2007; Dewhurst et al., 1998, 1999b) and permeability (Mesri and Olson, 1971; Coyner et al., 1993; Neuzil, 1994; Nagaraj et al., 1994; Yang and Aplin, 1998, 2007, 2010; Dewhurst et al., 1998, 1999a, 1999b; Hildenbrand et al., 2004; Kwon et al., 2004; Mallon et al., 2005) data on real rock samples (centimetre-scale) are available for clay-rich sediments, some of them even providing models as a function of effective stress and clay content (Aplin et al., 1995; Yang & Aplin, 1998, 2004, 2010), and sand-rich sediments (compare Nelson and Kibler, 2003). For silt-rich sediments only a few data sets are available (Bryant et al., 1975; Mitchell, 1976; Heard et al., 1988; Kitajima et al., 2004), but mostly for low pressures in the case of soil related studies (Heard et al., 1988) or uplifted sediments in the case of outcrop studies (Kitajima et al., 2004). In addition to real rock measurements experimental mechanical compaction data on pure and mixed aggregates (for porosity: Marion et al., 1992; Chuhan et al. 2003; Mondol et al., 2007; Mondol et al., 2008; Fawad et al., 2010; for permeability: Mondol et al., 2008; Mondol et al., 2011) provide an alternative, not at least due to their ability to serve as end-members and their reproducibility. Finally, theoretical compaction models are an additional option for both fine-grained (e.g. Terzaghi, 1943) and coarser grained material (e.g. Pettersen, 2007).

Most studies report sub-nano- to micro-darcy permeabilities and logarithmic porosity and permeability decrease with increasing effective stress for clay-rich sediments, which usually have high initial porosities (Aplin et al., 1995; Mondol et al., 2007). Additionally, clay rich sediments show anisotropic behaviour for vertical and horizontal permeabilities (Yang and Aplin, 1998; Armitage et al., 2011). For silt-rich sediments permeabilities in the micro- to

lower millidarcy range are usually reported (Bryant et al., 1975; Mitchell, 1976; Heard et al., 1988; Kitajima et al., 2004), whereas porosity cannot be narrowed to a certain threshold (Mitchell, 1976), which is probably due to the wide grain size spectrum of silts. However, from experimental mechanical compaction studies on fine silt sized Kaolinite and coarse silt sized quartz grains it appears that the compaction behaviour of fine silt tends to be more clay-like and the compaction behaviour of coarse silts tends to be more sand-like (Mondol et al., 2008; Fawad et al., 2010). Sand compaction on sample-scale (centimetre-scale) usually follows a linear (Pettersen, 2007; Chuhan et al., 2003) or slightly logarithmic (Zimmer, 2003) trend, whereas sand permeability decreases semi-logarithmic with increasing effective stress (Pettersen, 2007) or decreasing porosity (Chilingar, 1964).

Porosity and Permeability of Binary Mixtures

Variability in terms of spectra of grain size combinations in sediments makes it difficult to quantify physical properties of sedimentary rocks. A common technique to tackle this issue is to investigate sedimentary end-members, such as pure sands, silts or clays for the physical properties of interest and to combine them to physical properties of binary mixtures by use of theoretical packing models (Marion et al., 1992).

In detail, binary porosities and permeabilities are obtained by fractional mixing of the end-members (e.g. clay with sand), resulting in transitions between these end-members and their properties. It is therefore important to honour typical transition pathways for the respective properties (porosity and permeability as a function of effective stress). In particular, the transitions between cohesive fractions and sortable fractions show special features such as a porosity minimum (Marion et al., 1992; Revil and Cathles, 1999; Mondol et al., 2007; Mondol et al., 2008; Fawad et al., 2010) and a sudden permeability increase (Revil and Cathles, 1999; Mondol et al., 2011). It is obvious, that both should be correlated.

From a packing theory point of view this porosity minimum or sudden increase in permeability depicts the transition from a matrix- to a grain-supported framework at $\phi_{sortable}$, where the volume of the cohesive fraction $V_{cohesive}$ fills out all pores of the sortable fraction, characterised by its porosity $\phi_{sortable}$. Hereby, $V_{cohesive}$ is the normalized volume fraction of the cohesive material. Also, the sortable-to-cohesive ratio at the porosity minimum or sudden permeability increase is stress-dependent (e.g. Marion et al., 1992). Such a transition has also been described in classical sedimentology of shales at clay fractions of approximately 1/3 (Shepard, 1954; Folk, 1965; Blatt, 1980; Potter, 1980). Experimental mechanical compaction

experiments show minima between 15-40% of clay for clay-sand mixtures (Marion et al., 1992) and around 50% for clay-coarse silt mixtures (Fawad et al., 2010; Mondol et al., 2011). For transitions between finer fractions no minimum has been reported (compare Mondol et al., 2008). For binary mixtures of sortable particles a porosity minimum around 30% of the fraction of the larger particles has been found from numerical studies of random packing of unequal spheres (Visscher and Bolsterli, 1972; He et al., 1999; Kristiansen et al. 2005) and mixtures of different sized sands and sand sized glass beads (Zimmer, 2003). However, the influence of sorting of sands or sortable fractions on the extent of compaction is still in doubt (Lundegard, 1992; Zimmer, 2003). In this study we aim to extend these advances in porosity and permeability modelling of binary mixtures to the full grain size spectrum of siliclastic sediments (clay, fine silt, coarse silt, sand).

Methods and Data

The framework for modelling of physical properties (grain size fractions, porosity and permeability) of siliclastic sediments must honour three basic requirements:

1. Incorporate a wide range of lithological variability.
2. Account for compaction (mechanical compaction in this case)
3. Keeping the input as simple as possible and transferable to and from common quantitative measures (e.g. from wireline logs)

The first two requirements are solved by development of a modelling framework, which predicts porosity and permeability as a function of grain size fractions (clay, fine silt, coarse silt and sand) and effective stress. This modelling scheme will be outlined in detail in the next section. The third requirement is fulfilled by an algorithm to simulate regional grain size fraction trends from cohesive content only. Cohesive content consist of clay and fine silt sized particles and could be cross-correlated with common measures as vshale or net-gross (sand-shale) from wireline. The grain size simulation scheme is explained in the section after the porosity-permeability modelling framework.

Stress-Dependent Porosity and Permeability from Grain Size Fractions

In order to model porosity and permeability as a function of effective stress and grain size fraction combinations, we use a modified version of the sand-shale packing model for porosity (Marion et al., 1992) and permeability (Revil and Cathles, 1999) in this study. The classic sand-shale packing model is based on packing and volumetric theories: In a shaly-sand space between sand grains (sand pores) are filled with fine-grained particles (shale). The rock is supposed to be grain supported. If we increase the shale volume fraction we will reach a

situation, where all sand pores are filled with shale particles. This particular situation can also be described as the transition between a grain supported framework and a matrix supported framework. If we further increase the shale volume fraction, the sand grains will float in the shale matrix – the rock is supposed to be matrix supported (Marion et al. 1992). According to this model, the porosity ϕ of a sand-shale mixture becomes (Marion et al. 1992):

$$\phi = \begin{cases} \phi_{sand} - V_{shale} \cdot (1 - \phi_{shale}) & if \quad V_{shale} < \phi_{sand} \\ \phi_{sand} \cdot \phi_{shale} & if \quad V_{shale} \equiv \phi_{sand} \\ V_{shale} \cdot \phi_{sand} & if \quad V_{shale} > \phi_{sand} \end{cases} \qquad \text{Eq. 2.1}$$

Where ϕ_{sand} is the porosity of a clean sand, ϕ_{shale} is the porosity of a pure shale and V_{shale} is the volume fraction of shale of the sand-shale mixture. After Revil and Cathles (1999), the permeability of a sand-shale mixture can be calculated by:

$$K = \begin{cases} K_{sand} \cdot \left(1 - V_{shale} \cdot \left(\left(1 - \phi_{shale}\right) / \phi_{sand}\right)\right)^{3m_{ss}} & if \quad V_{shale} < \phi_{sand} \\ K_{sand} \cdot \left(\phi_{shale}\right)^{3m_{ss}} & if \quad V_{shale} \equiv \phi_{sand} \\ K_{shale} \cdot \left(V_{shale}\right)^{m_{sd}} & if \quad V_{shale} > \phi_{sand} \end{cases} \qquad \text{Eq. 2.2}$$

Where m_{ss} is the cementation exponent of the shaly sand domain, m_{sd} is the cementation exponent of a clean sand, K_{sand} is the permeability of a clean sand and K_{shale} is the permeability of a pure shale (Revil and Cathles, 1999).

As the porosity model seems to overestimate the stress dependent porosity reduction where the normalized shale volume fraction V_{shale} equals the sand porosity ϕ_{sand} Marion et al. (1992) introduced a perturbation factor, which corrects the model for non-ideal shale filling of the sand pores and framework perturbations. Koltermann and Gorelick (1995) expanded this approach by introducing a limit of how much shale can infill the sand pores. Both factors are highly sensitive and rely on further measurements on the shale end-member (in the case of the Koltermann-Gorelick approach) or on optimising the perturbation factor with measured porosities of sand-shale mixtures (in case of Marion et al.'s perturbation factor). Similar, for permeability calculations in the sand-shale system Revil's and Cathles' (1999) model predicts a permeability minimum, assuming a decrease in permeability with decreasing shale content in the sandy-shale domain, which only would be valid for an ideal filling of the sand pores, assuming zero perturbation. This is not well in concordance with more recent studies on

natural shales and mudstones (e.g. Yang and Aplin, 2010). To avoid the problems accompanying non-ideal pore filling, we substitute all calculations for sandy-shales by the porosity model proposed in Yang and Aplin (2004) and the permeability model from Yang and Aplin (2010), both of which are empirical relationships based on measurements on natural mudstones. In addition, we substitute the shale fraction by a cohesive fraction, summarizing the clay and fine silt contents. We perform the same substitution for the sand fraction of the sand-shale model by introducing a sortable fraction, consisting of the sand fraction and the coarse silt fraction (Figure 2.1). This unification has the advantage of differentiation between clay, fine silt, coarse silt and sand sized particles by simply changing the ratios of the sortable or cohesive fraction ingredients, respectively. In the same time, the approach is kept simple and allows for calibration with other (semi-)quantitative measurements (e.g. vshale from wireline logs). From here onwards we refer to our model as the cohesive-sortable grain packing model (CSGP model).

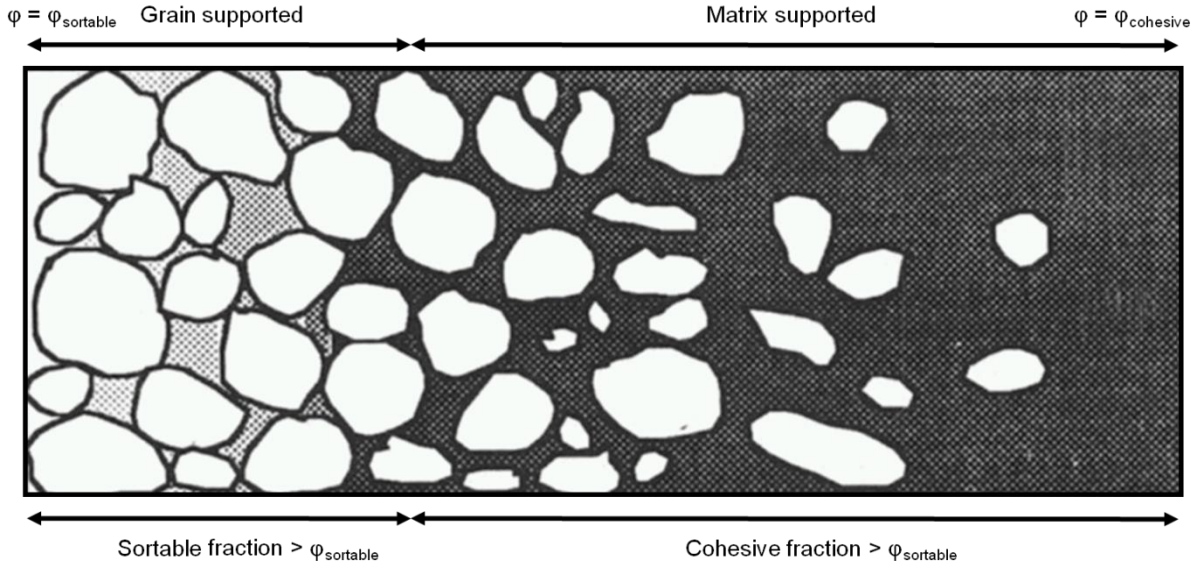

Figure 2.1: Cohesive-sortable grain packing (GSGP) model. The porosity of sortable particles (>10 µm), that are sand and coarse silt sized grains, are infilled by smaller cohesively behaving particles (clay and fine silt sized particles; < 10 µm). Illustration modified after Marion et al. (1992).

In order to extend the classic sand-shale packing model for porosity (Marion et al., 1992) and permeability (Revil and Cathles, 1999) prediction of mixtures of sand and shale to our CSGP model to calculate porosity and permeability from the full grain size spectrum of siliclastic sediments (clay, fine silt, coarse silt, sand), three steps are necessary:

- Define the porosity-permeability framework for matrix supported rocks, where the normalised volume fraction of the cohesive content $\overline{V}_{cohesive}$ is equal or greater than the

normalised volume of the pores of the sortable fraction, which is the porosity of the sortable fraction $\phi_{sortable}$.

- Define the porosity-permeability framework for grain supported rocks, where the normalised volume fraction of the cohesive content $\overline{V}_{cohesive}$ is less than the normalised volume of the pores of the sortable fraction, which is the porosity of the sortable fraction $\phi_{sortable}$.
- Apply end-member porosity and permeability compaction functions of pure aggregates (clay, fine silt, coarse silt, sand) to the whole framework

Framework for matrix supported rocks ***($\overline{V}_{cohesive} \geq \phi_{sortable}$)***

For matrix supported rocks we use Yang's and Aplin's models for porosity (2004) and permeability (2010). The porosity model requires clay content in weight percent and effective stress in MPa as input, whereas the permeability is calculated as a function of porosity and clay content in weight percent.

Thus, using the CSGP model, the porosity of a matrix supported rock ϕ_{matrix} is calculated by:

$$\phi_{matrix} = \phi_{YA}\left(W_{clay}, \sigma_{eff}\right) \qquad if \quad \overline{V}_{cohesive} \geq \phi_{sortable} \qquad \text{Eq. 2.3}$$

Where ϕ_{YA} is the porosity calculated after Yang and Aplin (2004), W_{clay} is the normalized weight fraction of clay content and σ_{eff} is the effective stress in MPa. The normalised volume fraction of the cohesive grain size fractions $\overline{V}_{cohesive}$ can be calculated from the normalised weight fraction $W_{cohesive}$ according to Marion et al. (1992):

$$\overline{V}_{cohesive} = \begin{cases} \dfrac{V_{cohesive}}{V_{cohesive} + vol_{sortable}} & if \quad V_{cohesive} \neq V_{\phi_{sortable}} \\ \phi_{sortable} & if \quad V_{cohesive} \equiv V_{\phi_{sortable}} \end{cases} \qquad \text{Eq. 2.4}$$

with

$$V_{sortable} = \begin{cases} \dfrac{(1-W_{cohesive})}{\rho_{sortable}\cdot(1-\phi_{sortable})} - V_{cohesive} & if \quad V_{cohesive} < V_{\phi_{sortable}} \\ \dfrac{1-W_{cohesive}}{\rho_{sortable}} & if \quad V_{cohesive} > V_{\phi_{sortable}} \end{cases} \qquad \text{Eq. 2.5}$$

and

$$V_{cohesive} = \frac{1-W_{cohesive}}{\rho_{cohesive}\cdot(1-\phi_{cohesive})} \qquad \text{Eq. 2.6}$$

$$V_{\phi_{sortable}} = \frac{1-W_{sortable}}{\rho_{sortable}\cdot(1-\phi_{sortable})} - \frac{1-W_{cohesive}}{\rho_{sortable}} \qquad \text{Eq. 2.7}$$

Thereby, $V_{sortable}$ and $V_{cohesive}$ are the actual volumes of the sortable and cohesive fraction normalized to 1 g, $W_{cohesive}$ and $W_{sortable}$ are the weight fractions of the cohesive and sortable fractions, $V_{\phi_{sortable}}$ is the sortable porosity volume normalized to 1 g of rock and $\rho_{sortable}$ is the density of the sortable fraction, which has been set to the mean density of quartz (2.64 g/cm^3). $\rho_{cohesive}$ is the density of the cohesive fraction (2.35 g/cm^3). The densities have been set according to Marion et al. (1992).

Accordingly, using the CSGP model, the permeability of of a matrix supported rock K_{matrix} then becomes:

$$K_{matrix} = K_{YA\_\mathrm{mod}}(W_{clay}, \sigma_{eff}) if \quad \overline{V}_{cohesive} \geq \phi_{sortable} \qquad \text{Eq. 2.8}$$

Where K_{YA_mod} is the permeability calculated from a modified empirical porosity-permeability relationship for mudstones (Yang and Aplin, 2010) as a function of the weight clay fraction W_{clay} and the effective stress σ_{eff} in MPa. As Yang and Aplin's model is designed for clay rich samples, the modification is set to extend the relationship linearly for clay fractions ≤ 50%. Hereby we extrapolate the permeability slope between clay fractions of 50 and 55% to avoid unreasonable results if $\overline{V}_{cohesive} < \phi_{sortable}$ and low clay contents (Figure 2.2).

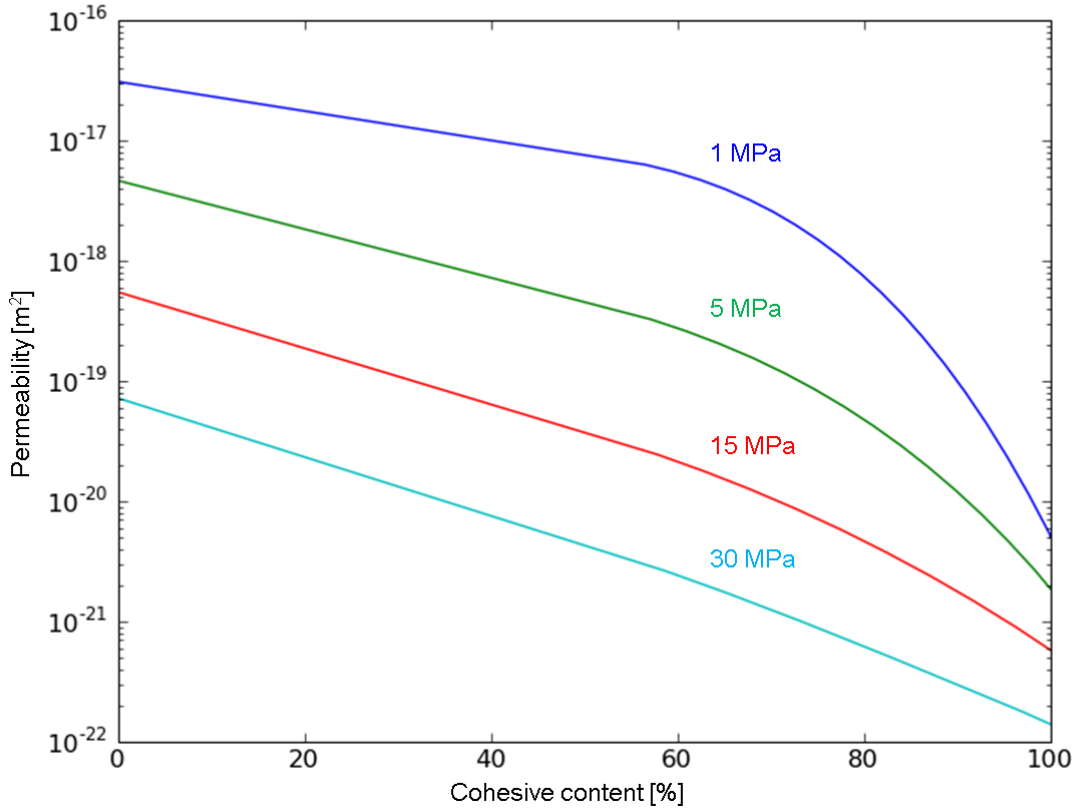

Figure 2.2: Permeability in m² modelled with extended relationships after Yang and Aplin (2004, 2010) vs. cohesive content in weight percent for effective stresses of 1 (blue), 5 (green), 15 (red) and 30 (cyan) MPa.

As stated previously, m_{ss} is a cementation factor, which is used for permeability calculation for cohesive volume fractions smaller than the porosity of the sortable fraction (Revil and Cathles, 1999). By solving Revil and Cathles' (1999) permeability model for shaly sands for m_{ss}, we can set m_{ss} in such a way that it fits the permeability K_{YA_mod} at the transition from a matrix to a grain supported rock frame work, where the normalised cohesive volume fraction $\overline{V}_{cohesive}$ equals the volume provided by the porosity of the sortable fraction $\phi_{sortable}$:

$$m_{ss} = \frac{\ln\left(\frac{K_{YA\_\mathrm{mod}}}{K_{sortable}}\right)}{3 \cdot \ln\left(\phi_{cohesive\_\mathrm{min}}\right)} \qquad \text{Eq. 2.9}$$

with

$$\phi_{cohesive\_\mathrm{min}} = \phi_{YA}\left(W_{clay}\right) \quad at \quad \overline{V}_{cohesive} = \phi_{sortable} \qquad \text{Eq. 2.10}$$

Where $\phi_{cohesive\_\min}$ is the cohesive porosity at the porosity minimum (that is the transition from a matrix to grain supported framwork) of a sortable-cohesive mixture and ϕ_{YA} is the porosity for the weight clay fraction W_{clay} at porosity minimum derived from Yang and Aplin's (2004) porosity model.

Framework for grain supported rocks ***($\overline{V}_{cohesive} \geq \phi_{sortable}$)***

A porosity minimum between differently sized sortable grains has been observed by various authors (Visscher and Bolsterli, 1972; He et al., 1999; Zimmer, 2003; Kristiansen et al. 2005). As a consequence, the physical properties (porosity and permeability) of the sortable fraction have to be determined honouring such a porosity minimum:

$$\phi_{sortable} = \begin{cases} \phi_{sortable\_\min} + \left(\phi_{coarseSilt} - \phi_{sortable\_\min}\right) \cdot \left(\dfrac{\overline{V}_{coarseSilt} - \phi_{sand}}{1 - \phi_{sand}} \right) & if \quad \overline{V}_{coarseSilt} \geq \phi_{sand} \\ \phi_{sortable\_\min} + \left(\phi_{sand} - \phi_{sortable\_\min}\right) \cdot \left(\dfrac{\left(1 - \overline{V}_{coarseSilt}\right) - \phi_{sand}}{1 - \phi_{sand}} \right) & if \quad \overline{V}_{coarseSilt} < \phi_{sand} \end{cases} \qquad \text{Eq. 2.11}$$

Where $\phi_{sortable}$ and $K_{sortable}$ are the porosity (fraction) and permeability of the sortable fraction. $\phi_{sortable\_\min}$ is the porosity minimum of a coarse silt-sand mixture. $\overline{V}_{coarseSilt}$ and $\overline{V}_{sand}$ are the volume grain size fractions normalised to the normalised sortable volume fraction of the whole rock $\overline{V}_{sortable}$.

The permeability of the sortable fraction is assumed to change log-linearly with a change in the normalised volume fractions of coarse silt $\overline{V}_{coarseSilt}$ and sand $\overline{V}_{sand}$:

$$\log10\left(K_{sortable}\right) = \overline{V}_{coarseSilt} \cdot \log10\left(K_{coarseSilt}\right) + \overline{V}_{sand} \cdot \log10\left(K_{sand}\right) \qquad \text{Eq. 2.12}$$

Finally, the porosity of a grain supported rock ϕ_{grain} can be calculated using linear interpolation adjusted to Yang's and Aplin's (2004) porosity model:

$$\phi_{grain} = \phi_{YA\_\min} + \left(\phi_{sortable} - \phi_{YA\_\min}\right) \cdot \left(\frac{\left(1 - \overline{V}_{cohesive}\right) - \phi_{sortable}}{1 - \phi_{sortable}} \right) \quad if \quad \overline{V}_{cohesive} < \phi_{sortable} \qquad \text{Eq. 2.13}$$

Where ϕ_{YA} is the porosity calculated from Yang and Aplin (2004), $\phi_{YA\_\min}$ is the minimum porosity calculated using the empirical relationship from Yang and Aplin (2004) for the clay weight fraction W_{clay} and the effective stress σ_{eff} in Megapascal, where the normalised cohesive volume fraction $\overline{V}_{cohesive}$ equals the volume provided by the porosity of the sortable fraction $\phi_{sortable}$.

Accordingly, the permeability of grain supported rock K_{grain} then becomes:

$$K_{grain} = K_{sortable} \cdot \left(1 - \overline{V}_{cohesive} \cdot \left(\frac{1 - \phi_{cohesive}}{\phi_{sortable}} \right)^{3m_{ss}} \right) \quad if \quad \overline{V}_{cohesive} < \phi_{sortable} \qquad \text{Eq. 2.14}$$

End-member porosity and permeability compaction functions of pure aggregates (clay, fine silt, coarse silt, sand)

As a next step, compaction functions for porosity and permeability have to be incorporated for the end-members clay, coarse silt and sand (Figure 2.3).

As end-member input, we used experimental mechanical compaction data for coarse silt (Fawad et al., 2010; Mondol et al., 2011) and sand porosity (Chuhan et al., 2003). For clay we used Yang and Aplin's (2004, 2010) empirical relationships by assuming 100% clay content, whereas for sand permeability we employed a theoretical model (Pettersen, 2007).

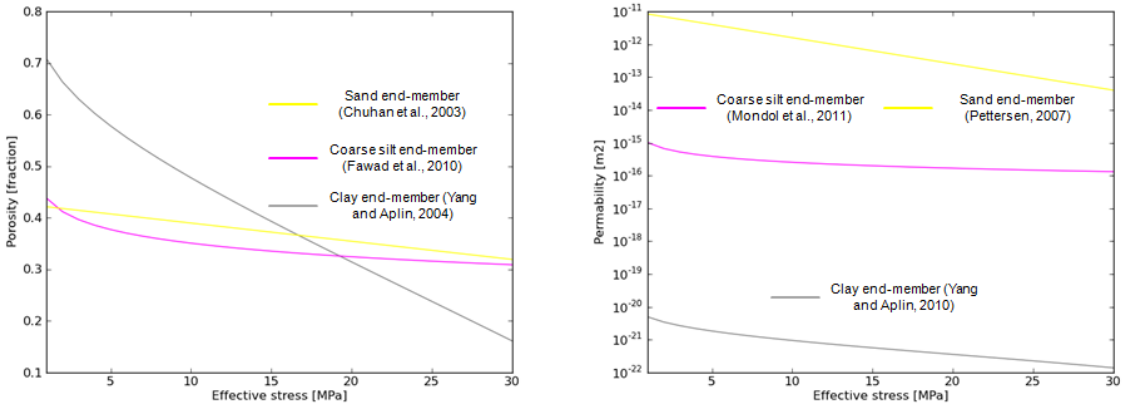

Figure 2.3: End-member porosities (left) and permeabilities (right) vs. effective stress.

The experimental mechanical compaction data suits our purposes well as the grain size of each end-member fits reasonably well our grain size fraction classification. Thus, for the

coarse silt end-member crushed quartz with grain sizes between 4-40 µm was used for both porosity (Fawad et al., 2010) and permeability (Mondol et al., 2011) measurements, whereas for sand a quartz sand with a mean grain size (D60) of 0.71 mm (Chuhan et al., 2003) was utilised to calculate porosity as a function of effective stress. For sand permeability a theoretical model based on critical state theory (Pettersen, 2007) has been employed. The latter predicts permeability directly as a function of effective stress. The relationships between porosity and effective stress for sand and coarse silt are:

$$\varphi_{sand} = -0.003522 \cdot \sigma_{\text{eff.}} + 0.425 \qquad \text{Eq. 2.15}$$

$$\varphi_{coarse\_silt} = -0.038 \cdot \ln(\sigma_{\text{eff.}}) + 0.4383 \qquad \text{Eq. 2.16}$$

Where φ_{sand} and φ_{coarse_silt} are the end-member porosities of pure sand and pure coarse silt and $\sigma_{\text{eff.}}$ is the effective stress in MPa. Equations 15 and 16 have been fitted to data of oed-243 from Chuhan et al. (2003) and data of crushed quartz from Fawad et al. (2010). The relationships between permeability and porosity and permeability and effective stress then are:

$$K_{sand} = K_{sand\,\min} \cdot K' \qquad \text{Eq. 2.17}$$

with

$$\log10(K') = \left(1 - \frac{\sigma_{\text{eff.}}}{50MPa}\right) \cdot \log10(K_{sand\,\max}) \qquad \text{Eq. 2.18}$$

$$K_{coarse\_silt} = 1e\text{-}18 \cdot \exp(15.789 \cdot \varphi_{coarse\_silt}) \qquad \text{Eq. 2.19}$$

Where K_{sand} and K_{coarse_silt} are the end-member permeabilities of pure sand and pure coarse silt in m^2, $K_{\text{sand min}}$ and $K_{\text{sand max}}$ are the minimum and maximum sand permeabilities at 0 and 50 MPa, respectively and $\sigma_{eff.}$ the effective stress in Megapascal. Equations 17 and 18 have been derived from Pettersen's (2007) permeability model and equation 19 has been fitted to silt permeability data from Mondol et al. (2011).

For cohesive permeabilities derived from clay content and effective stress we introduce a correction of the horizontal permeability K_h based on the model of Yang and Aplin (1998, 2007) and calibrated data from the Caprocks Project database:

$$K_h = K \cdot \tan(\alpha)^{-1.97} \qquad \text{Eq. 2.20}$$

with

$$\alpha = \begin{cases} 45^o \cdot \dfrac{\pi}{180^o} & for \quad \sigma_{eff.} < 0.1MPa \\ \left(45^o - 10.24 \cdot (e_{100} - e)\right) \cdot \dfrac{\pi}{180} & for \quad \sigma_{eff.} \geq 0.1MPa \end{cases} \qquad \text{Eq. 2.21}$$

Where e is the void ratio and e_{100} is the void ratio at 0.1 MPa, which can be calculated from clay content using the empirical relationship given in Yang and Aplin (2004). Then for clay and fine silt K becomes the vertical permeability, while for coarse siltstones and sandstones we assume pore isotropy, which is well confirmed for small volumes at effective stresses < yield stress (≈50 MPa) by experimental mechanical compaction tests of sandstones (e.g. Zhu et al., 1997, 2002; Dautrait et al., 2009).

In order to calculate porosity and permeability as a function of both effective stress and the different grain size fractions (clay, fine silt, coarse silt and sand), a behaviour for compaction of coarse silt-sand mixtures has to be defined. As our database lacks sand and coarse silt compaction data, we decided to define the porosity minimum of coarse silt-sand mixtures to be at $V_{coarseSilt} \equiv \phi_{sand}$, where $V_{coarseSilt}$ is the volume fraction of coarse silt and ϕ_{sand} is the sand porosity. Although ideal packing cannot be assumed for coarse silt-sand mixtures, as the grain size ratio is typically less than 10 (McGeary, 1964), porosity minima at fractions of the smaller particles close to the porosity of the larger particle aggregate have been reported from numerical studies of random packing of unequal spheres (Visscher and Bolsterli, 1972; He et al., 1999; Kristiansen et al. 2005) and laboratory experiments on mixtures of different sized sands and sand sized glass beads (Zimmer, 2003). In this study our end-member relationships for compaction and porosity loss of coarse silt and sand have been combined with Marion's packing model and a predefined decrease of the minimum sortable porosity $\phi_{sortable\_\min}$. The latter has been defined as a logarithmic function of effective stress $\sigma_{\text{eff.}}$, which has been derived from glass bead data (Zimmer, 2003) and modified for porosity data from experimental mechanical compaction data (Fawad et al., 2010; Chuhan et al., 2003). Hence, the minimum calculates as follows:

$$\phi_{sortable\_\min} = -0.03 \cdot \ln(\sigma_{\text{eff.}}) + 0.30 \qquad \text{Eq. 2.22}$$

For permeability change with increasing sand content and decreasing coarse silt content, we assume a log10-linear increase. Figure 2.4 summarizes the porosity-permeability modeling framework in a ternary grain size fraction diagram.

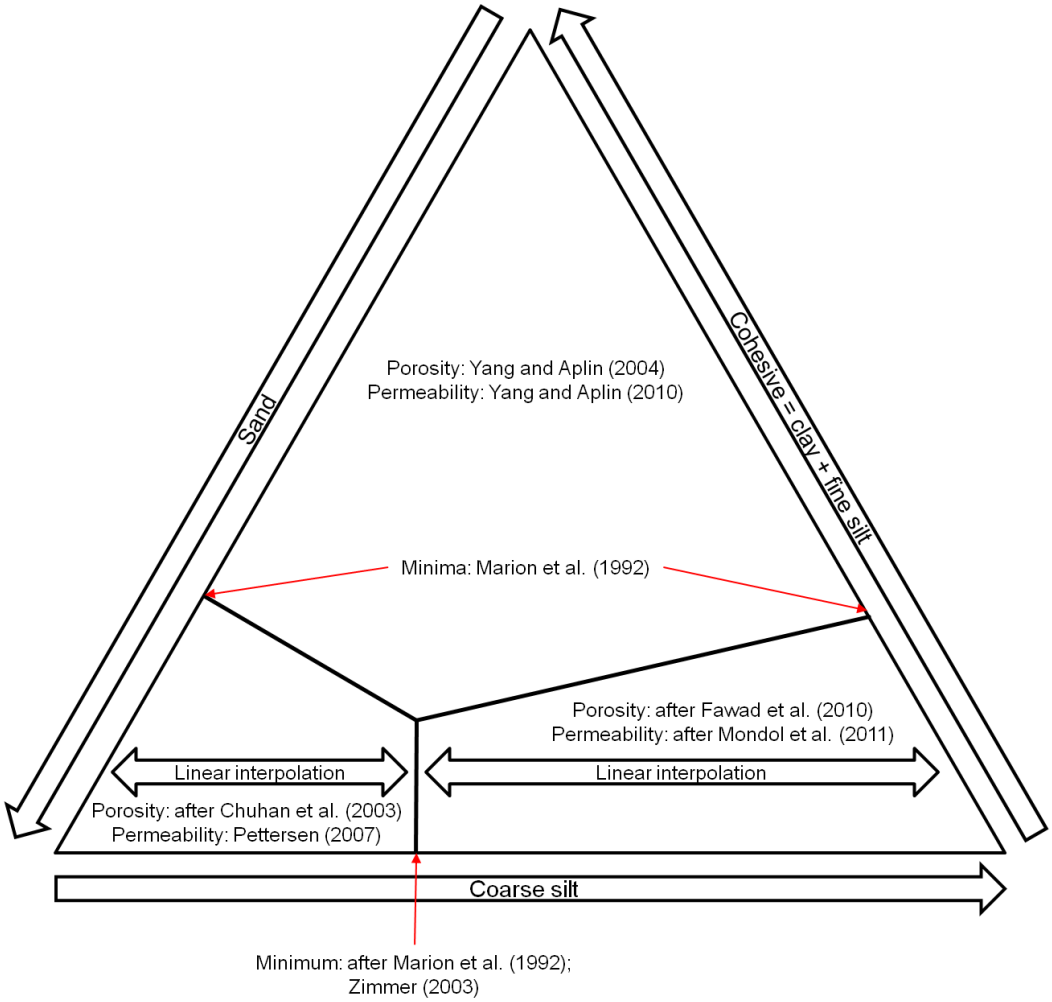

Figure 2.4: Modelling framework for porosity and permeability prediction from grain size fractions and effective stress.

Modelling and Simulating Grain Size Data from a Regional Data Base

The grain size data base used in this study is from an offshore gas field in the Nile Delta, Egypt. In total, 187 samples have been measured for grain size based on bulk density and grain density using the sedigraph technique (Coakley and Syvitski, 1991). The data base has been extended successively within the past three years by Boeker (2011) and others at Newcastle University (Aplin et al., 2011). The resulting grain size fractions follow a clear trend and are rich in silt sized grains (Figure 2.5).

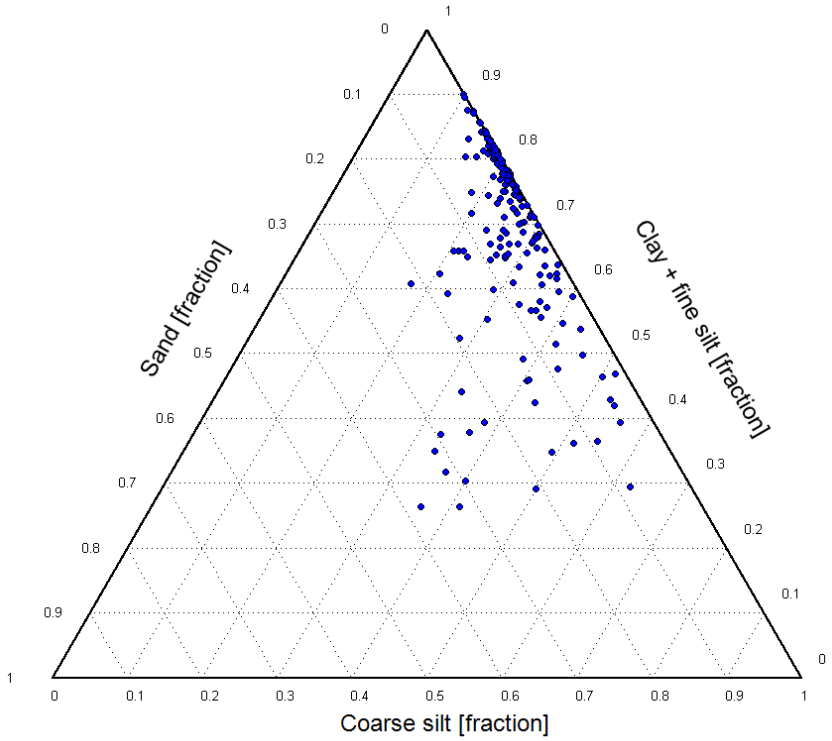

Figure 2.5: Ternary representation of the Nile Delta grain size fraction data base.

Table 2.2 summarizes general statistical moments of grain size fractions derived from the data base. On an average basis, fine silt and clay sized grains make up almost 70% of each sample, while coarse silt exceeds sand sized grains more than 5 times. Sand sized particles play only a minor role with less than 5% on average. Coarse silt and fine silt have an equal average share and make up more than 50% of grain size fractions in our data base. Clay fraction shows the highest variance followed by coarse silt, which is also reflected in Figure 2.5.

Table 2.2: Statistical overview of the Nile Delta grain size data base.

Statistical moment	Sand	Coarse Silt	Fine Silt	Clay
Minimum	0.04	9.96	10.32	11.07
Maximum	37.56	62.39	47.74	79.62
Arithmetic Mean	4.68	26.56	24.15	44.60
Variance	51.63	98.32	58.76	267.16

Regression models have been fitted to predict all grain size fractions as a function of the cohesive fraction. The regression models should fulfill the following conditions:

1. Sufficiently predict the grain size trend as a function of the cohesive fraction
2. Smoothly extrapolate to pure sand samples to ensure numerically stable results, when populating regional models with grain size fractions

The resulting models predict clay, fine silt, coarse silt and sand fractions from the cohesive fraction only (Figure 2.6):

$$W_{clay_{\mathrm{mod.}}} = 0.0075 \cdot W_{cohesive}^{\ 2} + 0.1108 \cdot W_{cohesive} \qquad R^2 = 0.80 \qquad \text{Eq. 2.23}$$

$$W_{fineSilt_{\mathrm{mod.}}} = W_{cohesive} - W_{clay_{\mathrm{mod.}}} \qquad R^2 = 0.11 \qquad \text{Eq. 2.24}$$

$$W_{coarseSilt_{\mathrm{mod.}}} = W_{sortable} - W_{sand_{\mathrm{mod.}}} \qquad R^2 = 0.79 \qquad \text{Eq. 2.25}$$

$$W_{sand_{\mathrm{mod.}}} = 0.5 \cdot \exp\left(W_{sortable} \cdot \ln\left(100 / 0.5\right)/100\right) - 0.5 \qquad R^2 = 0.61 \qquad \text{Eq. 2.26}$$

$$W_{sortable} = 100 - W_{cohesive} \qquad \text{Eq. 2.27}$$

Where, $W_{clay_{\mathrm{mod.}}}$ is the modelled clay weight fraction, $W_{fineSilt_{\mathrm{mod.}}}$ is the modelled fine silt weight fraction, $W_{coarseSilt_{\mathrm{mod.}}}$ is the modelled coarse silt weight fraction and $W_{sand_{\mathrm{mod.}}}$ is the modelled sand weight fraction. $W_{sortable}$ is the sortable weight fraction, which can be directly derived from the cohesive weight fraction $W_{cohesive}$.

Moreover, we used a simple technique to simulate the variability of the North African grain size data base. Hereby, the deviation dev_i at the i^{th} data point of a dataset with n individuals provides information about the variability of the data at this data point:

$$dev_i = x'_i - x_i \qquad \text{Eq. 2.28}$$

Where x_i is the original and x_i' the simulated data at the i^{th} data point. This results in a splitting of positive and negative deviations. Hence, fitting the positive and negative deviations of an established grain size fraction model allows for prediction and subsequent simulation of the variability of a grain size fraction database. Hereby, a random normal distributed positive or negative error $error_i^{+/-}$ of the modelled i^{th} grain size fraction is simulated as a function of the i^{th} positive or negative input grain size fraction deviation $gsf\_dev_i^{+/-}$:

$$error_i^{+/-}\left(gsf\_dev_i^{+/-}\right) = N\left(0, \left|gsf\_dev_i^{+/-}\right|\right) \qquad \text{Eq. 2.29}$$

Where $N\left(0, \left|gsf\_dev_i^{+/-}\right|\right)$ is the random normal distribution with mean 0 and standard deviation equal to the absolute value of deviation $gsf\_dev_i^{+/-}$. The simulated error $error_i$ is

obtained by a random Boolean decision, if a positive $gsf\_dev_i^+$ or negative $gsf\_dev_i^-$ deviation is used as input for the error simulation.

$$error_i = \begin{cases} error_{i\,i}^{+}\left(gsf\_dev_i^{+}\right) & if \quad bool_{random} = 1 \\ -error_{i\,i}^{-}\left(gsf\_dev_i^{-}\right) & if \quad bool_{random} = 0 \end{cases} \qquad \text{Eq. 2.30}$$

Where $bool_{random}$ is a random Boolean operator and yields uniformly either 0 or 1.
The simulated error is then added to the modelled grain size fraction:

$$gsf_{sim.i} = gsf_{\mathrm{mod}.i} + error_i \qquad \text{Eq. 2.31}$$

Four models have been established to predict the positive and negative deviations of clay and sand fractions (Figure 2.6), where the negative deviation models have been derived from regression models of the negative deviation. However, the models have to be optimized to guarantee the best simulation result with respect to all simulated grain size fractions:

$$clay\_dev_{i.}^{+} = -f_{clay} \cdot 0.01 \cdot W_{cohesive\,i}{}^{2} + \left(f_{clay} + 0.05\right) \cdot W_{cohesive\,i} \qquad \text{Eq. 2.32}$$

$$clay\_dev_{i.}^{-} = -0.0993 \cdot W_{cohesive\,i} \qquad \text{Eq. 2.33}$$

$$sand\_dev_i^{+} = -f_{sand} \cdot 0.0001 \cdot W_{sortable\,i}{}^{3} + f_{sand} \cdot 0.0005 \cdot W_{sortable\,i}{}^{2} + f_{sand} \cdot 0.005 \cdot W_{sortable\,i} \qquad \text{Eq. 2.34}$$

$$sand\_dev_i^{-} = -0.0011 \cdot W_{sortable\,i}{}^{2} - 0.0215 \cdot W_{sortable\,i} \qquad \text{Eq. 2.35}$$

Where $W_{cohesive}$ is the cohesive input weight fraction, $W_{sortable}$ is the sortable weight fraction, $clay\_dev^+$ is the positive standard clay error, $clay\_dev^-$ is the negative standard clay error, $sand\_dev^+$ is the positive standard sand error and $sand\_dev^-$ is the negative standard clay error. f_{clay} and f_{sand} are specific factors, which have to be optimised for a best fit of all grain size fractions.

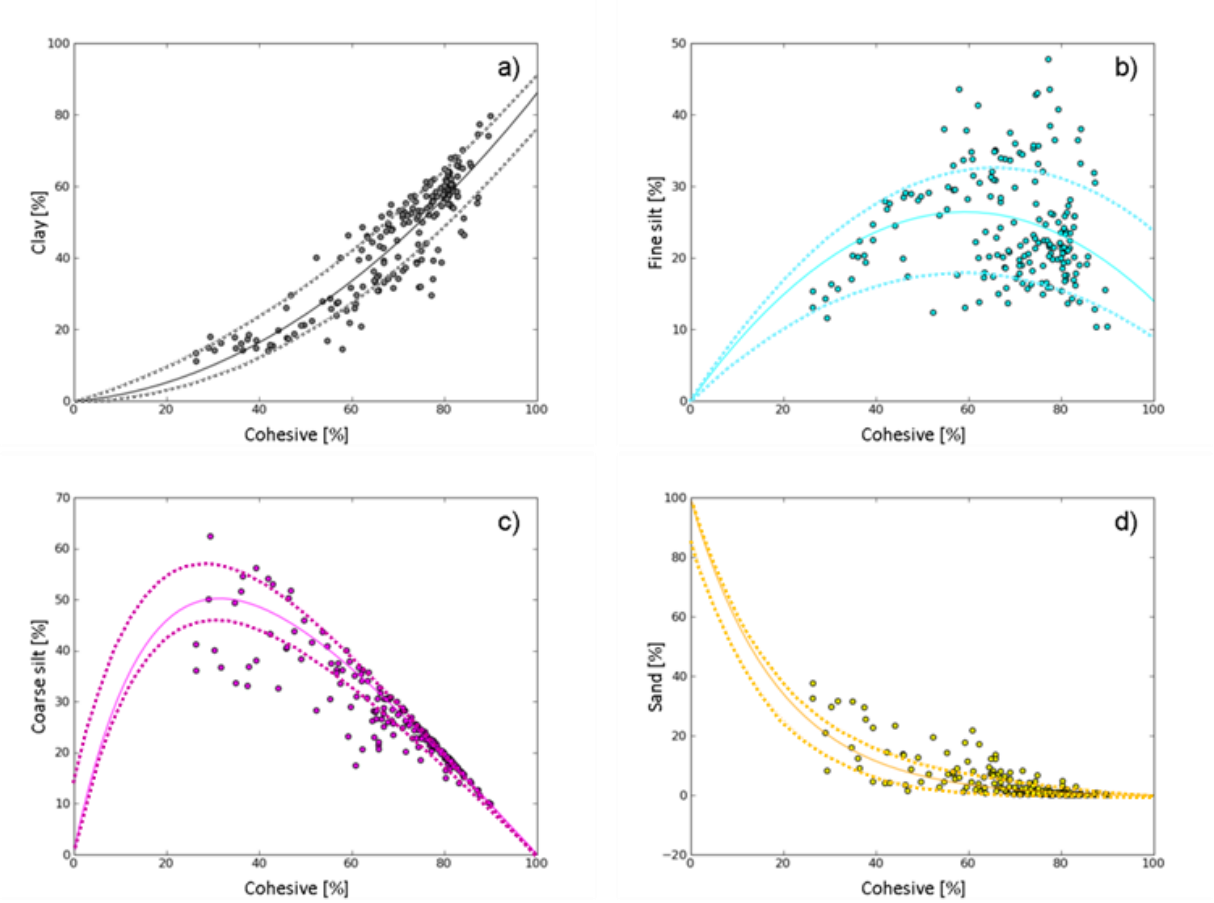

Figure 2.6: a)-d): Grain size fractions (clay, fine silt, coarse silt, sand) in weight percent as a function of cohesive fraction in weight percent. Circles represent the Nile Delta dataset, continuous lines show the grain size fraction models, while the error models are represented by dotted lines.

One possibility to test and optimize the simulation is to perform a two-sample Kolmogorov-Smirnov-Test and to calculate and compare p-values for different deviation models. To do so, the simulation is run with varying parameters of one of the deviation models. The parameter range is selected in such a way, that the deviation model covers the deviation data with maximum and minimum as input. The simulation is optimised, if the selected parameter yields the maximum p-value. Optimisation has been conducted by 1000 grain size fraction simulations for a range of f_{clay} and f_{sand} against Kolmogorov-Smirnov p-values. From this follows that the best simulation results will be achieved, if f_{clay} = 0.23 and f_{sand} = 0.17 (Figure 2.7).

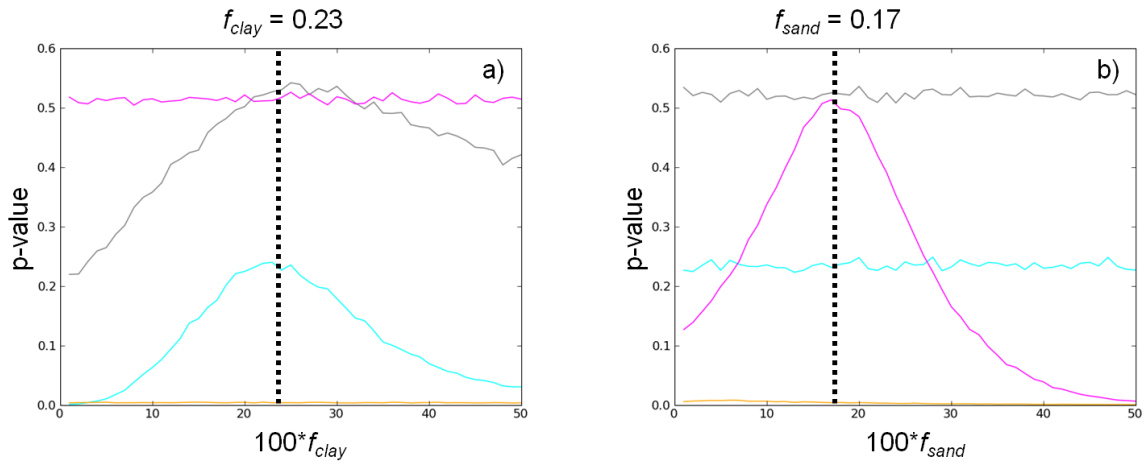

Figure 2.7: a) Optimisation of the standard deviation function for the simulation of clay and fine silt. b) Optimisation of the standard deviation function for the simulation of sand and coarse silt. The dotted lines mark the function parameters, which yield the highest p-values.

Results and Discussion

Physical properties of siliclastic sediments, such as porosity and permeability, are usually determined by laboratory measurements, which are time and cost consuming, in particular, when a large fraction of fine-grained material is involved. However, models to predict these properties in relation to lithology and grain size are available from a theoretical point of view (e.g. Marion et al., 1992; Revil and Cathles, 1999) or derived from laboratory measurements on real rocks (e.g. Yang and Aplin, 2004, 2010) or artificial aggregates (e.g. Mondol et al., 2008). Although these models have been proven to be useful and applicable, they only cover particular lithological types of siliclastic sediments, such as sandstones or mudstones. An integrated model, which allows for physical property prediction independent of the lithological type on the basis on these latest available models (e.g. Marion et al., 1992; Revil and Cathles, 1999; Chuhan et al., 2003; Yang and Aplin, 2004, Yang and Aplin, 2010), is not available, yet. Such a model would be of great importance to the modelling of fluid flow through heterogeneous sediments. Therefore, in this study available models have been integrated into a modelling framework to predict porosity and permeability from the full spectrum of grain size fraction combinations of fine-grained siliclastic sediments. It has been shown, that the modelling framework can reproduce porosity and permeability derived by laboratory measurements in a realistic way. Its flexibility to adjust or substitute the end-member functions of the pure lithological types (clay, fine silt, coarse silt, sand) to local requirements allows the framework to be transferable to any siliclastic sedimentary setting. Thereby, we used Yang's and Aplin's (2004, 2010) models for matrix supported rocks and adjusted the packing and pore filling models of Marion et al. (1992) and Revil and Cathles

(1999) to Yang's and Aplin's (2004, 2010) models in combination with laboratory data on coarse silts (Fawad et al., 2010; Mondol et al., 2011) and sands (Chuhan et al., 2003) as well as theoretical models on sands (Zimmer, 2003; Pettersen, 2007).

However, it should be mentioned, that for both porosity and permeability calculations, mainly experimental mechanical compaction data was used, which does not account for chemical compaction effects and should be therefore used with caution for depths > 2-3 km (Bjørlykke and Hoeg, 1997; Worden et al., 2005).

For clay compaction also different compaction curves have been reported showing a more rapid decrease in porosity at effective stresses below 5 MPa (Mondol et al., 2007, Mondol et al., 2008, Fawad et al., 2010) compared to Yang and Aplin's (2004) empirical relationship. In addition it has to be mentioned, that due to the nature of Yang and Aplin's (2004) porosity model porosities for effective stresses greater than 35 MPa appear to be unrealistically low or even negative. For future applications, we therefore suggest to refit the model and to introduce a double asymptotic model, allowing porosity calculations for higher effective stresses. Furthermore, the assumption for sortable mixtures (sand-coarse silt) to yield a porosity minimum where the volume of coarse silt grains fills the pore volume of sand grains has to be taken with caution, as ideal packing cannot be assumed for sortable mixtures. However, porosity minima have been reported from various authors (Visscher and Bolsterli, 1972; He et al., 1999; Zimmer, 2003; Kristiansen et al., 2005). An additional uncertainty is given by the difference of laboratory and natural mechanical compaction, as additional factors, such as hydrothermal fluid circulation, bioturbation, etc., might be involved in natural compaction, while experimental mechanical compaction involves only the study of the influence of stress and, in some cases, of different fluids.

For a better graphical overview of our stress and grain size dependent porosity-permeability modeling framework, we calculated porosities and permeabilities at different effective stresses (5, 15, 30 MPa) at a fixed ratio of clay to fine silt of 65:35%, which corresponds to the mean ratio of the Nile Delta grain size fraction data base. Visualisation of the results in ternary diagrams with the cohesive (clay + fine silt), coarse silt and sand fractions as end-members reveal theoretical stress-dependent porosity minima at a ratio of approximately 20%:40%:40% of cohesive:coarse_silt:sand at 5 MPa (Figure 2.8). Thereby, the porosity contrast decreases with increasing effective stress.

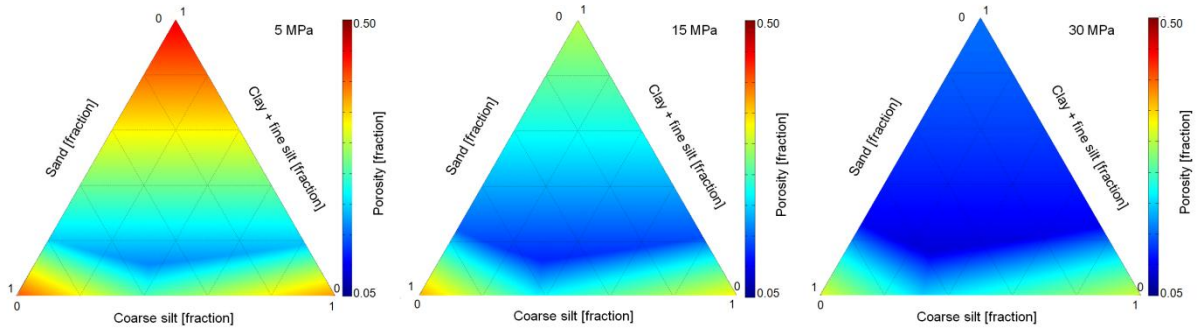

Figure 2.8: Ternary plots for porosity at different effective stresses (5 MPa, 15 MPa, 30 MPa). The clay-fine silt ratio of the cohesive fraction is fixed at 65% clay and 35% fine silt, which approximately corresponds to the mean of the ratio observed in the data base.

The minimum corresponds to the transition between a matrix and a grain supported rock framework and is the result of the binary minima incorporated by the models of Marion et al. (1992) and Zimmer (2003). Similar to Marion et al.'s (1992) and Revil and Cathles' (1999) models, our model yields porosity minima and a rapid increase of permeability between binary and ternary mixtures of different combinations of grain size fractions at $V_{cohesive} \equiv \phi_{sortable}$. The ternary graphical representation for a fixed clay-fine silt ratio demonstrates the strength of our approach and the importance of distinguishing between fine silt and coarse silt as both have an influence upon physical properties. Especially, a formation of a theoretical quaternary porosity minimum cannot be reproduced using the classic binary sand-shale model (Figure 2.9).

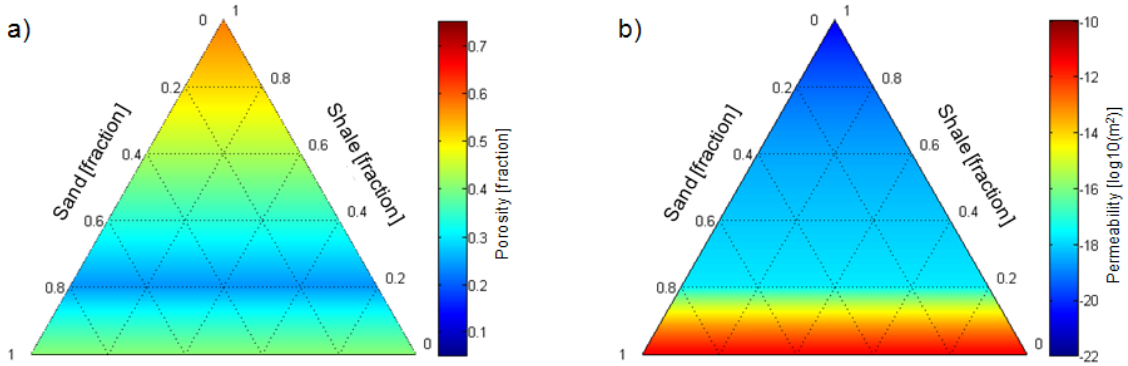

Figure 2.9: Ternary representation of the classic sand-shale model at 5MPa. The lower end-members are equal (sand). a): Porosity; b): permeability.

The model fails to distinguish between matrix supported rocks, which either are rich in coarse silt or sand sized grains, as the applied model of Yang and Aplin (2004, 2010) accounts for clay content only. Variations of coarse silt content with respect to sand content are only

reflected in grain supported rocks (Figure 2.10, left). However, from Figure 2.10 (centre) it becomes clear, that variation of the ratio between fine silt and clay content has a large influence upon the porosity of the whole system. For the unlikely combination of matrix supported rocks, whose matrix consists of fine silt sized particles only, our model fails to predict a porosity decrease, as clay content is the lithological input parameter. Variation of effective stress induces a change of the porosity minimum with respect to the cohesive fraction (Figure 2.10, right) according to Marion et al. (1992), while incorporating the reliable prediction of absolute values derived from Yang and Aplin's model (2004).

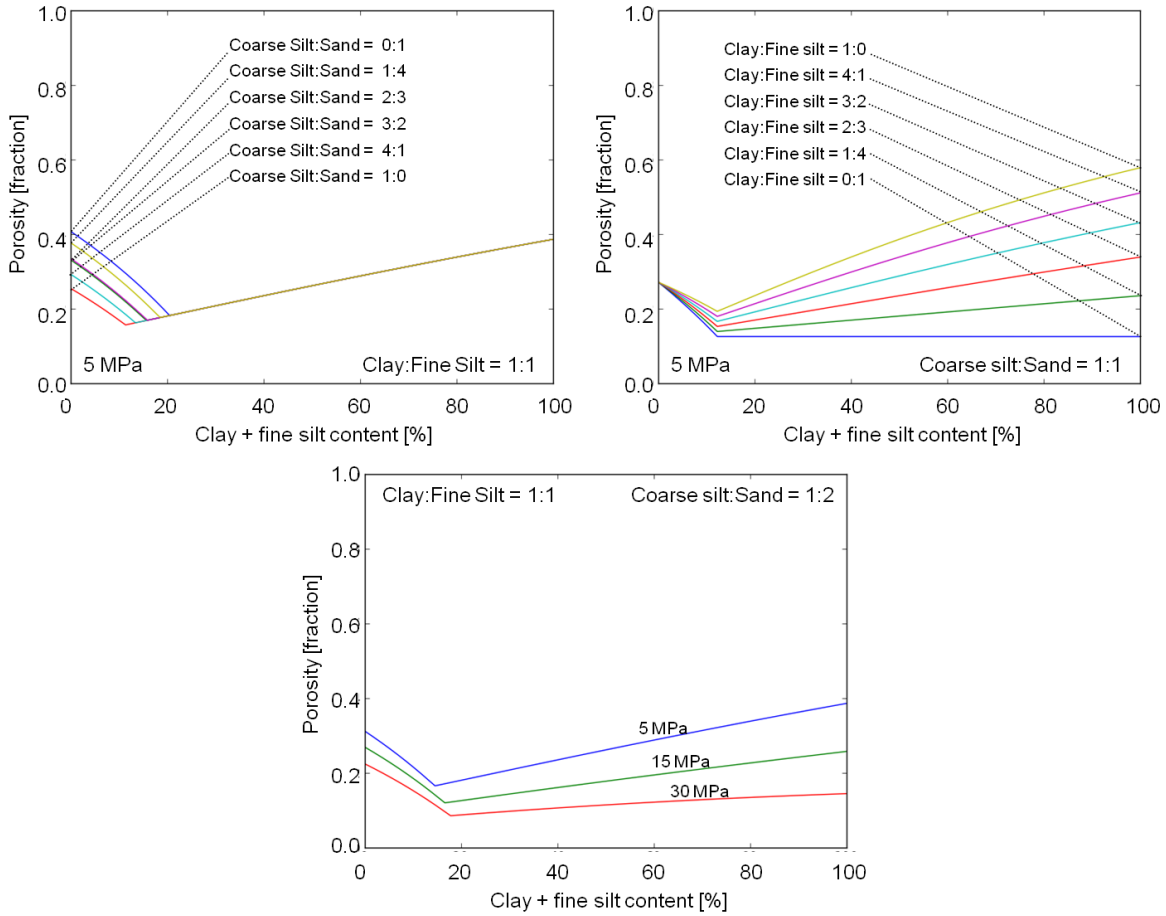

Figure 2.10: Porosity vs. cohesive content at constant effective stress and varying coarser fraction constitution (left), constant effective stress and varying cohesive fraction constitution (centre) and constant lithology and varying effective stress (right).

Looking at ternary representations of permeability as a function of grain size fractions, a sudden increase becomes visible at the border of the matrix to grain support-transition (Figure 2.11). Hereby, the permeability contrast increases with increasing effective stress.

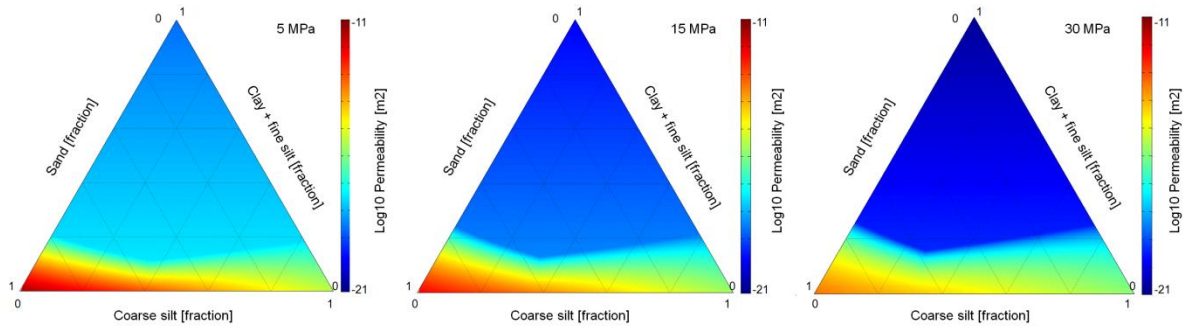

Figure 2.11: Ternary plots for log10 permeability at different effective stresses (5 MPa, 15 MPa, 30 MPa). The clay-fine silt ratio of the cohesive fraction is fixed at 65% clay and 35% fine silt, which approximately corresponds to the mean of the ratio observed in the data base.

As for the porosity, the rapid permeability increase corresponds to the transition between matrix and grain supported rock framework. Also, due to clay content being the lithological input for matrix supported rocks, coarse silt or sand has no influence upon the prediction of permeability of matrix supported rocks. Such variations are only reflected in grain supported rocks (Figure 2.12, left). On the other hand side, variation of the ratio between fine silt and clay content has a large influence upon the matrix supported part of the system (Figure 2.12, centre). However, it has to be tested, if a linear increase in permeability is valid in the range of low clay contents for matrix supported rocks. In concordance, Mondol et al. (2011) presented permeability data on clay-silt mixtures, which show a linear increase of permeability with increasing silt content up to a point, where the support state changes from matrix to grain support. On the opposite, Revil and Cathles (1999) suggest a permeability decrease with decreasing shale content until reaching a permeability minimum at $\phi_{sand} \equiv V_{shale}$. Our model fails to predict a permeability increase as a function of cohesive content for matrix supported rocks with zero clay content for equal reasons as stated above for porosity decrease prediction. Variation of effective stress induces a change of the matrix grain-support transition location with respect to the cohesive fraction (Figure 2.12, right), yielding a situation, where rocks with higher compaction (e.g. at 30 MPa) can have higher permeabilities with equal cohesive contents than rocks having seen less pressure. This effect results from negligence of chemical compaction and depicts the upper limit of our approach in terms of effective stress.

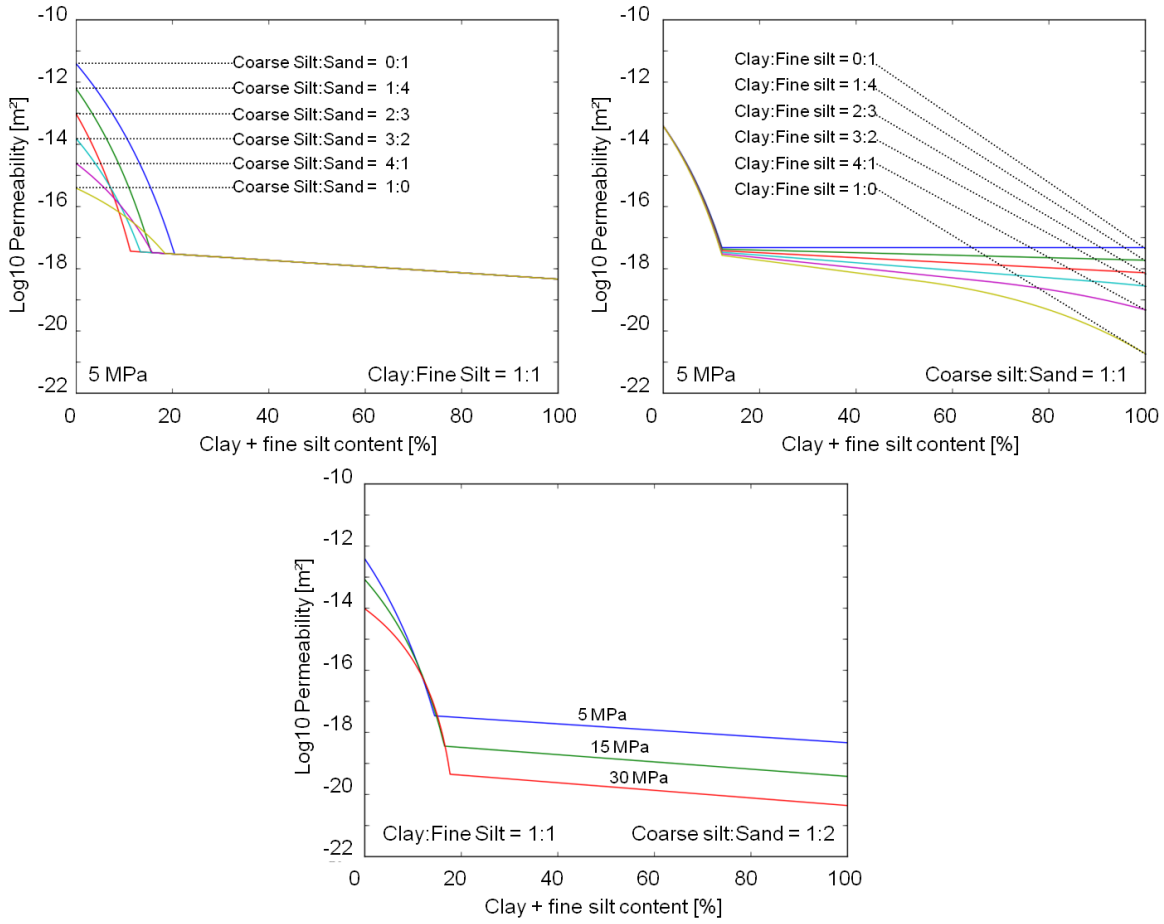

Figure 2.12: Permeability vs. cohesive content at constant effective stress and varying coarser fraction constitution (left), constant effective stress and varying cohesive fraction constitution (centre) and constant lithology and varying effective stress (right).

To test our model against real data we used grain size and porosity measurement data from published and unpublished sources from the Gulf of Mexico, the North Sea and West and Nile Delta, North Africa (Figure 2.13). All samples were taken from core or side wall core. As for our Nile Delta database the grain size data used in this section was analysed by the sedigraph technique and is based on bulk density and grain density (Coakley and Syvitski, 1991). Porosity was measured by employment of the mercury injection technique (a detailed description can be found in Boeker, 2011). The data displays a weak trend of decreasing porosity with decreasing clay content. Using the available grain size data as input for our modelling technique results in a similar trend, but with less scatter (Figure 2.14). Only for a fraction of the data effective stresses are available. For data with no information about the stress state we calculated the effective stress assuming hydrostatic pore pressure, a mean water density and a mean rock density. Then the effective stress becomes:

$$\sigma_{eff.} = \rho_{rock} \cdot g \cdot h_{sfl.} - \rho_{water} \cdot g \cdot \left(h_{water} + h_{sfl.}\right) \qquad \text{Eq. 2.36}$$

where, $\sigma_{eff.}$ is the effective stress in Pascal, ρ_{rock} is the mean rock density (here: 2500 kg/m^3), g is the Earth's mean gravitational acceleration (here: 9.81 m/s^2), $h_{sfl.}$ is the depth below sea floor, ρ_{water} is the mean water density (here: 1000 kg/m^3) and h_{water} is the water column above sea floor.

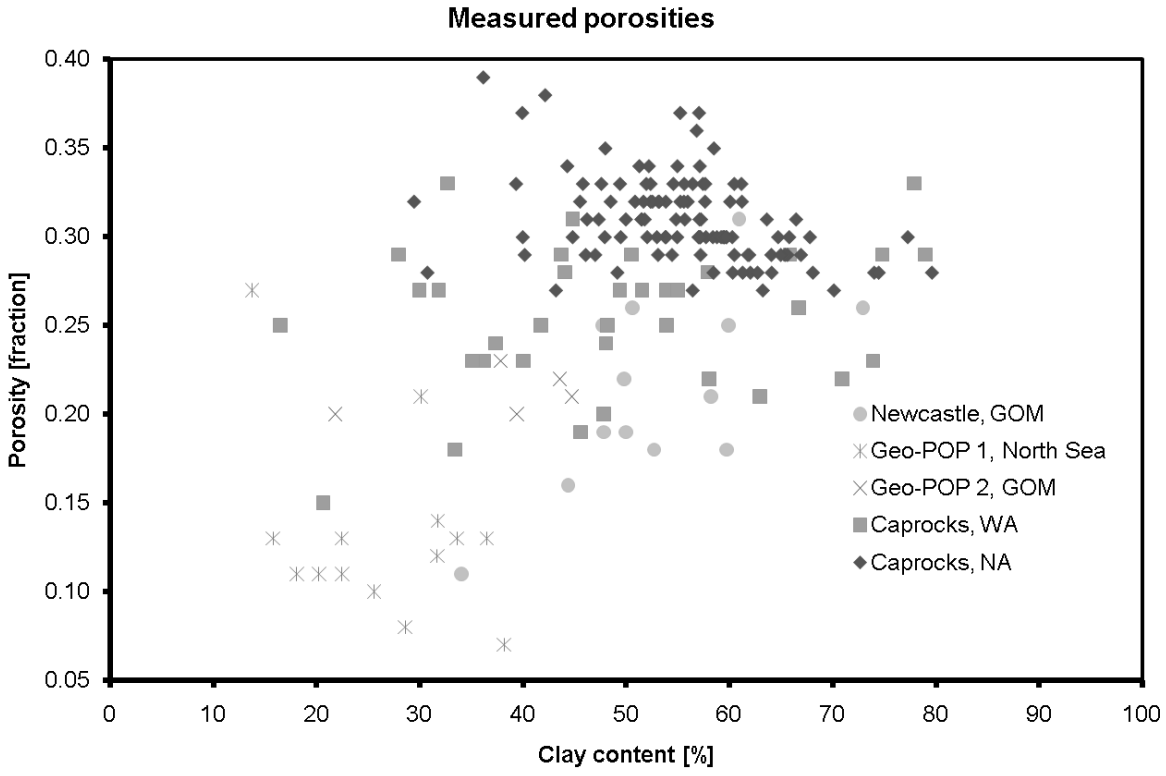

Figure 2.13: Porosity as a function of clay content for various data sets and effective stresses between 5-35 MPa.

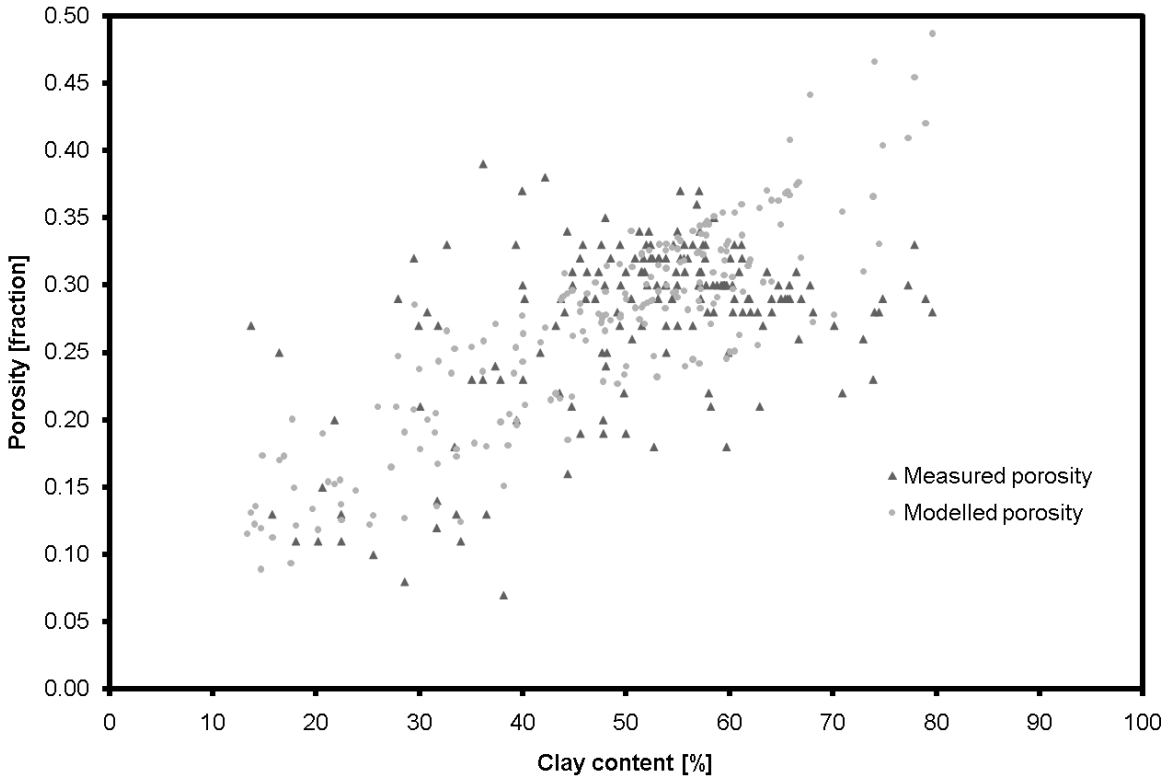

Figure 2.14: Measured (triangles) and modelled (dots) porosities as a function of clay content. The modelled porosities reproduce the general trend of the measured porosities, but show less scatter and large deviations at high clay contents.

In particular, the modelled porosities deviate from their measured counterparts at high clay contents (Figure 2.14). Figure 2.15 demonstrates a lot scatter when cross-plotting the modelled vs. the measured porosities. However, most of the scatter results for data with modelled stress states. The mean deviation is less than 5 percent points of porosity, approximately 65% of the modelled porosities deviate less than 5 percent points of porosity, approximately 85% of the modelled porosities deviate less than 7.5 percent points of porosity and more than 90% of the modelled porosities deviate less than 10 percent points of porosity from the measured porosities (Figure 2.16).

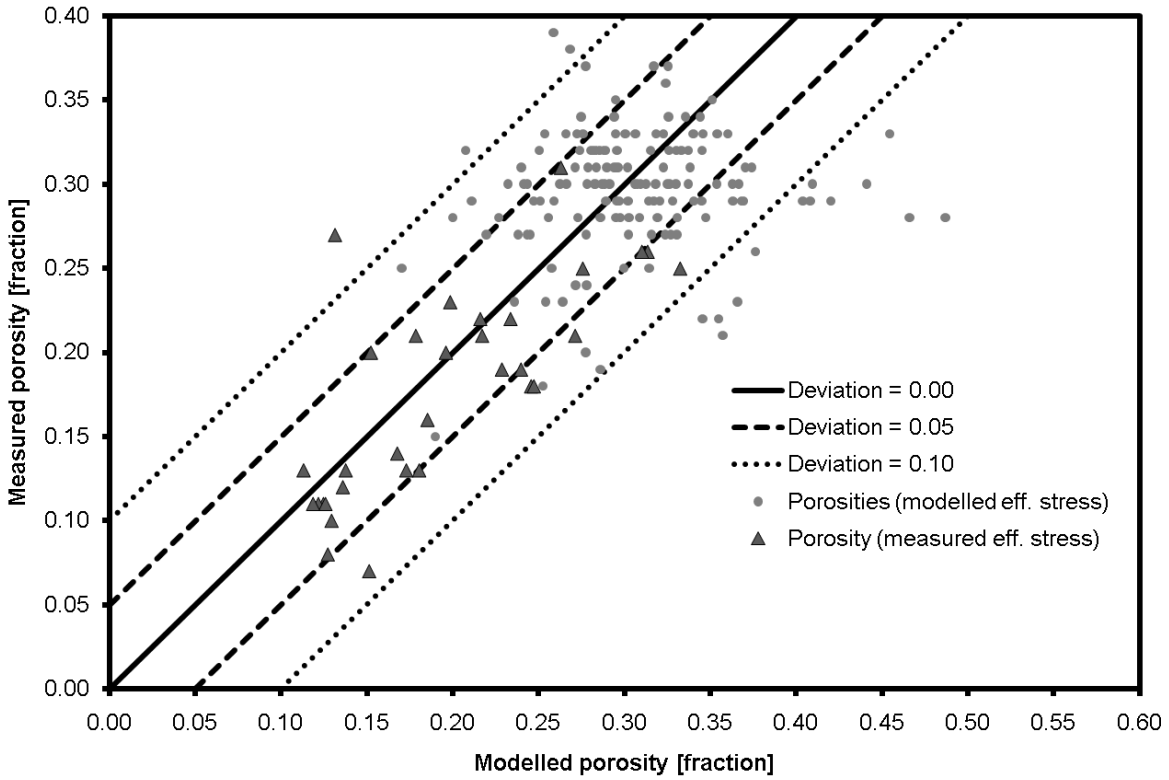

Figure 2.15: Measured vs. modelled porosities. The solid line represents the line of zero deviation, the dashed line marks a deviation of 5 percent points of porosity and the dotted line a 10 percent points of porosity deviation. Porosity data is divided into data with known stress state (triangles) and assumed stress state (dots).

Major differences between modelled and measured porosities might be the result of under- or overestimated effective stresses due to over pressure or deviating density profiles in depth, but also through time. Another parameter, which has the potential to lead to differences between modelled and measured porosities, could be early chemical compaction and related presence of cemented pores in sands and silts (Bjørlykke and Hoeg, 1997) or smectite-illite transition in clays (Bjørlykke , 1998; Worden et al., 2005). However, our model produces reasonable results for most of the measured porosity data. For permeability, our model could not be tested against real data, but input data are based on experimental mechanical compaction data and measured data from natural rocks and should therefore yield realistic results.

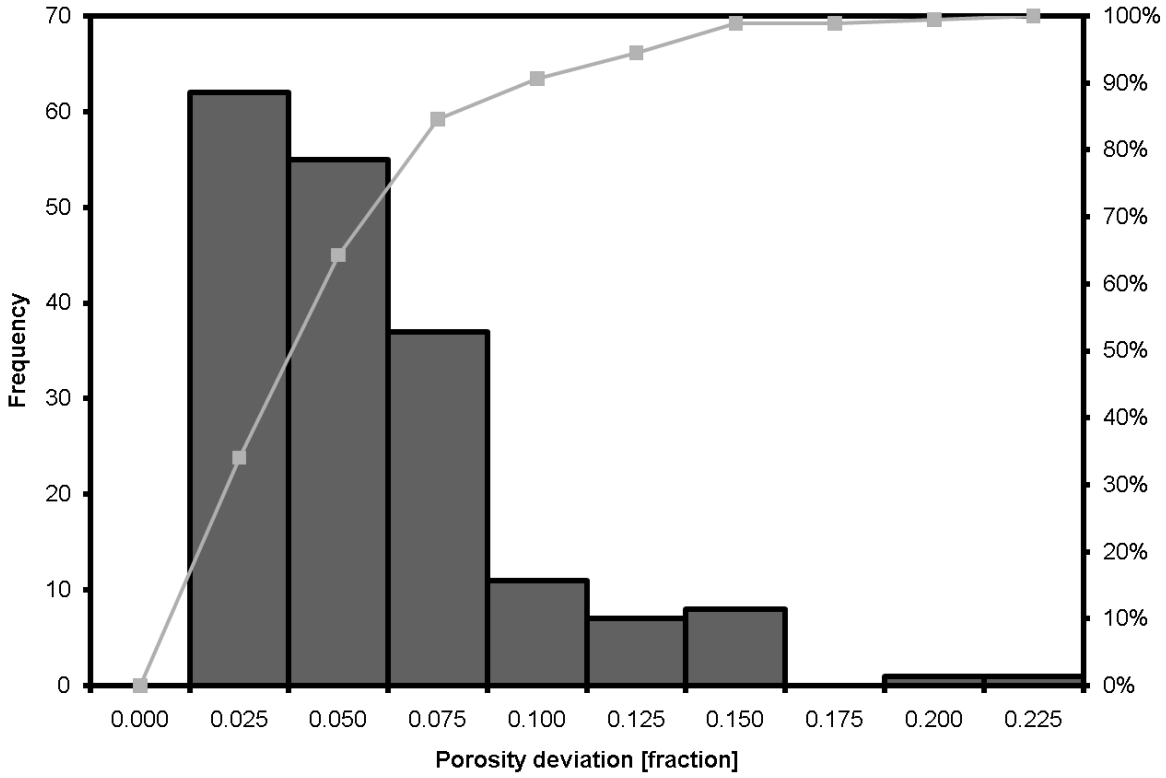

Figure 2.16: Histogram (bars) and cumulative histogram (brighter line plot) of absolute deviations of modelled porosities from measured porosities. Only 10 % of the modelled porosities show a deviation of more than 10 percent points of porosity.

The empirical models derived from the cohesive grain size fraction yielded good correlations and depict the depositional transition sequence from very fine-grained to coarser grained material. In that way, the grain size fraction trend follows a trend from clay and fine silt rich samples to samples with more coarse silt content to samples with more sand content.

Using the above explained simulation technique we ran 10000 simulations, yielding average p-values of 0.53, 0.24, 0.51 and 0.004 for the simulation of clay fraction distribution, fine silt fraction distribution, coarse silt fraction distribution and sand fraction distribution, respectively. Hence, for clay, fine silt and coarse silt fraction distribution the simulated distributions can be considered as statistically identical as their p-values are well above 0.1. The sand simulation does not yield sufficient similarity compared to the original sand fraction distribution, which becomes obvious from the p-value, but also from visual comparison of the cumulative distributions (Figure 2.17). The sand distribution comprises mainly of low sand fractions and forms a narrow and thus very sensitive distribution, which might explain the difference between original and simulated distributions. However, the general shape of the sand distribution is preserved (Figure 2.18).

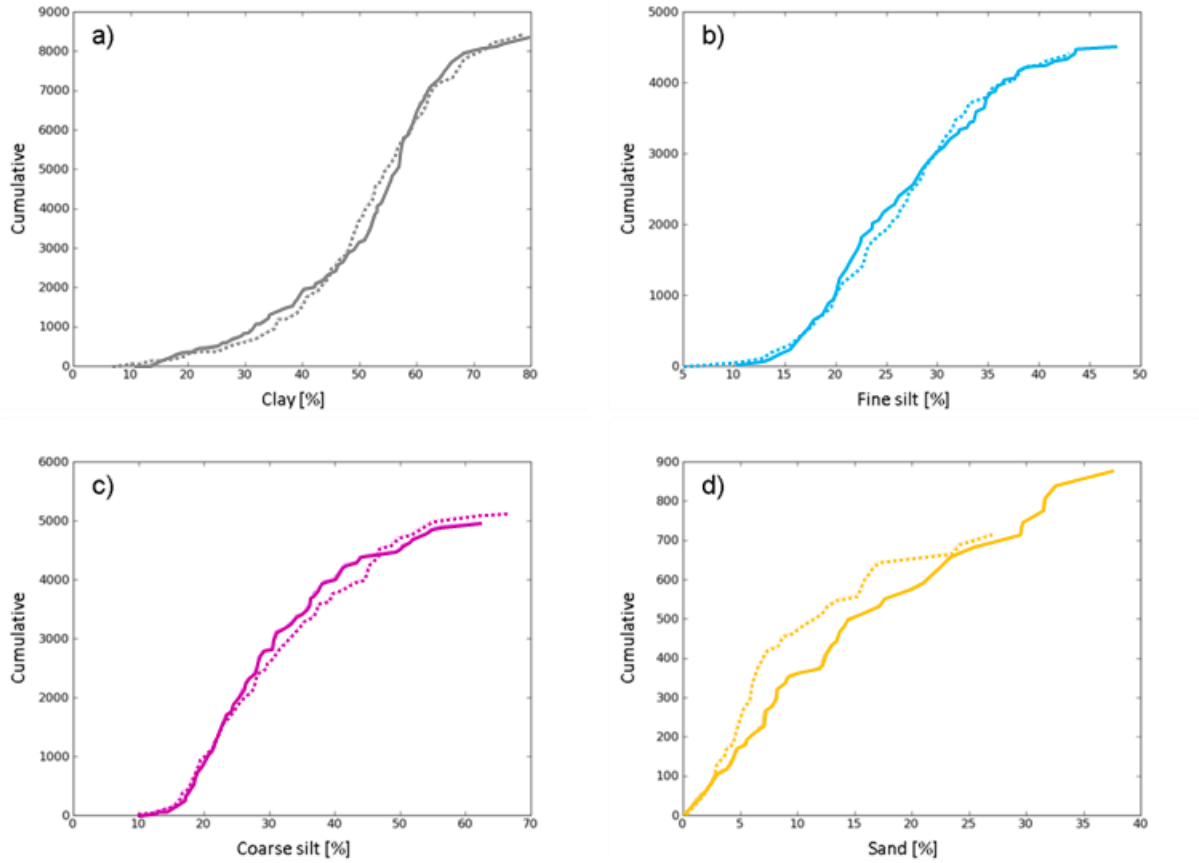

Figure 2.17: a)-d): Cumulatives of original grain size fraction distributions (solid lines) and a simulated grain size fraction realisation (dotted lines) for clay, fine silt, coarse silt and sand, respectively.

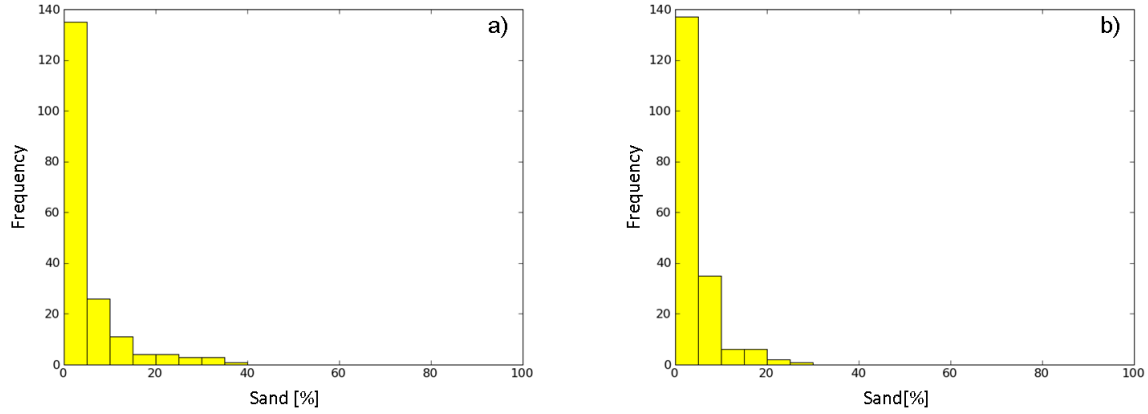

Figure 2.18: a): Original sand fraction distribution of the North African database in weight percent. b): Simulated counterpart. Note, that the general shapes are similar, although the statistical test failed.

Yang and Aplin (2010) have shown that by including a single lithological parameter such as clay content as a discriminator for permeability modelling the uncertainty for mudstone permeability can be reduced from 2-5 orders of magnitude to one order of magnitude. Yang and Aplin attributed the remaining one order of magnitude of permeability uncertainty to the complexity of mudstone lithology and grain size distribution. With the extension of Yang's

and Aplin's models for porosity (2004) and permeability (2010) to the whole grain size spectrum of fine-grained sediments we tried to further reduce this uncertainty. However, the absolute reliability of the modelling framework for porosity and permeability has to be proven by correlation with measured permeability data. Nevertheless, our modelling framework can be used for geological fluid flow modelling on different scales and is able to include a wide range of lithological variability. The lack of calibration data in our study can be addressed in future studies and the developed modelling framework can be easily adapted to new data and relationships by substitution of the end-members. Similar to Yang's and Aplin's models (2004, 2010) our modelling framework can be also used for porosity and permeability modelling based on shale estimates from geophysical well logs. Hereby, the cohesive content can be correlated with simple measures such as vshale from gamma ray. The resulting continuous porosity permeability depth profiles can then used to calibrate models of basin scale fluid flow and leakage rates of petroleum or stored CO_2.

Summary and Conclusions

We presented an extended version of Yang's and Aplin's porosity (2004) and permeability (2010) models, which can be used for porosity and permeability assignment for models of heterogeneous fine grained sediments. Thereby, the developed modelling framework allows for prediction of sample-scale (centimetre-scale) porosity and permeability data on the basis of grain size only and only requires laboratory data of the pure end-members (clay, fine silt, coarse silt, sand). In addition, the modelling framework is a first attempt to combine available data and theoretical models to a predictor of stress-dependent porosities and permeabilities from the full siliclastic grain size spectrum. The approach can also be used for geophysical well log based modelling of continuous porosity and permeability profiles, when combined with a grain size fraction model or simulation technique, which has also been presented in this study for a North African grain size fraction database.

The resulting modelling framework accounts for mechanical compaction and a wide range of lithological variety. Furthermore, the model does not only account for detailed property prediction of the sandy parts, but in particular for the shaly or mud-rich parts of heterogeneous fine-grained sediments. To do so, we linked the calculation of porosity and permeability to effective stress and to the whole spectrum of grain size fractions present in fine-grained sediments. Hereby, the modelling framework firstly combines existing theoretical models for binary lithological with Yang's and Aplin's models (2004, 2010) and latest measured data from natural rock and experimental mechanical compaction data. Taking

account for different grain size fractions has the advantage to reproduce a theoretical formation of a quaternary porosity minimum at dependent on the ratio of cohesive fraction:coarse silt fraction:sand fraction, which cannot be reproduced using the classic binary sand-shale model. Also, porosity and permeability variations due to different silt fraction compositions (sortable vs cohesive silt) can be incorporated. We showed the applicability of the porosity permeability modelling framework, as it delivers realistic results, while being very flexible, as end-member functions can be substituted easily, which enables the framework to being adaptable to different regions and depositional environments.

As our porosity-permeability model requires the full grain size fraction spectrum as input for each sample to be modelled, we developed a modelling/simulation scheme for grain size fractions on the basis of the cohesive (clay + fine silt) fraction only. This provides maximum flexibility, as grouping into sortable and cohesive fractions allows cross-calibration with common measurements such as vshale from geophysical well logs. We demonstrated the grain size modelling/simulation scheme by application to a grain size fraction data base of a case study from the Nile Delta, Egypt. Good to strong relationships ($R^2 \sim 0.8$) between the cohesive fraction and the individual grain size fractions have been found and modelled with polynomial regressions. The simulated grain size fraction distributions of the Nile Delta case study have been successfully reproduced for clay, fine silt and coarse silt fractions. The sand fraction distribution could only be approximated due to a lack of sand-rich samples in the data base.

Future work should involve extension of the modelling approach for chemical compaction and higher effective stresses. We plan to use the modelling approach to generate realistic rock models to upscale the sample properties to metre-scale properties of heterogeneous fine-grained sediments using numerical fluid flow simulation.

References

Aplin, A.C., Yang, Y.L. & Hansen, S. 1995. Assessment of , the compression coefficient of mudstones and its relationship to detailed lithology. Marine and Petroleum Geology, 12, 955–963.

Aplin, A. C., Fleet, A. J., MacQuaker, J. H. S. 1999. Muds and Mudstones: Physical and Fluid Flow Properties. Geological Society, Special Publications, 158. In: Aplin, A.C., Fleet, A.J. & MacQuaker, J.H.S. (eds) 1999. Muds and Mudstones: Physical and Fluid Flow Properties.Geological Society, Special Publications, 158, 1-8.

Aplin, A. C., Green, P. 2011. Caprocks grain size data base – unpublished data.

Armitage, P. J., Faulkner, D. R., Worden, R. H., Aplin, A. C., Butcher, A. R., Iliffe, J. 2011. Experimental measurement of, and controls on, permeability and permeability anisotropy of caprocks from the CO2 storage project at the Krechba Field, Algeria, J. Geophys. Res., 116, B12208, doi:10.1029/2011JB008385.

Bjørlykke, K., Hoeg, K. 1997. Effects of burial diagenesis on stresses, compaction and fluid flow in sedimentary basins. Marine and Petroleum Geology, 14, 3, 267-276.

Bjørlykke, K. 1998. Clay mineral diagenesis in sedimentary basins – a key to the prediction of rock properties. Examples from the North Sea Basin. Clay Minerals, 33, 1, 15–34.

Blatt, H., Middleton, G. V., Murray, R. C. 1980. Origin of Sedimentary Rocks. 2nd Edition, Prentice-Hall, Englewood Cliffs, NJ.

Boeker, U. 2011. Controls on Natural Gas Migration in the Western Nile Delta Fan. PhD Thesis, Newcastle University.

Bryant, W. R., Hottmann, A., Trabant, P. 1975, Permeability of unconsolidated and consolidated marine sediments, Gulf of Mexico. Marine Geotechnology, 1, 1, 1-14.

Chilingar, G. V. 1964. Relationship between porosity, permeability and grain size distribution of sands and sandstones. In: Deltaic and Shallow Marine Deposits, vol. 1, edited by L. M. J. U. Van Straaten, 71-75, Elsevier, New York.

Chuhan, F. A., Kjeldstad, A., Bjørlykke, K., Hoeg, K. 2003. Experimental compression of loose sands; relevance to porosity reduction during burial in sedimentary basins. Canadian Geotechnical Journal 40, 5, 995–1011.

Coakley, J. P., and Syvitski, J. P. M. 1991. Sedigraph techniques. In: Syvitski, J. P. M. (Ed.), Principles, Methods, and Application of Particle Size Analysis: New York (Cambridge Univ. Press), 129-142.

Coyner, K., Katsube, T. J., Best, M.E., Williamson, M. 1993. Gas and water permeability of tight shales from the Venture gas Field offshore Nova Scotia. In: Current Research, Part D. Geological Survey of Canada, 129–136.

Dautriat, J., Gland, N., Guelard, J., Dimanov, A., Raphanel, J. L. 2009. Axial and Radial Permeability Evolutions of Compressed Sandstones: End Effects and Shear-band Induced Permeability Anisotropy. Pure Appl. Geophys. 166, 1037–106.

Dewhurst, D. N., Aplin, A. C., Sarda, J. P., Yang, Y. L. 1998. Compaction-driven evolution of poroperm in natural mudstones: an experimental study. J. Geophys. Res., 103, 651–661.

Dewhurst, D. N., Yang, Y. L., Aplin, A. C. 1999a. Permeability and fluid flow in natural mudstones, in Muds and Mudstones: Physical and Fluid Flow Properties, edited by A.C. Aplin et al., Geol. Soc. Spec. Publ., 158, 23–43.

Dewhurst, D. N., Aplin, A. C., Sarda, J. P. 1999b. Influence of clay fraction on pore-scale properties and hydraulic conductivity of experimentally compacted mudstones. J. Geophys. Res., 104, B14, 29261–29274.

Fawad, M., Mondol, N. H., Jahren, J., Bjørlykke, K. 2010. Microfabric and rock properties of experimentally compressed silt-clay mixtures. Marine and Petroleum Geology, 27, 1698–1712.

Folk, R. L. 1965. Petrology of Sedimentary Rocks, 130p.

He, D., Ekere, N. N., Cai, L. 1999. Computer simulation of random packing of unequal particles. Physical Review E, 60, 6, 7098-7104.

Heard, J. R., Eileen, J. K., Mannering, J. V. 1988. Soil Macroporosity, Hydraulic Conductivity and Air Permeability of Silty Soils under Long-Term Conservation Tillage in Indiana. Soil & Tillage Research, 11, 1-18.

Hildenbrand, A., Schlomer, S., Krooss, B.M. 2004. Gas breakthrough experiments on fine-grained sedimentary rocks. Geofluids, 2, 1, 3–23.

Kitajima, H., Shimamoto, T., Tanikawa, W. 2004. Permeability Structure and Basin Analysis of Miyazaki Group. International symposium on methane hydrates and fluid flow in upper accretionary prisms. Japan Drilling Earth Science Consortium.

Kristiansen, K. d. L., Wouterse, A., Philipse, A. 2005. Simulation of random packing of binary sphere mixtures by mechanical contraction. Physica A, 358, 249–262.

Koltermann, C. E., Gorelick, S. 1995. Fractional Packing Model for Hydraulic Conductivity Derived from Sediment Mixtures. Water Resources Research, 31, 3283-3297.

Kwon, O., Kronenberg, A. K., Gangi, A. F., Johnson, B., Herbert, B. E. 2004. Permeability of illite-bearing shale: 1. Anisotropy and effects of clay content and loading. J. Geophys. Res., 109, B10, B10205.

Lundegard, P. D. 1992. Sandstone Porosity Loss – A "Big Picture" View of the Importance of Compaction. Journal of Sedimentary Petrology, 62, 2, 250-260.

Macquaker, J. H. S., Howell, J. K. 1999. Small-scale (<5.0 m) Vertical Heterogeneity in Mudstones: Implications for High-Resolution Stratigraphy in Siliclastic Mudstone Successions. J. of the Geol. Soc.London, 156, 105-112.

Mallon, A. J., Swarbrick, R. E., Katsube, T. J. 2005. Permeability of fine-grained rocks: new evidence from chalks. Geology 33, 21–24.

Marion, D., Nur, A., Yin, H., Han, D. 1992. Compressional velocity and porosity in sand-clay mixtures. Geophysics 57, 554–563.

McCave, I. N., Manighetti, B., and Robinson, S. G. 1995. Sortable silt and fine sediment size/composition slicing: parameters for palaeocurrent speed and palaeoceanography. Paleoceanography, 10, 593-610.

McGeary, R. K. 1961. Mechanical packing of spherical particles: J. Am. Ceram. Soc., 44, 513-522.

Mesri, G., Olson, R.E. 1971. Mechanisms controlling the permeability of clays. Clays Clay Min. 19, 151–158.

Mitchell, J. K. 1976, Fundamentals of Soil Behavior, Wiley, New York, 422 p.

Mondol, N. H., Bjørlykke, K., Jahren, J., Høeg, K. 2007. Experimental mechanical compaction of clay mineral aggregates - changes in physical properties of mudstones during burial. Marine and Petroleum Geology 24, 289–311.

Mondol, N. H., Bjørlykke, K., Jahren, J. 2008. Experimental compaction of clays: relationship between permeability and petrophysical properties in mudstones. Petroleum Geoscience 14, 319–337.

Mondol, N. H., Jahren, J., Berre, T., Grande, L., Bjørlykke, K. 2011. Permeability Anisotropy in Synthetic Mudstones − An Experimental Study. EAGE Vienna 2011. EarthDoc – Extended Abstract, D030.

Nagaraj, T. S., Pandian, N. S., Narasimha Raju, P. S. R., 1994. Stress-state-permeability relations for overconsolidated clays. Geotechnique, 44, 349–352.

Nelson, P. H., Kibler, J. E. 2003. A Catalog of Porosity and Permeability from Core Plugs in Siliciclastic Rocks. USGS - Open-file Report 03-420.

Neuzil, C.E. 1994. How permeable are clays and shales? Water Resour. Res. 30, 145–150.

Nordahl, K, Ringrose, P. S., Wen, R. 2005. Petrophysical characterization of a heterolithic tidal reservoir interval using a process-based modeling tool. Pet Geosci, 11,17–28.

Nordahl, K., Ringrose, P. S. 2008. Identifying the Representative Elementary Volume for Permeability in Heterolithic Deposits Using Numerical Rock Models Mathematical Geosciences, 40, 7, 753-771

Pettersen, O. 2007. Sandstone compaction, grain packing and Critical State Theory. Petroleum Geoscience, 13, 63–67.

Potter, E. P., Maynard, J. B., Pryor, W. A. 1980. Sedimentology of Shale. Springer, New York, Berlin, Heidelberg, Tokyo, 306 p.

Revil, A., Cathles, L. M. 1999. Permeability of Shaly Sands. Water Resources Research, 35, 3, 651-662.

Schieber, J. 1999. Distribution and Deposition of Mudstone Facies in the Upper Devonian Sonyea Group of New York. J. of Sedimentary Research, 69, 4, 909–925.

Shepard, F. P. 1954. Nomenclature based on sand-silt-clay ratios. Jour, Sed. Petrology, 24, 151-158.

Skempton, A.W. 1944. Notes on the compressibility of clay. Quarterly Journal of the Geological Society of London, 100, 119–135.

Terzaghi, K. 1943. Theoretical Soil Mechanics. John Wiley, New York.

Visscher, W. M., Bolsterli, M. 1972. Random Packing of Equal and Unequal Spheres in Two and Three Dimensions. Nature, 237, 504-507.

Wentworth, C. K. 1922. A scale of grade and class terms for clastic sediments. J. Geol., 30, 377-392.

Worden, R. H., Charpentier, D., Fisher, Q. J., Aplin, A. C. 2005. Fabric development and the smectite to illite transition in Upper Cretaceous mudstones from the North Sea: an image Analysis Approach. From: Shaw, R. P. (ed.) 2005. Understanding the Micro to Macro Behaviour of Rock-Fluid Systems. Geological Society, London, Special Publications, 249, 103-114.

Yang, Y. L., Aplin, A. C. 1998. Influence of lithology and effective stress on the pore size distribution and modelled permeability of some mudstones from the Norwegian margin. Mar. Petrol. Geol., 15, 163–175.

Yang, Y. L., Aplin, A. C. 2004. Definition and practical application of mudstone porosity–effective stress relationships. Petroleum Geoscience, 10, 153–162.

Yang, Y. L., Aplin, A. C. 2007. Permeability and petrophysical properties of 30 natural mudstones. Journal of Geophysical Research: Solid Earth, 112, B3, B03206.

Yang, Y. L., Aplin, A. C. 2010. A Permeability–Porosity Relationship for Mudstones. Marine and Petroleum Geology, 27, 8, 1692-1697.

Zhu, W., Montesi, L. G. J., Wong, T.-F. 1997. Shear-enhanced compaction and permeability reduction: Triaxial extension tests on porous sandstone. Mechanics of Materials, 25, 199-214.

Zhu, W., Montesi, L. G. J., Wong, T.-F. 2002. Effects of stress on the anisotropic development of permeability during mechanical compaction of porous sandstones. Geological Society, London, Special Publications; 200; 119-136.

Zimmer, M. A. 2003. Seismic Velocities in Unconsolidated Sands: Measurements of Pressure, Sorting, and Compaction Effects. PhD Thesis, Stanford University.

Chapter 3: Metre-Scale Heterogeneous Shales and Mudstones – Quantitative Extraction of High Resolution Variograms from Core and Borehole Images

Introduction

Shales and mudstones, which are important parts of petroleum systems as they can act as seals, source rocks and even reservoir rocks in case of unconventional systems, are the most abundant rock type in sedimentary basins (e.g. Potter et al., 1980). They also are of significance in other aspects of geosciences such as the storage of CO_2 and nuclear waste, hydrological issues and hydrothermal fluid circulation in sedimentary basins. It is well known and widely accepted from the basin and petroleum reservoir modelling community, that sub-metre scale heterogeneities can significantly influence migration and production of hydrocarbons from conventional reservoirs (e.g. Pickup et al., 2000, 2005; Mikes, 2006; Morton et al., 2002; Willis and White, 2000). Thereby, the experimental variogram as a geostatistical descriptor for spatial heterogeneity and related covariance function modelling has been widely used in the past to model and upscale these sub-metre scale heterogeneities for modelling of heterogeneous reservoirs (e.g. Deutsch, 2002; Chiles and Delfiner, 1999). However, despite the relevance of shales and mudstones, the influence of heterogeneity upon migration and hence seal integrity or unconventional reservoir quality, has usually been neglected in the past, although heterogeneous shales and mudstones have been qualitatively investigated and classified by many authors at different levels of detail (e.g. Cole and Picard, 1975; Potter et al., 1980; Schieber, 1999; Macquaker and Adams, 2003; Piper et al., 2010). Hence, when it comes to characterisation of physical properties of fine-grained sediments, shales and mudstones have been treated as homogeneous in the past - physical properties such as porosity and permeability or seismic velocities from measurements on spatially homogeneous samples have been directly upscaled to aquifer or geobody scale and beyond (e.g. Aplin and Macquaker, 2011; Huysmans et al., 2008). Sub-metre scale spatial heterogeneity present in shales and mudstones has usually been neglected, even in geostatistical studies - mainly due to the lack of appropriate data sources or due to a strict focus on the reservoir or aquifer geology.

The aim of this study is thus to fill this gap and to provide the geomodelling community with a set of representative high resolution variograms, which can be used to include Sub-metre scale heterogeneity in shales and mudstones into common basin and reservoir modelling workflows along with probable occurrence in associated seismic facies. Hereby, we use a

database of core and borehole images of heterogeneous mudstones derived from five wells of a producing offshore gas field in the Western Nile Delta, Egypt. The database is first interpreted on the basis of traditional classification schemes for sedimentary structures in fine-grained sediments. By doing so, only geometrical, flow relevant heterogeneities are considered. The interpretation is hence not a classical sedimentological interpretation, where detailed processes and paleo-environments are investigated, but an interpretation with focus on fluid flow through heterogeneous shales and mudstones. Geostatistical analysis techniques are used to quantify and enhance the sedimentological interpretation and to obtain the representative set of heterogeneities for extraction of the detailed variogram models (covariance functions).

Sub-Metre Scale Heterogeneities in Shales and Mudstones

Sedimentological Studies

Many investigative studies of heterogeneities present in shales and mudstones at different scales are available. An up-to-date review on mudstone diversity can be found in Aplin and Macquaker (2011).

Heterogeneities present in shales and mudstones have been investigated on different scales such as micrographs and thin sections (Potter et al., 1980; O'Brien and Slatt, 1990; Macquaker and Gawthorpe, 1993; Schieber, 1999; Rohl and Schmid-Rohl, 2005) and core slabs and images (e.g. Pe-Piper et al., 2005; Piper et al., 2010). Hereby, a range of sub-metre scale heterogeneities have been reported. Coarser grained material dispersed by storms and tides forms structures such as starved ripples (Macquaker and Bohacs, 2007; Schieber et al., 2007; Schieber and Southard, 2009) and intraclasts (Myrow, 1992; Schieber, 1994; Macquaker and Taylor, 1996; Macquaker et al., 2010a; Schieber et al., 2010). Clay-dominated ripples have been reported to form by flocculation (Schieber et al., 2007). Also, different forms of bioturbation (Droser and Bottjer, 1986), as well as coarser grained thin-beds as a result of turbiditic pollution of hemipelagites (e.g. Aplin and Macquaker, 2011) can be found. In addition, mass transport deposits, incorporate chaotic and brecciated mud-rich structures at different scales (e.g. Tripsanas et al., 2008). Finally, overpressure release can be associated with forming of sand injections through mud-rich sections with thicknesses ranging from few centimetres to hundreds of metres (Hurst et al., 2003, 2011).

According to these findings of shale and mudstone heterogeneity, classifications are available from many authors (for detailed reviews compare Potter et al., 1980; Collinson et al., 2006; Aplin and Macquaker, 2011). Thereby, two different approaches are usually taken: the first

approach addresses the sedimentological processes behind the forming of the heterogeneities. Usually studies based on process based classifications incorporate very detailed investigations on palaeontology, sequence stratigraphy and depositional environments (e.g. Piper et al., 2010), while the second approach is much more dedicated to the geometric shape of the heterogeneities and only marginally refers to sedimentological processes (e.g. Campbell, 1967; Reineck and Singh, 1973; Cole and Picard, 1975).

In both types of classifications, differentiation of respective scales is important, as classifications can address sub-millimetre-scale (e.g. Macquaker and Adams, 2003) to sub-metre scale (e.g. Schieber, 1999; Cole and Picard, 1975) heterogeneities. The classification of shale and mudstone heterogeneity on different scales goes hand in hand with different terminologies. In particular the term “texture” is usually used to indicate spatial alignment and elements on micrographs and thin-sections. In addition, “texture” can be also used to indicate grain size composition of the sediment (e.g. sandy texture, if the mud-rich sediment comprises a significant amount of sand grains). On larger scales the term "structure" is used to classify spatial heterogeneity. Both terms thus should not be mixed up as they refer to different scales of anisotropy. In this study we will investigate heterogeneities on the sub-metre scale and from a geometrical point of view only. We will therefore use the term “structure” only.

From a fluid flow point of view it might be argued, that the geometrical features play a more significant role, once the internal flow properties of the respective objects/structures are known, which has been shown in many studies on heterogeneous reservoir rocks (Pickup et al., 1995; Nordahl and Ringrose, 2008).

Geostatistical Studies

Geostatistical studies on heterogeneities in sediments usually address large scales and concern themselves with describing the heterogeneity of a whole depositional system or aquifer architecture on regional scale (e.g. Davis et al., 1993; Aggoun et al., 2006; Anderson, 1989; Klingbeil et al., 1999 and many others). Although heterogeneities from different scales and lithologies are mostly incorporated in these studies, the level of scale of considered heterogeneities usually exceeds the metre-scale. Sub-metre scale heterogeneities of mud-rich sections are only incorporated in very few cases in qualitative ways (e.g. Felletti, 2004). Other geostatistical studies incorporate or solely address sub-metre scale heterogeneities (1 mm – 1m), but deal with sandstone or carbonate reservoirs only (e.g. Pickup et al. 2000; Tilke et al., 2006; Huysmans et al., 2008; Huysmans and Dassargues, 2010). To the author's knowledge, this study is the first attempt to investigate and extract shale and mudstone heterogeneity from core and borehole images for further modelling using a quantitative approach.

Data Origin and Extent

The data used in this study originates from an off-shore gas field in the Western Nile Delta, Egypt. The sedimentation took place since the Messinian salinity crisis had subsided 5.3 Ma ago (Garfunkel, 1998, 2004). The deposition rate of the Pliocene and Pleistocene deltaic sediments was at an average rate of ~480 m/Ma (Vandré et al., 2007). On a regional scale, deposition can be seen as an analogue to a classic slope environment comprising channel and turbidite deposits, mud-rich units from widespread background sedimentation of hemipelagic fall-out as well as faulting and sliding (Mascle et al., 2001; Garziglia et al., 2008). The region has been target of gas exploration and exploitation in the past decade. A detailed study about gas migration and geochemistry in this area can be found in Boeker (2011).

The focus of this study is on visible heterogeneities on digital core images of four wells (B19, B20, B22 and B24) and borehole images of one additional well (B6). All wells are located at the delta front slope and transect sediments from the whole Piacenzian (first half of the Upper Pliocene). Water depth ranges from 339 m for well B20 to 646 m for well B19. The water depths of B6, B22 and B24 are 415 m, 580 m and 622.5 m, respectively. The data are of particular interest, as heterogeneities can be expected due to slope instabilities (Mascle et al., 2001; Garziglia et al., 2008), overpressure regimes as a result of the rapid sedimentation (Vandré et al., 2007) and eustatic cyclicity, which took place since the Upper Pliocene (Van der Zwaan and Gudjonsson, 1986).

Core images have been taken with a high resolution (< 0.3 mm/pixel) digital reflex camera and have been normalized to colour and light conditions with the help of an ink stripe. Borehole images were taken with a high resolution formation micro-imager (FMI; Safinya et al., 1991). The FMI measures electrical resistivity on four concentrically arranged flap and pad assemblies with 192 resistivity measuring buttons in total, yielding a technical resolution of 5 mm in vertical and horizontal direction and up to 50 µm by quantifying the current flow to the electrode (Schlumberger, 2004). The borehole coverage at 8 inch hole size is around 80%. FMI may be particularly useful in this study, due to potentially higher gas saturations in the coarser grained intervals (Boeker, 2011), emphasising lithological contrast.

In total, more than 425 m of usable core images and approximately 270 m of high resolution FMI output are available for interpretation (Figure 3.1), whereas the FMI output has already been pre-interpreted by the operator, which we used as guidance for our interpretation. From seismic interpretation (Georgiopoulou, 2009) we know, that all reservoirs, but the B22 reservoirs are channel fill reservoir rocks, vertically framed by hemipelagic sequences. The upper B22 core transects a levee reservoir, while the seismic facies of the lower B22 core is

unknown. The cored and imaged sections of these wells were especially suitable as they do not only cover the reservoir rocks (channels and levees), but also under- and overlying heterogeneous mud-rich hemipelagites (Figure 3.1). However, seismic facies can only be compared roughly to the image derived heterogeneity classes, as exact well-seismic depth correlations and well deviations have not been provided by the operator.

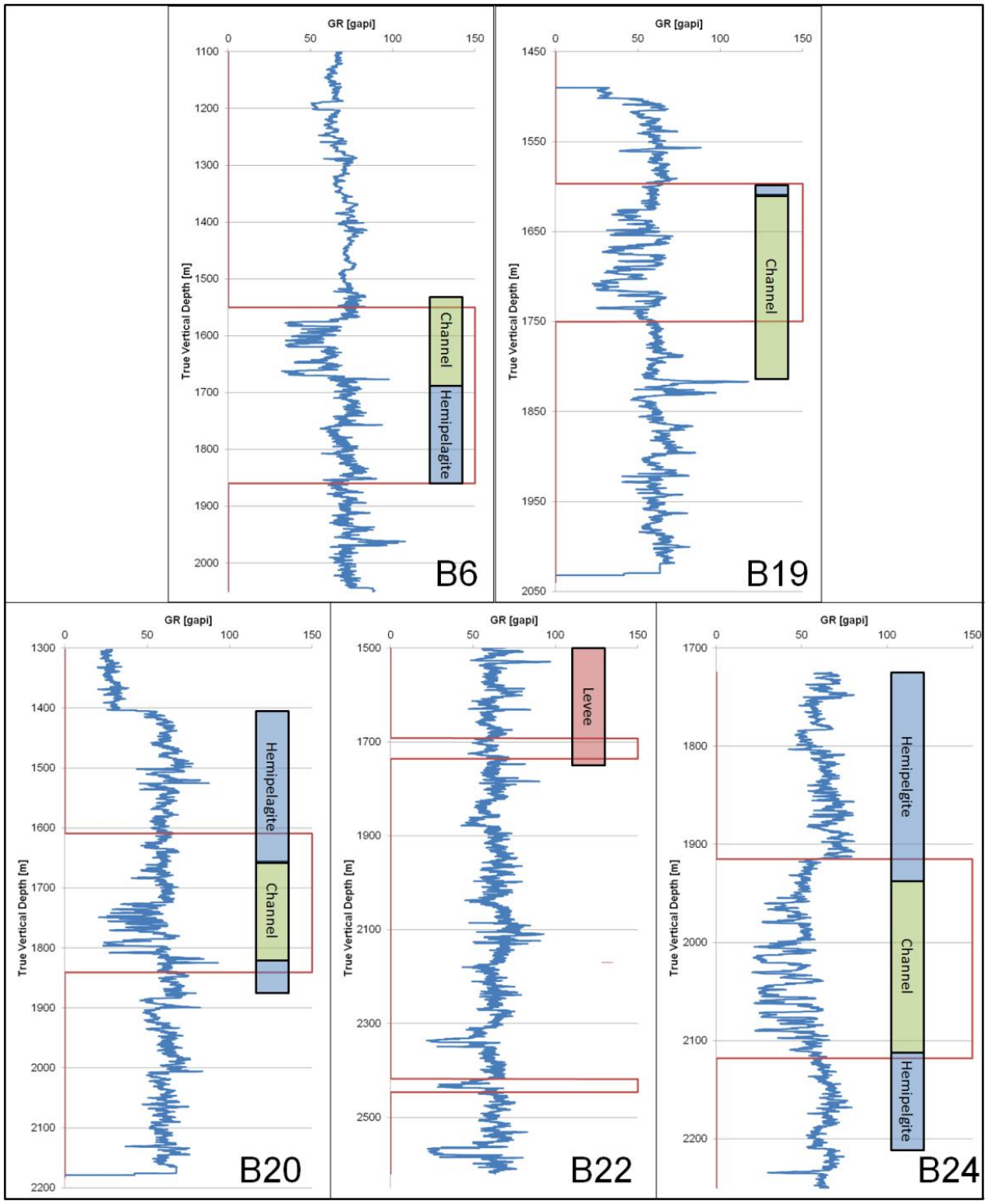

Figure 3.1: Gamma ray (blue lines) and cored/imaged sections (red lines) of the used wells of the Nile Delta case study. The colour bars indicate the approximate seismic facies association (blue: hemipelagite; red: levee; green: channel). The seismic facies of the lower cored section of well B22 is not known.

Methodology

The methodology splits up according to the two parts sedimentological interpretation and geostatistical analysis. Thereby, the geostatistical analyses will be applied to the results of the sedimentological interpretation. Hence, the geostatistical analysis will be used as a tool to quantify and enhance the sedimentological interpretation, which is focused on geometric properties of the observed heterogeneities. The main tool used for the geostatistical analysis is the semi-variogram or in short variogram, which has been proven to be a useful tool to describe sub-metre scale geological heterogeneity in previous papers (e.g., Jensen et al., 1996; McKinley et al., 2004). However, the quality of sampling and modelling of geological heterogeneity by utilisation of the semi-variogram is highly dependent on the size and scale of the sampling window (Jensen et al., 1996). It is therefore crucial to incorporate geological knowledge about the forming of the heterogeneities into sampling and modelling of geological heterogeneity (Jensen et al., 1996). In particular, where several scales of heterogeneity exist, the sampling and modelling should honour these scales (e.g. Kossack et al., 1990). To do so, sampling windows (intervals) have been derived from the sedimentological interpretation, which clearly separates different types of heterogeneity from each other.

It is another key point of the methodology, that geostatistical analysis is not used to correct the sedimentological interpretation, which we treat as superior to the geostatistical analysis. The geologist's eye is able to not only recognize features and their geometries, but also to combine them to a bigger picture - a crucial advantage, which automated geostatistical methods cannot deliver, yet. Instead, the goal of the geostatistical analysis is to enhance the sedimentological interpretation and to quantify differences within the individual interpreted structural classes. Moreover, we would like to test to what extent automated geostatistical analysis can recognize sedimentary structures present in shales and mudstones.

Finally, both sedimentary and geostatistical analyses are combined in detailed, manual geostatistical analysis (variogram modelling) to provide the geomodeller with a set of representative variogram models for modelling and simulating shale and mudstone heterogeneities.

Sedimentological Interpretation

The sedimentological interpretation is conducted in two steps. Prior to these steps a simple interpretation of core images, where we distinguish only between mud- ($\geq$ 50% mud) and non-mud-rich (< 50% mud) sections has been conducted. Thereby, we tested the reliability of

the lithological interpretation of core images. The minimum interpreted vertical interval size was set to 5 cm. In consequence, coarse grained material, which exceeds approximately 50% of image area over a vertical area of 5 cm is interpreted as non-mud section. To get an overview of the quality of interpretation, which is only based on the images, the resulting mud-non-mud profiles are compared with core gamma ray or conventional gamma ray profiles, where no core gamma ray has been measured (Figure 3.2). In general, the interpretation of mud-rich sections matches high gamma ray responses, confirming the rough reliability of the interpretation. Mismatches might result from dark coarse grained material (e.g. due to high organic content), core shifts, or averaging out of high frequency lithological contrasts due to limitation of the resolution of the gamma ray (core gamma ray: ~8-16 cm; conventional gamma ray: ~15 cm).

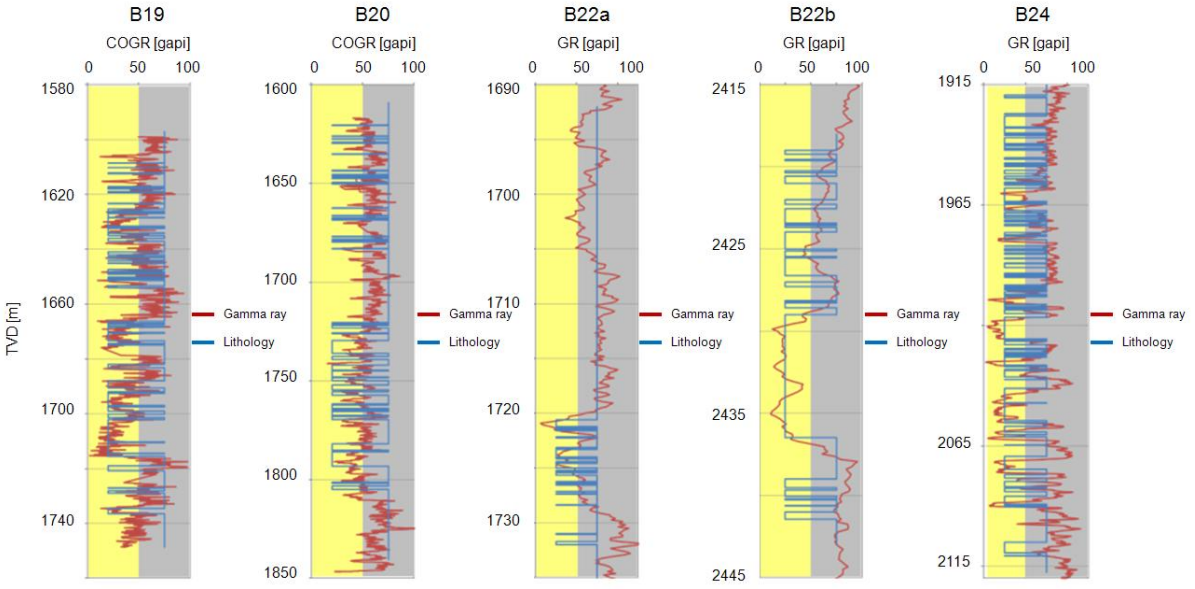

Figure 3.2: Sand-mud interpretation from core images (blue line; left-handed plotting = sand; right-handed plotting = mud) together with core gamma ray (red line; B19 and B20) or conventional gamma ray (red line; B22 and B24) to check the reliability of the core image interpretation. Preserved core sections have been assumed to be 50% of the preceding structure and 50% of the successive structure.

The first step of the actual sedimentological study was an interpretation of the mud-rich core images filtered out from the mud-non-mud profiles. The interpretation has been conducted on the basis of geometric properties only. We believe that such an abstraction is necessary to address the influence of spatial heterogeneity in mudstones on fluid flow. As bias in sedimentological interpretations can be high due to subjective decisions, we used a simplified version of Cole's and Picard's (1975) geometric classification scheme (Figure 3.3) to guide our interpretation. It is not the aim of this study to perform a full sedimentological study on shales and mudstones. Detailed descriptions and reconstructions of paleo-environments for

mud-rich slope settings can be found elsewhere (e.g. Pe-Piper et al., 2005; Piper et al., 2010 etc.). Table 3.1 compares the classification used in this study with the original classification scheme by Cole and Picard (1975).

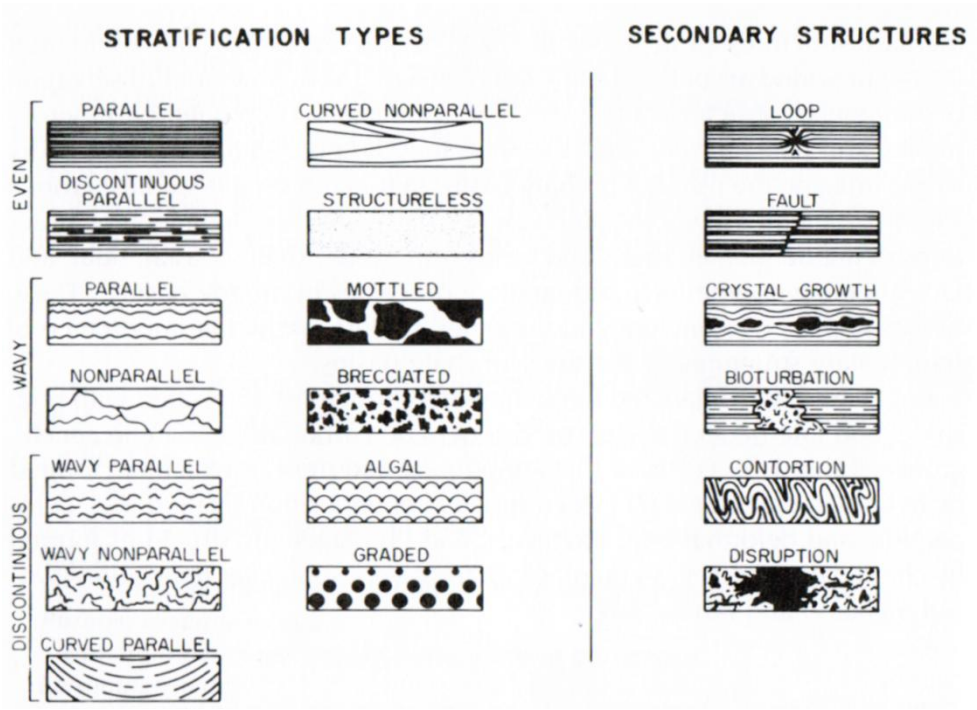

Figure 3.3: Geometric classification of shales and mudstones from Cole and Picard (1975; in: Potter et al., 1980, p. 24).

The second step is accomplished after interpretation of the core images. The observed heterogeneities from core are then assigned to the pre-interpreted FMI images from well B6 in order to re-interpret the FMI images, which have been pre-interpreted by the operator.

Table 3.1: Simplified classification scheme after Cole and Picard (1975). The unified classes used in this study are set in context to the more extensive classifications of Cole and Picard (1975).

Main classification	Homogeneous	Bedded	Chaotic	Clasts floating in a matrix
Cole and Picard (1975)	Structureless	Parallel, parallel wavy, parallel discontinuous	Curved nonparallel, mottled, nonparallel, contortion, discontinuous types	Brecciated, bioturbation, disruption

Geostatistical Analysis

The methodology for geostatistical analysis has been derived from many reviews (Marsily et al., 2005) and books (Chiles and Delfiner, 1999; Rivoirard, 1994; Armstrong, 1998; Deutsch, 2002; Wackernagel; 2003) on geostatistics to which we would like to refer for more detail on geostatistical analysis and modelling workflows. In this study, geostatistical analysis has been used to support the sedimentological interpretation of core images with a quantitative tool, namely the experimental variogram $\gamma(h)$ (Deutsch and Journel, 1998):

$$\gamma(h) = \frac{1}{N} \sum \left(z(h) - z(h+l) \right)^2 \qquad \text{Eq. 3.1}$$

Where *z(h)* is the value at position *h* and *z(h+l)* is the value at a position with distance *l* from *h*.

We calculated experimental variograms of heterogeneous core image sections in horizontal and vertical directions. We abstained from calculating experimental variograms in more directions for reasons of computing time, although heterogeneities with angularities around 45 degrees might not be covered by doing so. However, for the detailed manual fitting of the variograms (see below) a 45 degree experimental variogram was also calculated to capture not only horizontal and vertical heterogeneities. The quality of the images is crucial to keep error sources to a minimum. Typical core image quality limitations are scratches from slabbing, wetting stains, human hair and fissures due to core extraction. Based on these criteria a suite of high quality core images showing heterogeneous mudstones has to be selected. The resulting horizontal and vertical experimental variograms can be used in three different ways:

1. Exposure to **automated fitting** with a predefined covariance function to quantitatively obtain vertical and horizontal correlation lengths of observed heterogeneities along with other statistical moments such as the mean and variance of the image's RGB colour space.
2. **Semi-quantitative geostatistical interpretation** of horizontal vs vertical shapes of exponential variograms to identify different types of anisotropy.
3. **Manual fitting** with nested, angular covariance functions, which can be used for geomodelling of heterogeneities. Hereby, it is vital to include geological or sedimentological knowledge about the respective heterogeneities into the fitting process.

Automated fitting is useful to get a quantitative overview of the heterogeneities present in a large set of data, such as our core image data base. It has been employed previously to quantify heterogeneities in reservoir rocks from formation micro-images (e.g. Tilke et al., 2006). Hereby, not only the horizontal and vertical correlation lengths are calculated, but also general statistical moments such as the arithmetic mean and variance. However, the resulting correlation lengths and anisotropies only can be interpreted relative to each other, as the fits only roughly approximate the shape of the experimental variograms. Also, detailed information such as stationarity/instationarity, cyclicity, zonality etc. cannot be obtained (see below for more information about these terms). Thus, the results can deliver a rough idea of heterogeneity present in the system, but to draw more conclusions a more detailed analysis is required. Automated fitting requires a cost-criterion, which ensures the best fit is selected from an iterative process, where parameters of the fitting covariance function are changed successively. Here, we vary only one parameter, namely the range, which corresponds to the correlation length of the measured heterogeneity. We chose the exponential covariance function as we found most experimental variograms of this study to be best approximated by this function:

$$\gamma'(h) = C\left[1 - \exp\left(-\left(\frac{\delta h}{a}\right)^2\right)\right] \qquad \text{Eq. 3.2}$$

$$\delta = 2.996$$

Where C is the covariance, exp the exponential operator, h the position and a the range. δ is a correction factor. The range a is varied from 0 to the number of image pixels in vertical or horizontal direction, while C is kept constant at 1, which is acceptable as we transform the RGB-space of the respective image to a normal distribution with mean = 0 and variance = 1 prior to the calculation of the experimental variograms. To do so, the RGB-values, where unified to a single value $\overline{RGB}$ by taking the average of R (red), G (green) and B (blue). To find the best fit we use the cost criterion from Zhang et al. (1995), which is

$$J(r) = \sum_{i=1}^{k} \frac{N_{h(i)}}{h(i)} \left[\gamma(h(i)) - \gamma'(h(i)); a\right]^2 \qquad \text{Eq. 3.3}$$

Where $N_{h(i)}$ is the number of observation pairs present at the positions *h(i) (i = 1, ... , k)*, *γ(h(i))* is the experimental semi-variogram, *γ'(h(i))* is the value obtained by the fitted exponential covariance function with a range or correlation length *a (a = 0, 1,..., i_dim)*. *i_dim* is the image dimension in pixels in horizontal or vertical direction, respectively.

Semi-quantitative geostatistical interpretation is performed by visual analysis of the anisotropy behaviour of the vertical and horizontal variograms to each other. Grouping by anisotropy has the advantage of adding additional value to the sedimentological interpretation, even allowing distinguishing between subgroups for each class of heterogeneity on the basis of a semi-quantitative measure of anisotropy.
Basically, five different types of anisotropy behaviour (Figure 3.4) are possible (e.g. Armstrong, 1998):

1. Isotropic variograms, where the horizontal and vertical experimental variograms show similar correlation lengths (range) and maxima of variance (sill). Isotropic variograms can be for example expected from isotropic structures such as homogeneous or very chaotic rocks without preferred orientation or alignment.
2. Zonal anisotropic variograms in horizontal direction, where the horizontal sill is significantly lower than the vertical sill. Very continuous beds and laminas are a possible source of horizontal zonal anisotropy.
3. Geometrical anisotropic variograms in horizontal direction, where the horizontal range exceeds by far the vertical range, whereas the sill is the same for horizontal and vertical experimental variograms. Geometric anisotropy can be triggered for example by discontinuous horizontal structures, such as ripples and flaser bedding.
4. Zonal anisotropic variograms in vertical direction (vertical sill significantly smaller than horizontal sill). Vertical zonal anisotropy might be rather unusual, but could be observed, where extensive vertical sand injections or burrows are present.
5. Geometrical anisotropic variograms in vertical direction (vertical range greater than horizontal range with equal sills). Smaller vertical burrows or injectites could induce geometric anisotropy in vertical direction.

Similar to the automated fitting approach, semi-quantitative interpretation of the experimental variograms for different types of anisotropy gives only a rough, but semi-quantitative estimate of the heterogeneity in the studied sediment. Also, a degree of uncertainty is always involved due to subjective decision making; especially, where anisotropy types cannot be clearly

distinguished from each other (e.g. weak geometric anisotropy vs. isotropy). However, the method can help to identify additional differences between individual structural classes and thus to enhance the sedimentological interpretation.

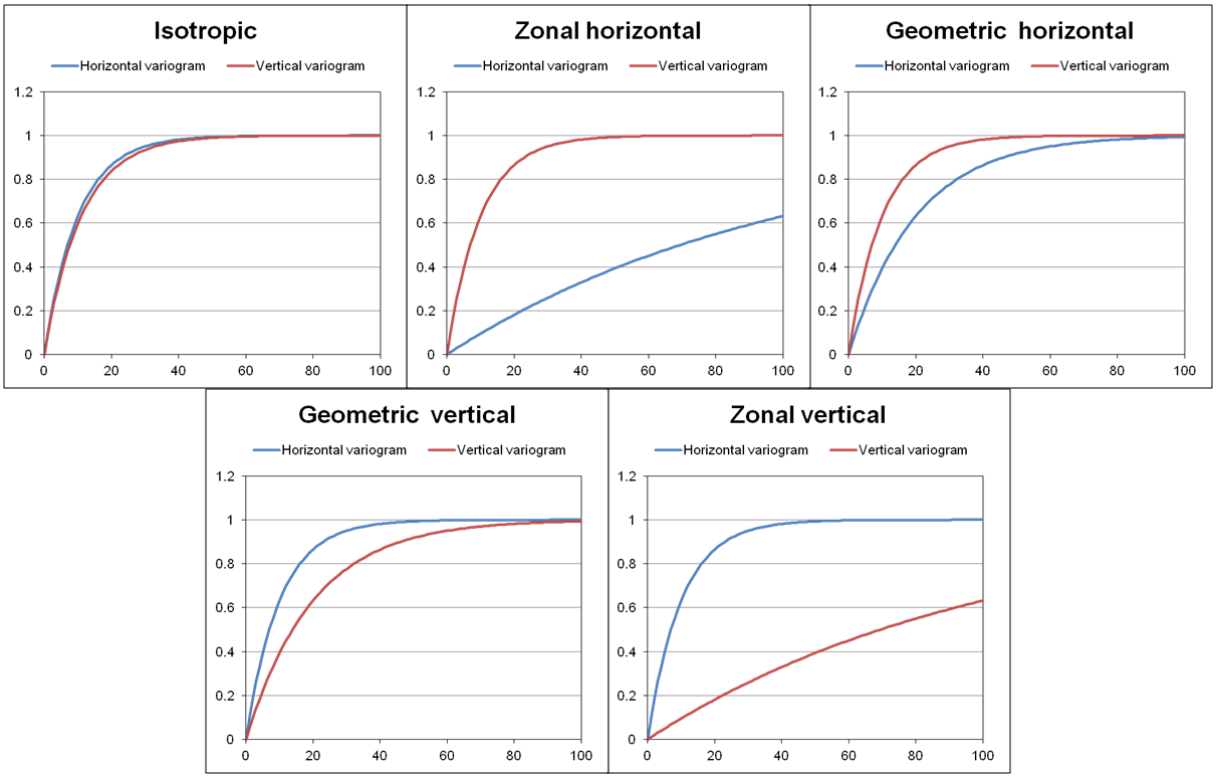

Figure 3.4: Anisotropy types from directional variograms. The parameters of interest are the variance (sill) reflected on the vertical axis and the correlation length (range) depicted on the horizontal axis.

To investigate the influence of the interval size upon the automated fitting procedure and semi-quantitative analysis, we applied these two methods not only to the original intervals, which resulted from the sedimentological interpretation and can be seen as the maximum available intervals (max intervals), but also to fixed intervals of 10 cm and 20 cm, respectively. The fixed intervals have been extracted from the original suite of images selected for the geostatistical analyses.

Manual fitting of experimental variograms derived from geological heterogeneity should always be conducted with having the related geological process, meaning and reasoning in mind (e.g. Jensen et al., 1996; Marsily et al., 2005). It is thus important to not only fit the experimental variogram in a best mathematical way, but also to calibrate the fitting with geological reasoning and experience according to the heterogeneity of interest.

Thereby, a few basic principles can help the geomodeller to sufficiently model spatial heterogeneity (e.g. Chiles and Delfiner, 1999):

1. Awareness of the scale of the heterogeneity
2. Understanding of the anisotropy of the heterogeneity
3. Knowledge about present cyclicity and/or instationarity (e.g. a general trend of upward fining, would cause local instationarity)
4. Addressing spatially random features such as mottling, distribution of pebbles/grains

The scales of heterogeneities range from sub-centimetre scale to several decimetres, and can be addressed using nested covariance functions, each representing a different scale. Anisotropy is handled (as already introduced above) by employing different ranges for the covariance functions. In order to account for inclined features, we also calculated a third experimental variogram in direction of 45 degrees. Also, different angularities can be applied to each nested covariance function. In this way, the variation of the range caused by non-ideally orientated experimental variograms can be taken into account. Zonality can be dealt with by applying a very high range to a horizontal or vertical covariance function of a nested heterogeneity. Different types of covariance functions are available. Hereby, the cardinal sine covariance function is in particular useful to approximate cyclicity (e.g. caused by periodic lamination), whereas the linear covariance function can near instationarity. The latter can also be addressed by the same technique used when modelling zonality in combination with an asymptotic covariance function (exponential, Gaussian or cubic), which is the method used in this study. Random features are usually modelled by adding the so called nugget effect, a covariance function with zero range, which mimics a pure random process. Finally, the following covariance functions have been used for variogram fitting (Geovariances, 2010):

Spherical (sph):

$$\gamma'(h) = C\left[\frac{3}{2}\left(\frac{\delta h}{a}\right) - \frac{1}{2}\left(\frac{\delta h}{a}\right)^3\right] \qquad (h < a)$$

$$\gamma'(h) = C \qquad (h \geq a) \qquad \text{Eq. 3.4}$$

$$\delta = 1$$

Exponential (exp):

$$\gamma'(h) = C\left[1 - \exp\left(\frac{-\delta h}{a}\right)\right] \qquad \text{Eq. 3.5}$$

$$\delta = 1.731$$

Gaussian (gau):

$$\gamma'(h) = C\left[1 - \exp\left(-\left(\frac{\delta h}{a}\right)^2\right)\right] \quad \text{Eq. 3.6}$$

$\delta = 2.996$

Cubic (cub):

$$\gamma'(h) = C\left[7\left(\frac{\delta h}{a}\right)^2 - \frac{35}{4}\left(\frac{\delta h}{a}\right)^3 + \frac{7}{2}\left(\frac{\delta h}{a}\right)^5 - \frac{3}{4}\left(\frac{\delta h}{a}\right)^7\right] \quad \text{Eq. 3.7}$$

$\delta = 1$

Cardinal Sine (sin):

$$\gamma'(h) = C\left[\frac{\sin\left(\frac{\delta h}{a}\right)}{\frac{\delta h}{a}}\right] \quad \text{Eq. 3.8}$$

$\delta = 20.371$

Nugget effect (nug):

$$\gamma'(h) = C \quad \text{Eq. 3.9}$$

Where $\gamma'(h)$ is the variogram model at position h with range a, C is the covariance and exp and sin are the exponential and sinus mathematical operators, respectively. δ is a correction factor.

Results

Core images interpreted as mud-rich exceed by far sand-rich images independent of seismic facies memberships (Figure 3.5, left). Channel fill is the most abundant seismic facies covered by core images, followed by hemipelagite and levee facies.

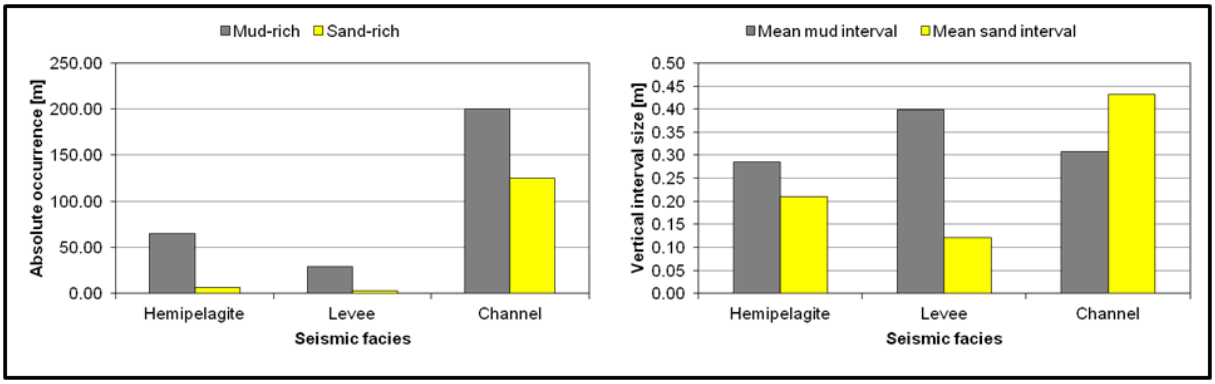

Figure 3.5: Bar charts comparing core images interpreted as either mud- or sand-rich (left) along with respective mean interval sizes (right) as a function of roughly attributed seismic facies.

The low mean thicknesses of mud- (~30-40 cm) and sand-rich (~10-45 cm) core image intervals indicate high heterogeneity in all seismic facies (Figure 3.5, right). However it should be kept in mind, that this result might be biased by preserved core sections, which artificially split up the intervals. While interval size of mud-rich core images shows only little variation with respect to seismic facies, for sand-rich core images the interval thickness is largest in channels and lowest in levee seismic facies. Also, a swap of the ratio between mud-rich and sand-rich intervals can be observed from hemipelagites and levees to channel seismic facies (Figure 3.5, right).

The mud-sand interpretation of the FMI data from well B6 shows slightly different results (Figure 3.6). The mud-rich image sections exceed the sand-rich sections in hemipelagites and channels (levee seismic facies are not covered by the FMI data), which is similar to the results from core images (Figure 3.6, left). However, differences are obvious in the ratio of sand-rich to mud-rich interval thicknesses, where mud-rich sections not only dominate in the hemipelagic seismic facies, but also in the channel seismic facies (Figure 3.6, right).

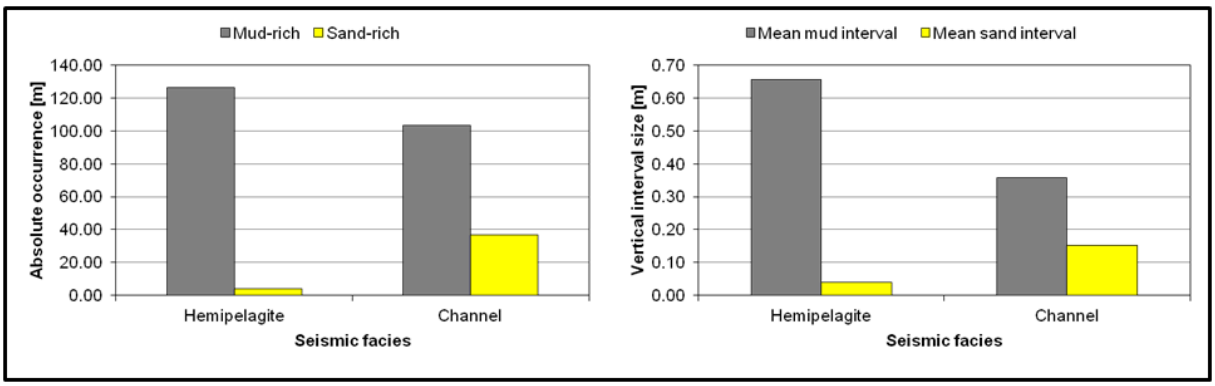

Figure 3.6: Bar charts comparing FMI sections interpreted as either mud- or sand-rich (left) along with respective mean interval sizes (right) as a function of roughly attributed seismic facies.

The observed heterogeneities fill the whole spectra of the simplified classification scheme after Cole and Picard (1975). Even more, the simplified classification scheme is not sufficient to cover the different types of observed heterogeneities. Therefore, the classification has been extended by sub-classes, which honour the observed heterogeneities (Table 3.2). We want to make a clear point that our classifications should not be considered as a new classification rather than an abstraction to pure geometric features according to existing classifications such as of Cole and Picard (1975), but tailored to the observed heterogeneities of this case study.
In the following we will present all heterogeneity classes in detail and relate the results to the geostatistical analyses afterwards, which yielded further sub-groups, based on the semi-quantitative analysis for anisotropy types (also see Figure 3.7, Figure 3.8 and Figure 3.9). The fraction of heterogeneous mud-rich core in relation to all mud-rich core is around 70% in hemipelagites, 63% in levees and 62% in channel seismic facies. The FMI interpretation shows even higher fractions of heterogeneous mud-rich core (94% in hemipelagic and 88% in channel seismic facies).

Homogeneous Mudstones

Homogeneous mud-rich images usually show no contrast on core images, but might contain unsupported grains and small pebbles, floating in a mud-rich matrix (Figure 3.7). On FMI, structureless mudstones only can be distinguished by resistivity magnitude, which is generally low, and the help of other measurements (caliper, gamma ray), as side wall holes can produce high, randomly distributed contrasts. Generally, deep water, calm sedimentation environments are a likely cause for structureless mudstones. However, other sedimentation processes, such as muddy debris flows or even low energy bottom currents (Schieber et al., 2007; Macquaker and Bohacs, 2007) are possible. In our case study structureless mudstones occur with almost equal probability in all covered seismic facies (Figure 3.11). Homogeneous mudstones have not been included in geostatistical analyses, as this part of the study has been reserved for heterogeneous mudstones only.

Bedded

Bedded structures mainly appear in two different forms. The first appearance is in the shape of parallel continuous beds and laminae, with sharp contact on the bottom of coarser grained laminae/beds and occasional upward fining or mottles (Figure 3.7). The spacing of the coarser grained parallel structures in the mud-rich matrix can vary from a few millimetres to several centimetres (Figure 3.7). In a general sense, the origin could be attributed to a rather calm

depositional environment with cyclic influx of coarser grained material, probably in a high-stand phase of the sea level.

The second observed parallel subtype incorporates lenticular- or flaser-shaped, continuous or discontinuous beds/laminae and ripples, with sharp or mottled boundaries (Figure 3.7). Bottom currents and/or tidal influence could be likely depositional processes related to these structures, which might represent a transition from high to low stands of the sea level. Bedded structures mostly occur in hemipelagites, but a significant fraction also can be assigned to channel structures and a minor fraction to levee seismic facies (Figure 3.11). From a fluid flow point of view, bedded structures might serve as horizontal conduits, whereas the risk for vertical flow can be expected to be close to a minimum for continuous beds and laminae. However, an increased chance of vertical flow should be attributed to lenticular, wavy beds and laminae, as the chance for vertical connectivity is increased.

Table 3.2: Extended classification for mudstone structures, tailored to this case study. The related sedimentological processes are kept as generic as possible.

Main structure class	Sub structure class	Geological features	Example related depositional process
Homogeneous	Homogeneous	Structureless, no contrast, might contain unsupported, floating grains	Deep sea; calm environment; muddy debris flows
Bedded	Laminated	Continuous, parallel laminas or beds, no interfering between individual layers	Deap sea, calm environment, but annual influx of coarser sediments
	Lenticular	Lenticalur, flasered, rippled, continuous or discontinuous beds or laminas	Shelf; bottom currents or wave base induced
Chaotic	Minor Slumped	Minor slumped, slurred or diffuse laminas or beds	Slope; initial state of gravity induced mass movement; dewatering due to overpressure; deformation
	Major Slumped	Major slumped, slurred or deformed chaotic features	Slope; gravity induced mass movement; deformation
Clasts	Small Clasts	Small (<3cm) clasts, burrows, or injections in a matrix	Slope bottom; shelf; debris flows; bioturbation; or sand injections
	Large Clasts	Large (>3cm) clasts, burrows, or injections in a matrix	Slope bottom; debris flows

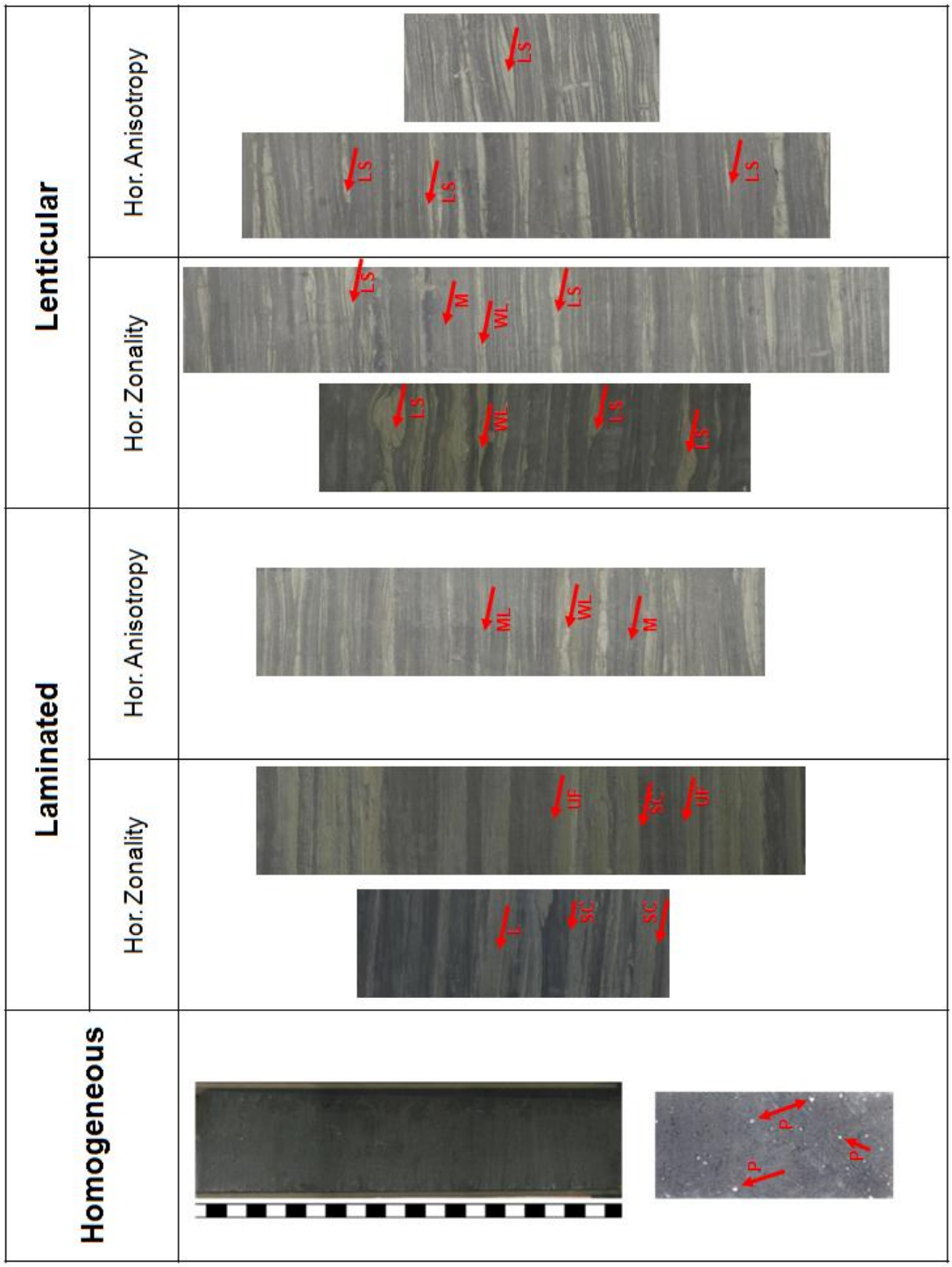

Figure 3.7: Examples of homogeneous and heterogeneous mudstones grouped for variogram types derived from geostatistical analysis. The images (except homogeneous mudstones) have been also subject to detailed geostatistical analysis. Homogeneous mudstones (left): completely structureless mudstones (top) or with grains and small pebbles (P) floating in a muddy matrix (below). Laminated mudstones (centre) can show very continuous beds and laminae (L) with sharp contacts on bottom of the coarser lamina (SC) and/or upward fining (UF). This is reflected in a horizontal zonality in geostatistical terms. A weaker but still pronounced horizontal anisotropy, induced by wavy continuous laminae (WL) and occasional mottles (M) and mottled laminae (ML) is also classified as laminated mudstone. Lenticular heterogeneities are also distinguished into either horizontal zonality with sharp lenses (LS) of coarser material and through going sharp wavy laminae (WL) and/or occasional mottles (M) or horizontal anisotropic variogram types omitting through going laminae.

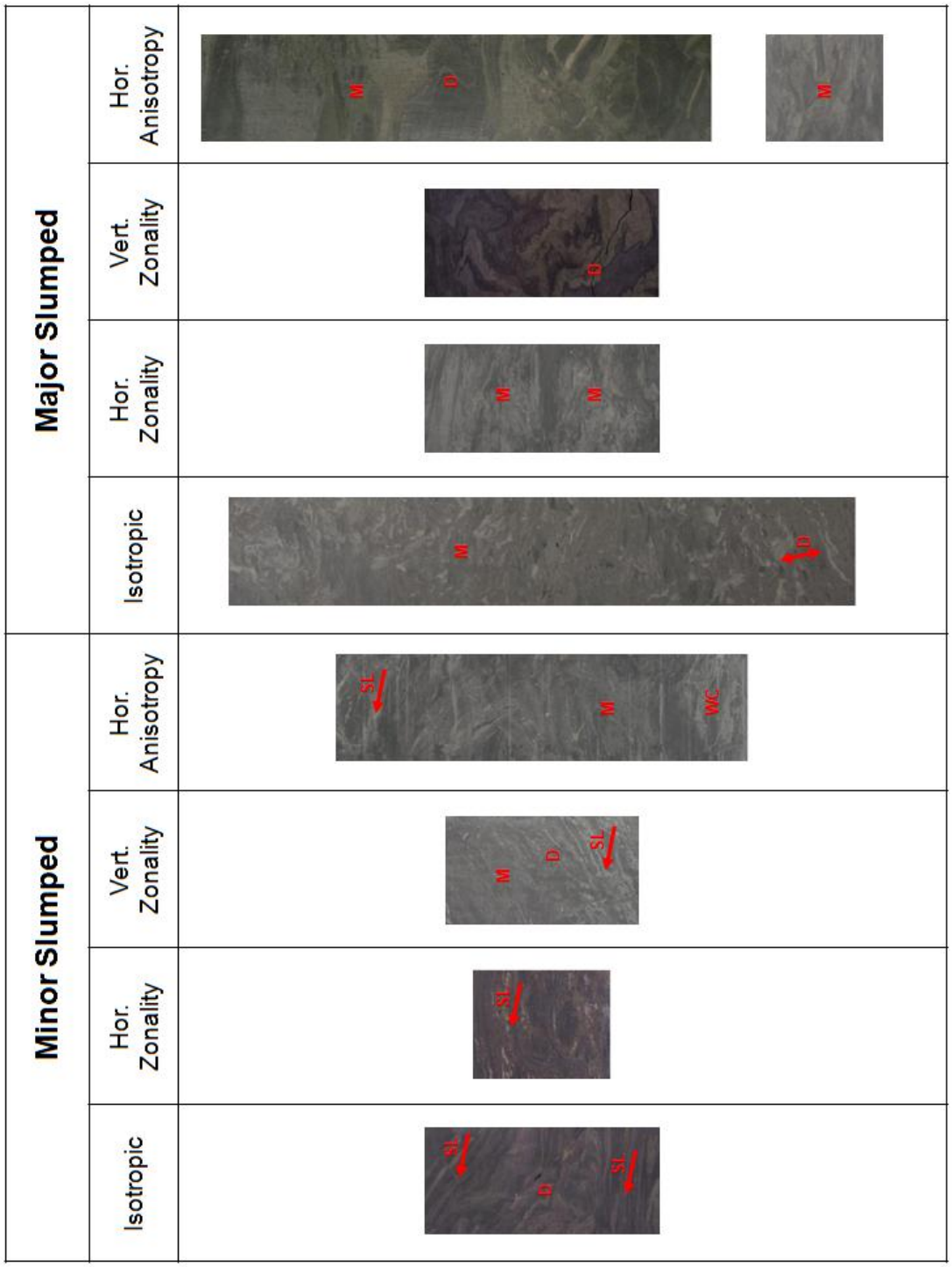

Figure 3.8: Examples of chaotic mudstones grouped for variogram types derived from geostatistical analysis. Minor slumped structures are present with different mean directions yielding four different anisotropy types. Usually they comprise structures, which can be still back related to its primary origin such as burrows or laminae (SL). Mottled (M) and distorted (D) features are also observed. However, the transition to major slumped structures and also to some types of small and large clasts bearing mudstones is floating and a sharp transition cannot be set. In general, major slumped mudstones are bare of any preferred direction or original structure, with an increased mottled and distorted appearance (M, D).

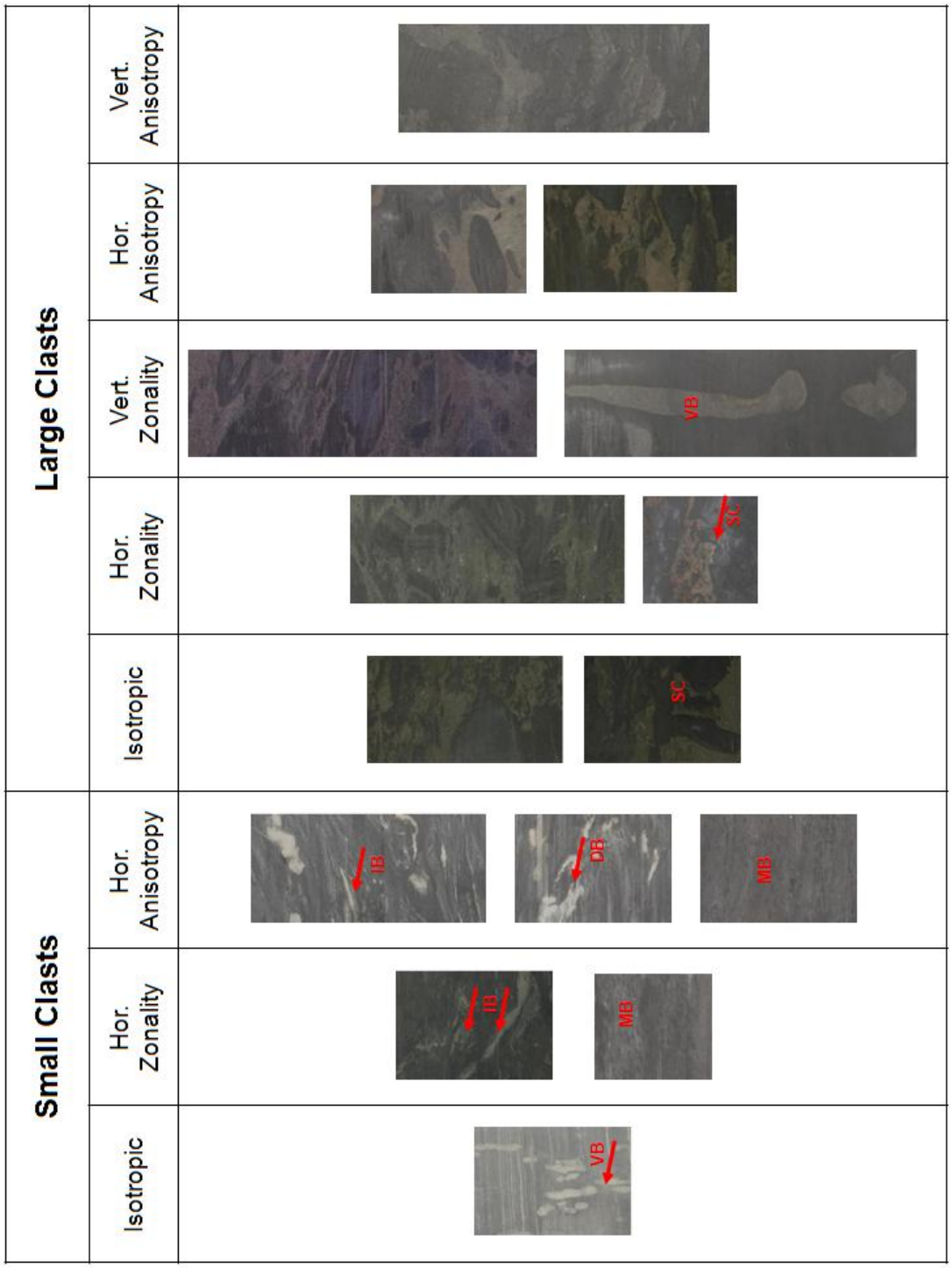

Figure 3.9: Examples of clasts bearing mudstones grouped for variogram types derived from geostatistical analysis. Small and large elongated or isotropic burrows in several orientations and alignments (VB, IB, DB) can be observed in small and large clasts bearing mudstones. Unique to small clasts bearing mudstones are small mud filled burrows, giving a mottled appearance (MB). The majority of large clasts bearing mudstones comprise of heavily disrupted or brecciated material with sharp contacts (SC) between coarser and finer clasts. Differentiation of the latter structures to slumped muds is difficult and sometimes purely subjective.

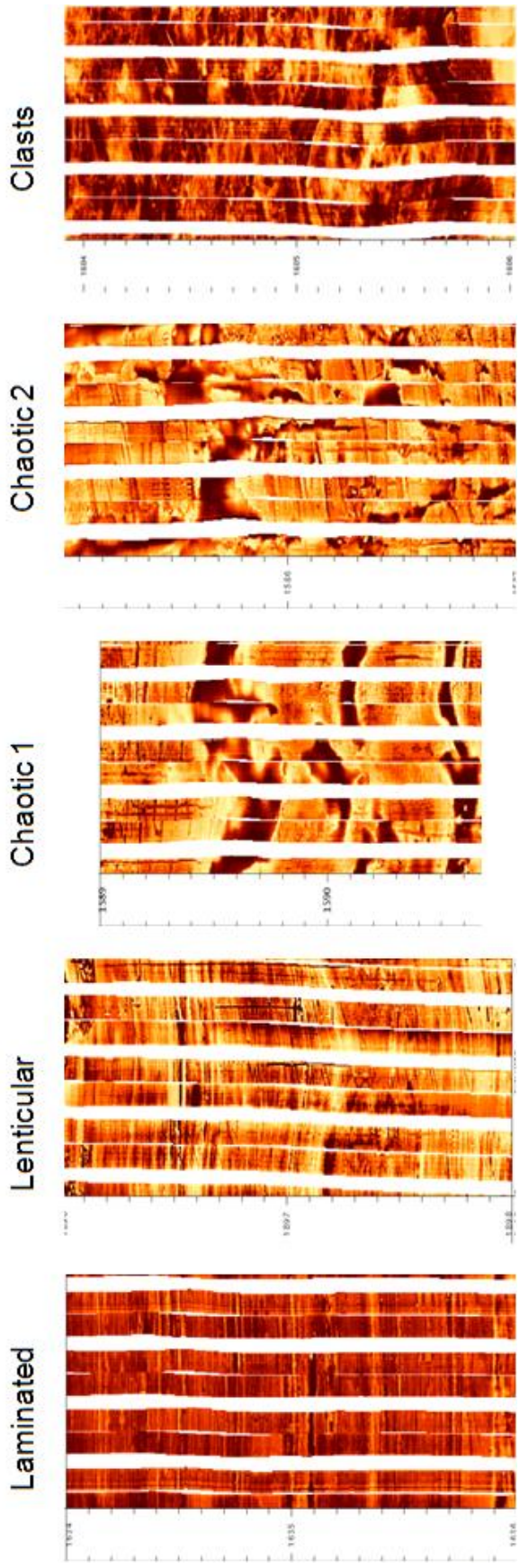

Figure 3.10: Examples from FMI for the heterogeneous structural classes Laminated, Lenticular, Chaotic and Clasts. The vertical extent of the images equals 2 m. Differentiation between different chaotic structures and different clasts was generally not possible on FMI. However, an example of chaotic mudstones with preserved original alignment could be found (Chaotic 1).

Chaotic Mudstones

The interpretation of core images resulted in two different types of chaotic structures - minor and major slumps (Figure 3.8). Minor slumps mainly contain features, whose origin can still be identified (e.g. laminae, burrows, etc.). Major slumps display chaos to a degree, where the original structure is not longer observable. Both types incorporate distorted and mottled features. The transition between both chaotic types is diffuse. Borderline decisions are hence common and cause uncertainty. Also, a clear differentiation from the structure class "clasts floating in a matrix" is sometimes difficult, as dimensions of very large clasts might exceed the image dimension, pretending a chaotic mixing from slumps and vice versa (see next section). Several sedimentological processes can be related to chaotic structures, ranging from soft sediment deformation and load casts to gravity induced mass movement and dewatering due to overpressure. Slightly instable slope systems or overpressured sediment packages could be possible depositional environments. In our case study chaotic structures are rare on core and even absent in levee seismic facies, but very common in hemipelagites and channels according to the FMI data of well B6 (Figure 3.11). Chaotic structures generate high uncertainties, when viewed from a fluid flow point of view. The chaotic alignment along with grain-scale mixing of finer and coarser material can produce preferred pathways for fluids and significantly reduce capillary entry pressures.

Clasts Floating in a Matrix

Different sizes of clasts made it necessary to distinguish between small clasts (< 3cm) and large clasts (> 3 cm). Hereby, clasts can be brecciated fragments from debris flows, burrows and shells, or injections of coarser material into a finer matrix caused by pressure release. Hence, almost the whole range of along-slope depositional environments must be considered for this structural class. However, in relation to the seismic facies assigned to the interpreted core and FMI data clasts bearing structures show the lowest occurrence (Figure 3.11). Large clasts are completely absent in hemipelagites, for example. From a fluid flow point of view clasts cause the highest threat and uncertainty, as vertical structures such as large burrows or sand injections can provide high permeability pathways through a mud-rich system (Hurst et al., 2011).

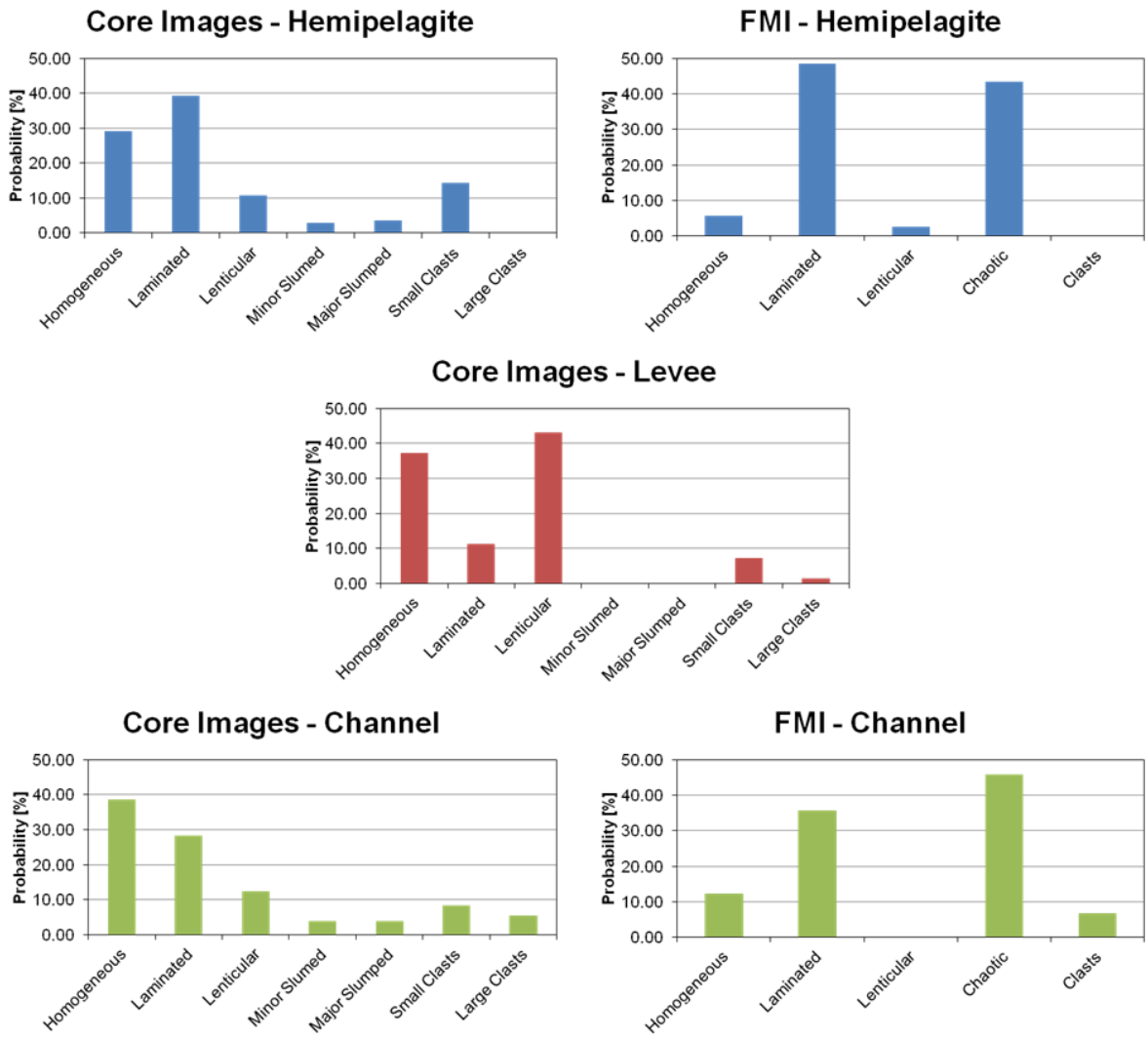

Figure 3.11: Probabilities in percentage to occur in covered seismic facies for each structural sub-class defined from core and borehole (FMI) images. The structural main classes chaotic and clasts have not been sub-divided on FMI.

Geostatistical Analyses

The automated geostatistical analysis resulted in a clear anisotropy difference between bedded structures and all other structures for all three runs (Figure 3.12). Table 3.3 summarizes the main differences of geometric image properties of the individual structural groups. Hereby, bedded structures show the highest anisotropy (horizontal range/vertical range). In addition, homogeneous mudstones show the lowest $\overline{RGB}$ standard deviation, while clasts and lenticular bedding depict the highest standard deviation of $\overline{RGB}$ values. However, mean $\overline{RGB}$ values remain almost constant for all structural groups. The vertical range differs for each structure for the respective interval sizes. Homogeneous mudstones always show the strongest

correlation length in the vertical direction, whereas minor slumped structures always show the weakest vertical correlation.

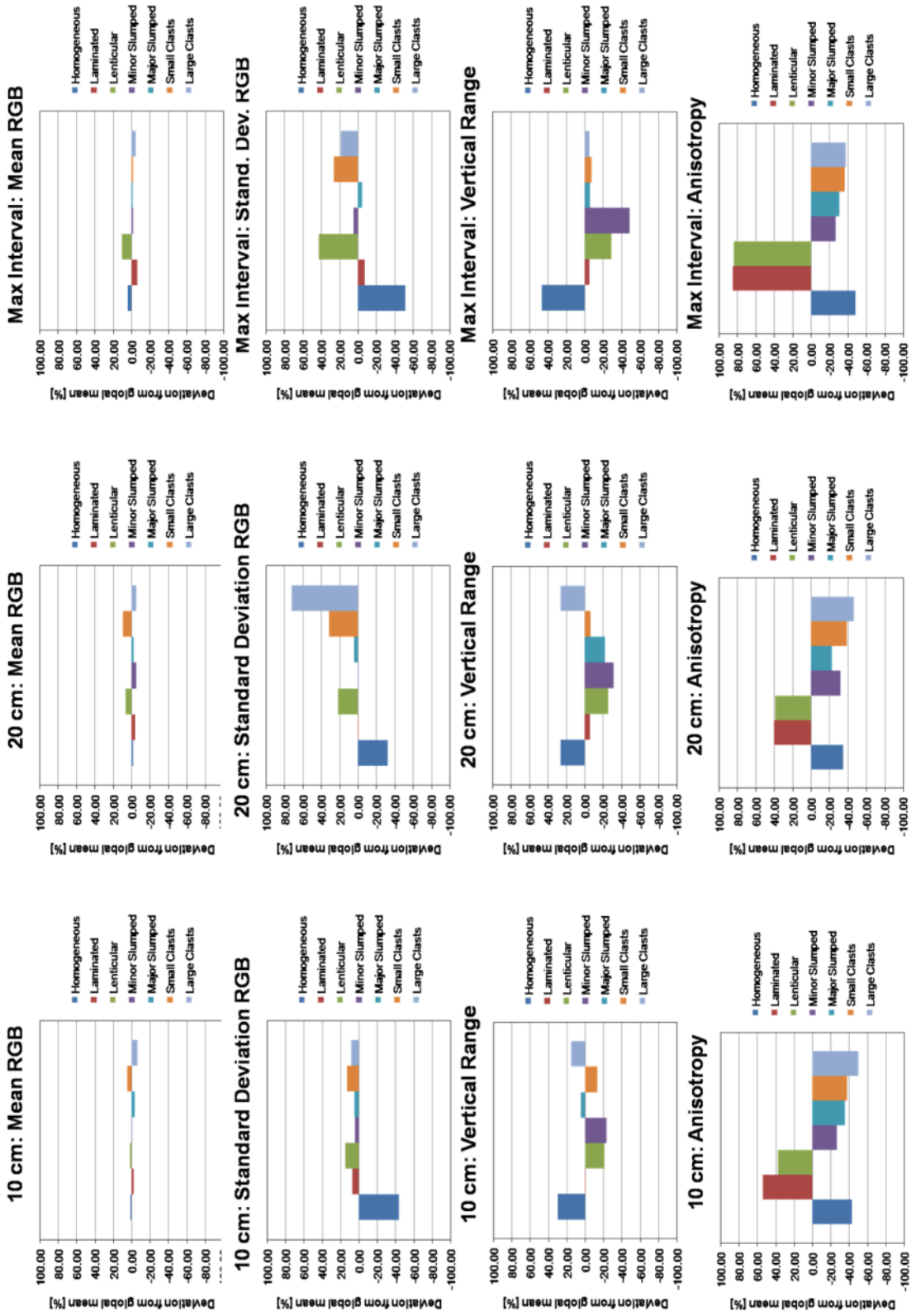

Figure 3.12: Deviations from global mean for each of the relevant results from the quantitative geostatistical analysis. The vertical interval size varies from left to right. The colours represent the respective structural classes.

Compared to the other structures, the vertical correlation length of large clasts varies most with interval size. Apart from vertical ranges or correlation lengths, the interval size only has a small effect on the results; only a weak increase of deviations from the global mean can be observed with increasing interval size.

Table 3.3: Table summarizing the most important results of the quantitative geostatistical analysis with qualitative classes (Low, Medium, High).

Structural Group	StDev RGB	Vertical Range	Anisotropy
Homogeneous	Low	High	Low
Bedded	Medium	Low-Medium	High
Chaotic	Medium	Low-Medium	Low
Clasts	High	Medium-High	Low

The semi-quantitative interpretation of the variographic data for specific variogram anisotropy types only yielded clear results for bedded structures (Figure 3.13): 100% of the variograms recorded a horizontal zonal or geometrical anisotropy, which is expected as horizontal correlation lengths of bedded structures should exceed vertical correlation lengths. The remaining structure classes comprise all variogram groups except vertical geometrical anisotropic variograms, which are only recorded in homogeneous and small clasts structures. This reflects the high variability of structures even if the heterogeneities have been already pre-classified into several groups (seven in or study). The results do not show significant differences for different image sizes. However a shift from horizontal zonal to horizontal geometric anisotropy with increasing interval size can be observed for bedded structures. This phenomenon is directly related to the interval size, as with increasing vertical interval size the vertical correlation length might also increase in some cases, yielding a less pronounced anisotropy.

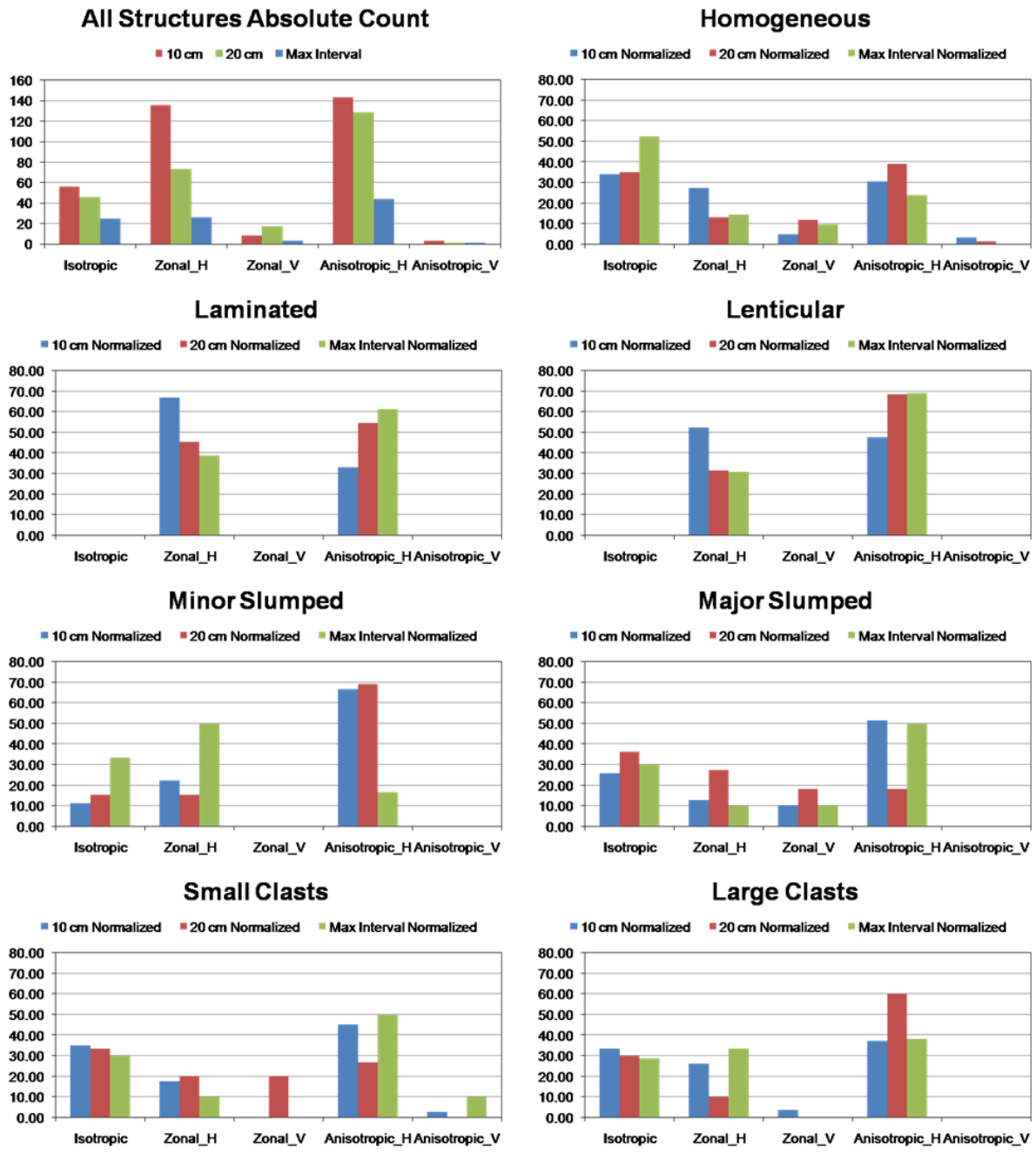

Figure 3.13: Normalized distributions of variogram types (isotropic, Zonal_H = horizontal zonal anisotropy, Zonal_V = vertical zonal anisotropy, Anisotropic_H = horizontal geometric anisotropy, Anisotropic_V = vertical geometric anisotropy) for each structural class. The vertical axis represents the probability of occurrence in percent. The top left histogram shows the absolute count (vertical axis) distribution of variogram types for all structural classes.

On the basis of the semi-quantitative geostatistical analysis for anisotropy behaviour, further subdivisions of the structural classes have been conducted (Figure 3.7, Figure 3.8 and Figure 3.9). For each of the resulting 20 structural classes derived from core images up to three images have been selected for manual fitting of the experimental variogram. In addition, a qualitatively selected set of heterogeneous images has been extracted from FMI data. Hereby, we kept the original interval sizes derived from the sedimentological interpretation (max interval), for both core images and FMI data (one image for each of the structural classes laminated, lenticular and clasts, whereas two images were selected for the class chaotic - the first one more similar to minor slumps, the second one more similar to major slumps). The selected images coincide with the images shown on Figure 3.7, Figure 3.8, Figure 3.9 and Figure 3.10.

The interval thicknesses of the selected core images and FMI sections for detailed variography range from 0.09 m to 0.52 m and 1.7 to 2.0 m, respectively. Table 3.4 summarizes the resulting variogram models along with origin (well, depth and data type), interval thickness and variogram anisotropy type. We used different covariance functions to best fit the experimental variograms in horizontal, vertical and diagonal (45 degrees) directions. In order to capture different scales of heterogeneities nested covariance functions have been modeled in most cases. Except of one example for small clasts, all examples comprise at least of two nested variograms. As most of the images of the selected structural classes do not show much inclination, angularity only had to be included in four cases. Zonality has been approximated with artificially high ranges of one nested structure in the direction of zonality.

Table 3.4: Data base table showing the parameters resulting from the detailed qualitative geostatistical analysis. The table comprises well origin, image type, interval size, structural class, variogram type (isotropic, Hor. Zonality = horizontal zonal anisotropy, Hor. Anisotropy = horizontal geometric anisotropy, Vert. Zonality = vertical zonal anisotropy, Vert. Anisotropy = vertical geometric anisotropy) and geostatistical parameters, which can serve as input for geostatistical simulation in geo-modelling.

Well	Image Type	Top [m]	Bottom [m]	Interval [m]	Structure	Variogram Type	Mod1	Rh1 [cm]	Rv1 [cm]	S1	Ang1	Mod2	Rh2 [cm]	Rv2 [cm]	S2	Ang2	Mod3	Rh3 [cm]	Rv3 [cm]	S3	Ang3
B24	Core	1935.23	1935.46	0.23	Laminated	Hor. Zonality	exp	2.02	0.29	0.40	90.00	sin	115.20	5.76	0.50	90.00	None	None	None	None	None
B24	Core	1986.03	1986.44	0.40	Laminated	Hor. Zonality	exp	0.86	0.14	0.14	90.00	exp	86.40	2.88	0.50	90.00	sin	288.00	23.04	0.36	90.00
B22	Core	1722.29	1722.67	0.37	Laminated	Hor. Anisotropy	exp	1.15	0.14	0.40	90.00	sin	37.44	5.76	0.50	90.00	None	None	None	None	None
B22	Core	1719.18	1719.69	0.52	Lenticular	Hor. Zonality	exp	0.58	0.03	0.25	90.00	exp	11.52	8.64	0.35	90.00	sin	288.00	2.88	0.40	90.00
B24	Core	1991.16	1991.48	0.32	Lenticular	Hor. Zonality	exp	4.32	1.44	0.70	90.00	sin	288.00	4.32	0.30	90.00	None	None	None	None	None
B22	Core	1712.04	1712.23	0.19	Lenticular	Hor. Anisotropy	exp	2.16	0.29	0.96	90.00	sin	28.80	2.16	0.04	90.00	None	None	None	None	None
B22	Core	1717.19	1717.62	0.43	Lenticular	Hor. Anisotropy	exp	7.20	0.29	0.60	90.00	sin	288.00	8.64	0.30	90.00	nug	0.00	0.00	0.10	90.00
B24	Core	2085.39	2085.57	0.17	Minor Slumped	Isotropic	exp	1.15	0.29	0.70	90.00	gau	6.34	3.46	0.20	90.00	sin	4.32	2.88	0.10	90.00
B24	Core	2085.59	2085.69	0.10	Minor Slumped	Hor. Zonality	exp	0.43	0.14	0.60	90.00	exp	10.08	2.16	0.40	90.00	None	None	None	None	None
B20	Core	1651.26	1651.40	0.14	Minor Slumped	Vert. Zonality	exp	0.49	0.58	0.75	90.00	gau	5.76	17.28	0.25	90.00	None	None	None	None	None
B20	Core	1641.39	1641.69	0.30	Minor Slumped	Hor. Anisotropy	exp	0.29	0.29	0.40	90.00	exp	7.78	2.02	0.58	90.00	None	None	None	None	None
B19	Core	1635.03	1635.49	0.46	Major Slumped	Isotropic	exp	0.58	0.29	0.30	90.00	exp	3.46	2.88	0.25	170.00	None	None	None	None	None
B20	Core	1682.34	1682.52	0.17	Major Slumped	Hor. Zonality	exp	0.58	0.43	0.40	90.00	exp	6.91	1.73	0.60	90.00	None	None	None	None	None
B24	Core	2002.51	2002.68	0.17	Major Slumped	Vert. Zonality	exp	1.15	0.86	0.80	90.00	sin	21.60	15.84	0.20	90.00	None	None	None	None	None
B19	Core	1716.06	1716.43	0.37	Major Slumped	Hor. Anisotropy	exp	1.73	0.86	0.45	90.00	sin	57.60	34.56	0.55	90.00	None	None	None	None	None
B20	Core	1682.03	1682.11	0.09	Major Slumped	Hor. Anisotropy	exp	0.86	0.29	0.50	90.00	exp	17.28	17.28	0.50	90.00	sin	14.40	2.88	0.20	90.00
B22	Core	1718.10	1718.22	0.12	Small Clasts	Isotropic	exp	0.86	0.29	0.50	90.00	exp	1.73	3.46	0.50	90.00	None	None	None	None	None
B24	Core	1964.08	1964.20	0.12	Small Clasts	Hor. Zonality	exp	0.58	0.29	0.40	90.00	exp	4.03	1.73	0.53	90.00	None	None	None	None	None
B22	Core	2437.02	2437.13	0.12	Small Clasts	Hor. Anisotropy	exp	2.88	1.15	1.00	90.00	None	None	None	None	None	None	None	None	None	None
B22	Core	2438.39	2438.57	0.17	Small Clasts	Hor. Anisotropy	exp	0.58	0.58	0.30	90.00	exp	4.61	1.15	0.70	90.00	None	None	None	None	None
B19	Core	1619.30	1619.39	0.09	Small Clasts	Hor. Zonality	exp	0.58	0.29	0.45	90.00	exp	16.56	2.02	0.55	90.00	None	None	None	None	None
B19	Core	1618.51	1618.63	0.12	Small Clasts	Hor. Anisotropy	exp	0.29	0.09	0.60	90.00	exp	4.32	0.86	0.40	90.00	None	None	None	None	None
B19	Core	1697.57	1697.69	0.12	Large Clasts	Isotropic	exp	0.58	0.58	0.50	90.00	exp	11.52	4.32	0.50	125.00	None	None	None	None	None
B19	Core	1651.49	1651.40	0.09	Large Clasts	Hor. Zonality	exp	0.86	0.58	0.55	90.00	exp	31.68	4.32	0.45	90.00	None	None	None	None	None
B20	Core	1658.14	1658.40	0.26	Large Clasts	Vert. Zonality	exp	2.88	2.88	0.40	90.00	exp	11.52	86.40	0.60	90.00	None	None	None	None	None
B19	Core	1634.08	1634.20	0.12	Large Clasts	Hor. Anisotropy	exp	1.73	0.86	0.60	90.00	sin	43.20	12.96	0.40	73.00	None	None	None	None	None
B20	Core	1720.17	1720.40	0.23	Large Clasts	Vert. Anisotropy	exp	0.43	0.43	0.50	90.00	sin	25.92	17.28	0.50	90.00	None	None	None	None	None
B19	Core	1699.18	1699.32	0.14	Large Clasts	Isotropic	exp	0.86	0.43	0.75	90.00	exp	7.78	7.78	0.25	90.00	None	None	None	None	None
B24	Core	1997.21	1997.41	0.20	Large Clasts	Hor. Zonality	exp	0.58	0.29	0.50	90.00	exp	5.76	8.64	0.35	90.00	sin	288.00	5.76	0.15	90.00
B24	Core	2062.42	2062.68	0.26	Large Clasts	Vert. Zonality	exp	1.15	0.43	0.70	90.00	sin	23.04	18.72	0.30	90.00	None	None	None	None	None
B19	Core	1691.55	1691.70	0.14	Large Clasts	Hor. Anisotropy	exp	1.44	0.43	0.60	90.00	exp	11.52	4.32	0.20	90.00	gau	7.20	7.20	0.30	90.00
B6	Borehole	1634.00	1636.00	2.00	Laminated	Hor. Zonality	sin	1000.00	13.68	0.65	90.00	cub	300.00	70.72	0.35	90.00	None	None	None	None	None
B6	Borehole	1896.00	1898.00	2.00	Lenticular	Hor. Anisptropy	sph	36.00	72.00	0.33	90.00	cub	144.00	1.20	0.33	65.00	cub	144.00	1.20	0.33	95.00
B6	Borehole	1589.00	1590.70	1.70	Minor Slumped	Hor. Anisotropy	exp	24.00	12.00	0.17	90.00	gau	168.00	8.40	0.42	105.00	gau	19.20	19.20	0.42	90.00
B6	Borehole	1585.00	1587.00	2.00	Major Slumped	Vert. Anisotropy	exp	6.00	13.90	1.00	90.00	None	None	None	None	None	None	None	None	None	None
B6	Borehole	1604.00	1606.00	2.00	Large Clasts	Vert. Anisotropy	cub	1.80	40.56	0.30	90.00	cub	13.40	19.20	0.59	90.00	cub	3.40	8.40	0.11	90.00

Discussion

The influence of sub-metre scale heterogeneities on larger scale fluid flow has been confirmed for heterogeneous systems previously (e.g. Pickup et al., 2000; Pickup et al., 2005). However, in addition to sub-metre scale heterogeneities, large scale heterogeneities can play a very crucial role in fluid flow in sedimentary basins. For example, large sand injections, which can form vertical conduits over several hundreds of metres have been reported on seismic and outcrop studies (e.g. Hurst et al., 2003, 2011). In addition, bypass systems by permeable faults or other vertical structures can ruin even the most homogeneous shale or mudstone sequence, when viewed from a seal or cap rock point of view (Cartwright et al., 2007).

Although our data set is narrowed to a channel dominated slope system, the heterogeneities observed cover almost the whole spectra of sub-metre scale sedimentary structures described in previous mudstone classifications (e.g. Schieber, 1999; Potter et al., 1980), reviews (e.g. Aplin and Macquaker, 2011) and investigative sedimentological studies (e.g. Pe-Piper et al., 2005; Piper et al., 2010). Nonetheless, we would like to encourage further studies on high quality data of heterogeneous shales and mudstones – not only on sub-metre scale, but also on outcrops and seismic data. To do so, more high resolution data of seal sections and fine-grained sediments in general is required from different depositional environments. We thus understand our study as a starting point for more quantitative work on shale and mudstone heterogeneity to fill the large gap of feasible descriptors of mudstone heterogeneity, as properties (e.g. porosity and permeability) of fine grained sediments are usually directly upscaled from sample to geobody scale or treated stochastically.

The observed heterogeneities comprise classic lamination and lenticular/flaser bedding, but also chaotic and brecciated features, and even sand injections. As the Nile Delta is an instable slope setting with rapid sedimentation and experienced different heights of sea levels, in particular in the Upper Pliocene, where our data originated from, it is an ideal case study to cover most heterogeneities of shales and mudstones induced by mass transport, overpressure, deep sea hemipelagic background sedimentation and tidal successions. Here, bedded structures mainly occur in hemipelagites, which has been also reported by other authors (compare Aplin and Macquaker, 2011). However, a very significant fraction of bedded structures could be also attributed to channel seismic facies by both data sources (core images and FMI), which has been also reported for other high energy depositional processes, such as debris flows and turbidites (e.g. Piper et al., 2010). The vast occurrence of chaotic mudstones in hemipelagites on FMI data is surprising and cannot be confirmed from core image data. An explanation might be inherited in the different measuring methods. While on core images

heterogeneity can only be seen by lithological contrast, resistivity can also capture heterogeneity, which becomes visible by different pore filling fluids, organic content or porosity (Safinya, 1991). Typical heterogeneities present in hemipelagic mudstones, which cannot be seen on core images due to a lack of lithological contrast, are contourites and related bioturbation (Faugères and Stow, 1993). Local biodegradation, which has been found to be significant in the Western Nile Delta gas field (Boeker, 2011) could appear as heterogeneity on FMI data, too. As this study has set a focus on flow relevant heterogeneities, which are usually dependent on lithological contrast we suggest neglecting the result for chaotic mudstones derived from FMI data. In case of clasts bearing structures, the results of both data sources are in concordance with previous studies. Hereby, only small clasts, presumably related to bioturbation and shell fragments, are reported with a small probability in hemipelagites and levees (compare Aplin and Macquaker, 2011; Potter et al., 1980; Schieber, 1999, Schieber et al., 2010). Minor probabilities have been reported for large clasts to be present in levees, probably due to overpressure release and gravity induced slumping. In channels, the probability is also low, but highest compared to the other seismic facies. Large clasts are common features in channels, induced by overpressure related sand injections (Hurst et al., 2003; 2011) or brecciation by mass movement and debris flows.

Even if statistics about frequency and occurrence of heterogeneous mudstones is only derived from point-wise datasets (wells), our case study shows, in relation to associated seismic facies, that mudstone heterogeneity is very common in deltaic slope settings (also compare Aplin and Macquaker, 2011). It should be mentioned, that sedimentological details, such as the particular type of bioturbation and paleo-environment were not distinguished or included in the sedimentological interpretation. However, the aim of the study was to abstract the sub-metre scale flow relevant geological features induced by these processes.

Even though the study could have been supported by more data sources (e.g. wireline logs) for a better correlation with lithology, we tested our interpretation of mud- and sand-rich intervals against core and conventional gamma ray logs and did not find significant deviations, which would imply misinterpretations. Nonetheless, it should be kept in mind, that core image and FMI data are limited in horizontal direction. It is therefore crucial to relate the presented results only to the scale of observation, which is the sub-metre scale. However, core and borehole image data are the best in situ measurements on sub-metre scale heterogeneities available.

FMI data can incorporate additional error sources, such as different pore-filling fluids, or holes in the borehole wall (Safinya et al., 1991). Hereby, we rely on the pre-interpretation by

the local operator. This pre-interpretation, was the basis for our interpretation of the FMI data. Furthermore, FMI images are drawn from the borehole wall, and thus incorporate the effect of an unfolded cylinder. In order to minimize this effect, experimental variograms were calculated from individual flap-pads only. Of course, this further reduced the lateral hard data information and the scale of observation should be kept in mind.

Although geostatistics have been widely used to model geological heterogeneities through different scales (Davis et al., 1993; Aggoun et al., 2006; Anderson, 1989; Klingbeil et al., 1999), sub-metre scale heterogeneities of shales and mudstones previously have only been included in very few geostatistical studies (e.g. Felletti, 2004). In combination with a quantitative approach to extract very detailed, representative variograms for heterogeneous shales and mudstones, this study provides a unique resource. The quantitative geostatistical analysis of heterogeneous, mud-rich core images supported our sedimentological interpretation, as the individual main structural classes (bedded, chaotic, clasts) were distinguished with combined geostatistical (range) and statistical parameters (mean and variance). It should be noted, that automated fitting of experimental variograms with a fixed sill (variance) and covariance function could yield misfits of the covariance function. Nevertheless, it is not crucial in a quantitative study to exactly reproduce each experimental variogram. Instead, the results should only reflect a tendency of anisotropy, which has to be set in a relative context. The results of our study for automated fitting show that in this way, anisotropy can be identified in most cases for rough grouping of shale and mudstone heterogeneity. The resulting trends of anisotropy and average RGB values and related standard deviations could be used to identify mudstone heterogeneity from one dimensional measurements such as geophysical well logs. To do so, a correlation between average RGB values and a geophysical well log measurement (e.g. gamma ray) has to be established.

The semi-quantitative geostatistical analysis for anisotropy types revealed additional differences, allowing definition of further structural sub-classes. However, it should also be mentioned, that calculation of experimental variograms in horizontal and vertical directions only reflects anisotropy in a biased way (apparent dip effect). This might trigger false anisotropy interpretations in our qualitative and semi-quantitative geostatistical analyses. Nevertheless, for the qualitative detailed manual variogram modelling, a 45 degree experimental variogram has been included, as well as angularity. Furthermore, we tried to keep obvious inclination and dip to a minimum in the selection process for the qualitative manual variogram modelling. FMI sections only were selected on a qualitative basis for qualitative manual variogram fitting. Usually, FMI data is used to gain information about

bedding dip and fractures (Safinya et al., 1991). While the main focus in the study has been set to extract sedimentary structures from core images, the extraction from FMI data has been a useful addition and to the author's knowledge the first attempt to extract heterogeneity from micro-formation images of mud-rich sequences. However, similar studies have been conducted for example in carbonate reservoirs (e.g. Tilke et al., 2006). We tried to select the FMI data sections on the basis of best quality and representativeness. Finally, manual fitting of experimental variograms is a subjective task with many degrees of freedom (incorporation of nested structures, angularity, range, sill, instationarity, nugget effect) on the one hand side, but allows - and requires - the geomodeller to include geological knowledge in the fitting process on the other hand side (Jensen et al. 1996), which has been done with great care in this study (compare methodology). We plan to use the obtained variogram models as input for geostatistical simulation to model sub-metre scale heterogeneous mudstones for subsequent numerical studies of effective permeabilities of heterogeneous mudstones using fluid flow simulation.

Conclusions

We investigated a large dataset of mud-rich core and borehole image data (> 500 m) from the Western Nile Delta, Egypt. Hereby, we set a focus on flow relevant heterogeneities in shales and mudstones. The heterogeneities have been first identified according to classic interpretation schemes and second quantified and enhanced by geostatistical analyses. Heterogeneous shales and mudstones are very common and exceed homogeneous fine-grained sediments in number in our case study. Here, this is even valid for reservoir rocks, which contain significant amounts of mud-rich sediments in our case study. Although our case study is limited to a channel dominated slope setting, the range of observed heterogeneities covers almost the full suite of heterogeneities identified, classified and summarized by previous sedimentological studies (compare Aplin and Macquaker, 2011). However, more studies on high resolution data with a focus on fluid flow are necessary not only on sub-metre scale, but also on micro- and seismic facies scales.

The resulting structural classes have been used for modelling of detailed multidirectional variograms, which can be used for modelling of metre-scale heterogeneous shales and mudstones. To allow for upscaling of these heterogeneities to seismic facies scale, probability density functions for different seismic facies (hemipelagite, levee, channel) have been provided for each structural class of heterogeneity.

References

Aggoun, R. C., Tiab, D., Owayed, J. F. 2006. Characterization of flow units in shaly sand reservoirs – Hassi R'mel Oil Rim, Algeria. J. Petr. Sci. Eng., 50, 211-226.

Anderson, M. 1989. Hydrogeological facies models to delineate large-scale spatial trends in glacial and glaciofluvial sediments. Geol. Soc. Am. Bull., 101, 501–511.

Aplin, A. C., Macquaker, J. 2011. Mudstone diversity: Origin and implications for source, seal, and reservoir properties in petroleum systems. AAPG Bulletin, 95, 12, 2031-2059.

Armstrong, M. 1998. Basic Linear Geostatistics. Springer Berlin Heidelberg, 155p.

Boeker, U. 2011. Controls on Natural Gas Migration in the Western Nile Delta Fan. PhD Thesis, Newcastle University, 196 p.

Campbell, C. V. 1967. Lamina, Laminaset, Bed and Bedset. Sedimentology, 8, 7-26.

Cartwright, J., Huuse, M, Aplin, A. C. 2007. Seal bypass systems. AAPG Bulletin, 91, 8, 1141–1166.

Chiles, J. P., Delfiner, P. 1999. Geostatistics: modeling spatial uncertainty. Wiley, New York, 695 p.

Cole, R. D., Picard, M. D. 1975. Primary and Secondary Sedimentary Structures in Oil Shale and Other Fine-Grained Rocks, Green River Formation (Eocene), Utah and Colorado. Utah Geol., 2, 49-67.

Collinson, J. D., Mountney, N., Thompson, D.B. 2006. Sedimentary Structures. Terra Publishing, 302 p.

Davis, J. M., Lohmann, R. C., Phillips, F. M., Wilson, J. L., Love, D. W. 1993. Architecture of the Sierra Ladrones Formation, central New Mexico: depositional controls on the permeability correlation structure. Geol. Soc. Am. Bull., 105, 998–1007.

Deutsch, C. V. 2002. Geostatistical Reservoir Modeling. Oxford University Press, USA, 384 p.

Deutsch, C. V., Journel, A. G., 1998. GSLIB Geostatistical Software Library and User's Guide. Oxford University Press, New York.

Droser, M. L., Bottjer, D. J. 1986. A semiquantitative field classification of ichnofabric. J Sed. Petr., 58, 558-559.

Faugères, J.-C., Stow, D. A. V. 1993. Bottom-current-controlled sedimentation: A synthesis of the contourite problem. Sed. Geol., 82, 287-297.

Felletti, F. 2004. Statistical modelling and validation of correlation in turbidites: an example from the Tertiary Piedmont Basin (Castagnola Fm., Northern Italy). Mar. Petr. Geol., 21, 23-39.

Garfunkel, Z. 1998. Constrains on the origin and history of the Eastern Mediterranean basin. Tectonophysics, 298, 1-3, 5-35.

Garfunkel, Z. 2004. Origin of the Eastern Mediterranean basin: a re-evaluation. Tectonophysics, 391, 1-4, 11-34.

Garziglia, S., Migeon, S., Ducassou, E., Loncke, L., Mascle, J. 2008. Mass-transport deposits on the Rosetta province (NW Nile deep-sea turbidite system, Egyptian margin): Characteristics, distribution, and potential causal processes. Marine Geology, 250, 180-198.

Georgiopoulou, A. 2009: Case study B. Presentation. Caprocks Project steering group meeting, Shell, The Hague, Netherlands.

Geovariances 2010. Isatis Technical References. Geovariances, Avon Cedex, France.

Hurst, A., Cartwright, J., Huuse, M., Jonk, R., Schwab, A., Duranti, D., Cronin, B. 2003. Significance of large-scale sand injectites as long-term fluid conduits: evidence from seismic data. Geofluids, 3, 4, 263–274.

Hurst, A., Scott, A., Vigorito, M. 2011. Physical characteristics of sand injectites. Earth-Science Reviews, 106, 215–246.

Huysmans, M., Peeters, L., Moermans, G., Dassargues, A. 2008. Relating Small-Scale Sedimentary Structures and Permeability in a Cross-Bedded Aquifer. J. Hydrol., 361, 41–51.

Huysmans, M., Dassargues, A. 2010. Application of Multiple-Point Geostatistics on Modelling Groundwater Flow and Transport in a Cross-Bedded Aquifer (Belgium). Hydrogeology Journal, 17, 1901–1911.

Jensen, J. L., Corbett, P. W. M., Pickup, G. E., Ringrose, P. S. 1996. Permeability semivariograms, geological structure and flow performance. Math. Geol., 28, 4, 419–435.

Klingbeil, R., Kleineidam, S., Asprion, U., Aigner, T., Teutsch, G. 1999. Relating lithofacies to hydrofacies: outcrop-based hydrogeological characterisation of quaternary gravel deposits. Sediment. Geol., 129, 3-4, 299–310.

Kossack, C. A., Aasen, J. O.. and Opdal, S, T. 1990. Scaling up heterogeneities with pseudofunctions. SPE Formation Evaluation, 5, 3, 226-232.

Macquaker, J. H. S., Gawthorpe, R. L. 1993. Mudstone lithofacies in the Kimmeridge Clay Formation, Wessex Basin, southern England: Implications for the origin and controls of the distribution of mudstones. J. Sed. Petr., 63, 1129-1143.

Macquaker, J. H. S., Adams, A. E. 2003. Maximizing Information from Fine-Grained Sedimentary Rocks: an Inclusive Nomenclature for Mudstones. J. Sed. Res., 73, 5, 735–744.

Macquaker, J. H. S., Taylor, K. G. 1996. A sequence-stratigraphic interpretation of a mudstone-dominated succession: The Lower Jurassic Cleveland Ironstone Formation, United Kingdom. J. Geol. Soc., 153, 759-770.

Macquaker, J. H. S., Bohacs, K. M. 2007. On the Accumulation of Mud. Science, 318, 1734-1735.

Macquaker, J. H. S., Bentley, S. J., Bohacs, K. M. 2010. Wave-enhanced sediment gravity flows and mud dispersal across continental shelves: Reappraising sediment transport processes operating in ancient mudstone successions. Geology, 38, 947-950.

Marsily, G. de, Delay, F.Goncalves, J., Renard, P., Teles, V., Violette, S. 2005. Dealing with spatial heterogeneity. Hydrogeol J, 13, 161–183.

Mascle, J., Zitter, T., Bellaiche, G., Droz, L., Gaullier, V., Loncke, L., Prismed Scientific Party 2001. The Nile deep-sea fan: preliminary results from a swath bathymetry survey. Marine and Petroleum Geology, 18, 471-477.

McKinley, J. M., Lloyd, C. D., Ruffell, A. H., 2004. Use of variography in permeability characterisation of visually homogeneous sandstone reservoirs with examples from outcrop studies. Math. Geol., 36, 7, 761–779.

Mikes, D. 2006. Sampling procedure for small-scale heterogeneities (cross-bedding) for reservoir modeling. Mar. Petrol. Geol., 23, 9–10, 961–977.

Morton, K., Thomas, S., Corbett, P., Davies, D. 2002. Detailed analysis of probe permeameter and vertical interference test permeability measurements in a heterogeneous reservoir. Petrol. Geosci., 8, 209–216.

Myrow, P. M. 1992. Bypass-zone tempestite facies model and proximality trends for an ancient muddy shoreline and shelf. J. Sed. Petr., 62, 99-111.

Nordahl, K., Ringrose, P. S. 2008. Identifying the Representative Elementary Volume for Permeability in Heterolithic Deposits Using Numerical Rock Models. Math. Geosci., DOI 10.1007/s11004-008-9182-4.

O'Brien, N. R., Slatt, R. M. 1990. Argilleceous rock atlas. New York, Springer-Verlag, 141 p.

Pe-Piper, G., Dolansky, L., Piper, D. J. W. 2005. Sedimentary Environment and Diagenesis of the Lower Cretaceous Chaswood Formation, Southeastern Canada: The Origin of Kaolin-Rich Mudstones. Sedimentary Geology, 178, 75–97.

Pickup, G. E., Stephen, K. D. Ma, J., Zhang, P., Clark, J. D. 2005. Multi-Stage Upscaling: Selection of Suitable Methods. Transp Porous Med, 58, 191–216.

Pickup, G. E., Ringrose, P. S., Sharif, A. 2000. Steady-state upscaling: from lamina-scale to full-field model. SPE J, 5, 2, 208–217.

Pickup, G. E., Ringrose, P. S., Corbett, P. W. M., Jensen, J. L., Sorbie, K. S. 1995. Geology, geometry and effective flow. Pet Geosci, 1, 37–42.

Piper, D. J. W., Noftall, R., Pe-Piper, G. 2010. Allochtonous Prodeltaic Sediment Facies in the Lower Cretaceous at the Tantallon M-41 Well: Implications for the Deep-Water Scotian Basin. AAPG Bulletin, 94, 1, 87-104.

Potter, E. P., Maynard, J. B., Pryor, W. A. 1980. Sedimentology of Shale. Springer, New York, Berlin, Heidelberg, Tokyo, 306 p.

Reineck, H. E., Singh, I. B. 1973. Depositional Sedimentary Environments. Springer, New York, Heidelberg, Berlin, 439 p.

Rivoirard, J. 1994. Introduction to disjunctive kriging and non-linear geostatistics. Oxford: Clarendon Press., 180 p.

Rohl, H.-J., Schmid-Rohl, A. 2005. Lower Toarcian (upper Liassic) black shales of the central European epicontinental basin: A sequence-stratigraphic case study from the southwestern German Posidonia Shale. In: Harris, N. (ed.). The deposition of organic-carbon-rich sediments: Models, mechanisms, and consequences. SEPM Special Publication, 82, 165-189.

Safinya, K. A., Le Lan, P., Villegas, M., and Cheung, P. S. 1991. Improved formation imaging with extended microelectrical arrays: Soc. Petrol. Eng., Paper no. 22726, 653–664.

Schieber, J. 1994. Evidence for high-energy events and shallow-water deposition in the Chattanooga Shale, Devonian, central Tennessee, U.S.A. Sedimentary Geology, 93, 193-208.

Schieber, J. 1999. Distribution and Deposition of Mudstone Facies in the Upper Devonian Sonyea Group of New York. J. Sed. Res., 69, 4, 909–925.

Schieber, J., Southard, J., Thaisen, K. 2007. Accretion of Mudstone Beds from Migrating Floccule Ripples. Science 318, 1760-1763.

Schieber, J., Southard, J. B. 2009. Bed-load transport of mud by floccule ripples: Direct observation of ripple migration processes and their implications. Geology, 37, 483-486.

Schieber, J., Southard, J. B., Schimmelmann, A. 2010. Lenticular shale fabrics resulting from intermittent erosion of water-rich muds: INterpreting the rock record in the light of recent flume experiments. J. Sed. Res., 80, 119-128.

Schlumberger 2004. FMI Fullbore Formation MicroImager Fact Sheet. www.slb.com/oilfield.

Tilke, P. G., Allen, D., Gyllensten, A. 2006. Quantitative Analysis of Porosity Heterogeneity: Application of Geostatistics to Borehole Images. Mathematical Geology, 38, 2, 155-174.

Tripsanas, E. K., Piper, D. J. W., Jenner, K. A., Bryant, W. R. 2008. Submarine mass-transport facies: new perspectives on flow processes from cores on the eastern North American margin. Sedimentology, 55, 97–136.

Van der Zwaan, G. J. and Gudjonsson, L. 1986. Middle Miocene--Pliocene stable isotope stratigraphy and paleoceanography of the Mediterranean. Mar. Micropaleontol., 10, 71-90.

Vandré, C., Cramer, B., Gerling, P., Winsemann, J. 2007. Natural gas formation in the western Nile delta (Eastern Mediterranean): Thermogenic versus microbial. Organic Geochemistry, 38, 4, 523-539.

Wackernagel, H. 2003. Multivariate Geostatistics. Springer Verlag, 403 p.

Willis, B.J., White, C.D., 2000. Quantitative outcrop data for flow simulation. J. Sediment. Res., 70, 788–802.

Zhang, X. F., Van Eijkeren, J. C. H., and Heemink, A.W. 1995. On the weighted least-squares method for fitting a semi-variogram model: Comput. Geosci., 21, 4, 605–608.

Chapter 4: Upscaling of Sub-Metre Scale Heterogeneities in Shales and Mudstones – Implications for Uncertainty and Dimensioning of Fluid Flow Models

Introduction

Shales and mudstones comprise the largest fraction of rocks of the Earth's sedimentary basins (e.g. Potter et al., 1980; Aplin et al., 1999) and are of direct relevance to many applied aspects of geosciences. Groundwater and conventional petroleum systems, CO_2 storage, and nuclear waste deposits are only the most prominent examples. Hereby, shales and mudstones usually serve as barrier rocks or seals, giving shales and mudstones at least the same importance for the groundwater or petroleum systems as the fluid bearing aquifer or reservoir rocks. Despite their relevance, shales and mudstones are only well understood on sample-scale (centimetre-scale), where many authors have published measurement results and models on physical properties such as porosity and permeability (e.g. Neuzil, 1994; Dewhurst et al., 1998; Yang and Aplin, 2004, 2010). On sub-metre scale, it can be argued, that these properties are highly dependent on spatial heterogeneity, which has been indicated from recent measurements on heterogeneous mud-rich samples (Armitage et al., 2011) and has been a long studied topic in the hydrocarbon and water reservoir community for sands and carbonates (e.g. Davis et al., 1993; Anderson, 1989; Klingbeil et al., 1999; Pickup et al., 2000, 2005). Although, heterogeneity in shales and mudstones has been extensively described on many scales, including the sub-metre scale (e.g. Cole and Picard, 1975; Potter et al., 1980; Schieber, 1999; Piper et al., 2010; Aplin and Macquaker, 2011), the influence of sub-metre scale heterogeneities in shales and mudstones upon fluid flow in sedimentary basins and hence seal (in case of hydrocarbon trapping, CO_2 and nuclear waste storage) and barrier (in case of groundwater flow) rock integrity has not been investigated systematically, yet.

Usually, the influence of heterogeneities on fluid flow is best described in a single, effective property (e.g. effective permeability). Such an effective property can then be used to upscale the influence of heterogeneity to the next level of scale (e.g. Pickup et al., 2005). Renard and Marsily (1997) provide a detailed review of upscaling methods such as percolation theory, where, from a geological fluid flow point of view, a certain threshold of highly permeable material guarantees for connectivity through a system (Begg and King, 1985), effective media theory (Dagan, 1979) and numerical methods. A critical parameter in upscaling, independent of the method, is the scale that the influence of heterogeneity should be upscaled to. This scale should ensure stable upscaling, and thus be a scale where the influence of the

heterogeneity of interest is considered to be stochastically stationary, or homogeneous in other words. This yields to the continuum approach, where a representative element or, in 3D, a representative elementary volume (Bear, 1972) fulfils these requirements. This approach is an approximation of the effective media theory, and assumes the representative element to be large enough to capture the relevant or representative heterogeneities (Bear, 1972). It is obvious that the size of the representative element is closely related to the length scale (or correlation lengths) of the modelled heterogeneities. Thus, the results of the upscaling method might be unstable, when these correlation lengths approach the observed scale (Sahimi, 1995). However, geological heterogeneities cannot be considered to be always present at representative scales, as natural discontinuities, such as fault zones, mud volcanoes, magmatic intrusions, etc. might produce the effect of a critical length scale compared to the domain of interest. In the field of characterisation of petroleum reservoirs the effect of length scales of heterogeneities on flow properties has been discussed (Hassanizadeh and Gray, 1983; Haldorsen, 1986) and studied numerically using stochastical (Desbarats, 1987; Begg et al., 1989; Deutsch, 1989) or process based (Wen et al., 1999; Nordahl et al., 2005; Scaglioni et al., 2006) modelling tools.

In this study, we aim to go the first step towards calculation of realistic effective flow properties, by determination of representative model sizes and resolutions of a set of sub-metre scale shale and mudstone heterogeneities. Hereby, the set of representative heterogeneities, which can be expected in seal and barrier rocks, will be modelled on the basis of quantitatively derived high resolution variogram models (Chapter 2). In order to study the interplay of these heterogeneities with model size and resolution in relation to effective permeability and connectivity, we use numerical fluid flow simulation. To do so, the effect of physical property variability of the respective lithologies present in shales and mudstones (sands, silts and muds) is neglected by assuming constant permeabilities, while the resolution and model size is varied for each heterogeneity type. This practice has been proven to be a useful method to investigate the influence of heterogeneity on fluid flow and to estimate representative model sizes (e.g. Nordahl and Ringrose, 2008).

The results can serve as guidance for model dimensioning of future numerical studies, which focus on the effect of shale and mudstone physical property variation. Hence, this study contributes to either producing numerical stable upscaling results or of including uncertainty measures into flow property upscaling of heterogeneous shales and mudstones.

Methods and Data

The methods used in this study follow three basic steps, which are required to assess influence of model size and resolution on upscaling of flow properties of sub-metre scale heterogeneous mudstones:

- Modelling heterogeneity of shales and mudstones for different model sizes and resolutions using geostatistical simulation
- Property assignment and numerical fluid flow simulation to obtain effective properties
- Post-processing of the results to assess the influence of model size and resolution

Modelling Sedimentary Structures

To model sedimentary structures we use nested variogram models (covariance functions) as input to geostatistical simulation. The used variogram models have been derived from experimental variograms calculated in horizontal, vertical and diagonal directions in Chapter 3 by carefully conducted, detailed geostatistical analysis (Table 4.1). Hereby, the geological character of the heterogeneities has been taken into account (Chapter 3), which is vital in manual variogram modelling (Jensen et al., 1996). The variograms account for anisotropy, angularity (inclination), cyclicity and instationarity (e.g. due to fining/sorting trends), nested covariance functions to include different structures and nugget effects to model geological random features, such as mottles and floating grains or pebbles. Also, the selection of the structural templates is based on the combined qualitative and quantitative analyses of more than 500 m of mud-rich image data.

The data set comprises a carefully selection of high quality core images and borehole images from high resolution formation micro imager, which measures electrical resistivity (Safinya, 1991), from 5 wells (B6, B19, B20, B22, B24) of an off shore gas field in the Western Nile Delta, Egypt. The total depth ranges from approximately 1500 – 2500 m and the data covers Upper Pliocene sediments, such as hemiplegic sections and channel-levee complexes, both highly heterogeneous on macro-scale (Figure 3.1). Water depths range from approximately 350-650 m. The selection was conducted on the basis of qualitative visual/geological along with semi-quantitative geostatistical anisotropy interpretation of the images (Chapter 2). The resulting heterogeneity classes follow common schemes for sedimentary structures in shales and mudstones (Campbell, 1967; Reineck and Singh, 1973; Cole and Picard, 1975; Potter et al., 1980; Collinson et al., 2006) and are with a strong focus on geometric properties, which can be back related to different depositional processes (Figure 4.2):

- Bedded structures were subdivided into continuous lamina or discontinuous, lenticular shaped beds or lamina. A deep sea to tidal influenced sedimentation environment with periodic influx of coarser material is a likely cause of origin for bedded structures.
- Chaotic structures pose a high uncertainty and depend critically on lithological composition. They are typical for slope and mass transport dominated settings. Chaotic structures are mostly caused by slumping and folding and range from small disturbed beds to mixing of different lithologies, which appear almost isotropic on the sub-metre scale. Hereby, minor slumps contain preserved structures, such as deformed beds, while major slumps are bare of any preferred orientation or primary structure.
- Clasts bearing structures span a wide range of possible structures from small bioturbation induced scattered clasts to mass transport related mixing of cm-dm sized sand and mud clasts to vertical sand-pipes in a mud-rich matrix caused by sand injection. They can be divided into small (< 3cm) and large (> 3cm) clasts, which can be differentiated from chaotic structures by the presence of sharp contacts between the clasts.

Finally, for selection of the core images, which best represent the spectra of sub-metre scale heterogeneities present in shales mudstones, a selection on the basis of image quality was conducted. In addition, these images were used to calculate experimental semi-variograms in horizontal and vertical directions. The resulting experimental variograms were then analysed for general anisotropy types, which allowed for further subdivision of the observed heterogeneity groups of the visual interpretation in a semi-quantitative way. The most different heterogeneities were finally selected for detailed variogram modelling (variography) to obtain nested variograms as input for geostatistical simulation. In order to cover the whole range of observed shale and mudstone heterogeneities, we preferred this rational rather than a selection based on the most common heterogeneities. Also, a set of borehole images, which represents the observed heterogeneities on core, has been selected manually for the detailed variography.

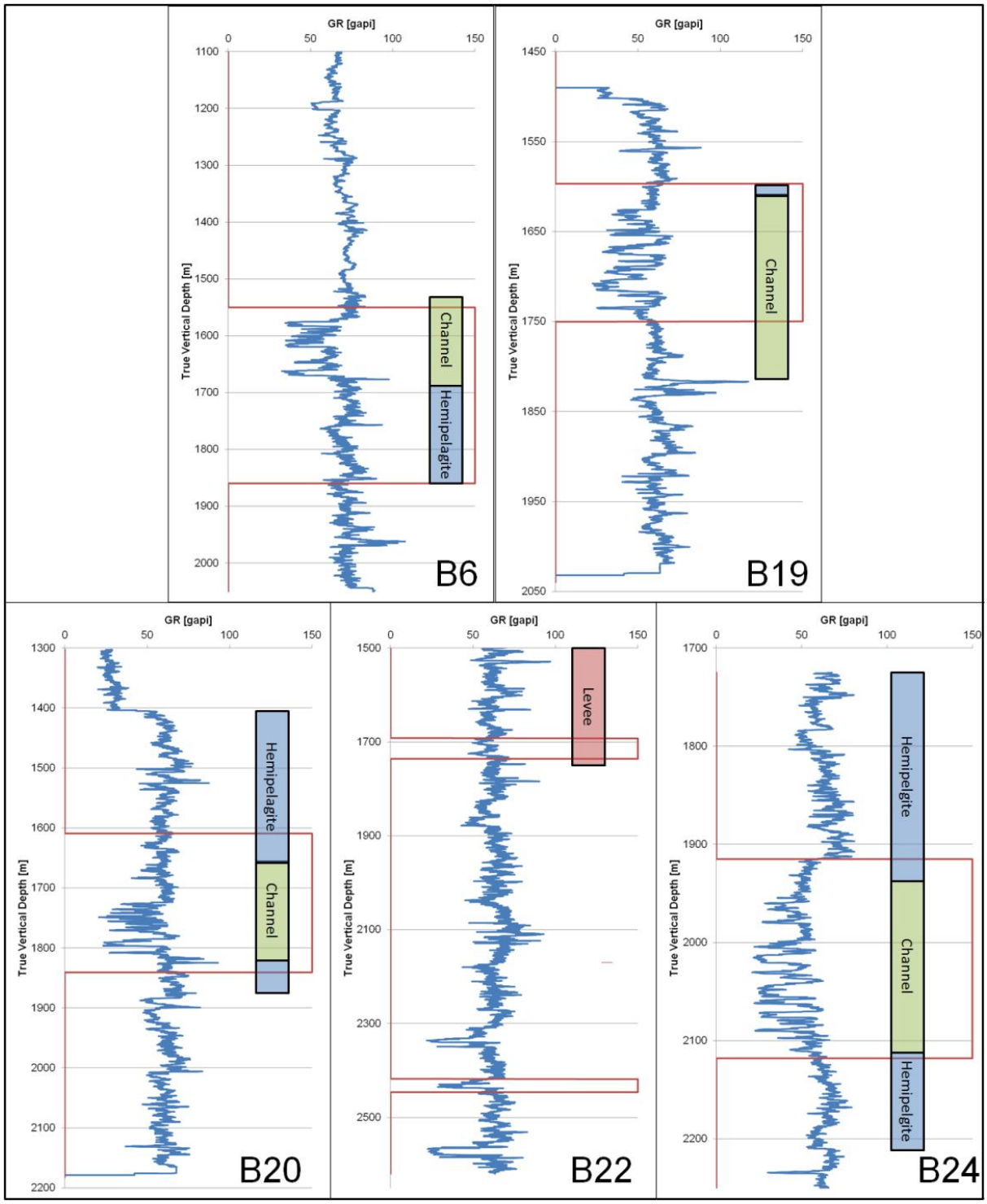

Figure 4.1: Gamma ray (blue lines) and cored/imaged sections (red lines) of the used wells of the Nile Delta case study. The colour bars indicate the approximate seismic facies association (blue: hemipelagite; red: levee; green: channel). The seismic facies of the lower cored section of well B22 is not known.

The simulation algorithm applied on the detailed variograms (Table 4.1) is the turning bands algorithm (Emery and Lantuéjoul, 2006) with 2000 turning bands. The turning bands method used in this study simplifies the simulation problem in 3D-space into a simulation problem in 1D space by performing simulations on lines (turning bands) randomly distributed in the 3D space. This has the advantage of simulating in 3D at the computational cost of one-dimensional simulations (Emery and Lantuéjoul, 2006). After the geostatistical simulation, the simulated data, following a normal distribution with mean 0 and variance 1, is back transformed to the initial distribution of mean RGB values of the original images, employing empirical Gaussian anamorphosis (e.g. Rivoirard, 1994; Wackernagel, 2003). Gaussian anamorphosis employs a transformation function between the cumulative of the normal distribution with mean 0 and variance 1 and any other monotonic cumulative distribution. The transformation function is modelled using a set (usually 30) of Hermite polynomials. The necessary Hermite polynomials have been extracted from the images prior to the simulation. To assess the influence of model size and resolution, we perform numerical simulations with different model sizes and resolutions. Hereby, the size of an edge of the square-shaped models (model edge length) is simultaneously varied for horizontal and vertical dimensions from 150, 300 and 600 to 1000 mm. The model resolution is varied in such a way that the cell size takes on values of 2, 5 and 10 mm. In addition, we would like to roughly investigate the influence of mud contents on the results of the numerical simulations. This is particular useful to give a first estimate of percolation thresholds (e.g. Begg and King, 1985) and their influence upon possible representative model sizes. 50% and 75% seemed to be a reasonable choice of mud contents in order to allow for sufficient lithological contrast, which is crucial for assessment of percolation thresholds on the one hand side, and to be well in the mud-rich range, on the other hand side. 36 images were selected for detailed variography and subsequent geostatistical simulation on the basis of qualitative and semi-quantitative interpretations. For each resulting structural template 10 stochastically equal geostatistical realisations were simulated and converted into flow models with mud contents of 50% and 75%, resulting in a total amount of 8640 models.

Table 4.1: Data base table showing the parameters resulting from the detailed qualitative geostatistical analysis. The table comprises well origin, image type, interval size, structural class, variogram type (isotropic, Hor. Zonality = horizontal zonal anisotropy, Hor. Anisotropy = horizontal geometric anisotropy, Vert. Zonality = vertical zonal anisotropy, Vert. Anisotropy = vertical geometric anisotropy) and geostatistical parameters, which served as input for geostatistical simulation in geo-modelling in this study.

Well	Image Type	Top [m]	Bottom [m]	Interval [m]	Structure	Variogram Type	Mod1	Rh1 [cm]	Rv1 [cm]	S1	Ang1	Mod2	Rh2 [cm]	Rv2 [cm]	S2	Ang2	Mod3	Rh3 [cm]	Rv3 [cm]	S3	Ang3
B24	Core	1935.23	1935.46	0.23	Laminated	Hor. Zonality	exp	2.02	0.29	0.40	90.00	sin	115.20	5.76	0.50	90.00	None	None	None	None	None
B24	Core	1986.03	1986.44	0.40	Laminated	Hor. Zonality	exp	0.86	0.14	0.14	90.00	exp	86.40	2.88	0.50	90.00	sin	288.00	23.04	0.36	90.00
B22	Core	1722.29	1722.67	0.37	Laminated	Hor. Anisotropy	exp	1.15	0.14	0.40	90.00	sin	37.44	5.76	0.50	90.00	None	None	None	None	None
B22	Core	1719.18	1719.69	0.52	Lenticular	Hor. Zonality	exp	0.58	0.03	0.25	90.00	exp	11.52	8.64	0.35	90.00	sin	288.00	2.88	0.40	90.00
B24	Core	1991.16	1991.48	0.32	Lenticular	Hor. Zonality	exp	4.32	1.44	0.70	90.00	sin	288.00	4.32	0.30	90.00	None	None	None	None	None
B22	Core	1712.04	1712.23	0.19	Lenticular	Hor. Anisotropy	exp	2.16	0.29	0.96	90.00	sin	28.80	2.16	0.04	90.00	None	None	None	None	None
B22	Core	1717.19	1717.62	0.43	Lenticular	Hor. Anisotropy	exp	7.20	0.29	0.60	90.00	sin	288.00	8.64	0.30	90.00	nug	0.00	0.00	0.10	90.00
B24	Core	2085.39	2085.57	0.17	Minor Slumped	Isotropic	exp	1.15	0.29	0.70	90.00	gau	6.34	3.46	0.20	90.00	sin	4.32	2.88	0.10	90.00
B24	Core	2085.59	2085.69	0.10	Minor Slumped	Hor. Zonality	exp	0.43	0.14	0.60	90.00	exp	10.08	2.16	0.40	90.00	None	None	None	None	None
B20	Core	1651.26	1651.40	0.14	Minor Slumped	Vert. Zonality	exp	0.49	0.58	0.75	90.00	gau	5.76	17.28	0.25	90.00	None	None	None	None	None
B20	Core	1641.39	1641.69	0.30	Minor Slumped	Hor. Anisotropy	exp	0.29	0.29	0.40	90.00	exp	7.78	2.02	0.58	90.00	None	None	None	None	None
B19	Core	1635.03	1635.49	0.46	Major Slumped	Isotropic	exp	0.58	0.29	0.30	90.00	exp	3.46	2.88	0.25	170.00	None	None	None	None	None
B20	Core	1682.34	1682.52	0.17	Major Slumped	Hor. Zonality	exp	0.58	0.43	0.40	90.00	exp	6.91	1.73	0.60	90.00	None	None	None	None	None
B24	Core	2002.51	2002.68	0.17	Major Slumped	Vert. Zonality	exp	1.15	0.86	0.80	90.00	sin	21.60	15.84	0.20	90.00	None	None	None	None	None
B19	Core	1716.06	1716.43	0.37	Major Slumped	Hor. Anisotropy	exp	1.73	0.86	0.45	90.00	sin	57.60	34.56	0.55	90.00	None	None	None	None	None
B20	Core	1682.03	1682.11	0.09	Major Slumped	Hor. Anisotropy	exp	0.86	0.29	0.50	90.00	exp	17.28	17.28	0.50	90.00	sin	14.40	2.88	0.20	90.00
B22	Core	1718.10	1718.22	0.12	Small Clasts	Isotropic	exp	0.86	0.29	0.50	90.00	exp	1.73	3.46	0.50	90.00	None	None	None	None	None
B24	Core	1964.08	1964.20	0.12	Small Clasts	Hor. Zonality	exp	0.58	0.29	0.40	90.00	exp	4.03	1.73	0.53	90.00	None	None	None	None	None
B22	Core	2437.02	2437.13	0.12	Small Clasts	Hor. Anisotropy	exp	2.88	1.15	1.00	90.00	None	None	None	None	None	None	None	None	None	None
B22	Core	2438.39	2438.57	0.17	Small Clasts	Hor. Anisotropy	exp	0.58	0.58	0.30	90.00	exp	4.61	1.15	0.70	90.00	None	None	None	None	None
B19	Core	1619.30	1619.39	0.09	Small Clasts	Hor. Zonality	exp	0.58	0.29	0.45	90.00	exp	16.56	2.02	0.55	90.00	None	None	None	None	None
B19	Core	1618.51	1618.63	0.12	Small Clasts	Hor. Anisotropy	exp	0.29	0.09	0.60	90.00	exp	4.32	0.86	0.40	90.00	None	None	None	None	None
B19	Core	1697.45	1697.57	0.12	Large Clasts	Isotropic	exp	0.58	0.58	0.50	90.00	exp	11.52	4.32	0.50	125.00	None	None	None	None	None
B19	Core	1651.40	1651.49	0.09	Large Clasts	Hor. Zonality	exp	0.86	0.58	0.55	90.00	exp	31.68	4.32	0.45	90.00	None	None	None	None	None
B20	Core	1658.14	1658.40	0.26	Large Clasts	Vert. Zonality	exp	2.88	2.88	0.40	90.00	exp	11.52	86.40	0.60	90.00	None	None	None	None	None
B19	Core	1634.08	1634.20	0.12	Large Clasts	Hor. Anisotropy	exp	1.73	0.86	0.60	90.00	sin	43.20	12.96	0.40	73.00	None	None	None	None	None
B20	Core	1720.17	1720.40	0.23	Large Clasts	Vert. Anisotropy	exp	0.43	0.43	0.50	90.00	sin	25.92	17.28	0.50	90.00	None	None	None	None	None
B19	Core	1699.18	1699.32	0.14	Large Clasts	Isotropic	exp	0.86	0.43	0.75	90.00	exp	7.78	7.78	0.25	90.00	None	None	None	None	None
B24	Core	1997.21	1997.41	0.20	Large Clasts	Hor. Zonality	exp	0.58	0.29	0.50	90.00	exp	5.76	8.64	0.35	90.00	sin	288.00	5.76	0.15	90.00
B24	Core	2062.42	2062.68	0.26	Large Clasts	Vert. Zonality	exp	1.15	0.43	0.70	90.00	sin	23.04	18.72	0.30	90.00	None	None	None	None	None
B19	Core	1691.55	1691.70	0.14	Large Clasts	Hor. Anisotropy	exp	1.44	0.43	0.60	90.00	exp	11.52	4.32	0.20	90.00	gau	7.20	7.20	0.30	90.00
B6	Borehole	1634.00	1636.00	2.00	Laminated	Hor. Zonality	sin	1000.00	13.68	0.65	90.00	cub	300.00	70.72	0.35	90.00	None	None	None	None	None
B6	Borehole	1896.00	1898.00	2.00	Lenticular	Hor. Anisptropy	sph	36.00	72.00	0.33	90.00	cub	144.00	1.20	0.33	65.00	cub	144.00	1.20	0.33	95.00
B6	Borehole	1589.00	1590.70	1.70	Minor Slumped	Hor. Anisptropy	exp	24.00	12.00	0.17	90.00	gau	168.00	8.40	0.42	105.00	gau	19.20	19.20	0.42	90.00
B6	Borehole	1585.00	1587.00	2.00	Major Slumped	Vert. Anisotropy	exp	6.00	13.90	1.00	90.00	None	None	None	None	None	None	None	None	None	None
B6	Borehole	1604.00	1606.00	2.00	Large Clasts	Vert. Anisotropy	cub	1.80	40.56	0.30	90.00	cub	13.40	19.20	0.59	90.00	cub	3.40	8.40	0.11	90.00

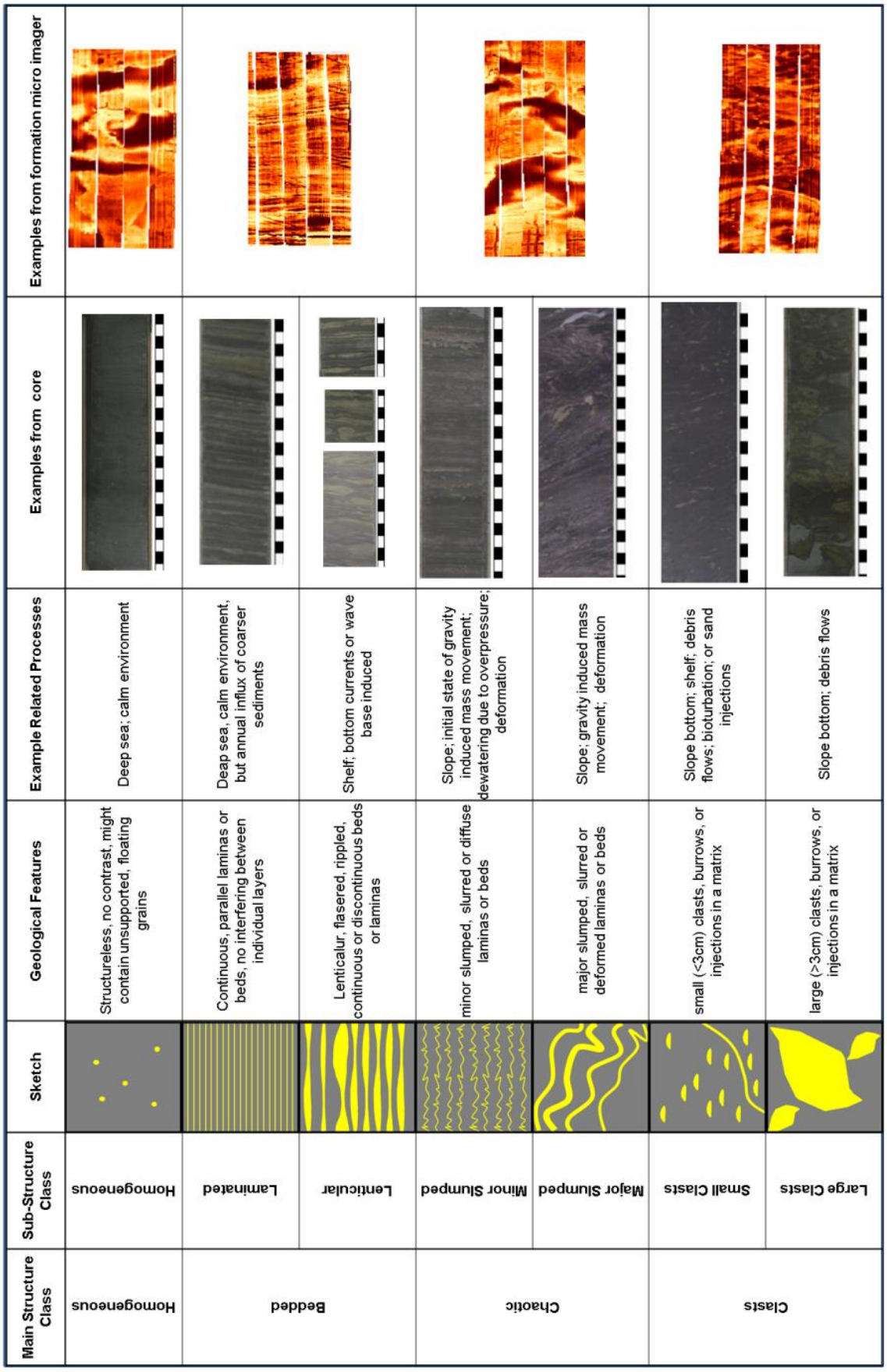

Figure 4.2: Classification scheme used in this study with examples from core and borehole images. Note that every heterogeneity or structure class can be related to geological features and possible depositional processes.

Fluid Flow Simulation

Effective permeabilities are calculated from the numerically simulated steady state flow rate through a 2D mixed finite element model with pressure boundary conditions by employing Darcy's law (Ma et al., 2006). The pressure boundary conditions are applied on the vertical boundaries, with no flow allowed on the horizontal boundaries to calculate vertical effective permeabilities and vice versa to calculate horizontal effective permeabilities. Thereby, only single phase fluid flow is considered. The permeability field required as input for the simulation has been derived from the image mean RGB distribution by setting the threshold of mud-rich cells to 50% or 75% of the mean RGB distribution, respectively. The mean RGB value $\overline{RGB}$ is given by:

$$\overline{RGB} = \frac{R+G+B}{3} \; with \quad R,G,B \quad \in \{0,255\} \qquad \text{Eq. 4.1}$$

The remaining cells are treated as sandstone cells. To omit the influence of petrophysical variation, the permeabilities are kept constant at 1 nD for mudstone cells and 1 D for sandstone cells. This allows a clear assignment of the results to the type of heterogeneity, model size and model resolution in the post processing step independent of further lithological variation. The high contrast also allows for estimating percolation thresholds and probabilities of connected pathways of sand through the system/model.

Post Processing

The large number of simulated flow models requires post processing techniques to extract meaningful results from the simulations. To do so, we mainly follow the workflow used by Nordahl and Ringrose (2008), employing the coefficient of variation C_V to estimate representative elementary domains (model edge lengths in our case). In addition, we provide the probability of connectivity *CP* for each structure, model size and cell size, to allow for an estimate of the uncertainty of the results, in particular for such structures whose correlation lengths are always larger or critically close to the observed model domain size.

The coefficient of variation C_V (e.g. Jensen et al., 2000) is given by

$$C_V = \frac{S_K}{\overline{K}} \qquad \text{Eq. 4.2}$$

S_K is the standard deviation and $\overline{K}$ is the arithmetic mean of the calculated effective permeabilities in a certain direction of a set of realisations of a model with certain structure, model size and cell size. For a number of realisations $N \leq 10$ a correction factor f_C has to be used (Jensen et al., 2000; Nordahl and Ringrose, 2008):

$$f_C = 1 + \frac{1}{4(N-1)} \qquad \text{Eq. 4.3}$$

For the coefficient of variation several classes of heterogeneity of the simulated results per structural class, model size and cell size can be defined (Corbett and Jensen, 1992):

$0.0 < C_V < 0.5$ → Homogeneous
$0.5 < C_V < 1.0$ → Heterogeneous
$1.0 < C_V$ → Very Heterogeneous

The probability of connectivity *CP* can be estimated from the fraction of realisations of a certain structure with equal model and cell size, which are characterised by a connected sand network in horizontal and/or vertical direction. This connectivity can be derived from the absolute value of effective permeabilities, which, in case of a connected network, should be close to the permeability of the sand fraction (1 D in this case). Vice versa, if no connection was established, the effective permeability should be close to the permeability of the mud fraction (1nD in this case). Thus, we consider a model to be connected, where the effective permeability exceeds the logarithmic upper quartile of the permeability range (1 nD – 1 D), which is 1 mD.
To ease the interpretation of the connectivity probability results we apply the following risk classification scheme:

$CP < 0.3$ → low probability of connectivity
$0.3 \leq CP < 0.5$ → medium probability of connectivity
$CP > 0.5$ → high probability of connectivity

The influence of the model resolution or cell size is assessed by calculating a mean connectivity probability $\overline{\overline{CP}}$ for all geostatistical realizations of all structural templates and

the standard deviation $s_{\overline{CP}}$ of mean connectivity probabilities $\overline{CP}$ in vertical and horizontal direction with respect to the different cell sizes. The cell size dependent mean connectivity probability $\overline{CP}$ is calculated for each model by averaging the connectivity probability *CP* of each geostatistical realization with equal model size:

$$\overline{CP} = \frac{1}{M}\sum_{j=1}^{M} CP_j \qquad \text{Eq. 4.4}$$

$$\overline{\overline{CP}} = \frac{1}{N}\sum_{i=1}^{N} \overline{CP}_i \qquad \text{Eq. 4.5}$$

$$s_{\overline{CP}} = \frac{1}{N}\sum_{i=1}^{N} \left| \overline{CP}_i - \overline{\overline{CP}} \right| \qquad \text{Eq. 4.6}$$

Where *N* is the number of models (36) and *M* is the number of model sizes (4).

The slope of both $\overline{\overline{CP}}$ and $s_{\overline{CP}}$ vs. cell size is an indicator of the robustness of the simulation results with respect to cell size or model resolution. A slope close to zero would therefore indicate no influence of the model resolution on the simulation results, whereas a positive or negative slope would indicate an influence.

Results

To test and demonstrate the geostatistical simulation for its capability to serve as a tool for modelling of sub-metre scale shale and mudstone heterogeneities, we clipped an original image except one vertical centred stripe, which covers approximately 12% of the whole image. The clipped area was then object of geostatistical simulation using the high resolution variogram model derived previously from the whole image in vertical, diagonal and horizontal direction. Finally the simulated area is conditioned to the vertical stripe of the original image. A visual comparison of the original and simulated image as well as their mean RGB distributions shows a good fit with the original unclipped core image, displaying similar geological features. In particular, the distribution of layers and lenses characteristic in the sample image were well reproduced. Also, the $\overline{RGB}$ distribution could be reproduced (Figure 4.3). The ability of the Turning Bands simulation algorithm (Emery and Lantuéjoul, 2006) to reproduce geological heterogeneity of shales and mudstones in a realistic way, encouraged us to further employ this technique in this study. In total, 8640 binary 2D flow models were subjected to numerical fluid flow simulation in this study. Examples for 600 mm model size

and 2 mm cell size of each structural template are shown in Figure 4.4 for 50% and 75% of mud content.

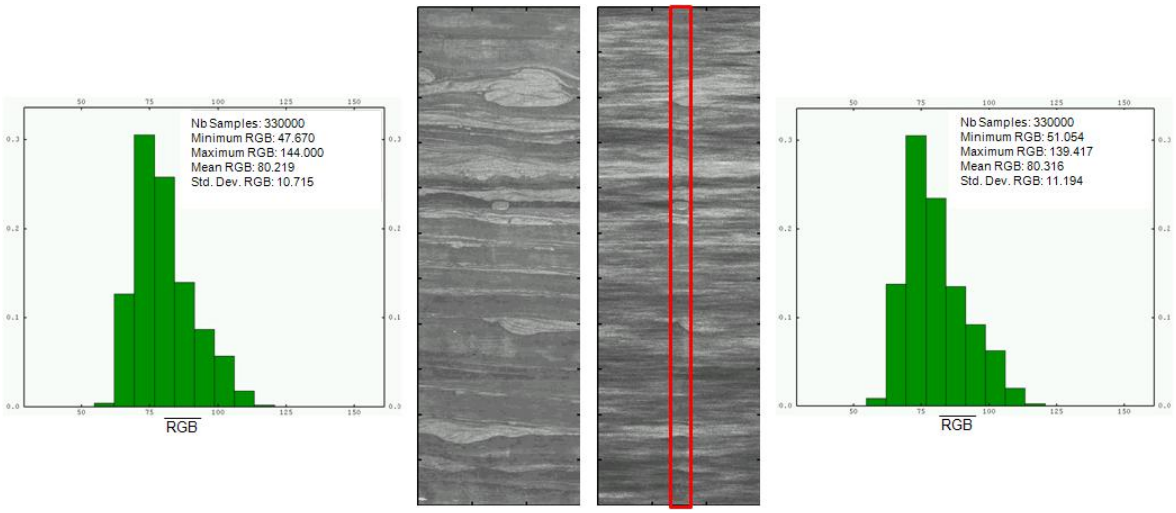

Figure 4.3: Result of qualitatively testing the simulation technique. The histograms show the original (left) and simulated (right) mean RGB distribution of the original (mid-left) and simulated (mid-right) images. The red rectangle indicates the preserved original part of the image in the simulated image.

The results of the calculations of coefficients of variation and connectivity probabilities in both horizontal and vertical direction have been plotted against the edge length of the model, which varies from 150, 300, 600 to 1000 mm for each mud content (Figure 4.5 and Figure 4.6). Table 4.2 and Table 4.3 provide an overview of the calculated coefficients of variation and connectivity probabilities for the individual model sizes and a cell size of 2 mm for 50% of mud content and 75% of mud content, respectively.

In the following the coefficient of variation and connectivity probability results for models with a mud content of 50% will be illustrated. The results of the 75% mud content simulations will be described afterwards briefly and only in relation to the 50% mud contents, as the 75% mud content run mainly serves for the assessment of the influence of mud content on the simulation results.

The following observations can be made for the respective structural classes:

- Laminated: High chance of horizontal connection, very low chance of vertical connection, general low variation in results, only little negative correlation of coefficient of variation on model edge length in vertical direction
- Lenticular: Mostly horizontally connected, very low chance of vertical connection, variation in horizontal results in only a few cases, no variation in vertical results, constant coefficients of variation with increasing model edge length

- Minor slumps: Mostly vertically sealed (zero to low connectivity probability), medium to high chance to be horizontally connected at small model edge lengths, low variation in vertical results, high variation in horizontal results, constant coefficient of variation with increasing model edge length in horizontal direction
- Major slumps: High variation in results, medium probability to be connected both horizontally and vertically, homogeneous coefficients of variation in vertical direction from 600 mm model edge length onwards for most models
- Small clasts: Good chance of horizontal connectivity at small model edge lengths (< 600 mm), low chance of vertical connectivity, generally high variation of horizontal results, variation of vertical results varies significantly itself, but approaches homogeneous coefficients of variation around 600 mm model edge length for most models
- Large clasts: Medium chance of vertical connectivity, high chance of horizontal connectivity, results are generally highly variable with constant coefficients of variation in horizontal direction and homogeneous coefficients of variation in vertical direction for half of the models

The simulations with mud contents of 75% have increasing C_{V_h} for laminated and lenticular structural models and decreasing C_{V_h} for the remaining structural types compared to models with a mud content of 50%. C_{V_v}, CP_h and CP_v are decreasing with increasing mud content for all structural classes. Also, most models reach a coefficient of variation below 0.5 at a model edge length of 600 mm.

On the basis of these results, the structural templates can be grouped, where they yield similar results. The resulting minimized number of structural templates can be used in studies where lithological variability is included (Chapter 5). Based on coefficients of variation and connectivity probabilities, we suggest further investigation of the following structural templates:

Laminated: Mod01, Mod03, Mod04

Lenticular: Mod05, Mod06, Mod07

Minor slumped: Mod10, Mod12, Mod14

Major slumped: Mod15, Mod16, Mod17, Mod18, Mod20

Small clasts: Mod21, Mod23, Mod25, Mod26

Large clasts: Mod28, Mod30, Mod27

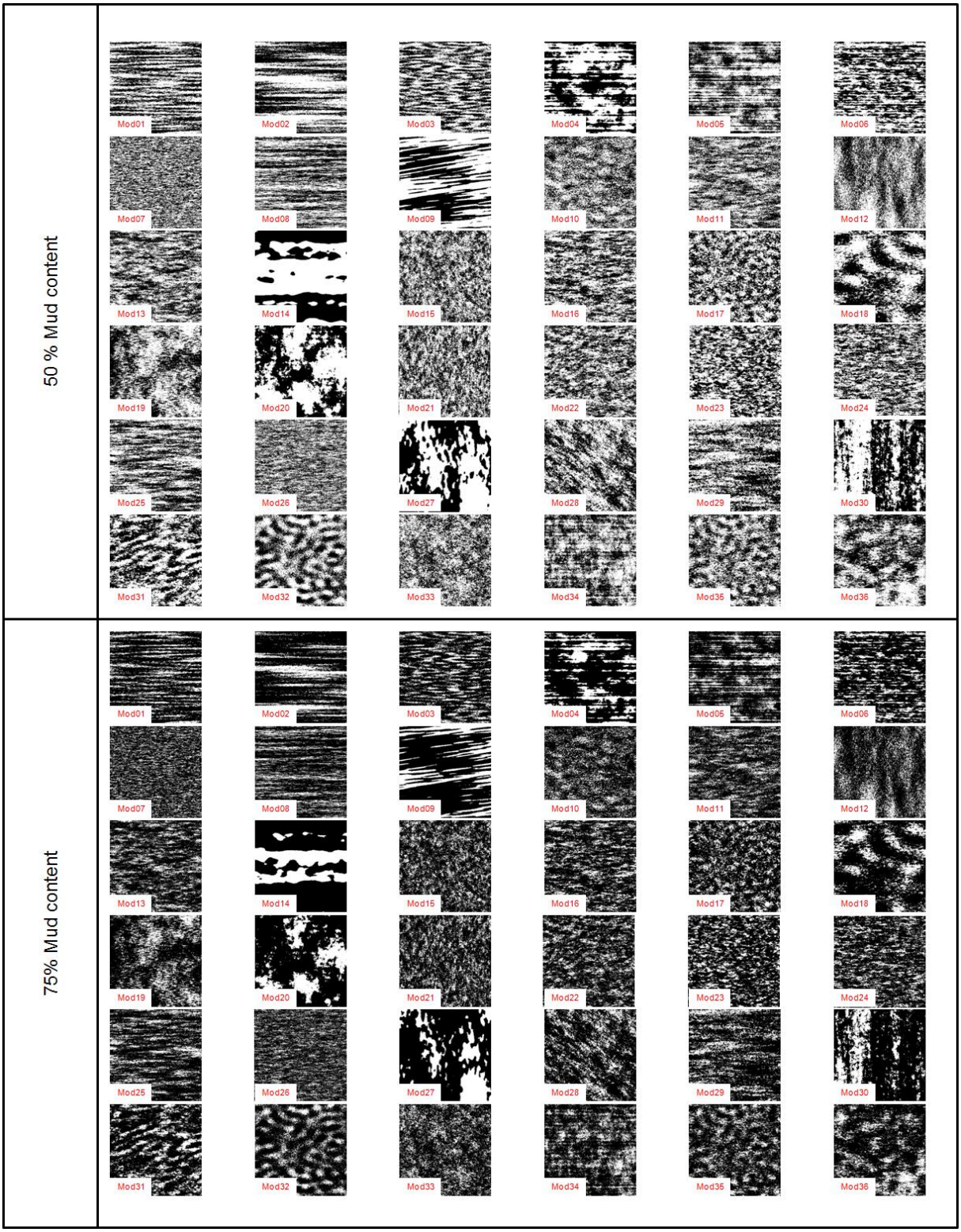

Figure 4.4: Example realisations of 600 mm x 600 mm permeability fields (white = 1nD; black = 1D) of each structural template for a mud content of 50% (top) and 75% mud content (bottom). The model ID is indicated in the lower left corner of each model and can be used to relate the images to the variogram and results Table 4.2 and Table 4.3. Models 1-9 represent different types of bedded structures from fine cm-scale lamination to large bed sets and ripples. Models 10-20 show chaotic structures, which can have relicts of primary orientation and structure or are completly overprinted by the mixing process (e.g. slumping, mass transport, deformation). The remaining models (21-36) incorporate different forms of clasts, which might have preffered orientations or are distributed completely randomly.

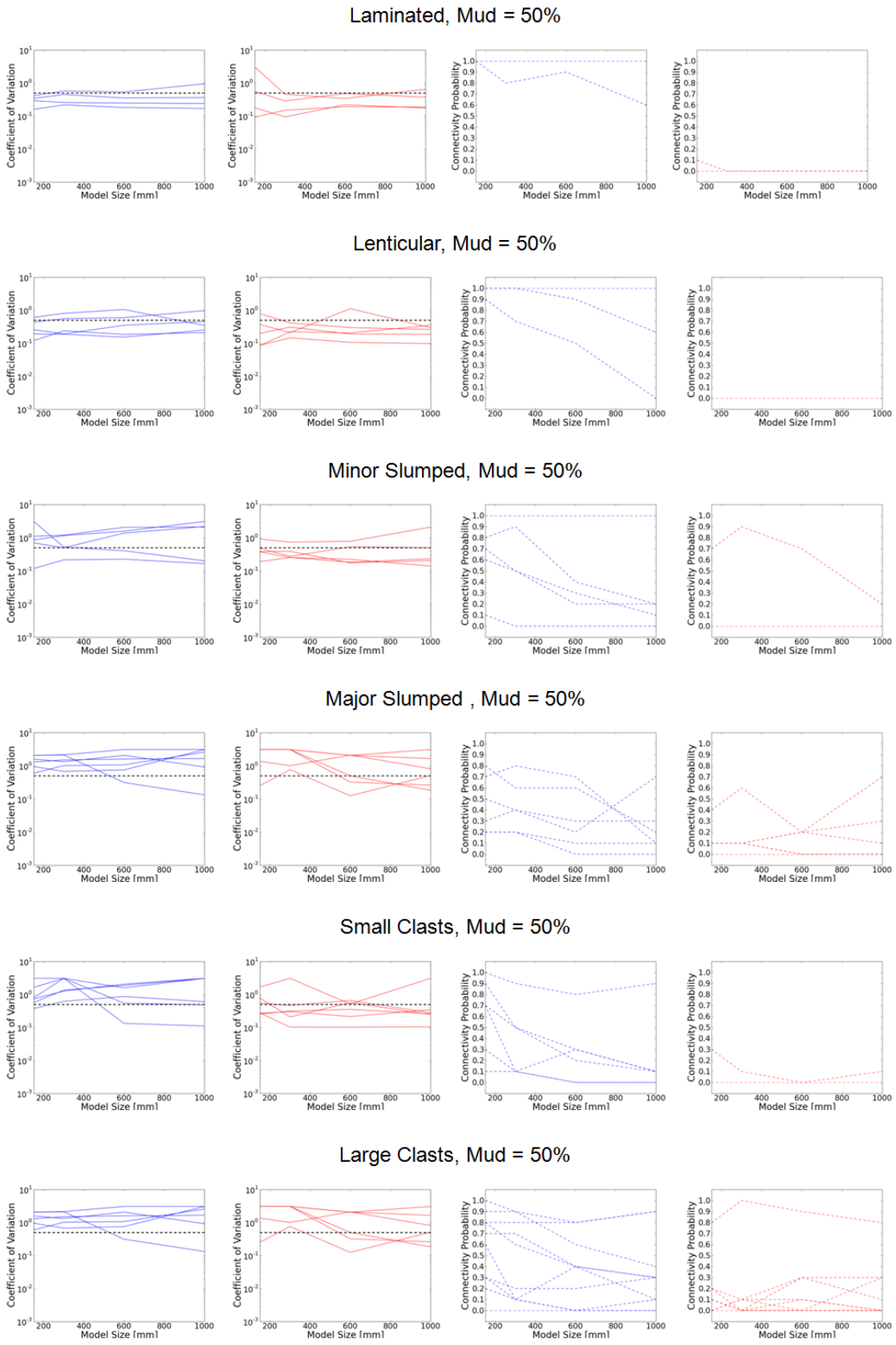

Figure 4.5: Coefficients of variation (straight lines) varying from 1e-3 to 1e+1 and connectivity probabilities (dotted lines) ranging from 0 to 1 in horizontal (blue) and vertical (red) directions at 50% of mud content as a function of model size (150, 300, 600 and 1000 mm) for each structural template and grouped after structural classes.

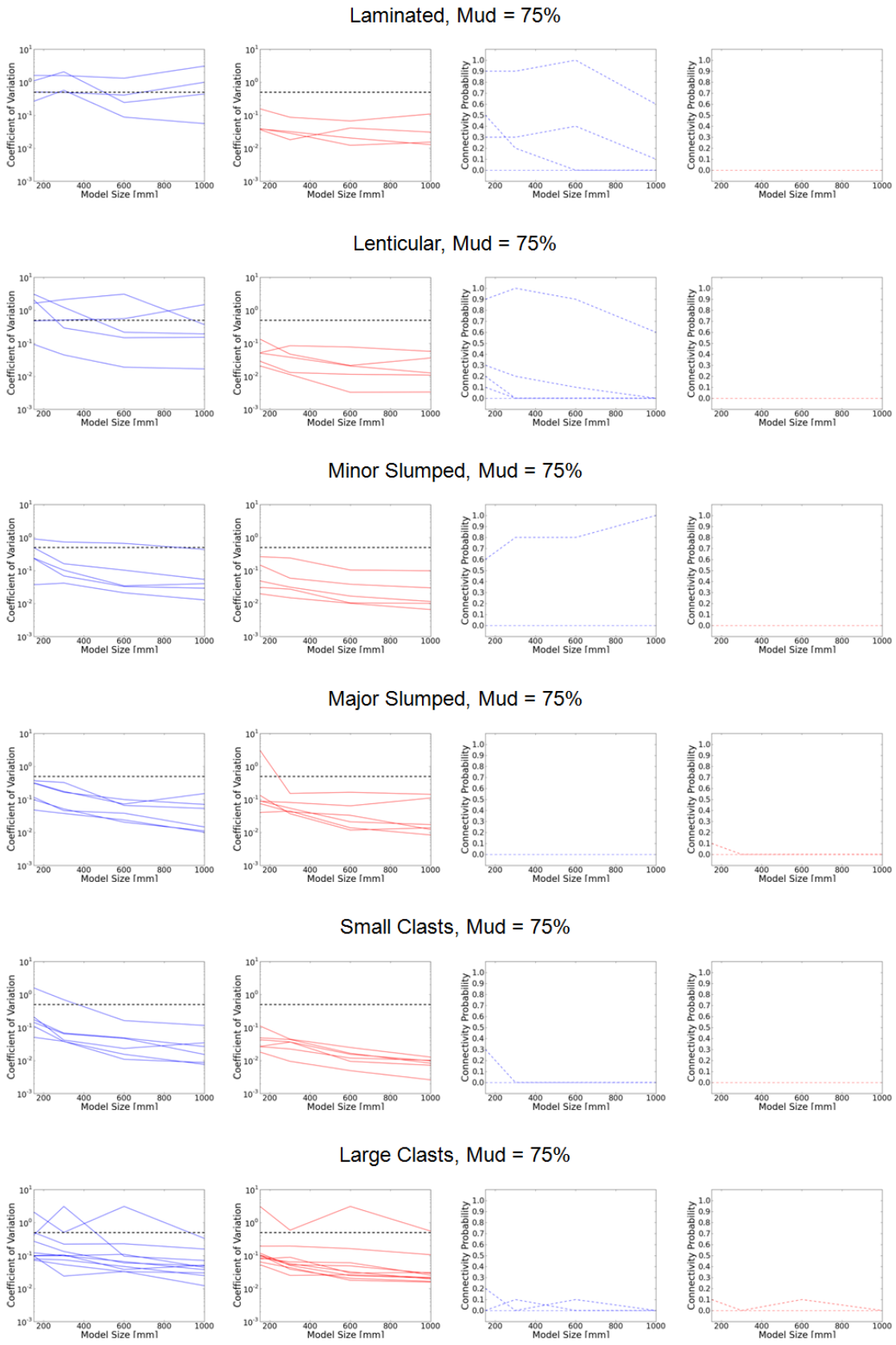

Figure 4.6: Coefficients of variation (straight lines) varying from 1e-3 to 1e+1 and connectivity probabilities (dotted lines) ranging from 0 to 1 in horizontal (blue) and vertical (red) directions at 75% of mud content as a function of model size (150, 300, 600 and 1000 mm) for each structural template and grouped after structural classes.

Table 4.2: Results data table together with basic geostatistical descriptions for 50% mud content. Hereby, coefficients of variation and connectivity probability results for each structural template were averaged from the respective geostatistical realisations. The table connects the results of this study with origin of the template (well, depth range, image type) and the visual and semi-quantitative interpretations (Chapter 3).

Template ID	Well	Image Type	Top [m]	Bottom [m]	Interval [m]	Structure	Variogram Type	Mud Content %	Cell Size [mm]	Model Edge Length: 150 mm				Model Edge Length: 300 mm				Model Edge Length: 600 mm				Model Edge Length: 1000 mm			
										CV_h	CV_v	CP_h	CP_v	CV_h	CV_v	CP_h	CP_v	CV_h	CV_v	CP_h	CP_v	CV_h	CV_v	CP_h	CP_v
Mod01	B24	Core	1935.23	1935.46	0.23	Laminated	Hor. Zonality	50	2	0.2929	0.1786	1.0	0.0	0.2566	0.0943	1.0	0.0	0.2478	0.2202	1.0	0.0	0.2403	0.1753	1.0	0.0
Mod02	B24	Core	1986.03	1986.44	0.40	Laminated	Hor. Zonality	50	2	0.1595	0.0929	1.0	0.0	0.2187	0.1498	1.0	0.0	0.1817	0.1919	1.0	0.0	0.1700	0.1864	1.0	0.0
Mod03	B22	Core	1722.29	1722.67	0.37	Laminated	Hor. Anisotropy	50	2	0.4119	0.5639	1.0	0.0	0.5750	0.2866	0.8	0.0	0.5363	0.4808	0.9	0.0	0.9508	0.3735	0.6	0.0
Mod04	B6	FMI	1634.00	1636.00	2.00	Laminated	Hor. Zonality	50	2	0.3444	3.0833	1.0	0.1	0.4473	0.4581	1.0	0.0	0.3538	0.3412	1.0	0.0	0.3638	0.6476	1.0	0.0
Mod05	B22	Core	1719.18	1719.69	0.52	Lenticular	Hor. Zonality	50	2	0.4401	0.7983	1.0	0.0	0.5567	0.4123	1.0	0.0	0.5975	0.2995	0.9	0.0	0.9763	0.2613	0.6	0.0
Mod06	B24	Core	1991.16	1991.48	0.32	Lenticular	Hor. Zonality	50	2	0.2569	0.3682	1.0	0.0	0.1921	0.2112	1.0	0.0	0.3510	1.1125	1.0	0.0	0.4555	0.2979	1.0	0.0
Mod07	B22	Core	1712.04	1712.23	0.19	Lenticular	Hor. Anisotropy	50	2	0.6091	0.2006	0.9	0.0	0.8073	0.3085	0.7	0.0	1.0499	0.1905	0.5	0.0	0.3476	0.1864	0.0	0.0
Mod08	B22	Core	1717.19	1717.62	0.43	Lenticular	Hor. Anisotropy	50	2	0.1905	0.0863	1.0	0.0	0.1885	0.1470	1.0	0.0	0.1531	0.1060	1.0	0.0	0.2510	0.0980	1.0	0.0
Mod09	B6	FMI	1896.00	1898.00	2.00	Lenticular	Hor. Anisotropy	50	2	0.1200	0.0847	1.0	0.0	0.2396	0.2231	1.0	0.0	0.1857	0.2056	1.0	0.0	0.2102	0.3515	1.0	0.0
Mod10	B24	Core	2085.39	2085.57	0.17	Minor Slumped	Isotropic	50	2	0.8590	0.4815	0.7	0.0	1.1582	0.2731	0.5	0.0	1.5759	0.5336	0.3	0.0	3.0830	0.4979	0.1	0.0
Mod11	B24	Core	2085.59	2085.69	0.10	Minor Slumped	Hor. Zonality	50	2	1.1083	0.1907	0.6	0.0	1.1893	0.2524	0.5	0.0	2.0631	0.2238	0.2	0.0	2.1029	0.1399	0.2	0.0
Mod12	B20	Core	1651.26	1651.40	0.14	Minor Slumped	Vert. Zonality	50	2	3.0833	0.9126	0.1	0.7	0.5228	0.7388	0.0	0.9	0.4047	0.7810	0.0	0.7	0.2014	2.0893	0.0	0.2
Mod13	B20	Core	1641.39	1641.69	0.30	Minor Slumped	Hor. Anisotropy	50	2	0.6957	0.3808	0.8	0.0	0.4986	0.3889	0.9	0.0	1.3831	0.1747	0.4	0.0	2.1725	0.2061	0.2	0.0
Mod14	B6	FMI	1589.00	1590.70	1.70	Minor Slumped	Hor. Anisotropy	50	2	0.1178	0.3752	1.0	0.0	0.2154	0.2534	1.0	0.0	0.2256	0.1830	1.0	0.0	0.1662	0.2339	1.0	0.0
Mod15	B19	Core	1635.03	1635.49	0.46	Major Slumped	Isotropic	50	2	2.0575	3.0833	0.2	0.1	2.1145	3.0833	0.2	0.1	0.3131	0.3216	0.0	0.0	0.1325	0.2617	0.0	0.0
Mod16	B20	Core	1682.34	1682.52	0.17	Major Slumped	Hor. Zonality	50	2	0.9514	0.2516	0.7	0.0	0.6757	0.7612	0.8	0.0	0.7512	0.1250	0.7	0.0	3.0831	0.5103	0.1	0.0
Mod17	B24	Core	2002.51	2002.68	0.17	Major Slumped	Vert. Zonality	50	2	2.0621	3.0833	0.2	0.1	2.1462	3.0833	0.2	0.1	3.0831	0.4986	0.1	0.0	3.0830	0.1832	0.1	0.0
Mod18	B19	Core	1716.06	1716.43	0.37	Major Slumped	Hor. Anisotropy	50	2	0.5988	3.0833	0.8	0.1	1.0173	3.0833	0.6	0.1	1.0686	2.0577	0.6	0.2	2.5774	1.6523	0.2	0.3
Mod19	B20	Core	1682.03	1682.11	0.09	Major Slumped	Hor. Anisotropy	50	2	1.2987	3.0833	0.5	0.1	1.5039	3.0833	0.4	0.1	1.5980	2.0591	0.3	0.2	1.6608	3.0832	0.3	0.1
Mod20	B6	FMI	1585.00	1587.00	2.00	Major Slumped	Vert. Anisotropy	50	2	1.5880	1.3575	0.3	0.4	1.3254	1.0066	0.4	0.6	2.0632	2.1020	0.2	0.2	0.9196	0.8140	0.7	0.7
Mod21	B22	Core	1718.10	1718.22	0.12	Small Clasts	Isotropic	50	2	3.0833	1.6816	0.1	0.3	3.0833	3.0833	0.1	0.1	0.5415	0.5119	0.0	0.0	0.4896	3.0831	0.0	0.1
Mod22	B24	Core	1964.08	1964.20	0.12	Small Clasts	Hor. Zonality	50	2	0.7966	0.2708	0.7	0.0	3.0833	3.0013	0.1	0.0	1.5907	0.2144	0.3	0.0	3.0831	0.3453	0.1	0.0
Mod23	B22	Core	2437.02	2437.13	0.12	Small Clasts	Hor. Anisotropy	50	2	0.7327	0.5511	0.7	0.0	1.2683	0.4682	0.5	0.0	2.0640	0.6567	0.2	0.0	3.0830	0.2792	0.1	0.0
Mod24	B22	Core	2438.39	2438.57	0.17	Small Clasts	Hor. Anisotropy	50	2	0.5696	0.7777	0.9	0.0	1.3531	0.2077	0.5	0.0	1.8728	0.5695	0.3	0.0	3.0827	0.2468	0.1	0.0
Mod25	B19	Core	1619.30	1619.39	0.09	Small Clasts	Hor. Zonality	50	2	0.3722	0.2556	1.0	0.0	0.6212	0.3132	0.9	0.0	0.8684	0.3533	0.8	0.0	0.6042	0.2605	0.9	0.0
Mod26	B19	Core	1618.51	1618.63	0.12	Small Clasts	Hor. Anisotropy	50	2	1.6378	0.2754	0.3	0.0	3.0832	0.1027	0.1	0.0	0.1329	0.1020	0.0	0.0	0.1114	0.1049	0.0	0.0
Mod27	B6	FMI	1604.00	1606.00	2.00	Large Clasts	Vert. Anisotropy	50	2	0.6703	0.3069	0.8	0.0	0.6262	3.0833	0.8	0.1	0.6820	1.5987	0.8	0.3	0.5067	1.6159	0.9	0.3
Mod28	B19	Core	1697.45	1697.57	0.12	Large Clasts	Isotropic	50	2	1.6327	3.0833	0.3	0.1	2.2025	0.3579	0.2	0.0	2.0592	1.5839	0.2	0.3	1.6226	3.0832	0.3	0.1
Mod29	B19	Core	1651.40	1651.49	0.09	Large Clasts	Hor. Zonality	50	2	0.4746	0.1660	0.9	0.0	0.5277	0.3265	0.9	0.0	0.9421	0.2148	0.8	0.0	0.7315	0.4587	0.9	0.0
Mod30	B20	Core	1658.14	1658.40	0.26	Large Clasts	Vert. Zonality	50	2	0.6286	0.6659	0.0	0.8	0.1336	0.3298	0.0	1.0	0.6407	0.6408	0.0	0.9	0.3521	0.6805	0.0	0.8
Mod31	B19	Core	1634.08	1634.20	0.12	Large Clasts	Hor. Anisotropy	50	2	0.7345	0.4074	0.8	0.0	0.9356	3.0833	0.6	0.1	1.2771	0.3871	0.4	0.0	1.5853	0.6302	0.3	0.0
Mod32	B20	Core	1720.17	1720.40	0.23	Large Clasts	Vert. Anisotropy	50	2	1.5847	2.4750	0.3	0.2	3.0833	3.0833	0.1	0.1	0.4120	3.0833	0.0	0.1	3.0831	0.2207	0.1	0.0
Mod33	B19	Core	1699.18	1699.32	0.14	Large Clasts	Isotropic	50	2	2.1001	3.0833	0.2	0.1	3.0833	0.2794	0.1	0.0	0.5251	0.5672	0.0	0.0	0.3742	0.3492	0.0	0.0
Mod34	B24	Core	1997.21	1997.41	0.20	Large Clasts	Hor. Zonality	50	2	0.7781	3.0833	0.7	0.1	0.7999	0.4564	0.7	0.0	1.3671	3.0833	0.4	0.1	1.5862	0.3574	0.3	0.0
Mod35	B24	Core	2062.42	2062.68	0.26	Large Clasts	Vert. Zonality	50	2	0.9678	2.1441	0.6	0.2	3.0833	0.5875	0.1	0.0	1.2699	0.7914	0.4	0.0	3.0831	0.2073	0.1	0.0
Mod36	B19	Core	1691.55	1691.70	0.14	Large Clasts	Hor. Anisotropy	50	2	0.4424	3.0833	1.0	0.1	0.7272	0.4072	0.9	0.0	1.2897	0.4175	0.6	0.0	1.3560	1.5885	0.4	0.3

Table 4.3: Results data table together with basic geostatistical descriptions for 50% mud content. Hereby, coefficients of variation and connectivity probability results for each structural template were averaged from the respective geostatistical realisations. The table connects the results of this study with origin of the template (well, depth range, image type) and the visual and semi-quantitative interpretations (Chapter 3).

Well	Image Type	Top [m]	Bottom [m]	Interval [m]	Structure	Variogram Type	Mod1	Rh1 [cm]	Rv1 [cm]	S1	Ang1	Mod2	Rh2 [cm]	Rv2 [cm]	S2	Ang2	Mod3	Rh3 [cm]	Rv3 [cm]	S3	Ang3
B24	Core	1935.23	1935.46	0.23	Laminated	Hor. Zonality	exp	2.02	0.29	0.40	90.00	sin	115.20	5.76	0.50	90.00	None	None	None	None	None
B24	Core	1986.03	1986.44	0.40	Laminated	Hor. Zonality	exp	0.86	0.14	0.14	90.00	exp	86.40	2.88	0.50	90.00	sin	288.00	23.04	0.36	90.00
B22	Core	1722.29	1722.67	0.37	Laminated	Hor. Anisotropy	exp	1.15	0.14	0.40	90.00	sin	37.44	5.76	0.50	90.00	None	None	None	None	None
B22	Core	1719.18	1719.69	0.52	Lenticular	Hor. Zonality	exp	0.58	0.03	0.25	90.00	exp	11.52	8.64	0.35	90.00	sin	288.00	2.88	0.40	90.00
B24	Core	1991.16	1991.48	0.32	Lenticular	Hor. Zonality	exp	4.32	1.44	0.70	90.00	sin	288.00	4.32	0.30	90.00	None	None	None	None	None
B22	Core	1712.04	1712.23	0.19	Lenticular	Hor. Anisotropy	exp	2.16	0.29	0.96	90.00	sin	28.80	2.16	0.04	90.00	None	None	None	None	None
B22	Core	1717.19	1717.62	0.43	Lenticular	Hor. Anisotropy	exp	7.20	0.29	0.60	90.00	sin	288.00	8.64	0.30	90.00	nug	0.00	0.00	0.10	90.00
B24	Core	2085.39	2085.57	0.17	Minor Slumped	Isotropic	exp	1.15	0.29	0.70	90.00	gau	6.34	3.46	0.20	90.00	sin	4.32	2.88	0.10	90.00
B24	Core	2085.59	2085.69	0.10	Minor Slumped	Hor. Zonality	exp	0.43	0.14	0.60	90.00	exp	10.08	2.16	0.40	90.00	None	None	None	None	None
B20	Core	1651.26	1651.40	0.14	Minor Slumped	Vert. Zonality	exp	0.49	0.58	0.75	90.00	gau	5.76	17.28	0.25	90.00	None	None	None	None	None
B20	Core	1641.39	1641.69	0.30	Minor Slumped	Hor. Anisotropy	exp	0.29	0.29	0.40	90.00	exp	7.78	2.02	0.58	90.00	None	None	None	None	None
B19	Core	1635.03	1635.49	0.46	Major Slumped	Isotropic	exp	0.58	0.29	0.30	90.00	exp	3.46	2.88	0.25	170.00	None	None	None	None	None
B20	Core	1682.34	1682.52	0.17	Major Slumped	Hor. Zonality	exp	0.58	0.43	0.40	90.00	exp	6.91	1.73	0.60	90.00	None	None	None	None	None
B24	Core	2002.51	2002.68	0.17	Major Slumped	Vert. Zonality	exp	1.15	0.86	0.80	90.00	sin	21.60	15.84	0.20	90.00	None	None	None	None	None
B19	Core	1716.06	1716.43	0.37	Major Slumped	Hor. Anisotropy	exp	1.73	0.86	0.45	90.00	sin	57.60	34.56	0.55	90.00	None	None	None	None	None
B20	Core	1682.03	1682.11	0.09	Major Slumped	Hor. Anisotropy	exp	0.86	0.29	0.50	90.00	exp	17.28	17.28	0.50	90.00	sin	14.40	2.88	0.20	90.00
B22	Core	1718.10	1718.22	0.12	Small Clasts	Isotropic	exp	0.86	0.29	0.50	90.00	exp	1.73	3.46	0.50	90.00	None	None	None	None	None
B24	Core	1964.08	1964.20	0.12	Small Clasts	Hor. Zonality	exp	0.58	0.29	0.40	90.00	exp	4.03	1.73	0.53	90.00	None	None	None	None	None
B22	Core	2437.02	2437.13	0.12	Small Clasts	Hor. Anisotropy	exp	2.88	1.15	1.00	90.00	None	None	None	None	None	None	None	None	None	None
B22	Core	2438.39	2438.57	0.17	Small Clasts	Hor. Anisotropy	exp	0.58	0.58	0.30	90.00	exp	4.61	1.15	0.70	90.00	None	None	None	None	None
B19	Core	1619.30	1619.39	0.09	Small Clasts	Hor. Zonality	exp	0.58	0.29	0.45	90.00	exp	16.56	2.02	0.55	90.00	None	None	None	None	None
B19	Core	1618.51	1618.63	0.12	Small Clasts	Hor. Anisotropy	exp	0.29	0.09	0.60	90.00	exp	4.32	0.86	0.40	90.00	None	None	None	None	None
B19	Core	1697.45	1697.57	0.12	Large Clasts	Isotropic	exp	0.58	0.58	0.50	90.00	exp	11.52	4.32	0.50	125.00	None	None	None	None	None
B19	Core	1651.40	1651.49	0.09	Large Clasts	Hor. Zonality	exp	0.86	0.58	0.55	90.00	exp	31.68	4.32	0.45	90.00	None	None	None	None	None
B20	Core	1658.14	1658.40	0.26	Large Clasts	Vert. Zonality	exp	2.88	2.88	0.40	90.00	exp	11.52	86.40	0.60	90.00	None	None	None	None	None
B19	Core	1634.08	1634.20	0.12	Large Clasts	Hor. Anisotropy	exp	1.73	0.86	0.60	90.00	sin	43.20	12.96	0.40	73.00	None	None	None	None	None
B20	Core	1720.17	1720.40	0.23	Large Clasts	Vert. Anisotropy	exp	0.43	0.43	0.50	90.00	sin	25.92	17.28	0.50	90.00	None	None	None	None	None
B19	Core	1699.18	1699.32	0.14	Large Clasts	Isotropic	exp	0.86	0.43	0.75	90.00	exp	7.78	7.78	0.25	90.00	None	None	None	None	None
B24	Core	1997.21	1997.41	0.20	Large Clasts	Hor. Zonality	exp	0.58	0.29	0.50	90.00	exp	5.76	8.64	0.35	90.00	sin	288.00	5.76	0.15	90.00
B24	Core	2062.42	2062.68	0.26	Large Clasts	Vert. Zonality	exp	1.15	0.43	0.70	90.00	sin	23.04	18.72	0.30	90.00	None	None	None	None	None
B19	Core	1691.55	1691.70	0.14	Large Clasts	Hor. Anisotropy	exp	1.44	0.43	0.60	90.00	exp	11.52	4.32	0.20	90.00	gau	7.20	7.20	0.30	90.00
B6	Borehole	1634.00	1636.00	2.00	Laminated	Hor. Zonality	sin	1000.00	13.68	0.65	90.00	cub	300.00	70.72	0.35	90.00	None	None	None	None	None
B6	Borehole	1896.00	1898.00	2.00	Lenticular	Hor. Anisptropy	sph	36.00	72.00	0.33	90.00	cub	144.00	1.20	0.33	65.00	cub	144.00	1.20	0.33	95.00
B6	Borehole	1589.00	1590.70	1.70	Minor Slumped	Hor. Anisotropy	exp	24.00	12.00	0.17	90.00	gau	168.00	8.40	0.42	105.00	gau	19.20	19.20	0.42	90.00
B6	Borehole	1585.00	1587.00	2.00	Major Slumped	Vert. Anisotropy	exp	6.00	13.90	1.00	90.00	None	None	None	None	None	None	None	None	None	None
B6	Borehole	1604.00	1606.00	2.00	Large Clasts	Vert. Anisotropy	cub	1.80	40.56	0.30	90.00	cub	13.40	19.20	0.59	90.00	cub	3.40	8.40	0.11	90.00

A general trend of decreasing coefficients of variation with increasing model domain size can only be observed for some models, but becomes more prominent, when averaging the results by structure (Figure 4.7). Hereby, it becomes obvious, that for most structural classes, the representative model size is not reached on the sub-metre scale at 50% mud contents. Thus, the probability of connectivity provides valuable additional information of uncertainty of each structural class. Generally, the connectivity probability is decreasing with increasing mud content and model edge length. At 75% mud content vertical connectivity probability is close to zero. Hereby it is important, that these results about connectivity only give an idea about possible percolation thresholds. The question, if these heterogeneous mudstone types provide reliable low permeability rocks at mud contents of 75% can only be answered, if lithological and thus petrophysical (grain size, porosity and permeability) variability is taken into account. Usually, the variability increases, when petrophysical variability is included (Norris and Lewis, 1991).

In order to evaluate the influence of model cell size on the results, we calculated mean connectivity probabilities in horizontal and vertical directions from all geostatistical realizations of all structural templates for each tested cell size (2 mm, 5 mm and 10 mm). In the horizontal direction both the mean and standard deviation of the connectivity probability display a significant negative slope, while in the vertical direction a slightly negative slope is only visible for the standard deviation. The vertical horizontal mean connectivity probability stays constant with respect to the cell size (Figure 4.8).

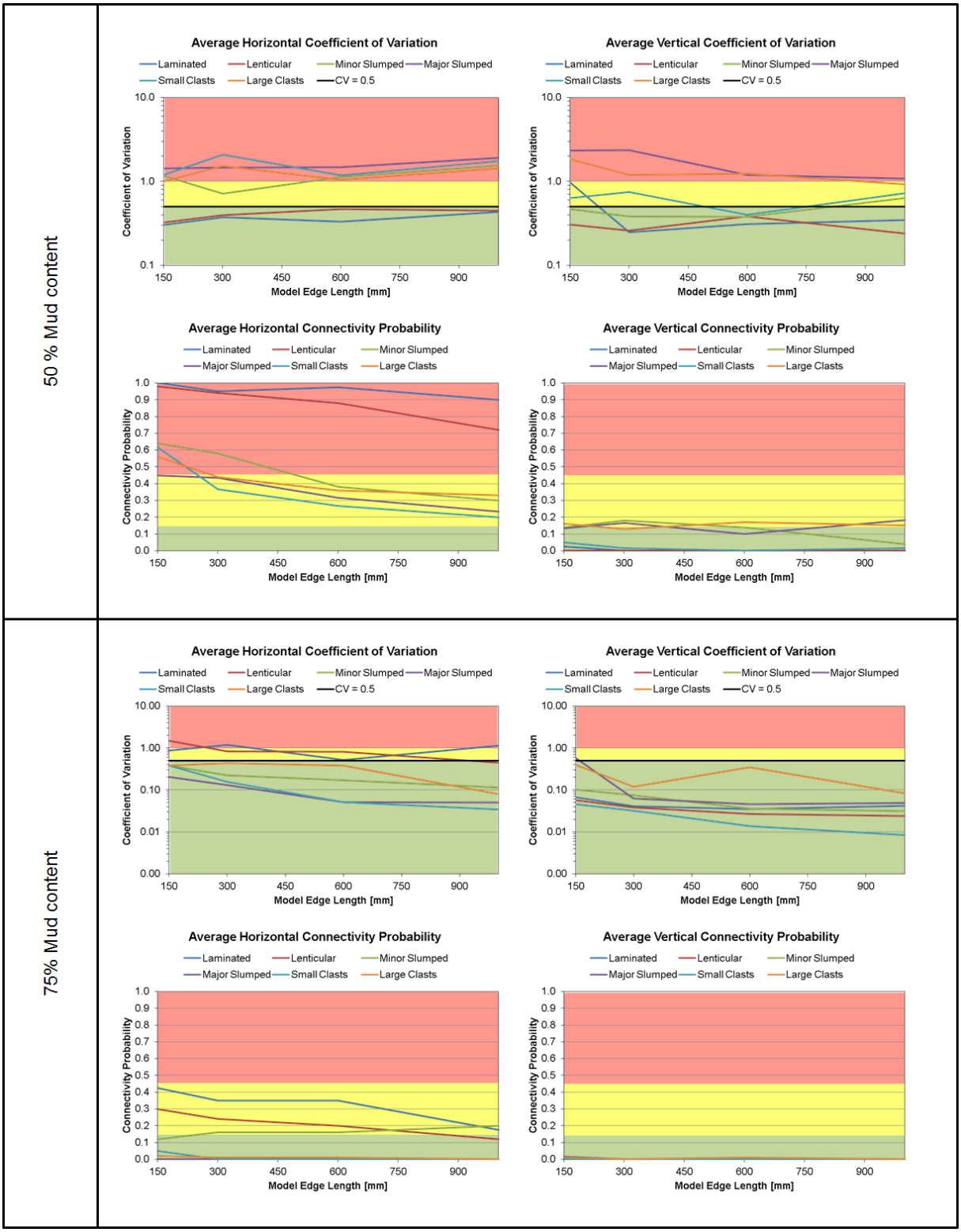

Figure 4.7: Structurally averaged coefficients of variation and connectivity probabilities in horizontal (left) and vertical (right) directions for 50% (top) and 75% (bottom) mud contents. The background colours indicate the coefficient of variation classes (green: homogeneous, yellow: heterogeneous, red: very heterogeneous) after Corbett and Jensen (1992) and the connectivity probability classes (green: low, yellow: medium, red: high).

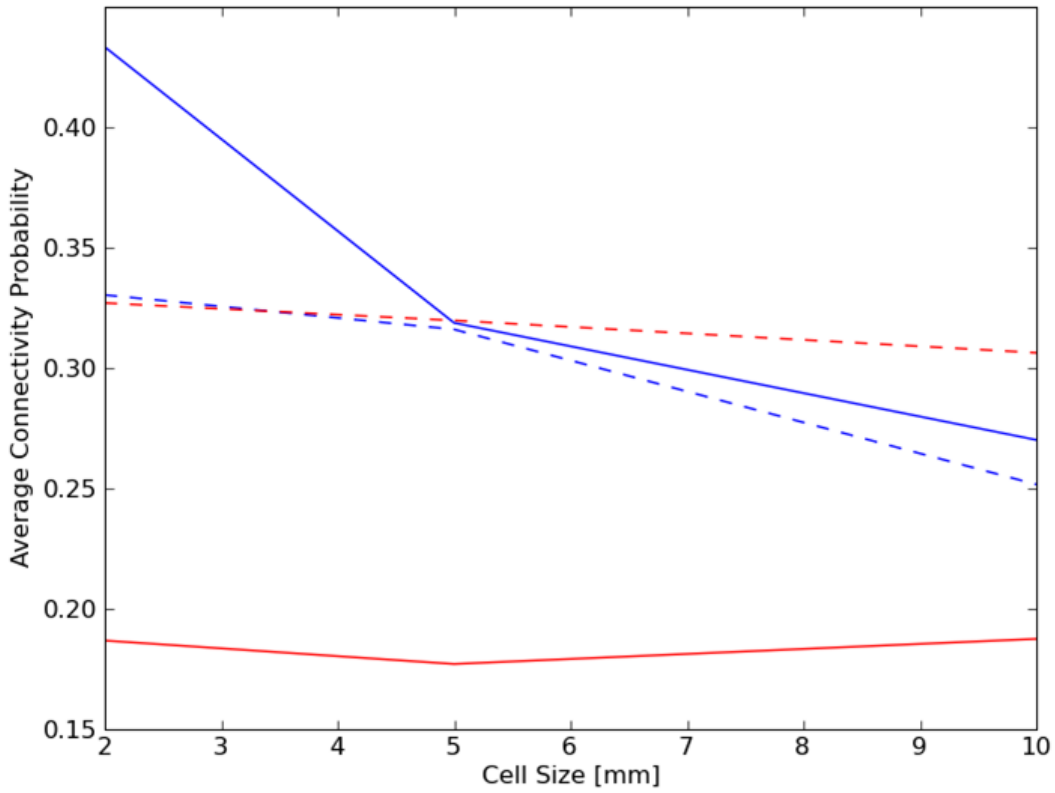

Figure 4.8: Mean (straight lines) and standard deviation (dotted lines) of horizontal (blue lines) and vertical (red lines) average connectivity probabilities of all geostatistical realizations of all structural templates as a function of cell size.

Discussion

Shales and mudstones have been mainly investigated on sample scale (centimetre-scale) for their physical properties in the past. However, heterogeneity can have significant influence upon effective rock properties (e.g. Weber, 1982). In most cases, and in particular in case of permeability evaluation, effective properties are calculated using numerical simulation (e.g. Renard and de Marsily, 1997). A common issue to overcome, when using numerical simulation is to choose the size of the numerical model in such a way, that it yields representative, reliable, stable results. Thus, the model size should represent the heterogeneity with respect to the investigated property and fulfil the requirements of a representative elementary volume (REV) or domain (Bear, 1972). Many studies have addressed the problem of REV estimation, mainly in relation to fractured rocks, carbonates or heterogeneous sandstones (e.g. Nordahl and Ringrose, 2008), as those were - and still are - of major economical and environmental interest. The role of shales and mudstones becomes increasingly important. Shale gas, drilling in overpressured petroleum systems and advanced

modelling of groundwater contamination are only some prominent examples. This increasing interest in shales and mudstones makes it necessary to study their heterogeneities and their influence on fluid flow, which is crucial for safe and successful hydrocarbon recovery and groundwater contamination predictions and investigations. Estimating the representative elementary domain for sub-metre scale shale and mudstone heterogeneity is therefore a vital step towards reliable flow modelling in sedimentary basins containing heterogeneous shales and mudstones.

We used a careful selected set of core and borehole images as templates to model sub-metre scale heterogeneous shales and mudstones and to evaluate representative model sizes and resolution, or a measure of uncertainty, where a representative elementary domain could not be obtained. Thereby, the coefficient of variation is a good measure to evaluate a representative size of an effective medium. However, in many cases the approach of an representative size for an effective medium might not be applicable, mainly due to two reasons. First, the representative size might be at a scale, which is not covered by any measurement in the field and/or laboratory. Second, the approach assumes a continuous or infinite medium, which, in geological systems, cannot always be guaranteed. Both cases have been observed in this study in particular for the structural classes “chaotic” and “clasts” at low mud contents (50%). In classical modelling approaches sample scale (centimetre-scale) measurements are upscaled by calculation of an effective property using numerical simulation. The effective property is then used as the property of a cell in a model representing the next larger scale. Hereby, the model dimensions should always by far exceed the correlation lengths to ensure robust results and to be in line with the rules of the classic continuum approach (Sahimi, 1995). By doing so, the cell size is usually chosen to be of the size of the previously evaluated representative domain (or REV). However, this implies that all occurrences of a certain structure appear at the size and scale of the respective representative scale (effective medium), which violates the principle that geological discontinuities might appear. Another way to upscale a property would be the combination of a probability density function (PDF) of the size of a certain structure with its PDF of the property of interest as a function of (cell) size (compare Durlofsky, 1991 and Pickup et al. 1994 on fluctuating boundary conditions). This technique requires a detailed investigation of the scales at which certain structures occur, which has been found to be between 300 mm and 700 mm on an average basis for shales and mudstones (Chapter 3). As we have shown that effective properties of mud-rich heterogeneous sediments might be variable at the scale of

measurement (e.g. wire line logs), we suggest a probabilistic upscaling method, rather than an effective medium upscaling with fixed element sizes and boundaries.

Despite, the significant influence of the size of the domain of interest (model) on effective permeability, a general trend of a decreasing coefficient of variation with increasing model size can only be observed in our study, when averaging the results per structure. Probably, this is related to the ratio between the average correlation lengths used in the geostatistical simulations and the domain sizes of some models. Nordahl and Ringrose (2008) found a general representative elementary volume for bedded around 5000 cm3, which corresponds to a model edge length of approximately 170 mm. All of our bedded structures display a coefficient of variation < 0.5 in vertical and horizontal direction at a model edge length between 150 mm and 300 mm, suggesting a representative size reached at a model edge length of 150-300 mm, which fits with the REV evaluated by Nordahl and Ringrose (2008).

We take this coincidence as encouragement to trust the results related to other heterogeneities investigated in our study. Furthermore, Nordahl and Ringrose (2008) found an increase of the horizontal coefficient of variation for their 3D models of tidal bedded, with increasing mud content. The same trend can be observed for our bedded type models, indicating a horizontal percolation threshold for bedded structures at mud contents well above 50%. However, for more chaotic structures (slumps and clasts) this trend cannot be confirmed, which is probably related to the smaller correlation length these structures involve, yielding generally lower horizontal connectivity probabilities compared to bedded structures.

Determining representative model sizes on the basis of the coefficient of variation for chaotic and clasts bearing mudstones has been not as unambiguous as for bedded structures. Although we would prefer probabilistic upscaling for heterogeneous shales and mudstones, we would like to suggest, as a general recommendation, to conduct further investigations of the studied shale and mudstone heterogeneities at a model edge length of 600 mm, as this size most corresponds to average interval sizes of heterogeneous shales and mudstones (Chapter 3) and yielded either coefficient of variation minima or coefficients of variation below 0.5 for most structural templates.

Moreover, the coefficient of variation and the connectivity probability might be good measures to select stable and unstable models at appropriate scales and to group models with similar connectivity probability for more advanced flow modelling (e.g. by implementing petrophysical and lithological variability). Based on these two measures it was possible to derive general trends of uncertainty and connectivity typical for the respective mudstone heterogeneities. The resulting trends are not of surprising nature, but this study quantifies the

proportional relation between uncertainty and structural complexity (either due to depositional energy or increase of secondary structures) and connectivity and structural complexity. The connectivity probability could also be read as an estimator of seal risk in petroleum or storage (CO_2, nuclear waste) systems, which have heterogeneous, mud-rich seal sections.

The significant slope of the mean and standard deviation of the averaged horizontal connectivity probability indicates an influence of the cell size on the simulated results. Thus, it seems appropriate to conduct more detailed future numerical calculations using a small cell size (2 mm). A resolution of 2 mm also honours the smallest used correlation length (range) of the nested covariance functions used for the geostatistical simulation. The smallest range used is 3 mm and covers best (but not fully) the resolution of the covariance functions (that is the scale at which the used covariance ranges differ), which is approximately 1 mm. Thus, the coarser resolutions of 5 and 10 mm would miss this scale of heterogeneity, which could be an explanation for the significant slope of the mean and standard deviation of the averaged horizontal connectivity probability. However, a cell size of 2 mm might be too small to represent sandstone sections in a model, as sand grain size might well reach the millimetre-scale. However, in this thesis we are using petrophysical sandstone data based on an aggregate with an average grain size of approximately 700 µm (Chapters 2 and 5). A finer resolution (e.g. of 1 mm) therefore would not be appropriate.

For reasons of computing time and the absence of a data source providing insights into the third spatial dimension, we decided to use 2D flow models. The third dimension is difficult to extract from image data and only assumptions could have been made. For ideal bedded structures, 2D models should give an answer close to models implementing the third dimension. However, in geometrically more complex models, 3D models can give a more accurate picture of the fluid flow through heterogeneous rocks. For example, this has been observed in the field of fluid migration modelling at basin-scale (e.g. Schneider et al., 2000). However, it has to be proven and should be object of future studies, if three dimensional models indeed yield different results and additional information about flow in heterogeneous shales and mudstones. Additionally, the method used to obtain effective permeabilities is based on numerical single phase Darcy flow simulation (Ma et al., 2006). Employment of other methods, such as percolation theory (e.g. Begg and King 1985), might yield differing results. This is also valid for simulations accounting for multi-phase flow (e.g. Pickup et al., 2000). The presented work should thus be understood as a starting point for understanding shale and mudstone heterogeneity from a fluid flow point of view using numerical methods.

Modelling of shale and mudstone heterogeneity has been conducted on detailed geostatistical analysis (variography) and simulation. Variography is easy to employ and has been used in several studies to successfully describe geological structures in relation to spatial flow property distributions (Jensen et al., 1996; McKinley et al., 2004). We showed the turning bands simulation algorithm (Emery and Lantuejoul, 2006) to be a fast and reliable simulation technique. In order to include discrete objects with sharp boundaries (e.g. burrows etc.) a post-simulation indicator technique has been applied with success (compare Marsily et al., 2005 for further reading on geostatistical indicator modelling). However, in some cases (in particular for the structural group clasts), an object-based modelling approach (Haldorsen and Chang, 1986) or multiple point statistics (e.g. Caers and Zhang, 2004) might yield more realistic results. In addition, fractal scaling methods provide an approach to model and describe geological heterogeneity (e.g. Chiles, 1988; Caniego et al., 2005; compare Molz et al., 2004 for a detailed review). This can be in particular useful to detect and simulate self-similar features and structures through different scales. In a multifractal approach these scaling properties are summarized by the multifractal spectrum. As the self-similarity opposed through fractals implies scale invariance, their correlation structure could be described by a power law covariance function in geostatistical terms (e.g. Molz et al., 2004; Eaton, 2006). In summary it can be said that for a large set of heterogeneities to be simulated the simulation technique used in this study provides a very good tool to capture and reproduce the main heterogeneities of mudstones in an economical (fast) way.

Conclusions

36 templates of 6 heterogeneous mudstone types were reproduced in 2D using geostatistical simulation. The studied heterogeneities range from continuous lamination, flaser bedding, slumping and deformation to brecciated clasts bearing mudstones, bioturbation and sand injections. We qualitatively showed that detailed variography combined with geostatistical simulation can realistically reproduce sub-metre scale heterogeneities in shales and mudstones. The 2D geostatistical realisations were converted to fluid flow models by assigning a binary permeability distribution for fictional mud (K_{Mud} = 1 nD) contents of 50% and 75% and respective sand contents (K_{Sand} = 1 D). The resulting flow models were object of numerical single phase fluid flow simulation to calculate effective permeabilities in horizontal and vertical direction. Hereby, the influence of model and cell size on the simulated effective permeabilities was investigated. The results coincide with previous studies on mud-rich

bedded structures using different (and often more complex) modelling approaches, which we take as confirmation of robustness and reliability for our geostatistical modelling approach.

Thus, we draw the following conclusions from the results of this study:

A dependence of the coefficient of variation on model size could only be observed for some models and as a general trend, when averaging the results for each structural type. Thereby, the trend is more prominent and absolute values are significantly lower for higher mud contents than for lower mud contents. In addition, this dependence varies in vertical and horizontal direction. Thereby, bedded structures show the most stable results, by already reaching a representative model size at a model edge length between 150 mm and 300 mm. High fluctuations of the coefficient of variation for chaotic and clasts bearing mudstones at 50% mud content indicate, that the representative model size exceeds the metre-scale at 50% mud content and might thus be located on a scale where no in situ measurements are available. However, many of chaotic and clasts bearing mudstones approach a coefficient of variation minimum at 600 mm model edge length for 50% mud content and almost all simulated structural templates of these shale and mudstone heterogeneities reach a coefficient of variation below 0.5 at 75% of mud content. We therefore suggest to conduct future studies on sub-metre scale heterogeneities in shales and mudstones with a model edge length of 600 mm along with an uncertainty measure such as the standard deviation or the coefficient of variation as a function of mud content. This will allow studying heterogeneities present in shales and mudstones, although the representative model size might not always be guaranteed (and measurable).

The probability of a vertically connected sand network through the whole model decreases with increasing mud content and increases with increasing structural complexity, either due to depositional energy involved in the genesis of the investigated mudstone heterogeneities (bedded < slumps < clasts) or an increase in secondary structure forming (bioturbation, dewatering, etc.). In horizontal direction the exact opposite is the case. Thus, chaotic and clasts bearing mudstones can pose significant vertical risk for preferred fluid flow in shales and mudstones, while bedded structures are unlikely to promote vertical fluid flow. Nevertheless, bedded structures show high anisotropies and very high chances of horizontal connectivity and thus support lateral flow through barrier and caprocks.

Cell size has an influence on the simulated effective permeabilities – in particular on horizontal effective permeabilities. For future studies using the same approach, we therefore suggest keeping the highest resolution, which is eligible for representing upscaled sample properties – 2 mm in case of this study.

References

Anderson, M. 1989. Hydrogeological facies models to delineate large-scale spatial trends in glacial and glaciofluvial sediments. Geol. Soc. Am. Bull. 101, 501–511.

Aplin, A. C., Fleet, A.J., Macquaker, J. H. S. 1999. Muds and Mudstones: Physical and Fluid Flow Properties. Geological Society, Special Publications, 158. In: Aplin, A.C., Fleet, A.J. & MacQuaker, J.H.S. (eds) 1999. Muds and Mudstones: Physical and Fluid Flow Properties.Geological Society, Special Publications, 158, 1-8.

Armitage, P. J., Faulkner, D. R., Worden, R. H., Aplin, A. C., Butcher, A. R., Iliffe, J. 2011. Experimental measurement of, and controls on, permeability and permeability anisotropy of caprocks from the CO2 storage project at the Krechba Field, Algeria, J. Geophys. Res., 116, B12208, doi:10.1029/2011JB008385.

Aplin, A. C., Macquaker, J. 2011. Mudstone diversity: Origin and implications for source, seal, and reservoir properties in petroleum systems. AAPG Bulletin, 95, 12, 2031-2059.

Bear, J. 1972. Dynamics of fluids in porous media. American Elsevier, New York.

Begg, S. H., King P. R. 1985. Modelling the effects of shales on reservoir performance: calculation of effective vertical permeability. Society of petroleum engineers paper 13529, presented at SPE symposium on reservoir simulation, Dallas, 10–13 February 1985.

Begg, S. H., Carter, R. R., Dranfield, P. 1989. Assigning effective values to simulator grid-lock parameters heterogeneous reservoirs. SPE reservoir engineering, paper 16754, pp 455–463.

Caers, J., Zhang, T. 2004. Multiple-point geostatistics: a quantitative vehicle for integrating geologic analogs into multiple reservoir models. In: Integration of outcrop and modern analog data in reservoir models. AAPG Mem, 80, 383–394.

Campbell, C. V. 1967. Lamina, Laminaset, Bed and Bedset. Sedimentology, 8, 7-26.

Caniego, F. J., Espejo, R., Martin, M. A., San José, F. 2005. Multifractal scaling of soil spatial variability. Ecological Modelling, 182, 291-303.

Chilès, J. P. 1988. Fractal and Geostatistical Methods for Modelling of a Fracture Network. Mathematical Geology, 20, 6, 631-654.

Cole, R. D., Picard, M. D. 1975. Primary and Secondary Sedimentary Structures in Oil Shale and Other Fine-Grained Rocks, Green River Formation (Eocene), Utah and Colorado. Utah Geol., 2, 49-67.

Collinson, J. D., Mountney, N., Thompson, D. B. 2006. Sedimentary Structures. Terra Publishing, 302 p.

Corbett, P. W. M., Jensen, J. L. 1992. Estimating the mean permeability: how many measurements do we need? First Break, 10, 3, 89–94.

Dagan, G. 1979. Models of groundwater flow in statistically homogeneous porous formations. Water Resour Res, 15, 1, 47–63

Davis, J.M., Lohmann, R.C., Phillips, F.M., Wilson, J.L., Love, D.W. 1993. Architecture of the Sierra Ladrones Formation, central New Mexico: depositional controls on the permeability correlation structure. Geol. Soc. Am. Bull., 105, 998–1007.

Desbarats, A. 1987. Support effects and the spatial averaging of transport properties. Math Geol, 21, 3, 383–389.

Deutsch, C. V. 1989. Calculating effective absolute permeability in sandstone/shale sequences. SPE Form Eval, 4, 3, 343–348.

Dewhurst, D. N., Aplin, A. C., Sarda, J. P., Yang, Y. L. 1998. Compaction-driven evolution of poroperm in natural mudstones: an experimental study. J. Geophys. Res., 103, 651–661.

Durlofsky, L. J. 1991. Numerical calculation of equivalent grid block permeability tensors for heterogeneous porous media. Water Resour Res, 27, 5, 699–708.

Emery, X., Lantuéjoul, C. 2006. TBSIM: a computer program for conditional simulation of three-dimensional Gaussian random fields via the turning bands method. Computers & Geosciences, 32, 10, 1615-1628.

Haldorsen, H. H. 1986. Simulator parameter assignment and the problem of scale in reservoir engineering. In: Lake LW, Caroll HB (eds) Reservoir characterization. Academic Press, Orlando, 293–340.

Haldorsen, H. H., Chang, D. M. 1986. Notes on stochastic shales; from outcrop to simulation mode. In: Lake LW, Caroll HB (eds) Reservoir characterization. Academic Press, Orlando, 445–485.

Hassanizadeh, M., Gray, W. G. 1983. General conservation equations for multi-phase systems, 1: averaging procedure. In: Pinder GF (ed) Flow through porous media, recent developments: a computational mechanics publications, 1–16.

Jensen, J. L., Corbett, P. W. M., Pickup, G. E., Ringrose, P. S. 1996. Permeability semivariograms, geological structure and flow performance. Math. Geol., 28, 4, 419–435.

Jensen, J. L., Lake, L. W., Corbett, P. W. M., Goggin, D. J. 2000. Statistics for petroleum engineers and geoscientists, 2nd edn. Elsevier, Amsterdam.

Klingbeil, R., Kleineidam, S., Asprion, U., Aigner, T., Teutsch, G. 1999. Relating lithofacies to hydrofacies: outcrop-based hydrogeological characterisation of quaternary gravel deposits. Sediment. Geol., 129, 3-4, 299–310.

Ma, J., Couples, G. D., Harris, S. D. 2006. A mixed finite element technique based on implicit discretization of faults for permeability upscaling in fault damage zones. Water Resour Res, 42, W08413, 12 p.

Marsily, G. de, Delay, F.Goncalves, J., Renard, P., Teles, V., Violette, S. 2005. Dealing with spatial heterogeneity. Hydrogeol J, 13, 161–183.

McKinley, J. M., Lloyd, C. D., Ruffell, A. H. 2004. Use of variography in permeability characterisation of visually homogeneous sandstone reservoirs with examples from outcrop studies. Math. Geol., 36, 7, 761–779.

Molz, F. J., Rajaram, H., Lu, S. L. 2004. Stochastic fractal-based models of heterogeneity in subsurface hydrology: origins, applications, limitations, and future research questions. Reviews of Geophysics, 42, 1, RG1002.

Neuzil, C.E. 1994. How permeable are clays and shales? Water Resour. Res. 30, 145–150.

Nordahl, K., Ringrose, P. S. 2008. Identifying the Representative Elementary Volume for Permeability in Heterolithic Deposits Using Numerical Rock Models. Mathematical Geosciences, 40, 7, 753-771.

Nordahl, K., Ringrose, P. S., Wen, R. 2005. Petrophysical characterization of a heterolithic tidal reservoir interval using a process-based modeling tool. Pet Geosci 11, 17–28.

Norris, R. J., Lewis, J. J. M. 1991. The geological modeling of effective permeability in complex heterolithic faces. Society of petroleum engineers paper 22692, presented at the 66th annual technical conference and exhibition, Dallas, TX, USA, 6–9 October 1991

Pickup, G. E., Ringrose, P. S., Jensen, J. L., Sorbie, K. S. 1994. Permeability tensors for sedimentary structures. Math Geol, 26, 2, 227–250.

Pickup, G. E., Ringrose, P. S., Sharif, A. 2000. Steady-state upscaling: from lamina-scale to full-field model. SPE J, 5, 2, 208–217.

Pickup, G. E., Stephen, K. D. Ma, J., Zhang, P., Clark, J. D. 2005. Multi-Stage Upscaling: Selection of Suitable Methods. Transp Porous Med, 58,191–216.

Piper, D. J. W., Noftall, R., Pe-Piper, G. 2010. Allochtonous Prodeltaic Sediment Facies in the Lower Cretaceous at the Tantallon M-41 Well: Implications for the Deep-Water Scotian Basin. AAPG Bulletin, 94, 1, 87-104.

Potter, E. P., Maynard, J. B., Pryor, W. A. 1980. Sedimentology of Shale. Springer, New York, Berlin, Heidelberg, Tokyo, 306 p.

Renard, P., Marsily, G. de 1997. Calculating equivalent permeability: a review, Adv.Water Resour., 20, 5–6, 253–278.

Reineck, H. E., Singh, I. B. 1973. Depositional Sedimentary Environments. Springer, New York, Heidelberg, Berlin, 439 p.

Rivoirard, J. 1994. Introduction to Disjunctive Kriging and Non-Linear Geostatistics. Oxford University Press, USA, 192 p.

Safinya, K. A., Le Lan, P., Villegas, M., and Cheung, P. S. 1991. Improved formation imaging with extended microelectrical arrays: Soc. Petrol. Eng., Paper no. 22726, 653–664.

Sahimi, M. 1995. Flow and transport in porous media and fractured rock. From classical methods to modern approaches. VCH, Weinheim.

Scaglioni, P., Ruvo, L., Cozzi, M. 2006. Implicit net-to-gross in the petrophysical characterization of thinlayered reservoirs. Pet Geosci, 12, 325–333

Schieber, J. (1999): Distribution and Deposition of Mudstone Facies in the Upper Devonian Sonyea Group of New York. J. Sed. Res., 69, 4, 909–925.

Schneider, F., Wolf, S., Faille, I., Pot, D. 2000. A 3D Basin Model for Hydrocarbon Potential Evaluation: Application to Congo Offshore. Oil & Gas Science and Technology – Rev. IFP, 55, 1, 3-13.

Wackernagel, H. 2003. Multivariate geostatistics. Third edition, Springer-Verlag, Berlin, 387 p.

Wen, R., Martinius, A. W., Næss, A., Ringrose, P. S. 1998. Three-dimensional simulation of small-scale heterogeneity in tidal deposits—a process-based stochastic simulation method. In: Buccianti A, Nardi G, Potenza R (eds): Proceedings of the 4th annual conference of the international association of mathematical geology (IAMG), Ischia, 129–134.

Yang, Y. L., Aplin, A. C. 2004. Definition and practical application of mudstone porosity–effective stress relationships. Petroleum Geoscience, 10, 153–162.

Yang, Y. L., Aplin, A. C. 2010. A Permeability–Porosity Relationship for Mudstones. Marine and Petroleum Geology, 27, 8, 1692-1697.

Chapter 5: Effective Porosity-Permeability Relationships of Metre-Scale Heterogeneous Mudstones

Introduction

Shales and mudstones comprise the largest fraction of rocks in the Earth's sedimentary basins (Aplin et al., 1999). They may serve as barrier rocks or seals in many applied aspects of geosciences, such as groundwater, conventional petroleum systems, CO_2 storage and nuclear waste deposits. From an economic perspective, their flow relevant physical properties, such as capillary entry pressures and permeability, play a key role. Hereby, permeability controls migration and leakage rates, and thus seal capacity and quality, once the critical capillary entry pressure of the seal is exceeded (e.g. Schowalter, 1979; Hildenbrand et al., 2002).

Current best practice for predicting seal capacity and flow in fine-grained sediments includes conventional log measurements for lithological interpretation in combination with lithologically dependent compaction curves and porosity-permeability models (e.g. Yang et al., 2004, 2010). However, conventional log measurements miss important sub-metre scale heterogeneities and the spatial component of rock property distributions. For example, Yang's and Aplin's (2004, 2010) models to predict porosity and permeability are based on measurements of samples, which are assumed to be homogeneous.

Heterogeneities of shales and mudstones appear at different scales (Schieber, 1999; McQuaker and Adams, 2003) and can incorporate wide ranges of grain size (Aplin et al., 1999) and spatially varying lithology (Potter, 1980; Aplin et al., 1999; Schieber, 1999). Fluid flow and seal capacity will be directly influenced by such heterogeneities (Weber, 1982), which can have significant influence on overall seal or reservoir performance (e.g. in case of thin bedded reservoirs), even if they occur on sub-metre scale (e.g. Pickup et al., 2000). However, incorporation of sub-metre scale heterogeneities present in seal sections into the common upscaling workflow is difficult, as the required high quality data, such as borehole images, well preserved core or lateral logs are rarely available due to economic reasons.

In this study we investigated a carefully selected group of mudstone heterogeneities from a case study from a gas field in the Western Nile Delta, Egypt, for effective permeability-porosity relationships at different stress-states. The dataset presents a unique opportunity to study these heterogeneities, as core and borehole images are available from highly heterogeneous sections, in many cases reaching well into seal or mud-rich sections. A combined probabilistic and geostatistical modelling approach was then chosen to reproduce

the observed heterogeneities at sub-metre scale by realistic rock property distributions at different stress states. The rock property population scheme extends Yang's and Aplin's (2004, 2010) porosity-permeability models for mudstones with published data and models of siltstone and sandstone porosities and permeabilities, as well as theoretical grain packing models. Finally, subsequent numerical fluid flow simulation has been used to calculate effective permeabilities and porosities. The resulting stress-dependent effective porosity permeability relationships can be used as input for larger scale flow models (e.g. on outcrop or seismic facies scale), 1D flow models for petroleum column height estimates or groundwater modelling. By doing so, the presented work contributes to understand the influence of mudstone heterogeneity on fluid migration through sub-metre scale pathways in sedimentary basins, fluid retention and sealing capacity of groundwater, CO_2 storage and petroleum system cap rocks.

Background

Published porosity and permeability data on natural fine-grained sediments are available for clay-rich sediments (Mesri and Olson, 1971; Coyner et al., 1993; Neuzil, 1994; Nagaraj et al., 1994; Aplin et al., 1995; Yang and Aplin, 1998, 2007; Dewhurst et al., 1998, 1999a, 1999b; Bjørlykke, 1998; Hildenbrand et al., 2004; Kwon et al., 2004; Mallon et al., 2005), some of them even providing porosity models as a function of effective stress and clay content (Aplin et al., 1995; Yang & Aplin, 1998, 2004) or permeability models as a function of porosity and clay content (Yang and Aplin, 2010). In addition to measurements on natural fine-grained sediments experimental, mechanical compaction data on pure and mixed aggregates of sand or silt and clay sized particles (Marion et al., 1992; Revil and Cathles, 1999; Mondol et al., 2007; Mondol et al., 2008; Fawad et al., 2010; Mondol et al., 2011) provide an alternative, not least due to their ability to serve as end-members of natural rock properties and their reproducibility.

Most studies report sub-nano- to micro-darcy permeabilities and a logarithmic porosity (e.g. Yang and Aplin, 2004; Mondol et al., 2007) and permeability (e.g. Mondol et al., 2008; Yang and Aplin, 2010) decrease with increasing effective stress for clay-rich sediments, which usually have high initial porosities (e.g. Aplin et al., 1995; Mondol et al., 2007).

Permeability measurements on natural, heterogeneous mudstones are very rare, as they are expensive and time consuming. However, Yang and Aplin (2007) measured horizontal and vertical permeabilities of samples of natural mudstones and found permeability anisotropies (K_h/K_v) between 1.7 and 11.2 for mudstones, and attributed this effect to particle alignment

and material heterogeneity. More recently, Armitage et al. (2011) also measured vertical and horizontal permeabilities of cap rock samples from the Krechba field within the Timimoun Basin, Algeria. Their measurements revealed a wide range of anisotropies (up to 4 orders of magnitude) independent of porosity and grain size. They ascribe the high range of anisotropy to the internal structures of the samples and to the fact, that with increasing heterogeneity, the effect of porosity and grain size decreases "*as vertical permeability is controlled by the least permeable layer, whereas the horizontal permeability is controlled by the most permeable layer*".

As the geometry of the "*least or most permeable layer*" is not always simple to describe and varies strongly with differing depositional processes, the influence of this geometry, or heterogeneity, is not easy to assess. To quantify this heterogeneity and its influence on fluid flow and effective permeability, at least four steps are required (e.g. Marsily et al., 2005):

1. Investigation of the heterogeneities (observation, description, interpretation)
2. Modelling of the heterogeneities
3. Population of relevant physical properties (lithology, porosity, permeability)
4. Upscaling of the influence of the heterogeneity on flow to appropriate scales

For investigation of geological heterogeneities the Geologist is the "tool" of choice. Geological heterogeneities must be described in detail and their origin has to be understood, before they can be modelled in a reasonable way.

Modelling of the heterogeneities also needs close supervision of a Geologist, but a set of different modelling approaches are available and should be selected carefully. Among many other reviews on modelling methodology, two recent examples are available from de Marsily et al. (2005) and Eaton (2006).

As geological heterogeneity is always associated to a certain degree of uncertainty due to incomplete data (Marsily et al., 2005), a stochastic part is usually involved in modelling procedures. Common uncertainties are the size and shape of geological features and in particular their spatial distribution in the subsurface. They can be addressed by three different approaches: classic geostatistical modelling, Boolean (zonal in hydrogeology) modelling or geostatistical discontinuous facies modelling (Marsily et al., 2005). Furthermore, the utilisation of fractal and multifractal scaling is increasingly used for modelling of geological heterogeneity through different scales (e.g. Molz et al., 2004).

Classic geostatistical modelling utilizes the semi-variogram for representing heterogeneities. A geostatistical simulation draws a continuous property field from a Gaussian random distribution. The resulting smoothness within the model yields problems where geological

facies change rapidly, for example due to erosion hiatus, faults and other discontinuities (Marsily et al., 2005; Eaton, 2006).

To overcome the issue of undesired smoothness, Boolean methods were introduced in 1986 by Haldorsen and Chang by development of the stochastic shale model. In contrast to classic geostatistical methods, which produce continuous models, the Boolean methods allow for the stochastic distribution of discrete geological objects (such as shale lenses in a sand body). The geometric object properties can be varied within the observed or assumed ranges by probability density functions and the spatial distribution might be described by a random stochastic or correlated field (Marsily et al., 2005) along with a general probability of occurrence. The resulting objects and confining matrix are then given fixed petrophysical properties (e.g. porosity and permeability) according to their geological meaning.

The geostatistical answer to Boolean methods is discontinuous facies modelling. In this case, the resulting Gaussian distribution is divided or truncated into several indicator thresholds, each representing a facies or lithological class. It was first developed as simple indicator modelling (Journel, 1983; Journel and Isaaks, 1984; Journel and Alabert, 1990; Journel and Gomez-Hernandez, 1993), where the Gaussian distribution drawn from the semi-variogram can either take on the value 0 or 1 and has been further developed to advanced facies modelling where mutiple facies proportions, which might vary with depth, are simulated (Matheron et al. 1987, 1988; see also Rivoirard 1994; Chiles and Delfiner 1999; Armstrong et al. 2003 – or see Marsily et al., 2005 for a detailed review).

The quality of sampling and modelling of geological heterogeneity through utilisation of the semi-variogram is highly dependent on the size and scale of the sampling window (Jensen et al., 1996). It is therefore crucial to incorporate geological knowledge of the genesis of the heterogeneities into sampling and modelling of heterogeneity (Jensen et al., 1996). In other words: where several scales of heterogeneity exist, the sampling and modelling should honour these scales (e.g. Kossack et al., 1990).

Recently, geostatistical facies modelling tools have been further extended by combination with process-based deterministic models (Wen et al., 1998), which has been successfully used at the sub-metre scale (e.g. Nordahl et al., 2005; Nordahl and Ringrose, 2008). Another increasingly important branch of geostatistics is multiple point statistics, which uses training images (based on outcrop/imaging data or expert knowledge) to reproduce geological heterogeneity (e.g. Caers and Zhang, 2004).

Also, fractal scaling methods are increasingly employed to describe and model geological heterogeneity (e.g. Chiles, 1988; Caniego et al., 2005). In a fractal scaling approach

geological features and structures are investigated for self-similarity through different scales, which leads to a multifractal approach, if these scaling properties for different features and structures are summarized in a so called multifractal spectrum. In geostatistical terms their correlation structure could be modelled by a power law covariance function, as the self-similarity opposed through fractals implies scale invariance (e.g. Molz et al., 2004; Eaton, 2006).

Once the heterogeneities are modelled, investigation of their influence on fluid flow and a description of this behaviour into a single variable or simple formulation is the next step. This process is also called averaging or, more recently, upscaling, as the influence of heterogeneities present at a certain scale on the next scale is described by a single property or formulation. In some cases upscaling may not be necessary, in particular when sub-metre scale heterogeneities are rare at the larger scale (Pickup et al., 2005). The converse argument, that upscaling of sub-metre scale heterogeneities is crucial in complex geological settings (Pickup et al., 2000; Pickup et al., 2005), where heterogeneity is high on all scales, is obvious.

Renard and Marsily (1997) provide a detailed review of upscaling methods such as effective media theory (Dagan, 1979), numerical methods and percolation theory, where, from a geological fluid flow point of view, a certain threshold of highly permeable material guarantees connectivity through a system (Begg and King, 1985). A critical parameter in upscaling, independent of the method, is the scale that the influence of heterogeneity should be upscaled to. A detailed study about finding appropriate model scales for the heterogeneities investigated in this study can be found in Chapter 3.

So far, most studies of the influence of sub-metre scale heterogeneities on fluid flow have focussed on reservoir modelling and performance. For example, Pickup et al. (1995) investigated the influence of spatial heterogeneity on the effective permeability of non-scaled models by deterministic modelling. They found that analytical solutions such as arithmetic, harmonic or geometric averaging fail, where heterogeneity goes beyond isotropy or simple structure such as perfectly parallel layering.

Nordahl et al. (2005) investigated the effect of mud content on effective vertical and horizontal permeabilities of heterogeneous, tidal, reservoir rocks using a process based modelling tool to generate near well bore models. They concluded that core plug measurements are not sufficient to calibrate and predict effective permeabilities from wireline data, as core plug measurements do not account for the heterogeneity present at wireline scale (sub-metre scale). In addition, they found percolation thresholds of 35% and 85% of mud content in form of mud drapes in layered and flasered tidal sediments for vertical and

horizontal effective permeabilities, respectively. However, in a study on the same type of tidal sediments, but with a binary permeability field, Nordahl and Ringrose (2008) established percolation thresholds of 80% and 50% mud content for horizontal and vertical effective permeabilities, respectively.

Similar percolation thresholds of mud contents have been also found by Scaglioni et al. (2006) for horizontal permeabilities, who investigated a thin layered reservoir at the same scale (sub-metre scale) and by using the same processed based modelling tool as Nordahl et al. (2005) and Nordahl and Ringrose (2008). However, for vertical permeabilities the percolation threshold seems to be less than 15% of mud content in their study, probably due to higher anisotropies of the layering system. The studies by Nordahl and co-workers (2005, 2008) and Scaglioni et al. (2006) are very close to the work presented in this study, in particular for bedded structures. We will thus use their results as a reference for the work presented in this study, although we employ a different modelling technique and extend the approach to other heterogeneities such as bioturbation, mass transport derived structures and injections of coarser material into mud-rich sequences.

Methods and Data

In the following we will describe the modelling workflow in detail, along with the data used in detail. The petrophysical model used for property assignment will be only explained briefly, as it has been described in detail elsewhere (Chapter 1). The modelling workflow follows the conventional route described above, but is specifically tailored to fine-grained sediments. Thus, the workflow comprises of four basic steps (Figure 5.1):

1. Interpretation and identification of the relevant structures/heterogeneities from core and borehole image data; selection of representative structural templates
2. Geostatistical simulation using manually fitted, nested covariance functions for each structural template and subsequent indicator super positioning according to a lithology scheme
3. Population of physical properties (grain size fractions, porosity and permeability) for different effective stresses using latest advances in fine-grained sediment physical property modelling and measurement results (Marion et al., 1992; Revil and Cathles, 1999; Yang and Aplin, 2004, 2010; Chuhan et al., 2003; Pettersen, 2007; Mondol et al., 2008; Fawad et al., 2010)
4. Numerical fluid flow simulation to calculate effective permeabilities in horizontal and vertical directions

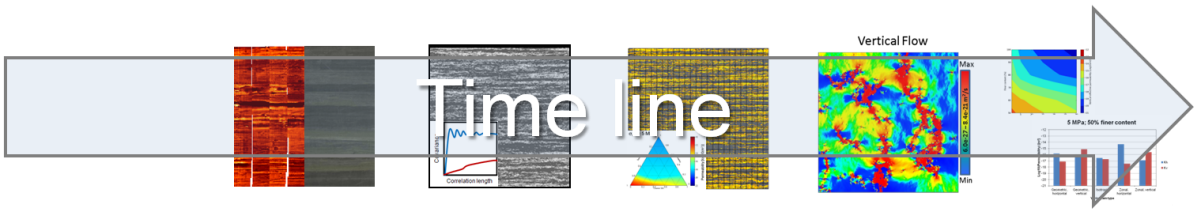

Task	Identify flow-relevant mudstone heterogeneity (MH)	Capture and model MHs	Populate MH models with reasonable, flow-relevant properties (lithology, K, phi)	Numerical simulation to calculate effective MH permeabilities	Post-processing
Intermediate steps	Reduce MHs to representative and manageable number		Calibrate numerical simulation for resolution and model size		
Data sources	Core images, log data, borehole image data, literature, etc.		Sample measurements, experimental data, theoretical models, literature	Ready flow models	Fluid flow simulation results (effective permeabilities)
Tools	Geologist's eyes, reading	Geostatistical analysis and simulation	Geologist, programming, some math, more reading	Mathematician, fluid flow simulator (2D)	Statistics, visualization, interpretation and relate results to initial problem (seal risk)

Figure 5.1: The workflow includes classical steps, but with special tailoring to mudstones. Thereby, different decision processes, data sources and methodological tools are used.

The data set comprises a careful selection of high quality core and borehole image data from 6 wells off shore Nile Delta, Egypt. The total depth ranges from approximately 1500 – 2500 m and the data covers parts of the top seal sections or highly heterogeneous mud-rich sections below the reservoirs (Figure 5.2). The selection of mud-rich core and borehole images was conducted on the basis of qualitative visual/geological interpretation of the images (high lithological contrast, presence of flow relevant features, minimum bias such as core slab scratches and artificial fractures). The images were then interpreted in terms of different types of heterogeneity (homogeneous, bedded, chaotic, clast bearing).

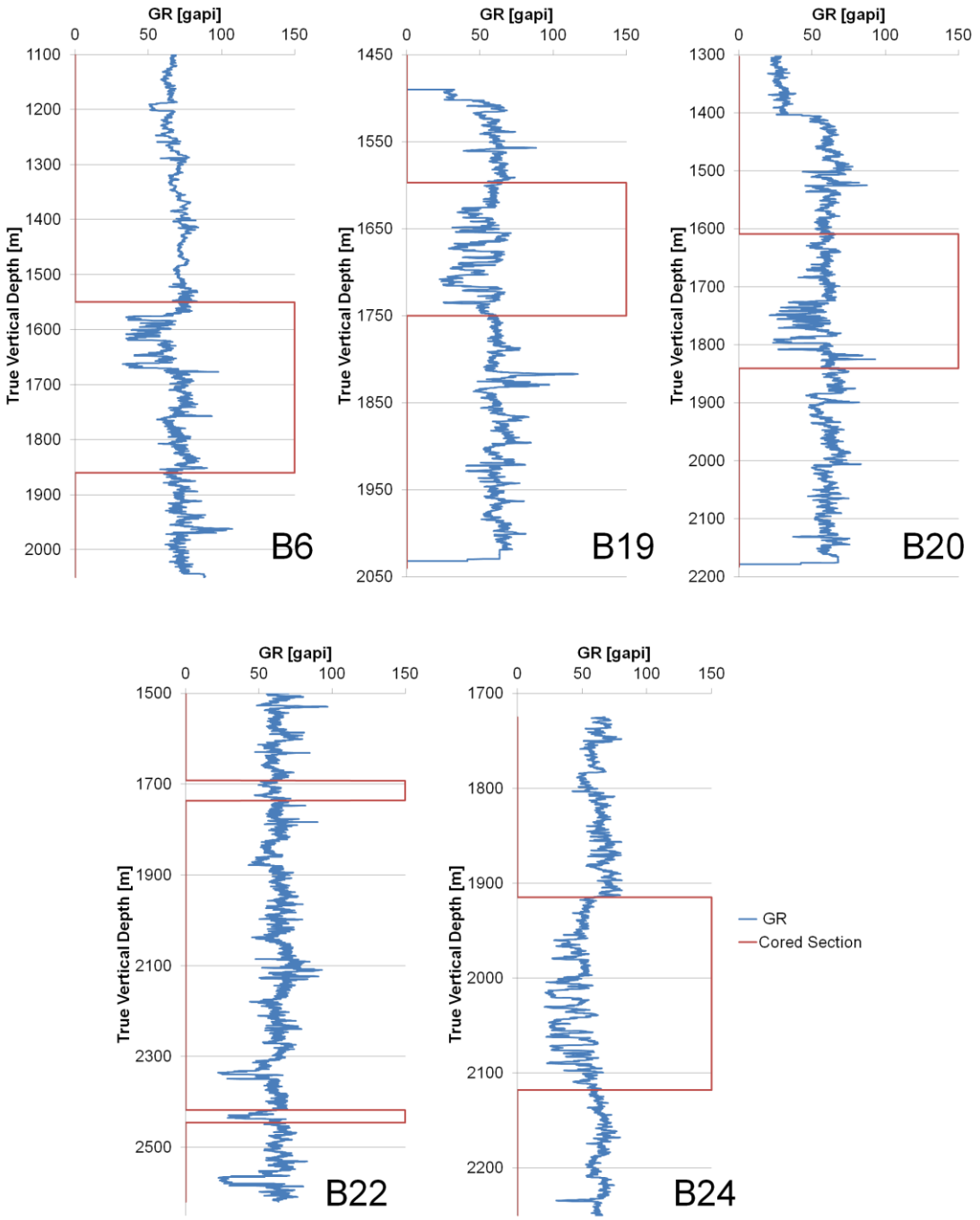

Figure 5.2: Gamma ray (blue lines) and cored/imaged sections (red lines) of the used wells of the Nile Data case study.

In the following we will briefly describe the interpretation process. More detail on the interpretation process is provided in Chapter 3. Figure 5.3 shows the interpretation scheme for the visual interpretation of the images. The structural classes are of an abstract nature, describing only geometric features, which can be back related to different depositional processes. Hereby, the classification scheme comprises a homogeneous structural class and

three heterogeneous structure classes, which can each be subdivided into two sub-structure classes. The classification scheme follows common schemes for sedimentary structures in fine grained sediments (Campbell, 1967; Reineck and Singh, 1973; Cole and Picard, 1975; Potter et al., 1980; Collinson et al., 2006). Homogeneous mudstones are only governed by its lithological composition. They do not exhibit any lithological contrast and consist of pure mud. Their origin is usually from deep sea or hemipelagic, calm depositional environments. Bedded structures can be subdivided into continuous lamina or discontinuous, lenticular shaped beds or lamina. A deep sea to tidal influenced sedimentary environment with periodic influx of coarser material is a likely cause of bedded structures. Chaotic structures may be typical of slope and mass transport dominated settings. The structures pose a high uncertainty in terms of vertical and horizontal connectivity of coarser material and depend critically on lithological composition. The chaotic structures are mostly caused by slumping and folding and range from small disturbed beds to mixing of different lithologies, which appear almost isotropic on the sub-metre scale. Clast bearing structures also span a wide range of possible structures from small bioturbation induced scattered clasts to mass transport related mixing of cm-dm sized sand and mud clasts to vertical sand pipes in a mud-rich matrix caused by sand injection.

Additionally, geostatistical study for lithological anisotropy has been conducted to support the visual/geological interpretation and to allow for further subdivision of the observed heterogeneity groups in a semi-quantitative way (Chapter 3). The group of images for this process has been selected on the basis of image quality in order to calculate experimental semi-variograms of average RGB values of the core images in horizontal and vertical directions with a minimum bias (e.g. slab scratches, human hair and artificial fractures). The resulting experimental variograms were then analysed for general anisotropy trends, such as isotropy, zonality, or geometric anisotropy by comparing the horizontal with the vertical experimental variogram of each image (Figure 5.4).

In order to cover the full range of observed heterogeneities present in our case study, the most different heterogeneities were finally selected for modelling of mudstone heterogeneity and subsequent numerical fluid flow simulation to calculate effective permeabilities. We preferred this rationale rather than a selection based on the most common heterogeneities, as - in a regional context - the data source is point-wise (wells) and cannot guarantee to deliver representative statistical distributions of heterogeneities of the case study. The number of subdivisions of the visual interpretation by geostatistical analysis also gives a first hint about

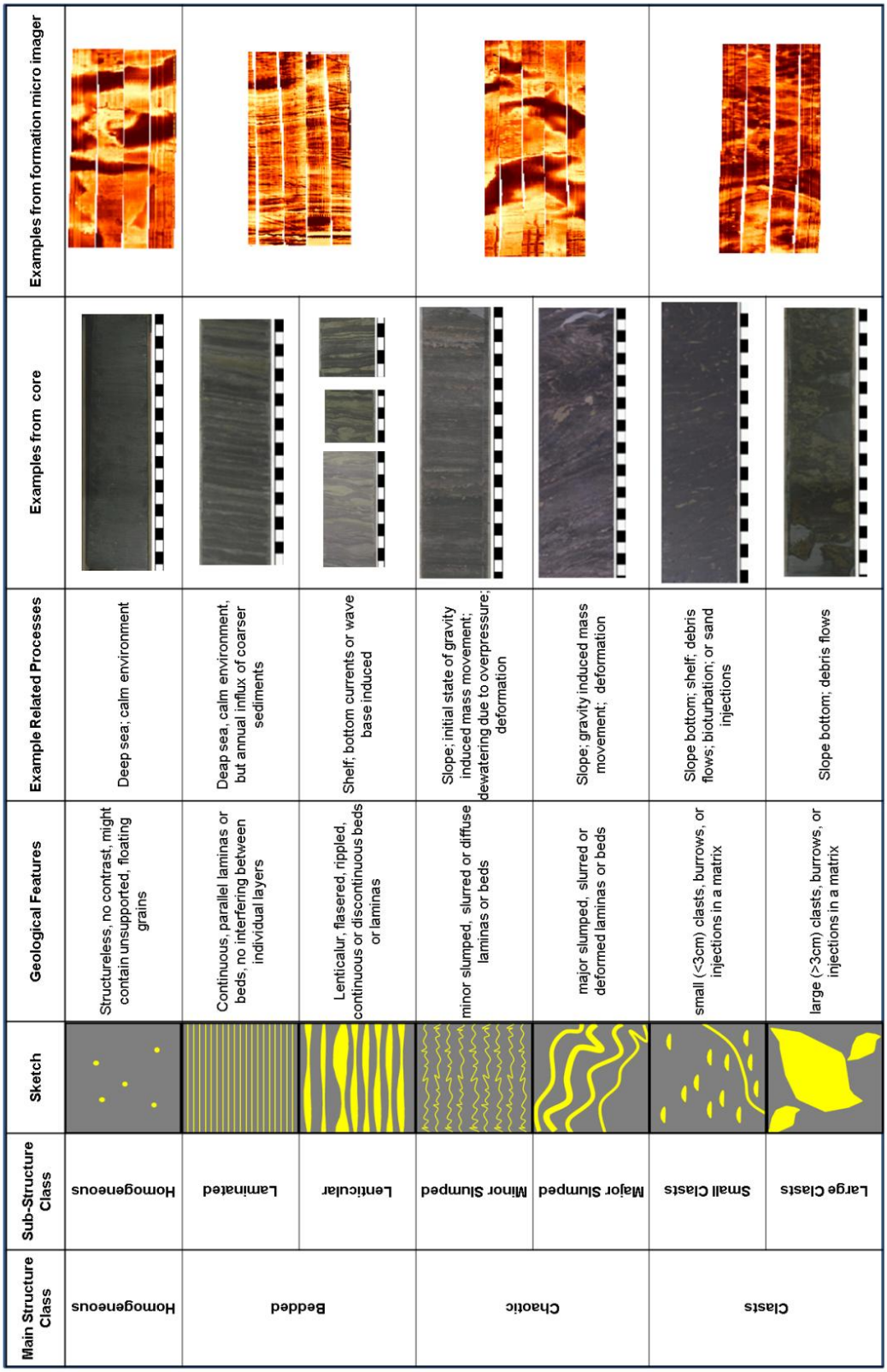

Figure 5.3: Classification scheme used in this study with examples from core and borehole images. Note that every heterogeneity or structure class can be related to geological features and possible depositional processes.

the uncertainty of the respective structural classes. Thereby, the number of subdivisions increases from bedded to chaotic to clast bearing mudstones (Compare Chapter 3).

Based on a study to estimate representative sizes of the models (Chapter 4), we decided to keep the resolution at 2 mm and the model edge length constant at 600 mm, as this size represented the influence of spatial heterogeneities best on an average basis for all structures. Together with the interpretation process the study on model size allowed for grouping of structural templates yielding similar results, yielding 21 structural templates for evaluation of stress-dependent effective porosity-permeability relationships (Table 5.1).

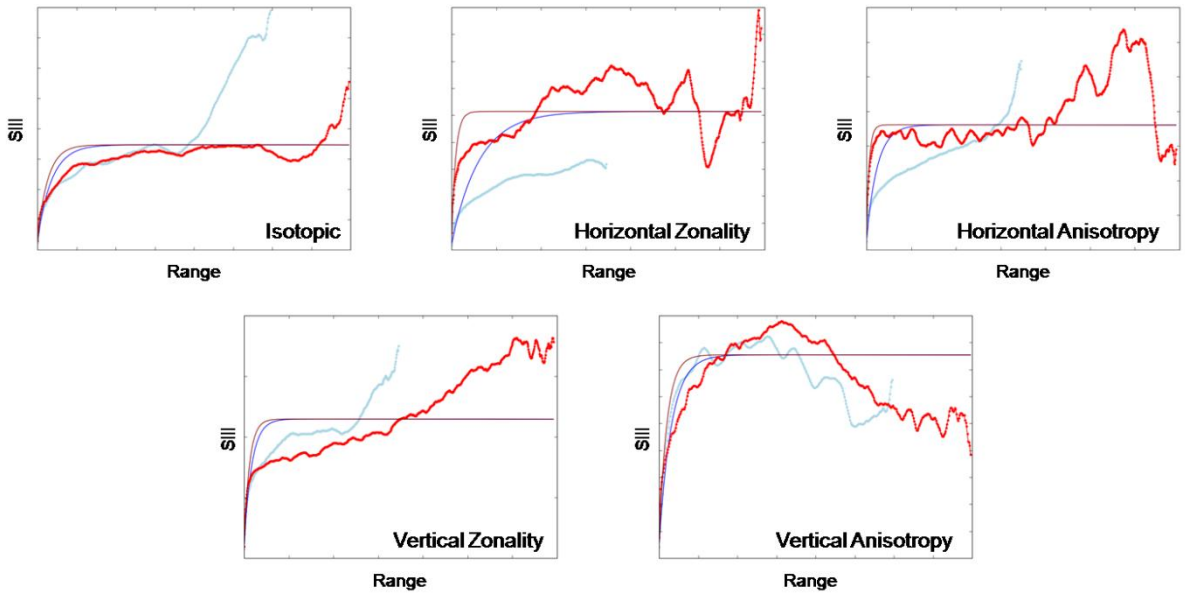

Figure 5.4: Examples for experimental variogram types (bold lines). The thin lines represent automatic fits with a single exponential covariance function and demonstrate the necessity of fitting variograms manually with nested covariance functions.

The nested covariance functions have been modelled interactively and with regard to the respective geological features visible on the images. This results in the most accurate fit of the experimental variograms, taking care of artefacts such as slab scratches on core (Figure 5.5a) or holes in the borehole wall (Figure 5.5b). For borehole image data the experimental variograms have been extracted from single flap/pads in order to minimize the effect of an unfolded cylinder (Figure 5.5c). The experimental variograms were calculated directly from the image data or RGB (Red Green Blue) colour space, whose average has been transformed to a Gaussian distribution (e.g. Rivoirard 1994 on anamorphosis modelling) to allow for subsequent geostatistical simulation. The covariance functions or variogram models were then used as inputs for geostatistical simulation. In this study the turning bands algorithm with 2000 turning bands was employed (Emery and Lantuejouel, 2006). Compared to other

simulation techniques such as the sequential Gaussian simulation, the turning bands algorithm has the advantage of working without a neighbourhood definition. Additionally, the method requires much less computational time, as it simplifies the simulation problem in 3D-space into a simulation problem in 1D space by simulating the problem on randomly distributed lines (turning bands) in the three-dimensional space. Thus, a turning bands simulation in 3D is performed at the computational cost of one-dimensional simulations (Emery and Lantuéjoul, 2006). The indicator superposition was conducted after the distribution of the simulated template was back transformed to its original average RGB colour space distribution using Gaussian anamorphosis modelling (Rivoirard 1994). Thereby, Gaussian anamorphosis transforms the cumulative of the simulated normal distribution with mean 0 and variance 1 to the cumulative of the initial distribution of the image's RGB colour space distribution. Hermite polynomials, which have been acquired from the images prior to simulation, are used to model the transformation function between the cumulative distributions. In this way, the indicator assignment varies according to desired mud contents for the whole model domain, while the average RGB colour space distribution is kept. The mud model cells are assigned to the respective percentile of the simulated average RGB colour space (Figure 5.6). The approach is superior to conventional indicator simulations, as nested structures can be incorporated, the initial distribution can be kept and the indicator internal structures are not lost.

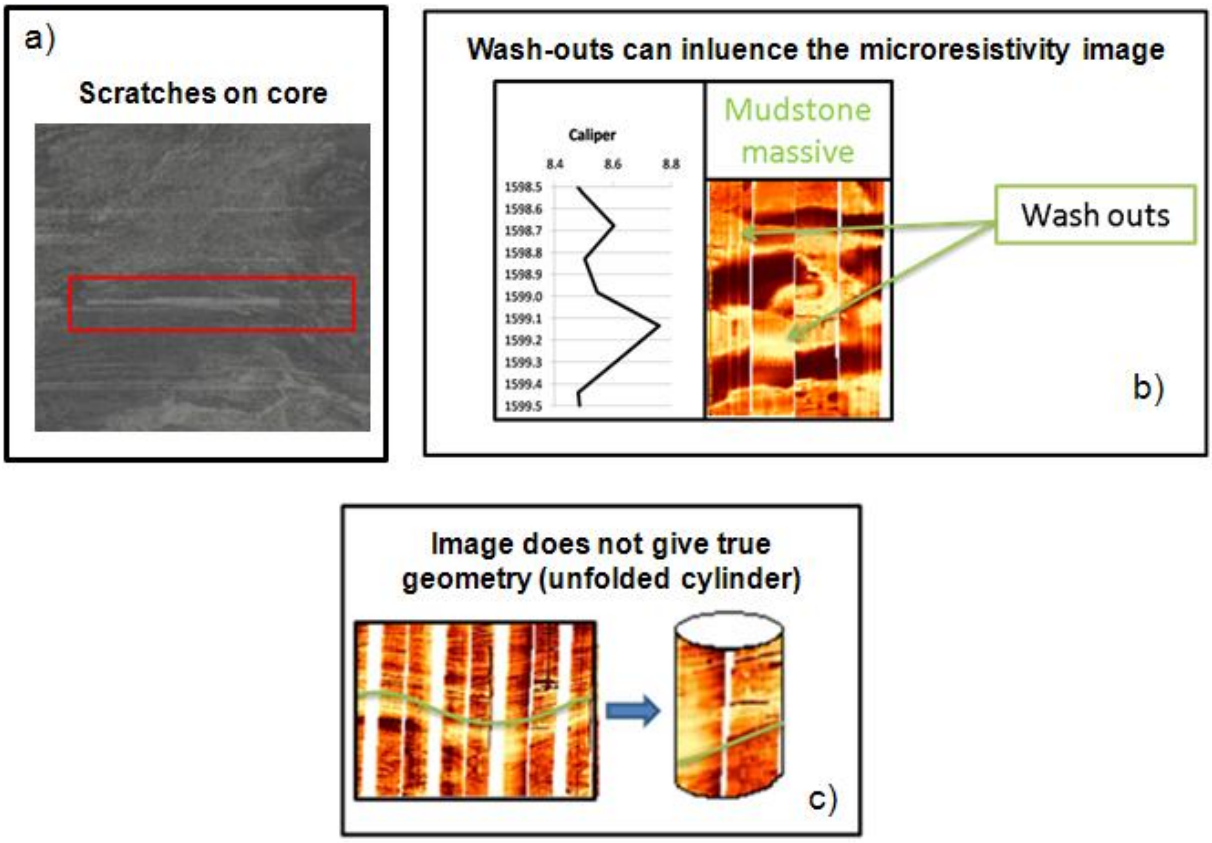

Figure 5.5: Possible error sources, when fitting covariance functions to experimental variograms of image data. a) scratches on core; b) wash outs; c) unfolded cylinder effect.

Based on the simulated average RGB colour space and indicator distributions (mud contents), the third step of the modelling workflow can be conducted, which is the propagation of petrophysical flow properties (porosity and permeability), which honour the lithological variability of the Nile Delta case study. The petrophysical properties are effective stress sensitive and are modelled using a grain size fraction dependent modelling framework (see Chapter 2 for a detailed description). The modelling framework integrates latest advances in shale and mudstone physical property modelling (Mondol et al., 2008, 2011; Yang and Aplin, 2004, 2010) with well established theoretical pore-filling models (Marion et al., 1992; Revil and Cathles, 1999), experimental mechanical compaction data for sands and silts (Fawad et al., 2010; Chuhan et al., 2002; Mondol et al., 2011) and theoretical permeability models for sandstones (Pettersen, 2007). Figure 5.7 shows the resulting porosity and permeability values at 5 MPa for a full range grain size fraction system, when using the modelling framework developed in Chapter 2.

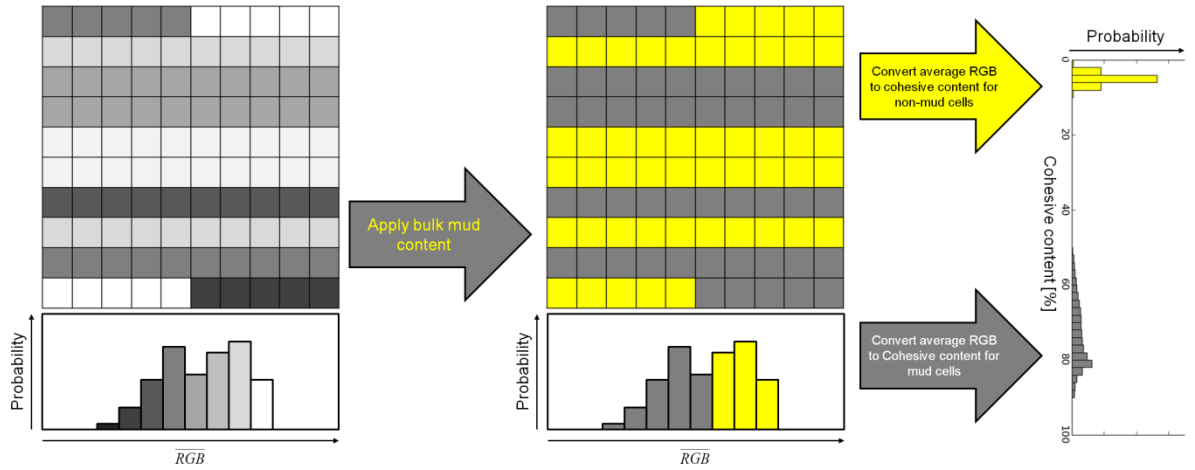

Figure 5.6: Schematic of indicator/mud content assignment to each model. The starting point is a simulated structural template with an averaged RGB distribution (left). According to the respective percentile the indicator function is applied to assign respective mud contents (here: 50%) (centre). The binary model is filled with lithological variety by simulating vshale contents (right).

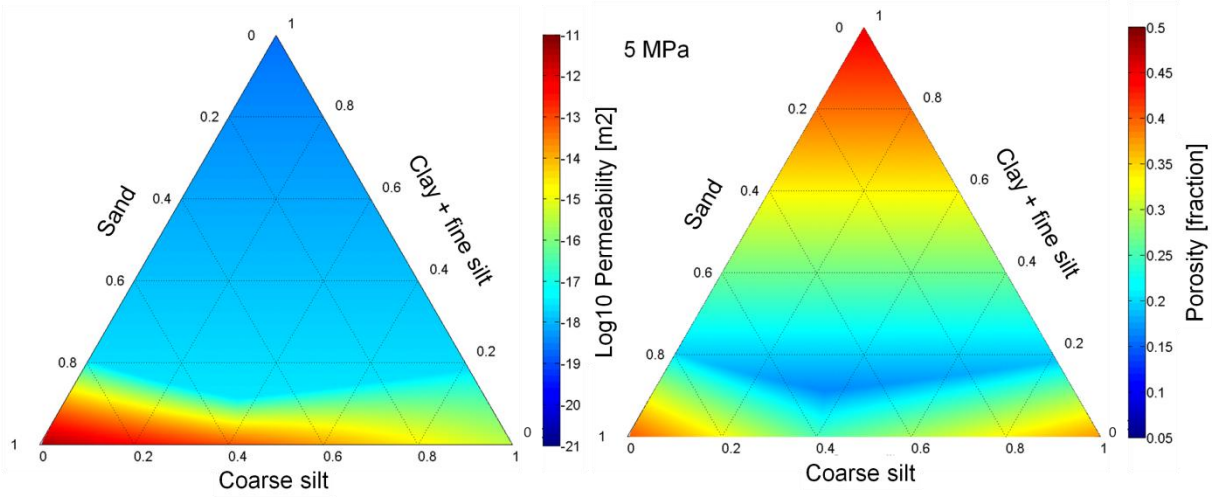

Figure 5.7: Example for the porosity-permeability modelling framework at 5 MPa. Porosity (left) and permeability (right) can be modelled from normalized grain size fraction combinations. The method incorporates more variety due to differences between sand-rich and coarse silt-rich sediments and is based on the combination of published data from natural rocks, experimental mechanical compaction of mixed aggregates and theoretical models (from Chapter 2).

Table 5.1: Variogram parameters of structural templates used in this study. Model_ID is a unique identification assigned to each structural template. The variogram parameters Variogram Type = type of geostatistical anisotropy, Mod (covariance function type, which can be either exp for exponential, sph for spherical, cub for cubic, gau for Gaussian or sin for cardinal sine), Rh and Rv (horizontal and vertical range or correlation length), S (sill or covariance), Ang (anisotropy angle) are shown next to geological interpretation (Structure), and origin (well, top and bottom depths and vertical interval size). A maximum of three nested structures have been modelled, which is indicated in the integer appendix of the parameters Mod, Rh, Rv, S and Ang.

Model_ID	Well	Image Type	Top [m]	Bottom [m]	Interval [m]	Structure	Variogram Type	Mod1	Rh1 [cm]	Rv1 [cm]	S1	Ang1	Mod2	Rh2 [cm]	Rv2 [cm]	S2	Ang2	Mod3	Rh3 [cm]	Rv3 [cm]	S3	Ang3
Mod01	B24	Core	1935.23	1935.46	0.23	Laminated	Hor. Zonality	exp	2.02	0.29	0.40	90.00	sin	115.20	5.76	0.50	90.00	None	None	None	None	None
Mod03	B22	Core	1722.29	1722.67	0.37	Laminated	Hor. Anisotropy	exp	1.15	0.14	0.40	90.00	sin	37.44	5.76	0.50	90.00	None	None	None	None	None
Mod05	B22	Core	1719.18	1719.69	0.52	Lenticular	Hor. Zonality	exp	0.58	0.03	0.25	90.00	exp	11.52	8.64	0.35	90.00	sin	288.00	2.88	0.40	90.00
Mod06	B24	Core	1991.16	1991.48	0.32	Lenticular	Hor. Zonality	exp	4.32	1.44	0.70	90.00	sin	288.00	4.32	0.30	90.00	None	None	None	None	None
Mod07	B22	Core	1712.04	1712.23	0.19	Lenticular	Hor. Anisotropy	exp	2.16	0.29	0.96	90.00	sin	28.80	2.16	0.04	90.00	None	None	None	None	None
Mod10	B24	Core	2085.39	2085.57	0.17	Minor Slumped	Isotropic	exp	1.15	0.29	0.70	90.00	gau	6.34	3.46	0.20	90.00	sin	4.32	2.88	0.10	90.00
Mod12	B20	Core	1651.26	1651.40	0.14	Minor Slumped	Vert. Zonality	exp	0.49	0.58	0.75	90.00	gau	5.76	17.28	0.25	90.00	None	None	None	None	None
Mod15	B19	Core	1635.03	1635.49	0.46	Major Slumped	Isotropic	exp	0.58	0.29	0.30	90.00	exp	3.46	2.88	0.25	170.00	None	None	None	None	None
Mod16	B20	Core	1682.34	1682.52	0.17	Major Slumped	Hor. Zonality	exp	0.58	0.43	0.40	90.00	exp	6.91	1.73	0.60	90.00	None	None	None	None	None
Mod17	B24	Core	2002.51	2002.68	0.17	Major Slumped	Vert. Zonality	exp	1.15	0.86	0.80	90.00	sin	21.60	15.84	0.20	90.00	None	None	None	None	None
Mod18	B19	Core	1716.06	1716.43	0.37	Major Slumped	Hor. Anisotropy	exp	1.73	0.86	0.45	90.00	sin	57.60	34.56	0.55	90.00	None	None	None	None	None
Mod21	B22	Core	1718.10	1718.22	0.12	Small Clasts	Isotropic	exp	0.86	0.29	0.50	90.00	exp	1.73	3.46	0.50	90.00	None	None	None	None	None
Mod23	B22	Core	2437.02	2437.13	0.12	Small Clasts	Hor. Anisotropy	exp	2.88	1.15	1.00	90.00	None	None	None	None	None	None	None	None	None	None
Mod25	B19	Core	1619.30	1619.39	0.09	Small Clasts	Hor. Zonality	exp	0.58	0.29	0.45	90.00	exp	16.56	2.02	0.55	90.00	None	None	None	None	None
Mod26	B19	Core	1618.51	1618.63	0.12	Small Clasts	Hor. Anisotropy	exp	0.29	0.09	0.60	90.00	exp	4.32	0.86	0.40	90.00	None	None	None	None	None
Mod28	B19	Core	1697.45	1697.57	0.12	Large Clasts	Isotropic	exp	0.58	0.58	0.50	90.00	exp	11.52	4.32	0.50	125.00	None	None	None	None	None
Mod30	B20	Core	1658.14	1658.40	0.26	Large Clasts	Vert. Zonality	exp	2.88	2.88	0.40	90.00	exp	11.52	86.40	0.60	90.00	None	None	None	None	None
Mod04	B6	Borehole	1634.00	1636.00	2.00	Laminated	Hor. Zonality	sin	1000.00	13.68	0.65	90.00	cub	300.00	70.72	0.35	90.00	None	None	None	None	None
Mod14	B6	Borehole	1589.00	1590.70	1.70	Minor Slumped	Hor. Anisotropy	exp	24.00	12.00	0.17	90.00	gau	168.00	8.40	0.42	105.00	gau	19.20	19.20	0.42	90.00
Mod20	B6	Borehole	1585.00	1587.00	2.00	Major Slumped	Vert. Anisotropy	exp	6.00	13.90	1.00	90.00	None	None	None	None	None	None	None	None	None	None
Mod27	B6	Borehole	1604.00	1606.00	2.00	Large Clasts	Vert. Anisotropy	cub	1.80	40.56	0.30	90.00	cub	13.40	19.20	0.59	90.00	cub	3.40	8.40	0.11	90.00

As input for the modelling framework we use cohesive content (clay + fine silt fractions; grain size < 10 µm) linearly derived from average RGB of the image (the higher the average RGB, the less the cohesive content) and stochastic simulation of a Nile Delta grain size fraction data base. Such a relationship is sufficient, where the average RGB of the image can be clearly assigned to lithological components. Figure 5.8 shows an example where the normalized average RGB of each horizontal pixel row well correlates with normalized core gamma ray derived shale content, which could be set equal to cohesive content, as most cohesive grains compose of clay minerals. Sections, from which the images used in this study as structural templates have been selected from, are from similarly well correlated sections.

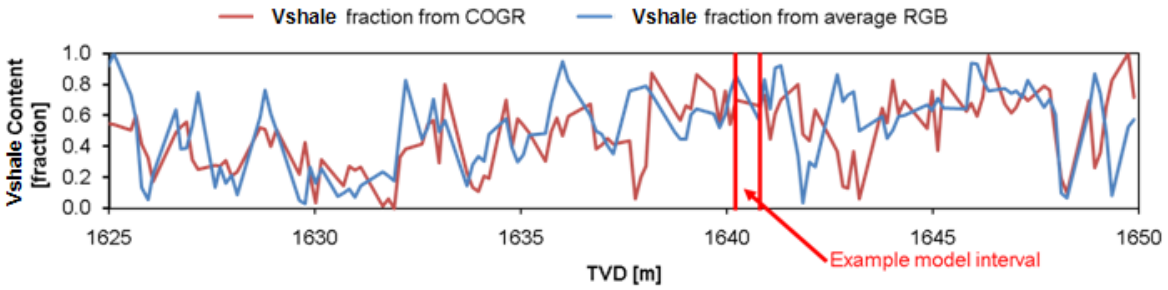

Figure 5.8: Example depth profile of vshale contents derived from core gamma ray (red line) and average RGB values (blue line). The 1-to-1 linear correlation works sufficiently for sections, where the interpretation of the image data is very clear.

The Nile Delta grain size fraction data base consists mainly of samples high in cohesive content. The samples of the database are therefore mudstones for the most part. The database shows a specific dependence of measured grain size fractions (clay, fine and coarse silt and sand) from measured cohesive content (Chapter 1). This dependence has been utilized in this study to reproduce realistic grain size fraction combinations for each model cell and to serve as input for the above described porosity permeability modelling framework. Hereby, we use a combination of a regression model of this dependency and a simulation of the model residuals to incorporate the natural variability in grain size fraction combinations (Figure 5.9). For cells, which will not be declared as mud-rich, the grain size fraction simulation scheme has been extended to low cohesive contents. Initial cohesive contents for mud-rich model cells have been derived from a combination of the above described relationship between average RGB and cohesive content and subsequent Gaussian anamorphosis modelling of the cohesive content distribution of the database (e.g. Rivoirard, 1994). For non-mud cells cohesive contents have been modelled with a truncated normal distribution with mean cohesive content of 5% and a narrow range of +/- 5% to allow a maximum permeability

contrast. Hereby, the cohesive contents are also dependent on the simulated average RGB value of the respective model cell in the same fashion as the mud-rich cells. To demonstrate the property assignment workflow, Figure 5.10a-c shows examples of cohesive content, porosity and vertical permeability distributions for 50% mud content.

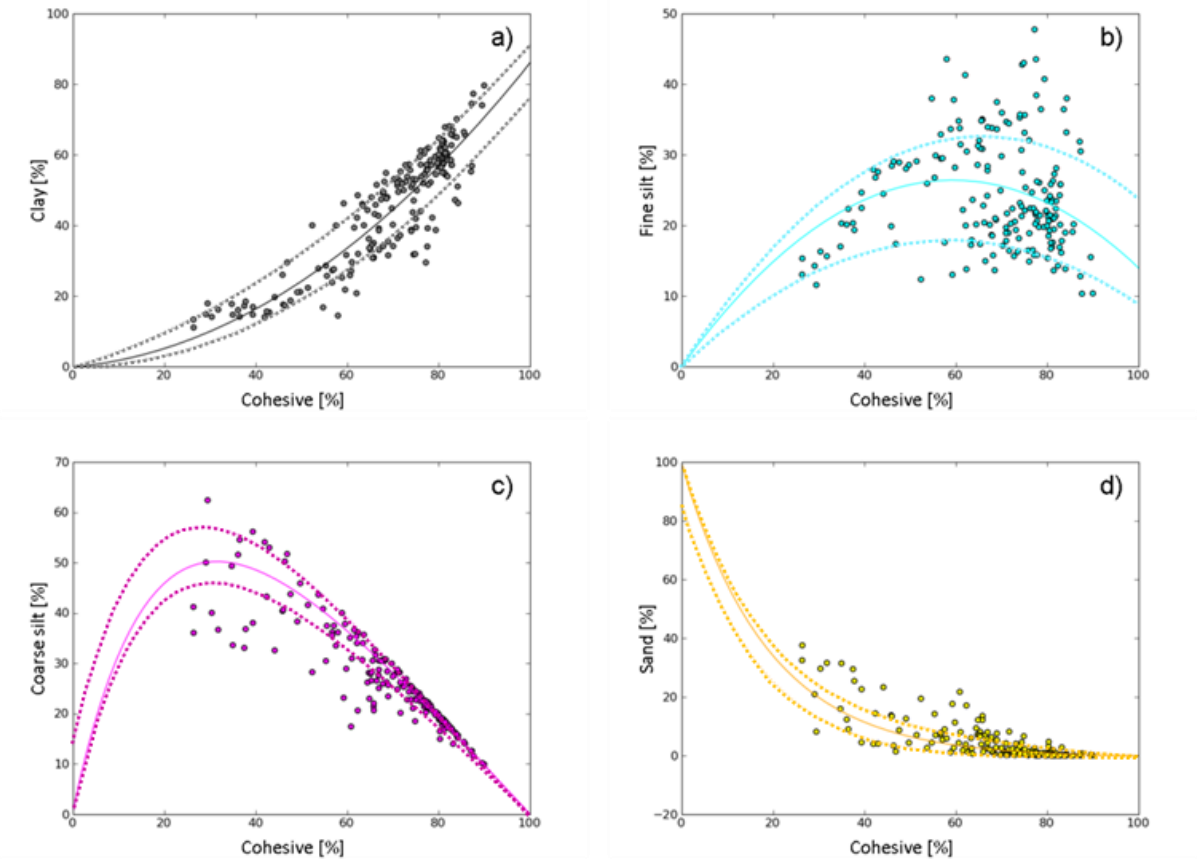

Figure 5.9: a)-d): Grain size fractions (clay, fine silt, coarse silt, sand) in weight percent as a function of cohesive content (clay + fine silt) fraction in weight percent. Circles represent the NA dataset, continuous lines show the grain size fraction models and the error models are represented by dotted lines.

To each of the 21 simulated structural templates a parameter matrix has been applied. This matrix varies two parameters, namely the overall mud content, that is the fraction of all cells of the simulated model, which have vshale contents above 50%, and effective stress to include the effect of mechanical compaction. Thereby, the mud content varies from 50% to 100% with a step size of 10%, whereas the effective stress ranges with a step size of 4 MPa from the minimum effective stress of 1 MPa to 5 MPa and a step size of 5 MPa from 5 MPa to the maximum applied effective stress of 30 MPa. As for each structural template ten stochastically equal realizations were simulated, the total number of models (8820) for fluid flow simulation results from the number of templates (21) times the number of mud contents (6) times the number of effective stresses (7) times the number of realizations (10).

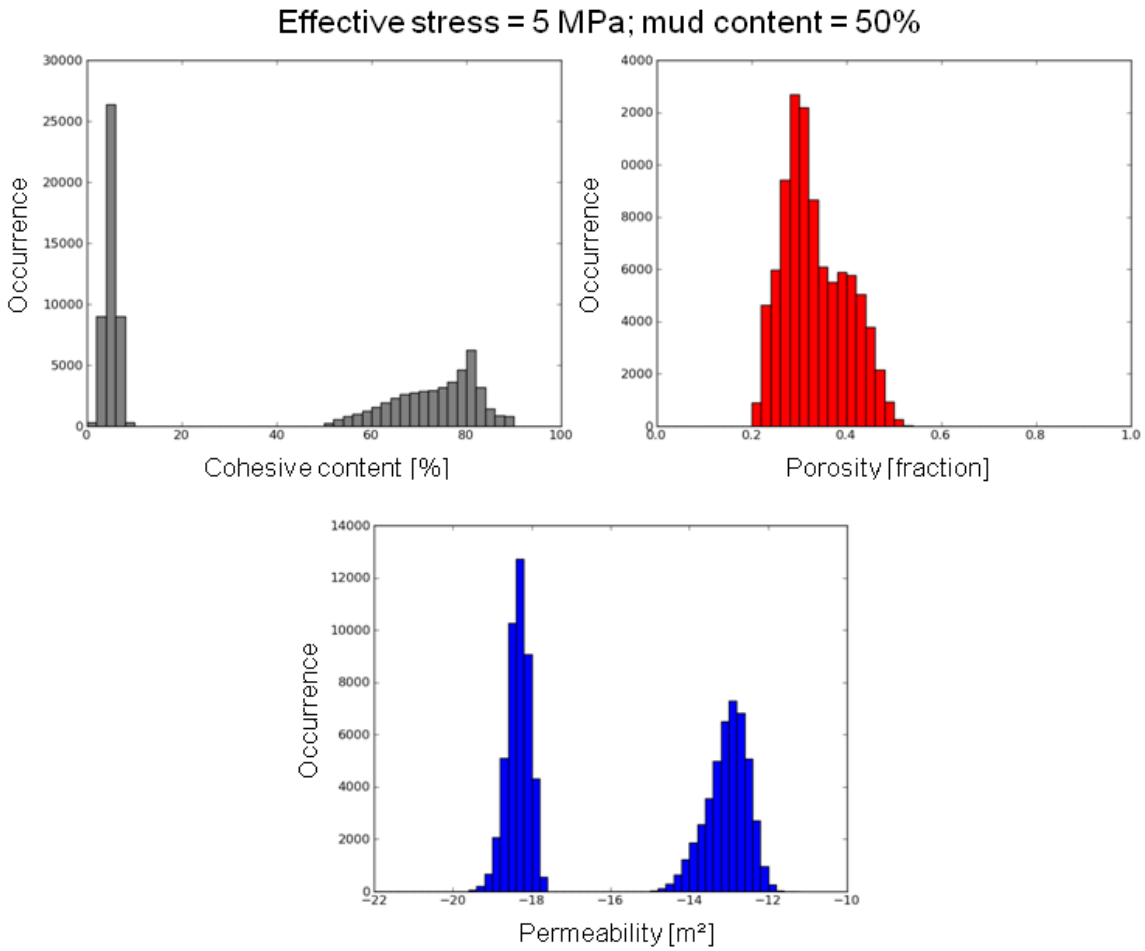

Figure 5.10: Example of property distribution (top left: cohesive content; top right: porosity; lower centre: vertical permeability) at 5MPa and 50% mud content for the ready-for-flow-simulation simulated structural template.

The resulting fluid flow models are then used to calculate effective horizontal and vertical permeabilities. To do so, a numerical fluid flow simulation is performed by using a 2D single phase fluid flow simulator based on a mixed finite element method (Ma et al., 2006). Effective permeabilities are then obtained from the numerically simulated steady state flow rate and pressure boundary conditions by employing Darcy's law (Ma et al., 2006). No flow is allowed on the boundaries parallel to the pressure gradient and the pressure boundary conditions are applied on the vertical boundaries to calculate vertical effective permeabilities and vice versa to calculate horizontal effective permeabilities. Effective porosity is calculated by arithmetic averaging of the porosities of all model cells as porosity is an additive property (Marsily et al., 2005). In the analysis of the results, the term percolation threshold is used for mud contents, where a significant change of effective permeability can be observed. Strictly spoken the term is not correctly used, as a percolation threshold refers to a certain point,

where a binary system changes from an unconnected state into a connected state. In contrast, this point is rather a transition from a less permeable to more permeable system in this study, as the components of the system (mud and sand) are defined by probability distributions of petrophysical properties, rather than by unique values. However, the term percolation threshold is used in this study for mud-sand ratios, where a sudden increase of effective permeability - and thus a sudden connected sand network - can be observed, as the term comes closest to this phenomenon.

Results

Due to the grain size simulation scheme used to populate the models with grain size fraction combinations on the basis of cohesive content only it is possible to calculate an average clay content for any mud content. By doing so, we can use these clay contents to calculate porosity and permeability with Yang's and Aplin's Models (2004, 2010) for a given effective stress and the mud contents investigated in this study (50, 60, 70, 80, 90 and 100 %). The results of this empirical porosity permeability calculation can be used as a homogeneous reference sample and for comparison with the numerical results. The resulting permeability plot (Figure 5.11) shows a strong relationship of effective stress and porosity or permeability and a minor influence of lithology on porosity or permeability. Thereby, at constant effective stress the corresponding porosities vary in a range of 5-10 %, while permeabilities vary with a maximum of 2 orders of magnitude. At constant mud content porosity varies with effective stress from 10 % to 55 %, while permeabilities range from 1e-21 m^2 to 1e-16 m^2.

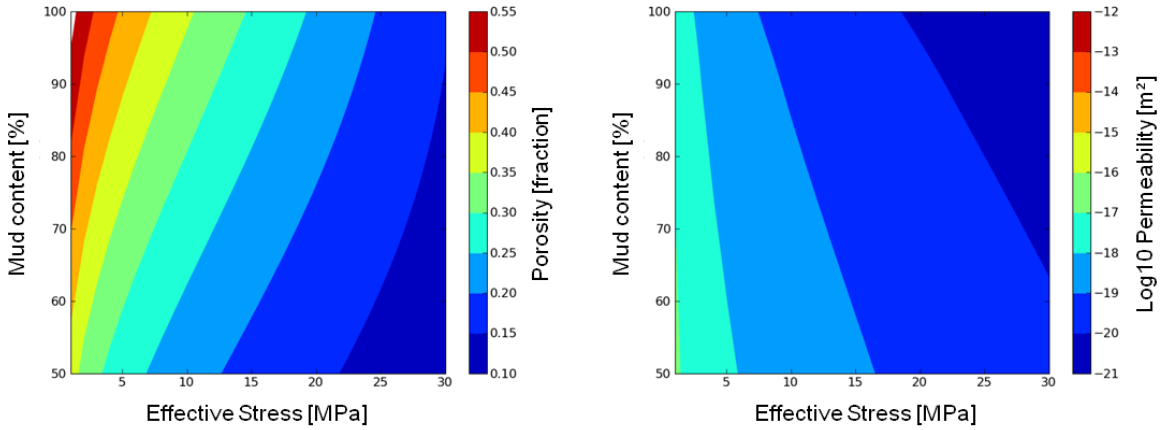

Figure 5.11: Porosity (left) and permeability (right) calculated for different effective stresses and mud contents by application of the petrophysical model to single values obtained by the Nile Delta grain size model (homogeneous reference sample).

The results of the numerical calculations have been divided into five groups and were compared to the homogeneous reference sample (Figure 5.12-4.16):

Group one (Figure 5.12) comprises structures with high horizontal permeabilities and vertical permeabilities similar to the homogeneous reference sample. Usually, the effective horizontal permeability of this group spans several orders of magnitude (1e-21 m^2 -1e-13 m^2 at 1 MPa effective stress) depending on mud content and effective stress. With decreasing mud content, the effective permeability switches from mud content-dependent to stress-dependent at mud contents between 50-80% (Figure 5.12, mid left). These mud contents depict the percolation threshold (content of coarse material, where connectivity through higher permeable coarser material through the model is provided) of this group and also corresponds to the highest standard deviation of effective horizontal permeability (Figure 5.12, mid right) with respect to the individual realizations and the approaching of a constant maximum anisotropy (Figure 5.12, top right). In vertical direction, the permeability changes as a function of effective stress only and spans a range from 1 e-21 m^2 to 1e-16 m^2 at an effective stress of 1 MPa (Figure 5.12, bottom left). In addition, very little variation can be observed within the vertical results of the individual geostatistical realizations (Figure 5.12, bottom right). The vertical results are of similar nature as the homogeneous analogous calculated reference sample and no percolation threshold (no vertically connected path of coarser, highly permeable material) is reached (Figure 5.12, bottom right). Group one mainly consists of bedded structures, but also some chaotic and small clasts structures.

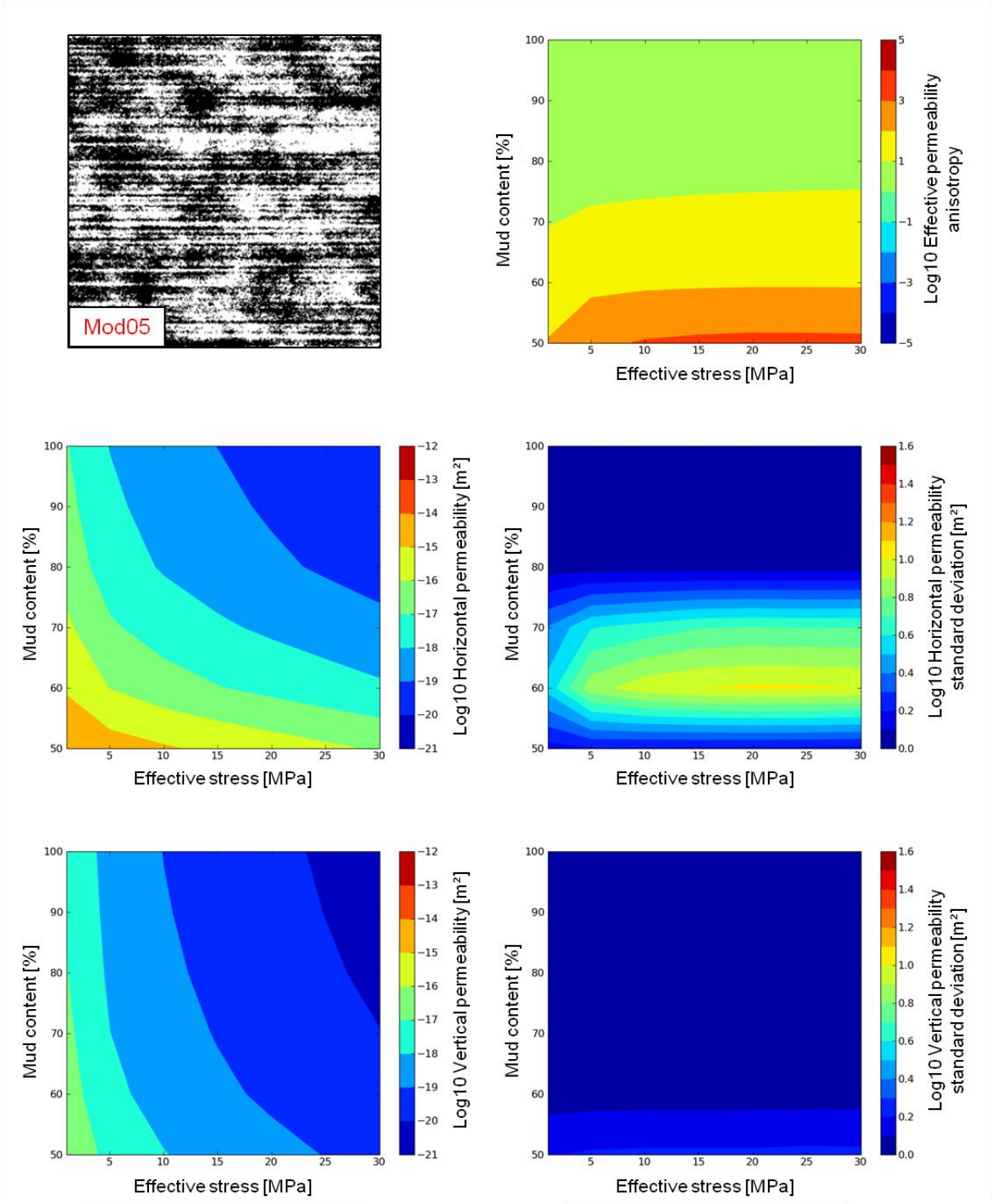

Figure 5.12: Example of result group 1 (high anisotropy → continuous horizontal structures). Explanation for Figures 4.12-4.16: On the upper left the binary representation of the simulated structural template is shown (600 mm edge length). Log10 effective permeability anisotropy (upper right), effective horizontal permeability (centre left), corresponding standard deviation (centre right) and effective vertical permeability (lower left) along with respective standard deviation (lower right) are represented as contour plots as a function of mud content and effective stress.

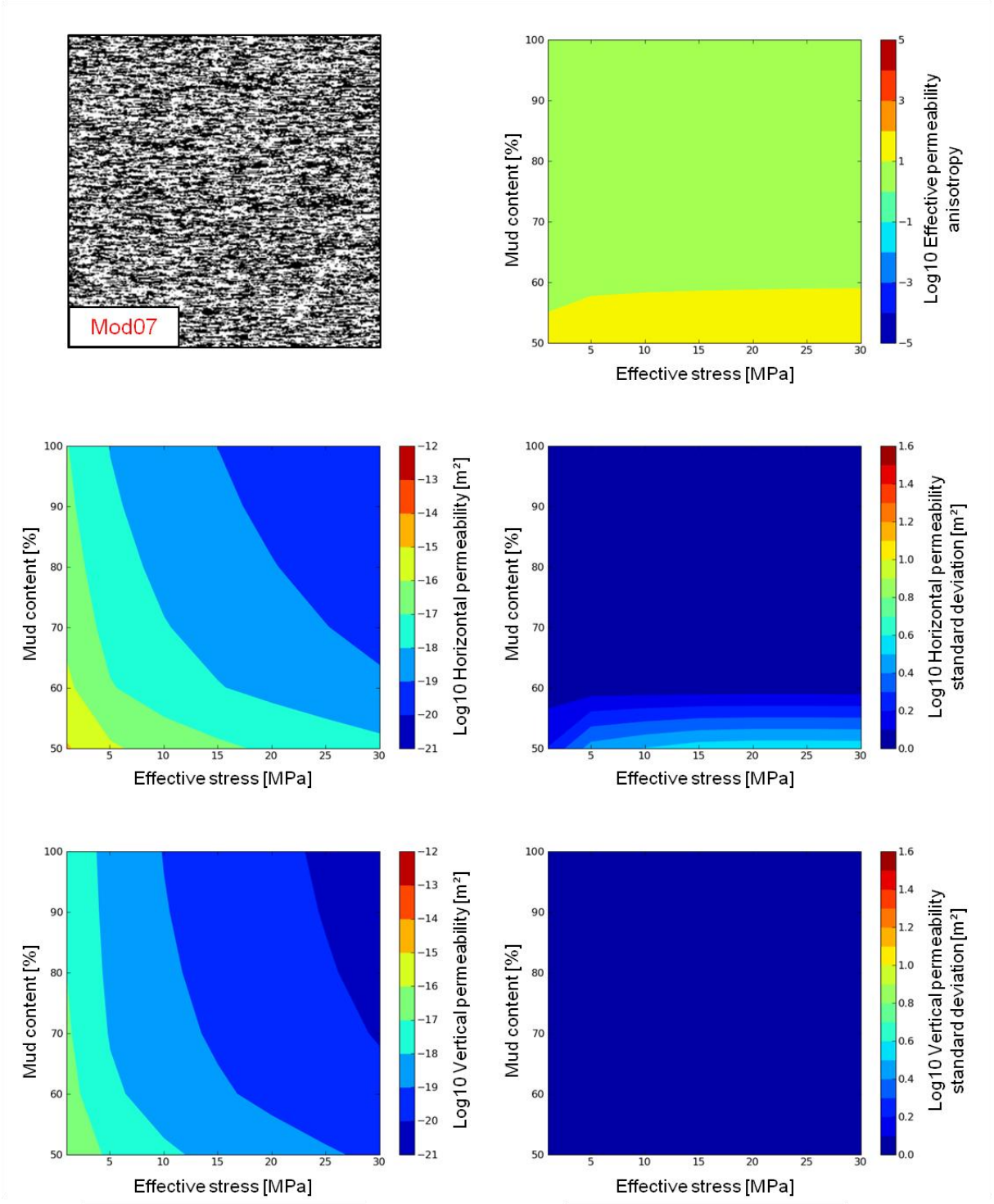

Figure 5.13: Example of result group 2 (medium-high anisotropy → discontinuous horizontal structures).

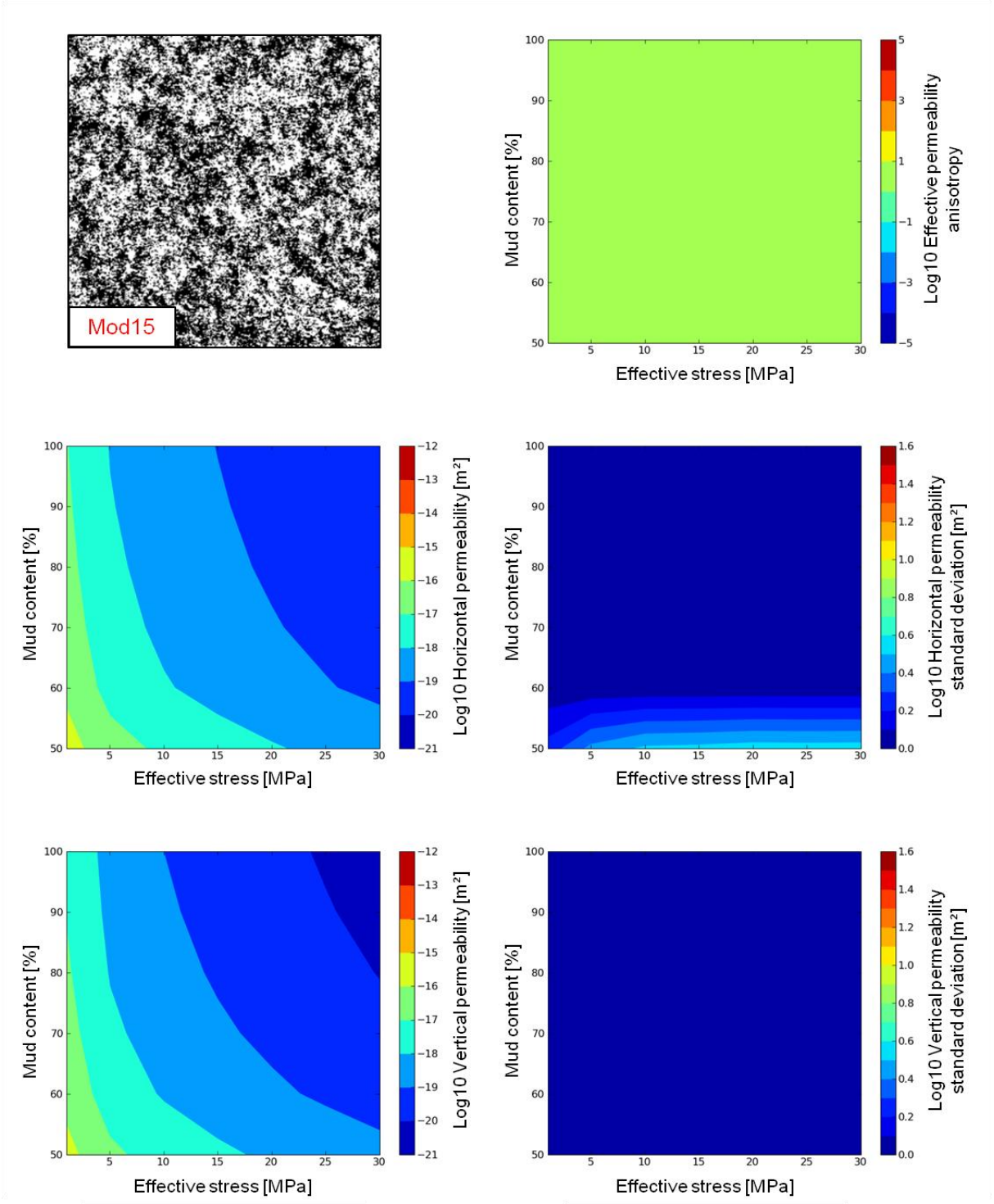

Figure 5.14: Example of result group 3 (anisotropy ~ 1 → isotropic structures).

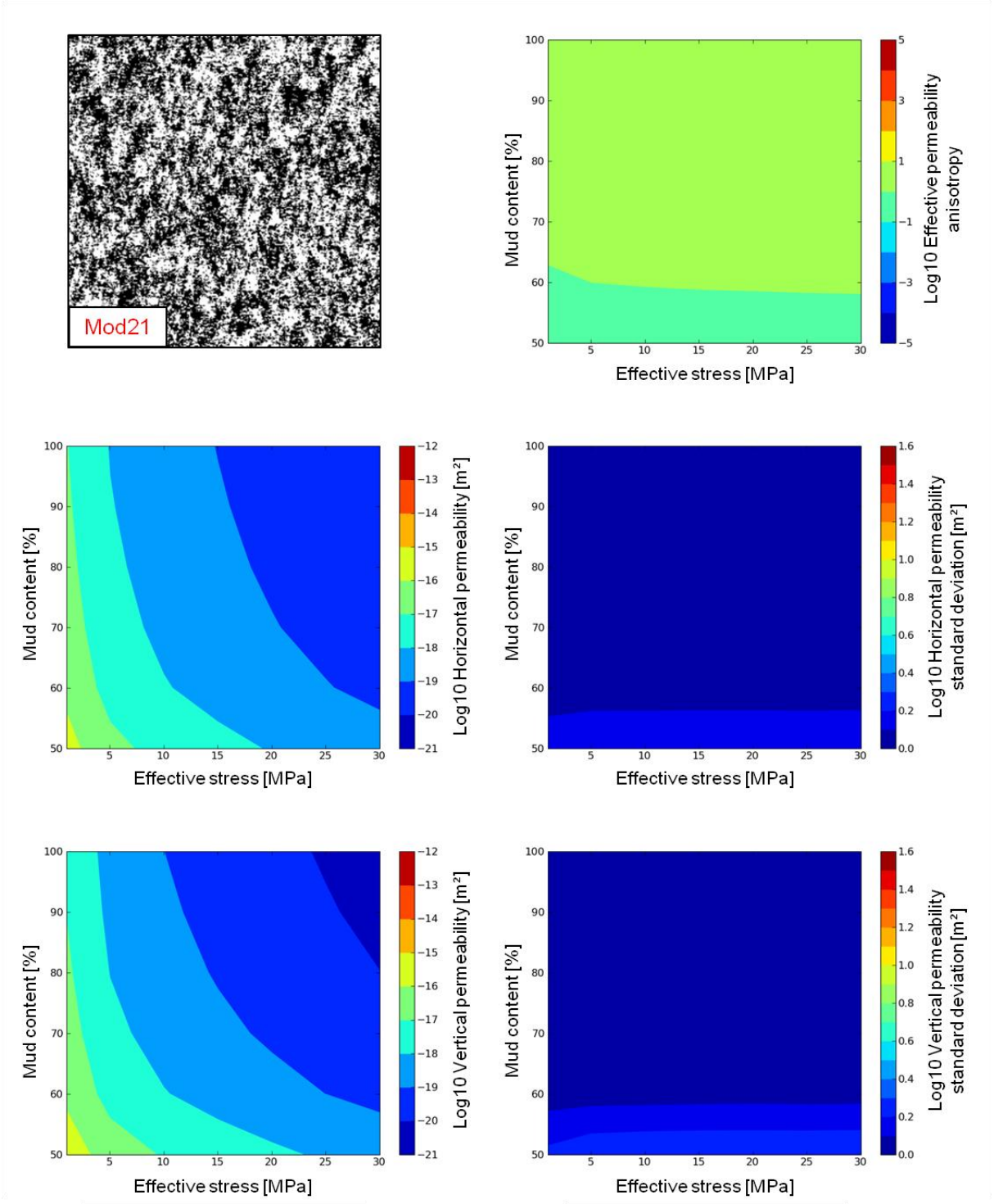

Figure 5.15: Example of result group 4 (low anisotropy → small vertical structures).

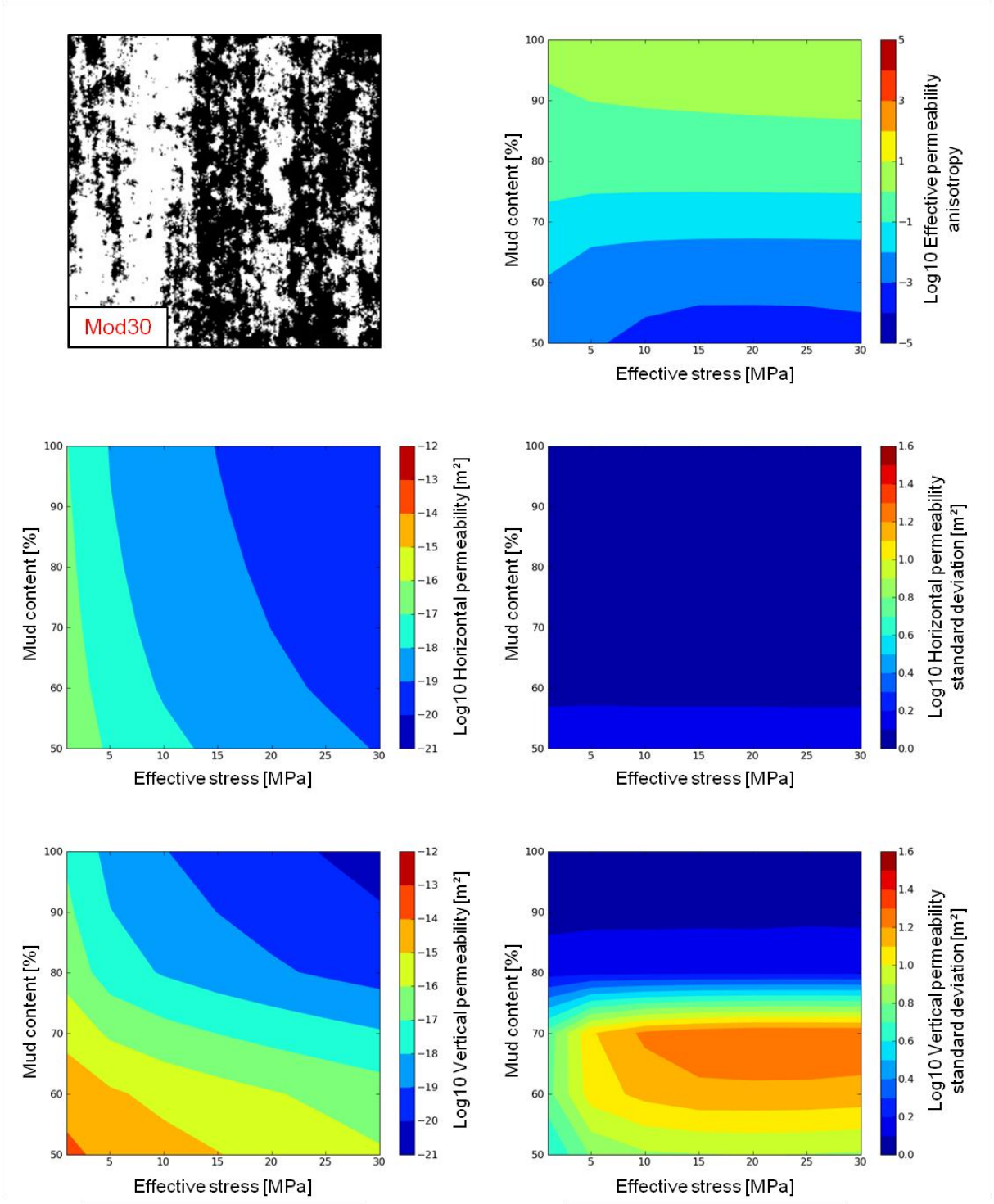

Figure 5.16: Example of result group 5 (very low anisotropy → large vertical structures).

Group two (Figure 5.13): the results of this group display high anisotropy (Figure 5.13, top right) with no or weak horizontally connected network of coarser, higher permeable material (Figure 5.13, mid right). The effective permeability in horizontal direction shows a lower maximum than the effective horizontal permeability of group one (max. 1e-15 m^2 at 1 MPa; Figure 5.13, mid left). In the vertical direction, the relationship between effective stress, mud content and effective permeability differs from the respective relationship of the homogeneous reference sample only for mud contents less than sixty percent. Group two cannot be assigned to a particular structure.

Group three (Figure 5.14) is featured by isotropic results with very similar behaviour in both horizontal and vertical directions (Figure 5.14, top right). The results are usually very robust with respect to the individual geostatistical realizations (Figure 5.14, mid right and bottom right), but do not reach high effective permeabilities compared to group one (max. 1e-15 m^2 at 1 MPa; Figure 5.14, mid left and mid right). In all cases, the influence of effective stress exceeds the influence of mud content on effective permeability. Similarities to the homogeneous reference sample are only observable at high mud contents. Group three only comprises chaotic and clast-bearing structures.

Group four (Figure 5.15) consists of structures yielding anisotropies less than or equal to 1 (Figure 5.15, top right). Therefore, the effective vertical permeability always exceeds the effective horizontal permeability (Figure 5.15, mid left and bottom left). However, the maximum effective permeabilities of this group reach only moderate values (1e-15 m^2 at 1 MPa). The results for the individual geostatistical realizations are more variable in the vertical direction when reaching a percolation threshold of approximately 60% mud content (Figure 5.15, bottom right). Also, the influence of effective stress on horizontal permeability is greater than vertical permeability. In the vertical direction, the effective permeability almost varies equally as a function of effective stress and mud content with a slightly higher variability of permeability as a function of effective stress (Figure 5.15, bottom left). Group four is the smallest group, comprising of minor slumped and small clasts bearing structures only.

Group five (Figure 5.16) consists of major slumped and large clasts bearing structures. They feature very low (<<1) anisotropies (Figure 5.16, top right). In the horizontal direction, the maximum effective permeabilities are quite variable (1e-16 m^2-1e-14 m^2 at 1 MPa; Figure 5.16, mid left). Equally, the influence of mud content and effective stress on effective permeability varies in horizontal direction. This is also reflected in the standard deviation of the effective horizontal permeabilities of the individual geostatistical realizations (Figure 5.16, mid right). The main feature of this group is a very high effective vertical permeability

(1e-14 m^2-1e-13 m^2 at 1 MPa; Figure 5.16, bottom left), which is reached at mud contents of 50-70%. At these percolation thresholds (Figure 5.16, bottom right), the influence of mud content on effective vertical permeability exceeds the influence of effective stress.

A different perspective upon the results can be established by grouping all structural templates by their geostatistical interpretation (variogroup) and respective averaging of the log10 effective horizontal and vertical permeabilities. With increasing mud content at constant effective stress (here: 5 MPa), the results become more and more similar as the percolation threshold increases and the respective permeability contrast decreases (Figure 5.17).

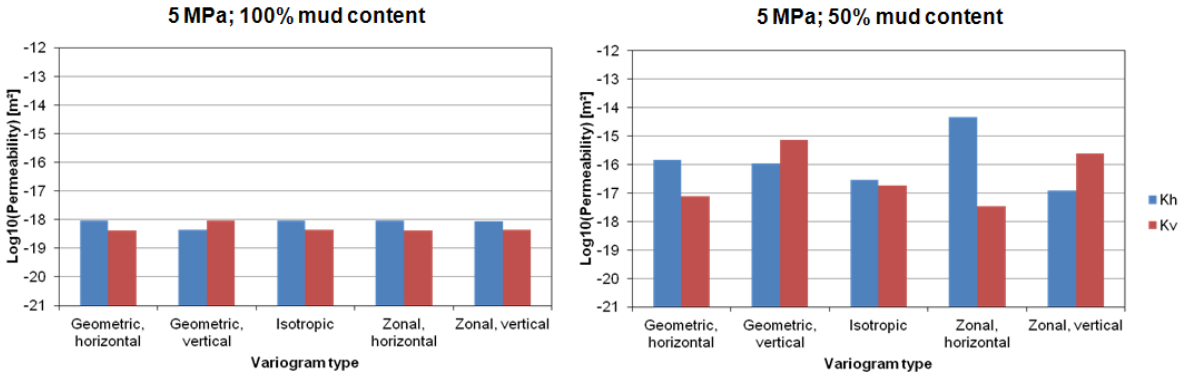

Figure 5.17: Grouping of the results into geostatistical groups (variogram types or variogroups) shows a dependence on geostatistical parameters (note the differences between Kh and Kv for the respective variogram types).

Plotting the averaged anisotropies for each variogroup vs. mud content depicts the dependence of anisotropy on geostatistical properties (Figure 5.18). Zonal horizontal and geometric horizontal structures display the highest anisotropy, while isotropic structures have constant anisotropies around 1. Structural templates with geostatistical properties that show a vertical dominance, show the lowest anisotropies. Note that the absolute values of individual templates could be higher as the averaging procedure might "damp" the result. However, even these averaged results demonstrate that effective permeability anisotropy might already vary by two orders of magnitude at very high mud contents around 80%, when compared for different geostatistical heterogeneity groups.

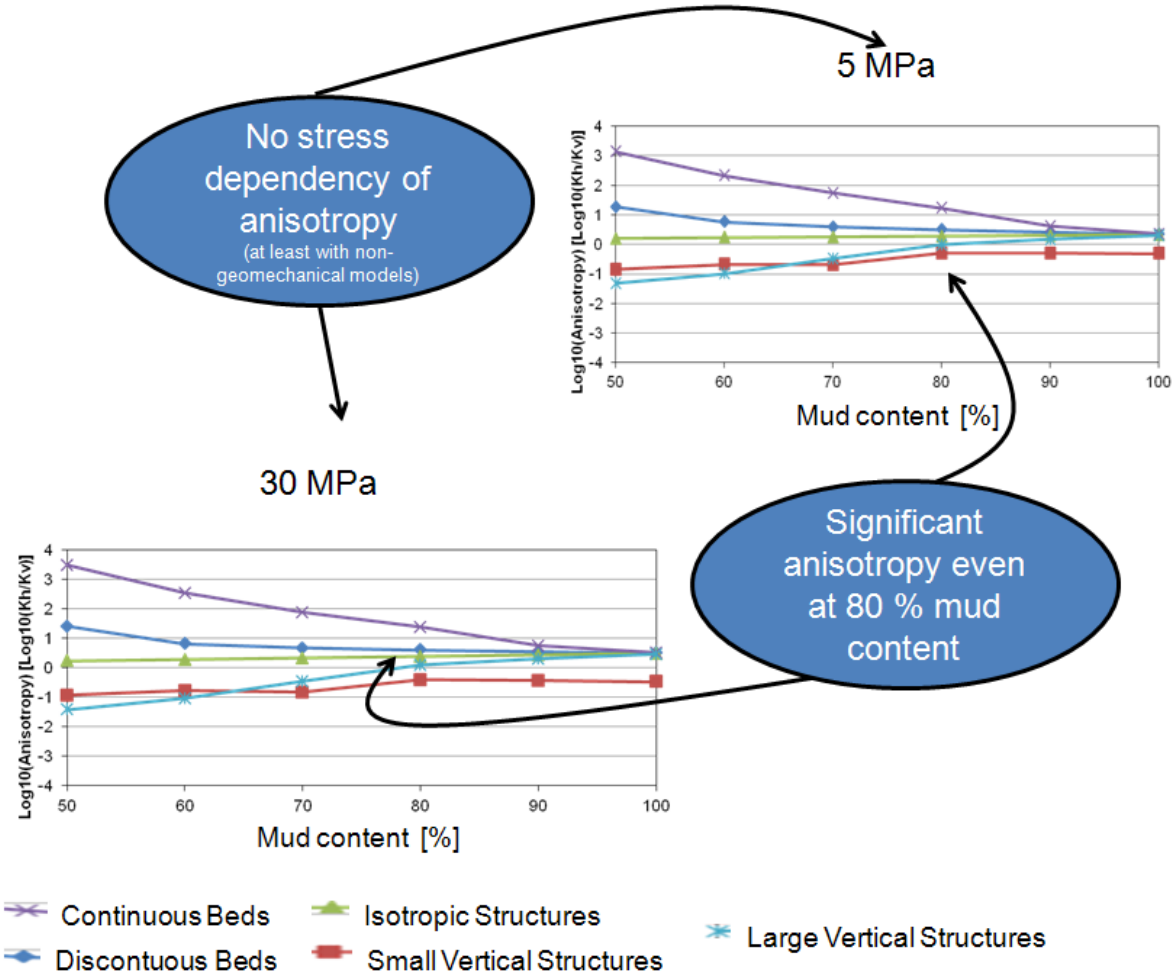

Figure 5.18: Average log10 effective permeability anisotropy of final heterogeneous mudstone groups as a function of mud content at 5 MPa (upper right) and 30 MPa (lower left). A stress dependency cannot be observed. Significant differences between anisotropies can be already observed at mud contents around 80%.

Finally, we modelled empirical relationships for calculation of porosity and effective permeabilities as a function of effective stress and lithology (mud content) with second order polynomials for one example of each structural template (Table 5.2 and Table 5.3). The resulting stress-dependent porosity-permeability relationships reveal a high variability due to heterogeneity and mud content. Porosity ranges between 15-42% and permeability spans values between 1e-21 m^2 and 1e-13 m^2. The shape of the porosity-permeability relationships are negatively curved for horizontal and vertical effective permeabilities lower than 1e-14 m^2 and positively curved for permeabilities > 1e-14 m^2 (Figure 5.19). The effective porosity-permeability relationships plot in the upper permeability third of published porosity-permeability data, or even exceed the majority of published data by up to 3 orders of

magnitude of permeability. Effective porosity spans a narrower range for effective porosity-permeability relationships (15-45%) than for measured published data (10-70%).

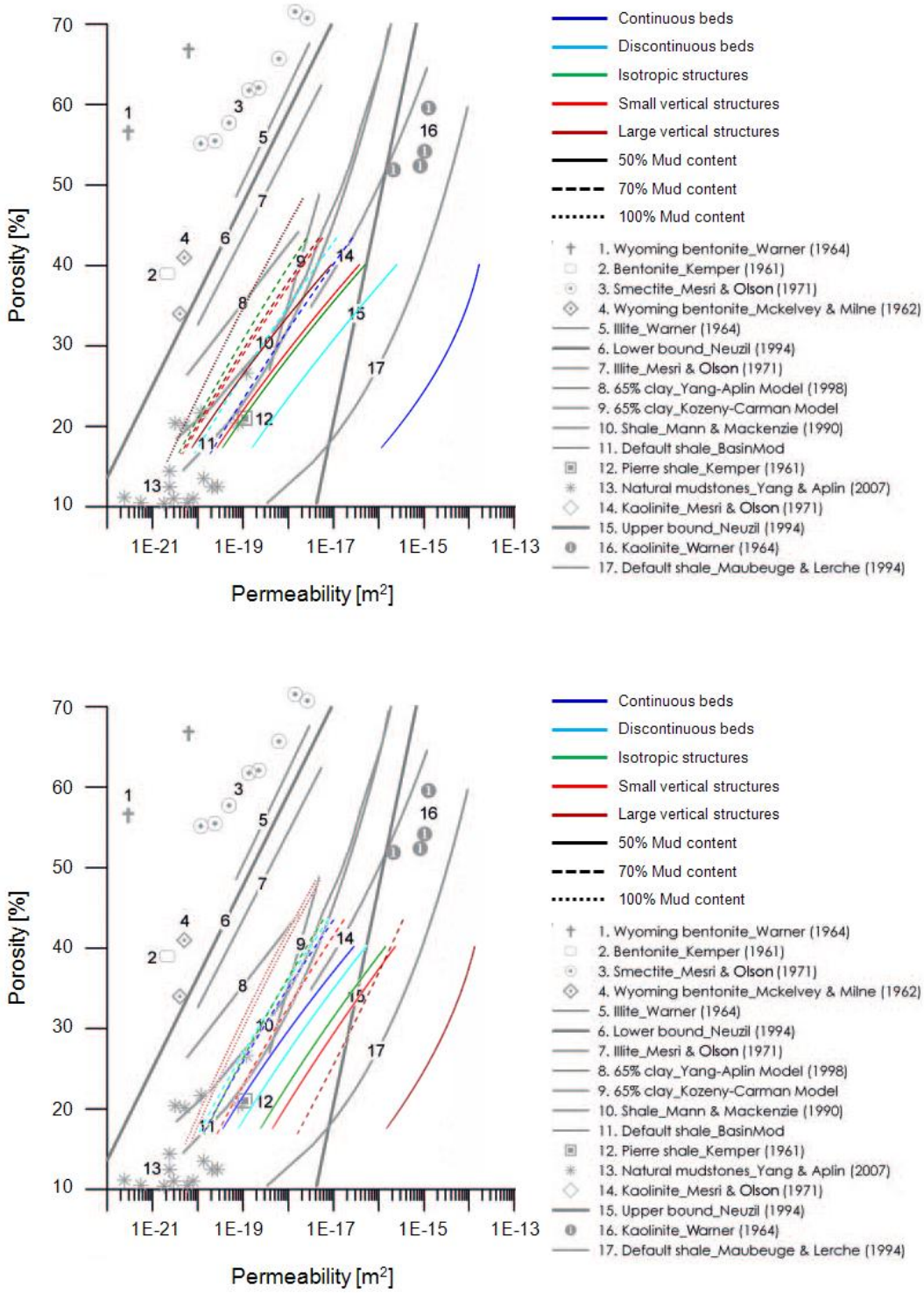

Figure 5.19: Comparison of a selection of the horizontal (top) vertical (bottom) effective porosity-permeability calculated in this study with published porosity permeability relationships derived from sample measurements (modified after Mondol et al., 2008). The colour of the lines represents the final structural class, whereas the line style represents the mud content.

Table 5.2: Modelled empirical effective stress σ – effective porosity φ relationships for different mud contents. The effective porosity is equal and therefore independent of heterogeneity as it is an additive property and calculated by the arithmetic average of the porosities of each model cell.

Mud content [%]	φ= f(σ)	R^2
50	$2.29e\text{-}004*\sigma^2$ -1.49e-002*σ + 4.16e-001	0.99
60	$2.53e\text{-}004*\sigma^2$ -1.64e-002*σ + 4.34e-001	0.99
70	$2.77e\text{-}004*\sigma^2$ -1.78e-002*σ + 4.52e-001	0.99
80	$3.01e\text{-}004*\sigma^2$ -1.93e-002*σ + 4.70e-001	0.99
90	$3.25e\text{-}004*\sigma^2$ -2.08e-002*σ + 4.87e-001	0.99
100	$3.49e\text{-}004*\sigma^2$ -2.23e-002*σ + 5.05e-001	0.99

Table 5.3: Results table showing the empirical relationships for all structural templates and mud contents between 50-100% to model porosity φ as a function of effective stress σ and to model horizontal and vertical effective permeabilities K_h and K_v as a function of porosity. R^2 gives the coefficient of correlation.

Final Group	Model_ID	Structure	Variogroup	Mud Content [%]	Kh = f(φ)	R²	Kv = f(φ)	R²	Kh/Kv = f(φ)	R²
Continous Beds	Mod01	Laminated	Zonal,horizontal	50	-1.86e+001*φ2 + 1.90e+001*φ - 1.87e+001	1	8.47e+000*φ2 + 7.97e+000*φ - 2.11e+001	1	1.53e+000*φ2 - 7.48e-001*φ + 9.01e-001	0.98
				60	5.64e+000*φ2 + 8.05e+000*φ - 1.97e+001	1	7.15e+000*φ2 + 7.60e+000*φ - 2.13e+001	1	2.66e-002*φ2 - 4.89e-002*φ + 9.23e-001	1
				70	4.28e+000*φ2 + 7.83e+000*φ - 2.01e+001	1	6.00e+000*φ2 + 7.32e+000*φ - 2.14e+001	1	6.67e-002*φ2 - 5.05e-002*φ + 9.41e-001	0.98
				80	3.47e+000*φ2 + 7.39e+000*φ - 2.04e+001	1	5.05e+000*φ2 + 7.08e+000*φ - 2.14e+001	1	7.61e-002*φ2 - 3.90e-002*φ + 9.55e-001	0.99
				90	2.77e+000*φ2 + 6.99e+000*φ - 2.06e+001	1	4.31e+000*φ2 + 6.79e+000*φ - 2.14e+001	1	8.61e-002*φ2 - 3.11e-002*φ + 9.65e-001	1
				100	2.23e+000*φ2 + 6.60e+000*φ - 2.08e+001	1	3.68e+000*φ2 + 6.55e+000*φ - 2.14e+001	1	9.11e-002*φ2 - 2.12e-002*φ + 9.75e-001	1
	Mod03	Laminated	Geometric,horizontal	50	6.64e+000*φ2 + 8.55e+000*φ - 1.98e+001	1	7.86e+000*φ2 + 8.11e+000*φ - 2.09e+001	1	2.20e-002*φ2 - 4.12e-002*φ + 9.49e-001	0.99
				60	5.58e+000*φ2 + 7.99e+000*φ - 2.02e+001	1	6.80e+000*φ2 + 7.67e+000*φ - 2.12e+001	1	4.02e-002*φ2 - 3.47e-002*φ + 9.54e-001	0.99
				70	4.47e+000*φ2 + 7.61e+000*φ - 2.05e+001	1	5.85e+000*φ2 + 7.33e+000*φ - 2.13e+001	1	6.39e-002*φ2 - 3.39e-002*φ + 9.60e-001	0.99
				80	3.41e+000*φ2 + 7.34e+000*φ - 2.06e+001	1	4.91e+000*φ2 + 7.09e+000*φ - 2.14e+001	1	8.09e-002*φ2 - 3.28e-002*φ + 9.66e-001	0.99
				90	2.69e+000*φ2 + 6.99e+000*φ - 2.08e+001	1	4.20e+000*φ2 + 6.83e+000*φ - 2.14e+001	1	8.95e-002*φ2 - 2.75e-002*φ + 9.71e-001	1
				100	2.26e+000*φ2 + 6.58e+000*φ - 2.08e+001	1	3.62e+000*φ2 + 6.56e+000*φ - 2.14e+001	1	8.58e-002*φ2 - 1.87e-002*φ + 9.76e-001	1
	Mod04	Laminated	Zonal,horizontal	50	-2.20e+001*φ2 + 2.10e+001*φ - 1.86e+001	1	8.61e+000*φ2 + 7.90e+000*φ - 2.11e+001	1	1.71e+000*φ2 - 8.65e-001*φ + 9.03e-001	0.99
				60	4.21e+000*φ2 + 8.59e+000*φ - 2.00e+001	1	7.14e+000*φ2 + 7.60e+000*φ - 2.12e+001	1	1.30e-001*φ2 - 8.00e-002*φ + 9.42e-001	0.76
				70	4.26e+000*φ2 + 7.69e+000*φ - 2.03e+001	1	5.82e+000*φ2 + 7.39e+000*φ - 2.13e+001	1	7.15e-002*φ2 - 3.87e-002*φ + 9.53e-001	0.97
				80	3.34e+000*φ2 + 7.31e+000*φ - 2.05e+001	1	4.89e+000*φ2 + 7.12e+000*φ - 2.14e+001	1	8.49e-002*φ2 - 3.23e-002*φ + 9.62e-001	0.99
				90	2.76e+000*φ2 + 6.94e+000*φ - 2.07e+001	1	4.20e+000*φ2 + 6.83e+000*φ - 2.14e+001	1	8.53e-002*φ2 - 2.53e-002*φ + 9.69e-001	1
				100	2.26e+000*φ2 + 6.58e+000*φ - 2.08e+001	1	3.58e+000*φ2 + 6.58e+000*φ - 2.14e+001	1	8.39e-002*φ2 - 1.76e-002*φ + 9.76e-001	1
	Mod05	Lenticular	Zonal,horizontal	50	-1.61e+001*φ2 + 1.76e+001*φ - 1.88e+001	1	8.27e+000*φ2 + 7.97e+000*φ - 2.09e+001	1	1.42e+000*φ2 - 6.65e-001*φ + 9.17e-001	1
				60	5.23e+000*φ2 + 8.05e+000*φ - 2.01e+001	1	7.00e+000*φ2 + 7.62e+000*φ - 2.12e+001	1	7.64e-002*φ2 - 4.57e-002*φ + 9.52e-001	0.98
				70	4.25e+000*φ2 + 7.63e+000*φ - 2.05e+001	1	5.77e+000*φ2 + 7.39e+000*φ - 2.13e+001	1	7.78e-002*φ2 - 3.40e-002*φ + 9.62e-001	0.99
				80	3.34e+000*φ2 + 7.32e+000*φ - 2.06e+001	1	4.81e+000*φ2 + 7.14e+000*φ - 2.14e+001	1	8.29e-002*φ2 - 2.91e-002*φ + 9.68e-001	1
				90	2.71e+000*φ2 + 6.94e+000*φ - 2.08e+001	1	4.13e+000*φ2 + 6.86e+000*φ - 2.14e+001	1	8.70e-002*φ2 - 2.33e-002*φ + 9.72e-001	1
				100	2.31e+000*φ2 + 6.55e+000*φ - 2.08e+001	1	3.58e+000*φ2 + 6.59e+000*φ - 2.14e+001	1	8.15e-002*φ2 - 1.60e-002*φ + 9.76e-001	1
	Mod06	Lenticular	Zonal,horizontal	50	7.63e+000*φ2 + 8.11e+000*φ - 1.97e+001	1	8.18e+000*φ2 + 8.02e+000*φ - 2.09e+001	1	-2.40e-002*φ2 - 2.00e-002*φ + 9.43e-001	1
				60	5.85e+000*φ2 + 7.82e+000*φ - 2.01e+001	1	6.86e+000*φ2 + 7.69e+000*φ - 2.12e+001	1	2.51e-002*φ2 - 2.77e-002*φ + 9.46e-001	0.97
				70	4.43e+000*φ2 + 7.58e+000*φ - 2.03e+001	1	5.79e+000*φ2 + 7.37e+000*φ - 2.13e+001	1	6.11e-002*φ2 - 3.27e-002*φ + 9.55e-001	0.92
				80	3.23e+000*φ2 + 7.45e+000*φ - 2.06e+001	1	4.91e+000*φ2 + 7.09e+000*φ - 2.14e+001	1	8.88e-002*φ2 - 3.92e-002*φ + 9.63e-001	1
				90	2.72e+000*φ2 + 6.97e+000*φ - 2.07e+001	1	4.20e+000*φ2 + 6.82e+000*φ - 2.14e+001	1	8.68e-002*φ2 - 2.72e-002*φ + 9.70e-001	1
				100	2.26e+000*φ2 + 6.59e+000*φ - 2.08e+001	1	3.60e+000*φ2 + 6.57e+000*φ - 2.14e+001	1	8.59e-002*φ2 - 1.88e-002*φ + 9.76e-001	1
	Mod14	MinorSlumped	Zonal,horizontal	50	-2.43e+001*φ2 + 2.24e+001*φ - 1.83e+001	1	9.91e+000*φ2 + 7.35e+000*φ - 2.14e+001	1	1.82e+000*φ2 - 9.55e-001*φ + 8.75e-001	0.99
				60	-1.83e+001*φ2 + 1.84e+001*φ - 1.79e+001	1	7.69e+000*φ2 + 7.39e+000*φ - 2.14e+001	1	1.38e+000*φ2 - 7.22e-001*φ + 8.51e-001	0.99
				70	-1.51e+001*φ2 + 1.61e+001*φ - 1.81e+001	1	6.26e+000*φ2 + 7.21e+000*φ - 2.14e+001	1	1.15e+000*φ2 - 5.90e-001*φ + 8.57e-001	0.99
				80	2.78e+000*φ2 + 7.59e+000*φ - 2.04e+001	1	5.13e+000*φ2 + 7.03e+000*φ - 2.14e+001	1	1.25e-001*φ2 - 5.56e-002*φ + 9.54e-001	0.99
				90	2.39e+000*φ2 + 7.12e+000*φ - 2.07e+001	1	4.32e+000*φ2 + 6.79e+000*φ - 2.14e+001	1	1.13e-001*φ2 - 3.89e-002*φ + 9.69e-001	1
				100	2.20e+000*φ2 + 6.62e+000*φ - 2.08e+001	1	3.68e+000*φ2 + 6.55e+000*φ - 2.14e+001	1	9.23e-002*φ2 - 2.20e-002*φ + 9.75e-001	1
	Mod16	MajorSlumped	Zonal,horizontal	50	5.49e+000*φ2 + 9.01e+000*φ - 1.99e+001	1	7.08e+000*φ2 + 8.40e+000*φ - 2.07e+001	1	6.15e-002*φ2 - 5.14e-002*φ + 9.62e-001	0.9
				60	5.43e+000*φ2 + 7.92e+000*φ - 2.03e+001	1	6.56e+000*φ2 + 7.70e+000*φ - 2.10e+001	1	4.96e-002*φ2 - 2.82e-002*φ + 9.67e-001	0.96
				70	4.25e+000*φ2 + 7.63e+000*φ - 2.06e+001	1	5.52e+000*φ2 + 7.43e+000*φ - 2.12e+001	1	6.74e-002*φ2 - 2.82e-002*φ + 9.71e-001	0.99
				80	3.38e+000*φ2 + 7.27e+000*φ - 2.07e+001	1	4.70e+000*φ2 + 7.15e+000*φ - 2.13e+001	1	7.80e-002*φ2 - 2.41e-002*φ + 9.74e-001	1
				90	2.73e+000*φ2 + 6.92e+000*φ - 2.08e+001	1	4.07e+000*φ2 + 6.86e+000*φ - 2.14e+001	1	8.33e-002*φ2 - 2.09e-002*φ + 9.76e-001	1
				100	2.35e+000*φ2 + 6.53e+000*φ - 2.08e+001	1	3.56e+000*φ2 + 6.58e+000*φ - 2.14e+001	1	7.78e-002*φ2 - 1.44e-002*φ + 9.76e-001	1
	Mod25	Small Clasts	Zonal,horizontal	50	5.90e+000*φ2 + 8.88e+000*φ - 1.99e+001	1	8.02e+000*φ2 + 8.06e+000*φ - 2.09e+001	1	7.61e-002*φ2 - 6.46e-002*φ + 9.51e-001	0.98
				60	5.63e+000*φ2 + 7.95e+000*φ - 2.02e+001	1	6.92e+000*φ2 + 7.62e+000*φ - 2.12e+001	1	5.25e-002*φ2 - 3.73e-002*φ + 9.54e-001	0.99
				70	4.31e+000*φ2 + 7.66e+000*φ - 2.05e+001	1	5.80e+000*φ2 + 7.35e+000*φ - 2.13e+001	1	7.35e-002*φ2 - 3.54e-002*φ + 9.62e-001	0.98
				80	3.35e+000*φ2 + 7.33e+000*φ - 2.07e+001	1	4.91e+000*φ2 + 7.09e+000*φ - 2.14e+001	1	8.73e-002*φ2 - 3.27e-002*φ + 9.68e-001	1
				90	2.61e+000*φ2 + 7.01e+000*φ - 2.08e+001	1	4.19e+000*φ2 + 6.83e+000*φ - 2.14e+001	1	9.50e-002*φ2 - 2.89e-002*φ + 9.73e-001	1
				100	2.30e+000*φ2 + 6.56e+000*φ - 2.08e+001	1	3.62e+000*φ2 + 6.57e+000*φ - 2.14e+001	1	8.41e-002*φ2 - 1.75e-002*φ + 9.76e-001	1

Continuation of table 4.3.

Final Group	Model_ID	Structure	Variogroup	Mud Content [%]	Kh = f(φ)	R²	Kv = f(φ)	R²	Kh/Kv = f(φ)	R²
Discontinuous Beds	Mod07	Lenticular	Geometric, horizontal	50	6.23e+000*φ2 + 8.71e+000*φ - 1.98e+001	1	7.20e+000*φ2 + 8.39e+000*φ - 2.08e+001	1	1.36e-002*φ2 - 3.40e-002*φ + 9.53e-001	1
				60	5.38e+000*φ2 + 8.04e+000*φ - 2.03e+001	1	6.75e+000*φ2 + 7.70e+000*φ - 2.12e+001	1	5.51e-002*φ2 - 3.69e-002*φ + 9.59e-001	0.98
				70	4.24e+000*φ2 + 7.89e+000*φ - 2.06e+001	1	5.75e+000*φ2 + 7.38e+000*φ - 2.14e+001	1	7.62e-002*φ2 - 3.58e-002*φ + 9.64e-001	0.99
				80	3.29e+000*φ2 + 7.35e+000*φ - 2.07e+001	1	4.90e+000*φ2 + 7.11e+000*φ - 2.14e+001	1	9.11e-002*φ2 - 3.28e-002*φ + 9.69e-001	1
				90	2.65e+000*φ2 + 6.99e+000*φ - 2.08e+001	1	4.17e+000*φ2 + 6.85e+000*φ - 2.14e+001	1	9.22e-002*φ2 - 2.84e-002*φ + 9.73e-001	1
				100	2.27e+000*φ2 + 6.58e+000*φ - 2.08e+001	1	3.61e+000*φ2 + 6.58e+000*φ - 2.14e+001	1	8.49e-002*φ2 - 1.78e-002*φ + 9.76e-001	1
	Mod18	Major Slumped	Geometric, horizontal	50	7.21e+000*φ2 + 8.10e+000*φ - 2.02e+001	1	4.56e+000*φ2 + 9.42e+000*φ - 2.04e+001	1	-.65e-001*φ2 + 8.10e-002*φ + 9.90e-001	0.99
				60	5.56e+000*φ2 + 7.84e+000*φ - 2.04e+001	1	4.20e+000*φ2 + 8.63e+000*φ - 2.07e+001	1	-8.29e-002*φ2 + 4.17e-002*φ + 9.85e-001	0.94
				70	4.45e+000*φ2 + 7.49e+000*φ - 2.06e+001	1	5.38e+000*φ2 + 7.44e+000*φ - 2.11e+001	1	5.58e-002*φ2 - 1.68e-002*φ + 9.80e-001	0.99
				80	3.52e+000*φ2 + 7.19e+000*φ - 2.08e+001	1	4.58e+000*φ2 + 7.17e+000*φ - 2.12e+001	1	6.54e-002*φ2 - 1.70e-002*φ + 9.78e-001	1
				90	2.85e+000*φ2 + 6.86e+000*φ - 2.08e+001	1	3.96e+000*φ2 + 6.89e+000*φ - 2.13e+001	1	7.06e-002*φ2 - 1.48e-002*φ + 9.77e-001	1
				100	2.41e+000*φ2 + 6.49e+000*φ - 2.08e+001	1	3.51e+000*φ2 + 6.60e+000*φ - 2.14e+001	1	7.19e-002*φ2 - 1.13e-002*φ + 9.76e-001	1
	Mod23	Small Clasts	Geometric, horizontal	50	6.78e+000*φ2 + 8.32e+000*φ - 2.01e+001	1	6.70e+000*φ2 + 8.51e+000*φ - 2.06e+001	1	-2.02e-002*φ2 + 4.67e-003*φ + 9.79e-001	0.75
				60	5.56e+000*φ2 + 7.89e+000*φ - 2.04e+001	1	6.28e+000*φ2 + 7.82e+000*φ - 2.10e+001	1	3.17e-002*φ2 - 1.65e-002*φ + 9.74e-001	0.87
				70	4.42e+000*φ2 + 7.52e+000*φ - 2.06e+001	1	5.42e+000*φ2 + 7.45e+000*φ - 2.12e+001	1	5.55e-002*φ2 - 1.93e-002*φ + 9.74e-001	0.99
				80	3.38e+000*φ2 + 7.27e+000*φ - 2.08e+001	1	4.59e+000*φ2 + 7.19e+000*φ - 2.13e+001	1	7.24e-002*φ2 - 2.14e-002*φ + 9.76e-001	1
				90	2.75e+000*φ2 + 6.92e+000*φ - 2.08e+001	1	4.01e+000*φ2 + 6.88e+000*φ - 2.13e+001	1	7.84e-002*φ2 - 1.92e-002*φ + 9.76e-001	1
				100	2.33e+000*φ2 + 6.54e+000*φ - 2.08e+001	1	3.52e+000*φ2 + 6.60e+000*φ - 2.14e+001	1	7.65e-002*φ2 - 1.40e-002*φ + 9.76e-001	1
Isotropic Structures	Mod10	Isotropic	Isotropic	50	5.98e+000*φ2 + 8.77e+000*φ - 2.01e+001	1	6.99e+000*φ2 + 8.42e+000*φ - 2.06e+001	1	4.01e-002*φ2 - 3.12e-002*φ + 9.75e-001	0.94
				60	5.58e+000*φ2 + 7.85e+000*φ - 2.05e+001	1	6.46e+000*φ2 + 7.75e+000*φ - 2.10e+001	1	4.25e-002*φ2 - 1.98e-002*φ + 9.74e-001	0.95
				70	4.30e+000*φ2 + 7.58e+000*φ - 2.07e+001	1	5.46e+000*φ2 + 7.45e+000*φ - 2.12e+001	1	6.57e-002*φ2 - 2.30e-002*φ + 9.75e-001	1
				80	3.45e+000*φ2 + 7.22e+000*φ - 2.08e+001	1	4.68e+000*φ2 + 7.16e+000*φ - 2.13e+001	1	7.43e-002*φ2 - 2.07e-002*φ + 9.75e-001	1
				90	2.74e+000*φ2 + 6.92e+000*φ - 2.08e+001	1	4.02e+000*φ2 + 6.90e+000*φ - 2.14e+001	1	8.07e-002*φ2 - 1.91e-002*φ + 9.76e-001	1
				100	2.32e+000*φ2 + 6.55e+000*φ - 2.08e+001	1	3.53e+000*φ2 + 6.60e+000*φ - 2.14e+001	1	7.80e-002*φ2 - 1.45e-002*φ + 9.76e-001	1
	Mod15	Major Slumped	Isotropic	50	6.80e+000*φ2 + 8.21e+000*φ - 2.03e+001	1	6.62e+000*φ2 + 8.46e+000*φ - 2.03e+001	1	-2.64e-003*φ2 + 1.11e-002*φ + 9.99e-001	0.98
				60	5.42e+000*φ2 + 7.84e+000*φ - 2.07e+001	1	6.04e+000*φ2 + 7.86e+000*φ - 2.08e+001	1	4.40e-002*φ2 - 8.40e-003*φ + 9.92e-001	1
				70	4.35e+000*φ2 + 7.47e+000*φ - 2.08e+001	1	5.14e+000*φ2 + 7.53e+000*φ - 2.11e+001	1	5.41e-002*φ2 - 9.26e-003*φ + 9.87e-001	1
				80	3.48e+000*φ2 + 7.16e+000*φ - 2.08e+001	1	4.43e+000*φ2 + 7.22e+000*φ - 2.12e+001	1	6.35e-002*φ2 - 1.14e-002*φ + 9.83e-001	1
				90	2.87e+000*φ2 + 6.82e+000*φ - 2.09e+001	1	3.88e+000*φ2 + 6.92e+000*φ - 2.13e+001	1	6.75e-002*φ2 - 1.05e-002*φ + 9.79e-001	1
				100	2.40e+000*φ2 + 6.49e+000*φ - 2.08e+001	1	3.43e+000*φ2 + 6.64e+000*φ - 2.14e+001	1	6.83e-002*φ2 - 9.01e-003*φ + 9.77e-001	1
	Mod17	Major Slumped	Zonal, vertical	50	7.37e+000*φ2 + 7.89e+000*φ - 2.03e+001	1	6.91e+000*φ2 + 8.31e+000*φ - 2.04e+001	1	-2.16e-002*φ2 + 2.06e-002*φ + 9.94e-001	0.99
				60	5.59e+000*φ2 + 7.79e+000*φ - 2.06e+001	1	6.10e+000*φ2 + 7.84e+000*φ - 2.09e+001	1	3.16e-002*φ2 - 6.92e-003*φ + 9.87e-001	0.99
				70	4.34e+000*φ2 + 7.52e+000*φ - 2.07e+001	1	5.25e+000*φ2 + 7.48e+000*φ - 2.11e+001	1	5.65e-002*φ2 - 1.54e-002*φ + 9.83e-001	1
				80	3.49e+000*φ2 + 7.17e+000*φ - 2.08e+001	1	4.51e+000*φ2 + 7.19e+000*φ - 2.12e+001	1	6.55e-002*φ2 - 1.43e-002*φ + 9.80e-001	1
				90	2.82e+000*φ2 + 6.85e+000*φ - 2.08e+001	1	3.91e+000*φ2 + 6.91e+000*φ - 2.13e+001	1	7.06e-002*φ2 - 1.33e-002*φ + 9.78e-001	1
				100	2.39e+000*φ2 + 6.50e+000*φ - 2.08e+001	1	3.47e+000*φ2 + 6.62e+000*φ - 2.14e+001	1	7.06e-002*φ2 - 1.07e-002*φ + 9.77e-001	1
	Mod26	Small Clasts	Geometric, horizontal	50	6.64e+000*φ2 + 8.32e+000*φ - 2.02e+001	1	7.38e+000*φ2 + 8.19e+000*φ - 2.08e+001	1	2.64e-002*φ2 - 1.99e-002*φ + 9.73e-001	0.86
				60	5.37e+000*φ2 + 7.89e+000*φ - 2.06e+001	1	6.58e+000*φ2 + 7.71e+000*φ - 2.12e+001	1	6.49e-002*φ2 - 2.63e-002*φ + 9.74e-001	0.99
				70	4.27e+000*φ2 + 7.53e+000*φ - 2.08e+001	1	5.57e+000*φ2 + 7.43e+000*φ - 2.13e+001	1	7.72e-002*φ2 - 2.36e-002*φ + 9.75e-001	1
				80	3.38e+000*φ2 + 7.22e+000*φ - 2.08e+001	1	4.74e+000*φ2 + 7.15e+000*φ - 2.14e+001	1	8.44e-002*φ2 - 2.20e-002*φ + 9.77e-001	1
				90	2.75e+000*φ2 + 6.89e+000*φ - 2.09e+001	1	4.06e+000*φ2 + 6.89e+000*φ - 2.14e+001	1	8.36e-002*φ2 - 1.83e-002*φ + 9.76e-001	1
				100	2.36e+000*φ2 + 6.52e+000*φ - 2.08e+001	1	3.52e+000*φ2 + 6.62e+000*φ - 2.14e+001	1	7.51e-002*φ2 - 1.23e-002*φ + 9.76e-001	1
	Mod28	Large Clasts	Isotropic	50	6.81e+000*φ2 + 8.19e+000*φ - 2.04e+001	1	4.01e+000*φ2 + 9.52e+000*φ - 2.02e+001	1	-1.66e-001*φ2 + 9.14e-002*φ + 1.01e+000	0.88
				60	5.84e+000*φ2 + 7.60e+000*φ - 2.06e+001	1	6.17e+000*φ2 + 7.72e+000*φ - 2.07e+001	1	2.55e-002*φ2 - 1.08e-003*φ + 9.92e-001	1
				70	4.37e+000*φ2 + 7.49e+000*φ - 2.07e+001	1	5.08e+000*φ2 + 7.51e+000*φ - 2.10e+001	1	4.88e-002*φ2 - 9.29e-003*φ + 9.89e-001	1
				80	3.53e+000*φ2 + 7.14e+000*φ - 2.08e+001	1	4.35e+000*φ2 + 7.22e+000*φ - 2.11e+001	1	5.58e-002*φ2 - 8.96e-003*φ + 9.86e-001	1
				90	2.87e+000*φ2 + 6.82e+000*φ - 2.08e+001	1	3.81e+000*φ2 + 6.92e+000*φ - 2.13e+001	1	6.28e-002*φ2 - 9.34e-003*φ + 9.80e-001	1
				100	2.41e+000*φ2 + 6.49e+000*φ - 2.08e+001	1	3.40e+000*φ2 + 6.64e+000*φ - 2.14e+001	1	6.63e-002*φ2 - 8.25e-003*φ + 9.77e-001	1

Continuation of table 4.3.

Final Group	Model_ID	Structure	Variogroup	Mud Content [%]	Kh=f(φ)	R²	Kv=f(φ)	R²	Kh/Kv=f(φ)	R²
Small Vertical Structures	Mod12	MinorSlumped	Zonal, vertical	50	7.03e+000*φ2 + 7.92e+000*φ - 2.07e+001	1	-4.42e+000*φ2 + 1.31e+001*φ - 1.95e+001	1	-7.60e-001*φ2 + 4.12e-001*φ + 1.05e+000	0.98
				60	5.62e+000*φ2 + 7.61e+000*φ - 2.08e+001	1	3.09e+000*φ2 + 9.02e+000*φ - 2.03e+001	1	-1.28e-001*φ2 + 9.50e-002*φ + 1.02e+000	0.99
				70	4.50e+000*φ2 + 7.32e+000*φ - 2.08e+001	1	4.69e+000*φ2 + 7.63e+000*φ - 2.08e+001	1	3.15e-002*φ2 + 1.12e-002*φ + 1.00e+000	1
				80	3.51e+000*φ2 + 7.10e+000*φ - 2.09e+001	1	4.05e+000*φ2 + 7.33e+000*φ - 2.10e+001	1	4.52e-002*φ2 + 1.91e-003*φ + 9.92e-001	1
				90	2.95e+000*φ2 + 6.74e+000*φ - 2.09e+001	1	3.62e+000*φ2 + 7.01e+000*φ - 2.12e+001	1	5.00e-002*φ2 + 3.87e-005*φ + 9.83e-001	1
				100	2.47e+000*φ2 + 6.45e+000*φ - 2.08e+001	1	3.35e+000*φ2 + 6.67e+000*φ - 2.13e+001	1	6.00e-002*φ2 - 4.36e-003*φ + 9.77e-001	1
	Mod21	Small Clasts	Isotropic	50	6.83e+000*φ2 + 8.17e+000*φ - 2.04e+001	1	5.13e+000*φ2 + 9.09e+000*φ - 2.01e+001	1	-8.40e-002*φ2 + 6.28e-002*φ + 1.01e+000	0.92
				60	5.36e+000*φ2 + 7.86e+000*φ - 2.07e+001	1	5.52e+000*φ2 + 8.06e+000*φ - 2.07e+001	1	2.10e-002*φ2 + 5.78e-003*φ + 9.99e-001	1
				70	4.28e+000*φ2 + 7.51e+000*φ - 2.08e+001	1	4.95e+000*φ2 + 7.80e+000*φ - 2.10e+001	1	4.91e-002*φ2 - 6.17e-003*φ + 9.90e-001	1
				80	3.50e+000*φ2 + 7.14e+000*φ - 2.08e+001	1	4.35e+000*φ2 + 7.25e+000*φ - 2.12e+001	1	5.88e-002*φ2 - 8.10e-003*φ + 9.84e-001	1
				90	2.85e+000*φ2 + 6.82e+000*φ - 2.09e+001	1	3.80e+000*φ2 + 6.96e+000*φ - 2.13e+001	1	6.43e-002*φ2 - 8.65e-003*φ + 9.80e-001	1
				100	2.43e+000*φ2 + 6.48e+000*φ - 2.08e+001	1	3.44e+000*φ2 + 6.63e+000*φ - 2.14e+001	1	6.68e-002*φ2 - 8.27e-003*φ + 9.77e-001	1
Large Vertical Structures	Mod20	MajorSlumped	Geometric, vertical	50	6.54e+000*φ2 + 8.21e+000*φ - 2.04e+001	1	-1.24e+001*φ2 + 1.66e+001*φ - 1.94e+001	1	-1.36e+000*φ2 + 6.86e-001*φ + 1.03e+000	1
				60	5.12e+000*φ2 + 7.96e+000*φ - 2.05e+001	1	8.15e-001*φ2 + 1.01e+001*φ - 2.03e+001	1	-2.55e-001*φ2 + 1.44e-001*φ + 1.01e+000	0.97
				70	4.14e+000*φ2 + 7.56e+000*φ - 2.07e+001	1	4.71e+000*φ2 + 7.67e+000*φ - 2.08e+001	1	4.69e-002*φ2 - 3.15e-003*φ + 9.98e-001	1
				80	3.47e+000*φ2 + 7.16e+000*φ - 2.08e+001	1	4.22e+000*φ2 + 7.25e+000*φ - 2.10e+001	1	5.53e-002*φ2 - 6.04e-003*φ + 9.91e-001	1
				90	2.87e+000*φ2 + 6.81e+000*φ - 2.08e+001	1	3.70e+000*φ2 + 6.95e+000*φ - 2.12e+001	1	5.79e-002*φ2 - 6.04e-003*φ + 9.83e-001	1
				100	2.39e+000*φ2 + 6.50e+000*φ - 2.08e+001	1	3.33e+000*φ2 + 6.67e+000*φ - 2.13e+001	1	6.32e-002*φ2 - 6.92e-003*φ + 9.77e-001	1
	Mod27	Large Clasts	Geometric, vertical	50	6.27e+000*φ2 + 8.55e+000*φ - 2.05e+001	1	1.80e+000*φ2 + 1.07e+001*φ - 2.04e+001	1	-2.72e-001*φ2 + 1.39e-001*φ + 9.99e-001	1
				60	5.34e+000*φ2 + 7.83e+000*φ - 2.06e+001	1	6.43e+000*φ2 + 7.77e+000*φ - 2.09e+001	1	7.12e-002*φ2 - 1.79e-002*φ + 9.85e-001	1
				70	4.29e+000*φ2 + 7.49e+000*φ - 2.07e+001	1	5.43e+000*φ2 + 7.46e+000*φ - 2.11e+001	1	7.60e-002*φ2 - 1.69e-002*φ + 9.84e-001	1
				80	3.33e+000*φ2 + 7.28e+000*φ - 2.08e+001	1	4.55e+000*φ2 + 7.20e+000*φ - 2.12e+001	1	7.67e-002*φ2 - 2.03e-002*φ + 9.80e-001	1
				90	2.92e+000*φ2 + 6.79e+000*φ - 2.08e+001	1	3.96e+000*φ2 + 6.89e+000*φ - 2.13e+001	1	6.82e-002*φ2 - 1.12e-002*φ + 9.77e-001	1
				100	2.38e+000*φ2 + 6.50e+000*φ - 2.08e+001	1	3.47e+000*φ2 + 6.61e+000*φ - 2.14e+001	1	7.13e-002*φ2 - 1.10e-002*φ + 9.77e-001	1
	Mod30	Large Clasts	Zonal, vertical	50	7.41e+000*φ2 + 7.59e+000*φ - 2.08e+001	1	-1.93e+001*φ2 + 1.98e+001*φ - 1.87e+001	1	-2.16e+000*φ2 + 1.15e+000*φ + 1.08e+000	0.99
				60	5.69e+000*φ2 + 7.48e+000*φ - 2.08e+001	1	-1.22e+001*φ2 + 1.54e+001*φ - 1.87e+001	1	-1.36e+000*φ2 + 7.23e-001*φ + 1.10e+000	0.99
				70	4.53e+000*φ2 + 7.25e+000*φ - 2.08e+001	1	-2.96e+000*φ2 + 1.06e+001*φ - 1.95e+001	1	-4.82e-001*φ2 + 2.68e-001*φ + 1.06e+000	0.99
				80	3.66e+000*φ2 + 6.99e+000*φ - 2.09e+001	1	3.58e+000*φ2 + 7.47e+000*φ - 2.06e+001	1	1.91e-002*φ2 + 2.38e-002*φ + 1.01e+000	1
				90	2.98e+000*φ2 + 6.72e+000*φ - 2.09e+001	1	3.32e+000*φ2 + 7.08e+000*φ - 2.10e+001	1	3.34e-002*φ2 + 8.42e-003*φ + 9.92e-001	1
				100	2.48e+000*φ2 + 6.43e+000*φ - 2.08e+001	1	3.23e+000*φ2 + 6.71e+000*φ - 2.13e+001	1	5.28e-002*φ2 - 7.01e-004*φ + 9.78e-001	1

Discussion

Mudstones are heterogeneous at different scales and their flow properties vary as a function of this heterogeneity, lithological composition and compaction (e.g. Aplin and Macquaker, 2011). Despite this common view, only little knowledge of stress-dependent flow properties such as permeability and porosity is available so far for heterogeneous mudstones. Yang and Aplin (2010) developed a permeability model for homogeneous mudstones at sample scale (centimetre-scale) as a function of porosity and clay content. In combination with their porosity model (Yang and Aplin, 2004), the model allows for including lithological variability and mechanical compaction through effective stress without spatial heterogeneity into mudstone porosity-permeability prediction workflows. The influence of sub-metre scale heterogeneity has long been noted and studied from the petroleum reservoir modelling community (e.g. Pickup et al., 2000) and in hydro-geological studies (Desbarats and Bachu, 1994; Huysmans and Dassargues, 2009). Previous numerical studies on sub-metre scale heterogeneity in mud-rich environments focused on tidal influenced (Nordahl et al., 2005; Nordahl and Ringrose, 2008) or thin-bedded (Scaglioni et al., 2006) sandstone reservoirs by using a process based modelling tool (Wen et al., 1999). However, the types of heterogeneity investigated by these studies were restricted to laminated and flaser-shaped sand-mudstone intercalations. We implemented an extended version of Yang's and Aplin's (2004, 2010) work into a geostatistical modelling workflow, which accounts for spatial lithological heterogeneity and variability present in mudstones at sub-metre scale (cm-m scale). Hereby, we regarded various types of mudstone heterogeneity (lamination, flaser bedding, bioturbation, soft sediment deformation, sand injections and mass movement). As Yang's and Aplin's (2004, 2010) models only include mechanical compaction in terms of effective stress, it has not been subject of this study to incorporate chemical compaction. Chemical compaction usually sets in at depths around 2-3 km roughly corresponding to 30 MPa in normal pressure or non-overpressured regimes and can significantly reduce porosity and permeability by cementation (Bjørlykke and Hoeg, 1997). It should also be mentioned, that the results presented here might be different when including the third spatial dimension, although our results correlate well with previous three-dimensional studies (Nordahl et al., 2005; Scaglioni et al., 2006; Nordahl and Ringrose, 2008). Also, the model size can have significant influence upon effective properties such as permeability. In particular, the model size should be chosen to be representative, yielding stable numerical results (e.g. effective permeabilities; compare Bear, 1972 on representative elementary volumes). In a previous study (Chapter 3) we investigated the influence of model size on effective permeability and found 600 mm of model edge length

(resulting in 600 mm x 600 mm model size) to yield sufficiently stable results for most heterogeneities. Heterogeneities yielding unstable results at this model size should be regarded with respect to an uncertainty measure. To do so, we provided standard deviations of the result distributions consisting of the 10 geostatistical realisations of the respective structural template.

The effective permeabilities obtained in this study by numerical fluid flow simulation significantly differ from Yang´s and Aplin´s (2010) results for homogeneous mudstones, which usually range between 1e-21 m² and 1e-16 m² depending on clay content and porosity and thus effective stress (1-30 MPa). In contrast, effective permeabilities of heterogeneous mudstones obtained in this study span values between 1e-21 m² and 1e-13 m² and thus exceed Yang's and Aplin's modelled permeabilities by up to three orders of magnitude, which can be attributed to the effect of geological heterogeneity included in this study. This is also reflected, when comparing the effective porosity-permeability relationships for heterogeneous mudstones obtained in this study with other published porosity and permeability data derived from measurements on homogeneous mudstone samples (Kemper, 1961; McKelvey and Milne, 1962; Warner, 1964; Mesri and Olson, 1971; Mann and McKenzie, 1990; Neuzil, 1994; Maubeuge and Lerche, 1994; Yang and Aplin, 1998; Yang and Aplin, 2007; Figure 5.19). The major difference between the "homogeneous" and "heterogeneous" permeability ranges exposes the influence of mud content and in particular the influence of heterogeneity. Hereby the heterogeneity is not only expressed by the larger range of permeabilities but also by the shape of the porosity permeability curves, which are not linear on a log-permeability plot – in contrast to porosity-permeability relationships of experimental mechanical compaction data on perfectly homogenous, artificial samples (e.g. Mondol et al., 2008). The different shapes reflect also the dominance of lithology (mud or sand in this case): a positive curve (that is the curvature is convex with respect to increasing permeability) is associated to a fully connected network of the coarser material. A negative curve (that is the curvature is concave with respect to increasing permeability) is associated to a "sealed" or only minor "connected" network of coarser and hence more permeable material. The implications for sealing or fluid retention capacity of heterogeneous mudstones are very obvious: though permeability measurements on homogeneous samples might suggest high sealing and fluid retention capacities, the influence of mudstone heterogeneity could yield significant lower capacities (three orders of magnitude in terms of permeability). Neglecting these effects in basin, reservoir or hydro-geological modelling can thus cause severe misinterpretations of fluid flow in the subsurface. Hence, the results of this study confirm the importance of sub-

metre scale heterogeneities and mud content for fluid flow as shown previously for modelling of heterogeneous sandstone reservoirs with deterministic (Pickup et al., 2000) or process-based (Nordahl et al., 2005; Scaglioni et al., 2006; Nordahl and Ringrose, 2008) modelling tools.

It should be mentioned that in this study the reproduced mudstone heterogeneities were generated with geostatistical tools, which are based on interpretation and simulation of geometric features only. Sedimentary processes are therefore only implemented indirectly. In some cases (flaser bedding, bioturbation and brecciation due to mass movement) process based tools (Wen et al., 1998), multiple point statistics (e.g. Caers and Zhang, 2004), fractal modelling (e.g. Molz et al., 2004) or a more object orientated, deterministic approach (Pickup et al., 1995) could have also been used. Additionally, the use of the geostatistical tools involves a process of averaging spatial correlations. It is known that the geostatistical correlation length is related to the observed effective property of a certain medium (Sahimi, 1995), which might imply a predisposition for numerical calculation of effective properties. In our study, this is only secondarily reflected, as we use complex nested covariance functions, which capture heterogeneities at different scales, to describe heterogeneous mudstones. Hence, the method used in this study is able to capture the most prominent and statistically relevant heterogeneities, no matter what the origin. Thereby, the incorporation of complex and realistic lithological variety is based on assumed mud contents of the whole model, similar to a net-to-gross (mud-to-sand) approach, which gives the approach a high flexibility to be correlated with conventional measurements, such as mud logs, wireline measurements, etc. Moreover, petrophysical properties have been assigned by a modelling and simulation technique, which honours latest advances in predicting porosity and permeability of fine grained sediments as a function of lithology and effective stress (Yang and Aplin, 2004, 2010), as well as Nile Delta specific variation of grain size fractions of fine grained sediments. Thus, the results should be seen as a first step towards a database of stress-dependent, effective permeabilities of heterogeneous mudstones at sub-metre scale.

In geometrically complex models, it has been shown, that 3D models can give a more accurate picture of the fluid flow through heterogeneous rocks (e.g. Schneider et al., 2000). However, the third dimension is difficult to extract from image data and only assumptions could have been made in this study. Also, the calculated effective permeabilities are in realistic ranges and the percolation thresholds are similar to previous studies (Nordahl et al., 2005; Nordahl and Ringrose, 2008), although connectivity as a function of mud content might evolve differently in 3D for complex models such as clasts and chaotic structures. In contrast,

for ideal bedded structures, 2D models should give an answer close to models implementing the third dimension. In addition, due to the large amount of models, which have been investigated in a quantitative way in this study, 2D models provide an economically (fast) way to firstly assess the effective flow properties of heterogeneous mudstones.

Five groups of mudstone heterogeneity, which can be distinguished by permeability anisotropy and absolute values of effective permeability, could be observed in this study. In this manner, effective permeability of heterogeneous mudstones is driven by connectivity of coarser grained and therefore higher permeable material through the system. As soon as the higher permeable material is connected through the system, the effective permeability jumps from values, which are close to the permeability of the finer material (mud), to values, which are close to the permeability of the coarser material (sand). The ratio of coarser to finer material (e.g. expressed by mud content) at which this connectivity is established, marks the heterogeneity-specific percolation threshold.

For very horizontal structures, such as undisturbed, deformed or flaser-shaped lamination or bedding these results correlate well with previous numerical studies on thin-bedded or tidal-influenced reservoirs (Nordahl et al., 2005; Scaglioni et al., 2006; Nordahl and Ringrose, 2008). These studies found similar percolation thresholds in horizontal direction (between 50-80% mud content) and suggest very low percolation thresholds in vertical direction (<< 50% mud content). As only mud contents ≥ 50% have been regarded in our study, the low vertical percolation thresholds can be confirmed indirectly by our study, too, as vertical connectivity in horizontal structures is never established in the investigated range of mud content (50-100%). Effective horizontal permeabilities of heterogeneous mudstones containing large vertical structures can easily reach values between 1e-16 m² (at 30 MPa) to 1e-13 m² (at 1 MPa) in case of horizontal connectivity. The high permeability anisotropy of the horizontal structures (up to five orders of magnitude) fits also very well with recent measurements of heterogeneous cap rock (mudstone) samples by Armitage et al. (2011), who found permeability anisotropies to vary by up to four orders of magnitude, even for samples with the same average lithological composition.

For vertical structures, the results of our study confirm, what has been expected by many authors of sedimentological studies on influence of sand injections (e.g. Hurst et al., 2003, 2011) and bioturbation (e.g. Kristensen and Hansen, 1999) on fluid flow in low permeability environments. Effective vertical permeabilities of heterogeneous mudstones containing large vertical structures can be as high as 1e-16 m² (at 30 MPa) to 1e-13 m² (at 1 MPa).

More isotropic structures (some clasts or brecciated structures and very chaotic slumps) were not found to provide sufficient high permeable networks in a mud-rich system in the present study. One reason for this phenomenon might be, that a spatially randomly distributed set of isotropic highly permeable features floating in a much less permeable matrix is less likely to be connected to each other than highly permeable non-isotropic features (Renard and Marsily, 1997). However, even if no percolation threshold is reached in these heterogeneities, permeabilities can still reach values up to 1e-15 m^2 at 1 MPa.

Viewing the vertical effective permeability results in the light of the initial depositional process involved in the forming of the structures/heterogeneities, a proportionality between effective vertical permeability and involved depositional energy (the higher the depositional energy, the higher the vertical permeability) is observable. The same can be confirmed for involvement of secondary depositional processes (the more overprinted by secondary depositional processes, the higher the vertical permeability), such as bioturbation, mass movement, deformation. Nevertheless, these are only general trends and are not always valid, as in the case of isotropic structures/heterogeneities.

The results for the structures with either very high (horizontal) or very low anisotropic (vertical) structures, show that high permeability pathways can govern the whole sub-metre scale system, once the percolation threshold is exceeded. This leads to anisotropy in general, which is a key parameter, promoting fluid flow in both vertical and horizontal directions. Even at very high mud contents, permeability anisotropy can vary already by several orders of magnitude depending on the respective spatial heterogeneity. In our study effective stress does not seem to have a significant effect on permeability anisotropy. This is mainly related to fact, that we did not implement physical deformation of the rock due to compaction. Geomechanical modelling accounting for such compactional deformation processes, might result in an increase of permeability anisotropy with increasing effective stress. Furthermore, all results of this study are based on numerical simulation of single phase fluid flow. Incorporation of multi-phase flow could add further value to the results (Pickup et al. 2000). In terms of leakage and fluid migration capillary entry pressures of different lithologies should also be regarded, as they might be the driving force to leakage and migration of fluids through heterogeneous mudstones (Schowalter, 1972). A study investigating the effective capillary entry pressures of sub-metre scale heterogeneous mudstones is currently undertaken at Newcastle University within the Caprocks Project (Kurtev et al., 2010a, 2010b).

Conclusions

Sub-metre scale heterogeneity significantly influences effective porosity-permeability relationships compared to porosity-permeability relationships obtained from measurements of "homogeneous" mudstone samples. Hence, the study of sub-metre scale mudstone heterogeneity is crucial to evaluate seal and barrier rocks in hydrocarbon and hydrological systems, but also for evaluation of CO_2 storage sites and in understanding fluid flow in sedimentary basins. We found effective permeabilities of heterogeneous mudstones to span values from 1e-21 m² up to 1e-13 m² in both vertical and horizontal direction, which exceeds permeabilities from homogeneous mudstone sample measurements by up to three orders of magnitude. In particular, for modelling fluid flow through barrier (hydrogeology, CO_2 and nuclear waste storage) and cap (petroleum systems) rocks this is an important finding, as in many modelling approaches mudstone permeability is upscaled directly from measurements on homogeneously treated samples to the cell scale of the model (1 m to several 100s of metres). Hereby, the mud content drives the effective permeability values for the respective structures. In many cases, mud contents as high as 50-80% are low enough to reach the percolation thresholds, where the effective permeability jumps from a low (in terms of fluid flow) to a high permeability forming a high permeability network through the mud-rich matrix. We found the effective permeability anisotropy to be the parameter, best ascribing the fluid flow behaviour of different heterogeneous mudstones as it relates back to the sedimentary structure involved in causing the heterogeneity and thus providing the best link to sedimentary environments. Hereby, a general trend relating effective vertical permeability to depositional energy or secondary processes involved in the sedimentation could be observed (the higher the energy or the more the secondary sedimentation overprint, the higher the effective vertical permeability). However, this trend is not valid for isotropic structures, which tend to behave similar to the results of sample measurements on homogeneous mudstones. Effective permeability anisotropies significantly vary (~ 2 orders of magnitude) even at high mud contents (80%) as a function of heterogeneity.

5 end-member structures have been identified based on effective permeability and anisotropy derived from numerical fluid flow simulation: continuous beds (lamination, parallel bedding), discontinuous beds (flaser and ripple structures), isotropic clasts/slumps (slumps, debris flows), small vertical structures (bioturbation, load casts, minor slumps), large vertical clasts (bioturbation, major slumps, sand injections). For each group, empirical relationships of porosity, effective permeability and effective permeability anisotropy were delivered for mud contents between 50-100% and mechanical compaction up to 30 MPa of effective stress.

Using wireline facies interpretation tools the results could be extrapolated to non-cored sections and might serve as a one-dimensional evaluation tool for seal risk and/or uncertainty. Automating of the approach might enhance uncertainty assessment in reservoir and basin modelling and might hence provide a greater variety of input functions. In addition, the results might serve as background models for complex basin or hydro-geological models or as direct upscaled input for geobody models or to feed in a database. The latter could be extended with new results from different locations, which might lead to better understanding of the influence of sub-metre scale heterogeneity on fluid flow through mud-rich sections in sedimentary basins and hydrological systems.

References

Aplin, A. C., Fleet, A. J., MacQuaker, J. H. S. 1999. Muds and Mudstones: Physical and Fluid Flow Properties. Geological Society, Special Publications, 158. In: Aplin, A.C., Fleet, A.J. & MacQuaker, J.H.S. (eds) 1999. Muds and Mudstones: Physical and Fluid Flow Properties.Geological Society, Special Publications, 158, 1-8.

Aplin, A. C., Yang, Y. L. & Hansen, S. 1995. Assessment of beta, the compression coefficient of mudstones and its relationship to detailed lithology. Marine and Petroleum Geology, 12, 955–963.

Armitage, P. J., D. R. Faulkner, R. H. Worden, A. C. Aplin, A. R. Butcher, and J. Iliffe 2011. Experimental measurement of, and controls on, permeability and permeability anisotropy of caprocks from the CO2 storage project at the Krechba Field, Algeria, J. Geophys. Res., 116, B12208, doi:10.1029/2011JB008385.

Armstrong, M., Galli, A., Le Loc'h, G., Geffroy, F., Eschard, F. 2003. Plurigaussian simulations in geosciences. Springer, Berlin Heidelberg New York

Bear, J. 1972. Dynamics of fluids in porous media. American Elsevier, New York.

Begg, S. H., King, P. R. 1985. Modelling the effects of shales on reservoir performance: calculation of effective vertical permeability. Society of petroleum engineers paper 13529, presented at SPE symposium on reservoir simulation, Dallas, 10–13 February 1985

Bjørlykke, K., Hoeg, K. 1997. Effects of burial diagenesis on stresses, compaction and fluid flow in sedimentary basins. Marine and Petroleum Geology, 14, 3, 267-276.

Bjørlykke, K. 1998. Clay mineral diagenesis in sedimentary basins – a key to the prediction of rock properties. Examples from the North Sea Basin. Clay Minerals, 33, 1, 15–34.

Campbell, C. V. 1967. Lamina, Laminaset, Bed and Bedset. Sedimentology, 8, 7-26.

Caers, J., Zhang, T. 2004. Multiple-point geostatistics: a quantitative vehicle for integrating geologic analogs into multiple reservoir models. In: Integration of outcrop and modern analog data in reservoir models. AAPG Mem, 80, 383–394.

Caniego, F. J., Espejo, R., Martin, M. A., San José, F. 2005. Multifractal scaling of soil spatial variability. Ecological Modelling, 182, 291-303.

Chiles, J. P., Delfiner, P. 1999. Geostatistics: modeling spatial uncertainty. Wiley, New York, 695 p.

Chilès, J. P. 1988. Fractal and Geostatistical Methods for Modelling of a Fracture Network. Mathematical Geology, 20, 6, 631-654.

Chuhan, F. A., Kjeldstad, A., Bjørlykke, K., Hoeg, K. 2003. Experimental compression of loose sands; relevance to porosity reduction during burial in sedimentary basins. Canadian Geotechnical Journal, 40, 5, 995–1011.

Cole, R. D., Picard, M. D. 1975. Primary and Secondary Sedimentary Structures in Oil Shale and Other Fine-Grained Rocks, Green River Formation (Eocene), Utah and Colorado. Utah Geol., 2, 49-67.

Collinson, J. D., Mountney, N., Thompson, D.B. 2006. Sedimentary Structures. Terra Publishing, 302 p.

Coyner, K., Katsube, T. J., Best, M. E., Williamson, M. 1993. Gas and water permeability of tight shales from the Venture gas Field offshore Nova Scotia. In: Current Research, Part D. Geological Survey of Canada, 129–136.

Dagan, G. 1979. Models of groundwater flow in statistically homogeneous porous formations. Water Resour Res, 15, 1, 47–63

Desbarats, A. J., Bachu, S. 1994. Geostatistical analysis of aquifer heterogeneity from the core scale to the basin scale: A cases study. Water Resources Research, 30, 3, 673-684.

Dewhurst, D. N., Aplin, A. C., Sarda, J. P., Yang, Y. L. 1998. Compaction-driven evolution of poroperm in natural mudstones: an experimental study. J. Geophys. Res., 103, 651–661.

Dewhurst, D. N., Yang, Y. L., Aplin, A. C. 1999a. Permeability and fluid flow in natural mudstones, in Muds and Mudstones: Physical and Fluid Flow Properties, edited by A.C. Aplin et al., Geol. Soc. Spec. Publ., 158, 23–43.

Dewhurst, D. N., Aplin, A. C., Sarda, J. P. 1999b. Influence of clay fraction on pore-scale properties and hydraulic conductivity of experimentally compacted mudstones. J. Geophys. Res., 104, B14, 29261–29274.

Eaton, T. T 2006. On the importance of geological heterogeneity for flow simulation. Sedimentary Geology, 184, 187–201

Emery, X., Lantuejoul, C. 2006. Tbsim: A computer program for conditional simulation of three-dimensional gaussian random fields via the turning bands method. Computers & Geosciences, 32, 1615–1628.

Fawad, M., Mondol, N. H., Jahren, J., Bjørlykke, K. 2010. Microfabric and rock properties of experimentally compressed silt-clay mixtures. Marine and Petroleum Geology, 27, 1698–1712.

Haldorsen, H. H, Chang, D. M. 1986. Notes on stochastic shales; from outcrop to simulation mode. In: Lake LW, Caroll HB (eds) Reservoir characterization. Academic Press, Orlando, 445–485

Hildenbrand, A., Schloemer, S., Krooss, B. M. 2002. Gas breakthrough experiments on fine-grained sedimentary rocks. Geofluids, 2, 3–23.

Hurst, A., Cartwright, J., Huuse, M., Jonk, R., Schwab, A., Duranti, D, Cronin, B. 2003. Significance of large-scale sand injectites as long-term fluid conduits: evidence from seismic data. Geofluids, 3, 263-274.

Hurst, A., Scott, A., Vigorito, M. 2011. Physical characteristics of sand injectites. Earth-Science Reviews, 106, 215–246.

Huysmans, M., Dasargues, A. 2009. Application of multiple-point geostatistics on modelling groundwater flow and transport in a cross-bedded aquifer (Belgium). Hydrogeology Journal, 17, 1901–1911.

Jensen, J. L., Corbett, P. W. M., Pickup, G. E., Ringrose, P. S., 1996. Permeability semivariograms, geological structure and flow performance. Math. Geol., 28, 4, 419–435.

Journel, A. G. 1983. Nonparametric estimation of spatial distribution. Math Geol, 15, 3, 445–468.

Journel, A. G., Alabert, F. G. 1990. New method for reservoir mapping. J Pet Technol February, 42, 2, 212–218.

Journel, A. G., Gomez-Hernandez, J. 1993. Stochatic imaging of the Wilmington clastic sequence. Soc Pet Eng Form Eval, 8, 1, 33–40.

Journel, A. G., Isaaks, E. K 1984. Conditional indicator simulation: application to a Saskatcheouan uranium deposit. Math Geol, 16, 7, 685–718.

Kemper, W.D. 1961. Movements of water as affected by free energy and pressure gradients. Proceedings – Soil Science Society of America, 25, 255–265.

Kossack, C. A., Aasen, J. O.. and Opdal, S, T., 1990. Scaling up heterogeneities with pseudofunctions: SPE Formation Evaluation, 5, 3, 226-232.

Kristensen, K., Hansen, K. 1999. Transport of carbon dioxide and ammonium in bioturbated (Nereis diversicolor) coastal, marine sediments. Biogeochemistry, 45, 147–168.

Kurtev, K. D., Drews, M., Aplin, A. C. 2010a. Critical Capillary Entry Pressure Upscaling in Heterogeneous Mudstones: A Scale-Invariant Stochastic Approach. 6th IMA Conference on Modelling Permeable Rocks.

Kurtev, K. D., Drews, M., Ma, J., Aplin, A. C. 2010b. Metre-scale Effective Flow Properties of Heterogeneous Fine-Grained Sediments. EAGE Shale Workshop 2010, EarthDoc Extended Abstract.

Kwon, O., Kronenberg, A.K., Gangi, A.F., Johnson, B., Herbert, B.E. 2004. Permeability of illite-bearing shale: 1. Anisotropy and effects of clay content and loading. J. Geophys. Res., 109, B10, B10205.

Ma, J., Couples, D. G., Harris, D. S. 2006. A mixed finite element technique based on implicit discretization of faults for permeability upscaling in fault damage zones. Water Resources Research, 42, 8, W08413.

Macquaker, J. H. S., Adams, A. E. 2003. Maximizing Information from Fine-Grained Sedimentary Rocks: an Inclusive Nomenclature for Mudstones. J. Sed. Res., 73, 5, 735–744.

Mallon, A.J., Swarbrick, R.E., Katsube, T.J., 2005. Permeability of fine-grained rocks: new evidence from chalks. Geology 33, 21–24.

Mann, D.M. & Mackenzie, A.S. 1990. Prediction of pore fluid pressure in sedimentary basins. Marine and Petroleum Geology, 7, 55–65.

Marion, D., Nur, A., Yin, H., Han, D. 1992. Compressional velocity and porosity in sand-clay mixtures. Geophysics, 57, 554–563.

Marsily, G., Delay, F.Goncalves, J., Renard, P., Teles, V., Violette, S. 2005. Dealing with spatial heterogeneity. Hydrogeol J, 13, 161–183.

Matheron, G., Beucher, H., de Fouquet, C., Galli, A., Guerillot, D., Ravenne, C. 1987. Conditional simulation of the geometry of fluvio-deltaic reservoirs. Society of Petroleum Engineers SPE, 16753.

Matheron, G., Beucher, H., de Fouquet, C., Galli, A., Ravenne, C. 1988. Simulation conditionnelle _ trois faci_s dans une falaise de la formation du Brent [Conditional simulations with three facies in a cliff of the Brent formation]. Sciences de la Terre, 28, 213–249.

Maubeuge, F., Lerche, I. 1994. Geopressure evolution and hydrocarbon generation in a North Indonesian basin; two-dimensional quantitative modelling. Marine and Petroleum Geology, 11, 104–115.

McCave, I. N., Manighetti, B., Robinson, S.G. 1995. Sortable silt and fine sediment size/composition slicing: parameters for palaeocurrent speed and palaeoceanography. Paleoceanography, 10, 593-610.

McKelvey, J. G. & Milne, I. H. 1962. The flow of salt solutions through compacted clay. In: Ingerson, E. (ed.) Clays and Clay Minerals. Proceedings –Ninth National Conference on Clays and Clay Minerals, 9, 248–259.

Mesri, G., Olson, R.E. 1971. Mechanisms controlling the permeability of clays. Clays Clay Min. 19, 151–158.

Molz, F. J., Rajaram, H., Lu, S. L. 2004. Stochastic fractal-based models of heterogeneity in subsurface hydrology: origins, applications, limitations, and future research questions. Reviews of Geophysics, 42, 1, RG1002.

Mondol, N. H., Bjørlykke, K., Jahren, J., Høeg, K. 2007. Experimental mechanical compaction of clay mineral aggregates - changes in physical properties of mudstones during burial. Marine and Petroleum Geology, 24, 289–311.

Mondol, N. H., Bjørlykke, K., Jahren, J. 2008. Experimental compaction of clays: relationship between permeability and petrophysical properties in mudstones. Petroleum Geoscience, 14, 319–337.

Mondol, N. H., Jahren, J., Berre, T., Grande, L., Bjørlykke, K. 2011. Permeability Anisotropy in Synthetic Mudstones − An Experimental Study. EAGE Vienna 2011. EarthDoc – Extended Abstract, D030.

Nagaraj, T. S., Pandian, N. S., Narasimha Raju, P. S. R. 1994. Stress-state-permeability relations for overconsolidated clays. Geotechnique, 44, 349–352.

Neuzil, C. E. 1994. How permeable are clays and shales? Water Resour. Res., 30, 145–150.

Nordahl, K., Ringrose, P. S., Wen, R. 2005. Petrophysical characterization of a heterolithic tidal reservoir interval using a process-based modeling tool. Pet Geosci, 11, 17–28.

Nordahl, K., Ringrose, P. S. 2008. Identifying the Representative Elementary Volume for Permeability in Heterolithic Deposits Using Numerical Rock Models Mathematical Geosciences, 40, 7, 753-771.

Pettersen, O. 2007. Sandstone compaction, grain packing and Critical State Theory. Petroleum Geoscience, 13, 63–67.

Pickup, G. E., Stephen, K. D. Ma, J., Zhang, P., Clark, J. D. 2005. Multi-Stage Upscaling: Selection of Suitable Methods. Transp Porous Med, 58, 191–216.

Pickup, G. E., Ringrose, P. S., Sharif, A. 2000. Steady-state upscaling: from lamina-scale to full-field model. Society of Petroleum Engineers Journal, 5, 2, 208–217.

Pickup, G. E., Ringrose, P. S., Corbett, P. W. M., Jensen, J. L., Sorbie, K. S. 1995. Geology, geometry and effective flow. Pet Geosci, 1, 37–42.

Potter, E. P., Maynard, J. B., Pryor, W. A. 1980. Sedimentology of Shale. Springer, New York, Berlin, Heidelberg, Tokyo, 306 p.

Reineck, H. E., Singh, I. B. 1973. Depositional Sedimentary Environments. Springer, New York, Heidelberg, Berlin, 439 p.

Renard, P., Marsily, G. de 1997. Calculating equivalent permeability: a review, Adv.Water Resour., 20, 5–6, 253–278.

Revil, A., Cathles, L. M. 1999. Permeability of Shaly Sands. Water Resources Research, 35, 3, 651-662.

Rivoirard, J. 1994. Introduction to disjunctive kriging and nonlinear geostatistics. Oxford University Press, Oxford.

Sahimi, M 1995. Flow and transport in porous media and fractured rock. From classical methods to modern approaches. VCH, Weinheim.

Scaglioni, P., Ruvo, L., Cozzi, M. 2006. Implicit net-to-gross in the petrophysical characterization of thinlayered reservoirs. Pet Geosci, 12, 325–333.

Schieber, J. 1999. Distribution and Deposition of Mudstone Facies in the Upper Devonian Sonyea Group of New York. J. Sed. Res., 69, 4, 909–925.

Schneider, F., Wolf, S., Faille, I., Pot, D. 2000. A 3D Basin Model for Hydrocarbon Potential Evaluation: Application to Congo Offshore. Oil & Gas Science and Technology – Rev. IFP, 55, 1, 3-13.

Schowalter, T. T. 1979. Mechanics of secondary hydrocarbon migration and entrapment. AAPG Bul., 63, 5, 723-760.

Warner, D. L. 1964. An analysis of the influence of physical-chemical factors upon theconsolidation of fine-grained elastic sediments PhD thesis, University of California, Berkeley, USA.

Weber, K. J. 1982. Influence of common sedimentary structures on fluid flow in reservoir models. J Pet Technol, 44, 665–672.

Wen, R., Martinius, A. W., Næss, A., Ringrose, P. 1998. Three-dimensional simulation of small-scale heterogeneity in tidal deposits—a process-based stochastic simulation method. In: Buccianti A, Nardi G, Potenza R (eds) Proceedings of the 4th annual conference of the international association of mathematical geology (IAMG), Ischia, 129–134.

Yang, Y., Aplin, A. C., Larter, S. 2004. Quantitative assessment of mudstone lithology using geophysical wireline logs and artificial neural networks. Petroleum Geoscience, 10, 2, 141-151.

Yang, Y. L., Aplin, A. C. 1998. Influence of lithology and effective stress on the pore size distribution and modelled permeability of some mudstones from the Norwegian margin. Mar. Petrol. Geol., 15, 163–175.

Yang, Y., Aplin, A. C. 1998. Influence of lithology and compaction on the pore size distribution and modelled permeability of some mudstones from the Norwegian margin. Marine and Petroleum Geology, 15, 163–175.

Yang, Y. L., Aplin, A. C. 2007. Permeability and petrophysical properties of 30 natural mudstones. Journal of Geophysical Research: Solid Earth, 112, B3, B03206.

Yang, Y. L., Aplin, A. C. 2010. A Permeability–Porosity Relationship for Mudstones. Marine and Petroleum Geology, 27, 8, 1692-1697.

Chapter 6: Summary and Conclusions

The physical properties of fine-grained sediments, such as shales and mudstones, are well understood on sample scale (centimetre-scale), as laboratory measurements of properties such as mineralogy, grain size, porosity and permeability are feasible and also available in the public domain. In particular, flow properties, such as porosity and permeability, of fine-grained sediments have been measured in the past in relation to understanding, prediction and modelling of petroleum migration, CO_2 and (nuclear waste) water retention capacities and - to a lesser extend - for modelling of subsurface ground water flow. Nevertheless, the properties have not been extensively investigated on larger scales, yet. Even more, physical properties, laboratorily measured from samples, are often directly upscaled to larger scales for the purpose of subsurface fluid flow modelling, assuming first that the sample measurements are representative for the whole fine-grained section to be modelled and second that the section is homogeneous over a large spatial domain of several metres (e.g. in case of ground water modelling) to 100s and 1000s of metres (e.g. in case of basin modelling). These assumptions indirectly imply, that the influence of heterogeneity, which appears on scales larger than the sample-scale (centimetre-scale) is insignificant, which can be doubted referring to studies demonstrating the influence of heterogeneity on fluid flow in petroleum reservoirs and groundwater aquifers. It is therefore crucial to investigate the influence of heterogeneity present in fine-grained sediments, such as shales and mudstones, on different scales.

As a starting point, this thesis concerned itself with the influence of sub-metre scale mudstone heterogeneities on effective flow properties (porosity and permeability) of metre-scale heterogeneous mudstones with respect to mechanical compaction and lithological variability. In order to investigate the influence of a variety of heterogeneity on fluid flow through mud-rich sections a modelling workflow has been developed. In principle, the workflow consists of four steps:

1. Development of a modelling framework to allow population of flow models with realistic porosity and permeability fields, predicted as a function of lithological (grain size fractions) and compactional (effective stress) parameters.
2. Identification and capturing of mudstone heterogeneity
3. Modelling of mudstone heterogeneity
4. Converting these models into fluid flow models, which can be used for numerical simulation to calculate effective permeabilities.

The workflow for upscaling of sub-metre scale heterogeneities in mudstones to the metre-scale is transferable to any location and geological setting, with adjustments according to data

availability. The development of this workflow and related sub-workflows for each step are one of the main outcomes of this thesis and the individual workflow steps are outlined on the following pages. As a case study, a unique dataset of high resolution core images and borehole images (electrical resistivity based formation micro imager) of heterogeneous mud-rich sections from the Piacenzian (Upper Pliocene) of the Western Nile Delta, offshore Egypt, was used.

Workflow Step 1 (Chapter 2)

Heterogeneous shales and mudstones comprise a range of different lithological units, such as mud, silt and sand. In this step, existing grain size, porosity and permeability models and measurements of these lithologies are reviewed and integrated in a modelling framework. The modelling framework allows prediction of porosity and permeability as a function of grain size fraction combinations and mechanical compaction (effective stress). This allows modelling of porosity and permeability for any lithological setup, as long as the end-member properties are known. Thereby, grain size related phenomena such as a porosity minimum and a sudden increase of permeability at a certain ratio of clay, fine silt, coarse silt and sand sized grain fractions can be modelled. These phenomena characterise the transition from a matrix to a grain supported rock framework. The sample-scale (centimetre-scale) modelling framework can be used to model stress-dependent porosity and permeability of siliclastic sediments independently of laboratory measurements. Only a lithological descriptor (e.g. vshale) and a grain size fraction trend (e.g. from clay and fine silt rich to coarse silt rich to sand rich) are required. The modelling framework can be used to populate porosity and permeability values along geophysical well logs, to create an artificial petrophysical database or to populate numerical models with petrophysical properties. The modelling frame work is transferable to other regions of the world, as end-member functions have been collected from various publications, which are not Nile Delta specific. Also, the end-member functions can be substituted easily.

The modelling frame work is adapted to the case study used in this study, an off-shore gas field from the Western Nile Delta, Egypt, by employing an algorithm to statistically simulate grain size fraction variations from input of a cohesive fraction (grain size < 10 μm) only. This allows the modelling framework to be adaptable to common continuous measures such as vshale from geophysical well logs. Thereby, the grain size simulation algorithm is also transferable and independent of the data. However statistics and trends (regressions) of a grain size fraction distribution is required. These properties might come from a real database or can

be assumed. The modelling framework along with the grain size fraction simulation algorithms have been used in this study to populate metre-scale heterogeneous mudstone models with petrophysical properties (grain size, porosity and permeability) as a function of effective stress. The models are then used to calculate effective permeabilities by numerical fluid flow simulation.

Workflow Step 2 (Chapter 3)

In the second workflow step sub-metre scale shale and mudstone heterogeneities have been studied and classified with a geometrical focus. To do so, existing classifications have been abstracted to geometric, flow-relevant features only in order to tailor the classifications to a fluid flow focus. More than 500 m of mud-rich core and borehole images have been examined using a combined visual and geostatistical interpretation workflow. In principle, this workflow is applicable to any region of the Earth, as long as a similar dataset (in terms of data types) is available. Thereby, visual interpretation supported by manual and automated geostatistical analyses of a high quality subset of core images are the core of the interpretation workflow. The results of the automated geostatistical analysis can be used for automated detection of mudstone heterogeneity on core and borehole images and to a certain extent even on geophysical well logs, by applying the general trends obtained for each structural class.

Additionally, based on the interpretation and analyses, examples for each resulting structural class were selected and analysed by detailed variography. As a final result, high resolution nested variogram models from core and borehole images, accounting for typical shale and mudstone heterogeneities, as well as distributions of mean intervals and occurrences of each structural class in different local depositional environments were provided. The nested variogram models and distributions can be used for modelling of shale and mudstone heterogeneities (e.g. for subsequent numerical simulation). For example, the high resolution nested variograms of heterogeneous mudstones obtained in this study can be used for modelling of mudstone heterogeneity on the sub-metre to metre-scale employing geostatistical simulation. The resulting models can be utilized for assessment of effective properties (other flow properties such as CEP, geomechanical properties, thermal properties, etc.) using numerical simulation. They can also serve as background geometries in high resolution larger scale models.

Workflow Step 3 (Chapter 4)

Prior to modelling of shale and mudstone heterogeneity, which accounts for lithological and petrophysical variability, it is necessary to investigate the effect of model dimensioning and

resolution on the uncertainty of the numerical results. To do so, we model shale and mudstone heterogeneities employing geostatistical indicator simulation. As input we use previously derived high resolution variogram models (workflow step 2). The resulting models are populated with two binary permeability fields representing 50% and 75% of mud content, respectively, to omit the influence of petrophysical variability. Thereby, the model size and resolution are varied independently. The results are investigated for uncertainty and connectivity, both as functions of model size and resolution.

Workflow Step 4 (Chapter 5)

Based on recommendations on model dimensioning (workflow step 3) and the modelling framework developed in workflow step 1, realistic heterogeneous mudstone models are produced with varying mud contents. To model the heterogeneities, we feed geostatistical indicator simulation with previously derived, representative variogram models (workflow step 2). Using numerical single phase fluid flow simulation, effective porosity-permeability relationships as a function of effective stress and mud content are calculated.

The calculated effective properties can be used for seal integrity analysis, as upscaled properties in larger scaled fluid flow models, column height predictions, pore pressure prediction and 1D permeability profiles along geophysical well logs using heterogeneity detection from well logs (e.g. by utilisation of artificial neural networks).

Key Results

The key results of this study should be seen in the light of the case study used. Although the Nile Delta provides a large range of sedimentological environments and thus geological heterogeneity, the results should be regarded as a starting point of a database of occurrence, appearance and effective flow properties of heterogeneous mudstones. Other sedimentological settings might yield different results in terms of absolute values, although the general trends for effective properties might be transferable to almost any sedimentological setting, where chemical compaction can be neglected.

For the Nile Delta case study, we found that sub-metre scale mudstone heterogeneity is very common, independent of the local depositional environment. However, the distributions of the respective mudstone heterogeneities within the seismic facies or geobodies are very dependent on the case study and in particular to the well location. Especially, the latter causes an uncertainty, as the internal of these geobodies cannot be assumed to be laterally homogeneous. This is above all valid for mass-transport complexes, channels and levees, while for hemipelagic sections a certain lateral continuity could be assumed.

We found that - in a rough manner - the observed mudstone heterogeneities can be identified using automated geostatistical analysis. However, for detailed analyses, geological knowledge is indispensable and should always be performed, when modelling and characterizing mudstone heterogeneity. Visual interpretation combined with geostatistical analyses techniques allowed for the extraction of a representative subset of mudstone heterogeneities from core images. The selection was supplemented by a qualitatively chosen suite of borehole images and was subjected to detailed geostatistical analysis. By doing so, we were able to show, the combination of detailed geostatistical analysis with geological knowledge can yield realistic models of mudstone heterogeneity. This can be performed with nested covariance functions to fit experimental variograms of mudstone heterogeneities and subsequent geostatistical simulation. The resulting models of heterogeneous mudstones were then used to investigate the influence of heterogeneity, model size and resolution on effective flow properties by means of numerical fluid flow simulation. A binary permeability field was applied to do so and the results were analysed by calculation of the coefficient of variation and a connectivity probability. As a result of this investigation, we recommend heterogeneous mudstone model sizes to have model edge lengths of 60 cm and a cell resolution of 2 mm for future numerical studies on shale and mudstone heterogeneity. Also, we show that at metre-scale the effective media theory has to be extended by a measure of uncertainty, as for many mudstone heterogeneities, which differ from bedded or laminated structures, the representative elementary volume/domain cannot be obtained at low mud contents (~50%) on sub-metre scale. Thus, mudstone heterogeneity poses a high risk in assessment of fluid flow in sedimentary systems and should not be neglected.

In a final step, petrophysical variability was added to the heterogeneous mudstone models. Inclusion of petrophysical variability is important in modelling of heterogeneous mudstones to account for (mechanical) compaction and regional lithological trends. In this study, we used grain size fraction regressions, which are specifically to the Nile Delta case study, as lithological trends. Though grain size fraction combinations in most cases trend from clay and fine silt rich via an increase of coarse silt and finally and increase of sand content, there can be geological settings, which promote different trends or even purely random distributions (e.g. glacial sedimentological environments or catastrophic events such as landslides, tsunamis and meteoric impacts). Again numerical fluid flow simulation was performed to calculate stress-dependent effective porosity-permeability relationships for different mud contents and types of heterogeneity. The model sizes and resolutions were chosen according to the results of the model size and resolution study conducted earlier in this thesis. Thereby,

5 different mudstone heterogeneity groups were identified by calculation of effective horizontal and vertical permeabilities. These groups are continuous beds, which strongly promote horizontal flow; discontinuous beds, which show a weaker permeability anisotropy and lower absolute values of horizontal permeability than continuous beds; isotropic structures, which have relatively low absolute values of effective permeability; small vertical structures, which promote vertical flow and large vertical structures, which act as vertical flow pipes throughout the investigated system on metre-scale.

The study demonstrated that effective permeability of heterogeneous mudstones is very dependent on the heterogeneity and overall mud content, which in the right combination can yield percolating systems promoting connectivity of high permeability pathways through the mud-rich matrix. The implications for fluid flow modelling of heterogeneous mud-rich environments are associated with a high uncertainty, as a minor change in mud content together with disregarding of mudstone heterogeneity can yield significantly misleading results. The demonstration that sub-metre scale heterogeneity can significantly influence fluid flow in terms of effective permeability and effective permeability anisotropy is a general result, which should alarm any modeller dealing with fine-grained, mud-rich sequences. For example, direct upscaling of laboratorial derived permeabilities might lead to significantly wrong results, as heterogeneity is neglected in such an approach. It has been shown in this study that effective permeabilities can vary by up to 3 orders of magnitude with respect to heterogeneity only. Additionally, effective permeability anisotropy differs even at very high mud contents (~80%) by almost two orders of magnitude as a function of mudstone heterogeneity. This has direct influence on fluid flow through various scales in sedimentary basins, as anisotropy promotes preferred fluid path ways. In order to allow inclusion of these effects of metre-scale heterogeneous mudstones on fluid flow, effective porosity-permeability and effective porosity-permeability anisotropy relationships for different mudstone heterogeneities and mud contents were provided as a final result. The relationships can be used for upscaling of flow properties of sub-metre scale heterogeneous mudstones - for example to populate larger scale models of depositional environments similar to the Nile Delta.

Limitations and Future Work

Although, the effective porosity-permeability relationships are based on high resolution image data and the calculation of the relationships honours lithological variability, it should be mentioned, that the models were simulated in 2D only. 3D modelling might give different

results, and should be addressed in future studies in particular in relation to chaotic and clasts bearing heterogeneity types. Also, the numerical simulation considers single phase fluid flow only. Two-phase or multi-phase flow should be considered in future studies and are likely to even more promote the influence of heterogeneity.

The sample-scale (centimetre-scale) modelling framework to predict porosity and permeability should be treated with care for burial depths greater than 2-3 km or effective stresses greater than 30 MPa, as chemical compaction becomes important in this depth range, which is not implemented in the frame work, yet. However, the end-member functions could be extended by a chemical compaction term, which sets in at 30 MPa in future studies. In addition, the modelling frame work does not consider mineralogical variations, as a grain size based approach has been taken. The integration of both mineralogical and grain size classification of siliclastic sediments is difficult, in particular for fine-grained sediments. Nevertheless, laboratory compaction experiments on pure aggregates have been numerously performed for coarse grained material in the past and are increasingly conducted for very fine-grained mineral mixtures by various research groups, which should shed light on this issue.

Different modelling methodologies might be more suitable for some types of heterogeneity investigated in this study. For example, a deterministic or multiple point statistics approach might be more suitable for the clasts bearing structures, as these methods might better reflect the sharp contacts and shape variations of the clasts with respect to the surrounding matrix. Also, fractal modelling could yield more realistic models of chaotic structures, such as sand injectites and slumps. In future work, the modelling method should be adapted to the respective type of heterogeneity.

Finally, the results refer to the metre-scale only. Vertically, the results could be extrapolated, as data sources such as geophysical well logs or the core profile itself exist. Horizontally, the results are difficult to extrapolate and need information from larger scales. Future work should therefore concern itself with the next larger scale of observation, which would be geological outcrops or micro-seismic data.

Future studies should also include a wider range of lithological combinations in order to receive a more complete picture on the influence of lithological components (mud, silt and sand). Appendix C shows some initial results using a different petrophysical modelling framework.

Going Beyond the Scope - (New) Questions for Future Research

The results of this thesis directly pose new questions, which could be addressed in continuative research. In the following, a small collection of questions, which arose during the research of this project, is outlined.

What is the overall contribution of small-scale (millimetre-metre scale) heterogeneity on fluid flow through mud-rich sections? This probably depends critically on the distribution of the small-scale heterogeneity units in the investigated system, leading directly to the next question: What is the influence of mudstone heterogeneity on other scales? For example, how are metre-scale heterogeneities distributed vertically AND horizontally in 100s of metre to km-scale geobodies (hemipelagites, mass transport complexes, channels, levees, etc.)? This could be useful to reliably populate upscaled properties derived in this study onto larger scale models. Is it possible to find some large scale indicators to address/identify this influence and the presence of small-scale heterogeneities (e.g. from seismic imaging)? Going downscale, the question could also be how homogeneous mudstone samples are? A similar study compared to the study presented in this thesis could be performed on thin sections to investigate the representativeness of mud-rich sample measurements.

What is the influence of mudstone heterogeneity on other (effective) properties such as geomechanical and thermal properties or seismic velocities? This might give new insights to fracture propagation in heterogeneous mudstones, and could enhance understanding of thermally driven conductive convection in geothermal ore depositioning systems.

How, if at all, can we reliably recognize mudstone heterogeneity from one dimensional measurements, such as geophysical well logs? Artificial neural networks are increasingly used to do so, but a calibration/validation study would be a great leap forward.

How to deal with the approach of a representative elementary volume/domain? A representative elementary volume cannot always be assumed in geological settings, as natural discontinuities may truncate heterogeneities. In numerical modelling this could be either solved with different realisations, which cover the range of sizes of appearances of certain heterogeneities. An elegant alternative to solve this issue could be given by adaptive gridding or intelligent grid refinement. However, detailed knowledge about the spatial distribution of heterogeneities dimensions would be necessary, but is very difficult to obtain.

Chapter 7: Appendices

Appendix A: Grain Size Data Base

The Nile Delta grain size database can be found in Microsoft Excel format on the attached compact disk. Only core plugs were used for grain size modelling and simulation.

Appendix B: Combined Results Table

The combined results table can be found in Microsoft Excel format on the attached compact disk. The table links geostatistical, lithological, modelled and simulated porosities and permeabilities of each structural template and provides information about well and depth origin.

Appendix C: Additional Contributions

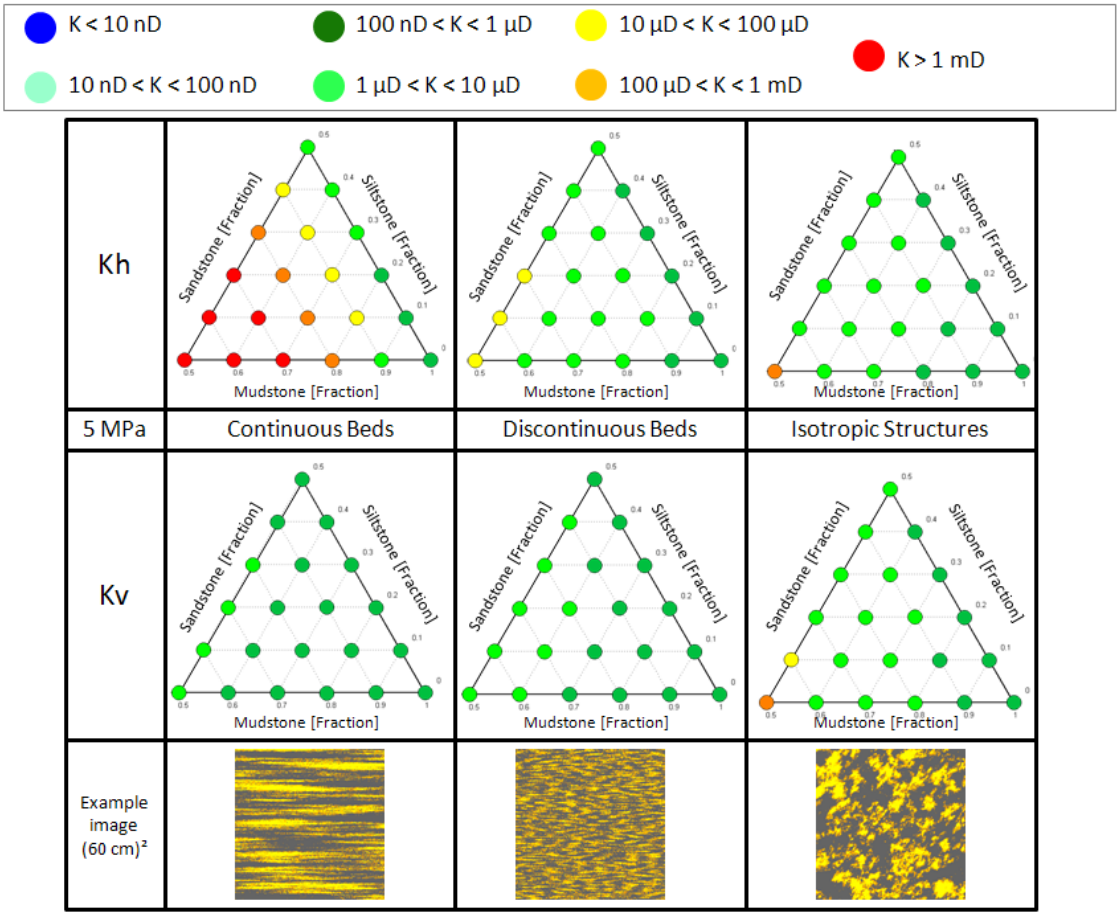

Figure 7.1: Example ternary representation of effective permeability results for a wider range of lithological combinations derived from numerical models with a different formulation of effective stress vs porosity vs permeability. The ternary representation can be a useful tool to directly link effective permeability to lithology and heterogeneity.

Core,Plug,SWC Samples from NA Only!!! No Sandstone Sa				X > 63 µ	63 µ >X> 10µ	10 µ >X> 2µ	2µ > X		
Region	No.	Depth [m or ft]	WaterColumn	Sand	Coarse Silt	Cohesive Silt	Clay	Cohesive	Sortable
NA	NA_1	1546.42	932.00	0.06	9.96	10.36	79.62	89.98	10.02
NA	NA_2	1547.65	932.00	0.27	10.21	15.49	74.03	89.52	10.48
NA	NA_3	1551.40	932.00	0.81	17.78	13.61	67.80	81.41	18.59
NA	NA_4	2004.46	764.00	0.46	17.67	22.36	59.50	81.86	18.14
NA	NA_5	2014.60	764.00	4.54	21.06	21.30	53.10	74.40	25.60
NA	NA_6	1580.00	595.00	1.43	22.54	32.06	43.97	76.03	23.97
NA	NA_7	1680.00	595.00	13.75	40.39	19.87	25.98	45.85	54.15
NA	NA_8	1780.00	595.00	2.66	43.63	25.93	27.78	53.70	46.30
NA	NA_9	2240.00	595.00	9.00	54.54	22.33	14.13	36.46	63.54
NA	NA_10	2350.00	595.00	4.41	45.88	28.56	21.16	49.72	50.28
NA	NA_11	2400.00	595.00	7.03	41.58	29.07	22.32	51.40	48.60
NA	NA_12	2500.00	595.00	7.07	36.21	29.45	27.27	56.72	43.28
NA	NA_13	2575.00	595.00	7.58	23.44	33.62	35.35	68.97	31.03
NA	NA_14	2625.00	595.00	29.61	40.03	16.29	14.08	30.36	69.64
NA	NA_15	2675.00	595.00	7.75	35.56	32.88	23.82	56.70	43.30
NA	NA_16	2745.00	595.00	23.29	32.57	24.46	19.67	44.13	55.87
NA	NA_17	2777.00	595.00	4.51	56.15	24.64	14.70	39.34	60.66
NA	NA_18	3430.00	595.00	1.14	40.01	33.64	25.21	58.86	41.14
NA	NA_19	4003.00	595.00	31.43	33.61	20.28	14.68	34.96	65.04
NA	NA_20	4006.00	595.00	13.38	40.64	28.42	17.56	45.98	54.02
NA	NA_21	4363.17	595.00	0.82	17.64	27.26	54.29	81.54	18.46
NA	NA_22	4373.08	595.00	0.63	15.19	33.17	51.01	84.18	15.82
NA	NA_23	4403.54	595.00	0.11	16.28	36.43	47.18	83.61	16.39
NA	NA_24	4436.24	595.00	12.83	21.40	35.03	30.75	65.77	34.23
NA	NA_25	4440.53	595.00	2.02	22.96	33.12	41.91	75.02	24.98
NA	NA_26	4454.54	595.00	1.11	24.39	42.76	31.74	74.51	25.49
NA	NA_27	4460.15	595.00	12.31	51.58	20.11	16.00	36.11	63.89
NA	NA_28	4473.37	595.00	2.51	20.27	47.74	29.47	77.22	22.78
NA	NA_29	4486.64	595.00	6.63	18.50	43.01	31.87	74.87	25.13
NA	NA_30	4496.52	595.00	21.72	17.44	33.76	27.08	60.85	39.15
NA	NA_31	4506.16	595.00	13.53	20.65	34.92	30.90	65.82	34.18

NA	NA_32	4515.00	595.00	37.56	36.06	15.31	11.07	26.38	73.62
NA	NA_33	4515.59	595.00	5.44	37.48	29.50	27.58	57.08	42.92
NA	NA_34	4600.00	595.00	3.40	50.24	29.05	17.31	46.36	53.64
NA	NA_35	4788.00	595.00	3.98	54.07	27.88	14.06	41.95	58.05
NA	NA_36	5000.00	595.00	4.06	52.99	27.57	15.38	42.95	57.05
NA	NA_37	5158.00	595.00	4.45	40.83	37.96	16.76	54.72	45.28
NA	NA_38	1598.72	646.00	0.04	18.76	17.57	63.63	81.20	18.80
NA	NA_39	1601.75	646.00	0.52	17.53	23.44	58.51	81.95	18.05
NA	NA_40	1605.70	646.00	0.13	24.05	16.44	59.38	75.82	24.18
NA	NA_41	1606.72	646.00	1.51	22.44	14.88	61.17	76.05	23.95
NA	NA_42	1607.74	646.00	0.74	28.25	17.81	53.21	71.01	28.99
NA	NA_43	1610.91	646.00	8.97	33.51	17.58	39.95	57.53	42.47
NA	NA_44	1615.77	646.00	1.11	21.14	20.60	57.14	77.75	22.25
NA	NA_45	1620.83	646.00	9.35	26.20	20.14	44.31	64.44	35.56
NA	NA_46	1625.80	646.00	0.16	19.88	23.51	56.45	79.96	20.04
NA	NA_47	1646.47	646.00	8.18	20.15	16.41	55.26	71.67	28.33
NA	NA_48	1654.35	646.00	0.79	11.62	10.32	77.28	87.60	12.40
NA	NA_49	1656.52	646.00	0.15	14.07	20.15	65.63	85.78	14.22
NA	NA_50	1658.48	646.00	2.82	14.00	17.79	65.39	83.18	16.82
NA	NA_51	1660.60	646.00	0.68	19.93	24.95	54.45	79.40	20.60
NA	NA_52	1661.25	646.00	0.54	23.18	22.42	53.85	76.27	23.73
NA	NA_53	1678.38	646.00	0.59	19.33	15.35	64.73	80.08	19.92
NA	NA_54	1678.38	646.00	0.28	17.02	16.90	65.80	82.70	17.30
NA	NA_55	1684.48	646.00	0.68	19.59	21.99	57.74	79.73	20.27
NA	NA_56	1686.60	646.00	17.62	23.15	13.01	46.22	59.23	40.77
NA	NA_57	1726.49	646.00	1.95	27.78	17.13	53.13	70.27	29.73
NA	NA_58	1737.46	646.00	2.83	28.39	20.78	48.00	68.78	31.22
NA	NA_59	1623.92	339.00	0.77	21.06	19.76	58.41	78.17	21.83
NA	NA_60	1633.35	339.00	5.12	26.28	20.99	47.61	68.60	31.40
NA	NA_61	1640.18	339.00	0.06	18.47	19.43	62.04	81.47	18.53
NA	NA_62	1647.49	339.00	17.08	20.62	13.79	48.51	62.30	37.70
NA	NA_63	1647.58	339.00	0.74	30.77	13.64	54.84	68.49	31.51
NA	NA_64	1649.47	339.00	7.03	26.53	14.94	51.49	66.44	33.56

NA	NA_65	1654.57	339.00	0.82	21.44	15.81	61.93	77.75	22.25
NA	NA_66	1664.44	339.00	19.40	28.25	12.35	40.00	52.35	47.65
NA	NA_67	1670.25	339.00	0.96	19.79	19.77	59.49	79.25	20.75
NA	NA_68	1674.90	339.00	3.23	16.49	18.49	61.79	80.28	19.72
NA	NA_69	1685.74	339.00	1.86	16.89	26.30	54.95	81.25	18.75
NA	NA_70	1699.04	339.00	0.48	18.64	23.66	57.22	80.88	19.12
NA	NA_71	1704.92	339.00	0.39	18.40	20.92	60.29	81.21	18.79
NA	NA_72	1707.93	339.00	8.12	26.59	17.35	47.94	65.30	34.70
NA	NA_73	1718.87	339.00	5.98	30.71	17.22	46.09	63.31	36.69
NA	NA_75	1728.85	339.00	4.08	22.78	19.35	53.80	73.14	26.86
NA	NA_76	1730.65	339.00	4.19	24.84	19.69	51.29	70.98	29.02
NA	NA_77	1783.89	339.00	1.78	21.39	16.50	60.33	76.83	23.17
NA	NA_78	1799.96	339.00	1.07	18.83	21.29	58.80	80.09	19.91
NA	NA_79	1805.89	339.00	0.30	22.22	21.51	55.97	77.48	22.52
NA	NA_80	1815.93	339.00	1.47	17.77	17.52	63.24	80.76	19.24
NA	NA_81	1817.79	339.00	3.90	30.53	34.81	30.77	65.57	34.43
NA	NA_82	1835.43	339.00	0.77	18.23	16.90	64.10	81.00	19.00
NA	NA_83	1836.84	339.00	0.15	17.13	24.26	58.47	82.72	17.28
NA	NA_84	1843.75	339.00	0.16	12.59	12.79	74.46	87.25	12.75
NA	NA_85	1693.38	580.00	0.15	17.00	25.79	57.07	82.85	17.15
NA	NA_86	1697.20	580.00	0.10	12.59	30.48	56.84	87.31	12.69
NA	NA_87	1705.35	580.00	0.83	17.21	28.09	53.87	81.96	18.04
NA	NA_88	1707.62	580.00	0.29	12.61	31.86	55.24	87.11	12.89
NA	NA_89	1709.21	580.00	0.70	25.51	18.16	55.63	73.79	26.21
NA	NA_90	1712.47	580.00	1.39	30.47	15.76	52.38	68.14	31.86
NA	NA_91	1713.47	580.00	0.33	19.19	19.26	61.22	80.48	19.52
NA	NA_92	1718.54	580.00	3.84	34.01	19.97	42.17	62.15	37.85
NA	NA_93	1721.40	580.00	2.50	34.03	17.92	45.55	63.46	36.54
NA	NA_94	1724.28	580.00	0.48	18.46	23.61	57.44	81.05	18.95
NA	NA_95	1730.49	580.00	0.85	18.75	20.67	59.74	80.40	19.60
NA	NA_96	2436.50	580.00	6.24	25.96	18.64	49.16	67.81	32.19
NA	NA_97	2437.42	580.00	0.34	15.70	13.83	70.13	83.96	16.04
NA	NA_98	2440.55	580.00	0.08	17.57	14.27	68.09	82.35	17.65

NA	NA_99	2440.67	580.00	0.73	18.67	24.15	56.45	80.60	19.40
NA	NA_100	1670.00	1162.00	8.02	30.97	31.46	29.56	61.02	38.98
NA	NA_101	1900.00	1162.00	15.94	49.33	16.99	17.73	34.73	65.27
NA	NA_102	2085.00	1162.00	20.88	50.04	14.26	14.82	29.08	70.92
NA	NA_103	2129.60	1162.00	0.07	21.67	26.05	52.21	78.26	21.74
NA	NA_104	2131.55	1162.00	0.04	22.23	26.21	51.52	77.73	22.27
NA	NA_105	2134.15	1162.00	0.14	19.08	25.81	54.97	80.78	19.22
NA	NA_106	2134.61	1162.00	0.13	20.13	22.07	57.67	79.74	20.26
NA	NA_107	2138.57	1162.00	0.11	18.95	23.29	57.65	80.94	19.06
NA	NA_108	2148.68	1162.00	0.07	18.11	21.34	60.48	81.82	18.18
NA	NA_109	2157.60	1162.00	0.05	14.40	19.08	66.47	85.55	14.45
NA	NA_110	2158.20	1162.00	1.02	24.43	27.53	47.02	74.55	25.45
NA	NA_111	2161.66	1162.00	7.12	28.14	28.56	36.18	64.74	35.26
NA	NA_112	2176.30	1162.00	0.24	18.98	16.71	64.07	80.78	19.22
NA	NA_113	2178.67	1162.00	2.13	24.35	16.26	57.26	73.52	26.48
NA	NA_114	2235.00	1162.00	22.61	38.03	22.46	16.90	39.36	60.64
NA	NA_115	2290.00	1162.00	6.99	27.91	32.02	33.08	65.09	34.91
NA	NA_116	2325.00	1162.00	0.59	24.17	25.34	49.90	75.24	24.76
NA	NA_117	2555.00	1162.00	7.99	25.07	27.77	39.16	66.93	33.07
NA	NA_118	2610.00	1162.00	11.29	28.92	28.18	31.61	59.79	40.21
NA	NA_119	2670.00	1162.00	14.19	30.47	26.76	28.58	55.34	44.66
NA	NA_120	2775.00	1162.00	8.16	62.39	11.56	17.89	29.45	70.55
NA	NA_121	2830.00	1162.00	5.33	25.70	37.46	31.51	68.97	31.03
NA	NA_122	2945.00	1162.00	3.17	22.85	35.25	38.73	73.98	26.02
NA	NA_123	3045.00	1162.00	2.22	22.71	35.63	39.44	75.07	24.93
NA	NA_124	1917.18	622.50	0.31	28.18	18.94	52.56	71.51	28.49
NA	NA_125	1918.34	622.50	0.54	25.44	23.16	50.87	74.02	25.98
NA	NA_126	1920.22	622.50	0.78	28.26	18.91	52.05	70.96	29.04
NA	NA_127	1920.64	622.50	0.21	26.89	20.53	52.38	72.91	27.09
NA	NA_128	1921.31	622.50	0.28	29.95	24.93	44.83	69.77	30.23
NA	NA_129	1921.53	622.50	2.15	31.64	20.39	45.82	66.21	33.79
NA	NA_130	1922.28	622.50	0.63	25.00	22.68	51.69	74.37	25.63
NA	NA_131	1922.53	622.50	0.56	28.27	21.69	49.48	71.18	28.82

NA	NA_132	1926.40	622.50	0.36	22.65	22.41	54.58	76.99	23.01
NA	NA_133	1926.56	622.50	1.43	51.72	17.37	29.48	46.85	53.15
NA	NA_134	1936.21	622.50	0.09	16.99	25.81	57.11	82.92	17.08
NA	NA_135	1942.10	622.50	1.22	30.82	18.54	49.42	67.96	32.04
NA	NA_136	1948.23	622.50	0.42	22.20	21.78	55.60	77.38	22.62
NA	NA_137	2036.45	622.50	0.34	16.59	16.13	66.94	83.07	16.93
NA	NA_138	2055.61	622.50	0.38	21.20	21.41	57.02	78.43	21.57
NA	NA_139	2064.56	622.50	2.25	25.72	20.24	51.80	72.03	27.97
NA	NA_140	2113.38	622.50	1.18	21.72	15.80	61.29	77.10	22.90
NA	NA_141	2116.26	622.50	0.16	22.45	20.20	57.18	77.39	22.61
NA	NA_142	2116.45	622.50	0.51	23.41	18.88	57.20	76.08	23.92
NA	NA_143	4394.31	476.00	0.97	24.69	30.66	43.69	74.35	25.65
NA	NA_144	4400.00	476.00	2.45	27.49	35.95	34.11	70.06	29.94
NA	NA_145	4406.38	476.00	12.14	22.05	30.83	34.99	65.81	34.19
NA	NA_146	4426.00	476.00	6.98	37.46	29.88	25.69	55.56	44.44
NA	NA_147	4430.31	476.00	1.48	30.64	33.79	34.09	67.88	32.12
NA	NA_148	4445.00	476.00	14.38	43.25	26.77	15.61	42.38	57.62
NA	NA_149	4447.40	476.00	0.79	20.60	36.44	42.18	78.62	21.38
NA	NA_150	4462.49	476.00	0.66	35.69	23.62	40.02	63.65	36.35
NA	NA_151	4483.00	476.00	12.60	38.31	28.02	21.06	49.08	50.92
NA	NA_152	4505.00	476.00	2.62	37.84	37.78	21.77	59.54	40.46
NA	NA_153	4530.52	476.00	0.10	15.63	37.98	46.30	84.27	15.73
NA	NA_154	4533.00	476.00	2.50	30.52	33.91	33.06	66.97	33.03
NA	NA_155	4538.56	476.00	0.75	21.64	38.42	39.19	77.61	22.39
NA	NA_156	4546.00	476.00	1.49	36.13	30.46	31.92	62.38	37.62
NA	NA_157	4559.42	476.00	6.50	28.18	30.92	34.40	65.32	34.68
NA	NA_158	4573.00	476.00	8.66	43.75	28.91	18.69	47.59	52.41
NA	NA_159	4587.34	476.00	29.45	33.06	20.31	17.17	37.48	62.52
NA	NA_160	4602.50	476.00	31.57	36.67	15.63	16.14	31.76	68.24
NA	NA_161	4618.60	476.00	4.33	35.05	34.78	25.84	60.62	39.38
NA	NA_162	4659.08	476.00	25.43	36.80	19.34	18.43	37.77	62.23
NA	NA_163	4687.00	476.00	0.23	20.38	40.72	38.67	79.39	20.61
NA	NA_164	4709.41	476.00	5.87	36.15	43.54	14.43	57.98	42.02

NA	NA_165	4762.42	476.00	2.56	35.40	41.29	20.76	62.04	37.96
NA	NA_166	4769.41	476.00	0.66	25.31	35.68	38.35	74.03	25.97
NA	NA_167	4775.61	476.00	0.20	28.75	34.66	36.38	71.04	28.96
NA	NA_168	4784.43	476.00	2.19	26.20	34.43	37.18	71.61	28.39
NA	NA_169	4801.49	476.00	0.43	22.05	43.52	34.01	77.53	22.47
NA	NA_170	1724.10	558.00	0.29	19.06	21.45	59.20	80.65	19.35
NA	NA_171	1730.22	558.00	0.13	15.92	18.97	64.98	83.95	16.05
NA	NA_172	1746.43	558.00	4.71	14.98	20.63	59.68	80.31	19.69
NA	NA_173	2302.75	558.00	1.30	32.69	22.80	43.21	66.01	33.99
NA	NA_174	2304.05	558.00	2.64	27.39	29.79	40.19	69.98	30.02
NA	NA_175	1585.75	415.00	0.91	22.46	24.67	51.96	76.63	23.37
NA	NA_176	1596.30	415.00	1.84	36.63	22.19	39.35	61.53	38.47
NA	NA_177	1620.73	415.00	2.32	25.32	22.37	49.98	72.36	27.64
NA	NA_178	1636.88	415.00	2.12	30.45	20.08	47.35	67.43	32.57
NA	NA_179	1818.00	29.00	5.51	27.61	24.18	42.69	66.87	33.13
NA	NA_180	1922.61	29.00	0.97	21.47	21.88	55.68	77.56	22.44
NA	NA_181	1924.27	29.00	0.26	19.73	19.93	60.08	80.01	19.99
NA	NA_182	1928.55	29.00	0.16	18.37	21.00	60.48	81.48	18.52
NA	NA_183	1934.56	29.00	0.18	17.00	20.09	62.73	82.82	17.18
NA	NA_184	1939.44	29.00	0.48	24.44	22.10	52.99	75.09	24.91
NA	NA_185	1942.22	29.00	0.97	26.30	15.65	57.08	72.73	27.27
NA	NA_186	2010.00	29.00	12.16	22.98	31.27	33.58	64.85	35.15
NA	NA_187	2175.00	29.00	4.33	28.73	28.36	38.58	66.94	33.06
NA	NA_188	2225.00	29.00	32.46	41.20	13.03	13.31	26.34	73.66

		X > 63 µ	63 µ >X> 2µ	63 µ >X> 10µ	10 µ >X> 2µ	2µ > X	10 µ >X	X> 10µ
Region	No.	Sand	Full Silt	Coarse Silt	Fine Silt	Clay	Finer	Coarser
NA	NA_1	0.06	20.32	9.96	10.36	79.62	89.98	10.02
NA	NA_2	0.27	25.70	10.21	15.49	74.03	89.52	10.48
NA	NA_3	0.81	31.40	17.78	13.61	67.80	81.41	18.59
NA	NA_4	0.46	40.03	17.67	22.36	59.50	81.86	18.14
NA	NA_5	4.54	42.36	21.06	21.30	53.10	74.40	25.60
NA	NA_6	1.43	54.60	22.54	32.06	43.97	76.03	23.97
NA	NA_7	13.75	60.26	40.39	19.87	25.98	45.85	54.15
NA	NA_8	2.66	69.56	43.63	25.93	27.78	53.70	46.30
NA	NA_9	9.00	76.87	54.54	22.33	14.13	36.46	63.54
NA	NA_10	4.41	74.44	45.88	28.56	21.16	49.72	50.28
NA	NA_11	7.03	70.65	41.58	29.07	22.32	51.40	48.60
NA	NA_12	7.07	65.66	36.21	29.45	27.27	56.72	43.28
NA	NA_13	7.58	57.06	23.44	33.62	35.35	68.97	31.03
NA	NA_14	29.61	56.31	40.03	16.29	14.08	30.36	69.64
NA	NA_15	7.75	68.43	35.56	32.88	23.82	56.70	43.30
NA	NA_16	23.29	57.04	32.57	24.46	19.67	44.13	55.87
NA	NA_17	4.51	80.79	56.15	24.64	14.70	39.34	60.66
NA	NA_18	1.14	73.65	40.01	33.64	25.21	58.86	41.14
NA	NA_19	31.43	53.88	33.61	20.28	14.68	34.96	65.04
NA	NA_20	13.38	69.05	40.64	28.42	17.56	45.98	54.02
NA	NA_21	0.82	44.89	17.64	27.26	54.29	81.54	18.46
NA	NA_22	0.63	48.36	15.19	33.17	51.01	84.18	15.82
NA	NA_23	0.11	52.71	16.28	36.43	47.18	83.61	16.39
NA	NA_24	12.83	56.42	21.40	35.03	30.75	65.77	34.23
NA	NA_25	2.02	56.07	22.96	33.12	41.91	75.02	24.98
NA	NA_26	1.11	67.15	24.39	42.76	31.74	74.51	25.49
NA	NA_27	12.31	71.69	51.58	20.11	16.00	36.11	63.89
NA	NA_28	2.51	68.01	20.27	47.74	29.47	77.22	22.78
NA	NA_29	6.63	61.51	18.50	43.01	31.87	74.87	25.13

NA	NA_30	21.72	51.20	17.44	33.76	27.08	60.85	39.15
NA	NA_31	13.53	55.57	20.65	34.92	30.90	65.82	34.18
NA	NA_32	37.56	51.37	36.06	15.31	11.07	26.38	73.62
NA	NA_33	5.44	66.99	37.48	29.50	27.58	57.08	42.92
NA	NA_34	3.40	79.29	50.24	29.05	17.31	46.36	53.64
NA	NA_35	3.98	81.95	54.07	27.88	14.06	41.95	58.05
NA	NA_36	4.06	80.56	52.99	27.57	15.38	42.95	57.05
NA	NA_37	4.45	78.79	40.83	37.96	16.76	54.72	45.28
NA	NA_38	0.04	36.33	18.76	17.57	63.63	81.20	18.80
NA	NA_39	0.52	40.97	17.53	23.44	58.51	81.95	18.05
NA	NA_40	0.13	40.49	24.05	16.44	59.38	75.82	24.18
NA	NA_41	1.51	37.32	22.44	14.88	61.17	76.05	23.95
NA	NA_42	0.74	46.06	28.25	17.81	53.21	71.01	28.99
NA	NA_43	8.97	51.08	33.51	17.58	39.95	57.53	42.47
NA	NA_44	1.11	41.75	21.14	20.60	57.14	77.75	22.25
NA	NA_45	9.35	46.34	26.20	20.14	44.31	64.44	35.56
NA	NA_46	0.16	43.39	19.88	23.51	56.45	79.96	20.04
NA	NA_47	8.18	36.56	20.15	16.41	55.26	71.67	28.33
NA	NA_48	0.79	21.94	11.62	10.32	77.28	87.60	12.40
NA	NA_49	0.15	34.22	14.07	20.15	65.63	85.78	14.22
NA	NA_50	2.82	31.79	14.00	17.79	65.39	83.18	16.82
NA	NA_51	0.68	44.87	19.93	24.95	54.45	79.40	20.60
NA	NA_52	0.54	45.60	23.18	22.42	53.85	76.27	23.73
NA	NA_53	0.59	34.69	19.33	15.35	64.73	80.08	19.92
NA	NA_54	0.28	33.92	17.02	16.90	65.80	82.70	17.30
NA	NA_55	0.68	41.58	19.59	21.99	57.74	79.73	20.27
NA	NA_56	17.62	36.16	23.15	13.01	46.22	59.23	40.77
NA	NA_57	1.95	44.91	27.78	17.13	53.13	70.27	29.73
NA	NA_58	2.83	49.17	28.39	20.78	48.00	68.78	31.22
NA	NA_59	0.77	40.82	21.06	19.76	58.41	78.17	21.83
NA	NA_60	5.12	47.27	26.28	20.99	47.61	68.60	31.40

NA	NA_61	0.06	37.90	18.47	19.43	62.04	81.47	18.53
NA	NA_62	17.08	34.41	20.62	13.79	48.51	62.30	37.70
NA	NA_63	0.74	44.41	30.77	13.64	54.84	68.49	31.51
NA	NA_64	7.03	41.48	26.53	14.94	51.49	66.44	33.56
NA	NA_65	0.82	37.25	21.44	15.81	61.93	77.75	22.25
NA	NA_66	19.40	40.60	28.25	12.35	40.00	52.35	47.65
NA	NA_67	0.96	39.55	19.79	19.77	59.49	79.25	20.75
NA	NA_68	3.23	34.98	16.49	18.49	61.79	80.28	19.72
NA	NA_69	1.86	43.19	16.89	26.30	54.95	81.25	18.75
NA	NA_70	0.48	42.30	18.64	23.66	57.22	80.88	19.12
NA	NA_71	0.39	39.32	18.40	20.92	60.29	81.21	18.79
NA	NA_72	8.12	43.94	26.59	17.35	47.94	65.30	34.70
NA	NA_73	5.98	47.93	30.71	17.22	46.09	63.31	36.69
NA	NA_75	4.08	42.12	22.78	19.35	53.80	73.14	26.86
NA	NA_76	4.19	44.52	24.84	19.69	51.29	70.98	29.02
NA	NA_77	1.78	37.89	21.39	16.50	60.33	76.83	23.17
NA	NA_78	1.07	40.12	18.83	21.29	58.80	80.09	19.91
NA	NA_79	0.30	43.73	22.22	21.51	55.97	77.48	22.52
NA	NA_80	1.47	35.30	17.77	17.52	63.24	80.76	19.24
NA	NA_81	3.90	65.33	30.53	34.81	30.77	65.57	34.43
NA	NA_82	0.77	35.13	18.23	16.90	64.10	81.00	19.00
NA	NA_83	0.15	41.38	17.13	24.26	58.47	82.72	17.28
NA	NA_84	0.16	25.39	12.59	12.79	74.46	87.25	12.75
NA	NA_85	0.15	42.78	17.00	25.79	57.07	82.85	17.15
NA	NA_86	0.10	43.06	12.59	30.48	56.84	87.31	12.69
NA	NA_87	0.83	45.30	17.21	28.09	53.87	81.96	18.04
NA	NA_88	0.29	44.47	12.61	31.86	55.24	87.11	12.89
NA	NA_89	0.70	43.67	25.51	18.16	55.63	73.79	26.21
NA	NA_90	1.39	46.24	30.47	15.76	52.38	68.14	31.86
NA	NA_91	0.33	38.45	19.19	19.26	61.22	80.48	19.52
NA	NA_92	3.84	53.98	34.01	19.97	42.17	62.15	37.85

NA	NA_93	2.50	51.95	34.03	17.92	45.55	63.46	36.54
NA	NA_94	0.48	42.07	18.46	23.61	57.44	81.05	18.95
NA	NA_95	0.85	39.41	18.75	20.67	59.74	80.40	19.60
NA	NA_96	6.24	44.60	25.96	18.64	49.16	67.81	32.19
NA	NA_97	0.34	29.53	15.70	13.83	70.13	83.96	16.04
NA	NA_98	0.08	31.83	17.57	14.27	68.09	82.35	17.65
NA	NA_99	0.73	42.82	18.67	24.15	56.45	80.60	19.40
NA	NA_100	8.02	62.42	30.97	31.46	29.56	61.02	38.98
NA	NA_101	15.94	66.33	49.33	16.99	17.73	34.73	65.27
NA	NA_102	20.88	64.30	50.04	14.26	14.82	29.08	70.92
NA	NA_103	0.07	47.72	21.67	26.05	52.21	78.26	21.74
NA	NA_104	0.04	48.44	22.23	26.21	51.52	77.73	22.27
NA	NA_105	0.14	44.89	19.08	25.81	54.97	80.78	19.22
NA	NA_106	0.13	42.20	20.13	22.07	57.67	79.74	20.26
NA	NA_107	0.11	42.25	18.95	23.29	57.65	80.94	19.06
NA	NA_108	0.07	39.45	18.11	21.34	60.48	81.82	18.18
NA	NA_109	0.05	33.48	14.40	19.08	66.47	85.55	14.45
NA	NA_110	1.02	51.96	24.43	27.53	47.02	74.55	25.45
NA	NA_111	7.12	56.70	28.14	28.56	36.18	64.74	35.26
NA	NA_112	0.24	35.69	18.98	16.71	64.07	80.78	19.22
NA	NA_113	2.13	40.61	24.35	16.26	57.26	73.52	26.48
NA	NA_114	22.61	60.49	38.03	22.46	16.90	39.36	60.64
NA	NA_115	6.99	59.93	27.91	32.02	33.08	65.09	34.91
NA	NA_116	0.59	49.51	24.17	25.34	49.90	75.24	24.76
NA	NA_117	7.99	52.85	25.07	27.77	39.16	66.93	33.07
NA	NA_118	11.29	57.11	28.92	28.18	31.61	59.79	40.21
NA	NA_119	14.19	57.23	30.47	26.76	28.58	55.34	44.66
NA	NA_120	8.16	73.95	62.39	11.56	17.89	29.45	70.55
NA	NA_121	5.33	63.16	25.70	37.46	31.51	68.97	31.03
NA	NA_122	3.17	58.10	22.85	35.25	38.73	73.98	26.02
NA	NA_123	2.22	58.35	22.71	35.63	39.44	75.07	24.93

NA	NA_124	0.31	47.12	28.18	18.94	52.56	71.51	28.49
NA	NA_125	0.54	48.59	25.44	23.16	50.87	74.02	25.98
NA	NA_126	0.78	47.17	28.26	18.91	52.05	70.96	29.04
NA	NA_127	0.21	47.41	26.89	20.53	52.38	72.91	27.09
NA	NA_128	0.28	54.89	29.95	24.93	44.83	69.77	30.23
NA	NA_129	2.15	52.03	31.64	20.39	45.82	66.21	33.79
NA	NA_130	0.63	47.68	25.00	22.68	51.69	74.37	25.63
NA	NA_131	0.56	49.96	28.27	21.69	49.48	71.18	28.82
NA	NA_132	0.36	45.06	22.65	22.41	54.58	76.99	23.01
NA	NA_133	1.43	69.09	51.72	17.37	29.48	46.85	53.15
NA	NA_134	0.09	42.80	16.99	25.81	57.11	82.92	17.08
NA	NA_135	1.22	49.36	30.82	18.54	49.42	67.96	32.04
NA	NA_136	0.42	43.98	22.20	21.78	55.60	77.38	22.62
NA	NA_137	0.34	32.72	16.59	16.13	66.94	83.07	16.93
NA	NA_138	0.38	42.60	21.20	21.41	57.02	78.43	21.57
NA	NA_139	2.25	45.95	25.72	20.24	51.80	72.03	27.97
NA	NA_140	1.18	37.53	21.72	15.80	61.29	77.10	22.90
NA	NA_141	0.16	42.66	22.45	20.20	57.18	77.39	22.61
NA	NA_142	0.51	42.30	23.41	18.88	57.20	76.08	23.92
NA	NA_143	0.97	55.34	24.69	30.66	43.69	74.35	25.65
NA	NA_144	2.45	63.44	27.49	35.95	34.11	70.06	29.94
NA	NA_145	12.14	52.87	22.05	30.83	34.99	65.81	34.19
NA	NA_146	6.98	67.34	37.46	29.88	25.69	55.56	44.44
NA	NA_147	1.48	64.43	30.64	33.79	34.09	67.88	32.12
NA	NA_148	14.38	70.02	43.25	26.77	15.61	42.38	57.62
NA	NA_149	0.79	57.04	20.60	36.44	42.18	78.62	21.38
NA	NA_150	0.66	59.32	35.69	23.62	40.02	63.65	36.35
NA	NA_151	12.60	66.33	38.31	28.02	21.06	49.08	50.92
NA	NA_152	2.62	75.62	37.84	37.78	21.77	59.54	40.46
NA	NA_153	0.10	53.61	15.63	37.98	46.30	84.27	15.73
NA	NA_154	2.50	64.44	30.52	33.91	33.06	66.97	33.03

NA	NA_155	0.75	60.06	21.64	38.42	39.19	77.61	22.39
NA	NA_156	1.49	66.59	36.13	30.46	31.92	62.38	37.62
NA	NA_157	6.50	59.10	28.18	30.92	34.40	65.32	34.68
NA	NA_158	8.66	72.65	43.75	28.91	18.69	47.59	52.41
NA	NA_159	29.45	53.37	33.06	20.31	17.17	37.48	62.52
NA	NA_160	31.57	52.29	36.67	15.63	16.14	31.76	68.24
NA	NA_161	4.33	69.83	35.05	34.78	25.84	60.62	39.38
NA	NA_162	25.43	56.14	36.80	19.34	18.43	37.77	62.23
NA	NA_163	0.23	61.10	20.38	40.72	38.67	79.39	20.61
NA	NA_164	5.87	79.69	36.15	43.54	14.43	57.98	42.02
NA	NA_165	2.56	76.68	35.40	41.29	20.76	62.04	37.96
NA	NA_166	0.66	61.00	25.31	35.68	38.35	74.03	25.97
NA	NA_167	0.20	63.41	28.75	34.66	36.38	71.04	28.96
NA	NA_168	2.19	60.63	26.20	34.43	37.18	71.61	28.39
NA	NA_169	0.43	65.57	22.05	43.52	34.01	77.53	22.47
NA	NA_170	0.29	40.51	19.06	21.45	59.20	80.65	19.35
NA	NA_171	0.13	34.89	15.92	18.97	64.98	83.95	16.05
NA	NA_172	4.71	35.61	14.98	20.63	59.68	80.31	19.69
NA	NA_173	1.30	55.49	32.69	22.80	43.21	66.01	33.99
NA	NA_174	2.64	57.17	27.39	29.79	40.19	69.98	30.02
NA	NA_175	0.91	47.13	22.46	24.67	51.96	76.63	23.37
NA	NA_176	1.84	58.81	36.63	22.19	39.35	61.53	38.47
NA	NA_177	2.32	47.70	25.32	22.37	49.98	72.36	27.64
NA	NA_178	2.12	50.53	30.45	20.08	47.35	67.43	32.57
NA	NA_179	5.51	51.80	27.61	24.18	42.69	66.87	33.13
NA	NA_180	0.97	43.36	21.47	21.88	55.68	77.56	22.44
NA	NA_181	0.26	39.66	19.73	19.93	60.08	80.01	19.99
NA	NA_182	0.16	39.37	18.37	21.00	60.48	81.48	18.52
NA	NA_183	0.18	37.09	17.00	20.09	62.73	82.82	17.18
NA	NA_184	0.48	46.54	24.44	22.10	52.99	75.09	24.91
NA	NA_185	0.97	41.95	26.30	15.65	57.08	72.73	27.27

NA	NA_186	12.16	54.25	22.98	31.27	33.58	64.85	35.15
NA	NA_187	4.33	57.09	28.73	28.36	38.58	66.94	33.06
NA	NA_188	32.46	54.23	41.20	13.03	13.31	26.34	73.66

Model NA with finer and coarser as input, where coarser = 100							
Sand	Residual	Tot. sum of sq.	Coarse Silt	Residual	Tot. sum of sq.	Fine Silt	Residual
0.85	0.63	21.38	9.17	0.63	275.65	19.29	79.61
0.87	0.36	19.46	9.61	0.36	267.44	19.50	16.05
1.34	0.28	15.03	17.25	0.28	77.09	22.68	82.21
1.31	0.71	17.80	16.83	0.71	78.97	22.53	0.03
1.94	6.75	0.02	23.66	6.75	30.27	24.64	11.16
1.78	0.12	10.56	22.19	0.12	16.17	24.25	60.92
8.81	24.46	82.29	45.34	24.46	191.31	25.00	26.36
5.81	9.90	4.08	40.48	9.90	291.39	26.12	0.04
14.49	30.15	18.65	49.05	30.15	782.94	22.45	0.01
7.18	7.69	0.08	43.11	7.69	373.14	25.67	8.34
6.57	0.21	5.49	42.04	0.21	225.45	25.89	10.13
4.95	4.48	5.70	38.33	4.48	93.14	26.31	9.89
2.59	24.95	8.41	28.44	24.95	9.72	25.65	63.50
20.01	92.10	621.45	49.62	92.10	181.30	20.08	14.43
4.96	7.78	9.40	38.35	7.78	80.92	26.31	43.16
9.65	186.23	346.41	46.22	186.23	36.11	24.64	0.03
12.44	62.90	0.03	48.22	62.90	875.61	23.37	1.60
4.42	10.79	12.56	36.72	10.79	180.76	26.35	53.12
15.69	247.95	715.57	49.35	247.95	49.62	21.92	2.70
8.75	21.47	75.69	45.27	21.47	198.11	25.03	11.47
1.33	0.26	14.95	17.13	0.26	79.60	22.64	21.32
1.16	0.28	16.43	14.67	0.28	129.21	21.71	131.29
1.19	1.18	20.93	15.20	1.18	105.60	21.92	210.60
3.07	95.34	66.38	31.16	95.34	26.68	26.04	80.79
1.88	0.02	7.09	23.10	0.02	12.99	24.50	74.31
1.93	0.68	12.79	23.56	0.68	4.72	24.62	329.31
14.76	6.01	58.18	49.13	6.01	625.97	22.33	4.93
1.67	0.71	4.71	21.11	0.71	39.55	23.94	566.43
1.89	22.42	3.79	23.23	22.42	65.00	24.53	341.31

3.98	314.60	290.18	35.17	314.60	83.25	26.34	55.14
3.06	109.57	78.20	31.12	109.57	34.89	26.04	78.92
24.71	164.99	1080.89	48.90	164.99	90.21	18.24	8.57
4.86	0.33	0.57	38.06	0.33	119.30	26.32	10.14
8.58	26.78	1.64	45.07	26.78	560.73	25.10	15.59
10.83	46.91	0.49	47.22	46.91	756.64	24.10	14.29
10.27	38.61	0.39	46.78	38.61	698.41	24.36	10.35
5.51	1.11	0.05	39.78	1.11	203.63	26.20	138.27
1.35	1.73	21.55	17.45	1.73	60.86	22.75	26.84
1.30	0.61	17.32	16.75	0.61	81.48	22.50	0.88
1.80	2.79	20.72	22.38	2.79	6.32	24.30	61.76
1.78	0.07	10.06	22.18	0.07	16.95	24.25	87.82
2.32	2.51	15.56	26.66	2.51	2.85	25.32	56.49
4.74	17.81	18.34	37.73	17.81	48.23	26.33	76.64
1.63	0.27	12.77	20.63	0.27	29.34	23.80	10.21
3.29	36.76	21.81	32.27	36.76	0.13	26.16	36.24
1.45	1.66	20.46	18.59	1.66	44.63	23.15	0.13
2.24	35.24	12.23	26.09	35.24	41.05	25.21	77.39
0.96	0.03	15.19	11.44	0.03	223.31	20.34	100.46
1.06	0.83	20.56	13.16	0.83	156.03	21.09	0.88
1.22	2.57	3.47	15.60	2.57	157.80	22.07	18.33
1.49	0.66	16.06	19.11	0.66	43.99	23.32	2.64
1.76	1.47	17.12	21.97	1.47	11.43	24.19	3.13
1.44	0.73	16.79	18.48	0.73	52.22	23.11	60.18
1.25	0.93	19.34	16.05	0.93	91.03	22.24	28.59
1.46	0.61	16.02	18.81	0.61	48.56	23.22	1.52
4.34	176.54	167.46	36.43	176.54	11.65	26.36	178.16
2.42	0.21	7.45	27.32	0.21	1.49	25.45	69.17
2.61	0.05	3.44	28.61	0.05	3.36	25.68	23.99
1.59	0.67	15.30	20.24	0.67	30.29	23.68	15.33
2.64	6.17	0.19	28.76	6.17	0.08	25.70	22.21

1.33	1.62	21.37	17.19	1.62	65.51	22.66	10.46
3.69	179.43	153.70	34.01	179.43	35.31	26.29	156.15
2.66	3.66	15.54	28.86	3.66	17.72	25.72	145.84
2.96	16.58	5.52	30.60	16.58	0.00	25.97	121.60
1.63	0.65	14.92	20.63	0.65	26.27	23.80	63.78
6.24	173.22	216.75	41.41	173.22	2.84	26.00	186.11
1.50	0.29	13.87	19.24	0.29	45.90	23.36	12.93
1.42	3.27	2.11	18.30	3.27	101.36	23.05	20.82
1.35	0.26	7.97	17.40	0.26	93.59	22.73	12.71
1.38	0.81	17.67	17.74	0.81	62.74	22.86	0.65
1.35	0.93	18.42	17.44	0.93	66.61	22.75	3.36
3.14	24.73	11.80	31.56	24.73	0.00	26.08	76.22
3.49	6.20	1.69	33.20	6.20	17.19	26.23	81.24
2.07	4.01	0.37	24.78	4.01	14.31	24.91	31.02
2.33	3.45	0.25	26.69	3.45	2.97	25.33	31.82
1.71	0.01	8.44	21.46	0.01	26.74	24.05	56.96
1.44	0.13	13.02	18.47	0.13	59.70	23.11	3.31
1.65	1.82	19.19	20.87	1.82	18.84	23.87	5.58
1.39	0.01	10.34	17.85	0.01	77.22	22.90	28.85
3.10	0.64	0.61	31.33	0.64	15.73	26.06	76.55
1.37	0.36	15.33	17.63	0.36	69.35	22.82	35.04
1.25	1.21	20.56	16.03	1.21	88.99	22.23	4.09
0.98	0.68	20.48	11.77	0.68	195.17	20.49	59.18
1.24	1.19	20.55	15.91	1.19	91.45	22.19	12.95
0.98	0.77	21.00	11.71	0.77	195.32	20.46	100.28
1.30	0.22	14.81	16.74	0.22	87.53	22.50	31.31
0.99	0.49	19.32	11.90	0.49	194.77	20.55	128.06
2.00	1.70	15.85	24.20	1.70	1.11	24.78	43.73
2.70	1.74	10.87	29.16	1.74	15.32	25.77	100.06
1.41	1.15	18.90	18.12	1.15	54.33	22.99	13.91
3.72	0.02	0.71	34.14	0.02	55.49	26.29	39.95

3.47	0.92	4.75	33.07	0.92	55.85	26.22	69.05
1.36	0.78	17.64	17.58	0.78	65.56	22.80	0.65
1.41	0.32	14.70	18.18	0.32	61.06	23.01	5.49
2.75	12.14	2.41	29.44	12.14	0.36	25.81	51.38
1.17	0.69	18.87	14.87	0.69	117.94	21.79	63.35
1.27	1.43	21.19	16.37	1.43	80.86	22.36	65.58
1.40	0.45	15.65	18.00	0.45	62.23	22.95	1.45
3.94	16.59	11.13	35.04	16.59	19.41	26.33	26.24
15.88	0.00	126.77	49.39	0.00	518.54	21.83	23.42
21.42	0.29	262.43	49.50	0.29	551.06	19.52	27.61
1.58	2.29	21.29	20.16	2.29	23.93	23.65	5.75
1.63	2.52	21.56	20.65	2.52	18.73	23.80	5.80
1.38	1.55	20.65	17.84	1.55	55.90	22.89	8.51
1.46	1.78	20.74	18.80	1.78	41.30	23.22	1.32
1.37	1.60	20.93	17.69	1.60	57.87	22.84	0.21
1.31	1.54	21.29	16.87	1.54	71.39	22.55	1.45
1.08	1.05	21.46	13.37	1.05	147.89	21.18	4.39
1.93	0.83	13.44	23.52	0.83	4.53	24.61	8.56
3.24	15.07	5.94	32.02	15.07	2.50	26.13	5.87
1.38	1.31	19.75	17.84	1.31	57.44	22.89	38.23
2.03	0.01	6.51	24.44	0.01	4.91	24.83	73.48
12.43	103.72	321.44	48.22	103.72	131.56	23.38	0.85
3.18	14.55	5.33	31.73	14.55	1.83	26.10	34.96
1.86	1.61	16.76	22.90	1.61	5.73	24.44	0.81
2.88	26.12	10.96	30.18	26.12	2.21	25.92	3.45
4.21	50.10	43.63	36.00	50.10	5.58	26.35	3.34
5.33	78.58	90.46	39.33	78.58	15.26	26.24	0.28
21.01	165.03	12.11	49.54	165.03	1283.71	19.68	66.00
2.59	7.51	0.42	28.44	7.51	0.75	25.65	139.48
1.98	1.39	2.30	24.03	1.39	13.77	24.73	110.66
1.87	0.12	6.08	23.06	0.12	14.80	24.49	124.26

2.26	3.80	19.09	26.23	3.80	2.62	25.23	39.60
1.98	2.08	17.17	24.00	2.08	1.26	24.73	2.46
2.33	2.41	15.26	26.71	2.41	2.89	25.33	41.26
2.10	3.59	20.03	24.99	3.59	0.11	24.96	19.67
2.48	4.85	19.39	27.75	4.85	11.51	25.53	0.36
3.00	0.71	6.40	30.79	0.71	25.76	26.00	31.41
1.94	1.73	16.43	23.69	1.73	2.43	24.65	3.89
2.30	3.05	17.03	26.52	3.05	2.91	25.29	12.98
1.69	1.78	18.71	21.32	1.78	15.28	24.00	2.55
8.36	48.01	10.60	44.79	48.01	633.13	25.20	61.34
1.24	1.31	21.09	15.84	1.31	91.63	22.16	13.31
2.73	2.28	11.98	29.31	2.28	18.15	25.79	52.54
1.66	1.53	18.15	20.96	1.53	19.03	23.90	4.49
1.23	0.79	18.86	15.70	0.79	99.44	22.11	35.72
1.57	1.42	18.54	20.00	1.42	28.78	23.61	4.84
2.20	0.00	5.93	25.77	0.00	0.71	25.14	24.00
1.68	0.25	12.27	21.22	0.25	23.39	23.98	66.80
1.66	2.25	20.49	20.95	2.25	16.87	23.90	13.63
1.78	1.61	17.43	22.15	1.61	9.90	24.24	28.71
1.95	0.96	13.79	23.71	0.96	3.52	24.65	36.04
2.44	0.00	4.98	27.50	0.00	0.86	25.48	109.58
3.06	82.49	55.64	31.13	82.49	20.38	26.04	22.95
5.27	2.92	5.26	39.17	2.92	118.80	26.25	13.15
2.74	1.60	10.28	29.37	1.60	16.63	25.80	63.86
10.59	14.33	93.97	47.03	14.33	278.48	24.21	6.52
1.55	0.58	15.17	19.83	0.58	35.57	23.55	166.07
3.43	7.67	16.17	32.92	7.67	83.38	26.21	6.70
7.42	26.83	62.73	43.49	26.83	138.14	25.58	5.97
4.26	2.71	4.26	36.19	2.71	127.16	26.36	130.47
1.15	1.11	21.02	14.58	1.11	119.47	21.67	265.81
2.88	0.14	4.75	30.15	0.14	15.71	25.91	64.00

1.64	0.79	15.47	20.76	0.79	24.18	23.84	212.71
3.67	4.75	10.20	33.95	4.75	91.49	26.28	17.45
3.14	11.26	3.29	31.54	11.26	2.64	26.08	23.40
8.03	0.39	15.82	44.37	0.39	295.32	25.33	12.78
13.73	247.36	613.62	48.79	247.36	42.30	22.79	6.18
18.58	168.69	723.02	49.65	168.69	102.10	20.68	25.50
4.03	0.09	0.12	35.35	0.09	72.10	26.34	71.16
13.52	141.95	430.52	48.71	141.95	104.80	22.89	12.58
1.49	1.58	19.80	19.12	1.58	38.21	23.32	302.54
4.63	1.54	1.42	37.39	1.54	91.93	26.34	295.87
3.74	1.39	4.52	34.22	1.39	78.08	26.30	224.61
1.98	1.75	16.21	23.99	1.75	1.56	24.72	120.13
2.32	4.47	20.06	26.64	4.47	4.80	25.32	87.31
2.25	0.00	6.23	26.14	0.00	0.13	25.21	84.99
1.64	1.48	18.11	20.83	1.48	20.39	23.86	386.54
1.39	1.23	19.33	17.96	1.23	56.21	22.93	2.19
1.17	1.08	20.73	14.88	1.08	113.23	21.79	7.94
1.42	10.80	0.00	18.27	10.80	134.08	23.04	5.80
3.03	2.99	11.46	30.96	2.99	37.58	26.02	10.37
2.45	0.03	4.19	27.57	0.03	0.68	25.50	18.40
1.72	0.66	14.24	21.64	0.66	16.84	24.10	0.33
3.84	3.99	8.08	34.63	3.99	101.31	26.32	17.08
2.16	0.03	5.57	25.48	0.03	1.54	25.07	7.29
2.81	0.47	6.57	29.76	0.47	15.13	25.86	33.42
2.89	6.86	0.69	30.23	6.86	1.11	25.92	3.03
1.64	0.46	13.82	20.80	0.46	25.87	23.85	3.86
1.44	1.40	19.56	18.55	1.40	46.70	23.13	10.24
1.33	1.39	20.48	17.19	1.39	67.14	22.66	2.77
1.24	1.14	20.30	15.94	1.14	91.36	22.20	4.44
1.87	1.95	17.69	23.04	1.95	4.51	24.48	5.69
2.12	1.32	13.76	25.15	1.32	0.07	25.00	87.43

3.22	80.02	55.98	31.93	80.02	12.80	26.12	26.47
2.88	2.10	0.12	30.18	2.10	4.70	25.92	5.97
24.77	59.14	771.59	48.89	59.14	214.32	18.22	26.93

-finer			
Tot. sum of sq.	Clay	Residual	Tot. sum of sq.
190.11	70.70	79.61	1226.01
75.02	70.02	16.05	865.91
111.03	58.73	82.21	537.96
3.21	59.33	0.03	221.96
8.13	49.76	11.16	72.19
62.50	51.77	60.92	0.40
18.34	20.85	26.36	346.71
3.15	27.58	0.04	283.08
3.32	14.01	0.01	928.80
19.42	24.05	8.34	549.72
24.22	25.51	10.13	496.41
28.08	30.41	9.89	300.60
89.64	43.32	63.50	85.58
61.88	10.28	14.43	931.94
76.10	30.39	43.16	431.98
0.10	19.50	0.03	621.72
0.24	15.97	1.60	894.20
90.08	32.50	53.12	376.01
15.01	13.04	2.70	895.22
18.19	20.95	11.47	731.18
9.63	58.91	21.32	93.78
81.24	62.47	131.29	41.05
150.74	61.69	210.60	6.62
118.29	39.73	80.79	192.05
80.37	50.53	74.31	7.27
346.41	49.89	329.31	165.44
16.34	13.78	4.93	818.25
556.54	53.27	566.43	228.99
355.52	50.34	341.31	162.28

Stat	Sand
Min	0.04
Max	37.56
Mean	4.68
Var	51.63
Mod_min	0.85
Mod_max	24.77
Mod_mean	3.82
Mod_var	20.05
R2	0.61

Coarser	Sand model
100-finer	0.5*exp(coarser*(ln(100/0.5)/100))

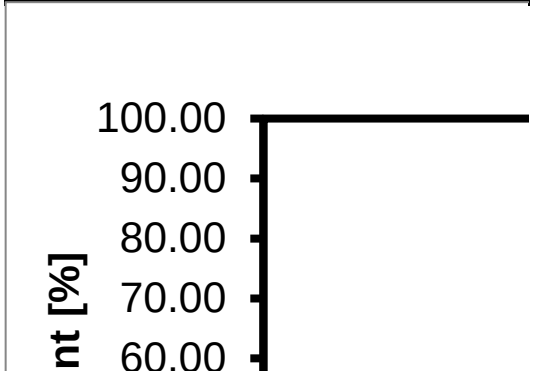

92.38	34.51	55.14	307.02
115.92	39.78	78.92	187.77
78.16	8.14	8.57	1124.55
28.65	30.76	10.14	289.99
24.01	21.25	15.59	745.21
13.92	17.84	14.29	932.72
11.71	18.60	10.35	854.12
190.62	28.52	138.27	775.45
43.30	58.45	26.84	361.89
0.51	59.44	0.88	193.26
59.40	51.52	61.76	218.23
86.03	51.80	87.82	274.37
40.25	45.69	56.49	73.99
43.21	31.20	76.64	21.66
12.59	53.95	10.21	157.22
16.13	38.29	36.24	0.09
0.41	56.81	0.13	140.24
59.97	46.46	77.39	113.50
191.34	67.25	100.46	1067.53
15.99	64.69	0.88	442.04
40.47	61.11	18.33	432.02
0.63	56.08	2.64	96.94
3.00	52.08	3.13	85.54
77.41	56.97	60.18	404.90
52.63	60.45	28.59	449.18
4.68	56.51	1.52	172.51
124.18	32.87	178.16	2.61
49.25	44.82	69.17	72.73
11.36	43.10	23.99	11.51
19.26	54.49	15.33	190.54
9.98	42.90	22.21	9.03

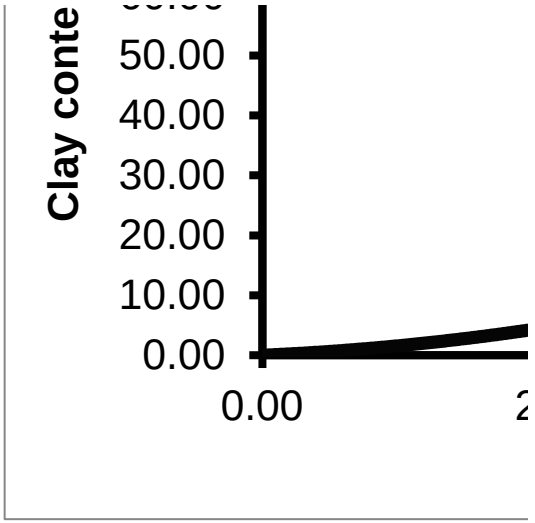

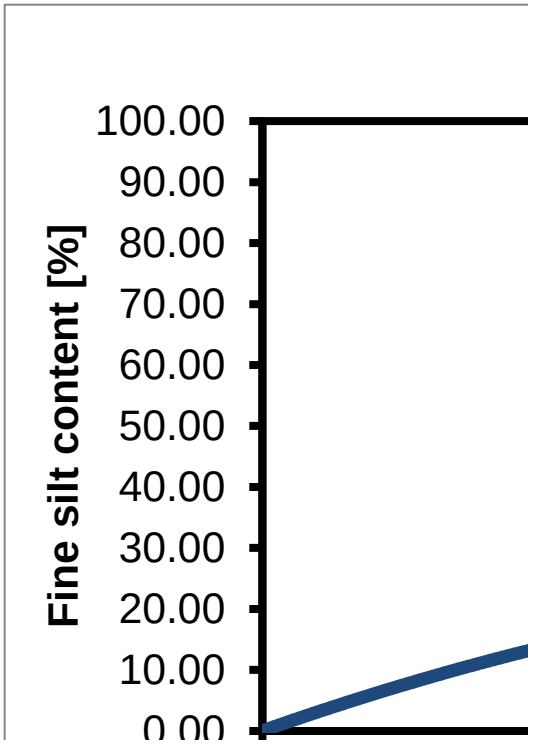

22.31	58.81	10.46	304.14
107.34	36.01	156.15	15.25
110.42	42.77	145.84	104.85
84.77	40.46	121.60	47.42
69.55	53.95	63.78	300.28
139.21	26.35	186.11	21.24
19.23	55.89	12.93	221.52
32.09	57.23	20.82	295.28
4.62	58.52	12.71	107.10
0.24	58.03	0.65	159.10
10.46	58.46	3.36	246.09
46.21	39.21	76.22	11.15
48.04	37.08	81.24	2.20
23.10	48.23	31.02	84.53
19.92	45.65	31.82	44.69
58.58	52.79	56.96	247.43
8.19	56.98	3.31	201.57
6.98	53.61	5.58	129.13
43.93	57.86	28.85	347.12
113.56	39.51	76.55	191.53
52.61	58.18	35.04	380.11
0.01	60.49	4.09	192.22
128.98	66.76	59.18	891.19
2.67	60.66	12.95	155.28
39.99	66.85	100.28	149.69
15.54	59.46	31.31	85.79
59.48	66.56	128.06	113.18
35.86	49.02	43.73	121.53
70.36	42.37	100.06	60.40
23.95	57.49	13.91	276.00
17.46	35.85	39.95	5.91

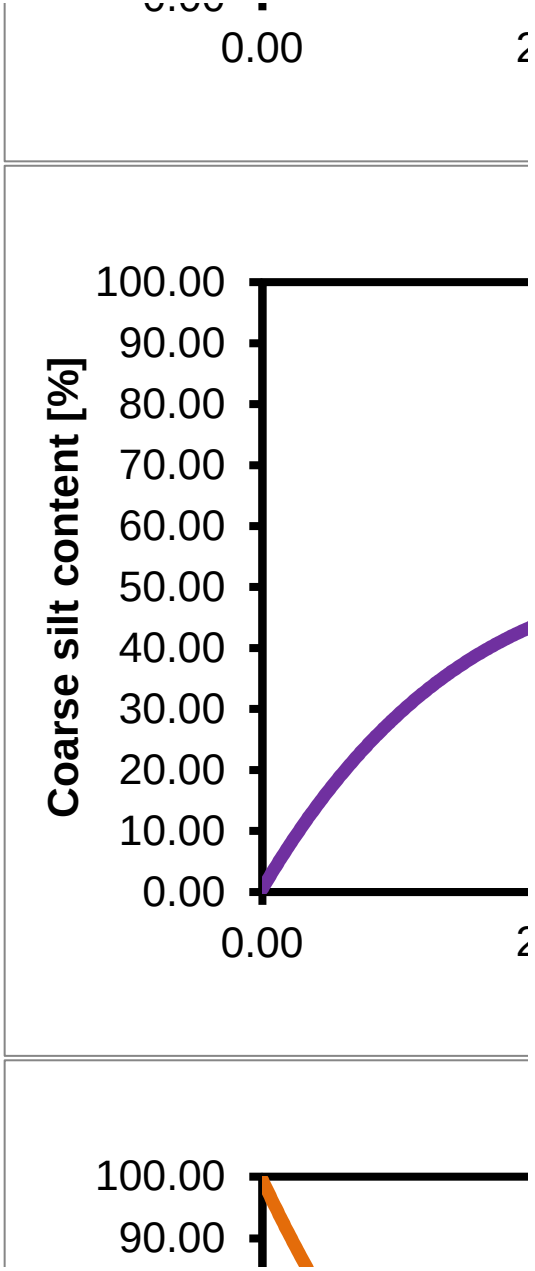

38.90	37.24	69.05	0.89
0.30	58.25	0.65	164.86
12.15	57.40	5.49	229.04
30.35	42.00	51.38	20.79
106.58	62.17	63.35	651.71
97.74	59.99	65.58	551.38
0.00	57.65	1.45	140.31
53.34	34.68	26.24	226.34
51.23	12.89	23.42	722.16
97.81	9.57	27.61	887.12
3.61	54.61	5.75	57.87
4.24	53.92	5.80	47.77
2.74	57.89	8.51	107.45
4.34	56.52	1.32	170.68
0.74	58.10	0.21	170.07
7.91	59.27	1.45	252.03
25.68	64.37	4.39	477.92
11.43	49.94	8.56	5.82
19.39	38.61	5.87	70.92
55.44	57.89	38.23	379.04
62.25	48.69	73.48	160.20
2.87	15.98	0.85	767.62
61.83	38.99	34.96	132.83
1.42	50.80	0.81	28.07
13.12	41.02	3.45	29.64
16.25	33.44	3.34	168.93
6.82	29.10	0.28	256.94
158.63	9.77	66.00	713.61
177.14	43.32	139.48	171.39
123.25	49.25	110.66	34.50
131.82	50.58	124.26	26.71

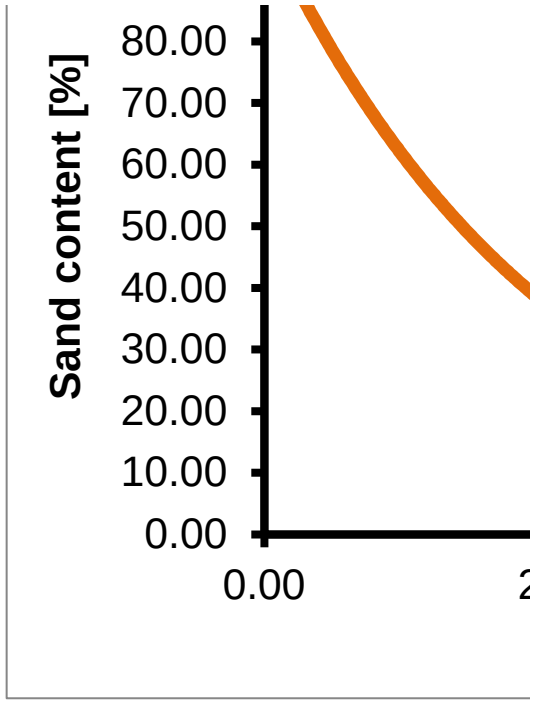

27.15	46.27	39.60	63.37
0.99	49.30	2.46	39.22
27.49	45.63	41.26	55.49
13.13	47.94	19.67	60.44
0.61	44.24	0.36	0.05
14.14	40.22	31.41	1.48
2.18	49.72	3.89	50.26
6.05	45.88	12.98	23.80
3.05	52.99	2.55	99.59
46.05	21.65	61.34	228.61
2.76	60.76	13.31	156.38
31.47	42.17	52.54	23.14
5.63	53.48	4.49	120.89
64.29	60.96	35.72	498.75
7.54	54.82	4.84	154.18
15.33	46.90	24.00	51.74
69.72	53.12	66.80	278.53
15.58	53.49	13.63	158.25
27.78	51.84	28.71	158.55
42.32	49.69	36.04	0.84
139.25	44.57	109.58	110.20
44.55	39.78	22.95	92.53
32.80	29.31	13.15	357.93
92.93	42.08	63.86	110.50
6.84	18.16	6.52	840.79
150.97	55.06	166.07	5.89
0.28	37.43	6.70	21.01
14.96	23.51	5.97	554.17
185.66	33.19	130.47	521.63
191.10	62.60	265.81	2.86
95.26	41.06	64.00	133.26

203.62	53.77	212.71	29.36
39.80	36.10	17.45	160.78
45.80	39.24	23.40	104.13
22.61	22.26	12.78	671.67
14.79	14.69	6.18	752.39
72.66	11.09	25.50	810.49
112.92	34.28	71.16	352.09
23.16	14.88	12.58	685.07
274.41	56.06	302.54	35.22
376.06	31.63	295.87	910.28
293.57	35.75	224.61	568.60
132.99	49.31	120.13	39.16
110.46	45.73	87.31	67.61
105.72	46.40	84.99	55.11
375.10	53.67	386.54	112.30
7.30	57.72	2.19	213.04
26.82	62.16	7.94	415.04
12.40	57.27	5.80	227.33
1.84	39.99	10.37	1.93
31.76	44.48	18.40	19.49
0.27	52.54	0.33	54.18
3.87	35.22	17.08	27.63
3.16	47.28	7.29	28.92
16.61	41.57	33.42	7.56
0.00	40.95	3.03	3.66
5.14	53.71	3.86	122.57
17.81	56.88	10.24	239.54
9.95	58.81	2.77	251.95
16.48	60.62	4.44	328.47
4.22	50.60	5.69	70.28
72.30	47.73	87.43	155.61

50.64	38.73	26.47	121.44
17.70	41.03	5.97	36.27
123.73	8.12	26.93	979.29

Coarse Silt	Fine Silt	Clay
9.96	10.32	11.07
62.39	47.74	79.62
26.56	24.15	44.60
98.32	58.76	267.16
9.17	18.22	8.12
49.65	26.36	70.70
27.43	24.11	44.65
112.17	3.39	221.78
0.79	0.11	0.80

Coarse Silt model	Cohesive Silt model	Clay model
coarser-sand	finer-clay	$0.0075*finer^2 + 0.1108*finer$

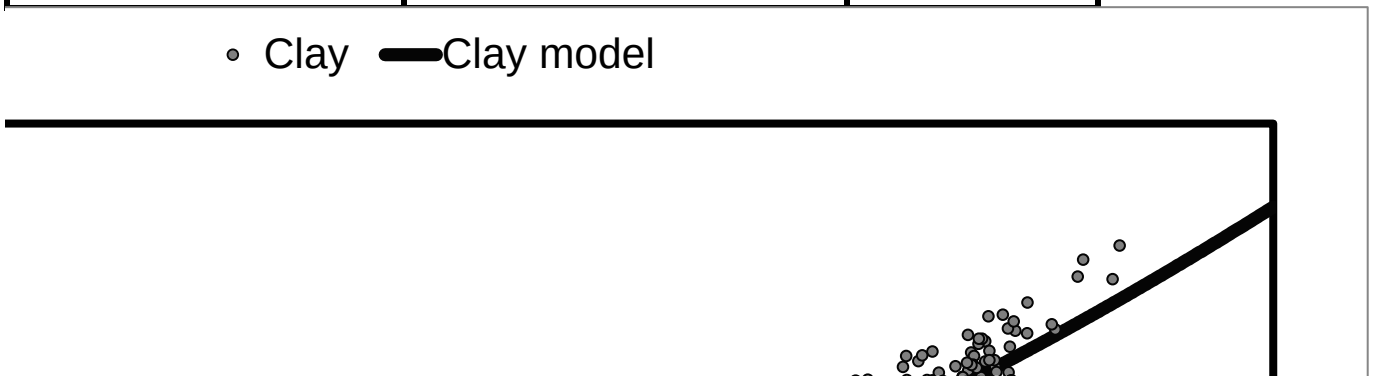

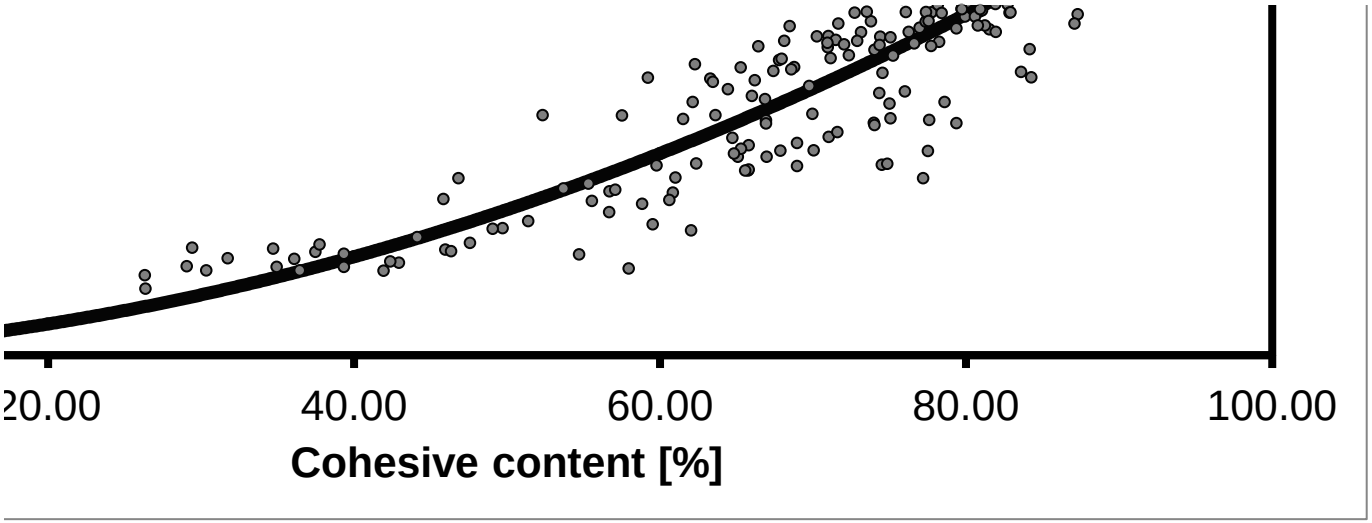
20.00
40.00
60.00
80.00
100.00
Cohesive content [%]

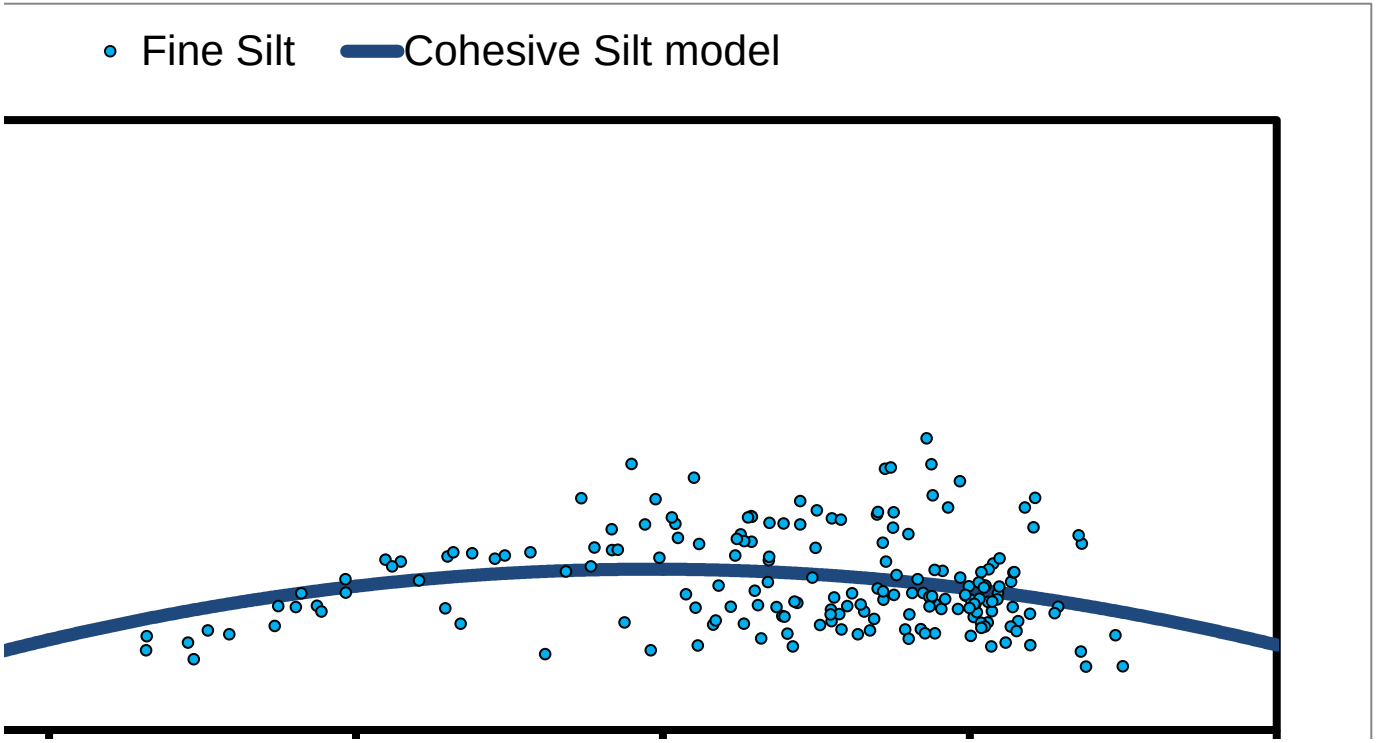
Fine Silt
Cohesive Silt model

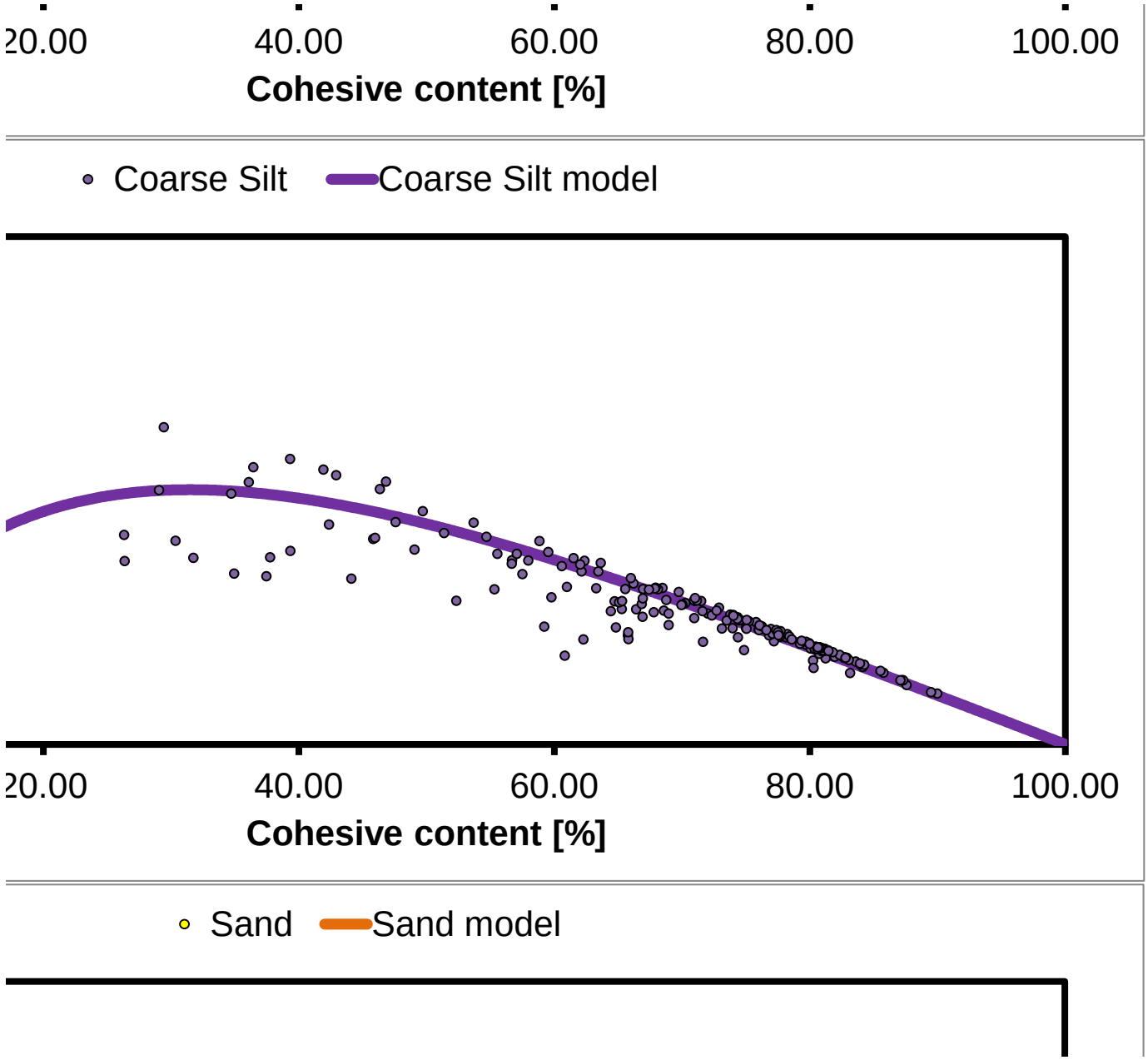
20.00
40.00
60.00
80.00
100.00
Cohesive content [%]
Coarse Silt
Coarse Silt model
20.00
40.00
60.00
80.00
100.00
Cohesive content [%]
Sand
Sand model

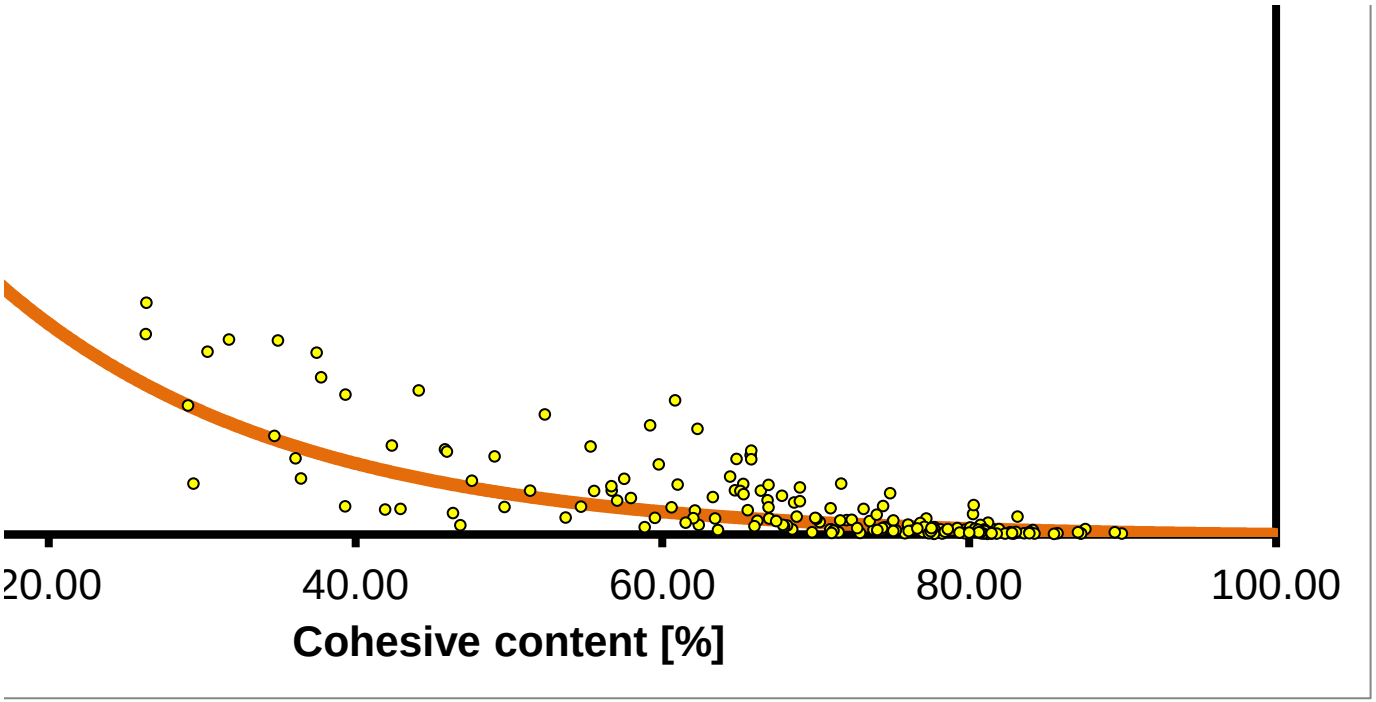
20.00
40.00
60.00
80.00
100.00
Cohesive content [%]

Model from 0-100					
Cohesive input	Sortable	Sand model	Coarse Silt model	Cohesive Silt model	Clay model
0.00	100.00	99.50	0.50	0.00	0.00
0.10	99.90	98.97	0.93	0.09	0.01
0.20	99.80	98.45	1.35	0.18	0.02
0.30	99.70	97.92	1.78	0.27	0.03
0.40	99.60	97.40	2.20	0.35	0.05
0.50	99.50	96.89	2.61	0.44	0.06
0.60	99.40	96.37	3.03	0.53	0.07
0.70	99.30	95.86	3.44	0.62	0.08
0.80	99.20	95.35	3.85	0.71	0.09
0.90	99.10	94.84	4.26	0.79	0.11
1.00	99.00	94.34	4.66	0.88	0.12
1.10	98.90	93.84	5.06	0.97	0.13
1.20	98.80	93.34	5.46	1.06	0.14
1.30	98.70	92.84	5.86	1.14	0.16
1.40	98.60	92.35	6.25	1.23	0.17
1.50	98.50	91.86	6.64	1.32	0.18
1.60	98.40	91.37	7.03	1.40	0.20
1.70	98.30	90.89	7.41	1.49	0.21
1.80	98.20	90.40	7.80	1.58	0.22
1.90	98.10	89.92	8.18	1.66	0.24
2.00	98.00	89.45	8.55	1.75	0.25
2.10	97.90	88.97	8.93	1.83	0.27
2.20	97.80	88.50	9.30	1.92	0.28
2.30	97.70	88.03	9.67	2.01	0.29
2.40	97.60	87.56	10.04	2.09	0.31
2.50	97.50	87.09	10.41	2.18	0.32
2.60	97.40	86.63	10.77	2.26	0.34
2.70	97.30	86.17	11.13	2.35	0.35
2.80	97.20	85.71	11.49	2.43	0.37

2.90	97.10	85.26	11.84	2.52	0.38
3.00	97.00	84.80	12.20	2.60	0.40
3.10	96.90	84.35	12.55	2.68	0.42
3.20	96.80	83.90	12.90	2.77	0.43
3.30	96.70	83.46	13.24	2.85	0.45
3.40	96.60	83.02	13.58	2.94	0.46
3.50	96.50	82.57	13.93	3.02	0.48
3.60	96.40	82.13	14.27	3.10	0.50
3.70	96.30	81.70	14.60	3.19	0.51
3.80	96.20	81.26	14.94	3.27	0.53
3.90	96.10	80.83	15.27	3.35	0.55
4.00	96.00	80.40	15.60	3.44	0.56
4.10	95.90	79.97	15.93	3.52	0.58
4.20	95.80	79.55	16.25	3.60	0.60
4.30	95.70	79.13	16.57	3.68	0.62
4.40	95.60	78.71	16.89	3.77	0.63
4.50	95.50	78.29	17.21	3.85	0.65
4.60	95.40	77.87	17.53	3.93	0.67
4.70	95.30	77.46	17.84	4.01	0.69
4.80	95.20	77.04	18.16	4.10	0.70
4.90	95.10	76.63	18.47	4.18	0.72
5.00	95.00	76.23	18.77	4.26	0.74
5.10	94.90	75.82	19.08	4.34	0.76
5.20	94.80	75.42	19.38	4.42	0.78
5.30	94.70	75.02	19.68	4.50	0.80
5.40	94.60	74.62	19.98	4.58	0.82
5.50	94.50	74.22	20.28	4.66	0.84
5.60	94.40	73.83	20.57	4.74	0.86
5.70	94.30	73.43	20.87	4.82	0.88
5.80	94.20	73.04	21.16	4.91	0.89
5.90	94.10	72.65	21.45	4.99	0.91

6.00	94.00	72.27	21.73	5.07	0.93
6.10	93.90	71.88	22.02	5.15	0.95
6.20	93.80	71.50	22.30	5.22	0.98
6.30	93.70	71.12	22.58	5.30	1.00
6.40	93.60	70.74	22.86	5.38	1.02
6.50	93.50	70.37	23.13	5.46	1.04
6.60	93.40	69.99	23.41	5.54	1.06
6.70	93.30	69.62	23.68	5.62	1.08
6.80	93.20	69.25	23.95	5.70	1.10
6.90	93.10	68.88	24.22	5.78	1.12
7.00	93.00	68.51	24.49	5.86	1.14
7.10	92.90	68.15	24.75	5.94	1.16
7.20	92.80	67.79	25.01	6.01	1.19
7.30	92.70	67.42	25.28	6.09	1.21
7.40	92.60	67.07	25.53	6.17	1.23
7.50	92.50	66.71	25.79	6.25	1.25
7.60	92.40	66.35	26.05	6.32	1.28
7.70	92.30	66.00	26.30	6.40	1.30
7.80	92.20	65.65	26.55	6.48	1.32
7.90	92.10	65.30	26.80	6.56	1.34
8.00	92.00	64.95	27.05	6.63	1.37
8.10	91.90	64.61	27.29	6.71	1.39
8.20	91.80	64.26	27.54	6.79	1.41
8.30	91.70	63.92	27.78	6.86	1.44
8.40	91.60	63.58	28.02	6.94	1.46
8.50	91.50	63.24	28.26	7.02	1.48
8.60	91.40	62.90	28.50	7.09	1.51
8.70	91.30	62.57	28.73	7.17	1.53
8.80	91.20	62.23	28.97	7.24	1.56
8.90	91.10	61.90	29.20	7.32	1.58
9.00	91.00	61.57	29.43	7.40	1.60

9.10	90.90	61.25	29.65	7.47	1.63
9.20	90.80	60.92	29.88	7.55	1.65
9.30	90.70	60.59	30.11	7.62	1.68
9.40	90.60	60.27	30.33	7.70	1.70
9.50	90.50	59.95	30.55	7.77	1.73
9.60	90.40	59.63	30.77	7.85	1.75
9.70	90.30	59.31	30.99	7.92	1.78
9.80	90.20	59.00	31.20	7.99	1.81
9.90	90.10	58.68	31.42	8.07	1.83
10.00	90.00	58.37	31.63	8.14	1.86
10.10	89.90	58.06	31.84	8.22	1.88
10.20	89.80	57.75	32.05	8.29	1.91
10.30	89.70	57.44	32.26	8.36	1.94
10.40	89.60	57.14	32.46	8.44	1.96
10.50	89.50	56.83	32.67	8.51	1.99
10.60	89.40	56.53	32.87	8.58	2.02
10.70	89.30	56.23	33.07	8.66	2.04
10.80	89.20	55.93	33.27	8.73	2.07
10.90	89.10	55.63	33.47	8.80	2.10
11.00	89.00	55.33	33.67	8.87	2.13
11.10	88.90	55.04	33.86	8.95	2.15
11.20	88.80	54.74	34.06	9.02	2.18
11.30	88.70	54.45	34.25	9.09	2.21
11.40	88.60	54.16	34.44	9.16	2.24
11.50	88.50	53.87	34.63	9.23	2.27
11.60	88.40	53.59	34.81	9.31	2.29
11.70	88.30	53.30	35.00	9.38	2.32
11.80	88.20	53.02	35.18	9.45	2.35
11.90	88.10	52.73	35.37	9.52	2.38
12.00	88.00	52.45	35.55	9.59	2.41
12.10	87.90	52.17	35.73	9.66	2.44

12.20	87.80	51.89	35.91	9.73	2.47
12.30	87.70	51.62	36.08	9.80	2.50
12.40	87.60	51.34	36.26	9.87	2.53
12.50	87.50	51.07	36.43	9.94	2.56
12.60	87.40	50.79	36.61	10.01	2.59
12.70	87.30	50.52	36.78	10.08	2.62
12.80	87.20	50.25	36.95	10.15	2.65
12.90	87.10	49.99	37.11	10.22	2.68
13.00	87.00	49.72	37.28	10.29	2.71
13.10	86.90	49.45	37.45	10.36	2.74
13.20	86.80	49.19	37.61	10.43	2.77
13.30	86.70	48.93	37.77	10.50	2.80
13.40	86.60	48.67	37.93	10.57	2.83
13.50	86.50	48.41	38.09	10.64	2.86
13.60	86.40	48.15	38.25	10.71	2.89
13.70	86.30	47.89	38.41	10.77	2.93
13.80	86.20	47.63	38.57	10.84	2.96
13.90	86.10	47.38	38.72	10.91	2.99
14.00	86.00	47.13	38.87	10.98	3.02
14.10	85.90	46.88	39.02	11.05	3.05
14.20	85.80	46.63	39.17	11.11	3.09
14.30	85.70	46.38	39.32	11.18	3.12
14.40	85.60	46.13	39.47	11.25	3.15
14.50	85.50	45.88	39.62	11.32	3.18
14.60	85.40	45.64	39.76	11.38	3.22
14.70	85.30	45.39	39.91	11.45	3.25
14.80	85.20	45.15	40.05	11.52	3.28
14.90	85.10	44.91	40.19	11.58	3.32
15.00	85.00	44.67	40.33	11.65	3.35
15.10	84.90	44.43	40.47	11.72	3.38
15.20	84.80	44.19	40.61	11.78	3.42

15.30	84.70	43.96	40.74	11.85	3.45
15.40	84.60	43.72	40.88	11.91	3.49
15.50	84.50	43.49	41.01	11.98	3.52
15.60	84.40	43.26	41.14	12.05	3.55
15.70	84.30	43.02	41.28	12.11	3.59
15.80	84.20	42.79	41.41	12.18	3.62
15.90	84.10	42.57	41.53	12.24	3.66
16.00	84.00	42.34	41.66	12.31	3.69
16.10	83.90	42.11	41.79	12.37	3.73
16.20	83.80	41.89	41.91	12.44	3.76
16.30	83.70	41.66	42.04	12.50	3.80
16.40	83.60	41.44	42.16	12.57	3.83
16.50	83.50	41.22	42.28	12.63	3.87
16.60	83.40	41.00	42.40	12.69	3.91
16.70	83.30	40.78	42.52	12.76	3.94
16.80	83.20	40.56	42.64	12.82	3.98
16.90	83.10	40.34	42.76	12.89	4.01
17.00	83.00	40.13	42.87	12.95	4.05
17.10	82.90	39.91	42.99	13.01	4.09
17.20	82.80	39.70	43.10	13.08	4.12
17.30	82.70	39.49	43.21	13.14	4.16
17.40	82.60	39.28	43.32	13.20	4.20
17.50	82.50	39.07	43.43	13.26	4.24
17.60	82.40	38.86	43.54	13.33	4.27
17.70	82.30	38.65	43.65	13.39	4.31
17.80	82.20	38.44	43.76	13.45	4.35
17.90	82.10	38.24	43.86	13.51	4.39
18.00	82.00	38.03	43.97	13.58	4.42
18.10	81.90	37.83	44.07	13.64	4.46
18.20	81.80	37.63	44.17	13.70	4.50
18.30	81.70	37.42	44.28	13.76	4.54

18.40	81.60	37.22	44.38	13.82	4.58
18.50	81.50	37.02	44.48	13.88	4.62
18.60	81.40	36.83	44.57	13.94	4.66
18.70	81.30	36.63	44.67	14.01	4.69
18.80	81.20	36.43	44.77	14.07	4.73
18.90	81.10	36.24	44.86	14.13	4.77
19.00	81.00	36.04	44.96	14.19	4.81
19.10	80.90	35.85	45.05	14.25	4.85
19.20	80.80	35.66	45.14	14.31	4.89
19.30	80.70	35.47	45.23	14.37	4.93
19.40	80.60	35.28	45.32	14.43	4.97
19.50	80.50	35.09	45.41	14.49	5.01
19.60	80.40	34.90	45.50	14.55	5.05
19.70	80.30	34.71	45.59	14.61	5.09
19.80	80.20	34.53	45.67	14.67	5.13
19.90	80.10	34.34	45.76	14.73	5.17
20.00	80.00	34.16	45.84	14.78	5.22
20.10	79.90	33.97	45.93	14.84	5.26
20.20	79.80	33.79	46.01	14.90	5.30
20.30	79.70	33.61	46.09	14.96	5.34
20.40	79.60	33.43	46.17	15.02	5.38
20.50	79.50	33.25	46.25	15.08	5.42
20.60	79.40	33.07	46.33	15.13	5.47
20.70	79.30	32.90	46.40	15.19	5.51
20.80	79.20	32.72	46.48	15.25	5.55
20.90	79.10	32.54	46.56	15.31	5.59
21.00	79.00	32.37	46.63	15.37	5.63
21.10	78.90	32.20	46.70	15.42	5.68
21.20	78.80	32.02	46.78	15.48	5.72
21.30	78.70	31.85	46.85	15.54	5.76
21.40	78.60	31.68	46.92	15.59	5.81

21.50	78.50	31.51	46.99	15.65	5.85
21.60	78.40	31.34	47.06	15.71	5.89
21.70	78.30	31.17	47.13	15.76	5.94
21.80	78.20	31.00	47.20	15.82	5.98
21.90	78.10	30.84	47.26	15.88	6.02
22.00	78.00	30.67	47.33	15.93	6.07
22.10	77.90	30.51	47.39	15.99	6.11
22.20	77.80	30.34	47.46	16.04	6.16
22.30	77.70	30.18	47.52	16.10	6.20
22.40	77.60	30.02	47.58	16.15	6.25
22.50	77.50	29.86	47.64	16.21	6.29
22.60	77.40	29.70	47.70	16.27	6.33
22.70	77.30	29.54	47.76	16.32	6.38
22.80	77.20	29.38	47.82	16.37	6.43
22.90	77.10	29.22	47.88	16.43	6.47
23.00	77.00	29.06	47.94	16.48	6.52
23.10	76.90	28.91	47.99	16.54	6.56
23.20	76.80	28.75	48.05	16.59	6.61
23.30	76.70	28.60	48.10	16.65	6.65
23.40	76.60	28.44	48.16	16.70	6.70
23.50	76.50	28.29	48.21	16.75	6.75
23.60	76.40	28.14	48.26	16.81	6.79
23.70	76.30	27.99	48.31	16.86	6.84
23.80	76.20	27.84	48.36	16.91	6.89
23.90	76.10	27.69	48.41	16.97	6.93
24.00	76.00	27.54	48.46	17.02	6.98
24.10	75.90	27.39	48.51	17.07	7.03
24.20	75.80	27.24	48.56	17.13	7.07
24.30	75.70	27.10	48.60	17.18	7.12
24.40	75.60	26.95	48.65	17.23	7.17
24.50	75.50	26.81	48.69	17.28	7.22

24.60	75.40	26.66	48.74	17.34	7.26
24.70	75.30	26.52	48.78	17.39	7.31
24.80	75.20	26.37	48.83	17.44	7.36
24.90	75.10	26.23	48.87	17.49	7.41
25.00	75.00	26.09	48.91	17.54	7.46
25.10	74.90	25.95	48.95	17.59	7.51
25.20	74.80	25.81	48.99	17.65	7.55
25.30	74.70	25.67	49.03	17.70	7.60
25.40	74.60	25.53	49.07	17.75	7.65
25.50	74.50	25.40	49.10	17.80	7.70
25.60	74.40	25.26	49.14	17.85	7.75
25.70	74.30	25.12	49.18	17.90	7.80
25.80	74.20	24.99	49.21	17.95	7.85
25.90	74.10	24.85	49.25	18.00	7.90
26.00	74.00	24.72	49.28	18.05	7.95
26.10	73.90	24.59	49.31	18.10	8.00
26.20	73.80	24.45	49.35	18.15	8.05
26.30	73.70	24.32	49.38	18.20	8.10
26.40	73.60	24.19	49.41	18.25	8.15
26.50	73.50	24.06	49.44	18.30	8.20
26.60	73.40	23.93	49.47	18.35	8.25
26.70	73.30	23.80	49.50	18.39	8.31
26.80	73.20	23.67	49.53	18.44	8.36
26.90	73.10	23.54	49.56	18.49	8.41
27.00	73.00	23.42	49.58	18.54	8.46
27.10	72.90	23.29	49.61	18.59	8.51
27.20	72.80	23.17	49.63	18.64	8.56
27.30	72.70	23.04	49.66	18.69	8.61
27.40	72.60	22.92	49.68	18.73	8.67
27.50	72.50	22.79	49.71	18.78	8.72
27.60	72.40	22.67	49.73	18.83	8.77

27.70	72.30	22.55	49.75	18.88	8.82
27.80	72.20	22.43	49.77	18.92	8.88
27.90	72.10	22.30	49.80	18.97	8.93
28.00	72.00	22.18	49.82	19.02	8.98
28.10	71.90	22.06	49.84	19.06	9.04
28.20	71.80	21.94	49.86	19.11	9.09
28.30	71.70	21.83	49.87	19.16	9.14
28.40	71.60	21.71	49.89	19.20	9.20
28.50	71.50	21.59	49.91	19.25	9.25
28.60	71.40	21.47	49.93	19.30	9.30
28.70	71.30	21.36	49.94	19.34	9.36
28.80	71.20	21.24	49.96	19.39	9.41
28.90	71.10	21.13	49.97	19.43	9.47
29.00	71.00	21.01	49.99	19.48	9.52
29.10	70.90	20.90	50.00	19.52	9.58
29.20	70.80	20.79	50.01	19.57	9.63
29.30	70.70	20.67	50.03	19.61	9.69
29.40	70.60	20.56	50.04	19.66	9.74
29.50	70.50	20.45	50.05	19.70	9.80
29.60	70.40	20.34	50.06	19.75	9.85
29.70	70.30	20.23	50.07	19.79	9.91
29.80	70.20	20.12	50.08	19.84	9.96
29.90	70.10	20.01	50.09	19.88	10.02
30.00	70.00	19.90	50.10	19.93	10.07
30.10	69.90	19.80	50.10	19.97	10.13
30.20	69.80	19.69	50.11	20.01	10.19
30.30	69.70	19.58	50.12	20.06	10.24
30.40	69.60	19.48	50.12	20.10	10.30
30.50	69.50	19.37	50.13	20.14	10.36
30.60	69.40	19.26	50.14	20.19	10.41
30.70	69.30	19.16	50.14	20.23	10.47

30.80	69.20	19.06	50.14	20.27	10.53
30.90	69.10	18.95	50.15	20.32	10.58
31.00	69.00	18.85	50.15	20.36	10.64
31.10	68.90	18.75	50.15	20.40	10.70
31.20	68.80	18.65	50.15	20.44	10.76
31.30	68.70	18.54	50.16	20.48	10.82
31.40	68.60	18.44	50.16	20.53	10.87
31.50	68.50	18.34	50.16	20.57	10.93
31.60	68.40	18.24	50.16	20.61	10.99
31.70	68.30	18.15	50.15	20.65	11.05
31.80	68.20	18.05	50.15	20.69	11.11
31.90	68.10	17.95	50.15	20.73	11.17
32.00	68.00	17.85	50.15	20.77	11.23
32.10	67.90	17.75	50.15	20.82	11.28
32.20	67.80	17.66	50.14	20.86	11.34
32.30	67.70	17.56	50.14	20.90	11.40
32.40	67.60	17.47	50.13	20.94	11.46
32.50	67.50	17.37	50.13	20.98	11.52
32.60	67.40	17.28	50.12	21.02	11.58
32.70	67.30	17.18	50.12	21.06	11.64
32.80	67.20	17.09	50.11	21.10	11.70
32.90	67.10	17.00	50.10	21.14	11.76
33.00	67.00	16.90	50.10	21.18	11.82
33.10	66.90	16.81	50.09	21.22	11.88
33.20	66.80	16.72	50.08	21.25	11.95
33.30	66.70	16.63	50.07	21.29	12.01
33.40	66.60	16.54	50.06	21.33	12.07
33.50	66.50	16.45	50.05	21.37	12.13
33.60	66.40	16.36	50.04	21.41	12.19
33.70	66.30	16.27	50.03	21.45	12.25
33.80	66.20	16.18	50.02	21.49	12.31

33.90	66.10	16.09	50.01	21.52	12.38
34.00	66.00	16.01	49.99	21.56	12.44
34.10	65.90	15.92	49.98	21.60	12.50
34.20	65.80	15.83	49.97	21.64	12.56
34.30	65.70	15.75	49.95	21.68	12.62
34.40	65.60	15.66	49.94	21.71	12.69
34.50	65.50	15.57	49.93	21.75	12.75
34.60	65.40	15.49	49.91	21.79	12.81
34.70	65.30	15.41	49.89	21.82	12.88
34.80	65.20	15.32	49.88	21.86	12.94
34.90	65.10	15.24	49.86	21.90	13.00
35.00	65.00	15.15	49.85	21.93	13.07
35.10	64.90	15.07	49.83	21.97	13.13
35.20	64.80	14.99	49.81	22.01	13.19
35.30	64.70	14.91	49.79	22.04	13.26
35.40	64.60	14.83	49.77	22.08	13.32
35.50	64.50	14.75	49.75	22.11	13.39
35.60	64.40	14.66	49.74	22.15	13.45
35.70	64.30	14.58	49.72	22.19	13.51
35.80	64.20	14.50	49.70	22.22	13.58
35.90	64.10	14.43	49.67	22.26	13.64
36.00	64.00	14.35	49.65	22.29	13.71
36.10	63.90	14.27	49.63	22.33	13.77
36.20	63.80	14.19	49.61	22.36	13.84
36.30	63.70	14.11	49.59	22.40	13.90
36.40	63.60	14.04	49.56	22.43	13.97
36.50	63.50	13.96	49.54	22.46	14.04
36.60	63.40	13.88	49.52	22.50	14.10
36.70	63.30	13.81	49.49	22.53	14.17
36.80	63.20	13.73	49.47	22.57	14.23
36.90	63.10	13.66	49.44	22.60	14.30

37.00	63.00	13.58	49.42	22.63	14.37
37.10	62.90	13.51	49.39	22.67	14.43
37.20	62.80	13.43	49.37	22.70	14.50
37.30	62.70	13.36	49.34	22.73	14.57
37.40	62.60	13.29	49.31	22.77	14.63
37.50	62.50	13.21	49.29	22.80	14.70
37.60	62.40	13.14	49.26	22.83	14.77
37.70	62.30	13.07	49.23	22.86	14.84
37.80	62.20	13.00	49.20	22.90	14.90
37.90	62.10	12.92	49.18	22.93	14.97
38.00	62.00	12.85	49.15	22.96	15.04
38.10	61.90	12.78	49.12	22.99	15.11
38.20	61.80	12.71	49.09	23.02	15.18
38.30	61.70	12.64	49.06	23.05	15.25
38.40	61.60	12.57	49.03	23.09	15.31
38.50	61.50	12.50	49.00	23.12	15.38
38.60	61.40	12.44	48.96	23.15	15.45
38.70	61.30	12.37	48.93	23.18	15.52
38.80	61.20	12.30	48.90	23.21	15.59
38.90	61.10	12.23	48.87	23.24	15.66
39.00	61.00	12.16	48.84	23.27	15.73
39.10	60.90	12.10	48.80	23.30	15.80
39.20	60.80	12.03	48.77	23.33	15.87
39.30	60.70	11.97	48.73	23.36	15.94
39.40	60.60	11.90	48.70	23.39	16.01
39.50	60.50	11.83	48.67	23.42	16.08
39.60	60.40	11.77	48.63	23.45	16.15
39.70	60.30	11.70	48.60	23.48	16.22
39.80	60.20	11.64	48.56	23.51	16.29
39.90	60.10	11.58	48.52	23.54	16.36
40.00	60.00	11.51	48.49	23.57	16.43

40.10	59.90	11.45	48.45	23.60	16.50
40.20	59.80	11.38	48.42	23.63	16.57
40.30	59.70	11.32	48.38	23.65	16.65
40.40	59.60	11.26	48.34	23.68	16.72
40.50	59.50	11.20	48.30	23.71	16.79
40.60	59.40	11.14	48.26	23.74	16.86
40.70	59.30	11.07	48.23	23.77	16.93
40.80	59.20	11.01	48.19	23.79	17.01
40.90	59.10	10.95	48.15	23.82	17.08
41.00	59.00	10.89	48.11	23.85	17.15
41.10	58.90	10.83	48.07	23.88	17.22
41.20	58.80	10.77	48.03	23.90	17.30
41.30	58.70	10.71	47.99	23.93	17.37
41.40	58.60	10.65	47.95	23.96	17.44
41.50	58.50	10.59	47.91	23.98	17.52
41.60	58.40	10.53	47.87	24.01	17.59
41.70	58.30	10.48	47.82	24.04	17.66
41.80	58.20	10.42	47.78	24.06	17.74
41.90	58.10	10.36	47.74	24.09	17.81
42.00	58.00	10.30	47.70	24.12	17.88
42.10	57.90	10.25	47.65	24.14	17.96
42.20	57.80	10.19	47.61	24.17	18.03
42.30	57.70	10.13	47.57	24.19	18.11
42.40	57.60	10.08	47.52	24.22	18.18
42.50	57.50	10.02	47.48	24.24	18.26
42.60	57.40	9.97	47.43	24.27	18.33
42.70	57.30	9.91	47.39	24.29	18.41
42.80	57.20	9.86	47.34	24.32	18.48
42.90	57.10	9.80	47.30	24.34	18.56
43.00	57.00	9.75	47.25	24.37	18.63
43.10	56.90	9.69	47.21	24.39	18.71

43.20	56.80	9.64	47.16	24.42	18.78
43.30	56.70	9.58	47.12	24.44	18.86
43.40	56.60	9.53	47.07	24.46	18.94
43.50	56.50	9.48	47.02	24.49	19.01
43.60	56.40	9.43	46.97	24.51	19.09
43.70	56.30	9.37	46.93	24.54	19.16
43.80	56.20	9.32	46.88	24.56	19.24
43.90	56.10	9.27	46.83	24.58	19.32
44.00	56.00	9.22	46.78	24.60	19.40
44.10	55.90	9.17	46.73	24.63	19.47
44.20	55.80	9.11	46.69	24.65	19.55
44.30	55.70	9.06	46.64	24.67	19.63
44.40	55.60	9.01	46.59	24.70	19.70
44.50	55.50	8.96	46.54	24.72	19.78
44.60	55.40	8.91	46.49	24.74	19.86
44.70	55.30	8.86	46.44	24.76	19.94
44.80	55.20	8.81	46.39	24.78	20.02
44.90	55.10	8.76	46.34	24.81	20.09
45.00	55.00	8.72	46.28	24.83	20.17
45.10	54.90	8.67	46.23	24.85	20.25
45.20	54.80	8.62	46.18	24.87	20.33
45.30	54.70	8.57	46.13	24.89	20.41
45.40	54.60	8.52	46.08	24.91	20.49
45.50	54.50	8.47	46.03	24.93	20.57
45.60	54.40	8.43	45.97	24.95	20.65
45.70	54.30	8.38	45.92	24.97	20.73
45.80	54.20	8.33	45.87	24.99	20.81
45.90	54.10	8.29	45.81	25.01	20.89
46.00	54.00	8.24	45.76	25.03	20.97
46.10	53.90	8.19	45.71	25.05	21.05
46.20	53.80	8.15	45.65	25.07	21.13

46.30	53.70	8.10	45.60	25.09	21.21
46.40	53.60	8.06	45.54	25.11	21.29
46.50	53.50	8.01	45.49	25.13	21.37
46.60	53.40	7.97	45.43	25.15	21.45
46.70	53.30	7.92	45.38	25.17	21.53
46.80	53.20	7.88	45.32	25.19	21.61
46.90	53.10	7.83	45.27	25.21	21.69
47.00	53.00	7.79	45.21	25.22	21.78
47.10	52.90	7.75	45.15	25.24	21.86
47.20	52.80	7.70	45.10	25.26	21.94
47.30	52.70	7.66	45.04	25.28	22.02
47.40	52.60	7.62	44.98	25.30	22.10
47.50	52.50	7.57	44.93	25.32	22.18
47.60	52.40	7.53	44.87	25.33	22.27
47.70	52.30	7.49	44.81	25.35	22.35
47.80	52.20	7.45	44.75	25.37	22.43
47.90	52.10	7.40	44.70	25.38	22.52
48.00	52.00	7.36	44.64	25.40	22.60
48.10	51.90	7.32	44.58	25.42	22.68
48.20	51.80	7.28	44.52	25.44	22.76
48.30	51.70	7.24	44.46	25.45	22.85
48.40	51.60	7.20	44.40	25.47	22.93
48.50	51.50	7.16	44.34	25.48	23.02
48.60	51.40	7.12	44.28	25.50	23.10
48.70	51.30	7.08	44.22	25.52	23.18
48.80	51.20	7.04	44.16	25.53	23.27
48.90	51.10	7.00	44.10	25.55	23.35
49.00	51.00	6.96	44.04	25.56	23.44
49.10	50.90	6.92	43.98	25.58	23.52
49.20	50.80	6.88	43.92	25.59	23.61
49.30	50.70	6.84	43.86	25.61	23.69

49.40	50.60	6.80	43.80	25.62	23.78
49.50	50.50	6.76	43.74	25.64	23.86
49.60	50.40	6.72	43.68	25.65	23.95
49.70	50.30	6.68	43.62	25.67	24.03
49.80	50.20	6.65	43.55	25.68	24.12
49.90	50.10	6.61	43.49	25.70	24.20
50.00	50.00	6.57	43.43	25.71	24.29
50.10	49.90	6.53	43.37	25.72	24.38
50.20	49.80	6.50	43.30	25.74	24.46
50.30	49.70	6.46	43.24	25.75	24.55
50.40	49.60	6.42	43.18	25.76	24.64
50.50	49.50	6.39	43.11	25.78	24.72
50.60	49.40	6.35	43.05	25.79	24.81
50.70	49.30	6.31	42.99	25.80	24.90
50.80	49.20	6.28	42.92	25.82	24.98
50.90	49.10	6.24	42.86	25.83	25.07
51.00	49.00	6.21	42.79	25.84	25.16
51.10	48.90	6.17	42.73	25.85	25.25
51.20	48.80	6.14	42.66	25.87	25.33
51.30	48.70	6.10	42.60	25.88	25.42
51.40	48.60	6.07	42.53	25.89	25.51
51.50	48.50	6.03	42.47	25.90	25.60
51.60	48.40	6.00	42.40	25.91	25.69
51.70	48.30	5.96	42.34	25.92	25.78
51.80	48.20	5.93	42.27	25.94	25.86
51.90	48.10	5.89	42.21	25.95	25.95
52.00	48.00	5.86	42.14	25.96	26.04
52.10	47.90	5.83	42.07	25.97	26.13
52.20	47.80	5.79	42.01	25.98	26.22
52.30	47.70	5.76	41.94	25.99	26.31
52.40	47.60	5.73	41.87	26.00	26.40

52.50	47.50	5.69	41.81	26.01	26.49
52.60	47.40	5.66	41.74	26.02	26.58
52.70	47.30	5.63	41.67	26.03	26.67
52.80	47.20	5.60	41.60	26.04	26.76
52.90	47.10	5.56	41.54	26.05	26.85
53.00	47.00	5.53	41.47	26.06	26.94
53.10	46.90	5.50	41.40	26.07	27.03
53.20	46.80	5.47	41.33	26.08	27.12
53.30	46.70	5.44	41.26	26.09	27.21
53.40	46.60	5.41	41.19	26.10	27.30
53.50	46.50	5.37	41.13	26.11	27.39
53.60	46.40	5.34	41.06	26.11	27.49
53.70	46.30	5.31	40.99	26.12	27.58
53.80	46.20	5.28	40.92	26.13	27.67
53.90	46.10	5.25	40.85	26.14	27.76
54.00	46.00	5.22	40.78	26.15	27.85
54.10	45.90	5.19	40.71	26.15	27.95
54.20	45.80	5.16	40.64	26.16	28.04
54.30	45.70	5.13	40.57	26.17	28.13
54.40	45.60	5.10	40.50	26.18	28.22
54.50	45.50	5.07	40.43	26.18	28.32
54.60	45.40	5.04	40.36	26.19	28.41
54.70	45.30	5.01	40.29	26.20	28.50
54.80	45.20	4.98	40.22	26.21	28.59
54.90	45.10	4.95	40.15	26.21	28.69
55.00	45.00	4.93	40.07	26.22	28.78
55.10	44.90	4.90	40.00	26.22	28.88
55.20	44.80	4.87	39.93	26.23	28.97
55.30	44.70	4.84	39.86	26.24	29.06
55.40	44.60	4.81	39.79	26.24	29.16
55.50	44.50	4.78	39.72	26.25	29.25

55.60	44.40	4.76	39.64	26.25	29.35
55.70	44.30	4.73	39.57	26.26	29.44
55.80	44.20	4.70	39.50	26.27	29.53
55.90	44.10	4.67	39.43	26.27	29.63
56.00	44.00	4.65	39.35	26.28	29.72
56.10	43.90	4.62	39.28	26.28	29.82
56.20	43.80	4.59	39.21	26.28	29.92
56.30	43.70	4.56	39.14	26.29	30.01
56.40	43.60	4.54	39.06	26.29	30.11
56.50	43.50	4.51	38.99	26.30	30.20
56.60	43.40	4.48	38.92	26.30	30.30
56.70	43.30	4.46	38.84	26.31	30.39
56.80	43.20	4.43	38.77	26.31	30.49
56.90	43.10	4.41	38.69	26.31	30.59
57.00	43.00	4.38	38.62	26.32	30.68
57.10	42.90	4.35	38.55	26.32	30.78
57.20	42.80	4.33	38.47	26.32	30.88
57.30	42.70	4.30	38.40	26.33	30.97
57.40	42.60	4.28	38.32	26.33	31.07
57.50	42.50	4.25	38.25	26.33	31.17
57.60	42.40	4.23	38.17	26.33	31.27
57.70	42.30	4.20	38.10	26.34	31.36
57.80	42.20	4.18	38.02	26.34	31.46
57.90	42.10	4.15	37.95	26.34	31.56
58.00	42.00	4.13	37.87	26.34	31.66
58.10	41.90	4.10	37.80	26.35	31.75
58.20	41.80	4.08	37.72	26.35	31.85
58.30	41.70	4.06	37.64	26.35	31.95
58.40	41.60	4.03	37.57	26.35	32.05
58.50	41.50	4.01	37.49	26.35	32.15
58.60	41.40	3.98	37.42	26.35	32.25

58.70	41.30	3.96	37.34	26.35	32.35
58.80	41.20	3.94	37.26	26.35	32.45
58.90	41.10	3.91	37.19	26.35	32.55
59.00	41.00	3.89	37.11	26.36	32.64
59.10	40.90	3.87	37.03	26.36	32.74
59.20	40.80	3.84	36.96	26.36	32.84
59.30	40.70	3.82	36.88	26.36	32.94
59.40	40.60	3.80	36.80	26.36	33.04
59.50	40.50	3.77	36.73	26.36	33.14
59.60	40.40	3.75	36.65	26.36	33.24
59.70	40.30	3.73	36.57	26.35	33.35
59.80	40.20	3.71	36.49	26.35	33.45
59.90	40.10	3.68	36.42	26.35	33.55
60.00	40.00	3.66	36.34	26.35	33.65
60.10	39.90	3.64	36.26	26.35	33.75
60.20	39.80	3.62	36.18	26.35	33.85
60.30	39.70	3.60	36.10	26.35	33.95
60.40	39.60	3.58	36.02	26.35	34.05
60.50	39.50	3.55	35.95	26.34	34.16
60.60	39.40	3.53	35.87	26.34	34.26
60.70	39.30	3.51	35.79	26.34	34.36
60.80	39.20	3.49	35.71	26.34	34.46
60.90	39.10	3.47	35.63	26.34	34.56
61.00	39.00	3.45	35.55	26.33	34.67
61.10	38.90	3.43	35.47	26.33	34.77
61.20	38.80	3.41	35.39	26.33	34.87
61.30	38.70	3.39	35.31	26.33	34.97
61.40	38.60	3.37	35.23	26.32	35.08
61.50	38.50	3.34	35.16	26.32	35.18
61.60	38.40	3.32	35.08	26.32	35.28
61.70	38.30	3.30	35.00	26.31	35.39

61.80	38.20	3.28	34.92	26.31	35.49
61.90	38.10	3.26	34.84	26.30	35.60
62.00	38.00	3.24	34.76	26.30	35.70
62.10	37.90	3.22	34.68	26.30	35.80
62.20	37.80	3.20	34.60	26.29	35.91
62.30	37.70	3.19	34.51	26.29	36.01
62.40	37.60	3.17	34.43	26.28	36.12
62.50	37.50	3.15	34.35	26.28	36.22
62.60	37.40	3.13	34.27	26.27	36.33
62.70	37.30	3.11	34.19	26.27	36.43
62.80	37.20	3.09	34.11	26.26	36.54
62.90	37.10	3.07	34.03	26.26	36.64
63.00	37.00	3.05	33.95	26.25	36.75
63.10	36.90	3.03	33.87	26.25	36.85
63.20	36.80	3.01	33.79	26.24	36.96
63.30	36.70	3.00	33.70	26.23	37.07
63.40	36.60	2.98	33.62	26.23	37.17
63.50	36.50	2.96	33.54	26.22	37.28
63.60	36.40	2.94	33.46	26.22	37.38
63.70	36.30	2.92	33.38	26.21	37.49
63.80	36.20	2.90	33.30	26.20	37.60
63.90	36.10	2.89	33.21	26.20	37.70
64.00	36.00	2.87	33.13	26.19	37.81
64.10	35.90	2.85	33.05	26.18	37.92
64.20	35.80	2.83	32.97	26.17	38.03
64.30	35.70	2.81	32.89	26.17	38.13
64.40	35.60	2.80	32.80	26.16	38.24
64.50	35.50	2.78	32.72	26.15	38.35
64.60	35.40	2.76	32.64	26.14	38.46
64.70	35.30	2.75	32.55	26.14	38.56
64.80	35.20	2.73	32.47	26.13	38.67

64.90	35.10	2.71	32.39	26.12	38.78
65.00	35.00	2.69	32.31	26.11	38.89
65.10	34.90	2.68	32.22	26.10	39.00
65.20	34.80	2.66	32.14	26.09	39.11
65.30	34.70	2.64	32.06	26.08	39.22
65.40	34.60	2.63	31.97	26.07	39.33
65.50	34.50	2.61	31.89	26.07	39.43
65.60	34.40	2.59	31.81	26.06	39.54
65.70	34.30	2.58	31.72	26.05	39.65
65.80	34.20	2.56	31.64	26.04	39.76
65.90	34.10	2.55	31.55	26.03	39.87
66.00	34.00	2.53	31.47	26.02	39.98
66.10	33.90	2.51	31.39	26.01	40.09
66.20	33.80	2.50	31.30	26.00	40.20
66.30	33.70	2.48	31.22	25.99	40.31
66.40	33.60	2.47	31.13	25.98	40.42
66.50	33.50	2.45	31.05	25.96	40.54
66.60	33.40	2.43	30.97	25.95	40.65
66.70	33.30	2.42	30.88	25.94	40.76
66.80	33.20	2.40	30.80	25.93	40.87
66.90	33.10	2.39	30.71	25.92	40.98
67.00	33.00	2.37	30.63	25.91	41.09
67.10	32.90	2.36	30.54	25.90	41.20
67.20	32.80	2.34	30.46	25.89	41.31
67.30	32.70	2.33	30.37	25.87	41.43
67.40	32.60	2.31	30.29	25.86	41.54
67.50	32.50	2.30	30.20	25.85	41.65
67.60	32.40	2.28	30.12	25.84	41.76
67.70	32.30	2.27	30.03	25.82	41.88
67.80	32.20	2.25	29.95	25.81	41.99
67.90	32.10	2.24	29.86	25.80	42.10

68.00	32.00	2.22	29.78	25.79	42.21
68.10	31.90	2.21	29.69	25.77	42.33
68.20	31.80	2.20	29.60	25.76	42.44
68.30	31.70	2.18	29.52	25.75	42.55
68.40	31.60	2.17	29.43	25.73	42.67
68.50	31.50	2.15	29.35	25.72	42.78
68.60	31.40	2.14	29.26	25.70	42.90
68.70	31.30	2.13	29.17	25.69	43.01
68.80	31.20	2.11	29.09	25.68	43.12
68.90	31.10	2.10	29.00	25.66	43.24
69.00	31.00	2.08	28.92	25.65	43.35
69.10	30.90	2.07	28.83	25.63	43.47
69.20	30.80	2.06	28.74	25.62	43.58
69.30	30.70	2.04	28.66	25.60	43.70
69.40	30.60	2.03	28.57	25.59	43.81
69.50	30.50	2.02	28.48	25.57	43.93
69.60	30.40	2.00	28.40	25.56	44.04
69.70	30.30	1.99	28.31	25.54	44.16
69.80	30.20	1.98	28.22	25.53	44.27
69.90	30.10	1.96	28.14	25.51	44.39
70.00	30.00	1.95	28.05	25.49	44.51
70.10	29.90	1.94	27.96	25.48	44.62
70.20	29.80	1.92	27.88	25.46	44.74
70.30	29.70	1.91	27.79	25.45	44.85
70.40	29.60	1.90	27.70	25.43	44.97
70.50	29.50	1.89	27.61	25.41	45.09
70.60	29.40	1.87	27.53	25.39	45.21
70.70	29.30	1.86	27.44	25.38	45.32
70.80	29.20	1.85	27.35	25.36	45.44
70.90	29.10	1.84	27.26	25.34	45.56
71.00	29.00	1.82	27.18	25.33	45.67

71.10	28.90	1.81	27.09	25.31	45.79
71.20	28.80	1.80	27.00	25.29	45.91
71.30	28.70	1.79	26.91	25.27	46.03
71.40	28.60	1.78	26.82	25.25	46.15
71.50	28.50	1.76	26.74	25.24	46.26
71.60	28.40	1.75	26.65	25.22	46.38
71.70	28.30	1.74	26.56	25.20	46.50
71.80	28.20	1.73	26.47	25.18	46.62
71.90	28.10	1.72	26.38	25.16	46.74
72.00	28.00	1.70	26.30	25.14	46.86
72.10	27.90	1.69	26.21	25.12	46.98
72.20	27.80	1.68	26.12	25.10	47.10
72.30	27.70	1.67	26.03	25.08	47.22
72.40	27.60	1.66	25.94	25.06	47.34
72.50	27.50	1.65	25.85	25.05	47.45
72.60	27.40	1.64	25.76	25.03	47.57
72.70	27.30	1.62	25.68	25.01	47.69
72.80	27.20	1.61	25.59	24.98	47.82
72.90	27.10	1.60	25.50	24.96	47.94
73.00	27.00	1.59	25.41	24.94	48.06
73.10	26.90	1.58	25.32	24.92	48.18
73.20	26.80	1.57	25.23	24.90	48.30
73.30	26.70	1.56	25.14	24.88	48.42
73.40	26.60	1.55	25.05	24.86	48.54
73.50	26.50	1.54	24.96	24.84	48.66
73.60	26.40	1.53	24.87	24.82	48.78
73.70	26.30	1.51	24.79	24.80	48.90
73.80	26.20	1.50	24.70	24.77	49.03
73.90	26.10	1.49	24.61	24.75	49.15
74.00	26.00	1.48	24.52	24.73	49.27
74.10	25.90	1.47	24.43	24.71	49.39

74.20	25.80	1.46	24.34	24.69	49.51
74.30	25.70	1.45	24.25	24.66	49.64
74.40	25.60	1.44	24.16	24.64	49.76
74.50	25.50	1.43	24.07	24.62	49.88
74.60	25.40	1.42	23.98	24.60	50.00
74.70	25.30	1.41	23.89	24.57	50.13
74.80	25.20	1.40	23.80	24.55	50.25
74.90	25.10	1.39	23.71	24.53	50.37
75.00	25.00	1.38	23.62	24.50	50.50
75.10	24.90	1.37	23.53	24.48	50.62
75.20	24.80	1.36	23.44	24.46	50.74
75.30	24.70	1.35	23.35	24.43	50.87
75.40	24.60	1.34	23.26	24.41	50.99
75.50	24.50	1.33	23.17	24.38	51.12
75.60	24.40	1.32	23.08	24.36	51.24
75.70	24.30	1.31	22.99	24.33	51.37
75.80	24.20	1.30	22.90	24.31	51.49
75.90	24.10	1.29	22.81	24.28	51.62
76.00	24.00	1.28	22.72	24.26	51.74
76.10	23.90	1.27	22.63	24.23	51.87
76.20	23.80	1.26	22.54	24.21	51.99
76.30	23.70	1.26	22.44	24.18	52.12
76.40	23.60	1.25	22.35	24.16	52.24
76.50	23.50	1.24	22.26	24.13	52.37
76.60	23.40	1.23	22.17	24.11	52.49
76.70	23.30	1.22	22.08	24.08	52.62
76.80	23.20	1.21	21.99	24.05	52.75
76.90	23.10	1.20	21.90	24.03	52.87
77.00	23.00	1.19	21.81	24.00	53.00
77.10	22.90	1.18	21.72	23.97	53.13
77.20	22.80	1.17	21.63	23.95	53.25

77.30	22.70	1.16	21.54	23.92	53.38
77.40	22.60	1.16	21.44	23.89	53.51
77.50	22.50	1.15	21.35	23.87	53.63
77.60	22.40	1.14	21.26	23.84	53.76
77.70	22.30	1.13	21.17	23.81	53.89
77.80	22.20	1.12	21.08	23.78	54.02
77.90	22.10	1.11	20.99	23.76	54.14
78.00	22.00	1.10	20.90	23.73	54.27
78.10	21.90	1.10	20.80	23.70	54.40
78.20	21.80	1.09	20.71	23.67	54.53
78.30	21.70	1.08	20.62	23.64	54.66
78.40	21.60	1.07	20.53	23.61	54.79
78.50	21.50	1.06	20.44	23.59	54.91
78.60	21.40	1.05	20.35	23.56	55.04
78.70	21.30	1.05	20.25	23.53	55.17
78.80	21.20	1.04	20.16	23.50	55.30
78.90	21.10	1.03	20.07	23.47	55.43
79.00	21.00	1.02	19.98	23.44	55.56
79.10	20.90	1.01	19.89	23.41	55.69
79.20	20.80	1.01	19.79	23.38	55.82
79.30	20.70	1.00	19.70	23.35	55.95
79.40	20.60	0.99	19.61	23.32	56.08
79.50	20.50	0.98	19.52	23.29	56.21
79.60	20.40	0.97	19.43	23.26	56.34
79.70	20.30	0.97	19.33	23.23	56.47
79.80	20.20	0.96	19.24	23.20	56.60
79.90	20.10	0.95	19.15	23.17	56.73
80.00	20.00	0.94	19.06	23.14	56.86
80.10	19.90	0.94	18.96	23.10	57.00
80.20	19.80	0.93	18.87	23.07	57.13
80.30	19.70	0.92	18.78	23.04	57.26

80.40	19.60	0.91	18.69	23.01	57.39
80.50	19.50	0.90	18.60	22.98	57.52
80.60	19.40	0.90	18.50	22.95	57.65
80.70	19.30	0.89	18.41	22.91	57.79
80.80	19.20	0.88	18.32	22.88	57.92
80.90	19.10	0.88	18.22	22.85	58.05
81.00	19.00	0.87	18.13	22.82	58.18
81.10	18.90	0.86	18.04	22.79	58.31
81.20	18.80	0.85	17.95	22.75	58.45
81.30	18.70	0.85	17.85	22.72	58.58
81.40	18.60	0.84	17.76	22.69	58.71
81.50	18.50	0.83	17.67	22.65	58.85
81.60	18.40	0.83	17.57	22.62	58.98
81.70	18.30	0.82	17.48	22.59	59.11
81.80	18.20	0.81	17.39	22.55	59.25
81.90	18.10	0.80	17.30	22.52	59.38
82.00	18.00	0.80	17.20	22.48	59.52
82.10	17.90	0.79	17.11	22.45	59.65
82.20	17.80	0.78	17.02	22.42	59.78
82.30	17.70	0.78	16.92	22.38	59.92
82.40	17.60	0.77	16.83	22.35	60.05
82.50	17.50	0.76	16.74	22.31	60.19
82.60	17.40	0.76	16.64	22.28	60.32
82.70	17.30	0.75	16.55	22.24	60.46
82.80	17.20	0.74	16.46	22.21	60.59
82.90	17.10	0.74	16.36	22.17	60.73
83.00	17.00	0.73	16.27	22.14	60.86
83.10	16.90	0.72	16.18	22.10	61.00
83.20	16.80	0.72	16.08	22.06	61.14
83.30	16.70	0.71	15.99	22.03	61.27
83.40	16.60	0.70	15.90	21.99	61.41

83.50	16.50	0.70	15.80	21.96	61.54
83.60	16.40	0.69	15.71	21.92	61.68
83.70	16.30	0.69	15.61	21.88	61.82
83.80	16.20	0.68	15.52	21.85	61.95
83.90	16.10	0.67	15.43	21.81	62.09
84.00	16.00	0.67	15.33	21.77	62.23
84.10	15.90	0.66	15.24	21.74	62.36
84.20	15.80	0.65	15.15	21.70	62.50
84.30	15.70	0.65	15.05	21.66	62.64
84.40	15.60	0.64	14.96	21.62	62.78
84.50	15.50	0.64	14.86	21.59	62.91
84.60	15.40	0.63	14.77	21.55	63.05
84.70	15.30	0.62	14.68	21.51	63.19
84.80	15.20	0.62	14.58	21.47	63.33
84.90	15.10	0.61	14.49	21.43	63.47
85.00	15.00	0.61	14.39	21.39	63.61
85.10	14.90	0.60	14.30	21.36	63.74
85.20	14.80	0.60	14.20	21.32	63.88
85.30	14.70	0.59	14.11	21.28	64.02
85.40	14.60	0.58	14.02	21.24	64.16
85.50	14.50	0.58	13.92	21.20	64.30
85.60	14.40	0.57	13.83	21.16	64.44
85.70	14.30	0.57	13.73	21.12	64.58
85.80	14.20	0.56	13.64	21.08	64.72
85.90	14.10	0.56	13.54	21.04	64.86
86.00	14.00	0.55	13.45	21.00	65.00
86.10	13.90	0.54	13.36	20.96	65.14
86.20	13.80	0.54	13.26	20.92	65.28
86.30	13.70	0.53	13.17	20.88	65.42
86.40	13.60	0.53	13.07	20.84	65.56
86.50	13.50	0.52	12.98	20.80	65.70

86.60	13.40	0.52	12.88	20.76	65.84
86.70	13.30	0.51	12.79	20.72	65.98
86.80	13.20	0.51	12.69	20.68	66.12
86.90	13.10	0.50	12.60	20.63	66.27
87.00	13.00	0.50	12.50	20.59	66.41
87.10	12.90	0.49	12.41	20.55	66.55
87.20	12.80	0.49	12.31	20.51	66.69
87.30	12.70	0.48	12.22	20.47	66.83
87.40	12.60	0.47	12.13	20.43	66.97
87.50	12.50	0.47	12.03	20.38	67.12
87.60	12.40	0.46	11.94	20.34	67.26
87.70	12.30	0.46	11.84	20.30	67.40
87.80	12.20	0.45	11.75	20.26	67.54
87.90	12.10	0.45	11.65	20.21	67.69
88.00	12.00	0.44	11.56	20.17	67.83
88.10	11.90	0.44	11.46	20.13	67.97
88.20	11.80	0.43	11.37	20.08	68.12
88.30	11.70	0.43	11.27	20.04	68.26
88.40	11.60	0.42	11.18	20.00	68.40
88.50	11.50	0.42	11.08	19.95	68.55
88.60	11.40	0.41	10.99	19.91	68.69
88.70	11.30	0.41	10.89	19.86	68.84
88.80	11.20	0.41	10.79	19.82	68.98
88.90	11.10	0.40	10.70	19.78	69.12
89.00	11.00	0.40	10.60	19.73	69.27
89.10	10.90	0.39	10.51	19.69	69.41
89.20	10.80	0.39	10.41	19.64	69.56
89.30	10.70	0.38	10.32	19.60	69.70
89.40	10.60	0.38	10.22	19.55	69.85
89.50	10.50	0.37	10.13	19.51	69.99
89.60	10.40	0.37	10.03	19.46	70.14

89.70	10.30	0.36	9.94	19.42	70.28
89.80	10.20	0.36	9.84	19.37	70.43
89.90	10.10	0.35	9.75	19.32	70.58
90.00	10.00	0.35	9.65	19.28	70.72
90.10	9.90	0.34	9.56	19.23	70.87
90.20	9.80	0.34	9.46	19.19	71.01
90.30	9.70	0.34	9.36	19.14	71.16
90.40	9.60	0.33	9.27	19.09	71.31
90.50	9.50	0.33	9.17	19.05	71.45
90.60	9.40	0.32	9.08	19.00	71.60
90.70	9.30	0.32	8.98	18.95	71.75
90.80	9.20	0.31	8.89	18.90	71.90
90.90	9.10	0.31	8.79	18.86	72.04
91.00	9.00	0.31	8.69	18.81	72.19
91.10	8.90	0.30	8.60	18.76	72.34
91.20	8.80	0.30	8.50	18.71	72.49
91.30	8.70	0.29	8.41	18.67	72.63
91.40	8.60	0.29	8.31	18.62	72.78
91.50	8.50	0.28	8.22	18.57	72.93
91.60	8.40	0.28	8.12	18.52	73.08
91.70	8.30	0.28	8.02	18.47	73.23
91.80	8.20	0.27	7.93	18.42	73.38
91.90	8.10	0.27	7.83	18.38	73.52
92.00	8.00	0.26	7.74	18.33	73.67
92.10	7.90	0.26	7.64	18.28	73.82
92.20	7.80	0.26	7.54	18.23	73.97
92.30	7.70	0.25	7.45	18.18	74.12
92.40	7.60	0.25	7.35	18.13	74.27
92.50	7.50	0.24	7.26	18.08	74.42
92.60	7.40	0.24	7.16	18.03	74.57
92.70	7.30	0.24	7.06	17.98	74.72

92.80	7.20	0.23	6.97	17.93	74.87
92.90	7.10	0.23	6.87	17.88	75.02
93.00	7.00	0.22	6.78	17.83	75.17
93.10	6.90	0.22	6.68	17.78	75.32
93.20	6.80	0.22	6.58	17.73	75.47
93.30	6.70	0.21	6.49	17.68	75.62
93.40	6.60	0.21	6.39	17.62	75.78
93.50	6.50	0.21	6.29	17.57	75.93
93.60	6.40	0.20	6.20	17.52	76.08
93.70	6.30	0.20	6.10	17.47	76.23
93.80	6.20	0.19	6.01	17.42	76.38
93.90	6.10	0.19	5.91	17.37	76.53
94.00	6.00	0.19	5.81	17.31	76.69
94.10	5.90	0.18	5.72	17.26	76.84
94.20	5.80	0.18	5.62	17.21	76.99
94.30	5.70	0.18	5.52	17.16	77.14
94.40	5.60	0.17	5.43	17.11	77.29
94.50	5.50	0.17	5.33	17.05	77.45
94.60	5.40	0.17	5.23	17.00	77.60
94.70	5.30	0.16	5.14	16.95	77.75
94.80	5.20	0.16	5.04	16.89	77.91
94.90	5.10	0.16	4.94	16.84	78.06
95.00	5.00	0.15	4.85	16.79	78.21
95.10	4.90	0.15	4.75	16.73	78.37
95.20	4.80	0.14	4.66	16.68	78.52
95.30	4.70	0.14	4.56	16.63	78.67
95.40	4.60	0.14	4.46	16.57	78.83
95.50	4.50	0.13	4.37	16.52	78.98
95.60	4.40	0.13	4.27	16.46	79.14
95.70	4.30	0.13	4.17	16.41	79.29
95.80	4.20	0.12	4.08	16.35	79.45

95.90	4.10	0.12	3.98	16.30	79.60
96.00	4.00	0.12	3.88	16.24	79.76
96.10	3.90	0.11	3.79	16.19	79.91
96.20	3.80	0.11	3.69	16.13	80.07
96.30	3.70	0.11	3.59	16.08	80.22
96.40	3.60	0.11	3.49	16.02	80.38
96.50	3.50	0.10	3.40	15.97	80.53
96.60	3.40	0.10	3.30	15.91	80.69
96.70	3.30	0.10	3.20	15.85	80.85
96.80	3.20	0.09	3.11	15.80	81.00
96.90	3.10	0.09	3.01	15.74	81.16
97.00	3.00	0.09	2.91	15.68	81.32
97.10	2.90	0.08	2.82	15.63	81.47
97.20	2.80	0.08	2.72	15.57	81.63
97.30	2.70	0.08	2.62	15.51	81.79
97.40	2.60	0.07	2.53	15.46	81.94
97.50	2.50	0.07	2.43	15.40	82.10
97.60	2.40	0.07	2.33	15.34	82.26
97.70	2.30	0.06	2.24	15.29	82.41
97.80	2.20	0.06	2.14	15.23	82.57
97.90	2.10	0.06	2.04	15.17	82.73
98.00	2.00	0.06	1.94	15.11	82.89
98.10	1.90	0.05	1.85	15.05	83.05
98.20	1.80	0.05	1.75	15.00	83.20
98.30	1.70	0.05	1.65	14.94	83.36
98.40	1.60	0.04	1.56	14.88	83.52
98.50	1.50	0.04	1.46	14.82	83.68
98.60	1.40	0.04	1.36	14.76	83.84
98.70	1.30	0.04	1.26	14.70	84.00
98.80	1.20	0.03	1.17	14.64	84.16
98.90	1.10	0.03	1.07	14.58	84.32

99.00	1.00	0.03	0.97	14.52	84.48
99.10	0.90	0.02	0.88	14.46	84.64
99.20	0.80	0.02	0.78	14.40	84.80
99.30	0.70	0.02	0.68	14.34	84.96
99.40	0.60	0.02	0.58	14.28	85.12
99.50	0.50	0.01	0.49	14.22	85.28
99.60	0.40	0.01	0.39	14.16	85.44
99.70	0.30	0.01	0.29	14.10	85.60
99.80	0.20	0.01	0.19	14.04	85.76
99.90	0.10	0.00	0.10	13.98	85.92
100.00	0.00	0.00	0.00	13.92	86.08

Model ID	Well	Image type	Top [m]	Bottom [m]	Interval [m]	Structural class	Geostatistical anisotropy type	Effective stress [MPa]
Mod01	B24	Core image	1935.23	1935.46	0.23	Laminated	Zonal, horizontal	1
Mod01	B24	Core image	1935.23	1935.46	0.23	Laminated	Zonal, horizontal	1
Mod01	B24	Core image	1935.23	1935.46	0.23	Laminated	Zonal, horizontal	1
Mod01	B24	Core image	1935.23	1935.46	0.23	Laminated	Zonal, horizontal	1
Mod01	B24	Core image	1935.23	1935.46	0.23	Laminated	Zonal, horizontal	1
Mod01	B24	Core image	1935.23	1935.46	0.23	Laminated	Zonal, horizontal	1
Mod01	B24	Core image	1935.23	1935.46	0.23	Laminated	Zonal, horizontal	5
Mod01	B24	Core image	1935.23	1935.46	0.23	Laminated	Zonal, horizontal	5
Mod01	B24	Core image	1935.23	1935.46	0.23	Laminated	Zonal, horizontal	5
Mod01	B24	Core image	1935.23	1935.46	0.23	Laminated	Zonal, horizontal	5
Mod01	B24	Core image	1935.23	1935.46	0.23	Laminated	Zonal, horizontal	5
Mod01	B24	Core image	1935.23	1935.46	0.23	Laminated	Zonal, horizontal	5
Mod01	B24	Core image	1935.23	1935.46	0.23	Laminated	Zonal, horizontal	10
Mod01	B24	Core image	1935.23	1935.46	0.23	Laminated	Zonal, horizontal	10
Mod01	B24	Core image	1935.23	1935.46	0.23	Laminated	Zonal, horizontal	10
Mod01	B24	Core image	1935.23	1935.46	0.23	Laminated	Zonal, horizontal	10
Mod01	B24	Core image	1935.23	1935.46	0.23	Laminated	Zonal, horizontal	10
Mod01	B24	Core image	1935.23	1935.46	0.23	Laminated	Zonal, horizontal	10
Mod01	B24	Core image	1935.23	1935.46	0.23	Laminated	Zonal, horizontal	15
Mod01	B24	Core image	1935.23	1935.46	0.23	Laminated	Zonal, horizontal	15
Mod01	B24	Core image	1935.23	1935.46	0.23	Laminated	Zonal, horizontal	15
Mod01	B24	Core image	1935.23	1935.46	0.23	Laminated	Zonal, horizontal	15
Mod01	B24	Core image	1935.23	1935.46	0.23	Laminated	Zonal, horizontal	15
Mod01	B24	Core image	1935.23	1935.46	0.23	Laminated	Zonal, horizontal	15
Mod01	B24	Core image	1935.23	1935.46	0.23	Laminated	Zonal, horizontal	20
Mod01	B24	Core image	1935.23	1935.46	0.23	Laminated	Zonal, horizontal	20
Mod01	B24	Core image	1935.23	1935.46	0.23	Laminated	Zonal, horizontal	20
Mod01	B24	Core image	1935.23	1935.46	0.23	Laminated	Zonal, horizontal	20
Mod01	B24	Core image	1935.23	1935.46	0.23	Laminated	Zonal, horizontal	20
Mod01	B24	Core image	1935.23	1935.46	0.23	Laminated	Zonal, horizontal	20
Mod01	B24	Core image	1935.23	1935.46	0.23	Laminated	Zonal, horizontal	25
Mod01	B24	Core image	1935.23	1935.46	0.23	Laminated	Zonal, horizontal	25

Mod01	B24	Core image	1935.23	1935.46	0.23	Laminated	Zonal, horizontal	25
Mod01	B24	Core image	1935.23	1935.46	0.23	Laminated	Zonal, horizontal	25
Mod01	B24	Core image	1935.23	1935.46	0.23	Laminated	Zonal, horizontal	25
Mod01	B24	Core image	1935.23	1935.46	0.23	Laminated	Zonal, horizontal	25
Mod01	B24	Core image	1935.23	1935.46	0.23	Laminated	Zonal, horizontal	30
Mod01	B24	Core image	1935.23	1935.46	0.23	Laminated	Zonal, horizontal	30
Mod01	B24	Core image	1935.23	1935.46	0.23	Laminated	Zonal, horizontal	30
Mod01	B24	Core image	1935.23	1935.46	0.23	Laminated	Zonal, horizontal	30
Mod01	B24	Core image	1935.23	1935.46	0.23	Laminated	Zonal, horizontal	30
Mod01	B24	Core image	1935.23	1935.46	0.23	Laminated	Zonal, horizontal	30
Mod03	B22	Core image	1722.29	1722.67	0.37	Laminated	Geometric, horizontal	1
Mod03	B22	Core image	1722.29	1722.67	0.37	Laminated	Geometric, horizontal	1
Mod03	B22	Core image	1722.29	1722.67	0.37	Laminated	Geometric, horizontal	1
Mod03	B22	Core image	1722.29	1722.67	0.37	Laminated	Geometric, horizontal	1
Mod03	B22	Core image	1722.29	1722.67	0.37	Laminated	Geometric, horizontal	1
Mod03	B22	Core image	1722.29	1722.67	0.37	Laminated	Geometric, horizontal	1
Mod03	B22	Core image	1722.29	1722.67	0.37	Laminated	Geometric, horizontal	5
Mod03	B22	Core image	1722.29	1722.67	0.37	Laminated	Geometric, horizontal	5
Mod03	B22	Core image	1722.29	1722.67	0.37	Laminated	Geometric, horizontal	5
Mod03	B22	Core image	1722.29	1722.67	0.37	Laminated	Geometric, horizontal	5
Mod03	B22	Core image	1722.29	1722.67	0.37	Laminated	Geometric, horizontal	5
Mod03	B22	Core image	1722.29	1722.67	0.37	Laminated	Geometric, horizontal	5
Mod03	B22	Core image	1722.29	1722.67	0.37	Laminated	Geometric, horizontal	10
Mod03	B22	Core image	1722.29	1722.67	0.37	Laminated	Geometric, horizontal	10
Mod03	B22	Core image	1722.29	1722.67	0.37	Laminated	Geometric, horizontal	10
Mod03	B22	Core image	1722.29	1722.67	0.37	Laminated	Geometric, horizontal	10
Mod03	B22	Core image	1722.29	1722.67	0.37	Laminated	Geometric, horizontal	10
Mod03	B22	Core image	1722.29	1722.67	0.37	Laminated	Geometric, horizontal	10
Mod03	B22	Core image	1722.29	1722.67	0.37	Laminated	Geometric, horizontal	15
Mod03	B22	Core image	1722.29	1722.67	0.37	Laminated	Geometric, horizontal	15
Mod03	B22	Core image	1722.29	1722.67	0.37	Laminated	Geometric, horizontal	15
Mod03	B22	Core image	1722.29	1722.67	0.37	Laminated	Geometric, horizontal	15
Mod03	B22	Core image	1722.29	1722.67	0.37	Laminated	Geometric, horizontal	15

Mod03	B22	Core image	1722.29	1722.67	0.37	Laminated	Geometric, horizontal	15
Mod03	B22	Core image	1722.29	1722.67	0.37	Laminated	Geometric, horizontal	20
Mod03	B22	Core image	1722.29	1722.67	0.37	Laminated	Geometric, horizontal	20
Mod03	B22	Core image	1722.29	1722.67	0.37	Laminated	Geometric, horizontal	20
Mod03	B22	Core image	1722.29	1722.67	0.37	Laminated	Geometric, horizontal	20
Mod03	B22	Core image	1722.29	1722.67	0.37	Laminated	Geometric, horizontal	20
Mod03	B22	Core image	1722.29	1722.67	0.37	Laminated	Geometric, horizontal	20
Mod03	B22	Core image	1722.29	1722.67	0.37	Laminated	Geometric, horizontal	25
Mod03	B22	Core image	1722.29	1722.67	0.37	Laminated	Geometric, horizontal	25
Mod03	B22	Core image	1722.29	1722.67	0.37	Laminated	Geometric, horizontal	25
Mod03	B22	Core image	1722.29	1722.67	0.37	Laminated	Geometric, horizontal	25
Mod03	B22	Core image	1722.29	1722.67	0.37	Laminated	Geometric, horizontal	25
Mod03	B22	Core image	1722.29	1722.67	0.37	Laminated	Geometric, horizontal	25
Mod03	B22	Core image	1722.29	1722.67	0.37	Laminated	Geometric, horizontal	30
Mod03	B22	Core image	1722.29	1722.67	0.37	Laminated	Geometric, horizontal	30
Mod03	B22	Core image	1722.29	1722.67	0.37	Laminated	Geometric, horizontal	30
Mod03	B22	Core image	1722.29	1722.67	0.37	Laminated	Geometric, horizontal	30
Mod03	B22	Core image	1722.29	1722.67	0.37	Laminated	Geometric, horizontal	30
Mod03	B22	Core image	1722.29	1722.67	0.37	Laminated	Geometric, horizontal	30
Mod04	B6	Borehole image	1634.00	1636.00	2.00	Laminated	Zonal, horizontal	1
Mod04	B6	Borehole image	1634.00	1636.00	2.00	Laminated	Zonal, horizontal	1
Mod04	B6	Borehole image	1634.00	1636.00	2.00	Laminated	Zonal, horizontal	1
Mod04	B6	Borehole image	1634.00	1636.00	2.00	Laminated	Zonal, horizontal	1
Mod04	B6	Borehole image	1634.00	1636.00	2.00	Laminated	Zonal, horizontal	1
Mod04	B6	Borehole image	1634.00	1636.00	2.00	Laminated	Zonal, horizontal	1
Mod04	B6	Borehole image	1634.00	1636.00	2.00	Laminated	Zonal, horizontal	5
Mod04	B6	Borehole image	1634.00	1636.00	2.00	Laminated	Zonal, horizontal	5
Mod04	B6	Borehole image	1634.00	1636.00	2.00	Laminated	Zonal, horizontal	5
Mod04	B6	Borehole image	1634.00	1636.00	2.00	Laminated	Zonal, horizontal	5
Mod04	B6	Borehole image	1634.00	1636.00	2.00	Laminated	Zonal, horizontal	5
Mod04	B6	Borehole image	1634.00	1636.00	2.00	Laminated	Zonal, horizontal	5
Mod04	B6	Borehole image	1634.00	1636.00	2.00	Laminated	Zonal, horizontal	10
Mod04	B6	Borehole image	1634.00	1636.00	2.00	Laminated	Zonal, horizontal	10

Mod04	B6	Borehole image	1634.00	1636.00	2.00	Laminated	Zonal, horizontal	10
Mod04	B6	Borehole image	1634.00	1636.00	2.00	Laminated	Zonal, horizontal	10
Mod04	B6	Borehole image	1634.00	1636.00	2.00	Laminated	Zonal, horizontal	10
Mod04	B6	Borehole image	1634.00	1636.00	2.00	Laminated	Zonal, horizontal	10
Mod04	B6	Borehole image	1634.00	1636.00	2.00	Laminated	Zonal, horizontal	15
Mod04	B6	Borehole image	1634.00	1636.00	2.00	Laminated	Zonal, horizontal	15
Mod04	B6	Borehole image	1634.00	1636.00	2.00	Laminated	Zonal, horizontal	15
Mod04	B6	Borehole image	1634.00	1636.00	2.00	Laminated	Zonal, horizontal	15
Mod04	B6	Borehole image	1634.00	1636.00	2.00	Laminated	Zonal, horizontal	15
Mod04	B6	Borehole image	1634.00	1636.00	2.00	Laminated	Zonal, horizontal	15
Mod04	B6	Borehole image	1634.00	1636.00	2.00	Laminated	Zonal, horizontal	20
Mod04	B6	Borehole image	1634.00	1636.00	2.00	Laminated	Zonal, horizontal	20
Mod04	B6	Borehole image	1634.00	1636.00	2.00	Laminated	Zonal, horizontal	20
Mod04	B6	Borehole image	1634.00	1636.00	2.00	Laminated	Zonal, horizontal	20
Mod04	B6	Borehole image	1634.00	1636.00	2.00	Laminated	Zonal, horizontal	20
Mod04	B6	Borehole image	1634.00	1636.00	2.00	Laminated	Zonal, horizontal	20
Mod04	B6	Borehole image	1634.00	1636.00	2.00	Laminated	Zonal, horizontal	25
Mod04	B6	Borehole image	1634.00	1636.00	2.00	Laminated	Zonal, horizontal	25
Mod04	B6	Borehole image	1634.00	1636.00	2.00	Laminated	Zonal, horizontal	25
Mod04	B6	Borehole image	1634.00	1636.00	2.00	Laminated	Zonal, horizontal	25
Mod04	B6	Borehole image	1634.00	1636.00	2.00	Laminated	Zonal, horizontal	25
Mod04	B6	Borehole image	1634.00	1636.00	2.00	Laminated	Zonal, horizontal	25
Mod04	B6	Borehole image	1634.00	1636.00	2.00	Laminated	Zonal, horizontal	30
Mod04	B6	Borehole image	1634.00	1636.00	2.00	Laminated	Zonal, horizontal	30
Mod04	B6	Borehole image	1634.00	1636.00	2.00	Laminated	Zonal, horizontal	30
Mod04	B6	Borehole image	1634.00	1636.00	2.00	Laminated	Zonal, horizontal	30
Mod04	B6	Borehole image	1634.00	1636.00	2.00	Laminated	Zonal, horizontal	30
Mod04	B6	Borehole image	1634.00	1636.00	2.00	Laminated	Zonal, horizontal	30

Mud content [%]	Mean cohesive content [%]	Mean porosity [fraction]	Minimum log10 effective Kh [m2]	Mean log10 effective Kh [m2]
50	39.18235161	0.413733872	-13.9898273	-13.71899112
60	46.01881599	0.431414766	-15.14212016	-14.66561783
70	52.85528036	0.449102641	-15.75518622	-15.46835709
80	59.69174474	0.466714947	-16.22462915	-16.10595072
90	66.52820912	0.484369983	-16.59026802	-16.5576085
100	73.36467349	0.501974301	-16.95733787	-16.95684071
50	39.18235161	0.33289634	-14.36539075	-14.11065594
60	46.01881599	0.342455709	-16.27434804	-15.38356061
70	52.85528036	0.35202319	-16.87326483	-16.5253286
80	59.69174474	0.361557665	-17.33392777	-17.21715729
90	66.52820912	0.371131674	-17.67979138	-17.6455327
100	73.36467349	0.380641357	-18.02598875	-18.02461944
50	39.18235161	0.283357146	-14.81899152	-14.48820112
60	46.01881599	0.288100878	-16.88444274	-15.86121072
70	52.85528036	0.292798907	-17.48585352	-17.11777293
80	59.69174474	0.297555005	-17.93424108	-17.82262428
90	66.52820912	0.30223752	-18.27107835	-18.23764569
100	73.36467349	0.306911885	-18.6062441	-18.6049098
50	39.18235161	0.247519473	-15.08688264	-14.80969025
60	46.01881599	0.248899787	-17.30971175	-16.22914721
70	52.85528036	0.250341894	-17.89962256	-17.52633882
80	59.69174474	0.251707898	-18.34899059	-18.23710225
90	66.52820912	0.253146032	-18.67830631	-18.64524231
100	73.36467349	0.254516932	-19.00485289	-19.00375971
50	39.18235161	0.217974339	-15.37267819	-15.12065637
60	46.01881599	0.216803392	-17.64918622	-16.56086406
70	52.85528036	0.215576375	-18.23451846	-17.86472267
80	59.69174474	0.214356193	-18.67969582	-18.57033135
90	66.52820912	0.213099329	-19.00499521	-18.97481622
100	73.36467349	0.211883434	-19.32758347	-19.32686595
50	39.18235161	0.192386554	-15.70151809	-15.42653264
60	46.01881599	0.188918717	-17.94252789	-16.83785172

70	52.85528036	0.185450307	-18.53660875	-18.15960867
80	59.69174474	0.182015216	-18.97166466	-18.86439596
90	66.52820912	0.178509968	-19.2932899	-19.26364398
100	73.36467349	0.175035116	-19.6110857	-19.61054475
50	39.18235161	0.169505053	-15.97521888	-15.71540956
60	46.01881599	0.164004666	-18.21544261	-17.12963699
70	52.85528036	0.158556315	-18.80549398	-18.42876847
80	59.69174474	0.153067379	-19.24469238	-19.13513752
90	66.52820912	0.147562772	-19.56123779	-19.53072965
100	73.36467349	0.142057261	-19.87406678	-19.87320511
50	39.18235161	0.413754493	-15.1214604	-14.62121878
60	46.01881599	0.431444672	-15.72032621	-15.5225457
70	52.85528036	0.448964423	-16.13794678	-16.08261794
80	59.69174474	0.466687845	-16.44922148	-16.43183262
90	66.52820912	0.484336821	-16.7325795	-16.72277222
100	73.36467349	0.502040423	-16.96123285	-16.9602095
50	39.18235161	0.332926257	-16.2391118	-15.28258549
60	46.01881599	0.342462833	-16.84654186	-16.57170518
70	52.85528036	0.352013854	-17.25417677	-17.19847187
80	59.69174474	0.361556712	-17.54584141	-17.53064117
90	66.52820912	0.371147384	-17.81274163	-17.80449703
100	73.36467349	0.380674855	-18.0310172	-18.03022988
50	39.18235161	0.283371151	-16.84702406	-15.73101726
60	46.01881599	0.288093208	-17.45188955	-17.16769115
70	52.85528036	0.292823522	-17.8533976	-17.8011002
80	59.69174474	0.297540015	-18.14310383	-18.12732463
90	66.52820912	0.302212796	-18.39921654	-18.39212399
100	73.36467349	0.306909476	-18.61208187	-18.61070765
50	39.18235161	0.247487727	-17.27196292	-16.0850059
60	46.01881599	0.248958558	-17.86570174	-17.57465623
70	52.85528036	0.250338469	-18.26605921	-18.21537124
80	59.69174474	0.251748659	-18.5513756	-18.53640243
90	66.52820912	0.253095003	-18.8031995	-18.79607427

100	73.36467349	0.254508888	-19.01009166	-19.00923423
50	39.18235161	0.217958857	-17.61495528	-16.410449
60	46.01881599	0.216777529	-18.20672032	-17.91242626
70	52.85528036	0.215601378	-18.60042491	-18.54810541
80	59.69174474	0.214356468	-18.88064842	-18.86617778
90	66.52820912	0.21311879	-19.12992457	-19.12316947
100	73.36467349	0.211872382	-19.33292079	-19.33190368
50	39.18235161	0.192382086	-17.90554984	-16.69223508
60	46.01881599	0.188924819	-18.49612083	-18.20086619
70	52.85528036	0.185477884	-18.89199004	-18.8401491
80	59.69174474	0.181993929	-19.17245756	-19.15570777
90	66.52820912	0.17852245	-19.415869	-19.40959133
100	73.36467349	0.175039436	-19.61644134	-19.61556146
50	39.18235161	0.169482104	-18.1782337	-16.98562792
60	46.01881599	0.164023203	-18.77162788	-18.47111557
70	52.85528036	0.158540118	-19.16161566	-19.11005211
80	59.69174474	0.153072176	-19.43922446	-19.42385108
90	66.52820912	0.147569374	-19.68155474	-19.67457154
100	73.36467349	0.142047981	-19.87847627	-19.87777365
50	39.18235161	0.413794189	-13.73698683	-13.48617224
60	46.01881599	0.43141808	-15.49197152	-13.96079894
70	52.85528036	0.449142777	-15.97075424	-14.77273641
80	59.69174474	0.466709042	-16.39566809	-15.91518901
90	66.52820912	0.484326311	-16.69459059	-16.59225752
100	73.36467349	0.502052635	-16.96076043	-16.95982448
50	39.18235161	0.332852222	-14.07756001	-13.84205746
60	46.01881599	0.342467287	-16.57804089	-14.39294426
70	52.85528036	0.352047484	-17.07590222	-15.44255602
80	59.69174474	0.361531609	-17.47890116	-16.9381034
90	66.52820912	0.371092156	-17.77475794	-17.67376467
100	73.36467349	0.380675596	-18.03126589	-18.028589
50	39.18235161	0.283363834	-14.47718032	-14.21025193
60	46.01881599	0.288054072	-17.18378522	-14.78805108

70	52.85528036	0.292776333	-17.67915815	-15.92253378
80	59.69174474	0.29752369	-18.07637989	-17.50460598
90	66.52820912	0.302258577	-18.36388839	-18.26329119
100	73.36467349	0.306918633	-18.61138023	-18.60883614
50	39.18235161	0.24748264	-14.7874635	-14.55176386
60	46.01881599	0.248913289	-17.58227428	-15.12307111
70	52.85528036	0.250335461	-18.08968942	-16.28113843
80	59.69174474	0.251691476	-18.47823056	-17.90492389
90	66.52820912	0.253108621	-18.76423175	-18.66720664
100	73.36467349	0.254518422	-19.00960742	-19.00713876
50	39.18235161	0.218032456	-15.13874107	-14.86883564
60	46.01881599	0.216810152	-17.89531491	-15.45139725
70	52.85528036	0.215550496	-18.42115801	-16.58939669
80	59.69174474	0.214357908	-18.81276702	-18.24467374
90	66.52820912	0.213132209	-19.09156109	-18.99468604
100	73.36467349	0.211861798	-19.33222028	-19.32980828
50	39.18235161	0.192413785	-15.43037097	-15.18090602
60	46.01881599	0.188906037	-18.20766926	-15.7575345
70	52.85528036	0.185474709	-18.71139088	-16.89217423
80	59.69174474	0.182002685	-19.09661425	-18.53016595
90	66.52820912	0.178508467	-19.37606672	-19.28243464
100	73.36467349	0.17503366	-19.61617207	-19.61343829
50	39.18235161	0.169478205	-15.70391206	-15.48032668
60	46.01881599	0.164037244	-18.49845602	-16.06010023
70	52.85528036	0.158530219	-18.98344298	-17.18103879
80	59.69174474	0.15304795	-19.35967362	-18.80338574
90	66.52820912	0.147568556	-19.64213373	-19.54944414
100	73.36467349	0.142060396	-19.8782498	-19.8759128

Mode log10 effective Kh [m2]	Maximum log10 effective Kh [m2]	Standard deviation log10 effective Kh [m2]	Minimum log10 effective Kv [m2]
-13.55853635	-13.48665453	0.163415999	-16.4430875
-15.14212016	-14.16684524	0.378018877	-16.73966144
-15.75518622	-14.64517537	0.307160862	-16.92207641
-16.19080365	-15.9878506	0.069516183	-17.02980241
-16.59026802	-16.47408877	0.032053117	-17.10977689
-16.95733787	-16.95629985	0.000352934	-17.17408922
-14.36539075	-13.86503283	0.1712409	-17.6481921
-16.27434804	-14.55726475	0.7071111	-17.94402187
-16.87326483	-15.04690361	0.512061742	-18.13429802
-17.23385663	-17.10042844	0.067675241	-18.24859309
-17.66509331	-17.57690493	0.027828176	-18.33146965
-18.02472493	-18.02377707	0.000634601	-18.39758512
-14.49256089	-14.24773792	0.181794303	-18.28428322
-16.88444274	-14.924391	0.822321503	-18.58011031
-17.48585352	-15.47059146	0.566375842	-18.77583224
-17.8381802	-17.71009904	0.065189586	-18.89229495
-18.25708859	-18.17314999	0.026811357	-18.97748915
-18.60454488	-18.60386519	0.000686925	-19.04484258
-15.08688264	-14.57482295	0.171311262	-18.71669877
-17.30971175	-15.26986804	0.871455055	-19.01150124
-17.89962256	-15.754707	0.605393961	-19.21035866
-18.25347159	-18.12611292	0.06375597	-19.3274856
-18.66471515	-18.58316818	0.025574613	-19.4123777
-19.00452014	-19.00252362	0.000754323	-19.47930821
-15.16188749	-14.88083322	0.16168676	-19.06641655
-17.64918622	-15.57553163	0.868487957	-19.3604916
-18.23451846	-16.07282167	0.611629594	-19.55816981
-18.58112543	-18.44969825	0.065821948	-19.67521151
-18.99209622	-18.91470228	0.024847913	-19.76019268
-19.32758347	-19.32605616	0.000473825	-19.82772408
-15.70151809	-15.18964447	0.169561905	-19.36918885
-17.94252789	-15.87069044	0.881955439	-19.65871587

-18.53660875	-16.3880803	0.605819306	-19.86212391
-18.87633083	-18.74921905	0.064468784	-19.97927834
-19.28036341	-19.2028045	0.024743639	-20.06551165
-19.6110857	-19.60983707	0.000427142	-20.13364176
-15.97521888	-15.47845136	0.164438733	-19.64963373
-18.21544261	-16.19567244	0.866038013	-19.94485876
-18.80549398	-16.62801093	0.615637809	-20.14090375
-19.14848427	-19.02020678	0.063576602	-20.25992167
-19.54857463	-19.47259568	0.024314091	-20.34577531
-19.87300084	-19.87257446	0.000493413	-20.41259214
-14.58537751	-14.18331535	0.347080095	-16.26710468
-15.72032621	-14.72740658	0.278699798	-16.64885911
-16.12129437	-16.02137993	0.03299348	-16.85387507
-16.4227403	-16.41832677	0.011644598	-17.00080506
-16.71851117	-16.71288383	0.006099826	-17.09526444
-16.96034017	-16.95967066	0.000457195	-17.16844055
-15.11586108	-14.66656079	0.629298464	-17.43283478
-16.84654186	-15.10461227	0.497182162	-17.83271516
-17.23860344	-17.14516341	0.032781318	-18.05180424
-17.51894816	-17.51446596	0.012032296	-18.20906423
-17.80239551	-17.79463592	0.005468796	-18.30962581
-18.0310172	-18.02916099	0.000515958	-18.38898765
-15.51786279	-14.98619828	0.735872383	-18.05864065
-17.45188955	-15.60232586	0.529335974	-18.46199716
-17.82425936	-17.75141376	0.030202738	-18.68949361
-18.11625681	-18.1117823	0.011580647	-18.84770248
-18.39921654	-18.38309303	0.005276308	-18.95263556
-18.61091982	-18.60937042	0.000743951	-19.03188566
-15.90446246	-15.35746228	0.775340983	-18.47482428
-17.86570174	-15.91270495	0.560740466	-18.88782414
-18.23740481	-18.16576882	0.02948656	-19.11892191
-18.52671776	-18.52260812	0.011004682	-19.28167605
-18.8031995	-18.78792165	0.004964902	-19.38679582

-19.00986601	-19.0085121	0.000496099	-19.46746346
-16.17909848	-15.60475575	0.785558804	-18.82226732
-18.20672032	-16.27541368	0.553020842	-19.23439626
-18.57137191	-18.49873939	0.030417433	-19.4658482
-18.85505032	-18.85078397	0.011328297	-19.62586963
-19.12031518	-19.11647143	0.004720204	-19.73526243
-19.33177129	-19.33090916	0.00052058	-19.816454
-16.51145503	-15.95381711	0.790682203	-19.11694928
-18.49612083	-16.52887412	0.564612669	-19.5327679
-18.84994002	-18.79387333	0.028202625	-19.76962773
-19.17245756	-19.13696518	0.012049957	-19.92842726
-19.415869	-19.40215021	0.004780886	-20.03805238
-19.61552562	-19.61515933	0.00039775	-20.12109348
-16.7713775	-16.20863502	0.781826338	-19.39955206
-18.77162788	-16.77041542	0.57402825	-19.81167067
-19.13327216	-19.06241341	0.028827508	-20.04567064
-19.43922446	-19.40615149	0.011445181	-20.208562
-19.67160144	-19.66762012	0.00452621	-20.31729549
-19.87818851	-19.87646195	0.000549229	-20.39969157
-13.43593563	-13.21014723	0.161018864	-16.58123151
-13.96710665	-13.3571607	0.55863612	-16.7319137
-15.97075424	-13.53783269	0.857175849	-16.87466515
-16.39566809	-13.97003214	0.667559683	-17.00319117
-16.69459059	-16.39464969	0.084783666	-17.09246181
-16.96076043	-16.95878502	0.000734853	-17.17003467
-14.07756001	-13.55843525	0.159856058	-17.78699254
-14.52136786	-13.69869866	0.763835843	-17.94619578
-17.07590222	-13.89478285	1.20157418	-18.07876574
-17.47890116	-14.39475531	0.864554956	-18.21751734
-17.77475794	-17.45622613	0.089006928	-18.30858164
-18.02751368	-18.02688832	0.001553178	-18.39083263
-14.15839441	-13.91930498	0.171511733	-18.43247489
-14.96220445	-14.07357214	0.829906163	-18.58413559

-17.67915815	-14.26081228	1.298631645	-18.71935107
-18.07637989	-14.71130374	0.946897624	-18.86021219
-18.36388839	-18.04207345	0.088671034	-18.95209849
-18.60862377	-18.60655642	0.001611789	-19.03407242
-14.49252483	-14.27132082	0.165996302	-18.86134369
-14.85920678	-14.40536219	0.849878935	-19.0235794
-18.08968942	-14.59597064	1.339095593	-19.14751757
-18.47823056	-15.04315615	0.969092311	-19.29387049
-18.76423175	-18.45317982	0.085991457	-19.38604196
-19.00684212	-19.00476814	0.001571891	-19.4688546
-15.13874107	-14.59604431	0.164325718	-19.2110218
-15.18696975	-14.73557889	0.846864767	-19.36871861
-18.42115801	-14.9247378	1.351447114	-19.49623927
-18.81276702	-15.37735086	0.968921951	-19.64435695
-19.09156109	-18.77269446	0.087924959	-19.73702001
-19.33222028	-19.32741453	0.001456083	-19.81931226
-15.43037097	-14.90889606	0.167436685	-19.51526608
-15.50871881	-15.05889373	0.848321675	-19.66899202
-18.71139088	-15.2528773	1.344800031	-19.80120275
-19.09661425	-15.6796792	0.964568214	-19.94603849
-19.37606672	-19.07220377	0.084435673	-20.04078683
-19.61617207	-19.61084101	0.001723529	-20.1213059
-15.70391206	-15.22368971	0.156862761	-19.79392737
-15.81104414	-15.36314216	0.84365225	-19.94961251
-18.98344298	-15.54891084	1.325554075	-20.08034672
-19.35967362	-15.997497	0.949698823	-20.22579701
-19.64213373	-19.34109516	0.082674902	-20.31967355
-19.87557926	-19.87357635	0.001347594	-20.40374388

Mean log10 effective Kv [m2]	Mode log10 effective Kv [m2]	Maximum log10 effective Kv [m2]	Standard deviation log10 effective Kv [m2]
-16.37396382	-16.41074762	-16.21670829	0.062118211
-16.70603162	-16.72577655	-16.64246725	0.026015579
-16.90259515	-16.90252502	-16.89470446	0.008024499
-17.02231374	-17.02346216	-17.01500849	0.004163565
-17.10650224	-17.10681427	-17.1028641	0.001732293
-17.17196865	-17.17140767	-17.17096074	0.000871871
-17.56076865	-17.61109289	-17.38849761	0.070746951
-17.90720549	-17.92812513	-17.83274471	0.029906308
-18.11382248	-18.11422917	-18.10620163	0.008083263
-18.23929009	-18.24145197	-18.23193048	0.004400009
-18.32776803	-18.32726774	-18.3241163	0.002220787
-18.39565469	-18.3964242	-18.3935219	0.001142338
-18.1952236	-18.24735773	-18.02580482	0.069775196
-18.54548781	-18.58011031	-18.46980543	0.030165858
-18.75426418	-18.75504829	-18.74673471	0.008746297
-18.88224559	-18.88269728	-18.87549904	0.004553469
-18.97256376	-18.97326772	-18.96763915	0.002492191
-19.04124776	-19.04201059	-19.0398866	0.001316132
-18.62778401	-18.68005631	-18.46020152	0.069399463
-18.97755085	-19.01150124	-18.89572121	0.032027118
-19.1881119	-19.1887685	-19.18013244	0.008738605
-19.31665408	-19.31715853	-19.30941323	0.004886365
-19.40754353	-19.4123777	-19.40248581	0.00291248
-19.47728471	-19.4773421	-19.47472061	0.001385415
-18.97244465	-19.02862669	-18.8018875	0.071136299
-19.32451778	-19.3604916	-19.24671653	0.031219858
-19.53536863	-19.5351608	-19.5259572	0.00893322
-19.66491793	-19.66536731	-19.65798417	0.004815164
-19.7559183	-19.75575317	-19.74983382	0.002722657
-19.82612416	-19.82618823	-19.82414043	0.001041599
-19.27658652	-19.33130109	-19.1039745	0.071334084
-19.62617084	-19.65871587	-19.54771357	0.030824301

-19.83856388	-19.83905211	-19.82982339	0.009436766
-19.96834344	-19.96888947	-19.96109782	0.004878607
-20.06005029	-20.05981189	-20.05553707	0.002572895
-20.13074666	-20.13055188	-20.12823448	0.001772586
-19.55490147	-19.61107897	-19.37975044	0.071725905
-19.90586385	-19.92816572	-19.82800749	0.031471346
-20.1172886	-20.11701947	-20.10746576	0.009497322
-20.24821278	-20.25143879	-20.24012827	0.005286646
-20.33988318	-20.34155264	-20.33592241	0.002992709
-20.41070022	-20.41122642	-20.40781214	0.001252424
-16.16180796	-16.23254103	-16.02515914	0.079134954
-16.60604987	-16.58826681	-16.56402989	0.027399679
-16.84260478	-16.83862357	-16.83608166	0.007160364
-16.9894226	-16.98995158	-16.98181147	0.00538176
-17.09116236	-17.09114961	-17.08806349	0.002290646
-17.16726942	-17.167469	-17.1661736	0.000594298
-17.32156016	-17.43283478	-17.16817884	0.088442633
-17.78976776	-17.82088055	-17.74987288	0.027525122
-18.04077593	-18.03628236	-18.03369538	0.006917035
-18.19617708	-18.19699938	-18.18795075	0.006073862
-18.30516226	-18.306839	-18.29987197	0.002797354
-18.3864245	-18.38689943	-18.38411515	0.001273032
-17.94754728	-18.05864065	-17.79468464	0.089661965
-18.41851713	-18.46199716	-18.37910225	0.027377279
-18.67522253	-18.67237974	-18.66553419	0.008357613
-18.83516034	-18.83493301	-18.8253559	0.00656606
-18.9467893	-18.94806905	-18.94198037	0.003048542
-19.03046441	-19.03011302	-19.02878355	0.000970371
-18.37147501	-18.47482428	-18.21649661	0.089045188
-18.84791407	-18.88782414	-18.80392611	0.026837138
-19.10616983	-19.10293479	-19.09653993	0.007764538
-19.26814174	-19.26867807	-19.25892959	0.006461186
-19.38100305	-19.37967245	-19.3768231	0.002954028

-19.46538511	-19.4652907	-19.4623937	0.001378024
-18.71488919	-18.82226732	-18.55805206	0.087200579
-19.19185225	-19.23439626	-19.1468855	0.027059905
-19.45182986	-19.44785381	-19.44065605	0.00823157
-19.61431745	-19.6148947	-19.6066635	0.006142171
-19.72936821	-19.73041708	-19.72395661	0.003214584
-19.81448086	-19.81526923	-19.81230729	0.001239766
-19.01449251	-19.11694928	-18.85870704	0.088518355
-19.49103994	-19.5327679	-19.45002251	0.026862468
-19.75296366	-19.74912565	-19.74092481	0.009067127
-19.91701623	-19.91920908	-19.90691818	0.00632759
-20.03276443	-20.03211818	-20.02766754	0.003145687
-20.11823753	-20.1173781	-20.11675887	0.001524668
-19.29036267	-19.39955206	-19.12686141	0.090995786
-19.76902132	-19.81167067	-19.72952613	0.026048341
-20.03009294	-20.02685817	-20.01933319	0.008882621
-20.19620936	-20.19622547	-20.18697307	0.006558308
-20.31165456	-20.31209746	-20.30516675	0.003470206
-20.39785098	-20.39859386	-20.39584958	0.000968012
-16.37184936	-16.38763962	-16.12951709	0.146381666
-16.62051349	-16.7319137	-16.5143467	0.070887645
-16.81018904	-16.87466515	-16.74617756	0.050655136
-16.97427232	-16.99389607	-16.9381255	0.024501642
-17.08191623	-17.09246181	-17.06225098	0.008592378
-17.16640932	-17.1675359	-17.1642042	0.001543184
-17.56352554	-17.57613004	-17.29498005	0.161726286
-17.82095843	-17.94619578	-17.70584914	0.078998802
-18.01421783	-18.07876574	-17.94187778	0.054808698
-18.18206223	-18.20661349	-18.1411904	0.028799256
-18.29562624	-18.30858164	-18.27428433	0.010323723
-18.38428026	-18.3816729	-18.38014628	0.003322131
-18.19921016	-18.21577383	-17.92683908	0.163542531
-18.45792212	-18.58413559	-18.33544734	0.080400654

-18.65247587	-18.71935107	-18.57966462	0.056819796
-18.82304	-18.84887481	-18.78085051	0.03032949
-18.93796446	-18.95209849	-18.91453103	0.011253947
-19.02764812	-19.02393646	-19.02224714	0.003715464
-18.62814671	-18.65271592	-18.37454555	0.164689824
-18.89136895	-19.0235794	-18.77122249	0.081809754
-19.08465308	-19.14751757	-19.01064497	0.057173459
-19.25506007	-19.2817986	-19.20936726	0.031450205
-19.3718374	-19.38604196	-19.34707615	0.011739567
-19.46327689	-19.45897543	-19.45732891	0.003964349
-18.97566326	-18.99168553	-18.69923718	0.167911173
-19.23747522	-19.36871861	-19.11139316	0.083128839
-19.43173708	-19.49623927	-19.35818791	0.058032157
-19.60335353	-19.63201131	-19.55793748	0.03187754
-19.72070659	-19.73702001	-19.69439931	0.012922186
-19.81179442	-19.81369367	-19.80620221	0.00391472
-19.27931801	-19.30059812	-19.01437416	0.165920791
-19.53931026	-19.66899202	-19.41569253	0.082180965
-19.73440097	-19.80120275	-19.66083487	0.058440059
-19.90609876	-19.93369625	-19.85964282	0.032053078
-20.02369965	-20.04078683	-19.99859516	0.012597595
-20.11607729	-20.11822553	-20.11052461	0.003622423
-19.55679222	-19.5805103	-19.29595421	0.166131095
-19.81756458	-19.94961251	-19.69323625	0.083304522
-20.01355413	-20.08034672	-19.93671169	0.058292071
-20.18529507	-20.21298491	-20.13611233	0.032884306
-20.30297254	-20.31967355	-20.27681533	0.012529711
-20.39595786	-20.39937627	-20.38845724	0.004564792

Model ID	Well	Image type	Top [m]	Bottom [m]	Interval [m]	Structural class	Geostatistical anisotropy type	Effective stress [MPa]
Mod05	B22	Core image	1719.18	1719.69	0.52	Lenticular	Zonal, horizontal	1
Mod05	B22	Core image	1719.18	1719.69	0.52	Lenticular	Zonal, horizontal	1
Mod05	B22	Core image	1719.18	1719.69	0.52	Lenticular	Zonal, horizontal	1
Mod05	B22	Core image	1719.18	1719.69	0.52	Lenticular	Zonal, horizontal	1
Mod05	B22	Core image	1719.18	1719.69	0.52	Lenticular	Zonal, horizontal	1
Mod05	B22	Core image	1719.18	1719.69	0.52	Lenticular	Zonal, horizontal	1
Mod05	B22	Core image	1719.18	1719.69	0.52	Lenticular	Zonal, horizontal	5
Mod05	B22	Core image	1719.18	1719.69	0.52	Lenticular	Zonal, horizontal	5
Mod05	B22	Core image	1719.18	1719.69	0.52	Lenticular	Zonal, horizontal	5
Mod05	B22	Core image	1719.18	1719.69	0.52	Lenticular	Zonal, horizontal	5
Mod05	B22	Core image	1719.18	1719.69	0.52	Lenticular	Zonal, horizontal	5
Mod05	B22	Core image	1719.18	1719.69	0.52	Lenticular	Zonal, horizontal	5
Mod05	B22	Core image	1719.18	1719.69	0.52	Lenticular	Zonal, horizontal	10
Mod05	B22	Core image	1719.18	1719.69	0.52	Lenticular	Zonal, horizontal	10
Mod05	B22	Core image	1719.18	1719.69	0.52	Lenticular	Zonal, horizontal	10
Mod05	B22	Core image	1719.18	1719.69	0.52	Lenticular	Zonal, horizontal	10
Mod05	B22	Core image	1719.18	1719.69	0.52	Lenticular	Zonal, horizontal	10
Mod05	B22	Core image	1719.18	1719.69	0.52	Lenticular	Zonal, horizontal	10
Mod05	B22	Core image	1719.18	1719.69	0.52	Lenticular	Zonal, horizontal	15
Mod05	B22	Core image	1719.18	1719.69	0.52	Lenticular	Zonal, horizontal	15
Mod05	B22	Core image	1719.18	1719.69	0.52	Lenticular	Zonal, horizontal	15
Mod05	B22	Core image	1719.18	1719.69	0.52	Lenticular	Zonal, horizontal	15
Mod05	B22	Core image	1719.18	1719.69	0.52	Lenticular	Zonal, horizontal	15
Mod05	B22	Core image	1719.18	1719.69	0.52	Lenticular	Zonal, horizontal	15
Mod05	B22	Core image	1719.18	1719.69	0.52	Lenticular	Zonal, horizontal	20
Mod05	B22	Core image	1719.18	1719.69	0.52	Lenticular	Zonal, horizontal	20
Mod05	B22	Core image	1719.18	1719.69	0.52	Lenticular	Zonal, horizontal	20
Mod05	B22	Core image	1719.18	1719.69	0.52	Lenticular	Zonal, horizontal	20
Mod05	B22	Core image	1719.18	1719.69	0.52	Lenticular	Zonal, horizontal	20
Mod05	B22	Core image	1719.18	1719.69	0.52	Lenticular	Zonal, horizontal	20
Mod05	B22	Core image	1719.18	1719.69	0.52	Lenticular	Zonal, horizontal	25
Mod05	B22	Core image	1719.18	1719.69	0.52	Lenticular	Zonal, horizontal	25

Mod05	B22	Core image	1719.18	1719.69	0.52	Lenticular	Zonal, horizontal	25
Mod05	B22	Core image	1719.18	1719.69	0.52	Lenticular	Zonal, horizontal	25
Mod05	B22	Core image	1719.18	1719.69	0.52	Lenticular	Zonal, horizontal	25
Mod05	B22	Core image	1719.18	1719.69	0.52	Lenticular	Zonal, horizontal	25
Mod05	B22	Core image	1719.18	1719.69	0.52	Lenticular	Zonal, horizontal	30
Mod05	B22	Core image	1719.18	1719.69	0.52	Lenticular	Zonal, horizontal	30
Mod05	B22	Core image	1719.18	1719.69	0.52	Lenticular	Zonal, horizontal	30
Mod05	B22	Core image	1719.18	1719.69	0.52	Lenticular	Zonal, horizontal	30
Mod05	B22	Core image	1719.18	1719.69	0.52	Lenticular	Zonal, horizontal	30
Mod05	B22	Core image	1719.18	1719.69	0.52	Lenticular	Zonal, horizontal	30
Mod06	B24	Core image	1991.16	1991.48	0.32	Lenticular	Zonal, horizontal	1
Mod06	B24	Core image	1991.16	1991.48	0.32	Lenticular	Zonal, horizontal	1
Mod06	B24	Core image	1991.16	1991.48	0.32	Lenticular	Zonal, horizontal	1
Mod06	B24	Core image	1991.16	1991.48	0.32	Lenticular	Zonal, horizontal	1
Mod06	B24	Core image	1991.16	1991.48	0.32	Lenticular	Zonal, horizontal	1
Mod06	B24	Core image	1991.16	1991.48	0.32	Lenticular	Zonal, horizontal	1
Mod06	B24	Core image	1991.16	1991.48	0.32	Lenticular	Zonal, horizontal	5
Mod06	B24	Core image	1991.16	1991.48	0.32	Lenticular	Zonal, horizontal	5
Mod06	B24	Core image	1991.16	1991.48	0.32	Lenticular	Zonal, horizontal	5
Mod06	B24	Core image	1991.16	1991.48	0.32	Lenticular	Zonal, horizontal	5
Mod06	B24	Core image	1991.16	1991.48	0.32	Lenticular	Zonal, horizontal	5
Mod06	B24	Core image	1991.16	1991.48	0.32	Lenticular	Zonal, horizontal	5
Mod06	B24	Core image	1991.16	1991.48	0.32	Lenticular	Zonal, horizontal	10
Mod06	B24	Core image	1991.16	1991.48	0.32	Lenticular	Zonal, horizontal	10
Mod06	B24	Core image	1991.16	1991.48	0.32	Lenticular	Zonal, horizontal	10
Mod06	B24	Core image	1991.16	1991.48	0.32	Lenticular	Zonal, horizontal	10
Mod06	B24	Core image	1991.16	1991.48	0.32	Lenticular	Zonal, horizontal	10
Mod06	B24	Core image	1991.16	1991.48	0.32	Lenticular	Zonal, horizontal	10
Mod06	B24	Core image	1991.16	1991.48	0.32	Lenticular	Zonal, horizontal	15
Mod06	B24	Core image	1991.16	1991.48	0.32	Lenticular	Zonal, horizontal	15
Mod06	B24	Core image	1991.16	1991.48	0.32	Lenticular	Zonal, horizontal	15
Mod06	B24	Core image	1991.16	1991.48	0.32	Lenticular	Zonal, horizontal	15
Mod06	B24	Core image	1991.16	1991.48	0.32	Lenticular	Zonal, horizontal	15

Mod06	B24	Core image	1991.16	1991.48	0.32	Lenticular	Zonal, horizontal	15
Mod06	B24	Core image	1991.16	1991.48	0.32	Lenticular	Zonal, horizontal	20
Mod06	B24	Core image	1991.16	1991.48	0.32	Lenticular	Zonal, horizontal	20
Mod06	B24	Core image	1991.16	1991.48	0.32	Lenticular	Zonal, horizontal	20
Mod06	B24	Core image	1991.16	1991.48	0.32	Lenticular	Zonal, horizontal	20
Mod06	B24	Core image	1991.16	1991.48	0.32	Lenticular	Zonal, horizontal	20
Mod06	B24	Core image	1991.16	1991.48	0.32	Lenticular	Zonal, horizontal	20
Mod06	B24	Core image	1991.16	1991.48	0.32	Lenticular	Zonal, horizontal	25
Mod06	B24	Core image	1991.16	1991.48	0.32	Lenticular	Zonal, horizontal	25
Mod06	B24	Core image	1991.16	1991.48	0.32	Lenticular	Zonal, horizontal	25
Mod06	B24	Core image	1991.16	1991.48	0.32	Lenticular	Zonal, horizontal	25
Mod06	B24	Core image	1991.16	1991.48	0.32	Lenticular	Zonal, horizontal	25
Mod06	B24	Core image	1991.16	1991.48	0.32	Lenticular	Zonal, horizontal	25
Mod06	B24	Core image	1991.16	1991.48	0.32	Lenticular	Zonal, horizontal	30
Mod06	B24	Core image	1991.16	1991.48	0.32	Lenticular	Zonal, horizontal	30
Mod06	B24	Core image	1991.16	1991.48	0.32	Lenticular	Zonal, horizontal	30
Mod06	B24	Core image	1991.16	1991.48	0.32	Lenticular	Zonal, horizontal	30
Mod06	B24	Core image	1991.16	1991.48	0.32	Lenticular	Zonal, horizontal	30
Mod06	B24	Core image	1991.16	1991.48	0.32	Lenticular	Zonal, horizontal	30
Mod07	B23	Core image	1712.04	1712.23	0.19	Lenticular	Geometric, horizontal	1
Mod07	B23	Core image	1712.04	1712.23	0.19	Lenticular	Geometric, horizontal	1
Mod07	B23	Core image	1712.04	1712.23	0.19	Lenticular	Geometric, horizontal	1
Mod07	B23	Core image	1712.04	1712.23	0.19	Lenticular	Geometric, horizontal	1
Mod07	B23	Core image	1712.04	1712.23	0.19	Lenticular	Geometric, horizontal	1
Mod07	B23	Core image	1712.04	1712.23	0.19	Lenticular	Geometric, horizontal	1
Mod07	B23	Core image	1712.04	1712.23	0.19	Lenticular	Geometric, horizontal	5
Mod07	B23	Core image	1712.04	1712.23	0.19	Lenticular	Geometric, horizontal	5
Mod07	B23	Core image	1712.04	1712.23	0.19	Lenticular	Geometric, horizontal	5
Mod07	B23	Core image	1712.04	1712.23	0.19	Lenticular	Geometric, horizontal	5
Mod07	B23	Core image	1712.04	1712.23	0.19	Lenticular	Geometric, horizontal	5
Mod07	B23	Core image	1712.04	1712.23	0.19	Lenticular	Geometric, horizontal	5
Mod07	B23	Core image	1712.04	1712.23	0.19	Lenticular	Geometric, horizontal	10
Mod07	B23	Core image	1712.04	1712.23	0.19	Lenticular	Geometric, horizontal	10

Mod07	B23	Core image	1712.04	1712.23	0.19	Lenticular	Geometric, horizontal	10
Mod07	B23	Core image	1712.04	1712.23	0.19	Lenticular	Geometric, horizontal	10
Mod07	B23	Core image	1712.04	1712.23	0.19	Lenticular	Geometric, horizontal	10
Mod07	B23	Core image	1712.04	1712.23	0.19	Lenticular	Geometric, horizontal	10
Mod07	B23	Core image	1712.04	1712.23	0.19	Lenticular	Geometric, horizontal	15
Mod07	B23	Core image	1712.04	1712.23	0.19	Lenticular	Geometric, horizontal	15
Mod07	B23	Core image	1712.04	1712.23	0.19	Lenticular	Geometric, horizontal	15
Mod07	B23	Core image	1712.04	1712.23	0.19	Lenticular	Geometric, horizontal	15
Mod07	B23	Core image	1712.04	1712.23	0.19	Lenticular	Geometric, horizontal	15
Mod07	B23	Core image	1712.04	1712.23	0.19	Lenticular	Geometric, horizontal	15
Mod07	B23	Core image	1712.04	1712.23	0.19	Lenticular	Geometric, horizontal	20
Mod07	B23	Core image	1712.04	1712.23	0.19	Lenticular	Geometric, horizontal	20
Mod07	B23	Core image	1712.04	1712.23	0.19	Lenticular	Geometric, horizontal	20
Mod07	B23	Core image	1712.04	1712.23	0.19	Lenticular	Geometric, horizontal	20
Mod07	B23	Core image	1712.04	1712.23	0.19	Lenticular	Geometric, horizontal	20
Mod07	B23	Core image	1712.04	1712.23	0.19	Lenticular	Geometric, horizontal	20
Mod07	B23	Core image	1712.04	1712.23	0.19	Lenticular	Geometric, horizontal	25
Mod07	B23	Core image	1712.04	1712.23	0.19	Lenticular	Geometric, horizontal	25
Mod07	B23	Core image	1712.04	1712.23	0.19	Lenticular	Geometric, horizontal	25
Mod07	B23	Core image	1712.04	1712.23	0.19	Lenticular	Geometric, horizontal	25
Mod07	B23	Core image	1712.04	1712.23	0.19	Lenticular	Geometric, horizontal	25
Mod07	B23	Core image	1712.04	1712.23	0.19	Lenticular	Geometric, horizontal	25
Mod07	B23	Core image	1712.04	1712.23	0.19	Lenticular	Geometric, horizontal	30
Mod07	B23	Core image	1712.04	1712.23	0.19	Lenticular	Geometric, horizontal	30
Mod07	B23	Core image	1712.04	1712.23	0.19	Lenticular	Geometric, horizontal	30
Mod07	B23	Core image	1712.04	1712.23	0.19	Lenticular	Geometric, horizontal	30
Mod07	B23	Core image	1712.04	1712.23	0.19	Lenticular	Geometric, horizontal	30
Mod07	B23	Core image	1712.04	1712.23	0.19	Lenticular	Geometric, horizontal	30

Mud content [%]	Mean cohesive content [%]	Mean porosity [fraction]	Minimum log10 effective Kh [m2]	Mean log10 effective Kh [m2]
50	39.18235161	0.413718677	-14.29647391	-14.11172023
60	46.01881599	0.431355565	-15.68243597	-15.12824632
70	52.85528036	0.448985592	-16.15837653	-15.83719612
80	59.69174474	0.466683872	-16.49434274	-16.41716264
90	66.52820912	0.484384893	-16.76354336	-16.73273735
100	73.36467349	0.501985241	-16.96359869	-16.96228831
50	39.18235161	0.33288469	-14.79633627	-14.54196561
60	46.01881599	0.342445611	-16.79049571	-16.03272998
70	52.85528036	0.35201332	-17.26176503	-16.87414672
80	59.69174474	0.361588306	-17.58433567	-17.50679008
90	66.52820912	0.371121761	-17.84033056	-17.80955807
100	73.36467349	0.380681159	-18.03485571	-18.0333208
50	39.18235161	0.283350738	-15.12118303	-14.89256206
60	46.01881599	0.288091244	-17.38694823	-16.5707544
70	52.85528036	0.292779955	-17.85118765	-17.45682212
80	59.69174474	0.29750675	-18.17264107	-18.09804082
90	66.52820912	0.302215206	-18.42424655	-18.3950234
100	73.36467349	0.306955429	-18.61567526	-18.61376504
50	39.18235161	0.247503028	-15.45548424	-15.21928763
60	46.01881599	0.248944962	-17.79506106	-16.96010389
70	52.85528036	0.250303272	-18.26685251	-17.85363396
80	59.69174474	0.25172668	-18.58154624	-18.50553643
90	66.52820912	0.25308895	-18.82611185	-18.79659308
100	73.36467349	0.254487028	-19.01389006	-19.0117159
50	39.18235161	0.218007027	-15.71803765	-15.51436171
60	46.01881599	0.216800613	-18.12941059	-17.28081044
70	52.85528036	0.215595951	-18.58917723	-18.18408701
80	59.69174474	0.214394073	-18.90833304	-18.83500087
90	66.52820912	0.213125346	-19.15217695	-19.12385125
100	73.36467349	0.211854378	-19.33604197	-19.33417458
50	39.18235161	0.192407313	-16.0442555	-15.82263781
60	46.01881599	0.188920705	-18.42519927	-17.57883029

70	52.85528036	0.185454866	-18.88301722	-18.47488943
80	59.69174474	0.181993477	-19.19614633	-19.12327683
90	66.52820912	0.178525481	-19.43632436	-19.40924986
100	73.36467349	0.175024213	-19.61922816	-19.61741163
50	39.18235161	0.169483878	-16.31931647	-16.12015991
60	46.01881599	0.164015642	-18.69330483	-17.8627647
70	52.85528036	0.158558727	-19.15266615	-18.74716432
80	59.69174474	0.153069938	-19.46379899	-19.38961734
90	66.52820912	0.147591019	-19.69977202	-19.67358902
100	73.36467349	0.142076765	-19.88167905	-19.88005543
50	39.18235161	0.413726569	-15.04730682	-13.97026147
60	46.01881599	0.431460043	-15.5822776	-15.03213524
70	52.85528036	0.449106137	-16.02636007	-15.81372202
80	59.69174474	0.466708004	-16.37762328	-16.2869406
90	66.52820912	0.484352752	-16.69750673	-16.64840959
100	73.36467349	0.502031145	-16.95990028	-16.95937374
50	39.18235161	0.332904503	-16.18865494	-14.4386609
60	46.01881599	0.342480295	-16.70391426	-15.9349781
70	52.85528036	0.351932154	-17.13344508	-16.92515931
80	59.69174474	0.361631014	-17.47150881	-17.38413245
90	66.52820912	0.371148597	-17.77966959	-17.73174024
100	73.36467349	0.380674024	-18.02982148	-18.0287019
50	39.18235161	0.28335392	-16.8157033	-14.83107981
60	46.01881599	0.288031821	-17.32424456	-16.47031627
70	52.85528036	0.292774873	-17.73765572	-17.52987747
80	59.69174474	0.297545947	-18.06660029	-17.98275962
90	66.52820912	0.302216658	-18.36860392	-18.32131069
100	73.36467349	0.30691486	-18.60973804	-18.60904673
50	39.18235161	0.247538419	-17.23126869	-15.16724031
60	46.01881599	0.248905536	-17.7325842	-16.87209463
70	52.85528036	0.250323837	-18.14416236	-17.9427536
80	59.69174474	0.251695061	-18.47323698	-18.39368658
90	66.52820912	0.253151079	-18.76972739	-18.72551616

100	73.36467349	0.254471672	-19.00857101	-19.00741695
50	39.18235161	0.217977343	-17.56753902	-15.48430484
60	46.01881599	0.216788915	-18.06252624	-17.18218939
70	52.85528036	0.215588886	-18.48155187	-18.28092565
80	59.69174474	0.214328044	-18.807558	-18.72364949
90	66.52820912	0.213146097	-19.09703489	-19.05305703
100	73.36467349	0.211853706	-19.33154606	-19.33027716
50	39.18235161	0.192404923	-17.86456838	-15.7896575
60	46.01881599	0.188914213	-18.35959311	-17.49188571
70	52.85528036	0.185470173	-18.77148929	-18.57238518
80	59.69174474	0.182006546	-19.09447557	-19.0164384
90	66.52820912	0.178528816	-19.38569243	-19.34046836
100	73.36467349	0.175028865	-19.61460467	-19.61383729
50	39.18235161	0.169497869	-18.14399655	-16.07528505
60	46.01881599	0.16404875	-18.63006092	-17.77844961
70	52.85528036	0.158526621	-19.03374842	-18.84352142
80	59.69174474	0.153052363	-19.36826612	-19.28507644
90	66.52820912	0.147579558	-19.64959884	-19.60599477
100	73.36467349	0.14206326	-19.87730584	-19.87652179
50	39.18235161	0.413770148	-15.13274411	-14.90463879
60	46.01881599	0.431385747	-15.86256993	-15.81205987
70	52.85528036	0.44902566	-16.2598711	-16.24518158
80	59.69174474	0.466705541	-16.56355746	-16.54838887
90	66.52820912	0.484394121	-16.78821757	-16.7856888
100	73.36467349	0.50195944	-16.96070885	-16.96009772
50	39.18235161	0.332879833	-16.23522703	-15.85756222
60	46.01881599	0.342381745	-16.97761287	-16.93068827
70	52.85528036	0.352014443	-17.36385125	-17.35014648
80	59.69174474	0.361517376	-17.6524885	-17.63845294
90	66.52820912	0.371093716	-17.86366318	-17.86189298
100	73.36467349	0.38068102	-18.0314358	-18.03071383
50	39.18235161	0.2833847	-16.8473723	-16.43147617
60	46.01881599	0.288099111	-17.58184792	-17.53668812

70	52.85528036	0.292819678	-17.96359869	-17.94973375
80	59.69174474	0.297574604	-18.24387074	-18.2313559
90	66.52820912	0.302231352	-18.44971415	-18.44756372
100	73.36467349	0.306879937	-18.61199654	-18.61118322
50	39.18235161	0.247528723	-17.26541857	-16.82421848
60	46.01881599	0.248909553	-17.99317469	-17.95238017
70	52.85528036	0.250320904	-18.37282265	-18.35944539
80	59.69174474	0.251721331	-18.64872176	-18.63740633
90	66.52820912	0.253114862	-18.85213825	-18.84980778
100	73.36467349	0.254498036	-19.01032064	-19.00981175
50	39.18235161	0.21800633	-17.60056166	-17.15644352
60	46.01881599	0.216776742	-18.32844119	-18.28689328
70	52.85528036	0.215558585	-18.70669491	-18.69229894
80	59.69174474	0.214323354	-18.97873212	-18.96657112
90	66.52820912	0.213093367	-19.17743182	-19.17549921
100	73.36467349	0.211872004	-19.3336524	-19.33264769
50	39.18235161	0.192394294	-17.89624416	-17.45309471
60	46.01881599	0.18892693	-18.62636539	-18.58073904
70	52.85528036	0.185436434	-18.99789012	-18.98335355
80	59.69174474	0.182019024	-19.26767943	-19.25584654
90	66.52820912	0.178529155	-19.46382931	-19.46180499
100	73.36467349	0.175047838	-19.61702173	-19.61622625
50	39.18235161	0.169474425	-18.17220698	-17.72943379
60	46.01881599	0.164011933	-18.89308871	-18.85120227
70	52.85528036	0.158544563	-19.26622593	-19.2526418
80	59.69174474	0.153061326	-19.53424251	-19.52156744
90	66.52820912	0.147564113	-19.72789836	-19.72595604
100	73.36467349	0.142071504	-19.87920569	-19.8787145

Mode log10 effective Kh [m2]	Maximum log10 effective Kh [m2]	Standard deviation log10 effective Kh [m2]	Minimum log10 effective Kv [m2]
-14.29647391	-13.81287427	0.161737581	-16.36138996
-15.68243597	-14.19298617	0.53579321	-16.62366398
-16.15837653	-14.69290207	0.402647458	-16.83157324
-16.42756178	-16.3385205	0.050598045	-16.98151587
-16.74148027	-16.68632256	0.022194296	-17.08792947
-16.96238527	-16.96147521	0.000580674	-17.16601763
-14.79633627	-14.20863712	0.192451149	-17.55396327
-16.79049571	-14.57904636	0.856014028	-17.82201933
-17.26176503	-15.14595644	0.590236137	-18.03311333
-17.54003061	-17.42926797	0.050127064	-18.19060528
-17.80930256	-17.76793188	0.021568508	-18.3007886
-18.033197	-18.03195297	0.000911932	-18.38335752
-15.04520413	-14.58933072	0.179164999	-18.1868622
-17.38694823	-14.99343128	0.958489825	-18.46055002
-17.85118765	-15.57146836	0.640607749	-18.66978312
-18.0443606	-18.02298052	0.049494864	-18.82938336
-18.40387575	-18.35294875	0.021214465	-18.94089118
-18.61304126	-18.61198766	0.001097232	-19.02824882
-15.45548424	-14.90090664	0.175612829	-18.60995735
-17.79506106	-15.31052776	0.998467561	-18.8847324
-18.26685251	-15.81394821	0.691114464	-19.10261101
-18.53696786	-18.42552193	0.048918641	-19.26473174
-18.82611185	-18.75194332	0.021600017	-19.37586751
-19.01132935	-19.01030507	0.001064721	-19.46286751
-15.71803765	-15.21420551	0.173364439	-18.9564334
-18.12941059	-15.58792604	1.018159061	-19.2328278
-18.58917723	-16.10306779	0.703337853	-19.44946347
-18.86550321	-18.75842862	0.048594437	-19.61054507
-19.13180282	-19.08086749	0.020784657	-19.72419128
-19.33358387	-19.33317419	0.000919775	-19.81362292
-16.0442555	-15.51785275	0.171708617	-19.26769793
-18.42519927	-15.90280171	1.014711408	-19.53106662

-18.88301722	-16.4249762	0.693969317	-19.75100232
-19.06766167	-19.04624755	0.047270301	-19.91721822
-19.43632436	-19.3680664	0.020136284	-20.02715407
-19.61737622	-19.61598727	0.00092547	-20.1164578
-16.31931647	-15.82877686	0.163113818	-19.5342648
-18.69330483	-16.20139631	0.996858217	-19.80629673
-19.15266615	-16.68206614	0.698322044	-20.02956479
-19.39907452	-19.31277524	0.047709569	-20.19426812
-19.69977202	-19.63207223	0.02020936	-20.30918394
-19.88042324	-19.87874883	0.000848953	-20.39666073
-14.05268909	-13.654842	0.378404697	-16.30438438
-15.5822776	-14.15577391	0.461390858	-16.65526593
-15.94676375	-15.46918581	0.162717728	-16.85414193
-16.37762328	-16.11189186	0.084042058	-16.99458781
-16.65211868	-16.53864856	0.044020858	-17.09475584
-16.95971331	-16.95859152	0.000426495	-17.16952746
-14.35875807	-14.05377526	0.593430029	-17.4848749
-16.70391426	-14.53084835	0.773979181	-17.84651136
-17.05822444	-16.60690059	0.158112334	-18.05541962
-17.47150881	-17.20832619	0.082540036	-18.20369076
-17.77966959	-17.62796852	0.041867251	-18.31009029
-18.0282348	-18.02797036	0.000649957	-18.3889366
-14.75169188	-14.40768998	0.674642528	-18.1164402
-17.32424456	-14.87904787	0.879716039	-18.47837426
-17.66300984	-17.21513461	0.158310046	-18.69180068
-18.06660029	-17.80916425	0.080025297	-18.84439375
-18.36860392	-18.22159404	0.040325351	-18.95231246
-18.60858648	-18.60839455	0.000570504	-19.03315645
-15.0767363	-14.71764756	0.698483159	-18.54459929
-17.7325842	-15.22974242	0.909344797	-18.91354407
-18.07389398	-17.65228368	0.156046707	-19.12481368
-18.47323698	-18.24198562	0.074436154	-19.27695583
-18.72758044	-18.62221308	0.040715034	-19.38617086

-19.00661364	-19.00628741	0.000743866	-19.46795814
-15.42248817	-15.0649797	0.70470095	-18.89059696
-18.06252624	-15.50346748	0.937935189	-19.25630997
-18.41099477	-17.98765216	0.153615706	-19.47096254
-18.807558	-18.56643817	0.075514486	-19.62253347
-19.05561893	-18.95207904	0.039734769	-19.73552692
-19.33083698	-19.32906428	0.000675303	-19.81608134
-15.70971489	-15.35057264	0.703314243	-19.19362125
-18.35959311	-15.85820857	0.920714381	-19.55840069
-18.70173543	-18.28321229	0.151364701	-19.77072014
-19.09447557	-18.86298789	0.072467668	-19.9255566
-19.34438059	-19.24110097	0.039465126	-20.03877355
-19.61460467	-19.61304112	0.000493333	-20.12274387
-16.00386562	-15.64717713	0.70091071	-19.46205756
-18.63006092	-16.14050564	0.907681521	-19.83736093
-18.96424571	-18.54722946	0.149146859	-20.05027342
-19.36826612	-19.12719656	0.074195697	-20.20433545
-19.60755902	-19.50245945	0.040140949	-20.31792716
-19.87678589	-19.87548599	0.000562863	-20.40081585
-15.13274411	-14.48967487	0.202786607	-16.12829808
-15.86256993	-15.70113819	0.045032088	-16.66157538
-16.2598711	-16.22431457	0.011477282	-16.87699491
-16.55570765	-16.53608313	0.007219723	-17.00922796
-16.78513367	-16.7839001	0.001453435	-17.10003731
-16.96070885	-16.95953216	0.000407238	-17.16686692
-16.23522703	-14.92027622	0.440985371	-17.27428107
-16.97761287	-16.8279169	0.0429646	-17.84347508
-17.36385125	-17.32988408	0.010687994	-18.07395199
-17.64543802	-17.62781181	0.006775025	-18.21703531
-17.86366318	-17.85984092	0.001323318	-18.31485146
-18.03056836	-18.02991778	0.000396185	-18.38689742
-16.8473723	-15.34347155	0.502137571	-17.90082368
-17.58184792	-17.43345292	0.042386516	-18.47439033

-17.95845698	-17.92760671	0.011424089	-18.71219827
-18.23090692	-18.22118406	0.006269036	-18.85713207
-18.44903032	-18.44492733	0.001418927	-18.95674385
-18.61175504	-18.61030599	0.000520177	-19.03087449
-17.26541857	-15.66574535	0.549877954	-18.31947685
-17.99317469	-17.85270095	0.041804702	-18.90431817
-18.36365401	-18.3407324	0.00979761	-19.14185818
-18.64218891	-18.62585679	0.00597207	-19.29019005
-18.85213825	-18.84660287	0.001721912	-19.39144616
-19.00979551	-19.00909533	0.000329698	-19.46737555
-17.60056166	-15.95132519	0.564140772	-18.66259665
-18.32844119	-18.19013336	0.041172972	-19.24673569
-18.70669491	-18.66829946	0.01157492	-19.48860198
-18.97191067	-18.95485704	0.006262026	-19.63764195
-19.17743182	-19.17378715	0.001320657	-19.73945401
-19.33256814	-19.33213443	0.000443007	-19.81612968
-17.89624416	-16.26059065	0.564484093	-18.96413019
-18.62636539	-18.48707025	0.041022879	-19.54982636
-18.98756764	-18.96176145	0.011275707	-19.78971359
-19.26142927	-19.24580385	0.005890364	-19.94179422
-19.46175557	-19.46020026	0.001117893	-20.04378353
-19.61626461	-19.61569678	0.00036684	-20.1204454
-18.17220698	-16.52276729	0.560174074	-19.2388129
-18.89308871	-18.7548601	0.040337474	-19.82039077
-19.26094728	-19.22927535	0.010986623	-20.06586024
-19.51801603	-19.51152543	0.006428041	-20.21912847
-19.7245552	-19.72399801	0.001338534	-20.32342527
-19.87884074	-19.87792836	0.000362754	-20.40092516

Mean log10 effective Kv [m2]	Mode log10 effective Kv [m2]	Maximum log10 effective Kv [m2]	Standard deviation log10 effective Kv [m2]
-16.15945118	-16.36138996	-15.76120645	0.191048565
-16.5666277	-16.62366398	-16.47607283	0.049135896
-16.79323451	-16.83157324	-16.7480067	0.026739234
-16.96835003	-16.98151587	-16.94204877	0.011280523
-17.0796065	-17.08264025	-17.06941719	0.005720839
-17.16437981	-17.16601763	-17.16290358	0.001074051
-17.33244035	-17.55396327	-16.86930286	0.211250988
-17.75804765	-17.82201933	-17.655997	0.053604552
-17.99214645	-18.03311333	-17.94752538	0.028857445
-18.17063317	-18.19060528	-18.14035622	0.015769818
-18.29115806	-18.29771018	-18.27923972	0.006659296
-18.38170203	-18.38335752	-18.37831284	0.001637218
-17.9633533	-18.1868622	-17.47862652	0.215676133
-18.39240234	-18.46055002	-18.29105758	0.056310601
-18.6269621	-18.59791584	-18.58593796	0.029395344
-18.80983891	-18.82938336	-18.77823638	0.015648003
-18.93271012	-18.94089118	-18.91787195	0.007553718
-19.02535942	-19.02824882	-19.02140913	0.002271701
-18.39155358	-18.60995735	-17.91062484	0.216127892
-18.82216379	-18.8847324	-18.71999333	0.055612184
-19.05935468	-19.10261101	-19.01774279	0.029769352
-19.24248882	-19.25714831	-19.21164776	0.016003725
-19.36667169	-19.37586751	-19.35241851	0.007527236
-19.46012435	-19.46286751	-19.45657146	0.002036315
-18.73461749	-18.9564334	-18.24125308	0.216272001
-19.16895944	-19.2328278	-19.06869624	0.056286727
-19.40651669	-19.3780856	-19.36618929	0.0306765
-19.58999344	-19.61054507	-19.55765352	0.016476851
-19.71538029	-19.72419128	-19.70136303	0.007695728
-19.80914268	-19.81021046	-19.80566052	0.002199893
-19.03517807	-19.26769793	-18.53319464	0.223032017
-19.46902916	-19.53106662	-19.36346597	0.056800207

-19.70802992	-19.67783871	-19.66564478	0.030410925
-19.89251686	-19.90928125	-19.8616594	0.016508309
-20.01844798	-20.02715407	-20.00484323	0.007583301
-20.11369025	-20.1164578	-20.10941692	0.002076745
-19.3118807	-19.5342648	-18.81343634	0.219693862
-19.7464933	-19.80629673	-19.63938387	0.057226132
-19.98539796	-19.95568314	-19.94336953	0.031022246
-20.17094067	-20.19426812	-20.13758833	0.017105567
-20.29783787	-20.30918394	-20.28422221	0.007941823
-20.39369439	-20.39666073	-20.38931855	0.00225755
-16.17065145	-16.16545292	-15.98021097	0.084836372
-16.59614827	-16.65526593	-16.43713163	0.058805805
-16.82896028	-16.84387846	-16.78229765	0.019284289
-16.98302595	-16.99458781	-16.95730638	0.010775011
-17.0904386	-17.08958241	-17.08570234	0.00274843
-17.16755955	-17.16727378	-17.16637231	0.000939382
-17.34339999	-17.33816754	-17.14255774	0.08890364
-17.78480756	-17.84651136	-17.61919924	0.060687001
-18.02847638	-18.04404095	-17.97576891	0.021244172
-18.1904854	-18.20369076	-18.16010483	0.012839443
-18.30467473	-18.31009029	-18.30028278	0.003783198
-18.38666439	-18.38658688	-18.38482459	0.00141478
-17.97269629	-17.96664804	-17.76692517	0.090584446
-18.41894086	-18.47837426	-18.25242895	0.061140872
-18.66445722	-18.68036912	-18.61177976	0.021655722
-18.82953376	-18.84439375	-18.79851821	0.013436925
-18.94626466	-18.95231246	-18.94011108	0.004062415
-19.03059952	-19.03315645	-19.0283253	0.001637211
-18.39994883	-18.39482162	-18.19511806	0.091127203
-18.84788969	-18.88038128	-18.68140456	0.061331396
-19.09628598	-19.11312352	-19.04298255	0.021372507
-19.26194696	-19.27695583	-19.23134192	0.013045424
-19.3807869	-19.38454965	-19.37482239	0.004134445

-19.46548903	-19.46795814	-19.46340495	0.001508448
-18.7436463	-18.74153185	-18.54277837	0.090068623
-19.19254	-19.22369373	-19.0279963	0.060976651
-19.44203544	-19.45914936	-19.38827032	0.0224433
-19.60934933	-19.62253347	-19.57798007	0.013070114
-19.72827209	-19.73161603	-19.72183881	0.004504743
-19.81428776	-19.81608134	-19.81147367	0.001357017
-19.04634325	-19.04612686	-18.84946767	0.089075473
-19.49438743	-19.52521939	-19.32613162	0.062094524
-19.74346547	-19.75960358	-19.69290421	0.021792256
-19.91170516	-19.9255566	-19.87923857	0.013611157
-20.03190366	-20.02948811	-20.02577394	0.004486036
-20.11867396	-20.11731687	-20.11641237	0.001956164
-19.32212451	-19.31228251	-19.11258245	0.09191033
-19.77216551	-19.83736093	-19.605095	0.061443007
-20.02135788	-20.03868139	-19.96912918	0.021778066
-20.19082616	-20.20433545	-20.1598437	0.013173538
-20.31140641	-20.30741834	-20.30566687	0.004626975
-20.39845842	-20.40081585	-20.39571993	0.001736039
-16.07780746	-16.12829808	-15.95812197	0.050429279
-16.64021428	-16.64642569	-16.60855146	0.014251386
-16.87096434	-16.87699491	-16.86344431	0.004172685
-17.00652179	-17.00661826	-17.00313867	0.001646002
-17.0987946	-17.10003731	-17.09683348	0.0008471
-17.16618425	-17.16570602	-17.16551254	0.000487148
-17.21877868	-17.27428107	-17.0818438	0.05719994
-17.82126921	-17.83442504	-17.78012482	0.017533993
-18.06698821	-18.06929572	-18.05765507	0.004696656
-18.21365238	-18.2159235	-18.20925263	0.001934143
-18.31300717	-18.31305234	-18.31170301	0.000845878
-18.38596191	-18.38660115	-18.38482353	0.000617631
-17.83763297	-17.90082368	-17.69644758	0.059693923
-18.45086307	-18.45628979	-18.41103845	0.017150683

-18.7027902	-18.70952677	-18.69349777	0.005526602
-18.85364375	-18.85413445	-18.85013762	0.001807314
-18.95534978	-18.95674385	-18.95387569	0.001034984
-19.03008048	-19.03087449	-19.0287622	0.000732371
-18.26122991	-18.31947685	-18.11951054	0.059477444
-18.87795776	-18.88584971	-18.83967856	0.0171971
-19.13354557	-19.14185818	-19.12373885	0.005439329
-19.28643208	-19.29019005	-19.28268407	0.002530959
-19.39004407	-19.39144616	-19.38762733	0.001239582
-19.46594312	-19.46614894	-19.46451347	0.000790119
-18.60301329	-18.66259665	-18.45725298	0.060521855
-19.22251138	-19.23757183	-19.18258868	0.017515177
-19.47964884	-19.48013279	-19.46884053	0.005419795
-19.63302478	-19.63200599	-19.6297516	0.00229871
-19.73817512	-19.73945401	-19.73649649	0.000992999
-19.81478073	-19.8150602	-19.81363423	0.000752734
-18.90135081	-18.96413019	-18.74968248	0.06269866
-19.52348518	-19.53045482	-19.48202597	0.018066181
-19.78120528	-19.78971359	-19.77001628	0.00547188
-19.93691853	-19.93934962	-19.93323814	0.00241552
-20.04215447	-20.04215199	-20.03997659	0.0009784
-20.11958875	-20.12016114	-20.11845558	0.000613242
-19.1781811	-19.2388129	-19.03781541	0.058881992
-19.79884898	-19.81138413	-19.7573443	0.017926707
-20.05875833	-20.06586024	-20.04958646	0.004992238
-20.21512961	-20.21428881	-20.21065906	0.002357522
-20.32180592	-20.32104979	-20.32065388	0.000915544
-20.39957441	-20.39973424	-20.39814635	0.000694047

Model ID	Well	Image type	Top [m]	Bottom [m]	Interval [m]	Structural class	Geostatistical anisotropy type	Effective stress [MPa]
Mod10	B24	Core	2085.39	2085.57	0.17	Minor slumped	Isotropic	1
Mod10	B24	Core	2085.39	2085.57	0.17	Minor slumped	Isotropic	1
Mod10	B24	Core	2085.39	2085.57	0.17	Minor slumped	Isotropic	1
Mod10	B24	Core	2085.39	2085.57	0.17	Minor slumped	Isotropic	1
Mod10	B24	Core	2085.39	2085.57	0.17	Minor slumped	Isotropic	1
Mod10	B24	Core	2085.39	2085.57	0.17	Minor slumped	Isotropic	1
Mod10	B24	Core	2085.39	2085.57	0.17	Minor slumped	Isotropic	5
Mod10	B24	Core	2085.39	2085.57	0.17	Minor slumped	Isotropic	5
Mod10	B24	Core	2085.39	2085.57	0.17	Minor slumped	Isotropic	5
Mod10	B24	Core	2085.39	2085.57	0.17	Minor slumped	Isotropic	5
Mod10	B24	Core	2085.39	2085.57	0.17	Minor slumped	Isotropic	5
Mod10	B24	Core	2085.39	2085.57	0.17	Minor slumped	Isotropic	5
Mod10	B24	Core	2085.39	2085.57	0.17	Minor slumped	Isotropic	10
Mod10	B24	Core	2085.39	2085.57	0.17	Minor slumped	Isotropic	10
Mod10	B24	Core	2085.39	2085.57	0.17	Minor slumped	Isotropic	10
Mod10	B24	Core	2085.39	2085.57	0.17	Minor slumped	Isotropic	10
Mod10	B24	Core	2085.39	2085.57	0.17	Minor slumped	Isotropic	10
Mod10	B24	Core	2085.39	2085.57	0.17	Minor slumped	Isotropic	10
Mod10	B24	Core	2085.39	2085.57	0.17	Minor slumped	Isotropic	15
Mod10	B24	Core	2085.39	2085.57	0.17	Minor slumped	Isotropic	15
Mod10	B24	Core	2085.39	2085.57	0.17	Minor slumped	Isotropic	15
Mod10	B24	Core	2085.39	2085.57	0.17	Minor slumped	Isotropic	15
Mod10	B24	Core	2085.39	2085.57	0.17	Minor slumped	Isotropic	15
Mod10	B24	Core	2085.39	2085.57	0.17	Minor slumped	Isotropic	15
Mod10	B24	Core	2085.39	2085.57	0.17	Minor slumped	Isotropic	20
Mod10	B24	Core	2085.39	2085.57	0.17	Minor slumped	Isotropic	20
Mod10	B24	Core	2085.39	2085.57	0.17	Minor slumped	Isotropic	20
Mod10	B24	Core	2085.39	2085.57	0.17	Minor slumped	Isotropic	20
Mod10	B24	Core	2085.39	2085.57	0.17	Minor slumped	Isotropic	20
Mod10	B24	Core	2085.39	2085.57	0.17	Minor slumped	Isotropic	20
Mod10	B24	Core	2085.39	2085.57	0.17	Minor slumped	Isotropic	25
Mod10	B24	Core	2085.39	2085.57	0.17	Minor slumped	Isotropic	25

Mod10	B24	Core	2085.39	2085.57	0.17	Minor slumped	Isotropic	25
Mod10	B24	Core	2085.39	2085.57	0.17	Minor slumped	Isotropic	25
Mod10	B24	Core	2085.39	2085.57	0.17	Minor slumped	Isotropic	25
Mod10	B24	Core	2085.39	2085.57	0.17	Minor slumped	Isotropic	25
Mod10	B24	Core	2085.39	2085.57	0.17	Minor slumped	Isotropic	30
Mod10	B24	Core	2085.39	2085.57	0.17	Minor slumped	Isotropic	30
Mod10	B24	Core	2085.39	2085.57	0.17	Minor slumped	Isotropic	30
Mod10	B24	Core	2085.39	2085.57	0.17	Minor slumped	Isotropic	30
Mod10	B24	Core	2085.39	2085.57	0.17	Minor slumped	Isotropic	30
Mod10	B24	Core	2085.39	2085.57	0.17	Minor slumped	Isotropic	30
Mod12	B20	Core	1651.26	1651.40	0.14	Minor slumped	Zonal, vertical	1
Mod12	B20	Core	1651.26	1651.40	0.14	Minor slumped	Zonal, vertical	1
Mod12	B20	Core	1651.26	1651.40	0.14	Minor slumped	Zonal, vertical	1
Mod12	B20	Core	1651.26	1651.40	0.14	Minor slumped	Zonal, vertical	1
Mod12	B20	Core	1651.26	1651.40	0.14	Minor slumped	Zonal, vertical	1
Mod12	B20	Core	1651.26	1651.40	0.14	Minor slumped	Zonal, vertical	1
Mod12	B20	Core	1651.26	1651.40	0.14	Minor slumped	Zonal, vertical	5
Mod12	B20	Core	1651.26	1651.40	0.14	Minor slumped	Zonal, vertical	5
Mod12	B20	Core	1651.26	1651.40	0.14	Minor slumped	Zonal, vertical	5
Mod12	B20	Core	1651.26	1651.40	0.14	Minor slumped	Zonal, vertical	5
Mod12	B20	Core	1651.26	1651.40	0.14	Minor slumped	Zonal, vertical	5
Mod12	B20	Core	1651.26	1651.40	0.14	Minor slumped	Zonal, vertical	5
Mod12	B20	Core	1651.26	1651.40	0.14	Minor slumped	Zonal, vertical	10
Mod12	B20	Core	1651.26	1651.40	0.14	Minor slumped	Zonal, vertical	10
Mod12	B20	Core	1651.26	1651.40	0.14	Minor slumped	Zonal, vertical	10
Mod12	B20	Core	1651.26	1651.40	0.14	Minor slumped	Zonal, vertical	10
Mod12	B20	Core	1651.26	1651.40	0.14	Minor slumped	Zonal, vertical	10
Mod12	B20	Core	1651.26	1651.40	0.14	Minor slumped	Zonal, vertical	10
Mod12	B20	Core	1651.26	1651.40	0.14	Minor slumped	Zonal, vertical	15
Mod12	B20	Core	1651.26	1651.40	0.14	Minor slumped	Zonal, vertical	15
Mod12	B20	Core	1651.26	1651.40	0.14	Minor slumped	Zonal, vertical	15
Mod12	B20	Core	1651.26	1651.40	0.14	Minor slumped	Zonal, vertical	15
Mod12	B20	Core	1651.26	1651.40	0.14	Minor slumped	Zonal, vertical	15

Mod12	B20	Core	1651.26	1651.40	0.14	Minor slumped	Zonal, vertical	15
Mod12	B20	Core	1651.26	1651.40	0.14	Minor slumped	Zonal, vertical	20
Mod12	B20	Core	1651.26	1651.40	0.14	Minor slumped	Zonal, vertical	20
Mod12	B20	Core	1651.26	1651.40	0.14	Minor slumped	Zonal, vertical	20
Mod12	B20	Core	1651.26	1651.40	0.14	Minor slumped	Zonal, vertical	20
Mod12	B20	Core	1651.26	1651.40	0.14	Minor slumped	Zonal, vertical	20
Mod12	B20	Core	1651.26	1651.40	0.14	Minor slumped	Zonal, vertical	20
Mod12	B20	Core	1651.26	1651.40	0.14	Minor slumped	Zonal, vertical	25
Mod12	B20	Core	1651.26	1651.40	0.14	Minor slumped	Zonal, vertical	25
Mod12	B20	Core	1651.26	1651.40	0.14	Minor slumped	Zonal, vertical	25
Mod12	B20	Core	1651.26	1651.40	0.14	Minor slumped	Zonal, vertical	25
Mod12	B20	Core	1651.26	1651.40	0.14	Minor slumped	Zonal, vertical	25
Mod12	B20	Core	1651.26	1651.40	0.14	Minor slumped	Zonal, vertical	25
Mod12	B20	Core	1651.26	1651.40	0.14	Minor slumped	Zonal, vertical	30
Mod12	B20	Core	1651.26	1651.40	0.14	Minor slumped	Zonal, vertical	30
Mod12	B20	Core	1651.26	1651.40	0.14	Minor slumped	Zonal, vertical	30
Mod12	B20	Core	1651.26	1651.40	0.14	Minor slumped	Zonal, vertical	30
Mod12	B20	Core	1651.26	1651.40	0.14	Minor slumped	Zonal, vertical	30
Mod12	B20	Core	1651.26	1651.40	0.14	Minor slumped	Zonal, vertical	30
Mod14	B6	FMI	1589.00	1590.70	1.70	Minor slumped	Zonal, horizontal	1
Mod14	B6	FMI	1589.00	1590.70	1.70	Minor slumped	Zonal, horizontal	1
Mod14	B6	FMI	1589.00	1590.70	1.70	Minor slumped	Zonal, horizontal	1
Mod14	B6	FMI	1589.00	1590.70	1.70	Minor slumped	Zonal, horizontal	1
Mod14	B6	FMI	1589.00	1590.70	1.70	Minor slumped	Zonal, horizontal	1
Mod14	B6	FMI	1589.00	1590.70	1.70	Minor slumped	Zonal, horizontal	1
Mod14	B6	FMI	1589.00	1590.70	1.70	Minor slumped	Zonal, horizontal	5
Mod14	B6	FMI	1589.00	1590.70	1.70	Minor slumped	Zonal, horizontal	5
Mod14	B6	FMI	1589.00	1590.70	1.70	Minor slumped	Zonal, horizontal	5
Mod14	B6	FMI	1589.00	1590.70	1.70	Minor slumped	Zonal, horizontal	5
Mod14	B6	FMI	1589.00	1590.70	1.70	Minor slumped	Zonal, horizontal	5
Mod14	B6	FMI	1589.00	1590.70	1.70	Minor slumped	Zonal, horizontal	5
Mod14	B6	FMI	1589.00	1590.70	1.70	Minor slumped	Zonal, horizontal	10
Mod14	B6	FMI	1589.00	1590.70	1.70	Minor slumped	Zonal, horizontal	10

Mod14	B6	FMI	1589.00	1590.70	1.70	Minor slumped	Zonal, horizontal	10
Mod14	B6	FMI	1589.00	1590.70	1.70	Minor slumped	Zonal, horizontal	10
Mod14	B6	FMI	1589.00	1590.70	1.70	Minor slumped	Zonal, horizontal	10
Mod14	B6	FMI	1589.00	1590.70	1.70	Minor slumped	Zonal, horizontal	10
Mod14	B6	FMI	1589.00	1590.70	1.70	Minor slumped	Zonal, horizontal	15
Mod14	B6	FMI	1589.00	1590.70	1.70	Minor slumped	Zonal, horizontal	15
Mod14	B6	FMI	1589.00	1590.70	1.70	Minor slumped	Zonal, horizontal	15
Mod14	B6	FMI	1589.00	1590.70	1.70	Minor slumped	Zonal, horizontal	15
Mod14	B6	FMI	1589.00	1590.70	1.70	Minor slumped	Zonal, horizontal	15
Mod14	B6	FMI	1589.00	1590.70	1.70	Minor slumped	Zonal, horizontal	15
Mod14	B6	FMI	1589.00	1590.70	1.70	Minor slumped	Zonal, horizontal	20
Mod14	B6	FMI	1589.00	1590.70	1.70	Minor slumped	Zonal, horizontal	20
Mod14	B6	FMI	1589.00	1590.70	1.70	Minor slumped	Zonal, horizontal	20
Mod14	B6	FMI	1589.00	1590.70	1.70	Minor slumped	Zonal, horizontal	20
Mod14	B6	FMI	1589.00	1590.70	1.70	Minor slumped	Zonal, horizontal	20
Mod14	B6	FMI	1589.00	1590.70	1.70	Minor slumped	Zonal, horizontal	20
Mod14	B6	FMI	1589.00	1590.70	1.70	Minor slumped	Zonal, horizontal	25
Mod14	B6	FMI	1589.00	1590.70	1.70	Minor slumped	Zonal, horizontal	25
Mod14	B6	FMI	1589.00	1590.70	1.70	Minor slumped	Zonal, horizontal	25
Mod14	B6	FMI	1589.00	1590.70	1.70	Minor slumped	Zonal, horizontal	25
Mod14	B6	FMI	1589.00	1590.70	1.70	Minor slumped	Zonal, horizontal	25
Mod14	B6	FMI	1589.00	1590.70	1.70	Minor slumped	Zonal, horizontal	25
Mod14	B6	FMI	1589.00	1590.70	1.70	Minor slumped	Zonal, horizontal	30
Mod14	B6	FMI	1589.00	1590.70	1.70	Minor slumped	Zonal, horizontal	30
Mod14	B6	FMI	1589.00	1590.70	1.70	Minor slumped	Zonal, horizontal	30
Mod14	B6	FMI	1589.00	1590.70	1.70	Minor slumped	Zonal, horizontal	30
Mod14	B6	FMI	1589.00	1590.70	1.70	Minor slumped	Zonal, horizontal	30
Mod14	B6	FMI	1589.00	1590.70	1.70	Minor slumped	Zonal, horizontal	30

Mud content [%]	Mean cohesive content [%]	Mean porosity [fraction]	Minimum log10 effective Kh [m2]	Mean log10 effective Kh [m2]
50	39.18235161	0.413802247	-15.40877952	-15.21158402
60	46.01881599	0.431459095	-16.03106198	-15.92268052
70	52.85528036	0.449078125	-16.38434975	-16.34190715
80	59.69174474	0.466694593	-16.63571548	-16.61536338
90	66.52820912	0.484341387	-16.82330115	-16.81791083
100	73.36467349	0.501993809	-16.96461429	-16.96411949
50	39.18235161	0.332828491	-16.50486656	-16.24920225
60	46.01881599	0.342467621	-17.14050984	-17.03165569
70	52.85528036	0.352034818	-17.48458187	-17.4430227
80	59.69174474	0.361563306	-17.72356577	-17.70486696
90	66.52820912	0.371087358	-17.9007131	-17.89579975
100	73.36467349	0.380635792	-18.03765056	-18.03681375
50	39.18235161	0.283339567	-17.10791932	-16.82548118
60	46.01881599	0.288072656	-17.7468147	-17.63567789
70	52.85528036	0.292762029	-18.07848103	-18.03866893
80	59.69174474	0.297470927	-18.31452429	-18.29496584
90	66.52820912	0.302157266	-18.48580301	-18.48061741
100	73.36467349	0.30693036	-18.61848783	-18.61780375
50	39.18235161	0.247519143	-17.51852584	-17.22429937
60	46.01881599	0.248906083	-18.15235147	-18.0471433
70	52.85528036	0.250278667	-18.48464683	-18.44694577
80	59.69174474	0.251730685	-18.71865751	-18.69999015
90	66.52820912	0.253075908	-18.88740505	-18.88170465
100	73.36467349	0.254488904	-19.01646482	-19.01575544
50	39.18235161	0.218018388	-17.86076654	-17.55924054
60	46.01881599	0.216775648	-18.48649474	-18.38069596
70	52.85528036	0.215602182	-18.81506736	-18.77782082
80	59.69174474	0.214312066	-19.04586366	-19.02713862
90	66.52820912	0.21314987	-19.21200637	-19.20702155
100	73.36467349	0.211897801	-19.33894871	-19.33830832
50	39.18235161	0.192387426	-18.15972637	-17.85862285
60	46.01881599	0.188921885	-18.77734855	-18.67275253

70	52.85528036	0.185451784	-19.10578643	-19.06798719
80	59.69174474	0.182027125	-19.33292453	-19.31476891
90	66.52820912	0.178525055	-19.49727116	-19.49181354
100	73.36467349	0.175036891	-19.62184384	-19.62124442
50	39.18235161	0.169499818	-18.42216481	-18.13005813
60	46.01881599	0.164022691	-19.0441228	-18.94132291
70	52.85528036	0.158555981	-19.36982545	-19.33528743
80	59.69174474	0.153044901	-19.59571891	-19.57985564
90	66.52820912	0.147588638	-19.76005769	-19.75580184
100	73.36467349	0.142071938	-19.88485232	-19.88362369
50	39.18235161	0.413724308	-16.20274908	-15.9665126
60	46.01881599	0.431415884	-16.43635282	-16.35665588
70	52.85528036	0.449039161	-16.63788147	-16.60880105
80	59.69174474	0.466694559	-16.78839362	-16.77392904
90	66.52820912	0.484418786	-16.89575879	-16.89062816
100	73.36467349	0.502023488	-16.97502613	-16.9738416
50	39.18235161	0.332899377	-17.29578769	-17.05190724
60	46.01881599	0.342442507	-17.53227353	-17.44568374
70	52.85528036	0.351987915	-17.72682504	-17.69623069
80	59.69174474	0.361559386	-17.87046478	-17.85727394
90	66.52820912	0.371103484	-17.97616339	-17.97003805
100	73.36467349	0.380630564	-18.05262216	-18.05108297
50	39.18235161	0.283303007	-17.88953824	-17.63997817
60	46.01881599	0.288052148	-18.11725126	-18.03492702
70	52.85528036	0.292812515	-18.31374458	-18.2828485
80	59.69174474	0.297491212	-18.4525022	-18.44097596
90	66.52820912	0.302248474	-18.55754532	-18.55180072
100	73.36467349	0.306971097	-18.6331439	-18.63156187
50	39.18235161	0.247484165	-18.28832856	-18.04430977
60	46.01881599	0.248928568	-18.52066227	-18.43696171
70	52.85528036	0.250322648	-18.713876	-18.68378845
80	59.69174474	0.251744943	-18.85367968	-18.84058386
90	66.52820912	0.253127423	-18.95518987	-18.94984408

100	73.36467349	0.254514306	-19.02956153	-19.02842363
50	39.18235161	0.217983979	-18.61394001	-18.37188183
60	46.01881599	0.216823348	-18.84487053	-18.76261205
70	52.85528036	0.215584172	-19.03742564	-19.00785261
80	59.69174474	0.214335589	-19.17578367	-19.16348388
90	66.52820912	0.213109378	-19.27679973	-19.27170526
100	73.36467349	0.211834122	-19.35095347	-19.34934939
50	39.18235161	0.192384694	-18.89941581	-18.66055223
60	46.01881599	0.188966767	-19.12899248	-19.04954483
70	52.85528036	0.185459198	-19.32112941	-19.29285689
80	59.69174474	0.182019482	-19.45972685	-19.44736539
90	66.52820912	0.178537255	-19.55933961	-19.55470276
100	73.36467349	0.175053876	-19.63315696	-19.63194539
50	39.18235161	0.16948369	-19.1661163	-18.92414156
60	46.01881599	0.164009878	-19.392987	-19.31267304
70	52.85528036	0.158552913	-19.58286391	-19.55620162
80	59.69174474	0.153068079	-19.72147046	-19.71019249
90	66.52820912	0.147583628	-19.8208304	-19.81684121
100	73.36467349	0.142058511	-19.89399279	-19.89335709
50	39.18235161	0.413671008	-13.19902187	-13.08798089
60	46.01881599	0.431439034	-13.39616196	-13.27634815
70	52.85528036	0.449049765	-13.94348009	-13.53992291
80	59.69174474	0.466705307	-16.26835323	-14.05918689
90	66.52820912	0.484375807	-16.70080442	-16.25382683
100	73.36467349	0.501978948	-16.95912483	-16.95625741
50	39.18235161	0.332961984	-13.54666637	-13.43971296
60	46.01881599	0.342410568	-13.77491827	-13.62892127
70	52.85528036	0.351968052	-14.34129715	-13.89400849
80	59.69174474	0.361524959	-17.33467047	-14.5053839
90	66.52820912	0.371089343	-17.76362651	-17.2478039
100	73.36467349	0.380653233	-18.02641268	-18.02317862
50	39.18235161	0.283321068	-13.9082592	-13.80290163
60	46.01881599	0.288050741	-14.14069054	-13.99211686

70	52.85528036	0.292799392	-14.6855513	-14.25851753
80	59.69174474	0.29748163	-17.91821358	-14.87695771
90	66.52820912	0.302242431	-18.34764341	-17.81641006
100	73.36467349	0.306848906	-18.60685843	-18.6031006
50	39.18235161	0.247491943	-14.24997245	-14.14256353
60	46.01881599	0.248906749	-14.48581099	-14.33325077
70	52.85528036	0.250323419	-15.03809552	-14.59841159
80	59.69174474	0.251713957	-18.32673666	-15.22046958
90	66.52820912	0.253142114	-18.75014641	-18.21327174
100	73.36467349	0.254511694	-19.0058294	-19.00203614
50	39.18235161	0.217971751	-14.5794238	-14.47018116
60	46.01881599	0.216775028	-14.79060296	-14.65621768
70	52.85528036	0.215561767	-15.35761166	-14.92612929
80	59.69174474	0.214330747	-18.65514224	-15.53935371
90	66.52820912	0.213110566	-19.07739909	-18.53928008
100	73.36467349	0.211863217	-19.32834128	-19.32507637
50	39.18235161	0.192382411	-14.89868262	-14.78515906
60	46.01881599	0.188898254	-15.10249992	-14.97466446
70	52.85528036	0.185451283	-15.64892103	-15.23735266
80	59.69174474	0.182001983	-18.94705609	-15.84236932
90	66.52820912	0.1785101	-19.36381612	-18.82731872
100	73.36467349	0.175034304	-19.61231659	-19.60905754
50	39.18235161	0.169481386	-15.20811575	-15.0922396
60	46.01881599	0.164016706	-15.40081476	-15.2807021
70	52.85528036	0.158519097	-15.94188918	-15.54282361
80	59.69174474	0.15304611	-19.20757819	-16.13872551
90	66.52820912	0.147583205	-19.62668333	-19.09537776
100	73.36467349	0.142064175	-19.87476604	-19.87174209

Mode log10 effective Kh [m2]	Maximum log10 effective Kh [m2]	Standard deviation log10 effective Kh [m2]	Minimum log10 effective Kv [m2]
-15.40877952	-14.59254451	0.239803153	-16.06532585
-15.94538841	-15.73120447	0.087886064	-16.52825076
-16.38434975	-16.29602976	0.026862963	-16.77474759
-16.61603846	-16.6012807	0.008964459	-16.95634305
-16.82043985	-16.81328658	0.003198311	-17.07739701
-16.96419444	-16.96363464	0.00028977	-17.16157597
-16.50486656	-15.20782691	0.374265692	-17.20578182
-17.0520664	-16.83095778	0.089566445	-17.69920893
-17.48458187	-17.3968892	0.027265245	-17.95992404
-17.70529105	-17.691585	0.008300139	-18.14995754
-17.89332619	-17.89209504	0.002929419	-18.28387808
-18.0367647	-18.03610031	0.000442109	-18.37659977
-17.10791932	-15.48570599	0.467812595	-17.8255593
-17.65992919	-17.44271542	0.087801673	-18.32300934
-18.07848103	-17.99669029	0.026580654	-18.58730767
-18.29572491	-18.28162538	0.008584833	-18.78627511
-18.47845793	-18.47723375	0.002826138	-18.92226882
-18.61764389	-18.61701094	0.000454082	-19.01961162
-17.51852584	-15.74974838	0.511670239	-18.25117418
-18.06800754	-17.8571477	0.086431781	-18.74601056
-18.48464683	-18.40582742	0.025302211	-19.01673013
-18.70498688	-18.68675937	0.008315553	-19.21627146
-18.87998794	-18.87702109	0.003145188	-19.35485687
-19.01624001	-19.01489117	0.000432724	-19.45330067
-17.86076654	-16.08366346	0.511826894	-18.58924975
-18.40125347	-18.1881503	0.086146841	-19.08849563
-18.78140631	-18.7365249	0.024554451	-19.36080746
-19.02766787	-19.01402102	0.008184896	-19.55916331
-19.20949569	-19.20321898	0.002775786	-19.70375395
-19.33799856	-19.33784021	0.000372465	-19.80318846
-18.15972637	-16.43052192	0.496507994	-18.88255635
-18.69437914	-18.48695562	0.085616138	-19.38880475

-19.10578643	-19.02928501	0.024247237	-19.65982368
-19.31648736	-19.30415948	0.007617596	-19.86315899
-19.49457543	-19.48783611	0.002694378	-20.00607464
-19.62114251	-19.62061652	0.000355653	-20.10635473
-18.42216481	-16.70292484	0.495208084	-19.15261245
-19.0016852	-18.74705963	0.08642561	-19.66568702
-19.36982545	-19.29601087	0.023888793	-19.93658782
-19.57998403	-19.56818288	0.007119874	-20.14114412
-19.75365173	-19.75258407	0.002500277	-20.28687082
-19.88375251	-19.88292766	0.000495523	-20.38626386
-16.11221418	-15.56900474	0.197742417	-15.53616671
-16.43635282	-16.1174988	0.091290711	-16.18810475
-16.62272662	-16.53179746	0.029456626	-16.55710182
-16.77832036	-16.7531372	0.010366843	-16.82939509
-16.89266835	-16.88494228	0.002936377	-17.01862134
-16.97436249	-16.97270341	0.000638179	-17.14956882
-17.20144046	-16.63535709	0.208488773	-16.6549813
-17.53227353	-17.19708062	0.095116614	-17.32720506
-17.71108006	-17.61661016	0.030389892	-17.70517458
-17.86552271	-17.8358703	0.010049152	-18.00263939
-17.97231244	-17.96268508	0.003384566	-18.20448077
-18.05105136	-18.04895697	0.000906559	-18.35420746
-17.79392356	-17.22023545	0.210488472	-17.25396473
-18.11725126	-17.78519852	0.094014997	-17.93442402
-18.2981951	-18.20489824	0.029786932	-18.32895126
-18.44783397	-18.41982457	0.009837792	-18.62465102
-18.55399743	-18.54512771	0.003147471	-18.83836851
-18.6331439	-18.6295998	0.001112542	-18.99396633
-18.19378523	-17.62652525	0.208887622	-17.66697009
-18.52066227	-18.18999545	0.093649913	-18.35605803
-18.69823648	-18.60439931	0.029976546	-18.75300438
-18.84887326	-18.82003479	0.009691882	-19.05171421
-18.95157433	-18.9425355	0.003206975	-19.26767782

-19.02904745	-19.02596293	0.001001192	-19.42723292
-18.51969199	-17.95420386	0.207960658	-18.00288983
-18.84487053	-18.51491771	0.093172002	-18.68959348
-19.02218311	-18.93072791	0.029268517	-19.09327556
-19.17126582	-19.14415873	0.009391624	-19.39645617
-19.27323696	-19.26433005	0.003142401	-19.61350817
-19.34945987	-19.34746841	0.00088827	-19.77511747
-18.80617185	-18.2467081	0.205100115	-18.29487556
-19.12899248	-18.80419718	0.091972883	-18.99242717
-19.30643753	-19.21828626	0.028195491	-19.3913745
-19.45533375	-19.42897517	0.008841095	-19.69582626
-19.55626908	-19.54859278	0.002853968	-19.9164723
-19.63278194	-19.63053181	0.000751683	-20.08085912
-19.07239795	-18.5100879	0.206917888	-18.56327298
-19.392987	-19.06667522	0.092423009	-19.24785241
-19.56852536	-19.482494	0.028011305	-19.66200394
-19.71706098	-19.69060407	0.008944421	-19.97052694
-19.81938971	-19.81074557	0.002671788	-20.19392183
-19.89399279	-19.89138424	0.000809088	-20.35847632
-13.11062767	-12.99276873	0.061348938	-16.76625024
-13.39616196	-13.12230622	0.086741255	-16.86929001
-13.52990146	-13.36447001	0.151560091	-16.97162398
-13.96875869	-13.58549293	0.75330849	-17.05140856
-16.70080442	-14.20794397	0.694432668	-17.11557851
-16.95641783	-16.95438759	0.001296483	-17.17769263
-13.54666637	-13.34013892	0.062402309	-18.00091559
-13.73208603	-13.47509263	0.086979406	-18.09252468
-13.88396438	-13.70103127	0.16632857	-18.200827
-14.40370376	-13.91520931	0.963115952	-18.2789705
-17.76362651	-14.59483812	0.89410655	-18.34151067
-18.0225918	-18.01972613	0.001886201	-18.40421728
-13.9082592	-13.70225699	0.062449516	-18.64807234
-14.01280565	-13.84229246	0.085636605	-18.74046585

-14.24011346	-14.06193833	0.161118212	-18.8476719
-14.80456764	-14.28562665	1.026986214	-18.92484006
-18.34764341	-15.0054884	0.946038754	-18.99044713
-18.60362268	-18.59930835	0.002201631	-19.0513807
-14.16288262	-14.04676284	0.060745763	-19.08319402
-14.35451024	-14.17944258	0.089505337	-19.17721754
-14.58227885	-14.39995219	0.165535504	-19.28327566
-15.14809851	-14.61832548	1.05017553	-19.3627475
-18.75014641	-15.32994535	0.969787176	-19.42469089
-19.0016164	-18.99845666	0.002044513	-19.48765186
-14.5794238	-14.36808769	0.061583196	-19.43228801
-14.79060296	-14.50565336	0.087399362	-19.52531909
-14.91676592	-14.74042762	0.160192447	-19.63267017
-15.4844098	-14.95595439	1.050802577	-19.71003221
-19.07739909	-15.62548077	0.979759194	-19.77419467
-19.32445529	-19.32154081	0.001943511	-19.83606081
-14.80718549	-14.68518932	0.062821595	-19.73405071
-15.10249992	-14.81455418	0.088013183	-19.83132283
-15.22385764	-15.05383228	0.155376936	-19.93589783
-15.79997403	-15.27546036	1.045130464	-20.01742577
-19.36381612	-15.9084491	0.981283973	-20.0791465
-19.60874839	-19.60607224	0.001893242	-20.14071756
-15.20811575	-14.98972549	0.063945416	-20.01465887
-15.40081476	-15.1188728	0.089101245	-20.1092605
-15.53369194	-15.37041305	0.149420946	-20.21621787
-16.09984492	-15.58188938	1.033269079	-20.29594391
-19.62668333	-16.19661732	0.974476328	-20.35984664
-19.87217964	-19.86873109	0.001707535	-20.42142955

Mean log10 effective Kv [m2]	Mode log10 effective Kv [m2]	Maximum log10 effective Kv [m2]	Standard deviation log10 effective Kv [m2]
-15.89510222	-16.01316077	-15.70017031	0.100044058
-16.46937951	-16.48805446	-16.38756372	0.037413481
-16.76188493	-16.77038873	-16.74423557	0.010119916
-16.94714881	-16.94942379	-16.94019811	0.004771688
-17.07441961	-17.0762558	-17.06940853	0.002425902
-17.16089865	-17.16116713	-17.16014502	0.00040866
-17.02441204	-17.03169962	-16.79959004	0.109910153
-17.63606499	-17.6579214	-17.55470256	0.038228694
-17.94358824	-17.93241573	-17.92783101	0.011028687
-18.14160625	-18.1475235	-18.13291925	0.005181605
-18.27960365	-18.28237293	-18.27334206	0.002829338
-18.37502954	-18.37551386	-18.37279908	0.001027616
-17.63957215	-17.64239582	-17.39817785	0.115001087
-18.25953139	-18.2812844	-18.17697203	0.038174224
-18.57248502	-18.58730767	-18.55727572	0.010868194
-18.77536784	-18.77763544	-18.76611589	0.005538125
-18.91831624	-18.92085944	-18.91240313	0.002920906
-19.01780422	-19.01961162	-19.01623664	0.001135107
-18.06255226	-18.06936789	-17.82695949	0.112350105
-18.68227014	-18.70323014	-18.59627909	0.040365291
-18.9988119	-18.98563434	-18.98045171	0.012539689
-19.2065411	-19.20752306	-19.19585852	0.005973132
-19.35176482	-19.35485687	-19.34648359	0.0026492
-19.45228155	-19.45330067	-19.45084341	0.000746302
-18.3994389	-18.5291433	-18.16850456	0.113854257
-19.02418171	-19.04597255	-18.93966485	0.039776662
-19.34423635	-19.33166632	-19.32680947	0.011522237
-19.55175258	-19.55916331	-19.54192597	0.005466588
-19.69971552	-19.7022652	-19.69333269	0.003048029
-19.80151818	-19.80318846	-19.7993273	0.001245293
-18.6998979	-18.70456276	-18.46723798	0.111748621
-19.32340689	-19.34589339	-19.23861499	0.039998466

-19.64333947	-19.62995499	-19.62497687	0.012302023
-19.8540854	-19.86040587	-19.84388718	0.005562006
-20.00227261	-20.00607464	-19.9961734	0.003208588
-20.10508973	-20.10552373	-20.10344623	0.000875258
-18.97038803	-18.97411477	-18.73611786	0.114399922
-19.59806455	-19.64438045	-19.51654108	0.039622534
-19.92011722	-19.90683454	-19.90187566	0.011895839
-20.13141971	-20.13341639	-20.12311275	0.00549481
-20.28155256	-20.28344748	-20.27488912	0.003098226
-20.38502124	-20.38594158	-20.38400789	0.000764362
-14.8799436	-15.53616671	-13.82696241	0.5889723
-15.78379318	-16.18810475	-14.44996498	0.490162509
-16.38943821	-16.44227606	-16.15521166	0.127937803
-16.73647068	-16.82939509	-16.61568064	0.066125315
-16.98082127	-16.99073877	-16.92103233	0.027428236
-17.14661572	-17.14570697	-17.14506332	0.001547406
-15.67876039	-16.6549813	-14.19607743	0.916052114
-16.82918838	-17.32720506	-14.8236222	0.701051257
-17.52439665	-17.58147946	-17.27224165	0.136584525
-17.89019467	-17.92977611	-17.74761791	0.077266586
-18.15765049	-18.17126612	-18.08822948	0.033069682
-18.34827325	-18.34657325	-18.34530089	0.002868493
-16.19260033	-17.25396473	-14.58405225	1.018909023
-17.3998543	-17.93442402	-15.10066767	0.797331163
-18.13656906	-18.19588043	-17.86320336	0.143132947
-18.51033175	-18.62465102	-18.35712512	0.080490279
-18.78680037	-18.80276455	-18.71375467	0.035257058
-18.98757955	-18.98679921	-18.98393237	0.002840363
-16.56784015	-17.66697009	-14.88814628	1.057763241
-17.8121329	-18.35605803	-15.49535247	0.803613686
-18.55536166	-18.6211834	-18.29163095	0.142419382
-18.93330193	-19.05171421	-18.77704434	0.081409423
-19.21493122	-19.23118508	-19.13995322	0.036128585

-19.42072432	-19.4211275	-19.41654843	0.002902938
-16.88538502	-18.00288983	-15.21283648	1.071072272
-18.14458587	-18.68959348	-15.802127	0.812026292
-18.89279798	-18.96035388	-18.62804966	0.145570093
-19.27516344	-19.31784591	-19.12132026	0.082154991
-19.55974962	-19.57620338	-19.48294141	0.036966709
-19.76845062	-19.7681885	-19.76541692	0.00305002
-17.1859518	-18.29487556	-15.51391539	1.064167677
-18.44044121	-18.99242717	-16.11209758	0.808319793
-19.18805434	-19.25616511	-18.91814163	0.146793617
-19.57364549	-19.61529976	-19.4139835	0.082137102
-19.86108643	-19.87774569	-19.78092918	0.03787966
-20.07292704	-20.07268668	-20.0694177	0.003286673
-17.45453596	-18.56327298	-15.82765691	1.063137468
-18.70803956	-19.24785241	-16.37869906	0.808892982
-19.46028317	-19.66200394	-19.18679409	0.147834221
-19.84689101	-19.89037504	-19.68999531	0.083300162
-20.13788998	-20.15580436	-20.0605107	0.037948072
-20.35170551	-20.35078273	-20.3477053	0.003075351
-16.66433652	-16.76625024	-16.3776554	0.111934442
-16.80144599	-16.86929001	-16.68267643	0.06542545
-16.92161963	-16.97162398	-16.86233579	0.034944172
-17.02289167	-17.04152505	-16.98222398	0.023702166
-17.10435258	-17.11557851	-17.08187316	0.009810134
-17.17286526	-17.17622578	-17.16742467	0.003052733
-17.89347005	-18.00091559	-17.60228762	0.114135544
-18.02399045	-18.09252468	-17.89383291	0.070978119
-18.14286932	-18.16268817	-18.06734109	0.04093338
-18.24339811	-18.26663315	-18.19260908	0.029318406
-18.32620347	-18.33498911	-18.29585978	0.014278952
-18.39660474	-18.39863378	-18.38467502	0.00556663
-18.53691072	-18.64807234	-18.24639932	0.115001469
-18.6680138	-18.74046585	-18.53529738	0.0729928

-18.78730063	-18.8476719	-18.70465285	0.043392437
-18.88765419	-18.91168738	-18.83277131	0.030357724
-18.9713592	-18.97598327	-18.93982363	0.015601212
-19.04132416	-19.04491774	-19.02876034	0.006193164
-18.97120706	-19.08319402	-18.67612321	0.116560551
-19.10195163	-19.17721754	-18.9659012	0.074298378
-19.22098657	-19.28327566	-19.13492032	0.045286418
-19.32244394	-19.33539826	-19.26702516	0.031238882
-19.4060957	-19.41712354	-19.3717194	0.016396008
-19.47779141	-19.48124065	-19.46521264	0.006555165
-19.32040088	-19.43228801	-19.02640345	0.115797364
-19.45023081	-19.52531909	-19.31487298	0.074699282
-19.56904737	-19.59003435	-19.4834448	0.045243707
-19.6707466	-19.6963637	-19.61435262	0.031573011
-19.75456958	-19.7666891	-19.72165574	0.016111906
-19.82660349	-19.82976071	-19.81401047	0.006383147
-19.62410443	-19.73405071	-19.33469675	0.114593279
-19.75316184	-19.83132283	-19.6130625	0.076596056
-19.87273511	-19.93589783	-19.78693936	0.045672029
-19.9740644	-19.98826905	-19.91537726	0.032742967
-20.05856023	-20.06419381	-20.02681209	0.016180762
-20.13066719	-20.13082986	-20.11764625	0.006562168
-19.90317335	-20.01465887	-19.61172114	0.115626316
-20.03318392	-20.1092605	-19.89419357	0.076606963
-20.15167846	-20.21621787	-20.0613302	0.047420102
-20.25382562	-20.26756313	-20.19661118	0.032894129
-20.33867115	-20.35172658	-20.30300618	0.017311942
-20.4107724	-20.41117192	-20.39749508	0.006829477

Model ID	Well	Image type	Top [m]	Bottom [m]	Interval [m]	Structural class	Geostatistical anisotropy type	Effective stress [MPa]
Mod15	B19	Core	1635.03	1635.49	0.46	Major Slumped	Isotropic	1
Mod15	B19	Core	1635.03	1635.49	0.46	Major Slumped	Isotropic	1
Mod15	B19	Core	1635.03	1635.49	0.46	Major Slumped	Isotropic	1
Mod15	B19	Core	1635.03	1635.49	0.46	Major Slumped	Isotropic	1
Mod15	B19	Core	1635.03	1635.49	0.46	Major Slumped	Isotropic	1
Mod15	B19	Core	1635.03	1635.49	0.46	Major Slumped	Isotropic	1
Mod15	B19	Core	1635.03	1635.49	0.46	Major Slumped	Isotropic	5
Mod15	B19	Core	1635.03	1635.49	0.46	Major Slumped	Isotropic	5
Mod15	B19	Core	1635.03	1635.49	0.46	Major Slumped	Isotropic	5
Mod15	B19	Core	1635.03	1635.49	0.46	Major Slumped	Isotropic	5
Mod15	B19	Core	1635.03	1635.49	0.46	Major Slumped	Isotropic	5
Mod15	B19	Core	1635.03	1635.49	0.46	Major Slumped	Isotropic	5
Mod15	B19	Core	1635.03	1635.49	0.46	Major Slumped	Isotropic	10
Mod15	B19	Core	1635.03	1635.49	0.46	Major Slumped	Isotropic	10
Mod15	B19	Core	1635.03	1635.49	0.46	Major Slumped	Isotropic	10
Mod15	B19	Core	1635.03	1635.49	0.46	Major Slumped	Isotropic	10
Mod15	B19	Core	1635.03	1635.49	0.46	Major Slumped	Isotropic	10
Mod15	B19	Core	1635.03	1635.49	0.46	Major Slumped	Isotropic	10
Mod15	B19	Core	1635.03	1635.49	0.46	Major Slumped	Isotropic	15
Mod15	B19	Core	1635.03	1635.49	0.46	Major Slumped	Isotropic	15
Mod15	B19	Core	1635.03	1635.49	0.46	Major Slumped	Isotropic	15
Mod15	B19	Core	1635.03	1635.49	0.46	Major Slumped	Isotropic	15
Mod15	B19	Core	1635.03	1635.49	0.46	Major Slumped	Isotropic	15
Mod15	B19	Core	1635.03	1635.49	0.46	Major Slumped	Isotropic	15
Mod15	B19	Core	1635.03	1635.49	0.46	Major Slumped	Isotropic	20
Mod15	B19	Core	1635.03	1635.49	0.46	Major Slumped	Isotropic	20
Mod15	B19	Core	1635.03	1635.49	0.46	Major Slumped	Isotropic	20
Mod15	B19	Core	1635.03	1635.49	0.46	Major Slumped	Isotropic	20
Mod15	B19	Core	1635.03	1635.49	0.46	Major Slumped	Isotropic	20
Mod15	B19	Core	1635.03	1635.49	0.46	Major Slumped	Isotropic	20
Mod15	B19	Core	1635.03	1635.49	0.46	Major Slumped	Isotropic	25
Mod15	B19	Core	1635.03	1635.49	0.46	Major Slumped	Isotropic	25

Mod15	B19	Core	1635.03	1635.49	0.46	Major Slumped	Isotropic	25
Mod15	B19	Core	1635.03	1635.49	0.46	Major Slumped	Isotropic	25
Mod15	B19	Core	1635.03	1635.49	0.46	Major Slumped	Isotropic	25
Mod15	B19	Core	1635.03	1635.49	0.46	Major Slumped	Isotropic	25
Mod15	B19	Core	1635.03	1635.49	0.46	Major Slumped	Isotropic	30
Mod15	B19	Core	1635.03	1635.49	0.46	Major Slumped	Isotropic	30
Mod15	B19	Core	1635.03	1635.49	0.46	Major Slumped	Isotropic	30
Mod15	B19	Core	1635.03	1635.49	0.46	Major Slumped	Isotropic	30
Mod15	B19	Core	1635.03	1635.49	0.46	Major Slumped	Isotropic	30
Mod15	B19	Core	1635.03	1635.49	0.46	Major Slumped	Isotropic	30
Mod16	B20	Core	1682.34	1682.52	0.17	Major Slumped	Zonal, horizontal	1
Mod16	B20	Core	1682.34	1682.52	0.17	Major Slumped	Zonal, horizontal	1
Mod16	B20	Core	1682.34	1682.52	0.17	Major Slumped	Zonal, horizontal	1
Mod16	B20	Core	1682.34	1682.52	0.17	Major Slumped	Zonal, horizontal	1
Mod16	B20	Core	1682.34	1682.52	0.17	Major Slumped	Zonal, horizontal	1
Mod16	B20	Core	1682.34	1682.52	0.17	Major Slumped	Zonal, horizontal	1
Mod16	B20	Core	1682.34	1682.52	0.17	Major Slumped	Zonal, horizontal	5
Mod16	B20	Core	1682.34	1682.52	0.17	Major Slumped	Zonal, horizontal	5
Mod16	B20	Core	1682.34	1682.52	0.17	Major Slumped	Zonal, horizontal	5
Mod16	B20	Core	1682.34	1682.52	0.17	Major Slumped	Zonal, horizontal	5
Mod16	B20	Core	1682.34	1682.52	0.17	Major Slumped	Zonal, horizontal	5
Mod16	B20	Core	1682.34	1682.52	0.17	Major Slumped	Zonal, horizontal	5
Mod16	B20	Core	1682.34	1682.52	0.17	Major Slumped	Zonal, horizontal	10
Mod16	B20	Core	1682.34	1682.52	0.17	Major Slumped	Zonal, horizontal	10
Mod16	B20	Core	1682.34	1682.52	0.17	Major Slumped	Zonal, horizontal	10
Mod16	B20	Core	1682.34	1682.52	0.17	Major Slumped	Zonal, horizontal	10
Mod16	B20	Core	1682.34	1682.52	0.17	Major Slumped	Zonal, horizontal	10
Mod16	B20	Core	1682.34	1682.52	0.17	Major Slumped	Zonal, horizontal	10
Mod16	B20	Core	1682.34	1682.52	0.17	Major Slumped	Zonal, horizontal	15
Mod16	B20	Core	1682.34	1682.52	0.17	Major Slumped	Zonal, horizontal	15
Mod16	B20	Core	1682.34	1682.52	0.17	Major Slumped	Zonal, horizontal	15
Mod16	B20	Core	1682.34	1682.52	0.17	Major Slumped	Zonal, horizontal	15
Mod16	B20	Core	1682.34	1682.52	0.17	Major Slumped	Zonal, horizontal	15

Mod16	B20	Core	1682.34	1682.52	0.17	Major Slumped	Zonal, horizontal	15
Mod16	B20	Core	1682.34	1682.52	0.17	Major Slumped	Zonal, horizontal	20
Mod16	B20	Core	1682.34	1682.52	0.17	Major Slumped	Zonal, horizontal	20
Mod16	B20	Core	1682.34	1682.52	0.17	Major Slumped	Zonal, horizontal	20
Mod16	B20	Core	1682.34	1682.52	0.17	Major Slumped	Zonal, horizontal	20
Mod16	B20	Core	1682.34	1682.52	0.17	Major Slumped	Zonal, horizontal	20
Mod16	B20	Core	1682.34	1682.52	0.17	Major Slumped	Zonal, horizontal	20
Mod16	B20	Core	1682.34	1682.52	0.17	Major Slumped	Zonal, horizontal	25
Mod16	B20	Core	1682.34	1682.52	0.17	Major Slumped	Zonal, horizontal	25
Mod16	B20	Core	1682.34	1682.52	0.17	Major Slumped	Zonal, horizontal	25
Mod16	B20	Core	1682.34	1682.52	0.17	Major Slumped	Zonal, horizontal	25
Mod16	B20	Core	1682.34	1682.52	0.17	Major Slumped	Zonal, horizontal	25
Mod16	B20	Core	1682.34	1682.52	0.17	Major Slumped	Zonal, horizontal	25
Mod16	B20	Core	1682.34	1682.52	0.17	Major Slumped	Zonal, horizontal	30
Mod16	B20	Core	1682.34	1682.52	0.17	Major Slumped	Zonal, horizontal	30
Mod16	B20	Core	1682.34	1682.52	0.17	Major Slumped	Zonal, horizontal	30
Mod16	B20	Core	1682.34	1682.52	0.17	Major Slumped	Zonal, horizontal	30
Mod16	B20	Core	1682.34	1682.52	0.17	Major Slumped	Zonal, horizontal	30
Mod16	B20	Core	1682.34	1682.52	0.17	Major Slumped	Zonal, horizontal	30
Mod17	B24	Core	2002.51	2002.68	0.17	Major Slumped	Zonal, vertical	1
Mod17	B24	Core	2002.51	2002.68	0.17	Major Slumped	Zonal, vertical	1
Mod17	B24	Core	2002.51	2002.68	0.17	Major Slumped	Zonal, vertical	1
Mod17	B24	Core	2002.51	2002.68	0.17	Major Slumped	Zonal, vertical	1
Mod17	B24	Core	2002.51	2002.68	0.17	Major Slumped	Zonal, vertical	1
Mod17	B24	Core	2002.51	2002.68	0.17	Major Slumped	Zonal, vertical	1
Mod17	B24	Core	2002.51	2002.68	0.17	Major Slumped	Zonal, vertical	5
Mod17	B24	Core	2002.51	2002.68	0.17	Major Slumped	Zonal, vertical	5
Mod17	B24	Core	2002.51	2002.68	0.17	Major Slumped	Zonal, vertical	5
Mod17	B24	Core	2002.51	2002.68	0.17	Major Slumped	Zonal, vertical	5
Mod17	B24	Core	2002.51	2002.68	0.17	Major Slumped	Zonal, vertical	5
Mod17	B24	Core	2002.51	2002.68	0.17	Major Slumped	Zonal, vertical	5
Mod17	B24	Core	2002.51	2002.68	0.17	Major Slumped	Zonal, vertical	10
Mod17	B24	Core	2002.51	2002.68	0.17	Major Slumped	Zonal, vertical	10

Mod17	B24	Core	2002.51	2002.68	0.17	Major Slumped	Zonal, vertical	10
Mod17	B24	Core	2002.51	2002.68	0.17	Major Slumped	Zonal, vertical	10
Mod17	B24	Core	2002.51	2002.68	0.17	Major Slumped	Zonal, vertical	10
Mod17	B24	Core	2002.51	2002.68	0.17	Major Slumped	Zonal, vertical	10
Mod17	B24	Core	2002.51	2002.68	0.17	Major Slumped	Zonal, vertical	15
Mod17	B24	Core	2002.51	2002.68	0.17	Major Slumped	Zonal, vertical	15
Mod17	B24	Core	2002.51	2002.68	0.17	Major Slumped	Zonal, vertical	15
Mod17	B24	Core	2002.51	2002.68	0.17	Major Slumped	Zonal, vertical	15
Mod17	B24	Core	2002.51	2002.68	0.17	Major Slumped	Zonal, vertical	15
Mod17	B24	Core	2002.51	2002.68	0.17	Major Slumped	Zonal, vertical	15
Mod17	B24	Core	2002.51	2002.68	0.17	Major Slumped	Zonal, vertical	20
Mod17	B24	Core	2002.51	2002.68	0.17	Major Slumped	Zonal, vertical	20
Mod17	B24	Core	2002.51	2002.68	0.17	Major Slumped	Zonal, vertical	20
Mod17	B24	Core	2002.51	2002.68	0.17	Major Slumped	Zonal, vertical	20
Mod17	B24	Core	2002.51	2002.68	0.17	Major Slumped	Zonal, vertical	20
Mod17	B24	Core	2002.51	2002.68	0.17	Major Slumped	Zonal, vertical	20
Mod17	B24	Core	2002.51	2002.68	0.17	Major Slumped	Zonal, vertical	25
Mod17	B24	Core	2002.51	2002.68	0.17	Major Slumped	Zonal, vertical	25
Mod17	B24	Core	2002.51	2002.68	0.17	Major Slumped	Zonal, vertical	25
Mod17	B24	Core	2002.51	2002.68	0.17	Major Slumped	Zonal, vertical	25
Mod17	B24	Core	2002.51	2002.68	0.17	Major Slumped	Zonal, vertical	25
Mod17	B24	Core	2002.51	2002.68	0.17	Major Slumped	Zonal, vertical	25
Mod17	B24	Core	2002.51	2002.68	0.17	Major Slumped	Zonal, vertical	30
Mod17	B24	Core	2002.51	2002.68	0.17	Major Slumped	Zonal, vertical	30
Mod17	B24	Core	2002.51	2002.68	0.17	Major Slumped	Zonal, vertical	30
Mod17	B24	Core	2002.51	2002.68	0.17	Major Slumped	Zonal, vertical	30
Mod17	B24	Core	2002.51	2002.68	0.17	Major Slumped	Zonal, vertical	30
Mod17	B24	Core	2002.51	2002.68	0.17	Major Slumped	Zonal, vertical	30
Mod18	B19	Core	1716.06	1716.43	0.37	Major Slumped	Geometric, horizontal	1
Mod18	B19	Core	1716.06	1716.43	0.37	Major Slumped	Geometric, horizontal	1
Mod18	B19	Core	1716.06	1716.43	0.37	Major Slumped	Geometric, horizontal	1
Mod18	B19	Core	1716.06	1716.43	0.37	Major Slumped	Geometric, horizontal	1
Mod18	B19	Core	1716.06	1716.43	0.37	Major Slumped	Geometric, horizontal	1

Mod18	B19	Core	1716.06	1716.43	0.37	Major Slumped	Geometric, horizontal	1
Mod18	B19	Core	1716.06	1716.43	0.37	Major Slumped	Geometric, horizontal	5
Mod18	B19	Core	1716.06	1716.43	0.37	Major Slumped	Geometric, horizontal	5
Mod18	B19	Core	1716.06	1716.43	0.37	Major Slumped	Geometric, horizontal	5
Mod18	B19	Core	1716.06	1716.43	0.37	Major Slumped	Geometric, horizontal	5
Mod18	B19	Core	1716.06	1716.43	0.37	Major Slumped	Geometric, horizontal	5
Mod18	B19	Core	1716.06	1716.43	0.37	Major Slumped	Geometric, horizontal	5
Mod18	B19	Core	1716.06	1716.43	0.37	Major Slumped	Geometric, horizontal	10
Mod18	B19	Core	1716.06	1716.43	0.37	Major Slumped	Geometric, horizontal	10
Mod18	B19	Core	1716.06	1716.43	0.37	Major Slumped	Geometric, horizontal	10
Mod18	B19	Core	1716.06	1716.43	0.37	Major Slumped	Geometric, horizontal	10
Mod18	B19	Core	1716.06	1716.43	0.37	Major Slumped	Geometric, horizontal	10
Mod18	B19	Core	1716.06	1716.43	0.37	Major Slumped	Geometric, horizontal	10
Mod18	B19	Core	1716.06	1716.43	0.37	Major Slumped	Geometric, horizontal	15
Mod18	B19	Core	1716.06	1716.43	0.37	Major Slumped	Geometric, horizontal	15
Mod18	B19	Core	1716.06	1716.43	0.37	Major Slumped	Geometric, horizontal	15
Mod18	B19	Core	1716.06	1716.43	0.37	Major Slumped	Geometric, horizontal	15
Mod18	B19	Core	1716.06	1716.43	0.37	Major Slumped	Geometric, horizontal	15
Mod18	B19	Core	1716.06	1716.43	0.37	Major Slumped	Geometric, horizontal	15
Mod18	B19	Core	1716.06	1716.43	0.37	Major Slumped	Geometric, horizontal	20
Mod18	B19	Core	1716.06	1716.43	0.37	Major Slumped	Geometric, horizontal	20
Mod18	B19	Core	1716.06	1716.43	0.37	Major Slumped	Geometric, horizontal	20
Mod18	B19	Core	1716.06	1716.43	0.37	Major Slumped	Geometric, horizontal	20
Mod18	B19	Core	1716.06	1716.43	0.37	Major Slumped	Geometric, horizontal	20
Mod18	B19	Core	1716.06	1716.43	0.37	Major Slumped	Geometric, horizontal	20
Mod18	B19	Core	1716.06	1716.43	0.37	Major Slumped	Geometric, horizontal	25
Mod18	B19	Core	1716.06	1716.43	0.37	Major Slumped	Geometric, horizontal	25
Mod18	B19	Core	1716.06	1716.43	0.37	Major Slumped	Geometric, horizontal	25
Mod18	B19	Core	1716.06	1716.43	0.37	Major Slumped	Geometric, horizontal	25
Mod18	B19	Core	1716.06	1716.43	0.37	Major Slumped	Geometric, horizontal	25
Mod18	B19	Core	1716.06	1716.43	0.37	Major Slumped	Geometric, horizontal	25
Mod18	B19	Core	1716.06	1716.43	0.37	Major Slumped	Geometric, horizontal	30
Mod18	B19	Core	1716.06	1716.43	0.37	Major Slumped	Geometric, horizontal	30

Mod18	B19	Core	1716.06	1716.43	0.37	Major Slumped	Geometric, horizontal	30
Mod18	B19	Core	1716.06	1716.43	0.37	Major Slumped	Geometric, horizontal	30
Mod18	B19	Core	1716.06	1716.43	0.37	Major Slumped	Geometric, horizontal	30
Mod18	B19	Core	1716.06	1716.43	0.37	Major Slumped	Geometric, horizontal	30
Mod20	B6	FMI	1585.00	1587.00	2.00	Major Slumped	Geometric, vertical	1
Mod20	B6	FMI	1585.00	1587.00	2.00	Major Slumped	Geometric, vertical	1
Mod20	B6	FMI	1585.00	1587.00	2.00	Major Slumped	Geometric, vertical	1
Mod20	B6	FMI	1585.00	1587.00	2.00	Major Slumped	Geometric, vertical	1
Mod20	B6	FMI	1585.00	1587.00	2.00	Major Slumped	Geometric, vertical	1
Mod20	B6	FMI	1585.00	1587.00	2.00	Major Slumped	Geometric, vertical	1
Mod20	B6	FMI	1585.00	1587.00	2.00	Major Slumped	Geometric, vertical	5
Mod20	B6	FMI	1585.00	1587.00	2.00	Major Slumped	Geometric, vertical	5
Mod20	B6	FMI	1585.00	1587.00	2.00	Major Slumped	Geometric, vertical	5
Mod20	B6	FMI	1585.00	1587.00	2.00	Major Slumped	Geometric, vertical	5
Mod20	B6	FMI	1585.00	1587.00	2.00	Major Slumped	Geometric, vertical	5
Mod20	B6	FMI	1585.00	1587.00	2.00	Major Slumped	Geometric, vertical	5
Mod20	B6	FMI	1585.00	1587.00	2.00	Major Slumped	Geometric, vertical	10
Mod20	B6	FMI	1585.00	1587.00	2.00	Major Slumped	Geometric, vertical	10
Mod20	B6	FMI	1585.00	1587.00	2.00	Major Slumped	Geometric, vertical	10
Mod20	B6	FMI	1585.00	1587.00	2.00	Major Slumped	Geometric, vertical	10
Mod20	B6	FMI	1585.00	1587.00	2.00	Major Slumped	Geometric, vertical	10
Mod20	B6	FMI	1585.00	1587.00	2.00	Major Slumped	Geometric, vertical	10
Mod20	B6	FMI	1585.00	1587.00	2.00	Major Slumped	Geometric, vertical	15
Mod20	B6	FMI	1585.00	1587.00	2.00	Major Slumped	Geometric, vertical	15
Mod20	B6	FMI	1585.00	1587.00	2.00	Major Slumped	Geometric, vertical	15
Mod20	B6	FMI	1585.00	1587.00	2.00	Major Slumped	Geometric, vertical	15
Mod20	B6	FMI	1585.00	1587.00	2.00	Major Slumped	Geometric, vertical	15
Mod20	B6	FMI	1585.00	1587.00	2.00	Major Slumped	Geometric, vertical	15
Mod20	B6	FMI	1585.00	1587.00	2.00	Major Slumped	Geometric, vertical	20
Mod20	B6	FMI	1585.00	1587.00	2.00	Major Slumped	Geometric, vertical	20
Mod20	B6	FMI	1585.00	1587.00	2.00	Major Slumped	Geometric, vertical	20
Mod20	B6	FMI	1585.00	1587.00	2.00	Major Slumped	Geometric, vertical	20
Mod20	B6	FMI	1585.00	1587.00	2.00	Major Slumped	Geometric, vertical	20

Mod20	B6	FMI	1585.00	1587.00	2.00	Major Slumped	Geometric, vertical	20
Mod20	B6	FMI	1585.00	1587.00	2.00	Major Slumped	Geometric, vertical	25
Mod20	B6	FMI	1585.00	1587.00	2.00	Major Slumped	Geometric, vertical	25
Mod20	B6	FMI	1585.00	1587.00	2.00	Major Slumped	Geometric, vertical	25
Mod20	B6	FMI	1585.00	1587.00	2.00	Major Slumped	Geometric, vertical	25
Mod20	B6	FMI	1585.00	1587.00	2.00	Major Slumped	Geometric, vertical	25
Mod20	B6	FMI	1585.00	1587.00	2.00	Major Slumped	Geometric, vertical	25
Mod20	B6	FMI	1585.00	1587.00	2.00	Major Slumped	Geometric, vertical	30
Mod20	B6	FMI	1585.00	1587.00	2.00	Major Slumped	Geometric, vertical	30
Mod20	B6	FMI	1585.00	1587.00	2.00	Major Slumped	Geometric, vertical	30
Mod20	B6	FMI	1585.00	1587.00	2.00	Major Slumped	Geometric, vertical	30
Mod20	B6	FMI	1585.00	1587.00	2.00	Major Slumped	Geometric, vertical	30
Mod20	B6	FMI	1585.00	1587.00	2.00	Major Slumped	Geometric, vertical	30

Mud content [%]	Mean cohesive content [%]	Mean porosity [fraction]	Minimum log10 effective Kh [m2]	Mean log10 effective Kh [m2]
50	39.18235161	0.413784241	-15.74627198	-15.59373398
60	46.01881599	0.431438315	-16.26353099	-16.22293551
70	52.85528036	0.44907567	-16.5435459	-16.5225837
80	59.69174474	0.466785315	-16.72765704	-16.72102328
90	66.52820912	0.484283425	-16.86793252	-16.86417811
100	73.36467349	0.50203489	-16.97032814	-16.96947174
50	39.18235161	0.332811755	-16.84922208	-16.6219025
60	46.01881599	0.342488895	-17.36224517	-17.32318373
70	52.85528036	0.35199946	-17.63757031	-17.61560292
80	59.69174474	0.361568255	-17.81168755	-17.80669972
90	66.52820912	0.371147258	-17.94685623	-17.94369612
100	73.36467349	0.380668927	-18.04599545	-18.04494284
50	39.18235161	0.283362656	-17.44457542	-17.1878531
60	46.01881599	0.288030996	-17.95831525	-17.91730444
70	52.85528036	0.292760565	-18.22569184	-18.20629454
80	59.69174474	0.297504998	-18.39907064	-18.39310542
90	66.52820912	0.302171598	-18.53032375	-18.52668304
100	73.36467349	0.30692893	-18.62633599	-18.62554739
50	39.18235161	0.247478697	-17.85569984	-17.595493
60	46.01881599	0.248931019	-18.36162557	-18.32440264
70	52.85528036	0.250354621	-18.63020918	-18.61075941
80	59.69174474	0.251765308	-18.80133742	-18.79546927
90	66.52820912	0.253104114	-18.92910917	-18.92595467
100	73.36467349	0.254514849	-19.02365598	-19.02308326
50	39.18235161	0.217995981	-18.19048203	-17.92202113
60	46.01881599	0.216805167	-18.69266017	-18.65391472
70	52.85528036	0.215565632	-18.95684214	-18.93780701
80	59.69174474	0.214342371	-19.1247309	-19.11966293
90	66.52820912	0.213110972	-19.25224183	-19.24924716
100	73.36467349	0.21188859	-19.34588606	-19.34482481
50	39.18235161	0.192366966	-18.47764707	-18.21194885
60	46.01881599	0.188927196	-18.98247001	-18.94232385

70	52.85528036	0.185462138	-19.24312969	-19.22496516
80	59.69174474	0.182007668	-19.41018774	-19.4050528
90	66.52820912	0.17850924	-19.53528695	-19.53288179
100	73.36467349	0.175035486	-19.62774914	-19.62737459
50	39.18235161	0.169499774	-18.74334478	-18.47886857
60	46.01881599	0.163997312	-19.24625153	-19.20938658
70	52.85528036	0.158534835	-19.50759585	-19.48949743
80	59.69174474	0.153040551	-19.67352896	-19.6687138
90	66.52820912	0.147570817	-19.7989417	-19.79571349
100	73.36467349	0.142071279	-19.88991895	-19.88943471
50	39.18235161	0.413740741	-15.20184953	-14.62191193
60	46.01881599	0.431471678	-15.89952951	-15.753248
70	52.85528036	0.449053002	-16.28755234	-16.23934253
80	59.69174474	0.466760723	-16.60143853	-16.56376624
90	66.52820912	0.484437342	-16.81506169	-16.7983829
100	73.36467349	0.502007191	-16.96452623	-16.96394918
50	39.18235161	0.332883589	-16.29361425	-15.19788029
60	46.01881599	0.342475557	-17.00717309	-16.8592261
70	52.85528036	0.351968394	-17.38829368	-17.33994746
80	59.69174474	0.361597949	-17.6901804	-17.65259605
90	66.52820912	0.371206556	-17.89116447	-17.87620919
100	73.36467349	0.380727554	-18.03808367	-18.03685132
50	39.18235161	0.283343733	-16.87431383	-15.63602747
60	46.01881599	0.288089756	-17.60641427	-17.45864393
70	52.85528036	0.292768395	-17.98547946	-17.9382037
80	59.69174474	0.297504361	-18.28008149	-18.24351194
90	66.52820912	0.302246517	-18.47633676	-18.46097597
100	73.36467349	0.306968385	-18.61843912	-18.61738018
50	39.18235161	0.247475665	-17.30430998	-15.98103723
60	46.01881599	0.248942115	-18.01695	-17.87378826
70	52.85528036	0.250299792	-18.39065963	-18.34657545
80	59.69174474	0.251730868	-18.68251332	-18.64914462
90	66.52820912	0.253125605	-18.87796443	-18.8626871

100	73.36467349	0.254512696	-19.01631915	-19.01537492
50	39.18235161	0.217980017	-17.64334898	-16.29953446
60	46.01881599	0.216821474	-18.35057654	-18.21189144
70	52.85528036	0.215564929	-18.72330388	-18.67869511
80	59.69174474	0.214357635	-19.01241238	-18.97770234
90	66.52820912	0.213132818	-19.20289457	-19.18757669
100	73.36467349	0.211859552	-19.33828384	-19.33753202
50	39.18235161	0.19237018	-17.94011865	-16.58109714
60	46.01881599	0.188900322	-18.63589384	-18.49894482
70	52.85528036	0.185488104	-19.0141565	-18.96787153
80	59.69174474	0.182022036	-19.29986764	-19.26557201
90	66.52820912	0.17854191	-19.48732094	-19.4731719
100	73.36467349	0.175051095	-19.62189294	-19.62088627
50	39.18235161	0.169492805	-18.20225064	-16.85999928
60	46.01881599	0.164004391	-18.90978781	-18.76763826
70	52.85528036	0.158535116	-19.28001859	-19.236451
80	59.69174474	0.153042833	-19.56390576	-19.5310092
90	66.52820912	0.147591966	-19.75064753	-19.7371307
100	73.36467349	0.142065461	-19.88363803	-19.88309966
50	39.18235161	0.413762956	-15.75805527	-15.45489179
60	46.01881599	0.431384345	-16.19170528	-16.12134776
70	52.85528036	0.449053553	-16.47200812	-16.44904257
80	59.69174474	0.466727393	-16.68335042	-16.67489555
90	66.52820912	0.48445138	-16.84642292	-16.84311107
100	73.36467349	0.501975154	-16.96841785	-16.96776395
50	39.18235161	0.332840387	-16.87263924	-16.53052244
60	46.01881599	0.342430997	-17.30153059	-17.22442959
70	52.85528036	0.352012778	-17.56849471	-17.54520462
80	59.69174474	0.361539994	-17.77018254	-17.76187773
90	66.52820912	0.371192294	-17.92560051	-17.92269976
100	73.36467349	0.380713562	-18.04328616	-18.04261643
50	39.18235161	0.283337625	-17.46815081	-17.12500165
60	46.01881599	0.28813278	-17.89556752	-17.82036237

70	52.85528036	0.29277166	-18.16175052	-18.13741776
80	59.69174474	0.2975321	-18.35786108	-18.34958666
90	66.52820912	0.302217374	-18.50904197	-18.5063746
100	73.36467349	0.306928874	-18.62425045	-18.62318291
50	39.18235161	0.247534647	-17.87684444	-17.53943192
60	46.01881599	0.248893953	-18.30534655	-18.22874433
70	52.85528036	0.25028711	-18.56733049	-18.54368157
80	59.69174474	0.251772448	-18.76063044	-18.75278101
90	66.52820912	0.253098704	-18.90921307	-18.90616697
100	73.36467349	0.254492176	-19.02137765	-19.02071619
50	39.18235161	0.218018948	-18.20610838	-17.87066379
60	46.01881599	0.216752889	-18.63550341	-18.55897503
70	52.85528036	0.215596121	-18.89548899	-18.87146469
80	59.69174474	0.214323954	-19.0870365	-19.07869923
90	66.52820912	0.213124541	-19.23282557	-19.22999803
100	73.36467349	0.211883826	-19.34360853	-19.34272816
50	39.18235161	0.192402817	-18.49556448	-18.16070739
60	46.01881599	0.188940439	-18.92147431	-18.85008542
70	52.85528036	0.185454143	-19.18372489	-19.15929065
80	59.69174474	0.182010597	-19.37172962	-19.36424939
90	66.52820912	0.178545208	-19.51695645	-19.51451805
100	73.36467349	0.175034096	-19.62626803	-19.62542252
50	39.18235161	0.169492052	-18.761229	-18.43214984
60	46.01881599	0.164025096	-19.19351816	-19.11509146
70	52.85528036	0.158557191	-19.44827682	-19.42482482
80	59.69174474	0.153055025	-19.63533833	-19.6283805
90	66.52820912	0.14755919	-19.77970881	-19.77758586
100	73.36467349	0.142065398	-19.88849217	-19.88747293
50	39.18235161	0.413709862	-15.65935564	-14.8434689
60	46.01881599	0.431362244	-16.01380936	-15.71725502
70	52.85528036	0.449030806	-16.37962343	-16.26388291
80	59.69174474	0.466735699	-16.61850045	-16.56334748
90	66.52820912	0.484406424	-16.81044232	-16.79301312

100	73.36467349	0.501927627	-16.96660037	-16.96499019
50	39.18235161	0.332890112	-16.77110454	-15.51132653
60	46.01881599	0.342490682	-17.11862162	-16.76196416
70	52.85528036	0.352034623	-17.47952826	-17.36888081
80	59.69174474	0.361578197	-17.70955579	-17.65559489
90	66.52820912	0.371102544	-17.89370709	-17.87482575
100	73.36467349	0.380697021	-18.04189885	-18.03847075
50	39.18235161	0.283344406	-17.38399001	-16.00847061
60	46.01881599	0.288045291	-17.71975636	-17.3390433
70	52.85528036	0.292822538	-18.0774676	-17.96647709
80	59.69174474	0.297543396	-18.30184811	-18.24708468
90	66.52820912	0.302240342	-18.47891424	-18.46030567
100	73.36467349	0.306921897	-18.62230408	-18.6189851
50	39.18235161	0.247506394	-17.79359244	-16.36492836
60	46.01881599	0.248902116	-18.13333585	-17.74826472
70	52.85528036	0.250300711	-18.48016282	-18.37256658
80	59.69174474	0.251746393	-18.7065822	-18.65214493
90	66.52820912	0.253119942	-18.88023949	-18.86177347
100	73.36467349	0.254525222	-19.02000254	-19.01693578
50	39.18235161	0.217996933	-18.12624881	-16.67182158
60	46.01881599	0.216811003	-18.45948909	-18.07489064
70	52.85528036	0.215573564	-18.8132216	-18.70308045
80	59.69174474	0.214342526	-19.03050441	-18.97972089
90	66.52820912	0.213094729	-19.20467624	-19.18616763
100	73.36467349	0.211900527	-19.34253205	-19.33912619
50	39.18235161	0.192385333	-18.41935781	-16.95119508
60	46.01881599	0.188931831	-18.7492995	-18.37019375
70	52.85528036	0.185450519	-19.09678246	-18.99370254
80	59.69174474	0.18200962	-19.31906288	-19.26690239
90	66.52820912	0.178525893	-19.48885891	-19.47114906
100	73.36467349	0.175030549	-19.62442051	-19.62199263
50	39.18235161	0.169507334	-18.68597258	-17.22875666
60	46.01881599	0.16403037	-19.01812479	-18.6341142

70	52.85528036	0.158557709	-19.36533636	-19.26031683
80	59.69174474	0.153066273	-19.58412726	-19.53238511
90	66.52820912	0.147578512	-19.75325283	-19.73499709
100	73.36467349	0.142065165	-19.88646441	-19.884243
50	39.18235161	0.41374278	-15.83151725	-14.64580406
60	46.01881599	0.431405673	-16.13200014	-15.7153063
70	52.85528036	0.449114736	-16.45273494	-16.35793811
80	59.69174474	0.466711847	-16.70367712	-16.64632179
90	66.52820912	0.484397897	-16.85444002	-16.83138123
100	73.36467349	0.502091014	-16.97212466	-16.97008953
50	39.18235161	0.332840372	-16.91402836	-15.31499411
60	46.01881599	0.342417351	-17.21976552	-16.72050713
70	52.85528036	0.351984198	-17.53813996	-17.44183717
80	59.69174474	0.361526081	-17.78860444	-17.73145803
90	66.52820912	0.37116255	-17.9329738	-17.91145979
100	73.36467349	0.380641246	-18.04697038	-18.04454157
50	39.18235161	0.28333494	-17.51229614	-15.78517473
60	46.01881599	0.288049491	-17.81038899	-17.29396128
70	52.85528036	0.292809678	-18.12632606	-18.02882754
80	59.69174474	0.297527123	-18.37387427	-18.31819912
90	66.52820912	0.302295238	-18.51586822	-18.49535007
100	73.36467349	0.306951132	-18.62763857	-18.6252125
50	39.18235161	0.247479064	-17.91247768	-16.15451002
60	46.01881599	0.24892264	-18.21377758	-17.68833754
70	52.85528036	0.250307906	-18.52825955	-18.43462298
80	59.69174474	0.25174065	-18.77564826	-18.71971794
90	66.52820912	0.253101419	-18.91459881	-18.8945531
100	73.36467349	0.254503126	-19.02443034	-19.02247045
50	39.18235161	0.218007432	-18.23313896	-16.45578822
60	46.01881599	0.216789169	-18.54603987	-18.01533992
70	52.85528036	0.215593138	-18.85602083	-18.76300655
80	59.69174474	0.214349584	-19.10092182	-19.04530756
90	66.52820912	0.213073247	-19.23588816	-19.21741512

100	73.36467349	0.211884347	-19.34557412	-19.3441715
50	39.18235161	0.192353733	-18.5279753	-16.74481462
60	46.01881599	0.188892227	-18.83995787	-18.31275427
70	52.85528036	0.185465119	-19.13980039	-19.04934721
80	59.69174474	0.182000935	-19.38473295	-19.33070677
90	66.52820912	0.178511021	-19.52032682	-19.5013481
100	73.36467349	0.175045705	-19.62869565	-19.6268134
50	39.18235161	0.169483221	-18.7925299	-17.02390358
60	46.01881599	0.16399966	-19.09383149	-18.57243857
70	52.85528036	0.158521367	-19.40723052	-19.31709577
80	59.69174474	0.153056666	-19.64932371	-19.59496696
90	66.52820912	0.147572507	-19.78347256	-19.76474447
100	73.36467349	0.142064726	-19.89052945	-19.88867444

Mode log10 effective Kh [m2]	Maximum log10 effective Kh [m2]	Standard deviation log10 effective Kh [m2]	Minimum log10 effective Kv [m2]
-15.74627198	-14.90684107	0.23828237	-15.77803835
-16.24935594	-16.16430562	0.025851529	-16.36834928
-16.52317718	-16.50790063	0.009700442	-16.69168749
-16.72513316	-16.70998989	0.005273801	-16.89402001
-16.86682737	-16.86019645	0.002518249	-17.04647032
-16.96938428	-16.96867638	0.000441877	-17.15480705
-16.84922208	-15.36055435	0.426811479	-16.8991093
-17.33554672	-17.26880058	0.024605962	-17.51554071
-17.61033776	-17.59944474	0.010300242	-17.85501504
-17.81168755	-17.79763158	0.004386842	-18.07431051
-17.94685623	-17.93915868	0.002469704	-18.24188934
-18.04569491	-18.04389163	0.000676541	-18.36478677
-17.44457542	-15.65048741	0.517320491	-17.51291821
-17.93116125	-17.86327626	0.024933977	-18.13239464
-18.20070075	-18.19070431	0.009728176	-18.47950992
-18.39672431	-18.38264628	0.0049639	-18.70224824
-18.52920437	-18.52248806	0.002234036	-18.87730912
-18.62567504	-18.62479378	0.000460622	-19.00386675
-17.85569984	-16.02627425	0.528110396	-17.93172135
-18.34919179	-18.27458907	0.023456453	-18.55561165
-18.60613384	-18.59650371	0.009302368	-18.90370886
-18.80133742	-18.78547139	0.004724296	-19.13354488
-18.92353247	-18.92260302	0.00214633	-19.30858959
-19.02365598	-19.02206433	0.000469271	-19.43804876
-18.19048203	-16.28927606	0.548989674	-18.27407694
-18.66648389	-18.6010432	0.024232647	-18.8901617
-18.93339701	-18.92401896	0.00887592	-19.24551941
-19.12271256	-19.11060248	0.004277914	-19.47700445
-19.25126762	-19.24542234	0.002151618	-19.65349837
-19.34510141	-19.34405522	0.000534609	-19.78717341
-18.47764707	-16.59090755	0.545174349	-18.56752458
-18.95717525	-18.89393836	0.023310997	-19.18665056

-19.22037758	-19.21127674	0.0087098	-19.54522067
-19.41018774	-19.39562597	0.004508988	-19.77629384
-19.53528695	-19.52997046	0.002024235	-19.95742449
-19.62754831	-19.62634334	0.000366873	-20.08960507
-18.74334478	-16.84879569	0.548042673	-18.83298707
-19.22169112	-19.1602901	0.023279315	-19.45789194
-19.49822181	-19.47478669	0.008855499	-19.81751116
-19.67352896	-19.65923871	0.004326653	-20.05297331
-19.79796612	-19.79211261	0.002191075	-20.23422717
-19.88991895	-19.8887274	0.000390971	-20.36988754
-14.52807693	-14.2585679	0.27548298	-16.09382933
-15.7095247	-15.67785723	0.066642081	-16.54059092
-16.28755234	-16.1569305	0.043342953	-16.78769518
-16.57962691	-16.52509786	0.022137482	-16.95173692
-16.80299103	-16.78689681	0.007945152	-17.07303126
-16.9638038	-16.96351483	0.000294154	-17.16262118
-15.1367061	-14.67394283	0.524713583	-17.25169799
-16.81549083	-16.78354379	0.068844028	-17.71054929
-17.38829368	-17.25517914	0.043392058	-17.97218984
-17.66924813	-17.61691745	0.020962103	-18.14764873
-17.88017129	-17.8655137	0.007198459	-18.27998797
-18.03740284	-18.03570076	0.000631212	-18.37757458
-15.32319713	-15.06467768	0.602431562	-17.87428782
-17.44039352	-17.37398522	0.070095503	-18.3300057
-17.98547946	-17.86462561	0.04064033	-18.60387915
-18.25981293	-18.20914155	0.020151515	-18.78410083
-18.4649386	-18.44974106	0.007257152	-18.91902737
-18.61707755	-18.61653293	0.00051885	-19.02039518
-15.91260357	-15.35592101	0.640797798	-18.29231403
-17.85202865	-17.78606011	0.067513563	-18.7604828
-18.39065963	-18.27203442	0.041310462	-19.03036606
-18.66368334	-18.61660837	0.019163853	-19.21402348
-18.86725129	-18.85296709	0.007051245	-19.35108698

-19.01509902	-19.01489566	0.000414274	-19.45406602
-16.24136337	-15.68056912	0.647739714	-18.63696747
-18.16199846	-18.13056879	0.066708384	-19.10177136
-18.72330388	-18.60467535	0.040182228	-19.37301022
-18.9829893	-18.94375853	0.019518693	-19.56009284
-19.19237726	-19.17835417	0.006961305	-19.69893526
-19.33735304	-19.33698073	0.000411141	-19.80504188
-16.29231247	-16.0176781	0.652365137	-18.93400598
-18.45360096	-18.42321882	0.06405446	-19.39688162
-19.0141565	-18.8945341	0.040399087	-19.67678504
-19.28089743	-19.2334719	0.018715628	-19.86144469
-19.47720599	-19.46371939	0.006755966	-20.00191947
-19.62072364	-19.61984667	0.000615665	-20.10726556
-16.56341055	-16.29027054	0.644944417	-19.21038686
-18.74668522	-18.68144419	0.06772318	-19.67074454
-19.28001859	-19.16099484	0.039758798	-19.94963185
-19.54525785	-19.49863807	0.018551304	-20.13859106
-19.74433359	-19.72854874	0.006456897	-20.28129906
-19.88324379	-19.8822582	0.000361677	-20.38707846
-15.59172432	-15.17589696	0.165332532	-15.89342837
-16.14508755	-16.02854323	0.041342662	-16.39686862
-16.45281427	-16.42722247	0.013172204	-16.70456926
-16.6689904	-16.66659706	0.005532131	-16.90148087
-16.84642292	-16.83788984	0.002644468	-17.04800668
-16.96774754	-16.9668538	0.000435158	-17.15544579
-16.67590169	-16.18405784	0.196976512	-17.02543443
-17.25342975	-17.13317766	0.042120591	-17.54580631
-17.54941651	-17.5239789	0.012946142	-17.87149088
-17.75588866	-17.75350634	0.005783506	-18.08529728
-17.92560051	-17.91785039	0.002393545	-18.24494346
-18.0425408	-18.04154697	0.000495896	-18.36521349
-17.27140604	-16.77954409	0.200556436	-17.62900607
-17.84883941	-17.73201913	0.040869862	-18.16737933

-18.1422323	-18.11620801	0.012945784	-18.49488124
-18.35786108	-18.3403823	0.005754371	-18.71380634
-18.50904197	-18.50080109	0.00254169	-18.88043071
-18.62425045	-18.62159301	0.000764988	-19.00665637
-17.78099799	-17.20591925	0.198717208	-18.05523611
-18.25853723	-18.14151393	0.040593533	-18.5882608
-18.54757751	-18.52124021	0.012948262	-18.9248291
-18.75574666	-18.74353723	0.005432395	-19.14513429
-18.90921307	-18.90118674	0.002335148	-19.31192027
-19.02103909	-19.02019267	0.000334788	-19.43926864
-18.10912414	-17.52721869	0.196332478	-18.38489833
-18.58780914	-18.46857346	0.041039843	-18.92911654
-18.87530026	-18.84838196	0.013061514	-19.26273498
-19.07967065	-19.06984952	0.005422787	-19.49017673
-19.23282557	-19.22502562	0.002271628	-19.65787155
-19.34248437	-19.34229701	0.000360826	-19.78745818
-18.30475461	-17.82772992	0.19878769	-18.68269525
-18.87607577	-18.76257943	0.03966035	-19.22821783
-19.16398862	-19.13767359	0.013025249	-19.56169978
-19.36701422	-19.35522573	0.005752496	-19.78929633
-19.51695645	-19.50946846	0.002243583	-19.96007455
-19.62529738	-19.62490912	0.00044625	-20.09063656
-18.57685624	-18.11592434	0.192527785	-18.94318659
-19.14530992	-19.0247893	0.041844477	-19.50060713
-19.42884169	-19.40292819	0.012760836	-19.83878777
-19.63091938	-19.61987201	0.00507917	-20.06530465
-19.77970881	-19.77375334	0.001788662	-20.23804962
-19.88735647	-19.88716719	0.000398835	-20.37070256
-14.43630138	-14.23245901	0.597202004	-16.04069239
-16.01380936	-14.75260127	0.369735818	-16.46841508
-16.33441066	-16.06313404	0.09285285	-16.76786062
-16.61850045	-16.48955419	0.040949878	-16.9416651
-16.81044232	-16.77727053	0.011592037	-17.06091026

-16.96563439	-16.96321945	0.000952633	-17.16109112
-16.77110454	-14.50258377	0.954964672	-17.19031507
-17.11862162	-15.22809959	0.545201797	-17.63316069
-17.4367796	-17.18028764	0.089159033	-17.94891311
-17.70955579	-17.58266451	0.040870027	-18.13815208
-17.86579395	-17.86114176	0.01198961	-18.26701873
-18.03862477	-18.03616922	0.001478629	-18.37428226
-17.38399001	-14.86960833	1.045300165	-17.80733221
-17.71975636	-15.59611456	0.611210468	-18.26513619
-18.03515932	-17.7813096	0.086633635	-18.57888822
-18.30184811	-18.17183783	0.040892376	-18.77207218
-18.45161007	-18.44705937	0.011442841	-18.90616873
-18.61831528	-18.61671976	0.001518414	-19.01591756
-17.79359244	-15.29243323	1.084761509	-18.23125981
-18.13333585	-15.92509218	0.634941856	-18.69007614
-18.43916788	-18.19319821	0.086401784	-19.00631825
-18.7065822	-18.58164733	0.039028558	-19.20120231
-18.85407691	-18.84971648	0.010865174	-19.33687034
-19.01644499	-19.01502197	0.001376145	-19.44997722
-15.96499452	-15.60478547	1.104831085	-18.56941706
-18.45948909	-16.24073794	0.638337162	-19.02246478
-18.77218487	-18.52596449	0.085190654	-19.34794618
-19.03050441	-18.90913203	0.038361268	-19.54683308
-19.17871789	-19.1743915	0.01075609	-19.68515146
-19.33917123	-19.33665061	0.001600496	-19.79805966
-18.41935781	-15.88219528	1.115159441	-18.8614226
-18.7492995	-16.54362941	0.635945909	-19.32808144
-19.05690001	-18.81760532	0.082719519	-19.64648961
-19.31906288	-19.1967109	0.038411372	-19.84705459
-19.46385102	-19.45968304	0.01026479	-19.98781259
-19.62174898	-19.61974533	0.00132964	-20.1007542
-16.55308461	-16.19760328	1.108264898	-19.1296476
-19.01812479	-16.77413012	0.646132504	-19.60499705

-19.32535993	-19.08550135	0.082264209	-19.92471223
-19.58412726	-19.46208273	0.037897363	-20.12522257
-19.72736386	-19.72304903	0.010264395	-20.26596866
-19.88378894	-19.88271876	0.001040724	-20.38134536
-14.26927357	-13.6443761	0.823664214	-15.84804209
-16.13200014	-13.96888251	0.608020836	-16.32951108
-16.45273494	-16.22452062	0.075467605	-16.64394927
-16.66353396	-16.56317607	0.03856801	-16.82935991
-16.84516128	-16.78948886	0.019119996	-17.00527427
-16.97156051	-16.96817562	0.001121566	-17.1509155
-16.91402836	-14.01497073	1.154680318	-16.95166309
-17.21976552	-14.34288484	0.815866642	-17.45497508
-17.53813996	-17.29087002	0.079705325	-17.80845956
-17.78860444	-17.64900037	0.038364752	-18.00646017
-17.92487268	-17.87626593	0.018225764	-18.19594512
-18.04697038	-18.04164256	0.001594869	-18.35679316
-17.51229614	-14.36997202	1.253679124	-17.57083094
-17.81038899	-14.7165789	0.878765097	-18.06995716
-18.12632606	-17.85897375	0.084191074	-18.43248547
-18.37387427	-18.2356064	0.037827659	-18.63875771
-18.50799267	-18.46073943	0.017507689	-18.83457463
-18.62763857	-18.62101193	0.001752143	-18.99526603
-17.91247768	-14.70415372	1.296218742	-17.9728013
-18.21377758	-15.03562721	0.905162789	-18.48552397
-18.52825955	-18.27555864	0.081682468	-18.86248765
-18.71662799	-18.6379343	0.037618291	-19.06738775
-18.90684998	-18.86035701	0.017350695	-19.26161032
-19.02288116	-19.0190082	0.001435801	-19.42932399
-15.48458093	-15.02648792	1.307740979	-18.31989847
-18.54603987	-15.34536822	0.909918311	-18.8171775
-18.85602083	-18.61324428	0.07852048	-19.20371853
-19.10092182	-18.96549587	0.036916575	-19.41242709
-19.22838277	-19.18335046	0.01689485	-19.60830995

-19.34437201	-19.34136672	0.001164525	-19.77736415
-15.79369537	-15.33798204	1.302302009	-18.61409715
-18.83995787	-15.65525611	0.905019715	-19.12361413
-19.13980039	-18.89308532	0.079824048	-19.49884759
-19.3272444	-19.25059301	0.036465507	-19.71226767
-19.51257046	-19.46603231	0.017154501	-19.91126872
-19.62671693	-19.62407863	0.001284251	-20.0810161
-16.08238735	-15.63069692	1.290970855	-18.89251868
-19.09383149	-15.93983875	0.898688649	-19.39788138
-19.40723052	-19.16257761	0.078567857	-19.77622639
-19.64932371	-19.51854734	0.035616106	-19.98614359
-19.77585085	-19.73012063	0.016912216	-20.18863281
-19.88861397	-19.88605999	0.001258403	-20.36086228

Mean log10 effective Kv [m2]	Mode log10 effective Kv [m2]	Maximum log10 effective Kv [m2]	Standard deviation log10 effective Kv [m2]
-15.69696302	-15.77803835	-15.60977164	0.05885714
-16.32466848	-16.35339231	-16.26365052	0.028482526
-16.65233415	-16.64976325	-16.61832007	0.017911212
-16.87780315	-16.88604115	-16.86609401	0.008901249
-17.03975813	-17.03919601	-17.03628629	0.002842915
-17.15387318	-17.15358969	-17.15310275	0.00053946
-16.80761266	-16.8991093	-16.70012894	0.070797763
-17.46900732	-17.48335629	-17.40289524	0.030477212
-17.81345386	-17.82034786	-17.77412495	0.01946837
-18.05527582	-18.06412468	-18.03866008	0.010706532
-18.23338683	-18.23414253	-18.22833243	0.003639994
-18.36160842	-18.36152604	-18.36022175	0.001187018
-17.41393059	-17.51291821	-17.31074443	0.067898534
-18.08498935	-18.10053507	-18.02088614	0.029394136
-18.43584304	-18.44168352	-18.39124832	0.021515837
-18.68316072	-18.69214975	-18.66690353	0.010553471
-18.86763756	-18.86726754	-18.8632509	0.003816001
-19.00212749	-19.00228683	-19.0011019	0.000859389
-17.82742751	-17.93172135	-17.71254764	0.073039955
-18.50499228	-18.52294462	-18.44127703	0.029629427
-18.86000229	-18.86573181	-18.81509573	0.021338203
-19.11155703	-19.12255185	-19.09506925	0.011093681
-19.29855903	-19.2982481	-19.2941115	0.004134217
-19.43631568	-19.43633722	-19.43505357	0.00084049
-18.16483593	-18.27407694	-18.04938983	0.07720692
-18.84522091	-18.85924647	-18.78195841	0.0285285
-19.20133101	-19.20715059	-19.15599217	0.021434029
-19.45451958	-19.46523965	-19.43582768	0.011752508
-19.64504037	-19.6444541	-19.64083639	0.003637422
-19.78475498	-19.78499588	-19.7820925	0.001303383
-18.45748605	-18.56752458	-18.35116789	0.07206279
-19.13988816	-19.15485621	-19.07537032	0.029405949

-19.49957303	-19.50664483	-19.45521039	0.021869154
-19.75493172	-19.76534394	-19.73796917	0.011028537
-19.94722189	-19.94810687	-19.94111866	0.004300691
-20.08852783	-20.08923783	-20.08703438	0.000825452
-18.73011186	-18.83298707	-18.62755383	0.070436928
-19.41293073	-19.45789194	-19.35077909	0.030426341
-19.77302656	-19.77753074	-19.7242235	0.022379608
-20.03062783	-20.04127395	-20.01202555	0.012073915
-20.22546624	-20.22599424	-20.21981955	0.003822707
-20.36802287	-20.36926255	-20.36551265	0.001340487
-15.97755515	-16.09382933	-15.69474969	0.131780247
-16.48796465	-16.49354626	-16.37593459	0.045136846
-16.76303265	-16.78769518	-16.72137671	0.020517892
-16.94514284	-16.95173692	-16.93892845	0.004519244
-17.07060544	-17.07303126	-17.06752776	0.001786153
-17.16136998	-17.16140125	-17.15977468	0.000764024
-17.11656064	-17.25169799	-16.76954597	0.157178002
-17.65567311	-17.66089811	-17.53677015	0.048430252
-17.9459912	-17.97218984	-17.8988615	0.02218971
-18.13963819	-18.13411006	-18.13185361	0.006136766
-18.27648535	-18.27862466	-18.27044484	0.002791862
-18.376008	-18.37627819	-18.37454967	0.000744435
-17.73090038	-17.87428782	-17.38102465	0.158173675
-18.27779494	-18.3300057	-18.15549549	0.048886578
-18.57462748	-18.60387915	-18.52304236	0.024662986
-18.77447043	-18.78133634	-18.76474939	0.006824542
-18.91500311	-18.91902737	-18.90941044	0.003373363
-19.01835863	-19.01878422	-19.01663626	0.000991215
-18.14666544	-18.29231403	-17.77823638	0.164460558
-18.70292462	-18.7604828	-18.57632823	0.050521926
-19.00350934	-19.03036606	-18.95056488	0.024126646
-19.2045692	-19.21402348	-19.19250421	0.007274285
-19.34743352	-19.35108698	-19.3436344	0.002808053

-19.45277143	-19.45324343	-19.45118694	0.000883996
-18.4889229	-18.63696747	-18.12309142	0.164083988
-19.04589567	-19.10177136	-18.92085857	0.04954937
-19.34620479	-19.37301022	-19.29324809	0.024223241
-19.55036891	-19.55482972	-19.54167193	0.006181615
-19.69486434	-19.69893526	-19.69041241	0.003088423
-19.80120588	-19.80107145	-19.79948328	0.001497413
-18.78934615	-18.93400598	-18.43220929	0.162101515
-19.3413454	-19.39688162	-19.2156916	0.050145399
-19.64618602	-19.67678504	-19.5894792	0.025579736
-19.85206296	-19.86144469	-19.84005702	0.007701699
-19.9981263	-20.00191947	-19.99128914	0.003315663
-20.10553017	-20.10726556	-20.10290648	0.001272375
-19.06573799	-19.21038686	-18.69620369	0.163455851
-19.61658377	-19.67074454	-19.49065363	0.049823077
-19.92237961	-19.94963185	-19.86801584	0.024840853
-20.12933121	-20.13859106	-20.11845558	0.007137278
-20.27643492	-20.27524102	-20.27069749	0.003126174
-20.38471292	-20.38486343	-20.38191005	0.001347272
-15.7716884	-15.86263131	-15.67784896	0.065720137
-16.35996857	-16.39686862	-16.31934999	0.025337867
-16.67735923	-16.67044712	-16.65679826	0.014758331
-16.88919469	-16.88380269	-16.88085633	0.007779177
-17.04316332	-17.04172141	-17.03920731	0.003045874
-17.15490575	-17.15480589	-17.15432597	0.000341597
-16.89102355	-16.88272908	-16.77570007	0.073640255
-17.50731331	-17.54580631	-17.46137977	0.027729169
-17.84360775	-17.83643422	-17.82241156	0.015667228
-18.07045216	-18.06762111	-18.06055064	0.00909312
-18.2381779	-18.24494346	-18.23148917	0.004487359
-18.36352997	-18.36430056	-18.36201822	0.000889814
-17.49467751	-17.51720867	-17.36814547	0.073343301
-18.12387163	-18.16737933	-18.07616558	0.029267082

-18.46614067	-18.47256676	-18.44281413	0.016400325
-18.70000743	-18.69775559	-18.69133529	0.008665261
-18.87311386	-18.8693666	-18.86752258	0.004735519
-19.00385514	-19.00393935	-19.00190159	0.001251474
-17.91174744	-17.90280195	-17.78847633	0.076029983
-18.54468587	-18.51351711	-18.50105983	0.029815374
-18.89075597	-18.89863145	-18.86370125	0.018097169
-19.12819303	-19.1250326	-19.11699192	0.010080244
-19.304108	-19.31192027	-19.29757291	0.004836848
-19.43757503	-19.43747384	-19.43508077	0.001093965
-18.24763884	-18.23936712	-18.13021872	0.075565056
-18.88342501	-18.9159212	-18.83674915	0.030274055
-19.23159272	-19.22764407	-19.20132588	0.01834021
-19.47163144	-19.4649297	-19.46072186	0.010532667
-19.65051845	-19.65787155	-19.64405259	0.004996816
-19.78599955	-19.78628216	-19.78471414	0.000798648
-18.54139178	-18.53353093	-18.42165768	0.075312185
-19.1806405	-19.2140088	-19.12875466	0.031367512
-19.52934906	-19.52027244	-19.50370151	0.01825378
-19.77153219	-19.76810645	-19.7596305	0.010655406
-19.95246313	-19.96007455	-19.94594645	0.005143666
-20.08968871	-20.09063656	-20.0882992	0.00087861
-18.81234425	-18.7967907	-18.68699379	0.073370299
-19.45323062	-19.48725446	-19.40713846	0.030109054
-19.80446994	-19.8108142	-19.77351609	0.019394504
-20.0486475	-20.03998001	-20.03575923	0.010496477
-20.23008334	-20.23804962	-20.22361848	0.004959025
-20.36909883	-20.37070256	-20.36757308	0.001110134
-15.73739821	-16.04069239	-14.21960563	0.518893486
-16.20956994	-16.46841508	-14.59036609	0.544441381
-16.65468979	-16.76786062	-16.3127449	0.12259208
-16.88035891	-16.8864182	-16.74830096	0.050275748
-17.03899227	-17.04001728	-17.01215996	0.013735109

-17.15709691	-17.15874149	-17.15286741	0.002185696
-16.7983002	-17.19031507	-14.59308019	0.744785005
-17.29613563	-17.63316069	-15.01245037	0.764826064
-17.82702442	-17.94891311	-17.46535718	0.130641164
-18.06570707	-18.10576546	-17.91144577	0.059194456
-18.23733321	-18.23772276	-18.19866147	0.018763335
-18.36724085	-18.36855989	-18.36093008	0.003979166
-17.38876372	-17.80733221	-14.94012621	0.825361042
-17.88657466	-18.26513619	-15.34277773	0.851558601
-18.45230994	-18.57888822	-18.09074894	0.131386156
-18.69736771	-18.73799703	-18.53354612	0.062433991
-18.87327483	-18.87479123	-18.83295455	0.020013556
-19.00807639	-19.01160219	-19.00081376	0.004462434
-17.80033232	-18.23125981	-15.27412592	0.850677036
-18.30102072	-18.69007614	-15.6769233	0.878381981
-18.87718922	-19.00631825	-18.50552954	0.135010546
-19.12474252	-19.1663786	-18.9574363	0.063700849
-19.30471687	-19.3153276	-19.26147074	0.02048525
-19.44219767	-19.44548681	-19.43426077	0.004647679
-18.13848537	-18.56941706	-15.59654487	0.856152262
-18.64046005	-19.02246478	-16.01278077	0.879294947
-19.21964555	-19.34794618	-18.85116607	0.133541672
-19.46908642	-19.511583	-19.30008253	0.064787375
-19.65119544	-19.65240452	-19.60874194	0.020818309
-19.79063966	-19.79408879	-19.78416159	0.004092328
-18.4352619	-18.8614226	-15.8924746	0.856588719
-18.94007937	-19.32808144	-16.33149947	0.873101322
-19.51792259	-19.64648961	-19.14348136	0.135475952
-19.76933607	-19.81215919	-19.60278674	0.063877118
-19.95304564	-19.95367158	-19.90815022	0.021999438
-20.09365578	-20.09633945	-20.08530257	0.004268089
-18.70705449	-19.1296476	-16.16368475	0.856496881
-19.20558815	-19.60499705	-16.51822211	0.899161999

-19.7931377	-19.85351563	-19.42633601	0.134120573
-20.04704267	-20.08945934	-19.87487998	0.065838367
-20.2313266	-20.23233684	-20.1874944	0.021642323
-20.37319224	-20.37672964	-20.36519033	0.004766811
-14.59468901	-14.38174514	-13.79522635	0.771052462
-15.75369037	-16.32951108	-14.22871318	0.732800407
-16.38752054	-16.48091179	-16.07331807	0.153080461
-16.69409499	-16.79282501	-16.57361563	0.086687887
-16.95353417	-16.97286671	-16.89184782	0.03199579
-17.14770662	-17.1509155	-17.14503906	0.00185223
-15.21093829	-14.56529564	-14.16756773	1.089924674
-16.72549751	-17.45497508	-14.56114766	1.041430978
-17.52828417	-17.6279337	-17.17661903	0.17106442
-17.85449131	-17.77855106	-17.7405662	0.092365744
-18.13159825	-18.1575805	-18.06166894	0.038366896
-18.3480738	-18.34657321	-18.34248522	0.003757928
-15.64507269	-14.95780076	-14.52229573	1.21000413
-17.29482832	-18.06995716	-14.96910896	1.124787443
-18.14501302	-18.242427	-17.76728081	0.180436882
-18.47775388	-18.40157728	-18.3620472	0.095536045
-18.76124357	-18.79355283	-18.69099831	0.041081097
-18.98640426	-18.98514437	-18.98109571	0.004171292
-15.98646743	-15.31435805	-14.87128417	1.240201549
-17.69967455	-18.48552397	-15.30674277	1.149976789
-18.5634592	-18.66680428	-18.17759587	0.185185402
-18.90072442	-18.82682112	-18.78672669	0.095758074
-19.18860026	-19.22002368	-19.11605707	0.041714582
-19.41920812	-19.42197232	-19.4121701	0.004570208
-16.30112818	-15.6343295	-15.18673467	1.256228961
-18.02686673	-18.8171775	-15.598777	1.162246047
-18.90300618	-19.00919495	-18.52288598	0.18473335
-19.2423317	-19.16242095	-19.12075326	0.098495556
-19.53274276	-19.56532269	-19.45785455	0.042913798

-19.76724036	-19.76493456	-19.75996272	0.004652648
-16.61837612	-15.94097594	-15.49545574	1.249832477
-18.32577802	-19.12361413	-15.92234145	1.155630294
-19.1986667	-19.30290926	-18.81306343	0.18678719
-19.54025936	-19.46066572	-19.41873206	0.098504903
-19.83315189	-19.86834081	-19.76102104	0.043398053
-20.07072821	-20.06885763	-20.06399424	0.004472297
-16.900336	-16.23185835	-15.78841496	1.235207196
-18.603195	-19.39788138	-16.20608465	1.157477626
-19.47451058	-19.57939962	-19.08733271	0.188155879
-19.81460071	-19.73575857	-19.69402773	0.098966417
-20.11044866	-20.14447458	-20.03407899	0.043445469
-20.34945324	-20.34794065	-20.34277199	0.004754166

Model ID	Well	Image type	Top [m]	Bottom [m]	Interval [m]	Structural class	Geostatistical anisotropy type	Effective stress [MPa]
Mod21	B22	Core	1718.10	1718.22	0.12	Small Clasts	Isotropic	1
Mod21	B22	Core	1718.10	1718.22	0.12	Small Clasts	Isotropic	1
Mod21	B22	Core	1718.10	1718.22	0.12	Small Clasts	Isotropic	1
Mod21	B22	Core	1718.10	1718.22	0.12	Small Clasts	Isotropic	1
Mod21	B22	Core	1718.10	1718.22	0.12	Small Clasts	Isotropic	1
Mod21	B22	Core	1718.10	1718.22	0.12	Small Clasts	Isotropic	1
Mod21	B22	Core	1718.10	1718.22	0.12	Small Clasts	Isotropic	5
Mod21	B22	Core	1718.10	1718.22	0.12	Small Clasts	Isotropic	5
Mod21	B22	Core	1718.10	1718.22	0.12	Small Clasts	Isotropic	5
Mod21	B22	Core	1718.10	1718.22	0.12	Small Clasts	Isotropic	5
Mod21	B22	Core	1718.10	1718.22	0.12	Small Clasts	Isotropic	5
Mod21	B22	Core	1718.10	1718.22	0.12	Small Clasts	Isotropic	5
Mod21	B22	Core	1718.10	1718.22	0.12	Small Clasts	Isotropic	10
Mod21	B22	Core	1718.10	1718.22	0.12	Small Clasts	Isotropic	10
Mod21	B22	Core	1718.10	1718.22	0.12	Small Clasts	Isotropic	10
Mod21	B22	Core	1718.10	1718.22	0.12	Small Clasts	Isotropic	10
Mod21	B22	Core	1718.10	1718.22	0.12	Small Clasts	Isotropic	10
Mod21	B22	Core	1718.10	1718.22	0.12	Small Clasts	Isotropic	10
Mod21	B22	Core	1718.10	1718.22	0.12	Small Clasts	Isotropic	15
Mod21	B22	Core	1718.10	1718.22	0.12	Small Clasts	Isotropic	15
Mod21	B22	Core	1718.10	1718.22	0.12	Small Clasts	Isotropic	15
Mod21	B22	Core	1718.10	1718.22	0.12	Small Clasts	Isotropic	15
Mod21	B22	Core	1718.10	1718.22	0.12	Small Clasts	Isotropic	15
Mod21	B22	Core	1718.10	1718.22	0.12	Small Clasts	Isotropic	15
Mod21	B22	Core	1718.10	1718.22	0.12	Small Clasts	Isotropic	20
Mod21	B22	Core	1718.10	1718.22	0.12	Small Clasts	Isotropic	20
Mod21	B22	Core	1718.10	1718.22	0.12	Small Clasts	Isotropic	20
Mod21	B22	Core	1718.10	1718.22	0.12	Small Clasts	Isotropic	20
Mod21	B22	Core	1718.10	1718.22	0.12	Small Clasts	Isotropic	20
Mod21	B22	Core	1718.10	1718.22	0.12	Small Clasts	Isotropic	20
Mod21	B22	Core	1718.10	1718.22	0.12	Small Clasts	Isotropic	25
Mod21	B22	Core	1718.10	1718.22	0.12	Small Clasts	Isotropic	25

Mod21	B22	Core	1718.10	1718.22	0.12	Small Clasts	Isotropic	25
Mod21	B22	Core	1718.10	1718.22	0.12	Small Clasts	Isotropic	25
Mod21	B22	Core	1718.10	1718.22	0.12	Small Clasts	Isotropic	25
Mod21	B22	Core	1718.10	1718.22	0.12	Small Clasts	Isotropic	25
Mod21	B22	Core	1718.10	1718.22	0.12	Small Clasts	Isotropic	30
Mod21	B22	Core	1718.10	1718.22	0.12	Small Clasts	Isotropic	30
Mod21	B22	Core	1718.10	1718.22	0.12	Small Clasts	Isotropic	30
Mod21	B22	Core	1718.10	1718.22	0.12	Small Clasts	Isotropic	30
Mod21	B22	Core	1718.10	1718.22	0.12	Small Clasts	Isotropic	30
Mod21	B22	Core	1718.10	1718.22	0.12	Small Clasts	Isotropic	30
Mod23	B22	Core	2437.02	2437.13	0.12	Small Clasts	Geometric, horizontal	1
Mod23	B22	Core	2437.02	2437.13	0.12	Small Clasts	Geometric, horizontal	1
Mod23	B22	Core	2437.02	2437.13	0.12	Small Clasts	Geometric, horizontal	1
Mod23	B22	Core	2437.02	2437.13	0.12	Small Clasts	Geometric, horizontal	1
Mod23	B22	Core	2437.02	2437.13	0.12	Small Clasts	Geometric, horizontal	1
Mod23	B22	Core	2437.02	2437.13	0.12	Small Clasts	Geometric, horizontal	1
Mod23	B22	Core	2437.02	2437.13	0.12	Small Clasts	Geometric, horizontal	5
Mod23	B22	Core	2437.02	2437.13	0.12	Small Clasts	Geometric, horizontal	5
Mod23	B22	Core	2437.02	2437.13	0.12	Small Clasts	Geometric, horizontal	5
Mod23	B22	Core	2437.02	2437.13	0.12	Small Clasts	Geometric, horizontal	5
Mod23	B22	Core	2437.02	2437.13	0.12	Small Clasts	Geometric, horizontal	5
Mod23	B22	Core	2437.02	2437.13	0.12	Small Clasts	Geometric, horizontal	5
Mod23	B22	Core	2437.02	2437.13	0.12	Small Clasts	Geometric, horizontal	10
Mod23	B22	Core	2437.02	2437.13	0.12	Small Clasts	Geometric, horizontal	10
Mod23	B22	Core	2437.02	2437.13	0.12	Small Clasts	Geometric, horizontal	10
Mod23	B22	Core	2437.02	2437.13	0.12	Small Clasts	Geometric, horizontal	10
Mod23	B22	Core	2437.02	2437.13	0.12	Small Clasts	Geometric, horizontal	10
Mod23	B22	Core	2437.02	2437.13	0.12	Small Clasts	Geometric, horizontal	10
Mod23	B22	Core	2437.02	2437.13	0.12	Small Clasts	Geometric, horizontal	15
Mod23	B22	Core	2437.02	2437.13	0.12	Small Clasts	Geometric, horizontal	15
Mod23	B22	Core	2437.02	2437.13	0.12	Small Clasts	Geometric, horizontal	15
Mod23	B22	Core	2437.02	2437.13	0.12	Small Clasts	Geometric, horizontal	15
Mod23	B22	Core	2437.02	2437.13	0.12	Small Clasts	Geometric, horizontal	15

Mod23	B22	Core	2437.02	2437.13	0.12	Small Clasts	Geometric, horizontal	15
Mod23	B22	Core	2437.02	2437.13	0.12	Small Clasts	Geometric, horizontal	20
Mod23	B22	Core	2437.02	2437.13	0.12	Small Clasts	Geometric, horizontal	20
Mod23	B22	Core	2437.02	2437.13	0.12	Small Clasts	Geometric, horizontal	20
Mod23	B22	Core	2437.02	2437.13	0.12	Small Clasts	Geometric, horizontal	20
Mod23	B22	Core	2437.02	2437.13	0.12	Small Clasts	Geometric, horizontal	20
Mod23	B22	Core	2437.02	2437.13	0.12	Small Clasts	Geometric, horizontal	20
Mod23	B22	Core	2437.02	2437.13	0.12	Small Clasts	Geometric, horizontal	25
Mod23	B22	Core	2437.02	2437.13	0.12	Small Clasts	Geometric, horizontal	25
Mod23	B22	Core	2437.02	2437.13	0.12	Small Clasts	Geometric, horizontal	25
Mod23	B22	Core	2437.02	2437.13	0.12	Small Clasts	Geometric, horizontal	25
Mod23	B22	Core	2437.02	2437.13	0.12	Small Clasts	Geometric, horizontal	25
Mod23	B22	Core	2437.02	2437.13	0.12	Small Clasts	Geometric, horizontal	25
Mod23	B22	Core	2437.02	2437.13	0.12	Small Clasts	Geometric, horizontal	30
Mod23	B22	Core	2437.02	2437.13	0.12	Small Clasts	Geometric, horizontal	30
Mod23	B22	Core	2437.02	2437.13	0.12	Small Clasts	Geometric, horizontal	30
Mod23	B22	Core	2437.02	2437.13	0.12	Small Clasts	Geometric, horizontal	30
Mod23	B22	Core	2437.02	2437.13	0.12	Small Clasts	Geometric, horizontal	30
Mod23	B22	Core	2437.02	2437.13	0.12	Small Clasts	Geometric, horizontal	30
Mod25	B19	Core	1619.30	1619.39	0.09	Small Clasts	Zonal, horizontal	1
Mod25	B19	Core	1619.30	1619.39	0.09	Small Clasts	Zonal, horizontal	1
Mod25	B19	Core	1619.30	1619.39	0.09	Small Clasts	Zonal, horizontal	1
Mod25	B19	Core	1619.30	1619.39	0.09	Small Clasts	Zonal, horizontal	1
Mod25	B19	Core	1619.30	1619.39	0.09	Small Clasts	Zonal, horizontal	1
Mod25	B19	Core	1619.30	1619.39	0.09	Small Clasts	Zonal, horizontal	1
Mod25	B19	Core	1619.30	1619.39	0.09	Small Clasts	Zonal, horizontal	5
Mod25	B19	Core	1619.30	1619.39	0.09	Small Clasts	Zonal, horizontal	5
Mod25	B19	Core	1619.30	1619.39	0.09	Small Clasts	Zonal, horizontal	5
Mod25	B19	Core	1619.30	1619.39	0.09	Small Clasts	Zonal, horizontal	5
Mod25	B19	Core	1619.30	1619.39	0.09	Small Clasts	Zonal, horizontal	5
Mod25	B19	Core	1619.30	1619.39	0.09	Small Clasts	Zonal, horizontal	5
Mod25	B19	Core	1619.30	1619.39	0.09	Small Clasts	Zonal, horizontal	10
Mod25	B19	Core	1619.30	1619.39	0.09	Small Clasts	Zonal, horizontal	10

Mod25	B19	Core	1619.30	1619.39	0.09	Small Clasts	Zonal, horizontal	10
Mod25	B19	Core	1619.30	1619.39	0.09	Small Clasts	Zonal, horizontal	10
Mod25	B19	Core	1619.30	1619.39	0.09	Small Clasts	Zonal, horizontal	10
Mod25	B19	Core	1619.30	1619.39	0.09	Small Clasts	Zonal, horizontal	10
Mod25	B19	Core	1619.30	1619.39	0.09	Small Clasts	Zonal, horizontal	15
Mod25	B19	Core	1619.30	1619.39	0.09	Small Clasts	Zonal, horizontal	15
Mod25	B19	Core	1619.30	1619.39	0.09	Small Clasts	Zonal, horizontal	15
Mod25	B19	Core	1619.30	1619.39	0.09	Small Clasts	Zonal, horizontal	15
Mod25	B19	Core	1619.30	1619.39	0.09	Small Clasts	Zonal, horizontal	15
Mod25	B19	Core	1619.30	1619.39	0.09	Small Clasts	Zonal, horizontal	15
Mod25	B19	Core	1619.30	1619.39	0.09	Small Clasts	Zonal, horizontal	20
Mod25	B19	Core	1619.30	1619.39	0.09	Small Clasts	Zonal, horizontal	20
Mod25	B19	Core	1619.30	1619.39	0.09	Small Clasts	Zonal, horizontal	20
Mod25	B19	Core	1619.30	1619.39	0.09	Small Clasts	Zonal, horizontal	20
Mod25	B19	Core	1619.30	1619.39	0.09	Small Clasts	Zonal, horizontal	20
Mod25	B19	Core	1619.30	1619.39	0.09	Small Clasts	Zonal, horizontal	20
Mod25	B19	Core	1619.30	1619.39	0.09	Small Clasts	Zonal, horizontal	25
Mod25	B19	Core	1619.30	1619.39	0.09	Small Clasts	Zonal, horizontal	25
Mod25	B19	Core	1619.30	1619.39	0.09	Small Clasts	Zonal, horizontal	25
Mod25	B19	Core	1619.30	1619.39	0.09	Small Clasts	Zonal, horizontal	25
Mod25	B19	Core	1619.30	1619.39	0.09	Small Clasts	Zonal, horizontal	25
Mod25	B19	Core	1619.30	1619.39	0.09	Small Clasts	Zonal, horizontal	25
Mod25	B19	Core	1619.30	1619.39	0.09	Small Clasts	Zonal, horizontal	30
Mod25	B19	Core	1619.30	1619.39	0.09	Small Clasts	Zonal, horizontal	30
Mod25	B19	Core	1619.30	1619.39	0.09	Small Clasts	Zonal, horizontal	30
Mod25	B19	Core	1619.30	1619.39	0.09	Small Clasts	Zonal, horizontal	30
Mod25	B19	Core	1619.30	1619.39	0.09	Small Clasts	Zonal, horizontal	30
Mod25	B19	Core	1619.30	1619.39	0.09	Small Clasts	Zonal, horizontal	30
Mod26	B19	Core	1618.51	1618.63	0.12	Small Clasts	Geometric, horizontal	1
Mod26	B19	Core	1618.51	1618.63	0.12	Small Clasts	Geometric, horizontal	1
Mod26	B19	Core	1618.51	1618.63	0.12	Small Clasts	Geometric, horizontal	1
Mod26	B19	Core	1618.51	1618.63	0.12	Small Clasts	Geometric, horizontal	1
Mod26	B19	Core	1618.51	1618.63	0.12	Small Clasts	Geometric, horizontal	1

Mod26	B19	Core	1618.51	1618.63	0.12	Small Clasts	Geometric, horizontal	1
Mod26	B19	Core	1618.51	1618.63	0.12	Small Clasts	Geometric, horizontal	5
Mod26	B19	Core	1618.51	1618.63	0.12	Small Clasts	Geometric, horizontal	5
Mod26	B19	Core	1618.51	1618.63	0.12	Small Clasts	Geometric, horizontal	5
Mod26	B19	Core	1618.51	1618.63	0.12	Small Clasts	Geometric, horizontal	5
Mod26	B19	Core	1618.51	1618.63	0.12	Small Clasts	Geometric, horizontal	5
Mod26	B19	Core	1618.51	1618.63	0.12	Small Clasts	Geometric, horizontal	5
Mod26	B19	Core	1618.51	1618.63	0.12	Small Clasts	Geometric, horizontal	10
Mod26	B19	Core	1618.51	1618.63	0.12	Small Clasts	Geometric, horizontal	10
Mod26	B19	Core	1618.51	1618.63	0.12	Small Clasts	Geometric, horizontal	10
Mod26	B19	Core	1618.51	1618.63	0.12	Small Clasts	Geometric, horizontal	10
Mod26	B19	Core	1618.51	1618.63	0.12	Small Clasts	Geometric, horizontal	10
Mod26	B19	Core	1618.51	1618.63	0.12	Small Clasts	Geometric, horizontal	10
Mod26	B19	Core	1618.51	1618.63	0.12	Small Clasts	Geometric, horizontal	15
Mod26	B19	Core	1618.51	1618.63	0.12	Small Clasts	Geometric, horizontal	15
Mod26	B19	Core	1618.51	1618.63	0.12	Small Clasts	Geometric, horizontal	15
Mod26	B19	Core	1618.51	1618.63	0.12	Small Clasts	Geometric, horizontal	15
Mod26	B19	Core	1618.51	1618.63	0.12	Small Clasts	Geometric, horizontal	15
Mod26	B19	Core	1618.51	1618.63	0.12	Small Clasts	Geometric, horizontal	15
Mod26	B19	Core	1618.51	1618.63	0.12	Small Clasts	Geometric, horizontal	20
Mod26	B19	Core	1618.51	1618.63	0.12	Small Clasts	Geometric, horizontal	20
Mod26	B19	Core	1618.51	1618.63	0.12	Small Clasts	Geometric, horizontal	20
Mod26	B19	Core	1618.51	1618.63	0.12	Small Clasts	Geometric, horizontal	20
Mod26	B19	Core	1618.51	1618.63	0.12	Small Clasts	Geometric, horizontal	20
Mod26	B19	Core	1618.51	1618.63	0.12	Small Clasts	Geometric, horizontal	20
Mod26	B19	Core	1618.51	1618.63	0.12	Small Clasts	Geometric, horizontal	25
Mod26	B19	Core	1618.51	1618.63	0.12	Small Clasts	Geometric, horizontal	25
Mod26	B19	Core	1618.51	1618.63	0.12	Small Clasts	Geometric, horizontal	25
Mod26	B19	Core	1618.51	1618.63	0.12	Small Clasts	Geometric, horizontal	25
Mod26	B19	Core	1618.51	1618.63	0.12	Small Clasts	Geometric, horizontal	25
Mod26	B19	Core	1618.51	1618.63	0.12	Small Clasts	Geometric, horizontal	25
Mod26	B19	Core	1618.51	1618.63	0.12	Small Clasts	Geometric, horizontal	30
Mod26	B19	Core	1618.51	1618.63	0.12	Small Clasts	Geometric, horizontal	30

Mod26	B19	Core	1618.51	1618.63	0.12	Small Clasts	Geometric, horizontal	30
Mod26	B19	Core	1618.51	1618.63	0.12	Small Clasts	Geometric, horizontal	30
Mod26	B19	Core	1618.51	1618.63	0.12	Small Clasts	Geometric, horizontal	30
Mod26	B19	Core	1618.51	1618.63	0.12	Small Clasts	Geometric, horizontal	30

Mud content [%]	Mean cohesive content [%]	Mean porosity [fraction]	Minimum log10 effective Kh [m2]	Mean log10 effective Kh [m2]
50	39.18235161	0.413767902	-15.82632433	-15.65572227
60	46.01881599	0.431367856	-16.30411136	-16.24489482
70	52.85528036	0.449038997	-16.56121882	-16.54376417
80	59.69174474	0.466731229	-16.7403058	-16.73308322
90	66.52820912	0.484390752	-16.87178819	-16.86949859
100	73.36467349	0.501934016	-16.9706284	-16.96985894
50	39.18235161	0.332846534	-16.93026532	-16.72957145
60	46.01881599	0.342474117	-17.39954552	-17.34291466
70	52.85528036	0.351995869	-17.65318363	-17.63550213
80	59.69174474	0.361558672	-17.82510905	-17.81760367
90	66.52820912	0.371147485	-17.95097202	-17.94849833
100	73.36467349	0.380702214	-18.04675849	-18.04599174
50	39.18235161	0.283362045	-17.5231901	-17.32582311
60	46.01881599	0.288103693	-17.99343128	-17.93625181
70	52.85528036	0.292748572	-18.24136739	-18.22425073
80	59.69174474	0.297548038	-18.4117451	-18.40383893
90	66.52820912	0.302200052	-18.53268646	-18.53095219
100	73.36467349	0.306897025	-18.6271745	-18.62639713
50	39.18235161	0.24747734	-17.93413657	-17.73173944
60	46.01881599	0.24893603	-18.39938427	-18.34226344
70	52.85528036	0.250326384	-18.64598189	-18.62876105
80	59.69174474	0.251680243	-18.81166785	-18.80454106
90	66.52820912	0.253125505	-18.93214462	-18.93014062
100	73.36467349	0.254522907	-19.02480999	-19.02386892
50	39.18235161	0.218023032	-18.26244639	-18.06037247
60	46.01881599	0.216767169	-18.72866033	-18.67168256
70	52.85528036	0.215563353	-18.97235281	-18.95469769
80	59.69174474	0.214318467	-19.1361872	-19.12908364
90	66.52820912	0.213090061	-19.25544261	-19.2529059
100	73.36467349	0.211907698	-19.34667265	-19.34564396
50	39.18235161	0.192396069	-18.54817674	-18.35323083
60	46.01881599	0.188928742	-19.01735977	-18.95930814

70	52.85528036	0.185430665	-19.25977157	-19.24081957
80	59.69174474	0.182021966	-19.42195477	-19.41448257
90	66.52820912	0.178558897	-19.53931109	-19.53699427
100	73.36467349	0.175027645	-19.62849621	-19.62793274
50	39.18235161	0.169472339	-18.82308436	-18.61699
60	46.01881599	0.164043788	-19.28198852	-19.22465511
70	52.85528036	0.158561611	-19.52382799	-19.50586701
80	59.69174474	0.153048527	-19.68450407	-19.67753863
90	66.52820912	0.147562268	-19.80123848	-19.79937587
100	73.36467349	0.142057813	-19.89050582	-19.88977384
50	39.18235161	0.413773727	-15.483917	-15.1082069
60	46.01881599	0.43139688	-15.97881484	-15.87866916
70	52.85528036	0.449017238	-16.34317379	-16.309114
80	59.69174474	0.466780917	-16.61092078	-16.58850512
90	66.52820912	0.484414078	-16.80872509	-16.79885944
100	73.36467349	0.50198557	-16.96525126	-16.96438275
50	39.18235161	0.332846631	-16.60137261	-16.01020635
60	46.01881599	0.34242899	-17.09064994	-16.97925229
70	52.85528036	0.351981027	-17.4441622	-17.41229271
80	59.69174474	0.361537244	-17.70074555	-17.67915798
90	66.52820912	0.371154784	-17.88754917	-17.87899282
100	73.36467349	0.380706267	-18.03861071	-18.03732445
50	39.18235161	0.283340366	-17.20320303	-16.52871235
60	46.01881599	0.288060867	-17.69636771	-17.58120268
70	52.85528036	0.292841042	-18.04145475	-18.00929979
80	59.69174474	0.297486355	-18.28987586	-18.27029672
90	66.52820912	0.302237157	-18.47351081	-18.4647368
100	73.36467349	0.30693691	-18.61857082	-18.61797533
50	39.18235161	0.247485869	-17.60380589	-16.92530779
60	46.01881599	0.248940924	-18.10622604	-17.99453245
70	52.85528036	0.250335016	-18.44693174	-18.41722945
80	59.69174474	0.251727275	-18.69451535	-18.67603824
90	66.52820912	0.253080668	-18.87484743	-18.86555438

100	73.36467349	0.254459557	-19.01627721	-19.01570931
50	39.18235161	0.218006598	-17.94985621	-17.23943421
60	46.01881599	0.216775288	-18.43721125	-18.32824345
70	52.85528036	0.215587444	-18.77909992	-18.74841471
80	59.69174474	0.214377644	-19.02282304	-19.00398345
90	66.52820912	0.213147482	-19.19936951	-19.19098861
100	73.36467349	0.211855115	-19.33854322	-19.33806921
50	39.18235161	0.19237998	-18.2368454	-17.54252137
60	46.01881599	0.188896295	-18.72680884	-18.62029132
70	52.85528036	0.185461322	-19.06677701	-19.03807115
80	59.69174474	0.181990402	-19.30973745	-19.29078088
90	66.52820912	0.178519651	-19.48470781	-19.47619499
100	73.36467349	0.175046611	-19.62199478	-19.62135862
50	39.18235161	0.169518977	-18.51359928	-17.81095219
60	46.01881599	0.164030882	-19.00060365	-18.88688299
70	52.85528036	0.158539325	-19.33177068	-19.30371914
80	59.69174474	0.153055103	-19.5753666	-19.55649157
90	66.52820912	0.147576797	-19.74901188	-19.73995707
100	73.36467349	0.142058905	-19.8845659	-19.8834125
50	39.18235161	0.413773816	-15.20609024	-14.22346113
60	46.01881599	0.431388559	-15.7305431	-15.24958429
70	52.85528036	0.449031791	-16.18283209	-16.04443371
80	59.69174474	0.466705769	-16.50553372	-16.44186781
90	66.52820912	0.484341099	-16.76807953	-16.75121895
100	73.36467349	0.501950307	-16.9626253	-16.96137266
50	39.18235161	0.332864426	-16.30818675	-14.70185541
60	46.01881599	0.342374321	-16.84699658	-16.21537414
70	52.85528036	0.351940289	-17.28823156	-17.15046831
80	59.69174474	0.361551185	-17.59611285	-17.53354142
90	66.52820912	0.371162299	-17.8432389	-17.82795024
100	73.36467349	0.380669338	-18.03344248	-18.03268591
50	39.18235161	0.283329598	-16.92021478	-15.07703411
60	46.01881599	0.288138149	-17.45138459	-16.76762661

70	52.85528036	0.292792518	-17.88608672	-17.75274673
80	59.69174474	0.297537407	-18.1902491	-18.12780631
90	66.52820912	0.302209347	-18.42953062	-18.41354085
100	73.36467349	0.306885638	-18.61429723	-18.61305724
50	39.18235161	0.247534367	-17.32497546	-15.44197609
60	46.01881599	0.248924337	-17.86144785	-17.15566132
70	52.85528036	0.250390245	-18.2973317	-18.16487162
80	59.69174474	0.251703745	-18.59620881	-18.53585181
90	66.52820912	0.25309618	-18.83092835	-18.81598559
100	73.36467349	0.254523079	-19.01295971	-19.01166487
50	39.18235161	0.21799477	-17.66735353	-15.75419301
60	46.01881599	0.216800146	-18.19767585	-17.49698445
70	52.85528036	0.215610178	-18.63285475	-18.4983392
80	59.69174474	0.214345699	-18.92454794	-18.8659836
90	66.52820912	0.213110124	-19.15767976	-19.14259021
100	73.36467349	0.211874514	-19.33491737	-19.33413419
50	39.18235161	0.19237557	-17.95744418	-16.03857951
60	46.01881599	0.188927055	-18.4917653	-17.78429796
70	52.85528036	0.185477848	-18.91954308	-18.78949199
80	59.69174474	0.18200566	-19.2143186	-19.1550925
90	66.52820912	0.178532259	-19.44328994	-19.42847903
100	73.36467349	0.175026173	-19.61825155	-19.61741579
50	39.18235161	0.169505079	-18.24784856	-16.32337721
60	46.01881599	0.163988846	-18.7598353	-18.05428048
70	52.85528036	0.158559626	-19.18823269	-19.05767951
80	59.69174474	0.153054413	-19.48103095	-19.42222262
90	66.52820912	0.147570361	-19.70970934	-19.69339558
100	73.36467349	0.142059917	-19.88060883	-19.87984732
50	39.18235161	0.413713638	-15.63534771	-15.47021861
60	46.01881599	0.431436357	-16.18994971	-16.14034327
70	52.85528036	0.449042624	-16.50054112	-16.48309728
80	59.69174474	0.466705869	-16.71548354	-16.70376203
90	66.52820912	0.48437434	-16.86288019	-16.85995914

100	73.36467349	0.501996977	-16.96762706	-16.96708896
50	39.18235161	0.332914973	-16.73655805	-16.56007336
60	46.01881599	0.342428271	-17.28814049	-17.2402084
70	52.85528036	0.352007982	-17.59165147	-17.57395066
80	59.69174474	0.361563489	-17.79826431	-17.78616328
90	66.52820912	0.371067528	-17.93831008	-17.93552295
100	73.36467349	0.38055432	-18.04217347	-18.04130296
50	39.18235161	0.28334768	-17.33086357	-17.15577628
60	46.01881599	0.288082246	-17.88462917	-17.83738816
70	52.85528036	0.292753034	-18.18378854	-18.16569523
80	59.69174474	0.297487394	-18.38578322	-18.37327767
90	66.52820912	0.302211361	-18.52133107	-18.51894779
100	73.36467349	0.306929601	-18.62329715	-18.62243856
50	39.18235161	0.247543833	-17.74441636	-17.56799544
60	46.01881599	0.248950793	-18.2944339	-18.24583188
70	52.85528036	0.250357944	-18.58781003	-18.57136149
80	59.69174474	0.251720865	-18.78629635	-18.77549472
90	66.52820912	0.253139777	-18.92119893	-18.9188744
100	73.36467349	0.254504104	-19.02089662	-19.02015464
50	39.18235161	0.217981979	-18.08268726	-17.90402205
60	46.01881599	0.216778123	-18.62417184	-18.577126
70	52.85528036	0.215563298	-18.91552382	-18.89924021
80	59.69174474	0.21436005	-19.11280764	-19.1012219
90	66.52820912	0.213116822	-19.24437665	-19.24234327
100	73.36467349	0.21187151	-19.34302929	-19.34205374
50	39.18235161	0.192391239	-18.36873689	-18.19467371
60	46.01881599	0.188921274	-18.91153078	-18.86666713
70	52.85528036	0.185463114	-19.20264173	-19.18709481
80	59.69174474	0.181990867	-19.39849517	-19.38703489
90	66.52820912	0.178525948	-19.5289343	-19.52668537
100	73.36467349	0.175058275	-19.62578339	-19.62506762
50	39.18235161	0.169504556	-18.63550529	-18.46279841
60	46.01881599	0.164018799	-19.17825858	-19.13393392

70	52.85528036	0.158549735	-19.46722906	-19.45287358
80	59.69174474	0.153059225	-19.66269252	-19.65129832
90	66.52820912	0.147574286	-19.79200499	-19.78980185
100	73.36467349	0.142070523	-19.88796169	-19.88717382

Mode log10 effective Kh [m2]	Maximum log10 effective Kh [m2]	Standard deviation log10 effective Kh [m2]	Minimum log10 effective Kv [m2]
-15.82632433	-15.36372379	0.161410246	-15.6882186
-16.30411136	-16.16937413	0.043261209	-16.27303086
-16.55494072	-16.51727216	0.012908118	-16.61900592
-16.7403058	-16.72030569	0.005459048	-16.85923749
-16.87090367	-16.86559656	0.0016533	-17.03306177
-16.9706284	-16.96920604	0.000465584	-17.15206414
-16.93026532	-16.35210186	0.191094471	-16.80496149
-17.39954552	-17.26725091	0.042740841	-17.41785251
-17.65318363	-17.60865551	0.012973558	-17.77908425
-17.82206277	-17.80378511	0.005753364	-18.03349924
-17.94907028	-17.94431594	0.001847128	-18.22401912
-18.04675849	-18.04531474	0.000464978	-18.35814332
-17.5231901	-16.94410205	0.191489858	-17.4052628
-17.97441257	-17.86030033	0.043497791	-18.03008065
-18.23522969	-18.19840354	0.012501236	-18.39729881
-18.40900591	-18.39257071	0.005126718	-18.6609403
-18.53268646	-18.52756976	0.001483145	-18.85750416
-18.62635127	-18.62602197	0.000348418	-18.99844367
-17.93413657	-17.34408783	0.194225923	-17.82227597
-18.38060412	-18.26792323	0.042616139	-18.45630188
-18.64598189	-18.60518597	0.011987091	-18.82426501
-18.80887963	-18.79215029	0.005211409	-19.08806456
-18.93214462	-18.92601785	0.001862343	-19.2879938
-19.02430966	-19.02305883	0.000531093	-19.43202017
-18.26244639	-17.67000042	0.195430879	-18.15566761
-18.70976342	-18.59638196	0.042106595	-18.79591802
-18.97235281	-18.92940069	0.012123644	-19.16728612
-19.13350336	-19.11740034	0.004867509	-19.43135482
-19.25350628	-19.24866546	0.001740502	-19.63515832
-19.34569925	-19.34496919	0.000467989	-19.7813516
-18.54817674	-17.97394501	0.190990097	-18.45023677
-18.9982078	-18.88329598	0.043550402	-19.08766898

-19.24703118	-19.21518023	0.012669429	-19.46106325
-19.4191304	-19.40218419	0.005267521	-19.7331782
-19.5378659	-19.53425291	0.001349171	-19.93794475
-19.62795027	-19.62722235	0.000386772	-20.0843364
-18.82308436	-18.22894855	0.196402366	-18.71848713
-19.26302407	-19.1492374	0.04211096	-19.35973328
-19.52382799	-19.48111509	0.011918368	-19.73569939
-19.68184063	-19.66586002	0.005007291	-20.00769838
-19.79983241	-19.79631725	0.001333667	-20.21603928
-19.88965838	-19.8893194	0.000348956	-20.3632514
-15.34396403	-14.5042462	0.329112602	-16.00218085
-15.97881484	-15.67775796	0.107163204	-16.48970438
-16.32540054	-16.21876106	0.032533897	-16.75143581
-16.60518142	-16.57074526	0.013100586	-16.93902656
-16.80017289	-16.78876996	0.006391995	-17.06754856
-16.9644028	-16.96376646	0.000384803	-17.16125352
-16.60137261	-14.93846836	0.610948077	-17.15143589
-17.09064994	-16.70890656	0.126290105	-17.65562934
-17.42734935	-17.32647225	0.031067955	-17.93128366
-17.68992235	-17.66286433	0.012194876	-18.12982501
-17.88754917	-17.86945075	0.005840458	-18.27158209
-18.03724551	-18.03622161	0.000611463	-18.3736083
-17.20320303	-15.25415572	0.735214272	-17.77508383
-17.69636771	-17.31846481	0.125971818	-18.27767381
-18.02495225	-17.92593728	0.02983058	-18.55851539
-18.26122534	-18.25645026	0.011634577	-18.76186353
-18.47351081	-18.45547185	0.006053048	-18.90849483
-18.61779586	-18.61748588	0.000322669	-19.01526392
-17.60380589	-15.6414142	0.760773726	-18.18425295
-18.10622604	-17.72627666	0.125357692	-18.70358932
-18.43094055	-18.33499345	0.029531164	-18.9846654
-18.69451535	-18.66157737	0.011033676	-19.19183091
-18.87484743	-18.85489376	0.006192203	-19.34114279

-19.01590958	-19.01499051	0.000356065	-19.44887462
-17.94985621	-15.87575995	0.788799893	-18.5280881
-18.43721125	-18.07269946	0.12328557	-19.04683346
-18.7626861	-18.66420322	0.030203555	-19.32845229
-19.02282304	-18.98807026	0.011253661	-19.53825693
-19.19936951	-19.18139146	0.005746946	-19.68775492
-19.33854322	-19.33727899	0.000458777	-19.79777605
-18.2368454	-16.20790682	0.775058521	-18.82152955
-18.72680884	-18.37017058	0.121610507	-19.34367848
-19.05129375	-18.95839417	0.028698125	-19.63060972
-19.28161849	-19.276932	0.011190099	-19.83915946
-19.47505931	-19.46782294	0.005570396	-19.99113593
-19.62165798	-19.62081599	0.000341884	-20.10065562
-18.51359928	-16.50716142	0.772554246	-19.10357245
-19.00060365	-18.61877117	0.125406942	-19.61907276
-19.31619963	-19.22277333	0.029077983	-19.90283643
-19.5474793	-19.54283142	0.010437579	-20.11590165
-19.74901188	-19.73145479	0.005746356	-20.26881429
-19.88309632	-19.88285139	0.000528048	-20.37991602
-13.96626546	-13.759628	0.403682999	-16.41349821
-15.7305431	-14.32381596	0.457872696	-16.67349414
-16.11254737	-15.93683559	0.075608298	-16.86307343
-16.48762137	-16.38014732	0.040253781	-16.99321317
-16.75237719	-16.73144075	0.009876149	-17.09063014
-16.96090782	-16.96062158	0.000569034	-17.16730974
-14.45716828	-14.1486652	0.589826263	-17.58998746
-16.54583332	-14.73885375	0.719572238	-17.8691968
-17.21664646	-17.03768371	0.075002214	-18.06564348
-17.49475976	-17.47786758	0.038344571	-18.20161941
-17.83339778	-17.80879499	0.009947037	-18.30544218
-18.03285701	-18.03207639	0.000365627	-18.38663183
-14.85929014	-14.51580269	0.652650072	-18.22062504
-17.45138459	-15.09244515	0.819527335	-18.50457917

-17.84998989	-17.63340896	0.074995338	-18.702835
-18.09076629	-18.07418582	0.037749218	-18.84345993
-18.41993401	-18.39594251	0.009510351	-18.94803755
-18.61332493	-18.61202854	0.000620496	-19.02976706
-15.18797315	-14.8318061	0.676872234	-18.64465769
-17.86144785	-15.39875508	0.859495388	-18.93311526
-18.22797032	-18.05456687	0.073236986	-19.13600658
-18.4987141	-18.48246498	0.036380226	-19.27639165
-18.82110469	-18.79654554	0.009810142	-19.38044026
-19.01120232	-19.01090942	0.000694671	-19.46576442
-15.50721662	-15.1471938	0.68502849	-18.99112742
-18.19767585	-15.77519769	0.854008452	-19.27785246
-18.56315109	-18.38889194	0.072593905	-19.48094945
-18.82898737	-18.81306061	0.035941325	-19.62219671
-19.14858918	-19.12586274	0.009095038	-19.73112963
-19.33491737	-19.33335287	0.000535148	-19.81471289
-15.82312584	-15.46740612	0.681877132	-19.29050532
-18.4917653	-16.00249435	0.869994178	-19.58078302
-18.85171938	-18.68216013	0.071284263	-19.78293212
-19.11786083	-19.10178454	0.036380232	-19.92417212
-19.4345355	-19.41264941	0.008880814	-20.03353443
-19.61746728	-19.61642159	0.000496027	-20.118661
-16.10265761	-15.74512578	0.682411409	-19.57126765
-18.7598353	-16.28864923	0.867424577	-19.855812
-19.11893466	-18.9456896	0.072130364	-20.05832462
-19.38479804	-19.36875922	0.036086584	-20.20287794
-19.69542039	-19.67636844	0.008995872	-20.31319398
-19.87994407	-19.87905773	0.000456702	-20.39778803
-15.63534771	-15.26951974	0.134001852	-16.24652419
-16.1488054	-16.09394632	0.029526194	-16.62689666
-16.47567502	-16.47153067	0.009000014	-16.83938143
-16.70432474	-16.69595563	0.00620827	-16.9772006
-16.86288019	-16.85694771	0.001874313	-17.08156755

-16.96748441	-16.96662852	0.000302496	-17.16095017
-16.73655805	-16.32482221	0.14892798	-17.4003647
-17.28814049	-17.19305187	0.02934624	-17.80039016
-17.57063417	-17.56222725	0.008868634	-18.02589654
-17.78722818	-17.77895109	0.005824078	-18.17703209
-17.93831008	-17.93259062	0.001811828	-18.28991904
-18.04113838	-18.04072434	0.000433321	-18.37514266
-17.33086357	-16.90476089	0.153101011	-18.01721425
-17.88462917	-17.79167422	0.02808104	-18.4258101
-18.15989591	-18.1559138	0.008675823	-18.65625867
-18.36888377	-18.3660672	0.005904739	-18.81319335
-18.52133107	-18.51658674	0.001441831	-18.92888789
-18.62256437	-18.62201478	0.000346196	-19.01899187
-17.74441636	-17.33019423	0.151412951	-18.43649162
-18.2944339	-18.20132036	0.028828889	-18.84914536
-18.56505958	-18.56126784	0.008178963	-19.08942095
-18.77131971	-18.76882361	0.005377675	-19.24285992
-18.92053957	-18.91658339	0.001426243	-19.36307201
-19.01973133	-19.01953711	0.000392933	-19.45407591
-18.08268726	-17.64579549	0.156234087	-18.77915737
-18.62417184	-18.52958804	0.028222938	-19.19397613
-18.89562814	-18.88766987	0.008545956	-19.4326301
-19.09698109	-19.09434333	0.00571008	-19.59064858
-19.24437665	-19.24015696	0.001437552	-19.71003889
-19.34209722	-19.34139817	0.000441403	-19.80297596
-18.36873689	-17.94594645	0.151977304	-19.0800239
-18.88622158	-18.82294856	0.027755451	-19.49315416
-19.18082606	-19.17719011	0.007800336	-19.72930254
-19.38806727	-19.38024633	0.005436754	-19.89102252
-19.5289343	-19.52447844	0.00148266	-20.013282
-19.62496026	-19.62482307	0.000281362	-20.10701545
-18.63550529	-18.21602	0.15243963	-19.3507898
-19.17825858	-19.09110876	0.026992862	-19.76684392

-19.46722906	-19.44037941	0.007814846	-20.00977662
-19.65246356	-19.64479184	0.005453414	-20.17054184
-19.78947832	-19.78758332	0.001428387	-20.29246389
-19.88771437	-19.8862304	0.000486288	-20.38782034

Mean log10 effective Kv [m2]	Mode log10 effective Kv [m2]	Maximum log10 effective Kv [m2]	Standard deviation log10 effective Kv [m2]
-15.41867682	-15.6882186	-14.99357247	0.225851867
-16.2206593	-16.27303086	-16.13517103	0.048276311
-16.60233387	-16.61197546	-16.56979268	0.012361475
-16.84902675	-16.84325327	-16.84058923	0.006800353
-17.0271206	-17.02990163	-17.02200128	0.002884839
-17.15086264	-17.15120128	-17.15005079	0.000571102
-16.48497321	-16.80496149	-15.93085381	0.275068214
-17.3425255	-17.28614076	-17.2641888	0.054587821
-17.75537357	-17.76340777	-17.72421659	0.015792042
-18.02157452	-18.03349924	-18.01088627	0.007950279
-18.21649033	-18.21402283	-18.21235678	0.003403087
-18.35741906	-18.35705546	-18.35687415	0.000417419
-17.08077082	-17.4052628	-16.49740357	0.286347431
-17.9543568	-17.89663592	-17.87439513	0.056014619
-18.3741526	-18.38097122	-18.34015223	0.016678539
-18.64827813	-18.65433158	-18.63780979	0.007648578
-18.84956303	-18.84808972	-18.84432395	0.003817512
-18.99720972	-18.99771879	-18.99590658	0.000739963
-17.48899353	-17.82227597	-16.90053	0.28994255
-18.37371144	-18.31110192	-18.28690193	0.059641455
-18.79767146	-18.8069426	-18.76363659	0.017511436
-19.07449082	-19.0671112	-19.06361898	0.008599302
-19.28074978	-19.28190493	-19.27378643	0.003709262
-19.43123063	-19.43202017	-19.43035226	0.000530783
-17.82511585	-18.15566761	-17.22804011	0.289286649
-18.70912761	-18.64502609	-18.61987744	0.061879633
-19.13765368	-19.14117029	-19.10634918	0.01726976
-19.41822279	-19.42434274	-19.40681255	0.0077571
-19.62616402	-19.62796434	-19.61837238	0.004184506
-19.77997192	-19.7813516	-19.77820771	0.000927537
-18.12448468	-18.45023677	-17.52435932	0.289739121
-19.00552832	-18.94388907	-18.91992575	0.059405223

-19.43510228	-19.43529119	-19.40092844	0.017388768
-19.71842732	-19.71096738	-19.70726558	0.008696217
-19.92925158	-19.92854136	-19.92148881	0.004275715
-20.08314112	-20.0843364	-20.08182283	0.000806516
-18.38621485	-18.71848713	-17.78170876	0.291788823
-19.27639975	-19.21376663	-19.18943886	0.060278415
-19.70951751	-19.71906437	-19.67747681	0.017409414
-19.99330179	-19.98572028	-19.98205727	0.008567758
-20.20622409	-20.20498476	-20.20056295	0.004393597
-20.36261557	-20.3632514	-20.36190029	0.000436046
-15.84064712	-16.00218085	-15.45704144	0.165019513
-16.42727593	-16.48970438	-16.26270158	0.065948271
-16.73553451	-16.75143581	-16.71454171	0.011784012
-16.92613486	-16.92625515	-16.91667658	0.006881386
-17.06066169	-17.06100063	-17.05608969	0.002851105
-17.1596149	-17.1592762	-17.15894665	0.000658782
-16.96036578	-17.15143589	-16.46776556	0.201729942
-17.58629092	-17.65562934	-17.41580338	0.069676008
-17.91258271	-17.93128366	-17.88988187	0.013361031
-18.11573889	-18.11438639	-18.10280742	0.008346787
-18.26255851	-18.26315177	-18.25682902	0.003762827
-18.37185711	-18.37199319	-18.3698397	0.001156749
-17.57037579	-17.77508383	-17.07101098	0.206256796
-18.20623714	-18.27767381	-18.02439175	0.073857826
-18.53919956	-18.55851539	-18.51227353	0.014942956
-18.74785461	-18.74326602	-18.73582702	0.008112715
-18.8999949	-18.90024878	-18.89406424	0.003788677
-19.01302569	-19.01277843	-19.01091432	0.001312452
-17.99107155	-18.18425295	-17.48386275	0.207157312
-18.63300934	-18.70358932	-18.45742103	0.072149779
-18.96605237	-18.97809167	-18.93864932	0.014254282
-19.17812454	-19.17366803	-19.16640288	0.007603625
-19.33132587	-19.33187442	-19.32492314	0.004002469

-19.44701377	-19.44708133	-19.44469027	0.001209866
-18.32960345	-18.5280881	-17.80760541	0.213045111
-18.97313338	-19.04683346	-18.79416523	0.073320673
-19.30997592	-19.32845229	-19.28253921	0.014175492
-19.52327249	-19.51780906	-19.50962991	0.008943955
-19.6788054	-19.67896432	-19.67237138	0.00398504
-19.79569957	-19.79488505	-19.79440322	0.001092071
-18.62707933	-18.82152955	-18.10153591	0.212569046
-19.26988214	-19.34367848	-19.08983094	0.074451105
-19.60976576	-19.63060972	-19.58140872	0.014796856
-19.82380579	-19.8307134	-19.80959826	0.008767786
-19.98105894	-19.98125412	-19.97384277	0.004403381
-20.09973492	-20.10065562	-20.09878696	0.000612215
-18.89725242	-19.10357245	-18.36501316	0.2152013
-19.5454965	-19.61907276	-19.37668867	0.071950034
-19.88458472	-19.90283643	-19.85595536	0.014372654
-20.10168017	-20.0974312	-20.09004302	0.008349766
-20.25955816	-20.26176372	-20.25236295	0.004123794
-20.37883628	-20.37991602	-20.37686447	0.000990476
-16.23204496	-16.12837092	-16.08084971	0.120885745
-16.60553104	-16.62057306	-16.48827034	0.055546761
-16.84023005	-16.83815382	-16.81946412	0.013803632
-16.98651429	-16.9911805	-16.97898445	0.004224994
-17.08925836	-17.08984378	-17.08787789	0.000898323
-17.16605762	-17.16656904	-17.16471729	0.000713884
-17.40026883	-17.58998746	-17.22897798	0.133989056
-17.79077055	-17.81003019	-17.66211364	0.062132584
-18.03763188	-18.04205323	-18.01059958	0.016765406
-18.19342049	-18.20161941	-18.18416799	0.00544384
-18.3035007	-18.30475754	-18.30064972	0.001298246
-18.38530232	-18.38663183	-18.38318118	0.00107106
-18.02482027	-18.22062504	-17.85984406	0.136467542
-18.42361582	-18.44507142	-18.29630204	0.062049531

-18.67333825	-18.66989322	-18.64518688	0.01753998
-18.83259218	-18.83547088	-18.82481882	0.005905286
-18.9448881	-18.94715161	-18.941836	0.001794259
-19.02877424	-19.02976706	-19.02725348	0.000763057
-18.45142228	-18.64465769	-18.28464524	0.13720762
-18.85098527	-18.87373804	-18.72529501	0.063920881
-19.10469491	-19.10214347	-19.07674613	0.018241465
-19.26481897	-19.27010939	-19.25440374	0.006565612
-19.37872692	-19.38044026	-19.37572822	0.001415729
-19.4643059	-19.4651183	-19.46124158	0.001264739
-18.79261024	-18.99112742	-18.63012022	0.139822682
-19.19475335	-19.21662494	-19.06355613	0.063767021
-19.44873479	-19.44553076	-19.41896675	0.018898719
-19.61176588	-19.60808396	-19.60243886	0.006261972
-19.72710299	-19.72996444	-19.72297329	0.002501015
-19.81291688	-19.81350235	-19.810476	0.001100431
-19.09360817	-19.29050532	-18.92586039	0.137925679
-19.4950264	-19.51866092	-19.36335567	0.064747575
-19.75121069	-19.74863584	-19.72291363	0.018517423
-19.91426801	-19.92417212	-19.90555333	0.005875752
-20.03084297	-20.03353443	-20.02732053	0.001949637
-20.11698911	-20.11759907	-20.11494425	0.001009348
-19.3715483	-19.57126765	-19.19629235	0.138060689
-19.77224805	-19.79526722	-19.64390527	0.06355786
-20.02825999	-20.02520233	-20.00036061	0.018394665
-20.19284182	-20.20287794	-20.18332793	0.006082409
-20.30971833	-20.31208357	-20.30542112	0.002222439
-20.39697991	-20.39778803	-20.39566593	0.000831333
-16.12961688	-16.20249791	-15.93834022	0.086808706
-16.60392908	-16.60879351	-16.58465599	0.011612216
-16.82943744	-16.83337756	-16.8183679	0.005716492
-16.97451623	-16.97305234	-16.97236096	0.001652962
-17.08020929	-17.07970862	-17.0793988	0.000625762

-17.16037652	-17.16042058	-17.15971445	0.000385861
-17.26493822	-17.34792761	-17.03330507	0.102151426
-17.77358619	-17.77370495	-17.75369103	0.012614699
-18.01564174	-18.02244352	-18.0017254	0.006692836
-18.17293634	-18.17149981	-18.1692869	0.002419173
-18.28746149	-18.28824371	-18.28600993	0.001044511
-18.37450142	-18.37493902	-18.37371713	0.000519564
-17.88034547	-17.96414208	-17.64570904	0.103068236
-18.3988789	-18.40511154	-18.37751346	0.013021963
-18.64644217	-18.64965445	-18.6331439	0.006420983
-18.80832016	-18.80582638	-18.80459855	0.00299735
-18.92721039	-18.92780027	-18.92508121	0.001188201
-19.01778297	-19.01736364	-19.01709227	0.000627137
-18.29766656	-18.38116253	-18.04918794	0.106862629
-18.824281	-18.82983205	-18.80408098	0.012754133
-19.07584595	-19.08160469	-19.06206406	0.007203208
-19.23993426	-19.24285992	-19.23610053	0.002578203
-19.36091014	-19.36083598	-19.35915895	0.001215568
-19.4528262	-19.4532803	-19.45129127	0.000789108
-18.63748846	-18.72397852	-18.39290543	0.106304525
-19.16516447	-19.1649549	-19.14318897	0.013388251
-19.42011776	-19.42518624	-19.40657658	0.006832086
-19.58650313	-19.58941314	-19.5820005	0.002565892
-19.70879555	-19.70914348	-19.70690496	0.000798479
-19.80169844	-19.8020195	-19.79962836	0.000835333
-18.93202785	-19.02435113	-18.69031448	0.107984783
-19.46458709	-19.46573704	-19.4451742	0.012817506
-19.72024902	-19.72930254	-19.70865335	0.00589177
-19.88820442	-19.89102252	-19.88419984	0.00242593
-20.01201383	-20.013282	-20.01028328	0.000825485
-20.10605201	-20.10635677	-20.10471008	0.000753773
-19.20659582	-19.29650539	-18.97079891	0.103987527
-19.73890129	-19.75257814	-19.71691371	0.013559823

-19.99716229	-19.99456882	-19.98316297	0.00720205
-20.16651115	-20.17054184	-20.16222854	0.003060751
-20.29121523	-20.29061438	-20.29030613	0.000711148
-20.38565959	-20.38629461	-20.38426031	0.000899565

Model ID	Well	Image type	Top [m]	Bottom [m]	Interval [m]	Structural class	Geostatistical anisotropy type	Effective stress [MPa]
Mod27	B6	FMI	1604.00	1606.00	2.00	Large Clasts	Geometric, vertical	1
Mod27	B6	FMI	1604.00	1606.00	2.00	Large Clasts	Geometric, vertical	1
Mod27	B6	FMI	1604.00	1606.00	2.00	Large Clasts	Geometric, vertical	1
Mod27	B6	FMI	1604.00	1606.00	2.00	Large Clasts	Geometric, vertical	1
Mod27	B6	FMI	1604.00	1606.00	2.00	Large Clasts	Geometric, vertical	1
Mod27	B6	FMI	1604.00	1606.00	2.00	Large Clasts	Geometric, vertical	1
Mod27	B6	FMI	1604.00	1606.00	2.00	Large Clasts	Geometric, vertical	5
Mod27	B6	FMI	1604.00	1606.00	2.00	Large Clasts	Geometric, vertical	5
Mod27	B6	FMI	1604.00	1606.00	2.00	Large Clasts	Geometric, vertical	5
Mod27	B6	FMI	1604.00	1606.00	2.00	Large Clasts	Geometric, vertical	5
Mod27	B6	FMI	1604.00	1606.00	2.00	Large Clasts	Geometric, vertical	5
Mod27	B6	FMI	1604.00	1606.00	2.00	Large Clasts	Geometric, vertical	5
Mod27	B6	FMI	1604.00	1606.00	2.00	Large Clasts	Geometric, vertical	10
Mod27	B6	FMI	1604.00	1606.00	2.00	Large Clasts	Geometric, vertical	10
Mod27	B6	FMI	1604.00	1606.00	2.00	Large Clasts	Geometric, vertical	10
Mod27	B6	FMI	1604.00	1606.00	2.00	Large Clasts	Geometric, vertical	10
Mod27	B6	FMI	1604.00	1606.00	2.00	Large Clasts	Geometric, vertical	10
Mod27	B6	FMI	1604.00	1606.00	2.00	Large Clasts	Geometric, vertical	10
Mod27	B6	FMI	1604.00	1606.00	2.00	Large Clasts	Geometric, vertical	15
Mod27	B6	FMI	1604.00	1606.00	2.00	Large Clasts	Geometric, vertical	15
Mod27	B6	FMI	1604.00	1606.00	2.00	Large Clasts	Geometric, vertical	15
Mod27	B6	FMI	1604.00	1606.00	2.00	Large Clasts	Geometric, vertical	15
Mod27	B6	FMI	1604.00	1606.00	2.00	Large Clasts	Geometric, vertical	15
Mod27	B6	FMI	1604.00	1606.00	2.00	Large Clasts	Geometric, vertical	15
Mod27	B6	FMI	1604.00	1606.00	2.00	Large Clasts	Geometric, vertical	20
Mod27	B6	FMI	1604.00	1606.00	2.00	Large Clasts	Geometric, vertical	20
Mod27	B6	FMI	1604.00	1606.00	2.00	Large Clasts	Geometric, vertical	20
Mod27	B6	FMI	1604.00	1606.00	2.00	Large Clasts	Geometric, vertical	20
Mod27	B6	FMI	1604.00	1606.00	2.00	Large Clasts	Geometric, vertical	20
Mod27	B6	FMI	1604.00	1606.00	2.00	Large Clasts	Geometric, vertical	20
Mod27	B6	FMI	1604.00	1606.00	2.00	Large Clasts	Geometric, vertical	25
Mod27	B6	FMI	1604.00	1606.00	2.00	Large Clasts	Geometric, vertical	25

Mod27	B6	FMI	1604.00	1606.00	2.00	Large Clasts	Geometric, vertical	25
Mod27	B6	FMI	1604.00	1606.00	2.00	Large Clasts	Geometric, vertical	25
Mod27	B6	FMI	1604.00	1606.00	2.00	Large Clasts	Geometric, vertical	25
Mod27	B6	FMI	1604.00	1606.00	2.00	Large Clasts	Geometric, vertical	25
Mod27	B6	FMI	1604.00	1606.00	2.00	Large Clasts	Geometric, vertical	30
Mod27	B6	FMI	1604.00	1606.00	2.00	Large Clasts	Geometric, vertical	30
Mod27	B6	FMI	1604.00	1606.00	2.00	Large Clasts	Geometric, vertical	30
Mod27	B6	FMI	1604.00	1606.00	2.00	Large Clasts	Geometric, vertical	30
Mod27	B6	FMI	1604.00	1606.00	2.00	Large Clasts	Geometric, vertical	30
Mod27	B6	FMI	1604.00	1606.00	2.00	Large Clasts	Geometric, vertical	30
Mod28	B19	Core	1697.45	1697.57	0.12	Large Clasts	Isotropic	1
Mod28	B19	Core	1697.45	1697.57	0.12	Large Clasts	Isotropic	1
Mod28	B19	Core	1697.45	1697.57	0.12	Large Clasts	Isotropic	1
Mod28	B19	Core	1697.45	1697.57	0.12	Large Clasts	Isotropic	1
Mod28	B19	Core	1697.45	1697.57	0.12	Large Clasts	Isotropic	1
Mod28	B19	Core	1697.45	1697.57	0.12	Large Clasts	Isotropic	1
Mod28	B19	Core	1697.45	1697.57	0.12	Large Clasts	Isotropic	5
Mod28	B19	Core	1697.45	1697.57	0.12	Large Clasts	Isotropic	5
Mod28	B19	Core	1697.45	1697.57	0.12	Large Clasts	Isotropic	5
Mod28	B19	Core	1697.45	1697.57	0.12	Large Clasts	Isotropic	5
Mod28	B19	Core	1697.45	1697.57	0.12	Large Clasts	Isotropic	5
Mod28	B19	Core	1697.45	1697.57	0.12	Large Clasts	Isotropic	5
Mod28	B19	Core	1697.45	1697.57	0.12	Large Clasts	Isotropic	10
Mod28	B19	Core	1697.45	1697.57	0.12	Large Clasts	Isotropic	10
Mod28	B19	Core	1697.45	1697.57	0.12	Large Clasts	Isotropic	10
Mod28	B19	Core	1697.45	1697.57	0.12	Large Clasts	Isotropic	10
Mod28	B19	Core	1697.45	1697.57	0.12	Large Clasts	Isotropic	10
Mod28	B19	Core	1697.45	1697.57	0.12	Large Clasts	Isotropic	10
Mod28	B19	Core	1697.45	1697.57	0.12	Large Clasts	Isotropic	15
Mod28	B19	Core	1697.45	1697.57	0.12	Large Clasts	Isotropic	15
Mod28	B19	Core	1697.45	1697.57	0.12	Large Clasts	Isotropic	15
Mod28	B19	Core	1697.45	1697.57	0.12	Large Clasts	Isotropic	15
Mod28	B19	Core	1697.45	1697.57	0.12	Large Clasts	Isotropic	15

Mod28	B19	Core	1697.45	1697.57	0.12	Large Clasts	Isotropic	15
Mod28	B19	Core	1697.45	1697.57	0.12	Large Clasts	Isotropic	20
Mod28	B19	Core	1697.45	1697.57	0.12	Large Clasts	Isotropic	20
Mod28	B19	Core	1697.45	1697.57	0.12	Large Clasts	Isotropic	20
Mod28	B19	Core	1697.45	1697.57	0.12	Large Clasts	Isotropic	20
Mod28	B19	Core	1697.45	1697.57	0.12	Large Clasts	Isotropic	20
Mod28	B19	Core	1697.45	1697.57	0.12	Large Clasts	Isotropic	20
Mod28	B19	Core	1697.45	1697.57	0.12	Large Clasts	Isotropic	25
Mod28	B19	Core	1697.45	1697.57	0.12	Large Clasts	Isotropic	25
Mod28	B19	Core	1697.45	1697.57	0.12	Large Clasts	Isotropic	25
Mod28	B19	Core	1697.45	1697.57	0.12	Large Clasts	Isotropic	25
Mod28	B19	Core	1697.45	1697.57	0.12	Large Clasts	Isotropic	25
Mod28	B19	Core	1697.45	1697.57	0.12	Large Clasts	Isotropic	25
Mod28	B19	Core	1697.45	1697.57	0.12	Large Clasts	Isotropic	30
Mod28	B19	Core	1697.45	1697.57	0.12	Large Clasts	Isotropic	30
Mod28	B19	Core	1697.45	1697.57	0.12	Large Clasts	Isotropic	30
Mod28	B19	Core	1697.45	1697.57	0.12	Large Clasts	Isotropic	30
Mod28	B19	Core	1697.45	1697.57	0.12	Large Clasts	Isotropic	30
Mod28	B19	Core	1697.45	1697.57	0.12	Large Clasts	Isotropic	30
Mod30	B20	Core	1658.14	1658.40	0.26	Large Clasts	Zonal, vertical	1
Mod30	B20	Core	1658.14	1658.40	0.26	Large Clasts	Zonal, vertical	1
Mod30	B20	Core	1658.14	1658.40	0.26	Large Clasts	Zonal, vertical	1
Mod30	B20	Core	1658.14	1658.40	0.26	Large Clasts	Zonal, vertical	1
Mod30	B20	Core	1658.14	1658.40	0.26	Large Clasts	Zonal, vertical	1
Mod30	B20	Core	1658.14	1658.40	0.26	Large Clasts	Zonal, vertical	1
Mod30	B20	Core	1658.14	1658.40	0.26	Large Clasts	Zonal, vertical	5
Mod30	B20	Core	1658.14	1658.40	0.26	Large Clasts	Zonal, vertical	5
Mod30	B20	Core	1658.14	1658.40	0.26	Large Clasts	Zonal, vertical	5
Mod30	B20	Core	1658.14	1658.40	0.26	Large Clasts	Zonal, vertical	5
Mod30	B20	Core	1658.14	1658.40	0.26	Large Clasts	Zonal, vertical	5
Mod30	B20	Core	1658.14	1658.40	0.26	Large Clasts	Zonal, vertical	5
Mod30	B20	Core	1658.14	1658.40	0.26	Large Clasts	Zonal, vertical	10
Mod30	B20	Core	1658.14	1658.40	0.26	Large Clasts	Zonal, vertical	10

Mod30	B20	Core	1658.14	1658.40	0.26	Large Clasts	Zonal, vertical	10
Mod30	B20	Core	1658.14	1658.40	0.26	Large Clasts	Zonal, vertical	10
Mod30	B20	Core	1658.14	1658.40	0.26	Large Clasts	Zonal, vertical	10
Mod30	B20	Core	1658.14	1658.40	0.26	Large Clasts	Zonal, vertical	10
Mod30	B20	Core	1658.14	1658.40	0.26	Large Clasts	Zonal, vertical	15
Mod30	B20	Core	1658.14	1658.40	0.26	Large Clasts	Zonal, vertical	15
Mod30	B20	Core	1658.14	1658.40	0.26	Large Clasts	Zonal, vertical	15
Mod30	B20	Core	1658.14	1658.40	0.26	Large Clasts	Zonal, vertical	15
Mod30	B20	Core	1658.14	1658.40	0.26	Large Clasts	Zonal, vertical	15
Mod30	B20	Core	1658.14	1658.40	0.26	Large Clasts	Zonal, vertical	15
Mod30	B20	Core	1658.14	1658.40	0.26	Large Clasts	Zonal, vertical	20
Mod30	B20	Core	1658.14	1658.40	0.26	Large Clasts	Zonal, vertical	20
Mod30	B20	Core	1658.14	1658.40	0.26	Large Clasts	Zonal, vertical	20
Mod30	B20	Core	1658.14	1658.40	0.26	Large Clasts	Zonal, vertical	20
Mod30	B20	Core	1658.14	1658.40	0.26	Large Clasts	Zonal, vertical	20
Mod30	B20	Core	1658.14	1658.40	0.26	Large Clasts	Zonal, vertical	20
Mod30	B20	Core	1658.14	1658.40	0.26	Large Clasts	Zonal, vertical	25
Mod30	B20	Core	1658.14	1658.40	0.26	Large Clasts	Zonal, vertical	25
Mod30	B20	Core	1658.14	1658.40	0.26	Large Clasts	Zonal, vertical	25
Mod30	B20	Core	1658.14	1658.40	0.26	Large Clasts	Zonal, vertical	25
Mod30	B20	Core	1658.14	1658.40	0.26	Large Clasts	Zonal, vertical	25
Mod30	B20	Core	1658.14	1658.40	0.26	Large Clasts	Zonal, vertical	25
Mod30	B20	Core	1658.14	1658.40	0.26	Large Clasts	Zonal, vertical	30
Mod30	B20	Core	1658.14	1658.40	0.26	Large Clasts	Zonal, vertical	30
Mod30	B20	Core	1658.14	1658.40	0.26	Large Clasts	Zonal, vertical	30
Mod30	B20	Core	1658.14	1658.40	0.26	Large Clasts	Zonal, vertical	30
Mod30	B20	Core	1658.14	1658.40	0.26	Large Clasts	Zonal, vertical	30
Mod30	B20	Core	1658.14	1658.40	0.26	Large Clasts	Zonal, vertical	30

Mud content [%]	Mean cohesive content [%]	Mean porosity [fraction]	Minimum log10 effective Kh [m2]	Mean log10 effective Kh [m2]
50	39.18235161	0.413766711	-15.87996269	-14.33869363
60	46.01881599	0.431417371	-16.22323201	-15.31143193
70	52.85528036	0.449050708	-16.49949595	-15.62268797
80	59.69174474	0.466729956	-16.65276954	-16.49452565
90	66.52820912	0.484355038	-16.81973359	-16.77532295
100	73.36467349	0.50198791	-16.96808684	-16.96499984
50	39.18235161	0.332878618	-16.97535427	-14.93335506
60	46.01881599	0.342478348	-17.31920505	-16.1899882
70	52.85528036	0.351993295	-17.59041851	-16.51381847
80	59.69174474	0.361552191	-17.73749433	-17.58005181
90	66.52820912	0.371096107	-17.90061981	-17.8556288
100	73.36467349	0.38062728	-18.04205479	-18.0376048
50	39.18235161	0.283358354	-17.57859023	-15.37125225
60	46.01881599	0.288092757	-17.90809047	-16.71492386
70	52.85528036	0.292773345	-18.17621027	-17.02700988
80	59.69174474	0.297451683	-18.32518753	-18.16559361
90	66.52820912	0.30220185	-18.48420031	-18.44088743
100	73.36467349	0.30697319	-18.62249705	-18.61838388
50	39.18235161	0.247541278	-17.98881031	-15.72278197
60	46.01881599	0.248921244	-18.31160154	-17.10470839
70	52.85528036	0.250356644	-18.5823025	-17.40854094
80	59.69174474	0.251716933	-18.72941898	-18.57051339
90	66.52820912	0.253165336	-18.88224495	-18.84285792
100	73.36467349	0.254526062	-19.02034193	-19.01612934
50	39.18235161	0.218028466	-18.3219617	-16.05781667
60	46.01881599	0.216753853	-18.64121264	-17.4333637
70	52.85528036	0.215577248	-18.90499463	-17.73399908
80	59.69174474	0.214359017	-19.05533822	-18.89727303
90	66.52820912	0.213133663	-19.20449746	-19.16699949
100	73.36467349	0.211849197	-19.34167373	-19.33800341
50	39.18235161	0.192368695	-18.61539572	-16.35227354
60	46.01881599	0.188899131	-18.92774275	-17.72981248

70	52.85528036	0.185475434	-19.19246159	-18.02391301
80	59.69174474	0.181993331	-19.34407152	-19.18792576
90	66.52820912	0.178509753	-19.48910528	-19.45203284
100	73.36467349	0.175031255	-19.62430713	-19.62114925
50	39.18235161	0.169511401	-18.88737154	-16.64124517
60	46.01881599	0.164011816	-19.1948493	-18.00616142
70	52.85528036	0.158526778	-19.45786826	-18.30473204
80	59.69174474	0.153058645	-19.60689532	-19.45393546
90	66.52820912	0.147547609	-19.75098763	-19.71592489
100	73.36467349	0.142060414	-19.88642428	-19.88336385
50	39.18235161	0.413738654	-15.83455386	-15.49906089
60	46.01881599	0.43139552	-16.18508216	-16.08155219
70	52.85528036	0.449049916	-16.48639491	-16.43042695
80	59.69174474	0.466693762	-16.69590603	-16.66701019
90	66.52820912	0.484425025	-16.85466061	-16.84560277
100	73.36467349	0.502039335	-16.97101417	-16.96964373
50	39.18235161	0.332877191	-16.93756469	-16.52533134
60	46.01881599	0.342460466	-17.2917083	-17.18262491
70	52.85528036	0.351985941	-17.58304345	-17.52682712
80	59.69174474	0.361578447	-17.78333013	-17.75466211
90	66.52820912	0.371147439	-17.93437174	-17.92519042
100	73.36467349	0.380709668	-18.04729084	-18.04535641
50	39.18235161	0.283387889	-17.5346112	-17.10208518
60	46.01881599	0.288107197	-17.8896157	-17.77854025
70	52.85528036	0.292774082	-18.1728156	-18.11742095
80	59.69174474	0.297512514	-18.37179709	-18.34264181
90	66.52820912	0.302267716	-18.51820492	-18.50892666
100	73.36467349	0.306911027	-18.62698864	-18.62551852
50	39.18235161	0.247501997	-17.94288948	-17.49961593
60	46.01881599	0.248916019	-18.29431329	-18.18595467
70	52.85528036	0.25034583	-18.57858036	-18.52283351
80	59.69174474	0.251698236	-18.77283601	-18.7449697
90	66.52820912	0.253125713	-18.91755574	-18.9084791

100	73.36467349	0.254444536	-19.02405561	-19.02286144
50	39.18235161	0.218039106	-18.26690389	-17.82474669
60	46.01881599	0.216770028	-18.62270468	-18.51519204
70	52.85528036	0.215574915	-18.90505396	-18.85057139
80	59.69174474	0.21433899	-19.09607047	-19.07000157
90	66.52820912	0.213092799	-19.24045982	-19.23164299
100	73.36467349	0.21188752	-19.34584753	-19.34487015
50	39.18235161	0.192367862	-18.56404103	-18.11480451
60	46.01881599	0.188937427	-18.90796747	-18.80484908
70	52.85528036	0.185482135	-19.19359005	-19.13757948
80	59.69174474	0.181995759	-19.38287065	-19.35581619
90	66.52820912	0.178512713	-19.52393537	-19.51569695
100	73.36467349	0.175048688	-19.6285516	-19.62751477
50	39.18235161	0.169481547	-18.83210989	-18.38429007
60	46.01881599	0.163999652	-19.17459336	-19.06906092
70	52.85528036	0.158536017	-19.45754183	-19.40322107
80	59.69174474	0.153056688	-19.64716556	-19.62029332
90	66.52820912	0.147573661	-19.78712287	-19.77891146
100	73.36467349	0.142064916	-19.89016844	-19.88923925
50	39.18235161	0.413776576	-16.35420255	-16.10743009
60	46.01881599	0.431387487	-16.51387144	-16.41874318
70	52.85528036	0.449053715	-16.64652617	-16.62312878
80	59.69174474	0.466674874	-16.79075315	-16.76927897
90	66.52820912	0.484378262	-16.89121518	-16.88229476
100	73.36467349	0.501972226	-16.97828986	-16.97609725
50	39.18235161	0.332926447	-17.44514999	-17.19178471
60	46.01881599	0.342512767	-17.60336135	-17.50635268
70	52.85528036	0.352000561	-17.73453594	-17.70922192
80	59.69174474	0.361562555	-17.87510795	-17.85305294
90	66.52820912	0.371130754	-17.97321759	-17.96299356
100	73.36467349	0.380690148	-18.05638629	-18.05340079
50	39.18235161	0.283397817	-18.03193053	-17.78020371
60	46.01881599	0.288062997	-18.18701716	-18.09203565

70	52.85528036	0.292792575	-18.3160196	-18.29282708
80	59.69174474	0.297524727	-18.45736127	-18.43594818
90	66.52820912	0.302209863	-18.55339605	-18.54420606
100	73.36467349	0.3068962	-18.63532333	-18.63305495
50	39.18235161	0.247540666	-18.4274955	-18.17970838
60	46.01881599	0.248922626	-18.58186616	-18.49230176
70	52.85528036	0.250309081	-18.71290625	-18.69162157
80	59.69174474	0.251761395	-18.85529506	-18.834216
90	66.52820912	0.253110667	-18.95066566	-18.94168163
100	73.36467349	0.254537197	-19.03173519	-19.02987709
50	39.18235161	0.217974861	-18.74795809	-18.50084974
60	46.01881599	0.216781494	-18.90368451	-18.81475974
70	52.85528036	0.21558221	-19.03416449	-19.01385061
80	59.69174474	0.214350114	-19.17636799	-19.15582933
90	66.52820912	0.213117289	-19.27296002	-19.26299774
100	73.36467349	0.211881058	-19.35281074	-19.35074067
50	39.18235161	0.192384496	-19.0314232	-18.78845391
60	46.01881599	0.188948013	-19.18443088	-19.09870442
70	52.85528036	0.185466709	-19.31651978	-19.29700799
80	59.69174474	0.181986713	-19.45856055	-19.43861432
90	66.52820912	0.178509528	-19.55382023	-19.54528271
100	73.36467349	0.175044489	-19.6341303	-19.63278003
50	39.18235161	0.1694899	-19.29227998	-19.05161654
60	46.01881599	0.164052995	-19.45029801	-19.36214343
70	52.85528036	0.158532088	-19.57961842	-19.55936086
80	59.69174474	0.153064756	-19.72110242	-19.70085435
90	66.52820912	0.147591108	-19.81656501	-19.80735905
100	73.36467349	0.14206746	-19.89602875	-19.89424357

Mode log10 effective Kh [m2]	Maximum log10 effective Kh [m2]	Standard deviation log10 effective Kh [m2]	Minimum log10 effective Kv [m2]
-13.79314641	-13.4453437	0.96805308	-16.46812274
-16.22323201	-13.65694608	1.050104296	-16.54570102
-16.49949595	-13.97263408	1.032839703	-16.68917079
-16.65276954	-16.04057889	0.189200853	-16.90089281
-16.80376008	-16.70791901	0.036050096	-17.05411505
-16.96808684	-16.9624739	0.001835568	-17.16039124
-14.2568451	-13.80376024	1.298328942	-17.67836222
-17.31920505	-14.02638453	1.388768693	-17.76142955
-17.59041851	-14.33455504	1.349004728	-17.87665479
-17.73749433	-17.10577092	0.193579662	-18.09237746
-17.88482693	-17.79006966	0.03603788	-18.25323584
-18.03856514	-18.03391226	0.002466162	-18.37053841
-14.65483969	-14.16754793	1.404283508	-18.31342093
-17.90809047	-14.3770124	1.50056045	-18.3960333
-18.17621027	-14.68482764	1.47049223	-18.50303024
-18.32518753	-17.65320513	0.20257478	-18.72439154
-18.46931193	-18.37998165	0.034886709	-18.88922516
-18.62045121	-18.61533661	0.002267225	-19.0121948
-14.99999259	-14.5018563	1.440561682	-18.7407383
-18.31160154	-14.71837585	1.529429819	-18.82099142
-18.5823025	-15.02866755	1.508303054	-18.93202948
-18.72941898	-18.06304816	0.200031817	-19.15208387
-18.86819946	-18.78392651	0.033052704	-19.32244232
-19.01724468	-19.01311501	0.002191974	-19.44522867
-15.31904305	-14.8185566	1.44197893	-19.07816116
-18.64121264	-15.03800829	1.533308396	-19.16837719
-18.90499463	-15.35445493	1.512086732	-19.27711857
-19.05533822	-18.38367365	0.1998744	-19.49781741
-19.19109686	-19.11069325	0.03206466	-19.66938333
-19.33988294	-19.33540597	0.002004237	-19.79344396
-15.62643988	-15.12828057	1.43792091	-19.37959533
-18.92774275	-15.34786587	1.520680371	-19.46768651

-19.19246159	-15.67149604	1.508773106	-19.58200216
-19.34407152	-18.70474086	0.190112036	-19.79877226
-19.47601253	-19.39745604	0.031154552	-19.97090043
-19.61983137	-19.61908541	0.001617832	-20.09766526
-15.93271144	-15.44026809	1.42442706	-19.65485573
-19.1948493	-15.64721568	1.508860561	-19.7401864
-19.45786826	-15.96589719	1.486957098	-19.85745099
-19.60689532	-18.97622094	0.187988214	-20.07620698
-19.73823068	-19.66168896	0.030236348	-20.25004736
-19.88345206	-19.88122289	0.001464694	-20.37730945
-15.68977361	-14.82109209	0.290080117	-15.95754656
-16.14209232	-15.88415327	0.078017195	-16.38611908
-16.44782325	-16.35139412	0.032535145	-16.64937601
-16.68665065	-16.63111834	0.021049347	-16.85634829
-16.85466061	-16.83069008	0.007967364	-17.02358307
-16.96978727	-16.9681514	0.000679346	-17.15421508
-16.93756469	-15.24621631	0.468711322	-17.08730032
-17.24711391	-16.97954756	0.080477949	-17.53341261
-17.54421413	-17.44714083	0.03277336	-17.80784529
-17.77398027	-17.71788112	0.020841711	-18.03143347
-17.93437174	-17.91053647	0.008050899	-18.21324361
-18.04626474	-18.04369948	0.001073496	-18.36071477
-17.5346112	-15.62409873	0.529913486	-17.70044258
-17.84521171	-17.57878777	0.079729988	-18.15003729
-18.13378012	-18.0361914	0.032851784	-18.43109576
-18.3620625	-18.30365497	0.020884573	-18.65961141
-18.51820492	-18.49322852	0.008113487	-18.84703933
-18.62698864	-18.62286502	0.001252234	-19.00017288
-17.94288948	-15.92531518	0.559338115	-18.11405728
-18.25067787	-17.98886534	0.078351701	-18.5654295
-18.53975836	-18.44270338	0.032387075	-18.85422575
-18.76342045	-18.70692707	0.020428594	-19.08600717
-18.91755574	-18.89361869	0.007867225	-19.2784408

-19.02405561	-19.02130056	0.000869484	-19.43415808
-18.26690389	-16.23252058	0.566127489	-18.44846949
-18.5787049	-18.31470622	0.079139361	-18.90574205
-18.86654997	-18.77029001	0.032143025	-19.19273294
-19.08712991	-19.03348658	0.019884467	-19.42532414
-19.24045982	-19.2180243	0.007368816	-19.62352342
-19.34584753	-19.34358458	0.000726679	-19.7836203
-18.56404103	-16.5025893	0.572372134	-18.7461582
-18.86626422	-18.61604468	0.075278981	-19.19911666
-19.15512144	-19.05894994	0.031966789	-19.49000222
-19.37378449	-19.31926755	0.019597115	-19.72919543
-19.52393537	-19.50215294	0.0072169	-19.92332315
-19.6285516	-19.62620375	0.000798418	-20.08637686
-18.83210989	-16.79993511	0.563678804	-19.01208583
-19.13115977	-18.87055825	0.078112153	-19.47108972
-19.42000578	-19.32616567	0.031161891	-19.76380043
-19.63841805	-19.58593293	0.019013856	-20.00578406
-19.78712287	-19.76548272	0.007102171	-20.20261472
-19.88982444	-19.88776042	0.000736492	-20.36577471
-16.27960271	-15.83200369	0.178272342	-15.4610645
-16.45296954	-16.30071481	0.063423873	-15.76526512
-16.64652617	-16.58829445	0.017236648	-16.19604401
-16.77721203	-16.74335921	0.013858951	-16.57746433
-16.89121518	-16.86460017	0.007278818	-16.9026212
-16.97638396	-16.97384277	0.001210057	-17.14063891
-17.36760771	-16.90235405	0.185279725	-16.5753568
-17.54225584	-17.38949208	0.064117231	-16.88817649
-17.72589764	-17.67406789	0.017649655	-17.31076664
-17.86144792	-17.82729785	0.014273915	-17.71589878
-17.97321759	-17.94368985	0.007884561	-18.06341237
-18.0535566	-18.04978367	0.00184069	-18.33660913
-18.03193053	-17.52330891	0.178849159	-17.18075293
-18.12481663	-17.96931529	0.06417902	-17.4845779

-18.3160196	-18.25778407	0.017212176	-17.92491678
-18.45048498	-18.40922725	0.014315509	-18.32653857
-18.54952955	-18.52633059	0.007261697	-18.686485
-18.63532333	-18.62975716	0.001624686	-18.97486625
-18.35294331	-17.90563021	0.181383559	-17.57252038
-18.58186616	-18.37600994	0.062593585	-17.90717763
-18.71290625	-18.65672536	0.016863175	-18.33989283
-18.84197737	-18.80868315	0.013828948	-18.7426959
-18.94685951	-18.92402261	0.007183809	-19.1102715
-19.03173519	-19.0269909	0.0014122	-19.40868714
-18.6710858	-18.20985211	0.183966239	-17.91113774
-18.8452505	-18.69916548	0.061983345	-18.23100174
-19.03416449	-18.97824855	0.017204583	-18.67359449
-19.16971264	-19.1297805	0.013581497	-19.08585896
-19.26904714	-19.24556986	0.007167795	-19.45334631
-19.35094836	-19.34846517	0.001220548	-19.7563965
-18.95901331	-18.52455401	0.177940714	-18.21109028
-19.18443088	-18.98247835	0.06166407	-18.53550896
-19.31651978	-19.26391678	0.017061648	-18.96614618
-19.45222412	-19.4142055	0.013101436	-19.38288953
-19.5500008	-19.52708419	0.007083658	-19.75399163
-19.6341303	-19.63006648	0.001225819	-20.05905541
-19.21968862	-18.78414046	0.178229596	-18.47486834
-19.45029801	-19.24165972	0.062568734	-18.80118901
-19.57961842	-19.5247735	0.017427761	-19.23825027
-19.70847392	-19.67690266	0.012964455	-19.65296482
-19.812855	-19.79059491	0.006765902	-20.02960663
-19.89447358	-19.89240002	0.001070893	-20.34018835

Mean log10 effective Kv [m2]	Mode log10 effective Kv [m2]	Maximum log10 effective Kv [m2]	Standard deviation log10 effective Kv [m2]
-15.71817744	-16.46812274	-14.11346303	0.791752636
-16.37541034	-16.54570102	-16.08155131	0.135394846
-16.62827655	-16.68917079	-16.43920177	0.07253229
-16.87093	-16.90089281	-16.83576912	0.022242755
-17.03463434	-17.042078	-17.01198537	0.012178735
-17.15557766	-17.15658384	-17.15150729	0.002725073
-16.71490695	-17.67836222	-14.47976152	1.106974554
-17.54027828	-17.76142955	-17.24087706	0.153602173
-17.80617032	-17.87665479	-17.58381233	0.083907839
-18.05789719	-18.05837197	-18.01303131	0.023317194
-18.23215511	-18.23456709	-18.20967542	0.012459678
-18.36373868	-18.36609927	-18.35500142	0.004575827
-17.28457253	-18.31342093	-14.84262484	1.203024451
-18.16543737	-18.3960333	-17.8761353	0.157214484
-18.4350147	-18.50303024	-18.20898693	0.085170118
-18.68973253	-18.68654768	-18.63608919	0.024959334
-18.86762639	-18.86990767	-18.84415101	0.012821083
-19.00467189	-19.00509249	-18.99562273	0.004679683
-17.68700986	-18.7407383	-15.17746123	1.238935665
-18.58593135	-18.82099142	-18.30032441	0.159439037
-18.86189338	-18.93202948	-18.63050027	0.087368636
-19.11796139	-19.15208387	-19.06325058	0.025324784
-19.30021978	-19.303756	-19.2788409	0.012690488
-19.43819092	-19.44522867	-19.4300178	0.004486898
-18.0251931	-19.07816116	-15.48382305	1.246150566
-18.93136978	-19.16837719	-18.63771549	0.161235798
-19.20526801	-19.27711857	-18.9709248	0.088762042
-19.46400305	-19.49781741	-19.40876394	0.025176269
-19.64667692	-19.65041872	-19.62513256	0.012770202
-19.78597062	-19.7867411	-19.77780395	0.004286462
-18.32160102	-19.37959533	-15.78521706	1.245332516
-19.2313095	-19.46768651	-18.94533716	0.159196287

-19.50522667	-19.58200216	-19.26531776	0.091362252
-19.7649585	-19.79877226	-19.70766195	0.025712583
-19.94804863	-19.95146266	-19.92554562	0.01238428
-20.08997333	-20.09032142	-20.08052965	0.004795375
-18.60490966	-19.65485573	-16.08631804	1.241787681
-19.50320364	-19.7401864	-19.21722792	0.162120173
-19.78120369	-19.85745099	-19.54170217	0.090461158
-20.04151361	-20.07620698	-19.98218647	0.026548779
-20.22632279	-20.22933665	-20.20172236	0.0128949
-20.36908331	-20.36956131	-20.35923045	0.004980108
-15.56798584	-15.95754656	-14.43318789	0.405890949
-16.23762521	-16.32323125	-15.94590427	0.117574557
-16.56745095	-16.64937601	-16.40136267	0.073400569
-16.82054498	-16.85634829	-16.73877759	0.034571819
-17.01183137	-17.01919079	-16.99283708	0.00883936
-17.15245821	-17.15421508	-17.15038652	0.001318486
-16.59478063	-17.08730032	-14.80719289	0.620961625
-17.37853278	-17.46863385	-17.07996124	0.121593502
-17.72254547	-17.80784529	-17.53739688	0.080780716
-17.99042287	-18.03143347	-17.89440126	0.041043194
-18.19845148	-18.21324361	-18.17076572	0.012681569
-18.35781729	-18.3575342	-18.35329345	0.002065752
-17.18519307	-17.70044258	-15.22384311	0.676258602
-17.99298641	-18.08437051	-17.69036983	0.123365116
-18.33980526	-18.43109576	-18.14833874	0.083347894
-18.61576818	-18.65961141	-18.51598219	0.042668897
-18.8305802	-18.84703933	-18.80115329	0.013727977
-18.99726454	-19.00017288	-18.99171928	0.002424125
-17.587074	-18.11405728	-15.55155031	0.700919195
-18.40761422	-18.49827998	-18.0953829	0.126846617
-18.76295032	-18.85422575	-18.56776851	0.086045391
-19.04034534	-19.08600717	-18.93943436	0.04356005
-19.25958197	-19.2784408	-19.22724861	0.015103632

-19.43039425	-19.43146736	-19.42474055	0.002740213
-17.92015001	-18.44846949	-15.83894061	0.714297938
-18.7444989	-18.83677253	-18.42295536	0.129224729
-19.10179853	-19.19273294	-18.90501208	0.085811273
-19.3829291	-19.42532414	-19.28225047	0.043748325
-19.60474417	-19.62352342	-19.57277201	0.015286059
-19.77901704	-19.78215549	-19.77336659	0.002718117
-18.20958592	-18.7461582	-16.13171184	0.714281088
-19.0397816	-19.1307441	-18.72050873	0.129215145
-19.39865022	-19.49000222	-19.20577414	0.085686907
-19.68222125	-19.72919543	-19.58063252	0.044107519
-19.9056623	-19.92332315	-19.87482138	0.014617404
-20.08278188	-20.08637686	-20.07665234	0.002789412
-18.48222252	-19.01208583	-16.42202018	0.711724717
-19.31021093	-19.4037391	-18.99963535	0.127364624
-19.67166964	-19.76380043	-19.4755143	0.086830924
-19.9571033	-20.00578406	-19.85156394	0.045866042
-20.18328869	-20.20261472	-20.14996674	0.015688722
-20.36137309	-20.36429317	-20.35540387	0.002958018
-13.80711063	-13.67246981	-13.37437069	0.593032622
-14.32356377	-13.96345917	-13.66315818	0.760103948
-15.33575443	-16.19604401	-14.32148526	0.736860115
-16.35733555	-16.49993113	-16.03473196	0.153723623
-16.81574954	-16.9026212	-16.66762618	0.066160979
-17.13775433	-17.13606753	-17.13530563	0.001776273
-14.24677057	-14.13392886	-13.72702421	0.807179827
-14.85994053	-14.43812681	-14.0297852	1.047606261
-16.15813012	-15.08866484	-14.71831454	1.085978797
-17.48432308	-17.63352791	-17.13930273	0.165557307
-17.96816522	-18.02715482	-17.80960947	0.071312119
-18.33154995	-18.33523472	-18.32698831	0.003021791
-14.63790886	-14.52044807	-14.07706393	0.882976007
-15.2801486	-14.84743579	-14.40791211	1.129789777

-16.65373364	-17.92491678	-14.93092419	1.221479928
-18.09774469	-18.24420067	-17.75017329	0.162596284
-18.59085041	-18.64968788	-18.4289052	0.073170408
-18.96760071	-18.97114929	-18.96185691	0.003773399
-14.96966966	-14.88043966	-14.43175954	0.892953077
-15.61557373	-15.19298433	-14.74061878	1.172669757
-17.02844594	-18.33989283	-15.21747721	1.270317794
-18.51119382	-18.65965006	-18.16137504	0.167759433
-19.01478529	-19.1102715	-18.85544447	0.073901475
-19.40056165	-19.40261614	-19.39452149	0.004128441
-15.29923545	-15.20194702	-14.75041523	0.901701004
-15.93067578	-15.50345897	-15.0488685	1.172118308
-17.34120311	-18.67359449	-15.54993112	1.293880571
-18.85335134	-19.00374446	-18.51105747	0.165696731
-19.35743739	-19.41635465	-19.19440468	0.073569845
-19.74808129	-19.75215587	-19.74155429	0.004257961
-15.60086582	-15.50744845	-15.05684148	0.894216485
-16.216655	-15.80894595	-15.35451878	1.17069612
-17.63499038	-18.96614618	-15.88529563	1.292375084
-19.14899567	-19.38288953	-18.79576332	0.169240938
-19.65610843	-19.75399163	-19.4815703	0.077751803
-20.05171524	-20.05509893	-20.04520773	0.004229805
-15.89507308	-15.81234642	-15.36859276	0.883713464
-16.51082493	-16.12230875	-15.67582871	1.157841764
-17.90907979	-16.63848911	-16.20519558	1.290919338
-19.42367527	-19.57034617	-19.07463427	0.165048655
-19.93018434	-19.99144301	-19.76246129	0.076213721
-20.33052022	-20.32724157	-20.32508377	0.004479623